29TH INTERNATIONAL TOWING TANK CONFERENCE

1st VIRTUAL CONFERENCE

Proceedings - Volume II

CENTRALE NANTES

DGA Hydrodynamics
FRANCE

29TH INTERNATIONAL TOWING TANK CONFERENCE

Organising Committee

Dr. Didier FRECHOU (Co-Chairman), DGA HYDRODYNAMICS
Prof. Pierre FERRANT (Co-Chairman), EC-NANTES

Jean-Baptiste AVRILLIER (Director), EC-NANTES
Laurent LE SAINT (Director), DGA HYDRODYNAMICS
Sandrine JAMET, EC-NANTES
Blandine MARIOT, EC-NANTES

Webinar support

Helena YANG (SeatoSky)
Ian HOLLIDAY (SeatoSky)

Sponsors

HR Wallingford
Qualisys Motion Capture
YLEC Consultants
General Acoustics
Sirehna NAVAL GROUP

Editor

Dr. Didier FRECHOU

Table of Content
Volume I

TABLE OF CONTENT VOLUME I ..... **IX**

TABLE OF CONTENT VOLUME II ..... **XIII**

THE EXECUTIVE COMMITTEE **1**

1. INTRODUCTION 1
2. OBITUARIES 1
3. COMMITTEE MEMBERSHIP 8
4. COMMITTEE MEETINGS 8
5. WORKING GROUP ON THE FUTURE OF ITTC 10
6. COMMITTEE ACTIVITIES 10
7. RECOMMENDATIONS TO THE FULL CONFERENCE 14

THE ADVISORY COUNCIL **15**

1. MEMBERSHIP AND MEETINGS 15
2. ACTIVITIES OF THE ADVISORY COUNCIL 15
3. OFFICERS FOR THE 30TH ITTC ADVISORY COUNCIL 17

RESISTANCE AND PROPULSION COMMITTEE **19**

1. INTRODUCTION 19
2. STATE OF THE ART 21
3. DEVELOPMENT OF PROCEDURE FOR WAVE PROFILE MEASUREMENT AND WAVE RESISTANCE ANALYSIS 39
4. VERIFICATION AND VALIDATION OF DETAILED FLOW FIELD DATA 39
5. INTERACTION WITH SHIPS IN OPERATION AT SEA COMMITTEE 43
6. HULL AND PROPELLER ROUGHNESS 44
7. UNEQUALLY LOADED MULTIPLE PROPELLER VESSELS 53
8. FULL SCALE DATA FOR PODDED PROPULSION 56
9. QUASI-STEADY PROPELLER AND PROPULSION TESTS 57
10. CAVITATION EROSION MODELLING AND PREDICTION 58
11. RIM DRIVE TESTING 63
12. INFLUENCE OF FD ON POWER PREDICTION 65
13. REYNOLDS NUMBER EFFECTS ON PROPELLER TESTING 69
14. SCALING METHODS FOR PROPULSORS 73
15. PROPULSOR PERFORMANCE IN WAVES 75
16. CONCLUSIONS AND RECOMMENDATIONS 78
17. REFERENCES 82

THE MANOEUVRING COMMITTEE **93**

1. INTRODUCTION 93
2. STATE OF THE ART 95
3. PROCEDURES 113
4. BENCHMARK DATA 117
5. UNDERWATER VEHICLES 118
6. CHALLENGES WITH RESPECT TO EXPERIMENTAL RESEARCH 132
7. CONCLUSIONS 139

8. RECOMMENDATIONS 142
9. REFERENCES 143

THE OCEAN ENGINEERING COMMITTEE 159

1. GENERAL 159
2. STATE-OF-THE-ART REVIEWS IN OFFSHORE STRUCTURES 161
3. REVIEW OF THE EXISTING PROCEDURES 196
4. STATE-OF-THE-ART REVIEW IN OFFSHORE AQUACULTURE SYSTEMS 196
5. STATE-OF-THE-ART REVIEW IN MODEL TESTS OF CABLE/PIPE DYNAMICS CLOSE TO THE SEA SURFACE 210
6. STATE-OF-THE-ART REVIEW IN HYBRID TESTING – SOFTWARE-IN-THE-LOOP TESTS FOR MODELLING WIND FORCES 215
7. EXPERIMENTAL BENCHMARK ON WAVE RUN-UP ON CYLINDERS 223
8. CFD BENCHMARK ON TWO-BODY INTERACTIONS 234
9. STATE-OF-THE-ART REVIEW IN LARGE DIAMETER FLEXIBLE RISERS FOR DEEP WATER MINING 247
10. PROCEDURE/GUIDELINE FOR MODEL CONSTRUCTION 254
11. CONCLUSIONS & RECOMMENDATIONS 254
12. REFERENCES 257

THE SEAKEEPING COMMITTEE 277

1. GENERAL 277
2. STATE OF ART REVIEW 279
3. DISCUSSION OF SPECIFIC TOPICS 322
4. COLLABORATION 331
5. ITTC RECOMMENDED PROCEDURES 332
6. CONCLUSIONS 335
7. ACKNOWLEDGEMENTS 342
8. REFERENCES 342

THE STABILITY IN WAVES COMMITTEE 367

1. INTRODUCTION 367
2. STATE-OF-THE-ART (TOR 1) 369
3. REVIEW ITTC RECOMMENDED PROCEDURES (TOR 2) 382
4. IMO 2ND GENERATION INTACT STABILITY CRITERIA (TOR 3) 385
5. RECOMMEDATION ON DEVELOPEING A SET OF PROCEDURES FOR DIRECT ASSESSMENT OF THE SECOND GENERATION IMO INTACT STABILITY CRITERIA (TOR 4) 394
6. FREE ROLL DECAY, FORCED ROLLING AND EXCITED ROLLING TESTS (TOR 5) 399
7. UPDATE PROCEDURE 7.5-02-07-04.5 ESTIMATION OF ROLL DAMPING (TOR 6) 402
8. UPDATING THE GUIDELINE 7.5-02-07-04.3 FOR PARAMETRIC ROLL (TOR 7) 403
9. UPDATE PROCEDURE 7.5-02-07-04.4 NUMERICAL SIMULATION OF CAPSIZE BEHAVIOUR OF DAMAGED SHIPS IN IRREGULAR BEAM SEAS (TOR 8) 406
10. DEVELOP/SUGGEST A METHOD FOR ESTIMATING TIME TO CAPSIZING AND / OR SINKING (TOR 9) 407
11. CONTINUE THE IDENTIFICATION OF BENCHMARK DATA FOR VALIDATION OF STABILITY IN WAVES PREDICTIONS (TOR 10) 408
12. RECOMMENDED PROCEDURES FOR INCLINING TESTS (TOR 11) 408
13. IMO LIAISON 409
14. CONCLUSIONS AND RECOMMEN-DATIONS 410
15. REFERENCES AND NOMENCLATURE 413

APPENDIX 1 COMMITTEES MEMBERS OF THE 29TH ITTC 427

APPENDIX 2 PROPOSED TASK AND STRUCTURE OF THE 30TH ITTC TECHNICAL COMMITTEES AND GROUPS 431

1. STRUCTURE OF TECHNICAL COMMITTEES 431
2. TERMS OF REFERENCE FOR THE GENERAL AND SPECIALIST TECHNICAL COMMITTEES AND GROUPS 431

3. MECHANISM FOR IDENTIFYING NEW SPECIALIST TECHNICAL COMMITTEES 432
4. TASKS OF THE TECHNICAL COMMITTEES AND GROUPS OF THE 30TH ITTC 433

APPENDIX 3 REVISED DESCRIPTION AND RULES OF THE ITTC 447
1. DESCRIPTION 447
2. AIMS 447
3. ACTIVITIES 447
4. MEMBERSHIP 448
5. FULL CONFERENCE 448
6. EXECUTIVE COMMITTEE 449
7. ADVISORY COUNCIL 450
8. TECHNICAL COMMITTEES 451
9. GROUPS 452
10. SERVING IN MORE THAN ONE CAPACITY 453
11. ITTC SECRETARY 453
12. MANAGEMENT OF ITTC FUNDS 453
13. THE CONFERENCE 454
14. COMMUNICATIONS 455

APPENDIX 4 ITTC MEMBER ORGANIZATIONS 461

APPENDIX 5 ITTC MEMBERS AND OBSERVERS INVITED TO ATTEND THE 29TH ITTC CONFERENCE 465

Table of Content
Volume II

TABLE OF CONTENT VOLUME I ..... **V**

TABLE OF CONTENT VOLUME II ..... **IX**

THE SPECIALIST COMMITTEE ON CFD AND EFD COMBINED METHODS **475**

1. INTRODUCTION 475
2. REVIEW OF RECENT STUDIES ON CLAIMED ISSUES OF MODEL TEST PREDICTION METHODS, FOR EXAMPLE SCALE EFFECTS 477
3. REVIEW OF BENCHMARK STUDIES, ACCURACY, ACHIEVEMENTS AND CHALLENGES OF FULL-SCALE SHIP CFD 496
4. REVIEW OF EFD/CFD COMBINATIONS FOR RELEVANT APPLICATIONS 501
5. SUGGESTED IMPROVEMENT OF CURRENT RECOMMENDED PROCEDURES BY USING CFD IN COMBINATION WITH MODEL TEST 504
6. REVIEW OF CURRENT ITTC PROCEDURES FOR POTENTIAL USE OF COMBINED EFD AND CFD 511
7. UNCERTAINTY ASSESSMENT METHODS FOR CFD SIMULATIONS 514
8. SUGGESTED PROCEDURES TO ENSURE THE QUALITY OF CFD/EFD COMBINED PREDICTIONS 544
9. LIAISON WITH THE ITTC TC OF RELATED TECHNICAL AREAS 548
10. LIAISON WITH OTHER GROUPS OUTSIDE ITTC 549
11. TOR 10 549
12. CONCLUSIONS AND RECOMMENDATIONS 550

THE SPECIALIST COMMITTEE ON ENERGY SAVING METHODS **571**

1. INTRODUCTION 571
2. SURVEY OF ENERGY SAVING METHODS 573
3. USE OF WIND ENERGY 587
4. CFD, EFD AND SCALING METHODS 590
5. RECOMMENDED GUIDELINE 602
6. FULL SCALE DATA 604
7. CONCLUSIONS 606
8. REFERENCES 607

THE SPECIALIST COMMITTEE ON HYDRODYNAMIC NOISE **623**

1. OVERVIEW 623
2. INTRODUCTION 624
3. REGULATION 626
4. FULL-SCALE MEASUREMENT 630
5. MODEL-SCALE MEASUREMENT 636
6. COMPUTATIONAL PREDICTION 657
7. BENCHMARKING (MV) 669
8. SUMMARY AND CONCLUSIONS 675
9. RECOMMENDATIONS 676
10. REFERENCES 677

THE SPECIALIST COMMITTEE ON ICE **693**

1. INTRODUCTION 693
2. MATERIALS 694
3. UPDATES ON THE REVISED GUIDELINES 694

4. References 703
5. COmpressive ICE 706
6. SNOW-COVERED ICE 707
7. References 709
8. Future work 710

THE SPECIALIST COMMITTEE ON MANOEUVRING IN WAVES 711

1. INTRODUCTION 711
2. GENERAL 712
3. State-of-the ART of predicTION METHODS of SHIP MANOEUVRING in WAVES 714
4. MINIMUM ENGINE POWER REQUIREMENT 730
5. CONCLUSIONS 737
6. RECOMMENDATIOnS 738
7. References 738

THE SPECIALIST COMMITTEE ON MODELLING OF ENVIRONMENTAL CONDITIONS 747

1. GEneral 747
2. Modelling of extreme environments 749
3. Breaking waves 753
4. State-of-the-art review of wind-wave interactions and the effects on the generation of extreme waves 755
5. State-of-the-art review of wave-current interactions and the effects on wave breaking 758
6. References 760

THE SPECIALIST COMMITTEE ON SHIPS IN OPERATION AT SEA (SOS) 767

1. Introduction 767
2. Shallow Water Corrections 771
3. Wave correction 777
4. Monitoring the development of CFD methods for added resistance due to waves 784
5. Wind Correction - Guidance on the Location and Height of the Anemometer 788
6. Limitations of averaging wind correction method 789
7. Guideline For CFD-Based Determination of Wind Resistance Coefficients 793
8. Study on CFD Computations of Wind forces 793
9. Current Correction 797
10. Comprehensive Correction 799
11. model-ship correlation factors at different drafts 802
12. SHaFT G-modulus 803
13. Water Temperature and density correction 804
14. Noise in the measured data and measurement error 806
15. Update the speed/power sea trial procedures 7.5-04-01-01.1 807
16. Updates to the guideline on the determination of model-ship correlation factors 807
17. Key Performance Indicators for Ships in Service 809
18. More accurate measurement of environmental data 811
19. Speed power performance related monitoring 813
20. Possibilities to analyse ship performance on a single run 816
21. Explore 'ship in service' issues to get feedback to towing tanks 818
22. Monitoring the new information and communication technologies applied on board ships 819
23. CONCLUSIONS AND RECOMMENDATIONS 819
24. References 821

THE SPECIALIST COMMITTEE ON HYDRODYNAMIC MODELLING OF MARINE RENEWABLE ENERGY DEVICES 829

1. Introduction 829
2. Tasks 830

3. PROCEDURES AND GUIDELINES 830
4. COOPERATION WITH OTHER COMMITTEES 832
5. BENCHMARK DATA 832
6. FULL SCALE INSTALLATIONS 838
7. WAVE ENERGY CONVERTERS 846
8. CURRENT TURBINES 851
9. OFFSHORE WIND TURBINES 860
10. CLOSING SUMMARY 869
11. RECOMMENDATIONS 872
12. REFERENCE 874

THE QUALITY SYSTEMS GROUP 887

1. GENERAL 887
2. TASKS PERFORMED 888
3. CONCLUSIONS 901
4. RECOMMENDATIONS TO THE CONFERENCE 901
5. RECOMMENDATIONS FOR FUTURE WORK 901

The Specialist Committee on CFD and EFD Combined Methods

Final Report and Recommendations to the 29th ITTC

1. INTRODUCTION

1.1 MEMBERSHIP AND MEETINGS

The members (Figure 1) of the Specialist Committee on CFD and EFD Combined Methods of the 29th ITTC are:

- Chair: Sofia Werner, SSPA, Sweden
- Secretary: Ayhan Akinturk, National Research Council of Canada (NRC), Canada
- Secretary: Joe Banks, Southampton University, U.K.
- Kevin Maki, University of Michigan, USA
- Takanori Hino, Yokohama National University, Japan
- Feng Zhao, China Ship Scientific Research Centre (CSSRC), China
- Shin Hyung Rhee, Seoul National University, South Korea
- Hyung Taek Ahn, University of Ulsan, South Korea
- Peter Horn, Hamburgische Schiffbau-Versuchsanstalt (HSVA), Germany
- Tahsin Tezdogan, Strathclyde University, U.K.

Figure 1: The members of the Specialist Committee on CFD and EFD Combined Methods of the 29th ITTC

Four physical meetings were held:

- January 17-19, 2018, SSPA Sweden, 10 members attended
- July 3-4, 2018, NRC, Canada, 9 members attended
- January 22-23, 2019 Yokohama, Japan, 9 members attended
- January 13-14, 2020, Glasgow, U.K. 6 members attended, 1 additional online

1.2 TERMS OF REFERENCE ASSIGNED BY THE 28TH ITTC

Combined methods

1. Review recent studies on claimed problems of the current model test prediction methods, for example scale effects. Assess their levels of impact.
2. Review benchmark studies, accuracy achievements and challenges of full scale ship CFD.
3. Review work on EFD/CFD combinations for relevant applications.
4. Suggest ways to improve the current recommended procedures by using CFD in combination with model test. Especially focusing on scaling procedures, starting with but not limited to the calm water speed power prediction.
5. Suggest which other parts of the ITTC procedures that could benefit from combined methods in future work.

Confidence of predictions

6. Review past work and procedures, within and outside ITTC, on CFD uncertainty, validation & verification (V&V), applied to the marine and other business sectors.
7. Suggest practical procedures to ensure the quality of CFD/EFD combined predictions to the end user, especially when applied to speed power predictions. This includes the demonstration of V&V and uncertainty assessment of commercially or legally valid predictions.

Interactions

8. Liaise and cooperate actively with the ITTC TC of related technical areas. Suggest modifications of the relevant Recommended Procedures related to CFD/EFD combinations where applicable.
9. Liaise and cooperate actively with the "CFD Workshop" committee and other groups that deal with CFD benchmark and V&V. Consider their results and suggest further work.
10. Act as a research coordinator for other researchers who wish to contribute: Suggest research topics that lead towards the given committee goals, assembly and review ongoing work.

Presentation of result

11. Apart from the normal committee report, the work should also be presented in a format directed towards the typical receiver of ship predictions including both ship owners and authorities. This should include discussions on accuracy of respective method (CFD and EFD), reasonable requirements to uncertainty demonstration, and description of new combined methods.

1.3 GENERAL REMARKS

CFD offers new possibilities to improve the EFD based predictions, for example with new treatment of scale effects. On the other hand, we can still not in general rely purely on CFD for ship hydrodynamic predictions for commercial or legal purposes. By using the best combination of CFD and EFD, rather than viewing them as competing methods, we can deliver even better prediction.

New methods based on EFD/CFD combinations need to have the same confidence level as the existing Recommended Procedures give to the end client today.

The purpose of this new Specialist Committee is to initiate and support the process of introducing combined EFD/CFD methods in ITTC's procedures, with a focus on the predictions confidence level.

2. REVIEW OF RECENT STUDIES ON CLAIMED ISSUES OF MODEL TEST PREDICTION METHODS, FOR EXAMPLE SCALE EFFECTS

Within this section, the focus is laid on calm water speed power prediction based on model tests. Results derived from model tests for manoeuvring, sea keeping or cavitation are not subject to this section.

There are various flaws in current calm water model test scaling methodologies that affect the design of the vessel, credibility of the institute and comparability of results. Some customers see a significant difference among predictions of different model basins. – not only at the trial or ballast draught but also at the load draught. Different model basins have their individual correlation strategy deviating from ITTC recommended procedures bringing different possibilities for correlations, namely correlation allowance (c_A), form factor (1+k), correction on power (c_P), correction on propeller revolution (c_N), correction on friction (c_{FC}) or correction on wake (w_c).

Well-adjusted scaling and correlation strategies and techniques have been established and in the end there is a final correlation allowance derived from model test results in relation with sea trial results. The correlation allowance is therefore only applicable for the scaling method applied to this correlation allowance determination method.

The accuracy of a power prediction depends on the accuracy of the measured values and the complex scaling procedure. Helma et al. (2017) point it out when they say: "An inherent problem of this approach is, that it is virtually

impossible to verify each single step, because of the complex nature of the underlying problem."

Not stated to be complete, this overview shows aspects of experimental as well as computational problems, challenges and hopes in better predictions. Each topic requires more detailed study to conclude with a sophisticated opinion. Some topics are only touched on and not worked out in complete detail.

To each major topic in the ship prediction methods, shortcomings and advantages are noted below for the EFD as well as for the CFD methods. Challenges and dangers in combining them are not fully assessed in this document.

Generally, problems in the model testing procedure or in the evaluation strategies are not always described in detail in published articles. Therefore the following section summarizes also the authors' experiences and impressions of the latest developments which are not substantiated by scientific investigations.

2.1 RESISTANCE RELATED ISSUES

2.1.1 FROUDE SCALING, ITTC-1957 CORRELATION LINE AND FORM FACTOR METHOD (1978 ITTC PERFORMANCE PREDICTION METHOD)

Extrapolating model-scale resistance according to Froude's Hypothesis follows the principle of scaling the frictional part of the resistance to larger Reynolds number flows by applying friction lines and keeping residuary resistance constant. "A standard extrapolation method applied to the model-scale resistance here underestimates the full-scale resistance by 10%, but the empirical correlation allowance approximately corrects for that difference" (Raven et al., 2008). Raven (2017) claims that extrapolation method according to 1978 ITTC Performance Prediction Method disregards scale effects in form factor and wave resistance, the correlation allowance c_A makes up for this on average. CFD can help to estimate scale effects more precisely and reduce magnitude of c_A. Full-scale CFD calculations claim to be capable of investigating Reynolds scale effects.

Model basins use different scaling and correction methods developed overtime. Some of them have been mutually agreed upon and introduced in the recommended procedures of the ITTC but not all basins following these recommendations strictly. Two major extrapolation strategies exist and are both in use: namely the 2D method (ITTC, 1957) and the 3D method or form factor method (ITTC, 1978).

The ITTC-1957 correlation line was introduced during the 8th ITTC 1957 (ITTC, 1957) as a model-ship correlation line based on empirical investigations. Strictly speaking, ITTC-1957 model-ship correlation line embeds a form factor of about 1.09 which is the reason why it is called the Model Ship Correlation Line, not a friction line. It was stated that this correlation line was regarded only as an interim solution to this problem for practical engineering purposes (Strasser, 2018). It affects the balance between residual and frictional parts of the total resistance and has therefore a significant impact on the predicted power for the full-scale vessel. Model basins have derived different principles of determining a correlation allowance (c_A) based on full-scale sea trial statistics to overcome this shortage for practical engineering purposes. The method is known to be simple and reliable due to the good database for the determination of the correlation allowance.

ITTC78 overlays yet another form factor. The method of the form factor 1+k, introduced in 15th ITTC 1978 (ITTC, 1978), is also known as the three-dimensional analysis method because a form dependent factor is included. It claims to comprise the form dependent scale effects into the form factor which is set constant for the model and the full-scale ship. The

determination of the form factor, derived from model test, faces significant problems when using the Prohaska method (ITTC, 2017a): submergence of the bulbous bow and the transom, flow separation and the presence of appendages lead to difficulties in a doubtless determination of the form factor (Hollenbach, 2009, Wang 2016a). This uncertainty in the determination of the form factor will directly affect accuracy of the full-scale resistance prediction as the form factor accounts for the relation of the wave and frictional resistance. Experience and impressions from results of different towing tank institutes show a significant spread of the form factor and therefore of the extrapolated full-scale results, when the 3D method is used.

It was found that if ITTC-1957 correlation line is used in combination with the form factor, "1 + k increases substantially from model to ship. An extrapolation using a fixed form factor would underestimate the ship viscous resistance by 7%" (Raven et al., 2008). García-Gómez (2000), Kouh et al. (2009), Park (2015), Wang et al. (Wang, 2015a), Kinaci et al. (2016), Lee et al. (2018) and Korkmaz et al. (2019a) demonstrate, using CFD, that the form factor is scale dependent if derived using the ITTC-1957 model-ship correlation line (Figure 2). The use of flat plate friction lines (like Grigson (Grigson, 1999), Katsui (Tahara et al., 2003) or a numerical derived friction line leads to comparable form factors for model and full-scale ships (Eça et al. 2005, Eça et al. 2008, Raven 2017, Park 2015).

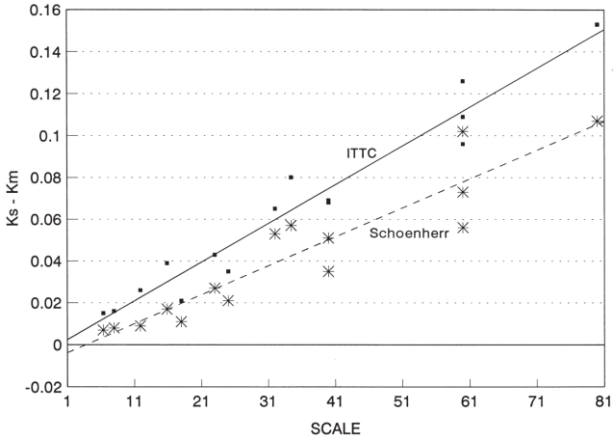

Figure 2: Form factor scale effect dependence on ITTC-1957 correlation line and Schoenherr friction line. K_s is the form factor of the ship and K_m that of the model. García-Gómez (2000).

Determining the form factor with CFD faces problems as well. The handling of the flow separation of an immersed transom or a bulbous bow is still a problem and Pereira et al. (2017) show that the predicted scale effect of a form factor differs depending on which turbulence model is used. The challenges of calculating the form factor with CFD methods is later described in section 5 of this specialist committee report.

When Toki (2008) asked "Should ITTC-1957 correlation line be revised?" they concluded, it is "Yes" in a sense that ITTC-1957 model-ship correlation line, which is prepared for two-dimensional analysis, is used in the three-dimensional form factor method analysis (1978 ITTC Performance Prediction Method). It is "No" in another sense, because towing tanks using the two-dimensional method with its correlation allowance would lose all of the full scale trial basis of making predictions. The expected gain by the revision of the friction line would be almost negligible and we have to expect the setback in power prediction accuracy caused by changing from the well accustomed line to new one.

Raven (2017) concluded that the scale effects of the form factor related to the ITTC-1957 model ship correlation line is not anything

physical but an effect of the usage of the ITTC-1957 line. For slender ships the form factor, related to modern friction lines, seems to be more equal for changing Reynold numbers. For full block vessels with flow separation the form factor changes for a varying Reynolds number and is affected by scale effects. He concluded, that CFD can contribute here to capture this scale effect. Changing to a physically correct flat-plate friction line must be followed by an adjustment of the correlation allowance c_A.

Studies of Kormaz et al. (Kormaz, 2019a, 2019b) was focused on the numerical determination of the form factor and numerical friction lines. They showed that the form factor is scale dependent when using the ITTC-1957 correlation line and scale effects are reduced significantly when a numerical friction line based on the same CFD code is used. A joint research study of 9 different organizations and 7 different CFD codes results in a comparison of the determination of form factors by different approaches (Korkmaz et al., 2020). They showed that the full-scale resistance predictions will scatter less when they used numerically derived form factors for extrapolating towing tank test results. It is shown that the combination of experiments and CFD can provide improvement to the 1978 ITTC Performance Prediction Method (Kormaz et al. 2021).

Wang et al. (Wang, 2015a) calculated numerical friction lines by CFD and compared them with available friction lines from literature. Full-scale resistance values for different hull forms were derived and they showed, that the form factor keeps relatively constant when they use numerical friction lines and bare hull forms, but not for appended hull forms. Generally, they concluded to use numerical friction lines when using form factors based on CFD.

Wang et al. (Wang, 2015c) presents a way of calculating the form factor based on energy conservation of ship wave making.

Wang et al. (Wang, 2016a) investigated the form factor derived numerically for different hull forms at various draughts and compared them with model test results. They concluded that the form factor is in line with the experimentally results, when the bulbous bow is totally immersed and the transom not. They claimed that when the bulbous bow is pronounced or the transom immersed and the experimental results are doubtful, numerical results are still reasonable.

Conclusively it can be said that CFD can be supportive in determining the form factor and increasing the accuracy of 1978 ITTC Performance Prediction Method but it is too early to state new procedures and should be re-evaluated when there are more data available. An introduction of a new ship-model correlation line or the revision of the ITTC-1957 ship-model correlation line needs more in depth study as well.

2.1.2 WAVE RESISTANCE

Raven et al. (2004) show that there is a scale effect on the stern wave elevation, though it is not large for slender ships. Raven et al. (2008) indicates that “the boundary layer around the hull is thin over the forward part of the hull, and in that region the pressure field is hardly affected by viscous effects. On the other hand, along the aft body, the boundary layer thickens quickly due to the decreasing girth length and the increasing pressure towards the stern. The displacement thickness of the boundary layer and wake reduce that pressure increase, and more so at model-scale than at full-scale. The reduced pressure increase in most cases leads to a reduced stern wave generation, again more pronounced at model than at full-scale; but this depends on the stern shape.” Raven (2017) claims that the wave resistance coefficient, C_W, is 20% larger for the full-scale ship than for model-scale. This increase, which is contrary to the common assumption in Froude’s hypothesis, seems consistent with the increase of the stern

wave system (Raven et al. 2008) (see also Figure 3).

Van der Ploeg et al. (2011) investigated scale effect of the free-surface and concluded that the scale effects occur only in the stern wave system: namely the stern wave length is longer, the amplitude is larger and waves are less steep in full-scale. Further scale effects are recognized at the transom as the full-scale transom is dry while the model-scale transom is partly wetted.

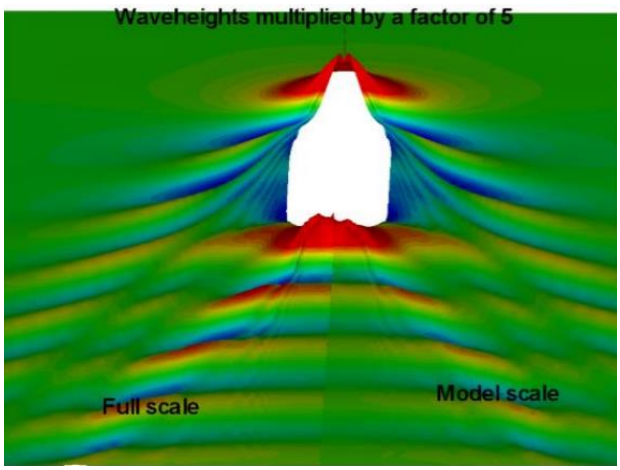

Figure 3: Stern view of computed wave patterns of Hamburg Test Case at Fn=0.238, for full-scale (left) and model-scale (right). Wave heights multiplied by 5 (Raven, 2008)

Kinaci et al. (2016) reviewed the determination of the wave resistance by CFD with the use of the form factor method in comparison to the wave resistance derived from model tests. They concluded a different value and slope of the wave resistance over the Reynolds and Froude numbers, was crucial in hull optimization processes.

Farkas et al. (2017) show that there is a scale effect on the wave resistance coefficient for tankers in dependent on the vessel's speed. They concluded that, for the investigated hull form, these scale effects have a minor impact on the final result.

2.1.3 ROUGHNESS CORRECTION

The roughness correction allowance used in ship powering prediction is based on an empirical formula (ITTC, 1990, Townsin et al., 1984). As experimental results for the determination of the roughness allowance are challenging to get for full-scale ship Reynolds numbers, this formula is based on extrapolation. Although this formula suffers from an insufficient experimental basis, the common performance prediction method agrees satisfyingly with sea trial results. To overcome the deficiency of the roughness correction method, CFD methods can contribute here as CFD methods are capable to simulate in full-scale ship size, but suffer as well from missing experimental validation data in full-scale.

Full-scale CFD calculations have been performed for ships (Tahara et al. 2003, Eça et al. 2010, Pereira et al. 2017, Ponkratev 2017, Guiard 2017, Kim et al. 2019a) or for full-scale flat plate to derive a numerical friction line (Kouh et al. 2009, Wang et al. 2015a, Korkmaz et al. 2019b). Additional data is required to determine a recommended value for the hull roughness in CFD calculations (Ponkratev, 2017). Guiard (2017) found as well, that applying reasonable values for the roughness in a simulation, the result does not tend to predict the full-scale resistance as expected.

Eça et al. (2010) performed full-scale ship CFD calculations with different roughness values and concluded a good agreement with empirical formula of Townsin et al. (1984). Furthermore, they concluded, that the empirical formula accounts not for different hull forms whereas CFD calculations can make a benefit here in providing hull dependent roughness allowances and therefore improving the full-scale resistance predictions.

Further studies on full-scale CFD computation for ships with implementation of the roughness are currently addressed in the

International Joint Research Project (JoRes) workshop lead by Ponkratov (Ponkratov, 2021). Results are expected in 2022.

Mikkelsen et al. (2020) have validated full-scale CFD calculations with sea trial results and have shown that a wall function considering roughness is important to get proper results in this scale.

Demirel et al. (2014 and 2017) as well as Oliveira et al. (2018) investigated the use CFD to predict hull resistance for varying roughness of the hull coating and bio-fouling.

The effect of air lubrication systems on the hull friction was investigated with CFD methods by Kim et al. (2019b)

2.1.4 TRANSOM IMMERSION

The transom immersion is affected by the scale effects. The speed at which a transom runs dry differs from model to full-scale (see also Section 2.1.2, especially van der Ploeg et al. (2011)). These observations are directly connected to the scale effects of the stern wave system. These effects are currently not addressed in the 1978 ITTC Performance Prediction Method (ITTC, 2017b).

Yamano et al. (2000) show that the forward facing breaking wave behind a submerged transom is scale dependent. The resistance coefficient is stated to decrease with increasing Reynolds number and is dependent on the type of stern wave: if it is a forward facing breaking wave or a following wave.

Starke et al. (2007) show that the clearance when the transom gets dry occurs at lower speed in full-scale than in model-scale. They investigated different transom depths, speeds and scales of 2-D transom stern flows. It was shown that this effect is substantially dependent on viscous effects and therefore on the Reynolds number. Due to the velocity defect in the wake of model-scale flows, the trailing wave length is reduced.

A trim wedge optimization study performed by Gornicz et al. (2016) shows that the improvement of the resistance is larger for full-scale flows than for model-scale flows due to transom flow scale effects.

Duy et al. (2017) investigated different transom shapes for the KCS container ship in model-scale.

Song et al. (2019) investigated the effect of a stern flap (or “duct tail”) on the DTMB5415 in model and full-scale in CFD and experiments. They found that the full-scale simulation lead to larger improvements than the extrapolated values from model-scale investigations. They stated that the current model extrapolation method cannot account for the effect of the resistance reduction of the stern flap.

The scale effects of the stern waves seem to be very complex but CFD has already shown that it can provide a good insight in these scale effects. A derivation of correction factors to account for the different scale effects and to improve the performance prediction might be reasonable in the future.

2.1.5 NOMINAL WAKE SCALING

This section deals with the nominal wake scale effects in the propeller plane. Section 2.2.3 accounts for the scale effects of the effective wake including propeller operation used for the performance prediction.

The Specialist Committee on Scaling of Wake Field of 26th ITTC (ITTC , 2011) made comparisons between full-scale CFD results and extrapolated full-scale wake fields from model-scale according to different methods. The method according to Sasajima and Tanka (1966) was found to be suitable for scaling the model-scale wake. The specialist committee concluded

that the best approximation of the full-scale nominal wake can be obtained using high resolution CFD calculations.

Van et al. (2011) use geosim models of KVLCC2 and KCS. They show the scale effect on the flow using CFD. It is shown that for larger Reynolds numbers, the flow near the hull surface around the stern accelerates more and the pressure recovery is larger. This delays the three-dimensional flow separation and reduces the bilge vortex formation. In the wake, the axial flow component is larger and the hook shape disappears for larger Reynolds numbers. This effect is larger on full block hulls.

In a full-scale CFD study with different hull roughness settings, Eça et al. (2010) showed a dependency of the nominal wake on the applied roughness in the calculation.

Wang et al. (2015b) calculated the nominal axial wake fraction of a container ship at different scales and derived a simple relationship to describe scale effects on wake fraction.

Pereira (2017) showed with RANS simulations that the predicted wake scale effect depends on the turbulence model (Figure 4). The difference in wake prediction between the turbulence models is smaller at full-scale. The dependency of the calculated nominal wake on the turbulence model is also shown by Guiard (2017).

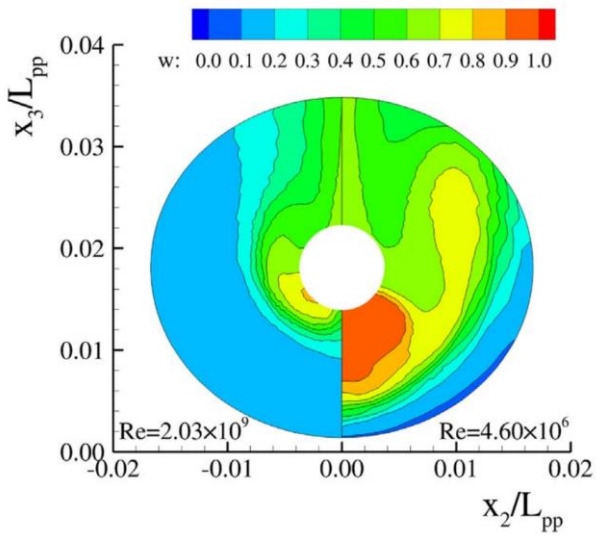

Figure 4: Stream-wise velocity deficit at the propeller at model (right) and full-scale (left) Reynolds number. (Pereira, 2017)

The aim of the international JoRes workshop led by Ponkratov (Ponkratov, 2021) is to measure a full-scale wake and to compare it with full-scale wake measurements. As this will be with an operating propeller, the findings might only be partial beneficial for improving the nominal wake scaling. Results are expected in 2022.

Experimental wake measurements in cavitation tunnels with a model running at larger Reynolds number than models running in the towing tank can help improve the scaling methods for the nominal wake.

The Tokyo 2015 Workshop on CFD methods in ship hydrodynamics (Hino et al. 2021) indicated that CFD methods can help to understand flow phenomena in the wake.

2.1.6 HIGH SPEED VESSELS

For high speed vessels like planing boats or catamarans the ITTC provides procedures in 7.5-02-05 “High Speed Marine Vehicles”. In contrast to the classical performance prediction of displacement hulls, the prediction for high speed vessel requires special attention to several

aspects which could be challenging during the experimental studies. To list some issues, CFD could assist here to improve the predictions: the wetted area for the scaling process could be estimated, the final dynamic floating position could be predicted to install turbulence stimulators, load cells or other measurement devices properly. For high speed vessels the air resistance plays a substantial role where CFD could help to determine the air resistance during the model tests or for the final full-scale vessel.

Lift producing appendages like foils suffer from scale effects due to different Reynolds number in model and full-scale. Lifting forces could be investigated in CFD in model and full-scale, to adjust the lifting devices for the model-scale experiments to represent the equivalent lift effect as for the full-scale vessel.

A further scale dependent effect is the spray of the bow wave or other waves. Due to the surface tension of the water, the spray requires the attention on other scale effects.

Conclusively it can be said, that the topic of high speed vessel needs further attention on investigating the scale effects of the model test procedure including a literature review and assessing the benefits of possible assistance by CFD calculation methods what might be addressed in future ITTC committees.

2.1.7 SCALING OF SMALL APPENDAGES

Smaller appendages like small bow thrusters, small bilge keels or sea chests may not be applied on the model for towing tank tests and are included in the performance prediction methods by towing tank facilities differently. Typically, an additional correlation allowance is applied following different principles. A common strategy among the towing tank facilities is not present and detailed studies are not available.

As these appendages have not been present at the model tests, the issue is not based on scaling problems but rather on the estimation of the additional resistance in the full-scale.

However, Krasilnikov et al. (2017) studied scale effects on bow thruster tunnels and found their relative resistance to be twice as large in full-scale than in model-scale.

For a better understanding of the full-scale behavior of these appendages, CFD calculation can assist.

2.1.8 SCALING OF LARGE APPENDAGES

Appendages typically mounted on the model like rudders, twin screw appendages, stabilizer fins, large bow thrusters or large bilge keels can be scaled individually, partially and independent of the bare hull resistance according to the 1978 ITTC Performance Prediction Method (ITTC, 2017b).

Scale effects on the wake of appendages have been investigated by Visonneau et al. (2006). A scale effect on the resistance of the appendages has not been subject to this study. The Beta-Method (ITTC, 2017b) for predicting the appendage resistance has been reviewed and numerical simulations have been carried out for validation by Oliva-Remolà et al. (2013). They compared experimental and extrapolated results with the results obtained from CFD simulations. They report that due to the complex geometry the validation of the Beta-Method with computational methods has not been successful.

An investigation on the scale effects on rudder lift and drag forces with operating propeller has been performed by Nguyen et al. (2016). Van Hoydonck et al. (2018) investigated the rudder drag and lift on a free-stream full-scale computation and found that the drag values for the full-scale computation are

significantly lower than those obtained from the towing tank results.

Sasaki et al. (2019) and Tacar et al. (2019) investigated scale effects on a Gate Rudder.

A proper scaling procedure for appendages of different types at different positions and flow regimes seems not to be investigated very much. A profound understanding of the scale effects require further studies where full-scale CFD calculations can assist.

2.1.9 FLOW SEPARATION OR VORTEX GENERATION ON THE HULL

This topic has hardly been investigated towards its effect in the scaling procedure of the resistance. Exemplary, it can be seen in model and full-scale wake calculation, that hook vortices (bilge vortex) will have different extents at different scales. The issue of flow separation on the aft part of the hull has barely been investigated.

To further understand the scale characteristics of vortices and flow separation and their effect on the resistance scaling and prediction, more investigation must be done. CFD methods (RANS) may only be of limited use as flow separation is very complex.

2.2 PROPULSION RELATED ISSUES

The performance prediction method according to the 1978 ITTC Performance Prediction Method (ITTC, 2017b) introduces several simplified mathematical formulations to the scaling procedure. It is known that the complex and very diverse flow phenomena at the propeller and the hull will interact with each other and may not be broken down to a simplified mathematical formulation. Therefore, it could not always be distinguished which part of the scaling process is affected by a minor change in the propulsion settings, for example, a change in the propeller diameter. The changed propeller diameter will modify the wake scaling and the open water test scaling as well. But will they always change the prediction in the same direction? Nevertheless, the following section will focus on specific issues of the propulsion prediction, although it is known that specific aspects that contribute to the overall performance prediction need to be analysed in a holistic way. Subsequently, the final overall performance prediction will always require a certain amount of judgment.

2.2.1 PROPELLER SCALING

The scaling of the propeller open water test results to other Reynolds numbers like those during the propulsion test or those in full-scale are a crucial part of the performance prediction method for ships. Although the 1978 ITTC Performance Prediction Method (ITTC, 2017b) provides simple mathematical formulations to account for scale effects for the full-scale propeller open water performance, other available methods in literature and in use differ in their level of detail. Streckwall et al. (2013) stated that the results of the existing methods differ significantly. In particular, modern blade geometries require modern scaling methods which are using scaling procedures depending on the variation of blade geometry over the radius or even more complex methods. CFD can contribute here to improve the scaling procedure as it gives insight into the flow on the propeller blades on different scales.

As the flow on the propeller blade features the transition of laminar to turbulent flow at model-scale, CFD calculations have to make use of turbulence transition models. Experimental paint flow tests on propeller blades have been performed to validate the findings made in CFD (Figure 5).

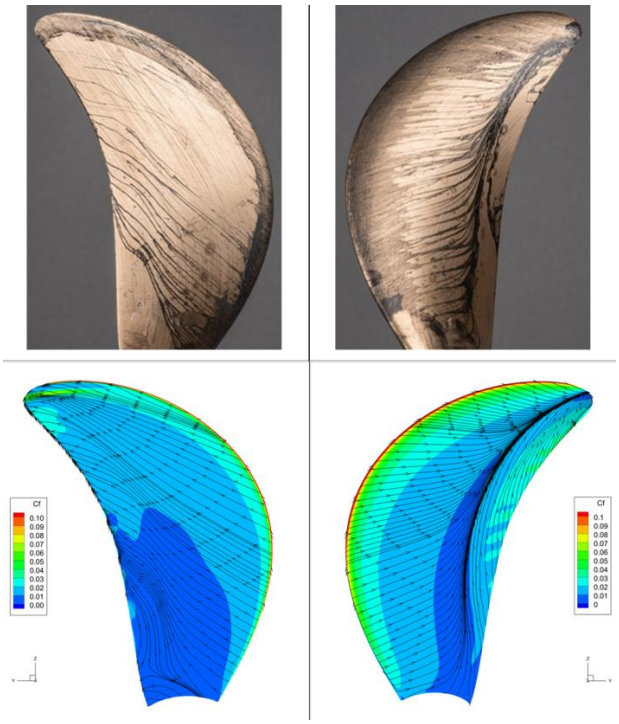

Figure 5: Propeller at low Reynolds numbers. Paint test (row 1) vs. limiting streamlines by CFD (transition γ-model) (row 2). Left: Pressure side. Right: Suction side. (Li, 2019)

Following this approach, Müller et al. (2009) investigated the flow on propeller blades and found that the three-dimensional flow effects play an important role and that a reduction to a two-dimensional problem related to the blade profile will not be sufficient to capture all effects for the scaling procedure. They proposed a scaling method applying a change of the magnitude of the force and the angle at each radius.

Streckwall et al. (2013) developed a "stripe method" to better predict the propeller scaling, especially for modern types of propeller blade profiles.

Rijpkema et al. (2015) and Baltazar et al. (2017) investigated different numerical strategies, in particular different turbulence models (including turbulence transition models) for varying Reynolds numbers. They show an increasing thrust and a decreasing torque with increasing Reynolds numbers. Different turbulence models have been investigated by Bonfiglio et al. (2015) especially for transient flows on the propeller blade. The prediction of the wake behind a propeller open water test with different turbulence closures have been investigated by Guilmineau et al. (2015)

Amadeo et al. (2017) and Quereda et al. (2019) focused on the application of turbulence transition models for unconventional propellers and the resulting performance prediction.

Other unconventional propellers have been subject to the studies of Peravali et al. (2016). The study evaluated propeller scaling procedures with the 1978 ITTC Performance Prediction Method and RANS methods in open water and in-behind condition. They have shown that there is a Reynolds number effect on blade pressure distribution which is not taken into account by the ITTC 1978 method related to the effective wake scaling. This will especially affect unconventional propellers.

The scaling of tip-rake propellers has been investigated by Okazaki et al. (2015), Dong et al. (2017), Shin et al. (2017) and Klose et al. (2017), where the latter proposed a modification to the ITTC 1978 scaling method.

Helma (2015) introduced a new scaling method and compared the results with other scaling methods specifically focusing on the overall performance prediction (Helma et al. 2017).

Hasuike et al. (2017) and Li et al. (2019) investigated the propeller scaling process and recommend using the "2 propeller open water test method" (2POT) introduced by Tamura (1977).

Heinke at al. (2019) showed the application of at least three propeller open water tests to identify the Reynolds dependency of the propeller open water tests performed at very low

Reynolds numbers and to improve the performance prediction. This method is supplemented with CFD calculations

By the latest research it is shown that the classical propeller scaling methods do not properly predict the full-scale open water performance, especially those of unconventional designs like tip modified propellers or small blade area propellers. Many studies mentioned here applied sophisticated CFD methods including transition turbulence models to account for the correct transition of laminar flow to turbulent flow for model-scale Reynolds numbers. Although some flow phenomena have been well predicted by CFD, not all results are fully satisfying when CFD methods are applied. The simulation of the laminar-turbulent transition is still a demanding task. Ongoing studies where CFD methods might be a part of have to be made to possibly conclude with an updated scaling procedure within the ITTC recommendation.

2.2.2 PROPELLER HULL INTERACTION

The understanding of the scale effects of the propeller-hull interaction requires model tests or CFD computations of the sailing hull with running propeller. The propeller-hull interaction is expressed by the overall propulsive efficiency (ETAD, η_D) influenced by the hull efficiency (ETAH, η_H, defined by the wake fraction w and the thrust deduction factor t) and the relative rotative efficiency (ETAR, η_R). The scale effects of the rotative efficiency and the thrust deduction factor are defined to be zero or negligible in the 1978 ITTC Performance Prediction Method. The scale effect of the wake fraction has a major influence. In addition to the reference made in this section, studies presented in Section 2.1.5 should be considered as well.

In the report of the Specialist Committee on Scaling of Wake Field of 26th ITTC (ITTC, 2011)) participants of a survey stated that the typical scaling on wake was performed for nominal wakes as well as distributions. Effective wake and average values were of secondary importance. Procedures of scaling the effective wake are provided by 1978 ITTC Performance Prediction Method (ITTC, 2017b) or Yazaki (1969).

Numerical and experimental investigations have been performed by Pecoraro et al. (2013) to investigate the effect of the propeller on the detached flow in the stern region of the hull and to quantify the propeller influence upstream.

Krasilnikow (2013) showed that numerical self-propulsion tests in model-scale are suitable to capture the propeller-hull interactions properly.

Hally (2017) showed a method to determine the effective wake by a RANS-BEM coupling method. A similar method has also been used by Regener et al. (2017) to investigate and evaluate nominal and effective wakes in model and full-scale with respect to propeller design.

Sun et al. (2019) performed model and full-scale CFD calculations and investigated the scale effects of the propeller-hull interaction coefficients (Figure 6). They showed that the scale dependency of the wake is one of the main reasons for the propeller working at higher advance ratio and having a lower thrust coefficient in full-scale than in model-scale.

The effect on the rotative efficiency has been investigated by means of experimental data and RANS calculation by Lücke et al. (2017). They recommended an introduction of an efficiency factor η_N in case of rotating wakes in case of using pre swirl stators or asymmetric aft bodies.

Lin et al. (2014) evaluated the scale dependency of the thrust deduction.

By separating the free surface calculation from the propeller calculation, an alternative approach to derive propeller hull interaction and

final performance was applied by Giannoulis (2019).

An alternative principle of the computational set up to derive propeller hull interaction and a final performance prediction was applied by Giannoulis (2019).

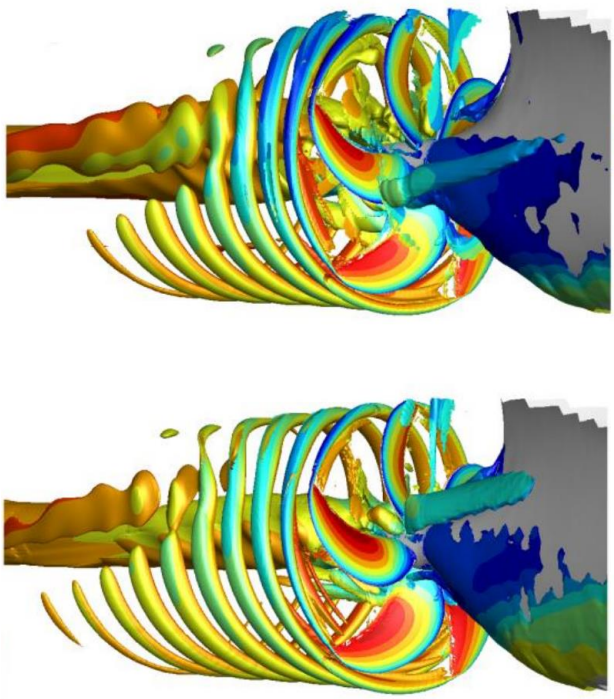

Figure 6: Propeller operating behind a hull. Instantaneous iso-surface of nondimensional Q-criterion, colored by axial velocity ratio. Top: Model-scale. Bottom: Full-scale. (Sun, 2019)

The scaling methods for wake are very basic but directly affect the final performance prediction. Further CFD simulations with propeller operation might by helpful in the future to investigate these scaling issues in more detail and to improve the accuracy of the performance prediction.

2.2.3 ESD SCALING

Energy Saving Devices (ESD) or Propulsion Improving Devices (PID) are mostly operating near the propeller and are found to be effective in model tests, as well as full-scale sea trials or monitoring data. As they are working in the wake region of the hull they are affected by Reynolds number effects (scale effects). ITTC provides no standardized procedures to account for these special scale effects (Kim, 2017). A Specialist Committee on Unconventional Propellers at the 22nd ITTC (ITTC, 1999) reviewed experimental methods and extrapolation strategies for different kinds of energy saving devices in detail. Scale effects mainly due to a modified wake in full-scale are affecting the friction on the device, the modified propeller revolution due to the device or the generation of vortices at the device.

It was shown by Hafermann et al. (2010) that self-propulsion RANS calculations are capable to predict the power gains by a combination of fins and ducts in front of the propeller in model-scale. A closer look on the scale effects of ducts and fins has been made by Heinke et al. (2011) mentioning as well the influence on the cavitation, pressure pulses and design of fins in terms of angle of attack difference between model and full-scale. The need of adapting the design of ESDs towards the full-scale wake is described by Guiard et al. (2013). A design process for pre swirl stators including the validation with trial results was performed by Kim et al. (2012) as well as by Xing-Kaeding et al. (2015). Visonneau et al. (2016) concluded the need for a design of an ESD in full-scale too. They showed as well by unsteady hybrid LES computation an unsteady separation zone characterized by a wake of coherent ring vortices.

A propeller cap fin recovering energy from the hub vortex was investigated by Kim et al. (2016). They pointed out the difficulty to reproduce the cap vortex effects in model-scale (experimental and numerical). They show by computation that the power saving effect is larger in full-scale, a result verified by sea trials.

Kim et al. (2017) proposed an extrapolation method for model-scale results by taking into account the tangential velocity components into account, calculated by CFD methods.

The effect of a combination of different ESDs has been investigated by Okada et al. (2017) and Lee at al. (2017). The latter have shown that the efficiency gain by a combination of three devices is smaller than sum of the efficiency gain by each device.

Further studies on the design, performance and scale effects with full-scale CFD calculations have been made by Wawrzusiszyn (2018), Krasilnikov et al. (2019) and Sakamoto et al. (2019).

Although it is well known that there are significant scale effects on energy saving devices, not all flow phenomena are fully understood. Therefore suitable and commonly agreed extrapolation methods may not be available. Further studies should be made here including the use of full-scale CFD to better understand the physics and to provide sophisticated power prediction guidelines.

2.2.4 PODDED PROPULSION

Scaling procedures for podded propulsion or azimuthing drive units are addressed in the ITTC Recommended Procedures and Guidelines "Podded Propulsion Tests and Extrapolation" (ITTC 2017c and ITTC 2017d) and its contribution by "The Specialist Committee on Azimuthing Podded Propulsion of the 24th and the 25th ITTC" (ITTC 2005 and ITTC 2008). The Procedure "describes the best possible methodology based on information currently available. However, users should be aware that a clear scaling procedure has not yet been developed due to the lack of model-scale and full-scale supporting data the public domain. The Procedure may be changed when such data becomes available" (ITTC 2017c). Although, commonly agreed procedures have been defined, difficulties are still to fully understand and account for scaling effects of the pod housing resistance, complex pod units (like contra rotating pod units), off-design conditions or aspects of cavitation and manoeuvring. The community was encouraged to investigate more on full-scale problems including the assistance with RANS CFD methods.

Sanchez-Caja et al. (2003) investigated the performance of POD units by means of model and full-scale CFD calculation and found large differences in the scaling of passive components of the thruster showing that the available scaling procedures are not adequate.

Choi et al. (2014) investigated scale effects of pulling type podded propeller with CFD analysis performed at different Reynolds numbers. They concluded that the pod housing resistance under the presence of the propeller slipstream is a major factor of the scale effects. An extrapolation method for these types of podded propulsors is suggested by Park et al. (2016).

Contra rotating PODs (CRP) have been investigated by Wang et al. (2016b). They proposed for the extrapolation and performance prediction using thrust and torque coefficients for the aft propeller to account for the forwards propeller wake and pod blockage effect. Krasilnikov et al. (2017) had a focus on scale effects of a CRP as well performing self-propulsion CFD simulations. They found that propulsive factors do not show large variation with scale, however they suggest performing more investigation on the wake fraction and the thrust deduction factor as they have been under-predicted by the CFD calculations compared to measurements.

A hybrid design of a shaft line propeller in front of a podded propeller has been investigated experimentally by Quereda et al. (2017). They proposed an extrapolation method for these kind of propulsion system.

A POD housing with a nozzle around the propeller and a stator has been investigated by Veikonheimo et al. (2017) using CFD and model-scale test. A new extrapolation method has been introduced for this kind of propulsion system.

To understand the flow physics and provide advanced extrapolation methods for the variety of podded propulsion systems more in depth studies are needed. CFD methods can assist here to understand the complex flow and interaction effect between hull, POD housing and propeller as well as to investigate effects in the scale.

2.2.5 DUCTED PROPELLERS

The performance of model tests (propulsion and bollard pull) and the principle evaluation of ducted propellers is addressed in the ITTC procedures and guidelines (ITTC, 2017e).

Bulten et al. (2011 and 2017) investigated scale effects on ducted propellers by model and full-scale CFD calculations. Scale effects have been identified and explained based on the theory of loss coefficients and pump efficiency. They stated that the "conventional extrapolation method based on wake fraction, thrust deduction and relative rotative efficiency does not always give clear trends for ducted propellers" and that the "possible differences between laminar and turbulent flow regimes are not explicitly captured in the extrapolation methodology".

Rijpkema et al. (2011) investigated open and ducted propellers with potential flow and RANS methods for different scales (Figure 7). They found, that all open water coefficients increase depending on the propeller loading.

Xia et al. (2012) investigated ducted propellers and was checking the numerical set-up as well as the cavitation and thrust breakdown behaviour.

Bhattacharyya et al. (2015a and 2015b) investigated the laminar turbulent transition of open and ducted propellers with RANS methods including transition modelling. They showed that it is important to use CFD with transitional effects as it directly affects the interpretation of the scale effects. The scale effects were found to be similar for different duct designs. They found significant scale effects for the duct thrust depending on the propeller loading. The interaction between the propeller tip and the duct is important because it influences the scale effects due to propeller tip loading.

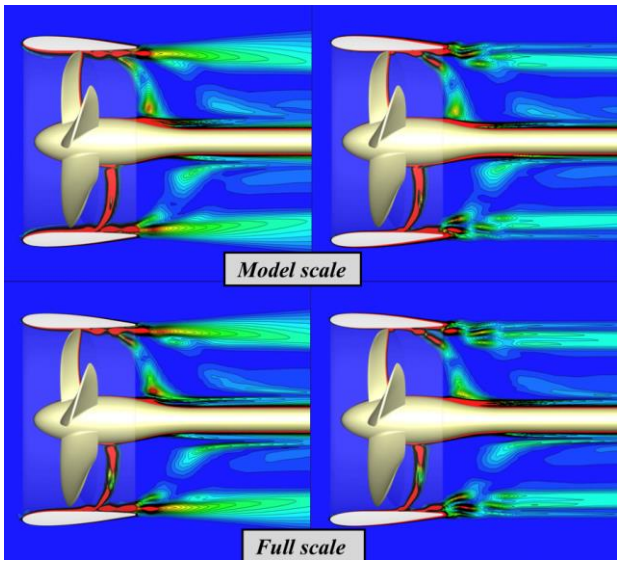

Figure 7: Slice of vorticity field for J=0.30 (left), J=1.0 (right). Model-scale results (top) and full-scale results (bottom). (Rijpkema et al. 2011)

Zondervan et al. (2019) compared the performance of ducted controllable pitch propellers calculated with BEM and URANS including sliding interface. They found that BEM method is an adequate choice for the design of ducted propellers in reasonable calculation times although it has its limitations.

The complex flow of the propeller interacting with a duct can be further investigated with CFD calculations to better understand the flow phenomena and scale effects and to improve the extrapolation methods for ducted propellers.

2.3 ASSESSMENT OF LEVEL OF IMPACT ON SPEED POWER PREDICTION

The following chapter is based on literature review, as well as own experience from commercial work and interviews with yards, propeller designers, ship owners. The aim of this chapter is to identify the different mentioned difficulties with the scale effects and their "level of impact" towards the general performance prediction of vessels.

The impact can be judged in different ways. For example:

1. Impact on trends in full-scale performance. When the optimum design in model-scale is not the optimum in full-scale. The prediction in model-scale drives the design in the wrong direction, leading to ships that work not in the optimum in reality.
2. Error in predicting the energy saving of new concept.
   a. Show large potential in model-scale, but gives no gain in full-scale. Leads to increased energy consumption.
   b. Show no potential in model-scale, but gives in fact good saving in full-scale. Leads to missed opportunities, since these concepts are not realized.
3. Error in predicting the absolute value of power. This leads to issues for the next link in the chain, for example that cavitation tests are done at incorrect condition which may lead to unnecessary safe propeller or opposite, propeller damage because risk was not detected. It can give error in selecting main engine and other design choices depending on the total power. It affects the regulations like EEDI, EEXI and contracts.

The following paragraphs summarize the "level of impact" for some of the individual topics mentioned in the forgoing chapters.

Hull friction determination using alternative friction or correlation line

On average level, the effect of using an unsuitable friction or correlation line and the form factor concept is small. If a model basin uses similar scale factors and similar type of ships, the average error is well corrected with correlation factors. For individual ships deviating from the standard and for model basins without extensive correlation statistics, the error might be larger.

Determination of the form factor

Difficulties to determine the form factor due to the applicability of the experimental procedure (Prohaska method) can fail for some ship types and lead to errors in the magnitude 5% even up to 10% on total power. It can affect the trends so that the best hull form is not selected, for example when balancing the wave resistance against viscous resistance. This effect can be significant for some ship types operating at Froude numbers around 0.2-0.3, like RoRo, LNG-carriers, container vessels, but less important for tankers, bulk carriers and others operating at lower Froude number. It has also consequence on defining the EEDI as the form factor has a large effect here.

Wave resistance and transom drag

Scale effects of wave resistance could also affect the trends, for example comparing ship hulls forms with different stern shape. This is linked to the transom resistance scaling, since the scale effect on wave resistance occurs mainly in the aft body. The magnitude of the error could be significant and affects ship types like RoRo or container vessels.

Roughness allowance

The roughness allowance is applied on all full-scale ship prediction procedures. As the overall frictional resistance due to roughness is rather small compared to other parts of the

resistance the impact on trends and absolute power is low when improving this issue.

Appendage resistance

Appendages could be very different and scaling procedures are not individually enough to account for different scale effects. Therefore there might be an impact on trends, optima of designs and overall power consumption. For a better understanding of the full-scale behaviour of appendages and the flow, CFD calculation can assist. Proper scaling procedure for appendages of different types at different positions and flow regimes can investigated.

Flow separation or vortex on the hull

For models of full ships, there may be flow separation or string bilge vortices, which do not occur in full-scale. Sometimes this is stronger in towed condition during the resistance test but less so in the self-propelled condition. These phenomena may lead to:

- Form factor can be too high, which may give too optimistic power prediction.
- A duct ahead of propeller stabilizes the flow and reduces separation what affects the evaluation of this energy saving device.
- Separation around U-shaped aft body with flow separation in resistance test underestimates the thrust deduction coefficient t and overestimates of wake fraction w, leading to too optimistic power prediction.

Propeller Open Water Scaling

Several propeller designers express their concern that some actors (always the others) deliberately optimize propeller blades for model-scale condition. One example is the problem of a possible laminar boundary layer in self-propulsion test and the usage of two propeller open water test (POT) at different Reynolds number to overcome this. It is claimed that this method can be utilized to achieve higher efficiency on paper. On the other hand, others claim that the 1978 ITTC Performance Prediction Method (ITTC, 2017b) with one POT penalizes low blade area propeller.

In both ways, this may lead to suboptimal propeller designs. The magnitude is approximately up to 3% and can affect most common ship types.

Effective wake scaling

The scaling according to 1978 ITTC Performance Prediction Method (ITTC, 2017b) is sometimes claimed to penalize some concepts:

- Unconventional propellers
- Increasing propeller diameter

Energy saving devices

Different ESDs recover energy from different sources to improve the performance. The individuality of the devices makes it difficult to find common scaling procedures and to predict the absolute power level. The influence on the optima in design between model and full-scale is noticeable.

Ducted propellers

This is indicated here as an example where the usage of model tests may hinder the possible development of energy savings due to significant scale effects. It is suspected, that ducted propellers perform in general better in full-scale than in model-scale.

2.4 RANKING OF THE LEVEL OF IMPACT

The committee has proposed a ranking of different challenges in scaling to determine the future focus for investigations. The choice of issues to rank has been mutually agreed upon.

For this ranking, three different criteria have been evaluated for each issue separately. A rating of zero to two has been applied after a common discussion in the committee. These ratings have been summed up equally weighted to get an overall ranking and to find the issue most suitable for future investigations. As the ranking is based on personal impression and experience of each committee's member daily work and the input of interviews made by the committee, the result is quite subjective and controversial to a certain degree. Nevertheless it was found that this is a simple, practical and good starting point to get a ranking at all.

The three criteria are:

1. Impact on trends and design
2. Impact on absolute power
3. Frequency of occurrence

Criteria one and two have been discussed in the introduction of this chapter. The ranking for the third criteria "frequency of occurrence" tries to classify how often this issue is coming up during typical daily work for performance prediction of ships. Therefore, more frequent issues are rated higher than more seldom issues what addresses the urgency for further improvement.

A table giving an overview of these rankings is found in the appendix of this chapter (See Appendix A). From this tabular overview the committee concluded to suggest the community to focus on five different issues:

- Numerical determination of the form factor
- Full-scale calculations of energy saving devices
- Improving wake scaling methods
- Improving propeller open water scaling methods
- Understanding scale effects of transom immersion (linked to wave resistance scale effects)

In addition to this ranking, the possibility to improve each issue with CFD methods was classified. This result is included in the table as well and, as for the other ranking, is strongly based on personal impressions and experiences.

The committee decided to investigate whether a modification of the 1978 ITTC Performance Prediction Method (ITTC, 2017b) regarding the possibility to use CFD for the form factor could be beneficial. The motivation for selecting this issue from the list is that it was regarded as a major error source in EEDI and contract power prediction, and it is believed to have a potential to be improved with CFD, since state-of-the-art CFD can handle model-scale resistance computations well.

The community is not bound to this ranking and classification and could make their individual ranking based on their experience and therefore their choice of the path of future investigations.

2.5 ISSUES NOT CONSIDERED

There have been many issues reviewed in this chapter in detail having more or less a significant effect on the speed power performance prediction. Nevertheless, some other issues do affect the prediction methods as well and are influenced by scale effects. But it was found that these issues have a minor effect on the speed power prediction and will therefore only be mentioned here shortly.

Some of the issues are from the perspective of sea trials. Sea trials are important to mention here, because they are the basis for the correlation strategy of model tests. The following three topics are mostly vessel specific issues and are determined individually to correct sea trials properly. These are:

- Added resistance of wind
- Added resistance of waves
- Added resistance due to shallow water

There are suitable methods either empirically or by means of CFD methods, to determine the value of these added resistances. These fields already have or will have a certain potential where CFD methods could improve the sea trial evaluation and therefore the correlation of model tests.

There are further model test procedures affected from scale effects:

- Sea-keeping tests
- Manoeuvring tests
- Cavitation tests

These tests have not been part of the review as they are not part of the calm water speed power prediction. Nevertheless, these methods already do or will benefit from the application of CFD methods.

2.6 ADVANTAGES OF MODEL TESTS

Experimental model tests are still the most trusted method for power predictions for ships. This is mainly due to the profound experience for the application of performance prediction methods applied among different towing tank facilities. Based on these experiences, good correlation strategies are available giving reliable prediction for the absolute powering of ships. A good correlation between sea trials and scaled tank results has been established over the decades. Werner et al. (2020) shows that towing tank predictions and corresponding sea trials match within 1% on average for a population of 183 ships. (Figure 8). Furthermore experimental tests will still benefit from the inherently correct physical water properties like turbulence, boundary layer development, flow separation or vortex generation where CFD methods may suffer from the necessary approximations.

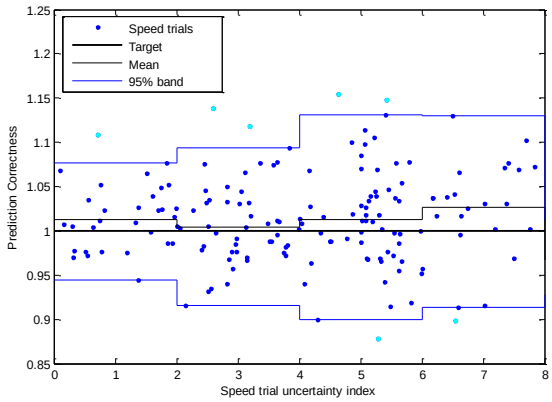

Figure 8: Confirmation of model test power prediction correlation show that the average difference is about 1% on the power. (Note that the spread is due to precision error in speed trial test and building process.) (Werner et al. 2020)

2.7 OUTLOOK

Besides the aforementioned encouragement in further CFD investigation in model and full-scale for the variety of different issues of the scaling and performance prediction methods, a certain focus should be laid on the checking and adaptation of the correlation allowance of an individual towing tank facilities by applying new methods like CFD. The link to the ITTC Guideline on the determination of model-ship correlation factors (ITTC, 2017f) is made here. Currently there is no procedure indicating when a correlation factor has to be adjusted when changing scaling procedures.

The committee identified scaling processes to be addressed in future for the consideration if CFD methods can be used in assistance for a more precise speed power prediction. These problems are:

- Numerical determination of the form factor
- Full-scale calculations of energy saving devices
- Improving wake scaling methods
- Improving propeller open water scaling methods

- Understanding scale effects of transom immersion (linked to wave resistance scale effects)

Unless these emphasized scaling issues, all other items mentioned in this chapter merit more in-depth investigation with CFD methods. CFD tools can be useful for understanding scale effects and will give an insight into flow superior to that obtained from experimental model tests alone. The items that need more in-depth investigation are:

- Appendage drag scale effects
- Nominal wake scale effects
- Ducted propeller scale effects
- Podded propulsor scale effects
- High speed vessel scale effects
- Flow separation and vortex generation scale effects
- Full-scale roughness effects
- Application of numerical friction lines within the 1978 ITTC Performance Prediction Method

It should be kept in mind that these individual problems should not be considered separately. There might be scaling problems interacting with each other. The indication of interaction effects should be addressed in further studies as well.

Besides the scaling problems in the calm water speed power prediction, scaling problems in the fields of manoeuvring, sea keeping and cavitation are worth more detailed investigation. Determination of added resistance due to wind, waves and shallow waters is needed to properly evaluate sea trials and should be investigated in detail. From these investigation, updated procedures and guidelines should be worked out by the ITTC to address the potential which CFD methods can provide.

The committee concluded to keep on working on the above mentioned fields. The committee can liaise benchmark cases of CFD methods which can be used for the power prediction. Other committees should have a task to review possible application of CFD methods within their field of work. They should contact the EFD/CFD specialist committee and inform them on these possibilities and EFD/CFD specialist committee summarizes these methods.

2.8 CONCLUSION

Model tests are still an accurate reliable way to predict the speed and power for ships. Nevertheless the computational methods can truly assist to improve the applied methods during the general scaling process by assisting and improving an individual scaling problem.

To identify which of the scaling problems would be the most suitable to be used for applying a CFD method to its improvement, it is necessary to organize these individual problems and rank them on different aspects. Different individual scaling problems for the calm water speed power prediction have been identified and their general uncertainty has been assessed to the level of impact on the prediction of correct trends in design as well as on the absolute powering level. The scaling problems have been rated on their frequency of occurrence in the typical business of towing tank facilities. The CFD method, which could be used in a certain scaling problem, has been assessed if it is easy to be used and state of the art for industrial CFD application. The possible improvement of the accuracy of a certain scaling problem by using CFD methods was judged as well.

All these aspects have been collected in a matrix-like overview. The determination of the form factor was addressed to be the most valuable one for further investigation to be used in combination with CFD methods.

It has to be noted here, that scaling effects and their possible assistance by CFD methods have been investigated separately here and not

the combination of different scaling processes. It is known that scale effects have impact on the ranking: some scale effects are over predicting and some are under predicting. Effects are mixed and can interact in the end of a complete speed power prediction process and CFD methods could help to become aware of these effects. Picking out one scale effect and make it more robust by insights from CFD methods can result in that the final speed power prediction is not even more correct, because all scaling effects are mixed and working together hand in hand. The use of a correlation allowance finally corrects it. You have to be very careful by changing single scaling methods without checking the overall accordance with a modified correlation allowance value. Methods for checking and adapting the correlation allowance have to be available when changing individual parts of the scaling process.

The work on determining the form factor by CFD methods and comparing these results with the form factor derived from towing tank showed a good agreement. Despite that, a quite significant spread was observed among the participants. That shows that CFD methods are promising but results have to be handled carefully.

The committee identified further scaling processes to be addressed in future for the consideration if CFD methods to be used in assistance for a more precise speed power prediction. These problems are: propeller-open-water scaling, effective wake scaling, scaling problems of immersed transoms and scaling of energy saving devices. Besides the scaling problems in the calm water speed power prediction, scaling problems in fields of manoeuvring, sea keeping and cavitation are also worth to look into them more in detail.

3. REVIEW OF BENCHMARK STUDIES, ACCURACY, ACHIEVEMENTS AND CHALLENGES OF FULL-SCALE SHIP CFD

3.1 SCOPE

In this section, a review of the full-scale benchmark studies is outlined. Emphasis is placed on the achieved predictive accuracy. Studies reporting on the challenges associated with performing full-scale simulations are also given. The purpose of doing so is to enable a summary based on a broad overview of the current progress within the community.

3.2 ACHIEVEMENTS OF FULL-SCALE CFD WITH FOCUS ON LLOYD'S REGISTER 2016 WORKSHOP.

In view of the constant increase of available computational power, several workshops have been organized to gauge the performance of modern computational tools. Accurate prediction of ship hydrodynamics has come a long way in recent years, especially with the advent of Computational Fluid Dynamics (CFD). However, confidence in this technique is not sufficient, particularly for full-scale predictions, which is what the 2016 Lloyd's Register workshop aimed at improving. Full-scale data is notoriously difficult to obtain, for this reason, the abovementioned workshop focused participants investigations in this direction. The organisers (Ponkratov, 2016) provided the required characteristics and 3D model of the ship and received sixty sets of results with varying degrees of setup complexity. For instance, some included surface roughness, superstructure aerodynamics, while others made simplifications. The workshop also included propeller cavitation comparisons.

Challenges associated with full-scale CFD computations are discussed starting with the 3D laser scan of the ship, which revealed some small deviations between the original drawings and actual ship. High curvature areas, such as

bilge keels, were manually adjusted because the scanning method ran into difficulty when applied to these features. The adoption of similar corrections was necessary to ensure the accurate description of the propeller geometry, where the scan showed the four propeller blades are not identical – an assumption usually made in hydrodynamic analysis. This same assumption was made during the workshop for the sake of simplicity. All sensors had to be checked against each other and verified for the correct outputs.

As part of the workshop, submitted resistance calculations were compared to established methods to determine each model's suitability. While most research into the resistance of ships is focused solely on the underwater shape, the organizers included the vessel's cranes and superstructure. The former was shown to be negligible. These parameters are expected to be strongly dependent on the ship characteristics and can be excluded if their contribution is known to be small. Furthermore, neglecting the superstructure was shown to influence dynamic trim, which, if ignored, can also impact predictive accuracy. The received trim amplitudes were very small and scattered, while the sinkage values agreed well between participants. This suggests that trim is more challenging than sinkage to capture numerically in full-scale.

In terms of self-propulsion simulations, it was established that allowing the ship to surge freely can be beneficial in cases where propeller RPM cannot be gradually adjusted to achieve thrust/effective resistance balance. One set of submitted results employed a novel approach where the setup is split into four stages, each with a different turbulence treatment. However, this methodology is more resource consuming, thus recommended in cases where no alternative is available. In terms of accuracy, the participants reported values with a scatter between -30% and +10%. An assessment of the CFD power predictions, compared to the sea trial data is shown in Figure 9.

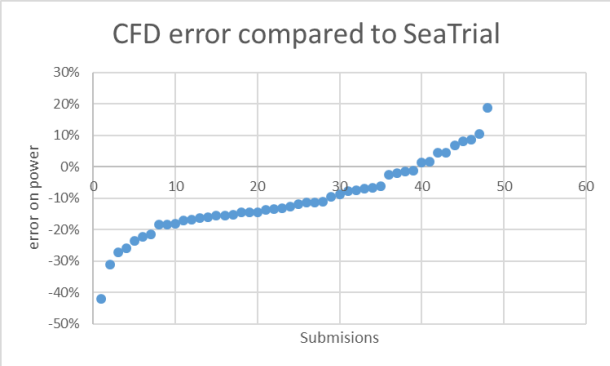

Figure 9. CFD error of predicted power for a given speed compared to sea trial result.

Overall, based on the scatter of results submitted by the participants, it is not possible to conclude that current CFD practices are sufficiently mature to be applied directly at full-scale with confidence. Further investigations are required to determine the best approach to achieve a good prediction. For example, a fine mesh of as many as 35 million cells and a small time step were not sufficient to capture propeller tip vortex cavitation detaching form the blades. Only the early stage tip vortex detachment was resolved. Thus, further efforts are required to establish higher predictive capabilities and increase confidence to allow routine applications of full-scale CFD. An example of such research is the work of Starke et al. (2017), who participated in the full-scale workshop. According to their study, the free surface fitting method was not capable of capturing overturning bow wave features. Thus, making the Volume of Fluid (VOF) method more applicable to full-scale ship CFD.

3.3 CHALLENGES OF FULL-SCALE CFD

One aspect reported as a challenge in much of the research work reviewed in this section relates to the number of cells required to perform a full-scale simulation. For instance, as

stated earlier, the full-scale workshop, organised by Lloyd's Register, received submissions ranging from a few million to 35 million cells. Thus, the approaches to full-scale CFD relating to mesh vary significantly across the research community. One approach to circumvent large cell numbers was devised by Haase et al. (2016). Specifically, Haase et al. (2016) proposed the validation of a grid in model scale Reynolds numbers, which is then scaled solely by a change in the value of viscosity.

Sezen and Cakici (2019) re-constructed the near-wall mesh in order to match the y^+ values in model- and full-scale. They determined that the method exhibits slight variations in the computed residual resistance coefficient. According to Terziev et al. (2019) such differences in the residual resistance coefficients may safely be attributed to scale effects. The procedure of Haase et al. (2016) can be implemented in multiphase and double body conditions, even when the mesh is kept identical between model- and full-scales, as shown by Terziev et al. (2019). Thus, computational savings are possible when adopting this technique. However, further studies are required to determine the confidence levels attributable to this technique.

To alleviate the computational load, a widely resorted to assumption is that of double body flow. Indeed, several RANS-based works referred previously have made use of this simplification. The literature also offers examples of full-scale computations which have modelled all physical phenomena. For instance, Tezdogan et al. (2016) provided a useful starting point for full-scale simulations in the arguably more complex unsteady case of shallow water vertical motions due to waves. Recent work exploring the added layer of complexity introduced when considering calm shallow water cases at full-scale can be found in Garenaux et al. (2019) and Terziev et al. (2020). The apparent scarcity of experimental data did not allow comparisons in these cases. Therefore, no validation was made against full-scale measurements.

In cases where self-propulsion is modelled, a variety of simplifications are applied by researchers to reduce the computational load required in discretising a ship's propeller (K. S. Kim et al., 2019). The accurate modelling of the propeller is critical to assess performance and devise intervention strategies, such as the inclusion of an energy saving device, to improve performance (Gudla et al., 2019; Huang and Lin, 2019).

Near-wall cells are of particular importance in resistance predictions, especially in full-scale. The aspect ratio of cells within the boundary layer of a ship can be too large, causing stability problems. For this reason, most researchers opt to use wall functions and prescribe the near-wall mesh so that wall functions are used (Peric, 2019). Although the computed forces can be predicted with reasonable accuracy when using wall functions, the flow properties within the wake field may not be modelled accurately. Therefore, a comparison between the wall function, and the resolved approach is necessary at full-scale to determine the former's suitability.

Turbulence modelling is typically a source of modelling error, which is difficult to quantify at full-scale (Bhushan et al., 2009, 2007; Duvigneau et al., 2003; Pereira et al., 2017). Thus, alternatives to RANS techniques, which resolve at least part of the turbulent kinetic energy spectrum have emerged and are rapidly gaining popularity. In this respect, Liefvendahl and Fureby (2017) estimated that a full-scale Large Eddy Simulation (LES) for the Japan Bulk Carrier (JBC) would require between 9.7×10^9 and 67×10^{12} cells, depending on the approach (wall-modelled LES vs. wall-resolved LES). For example, Fujisawa et al. (2020) resolved the flow around a model-scale propeller in open water via the LES approach using grids numbering between 0.1 and 6.4

billion cells. Such grids are difficult to handle, even in academic contexts, demonstrating that resolving the turbulent kinetic energy spectrum in full-scale is not currently practical. According to Pena et al. (2019), the bridging alternative, known as Detached Eddy Simulation (DES), can be successfully employed to predict full-scale ship performance. For instance, the authors gave Figure 10 as an example of the generated vortices in the aft region of the ship.

Zhang et al. (2018) summarised the challenges related to full-scale simulations of ship hydrodynamics as follows.

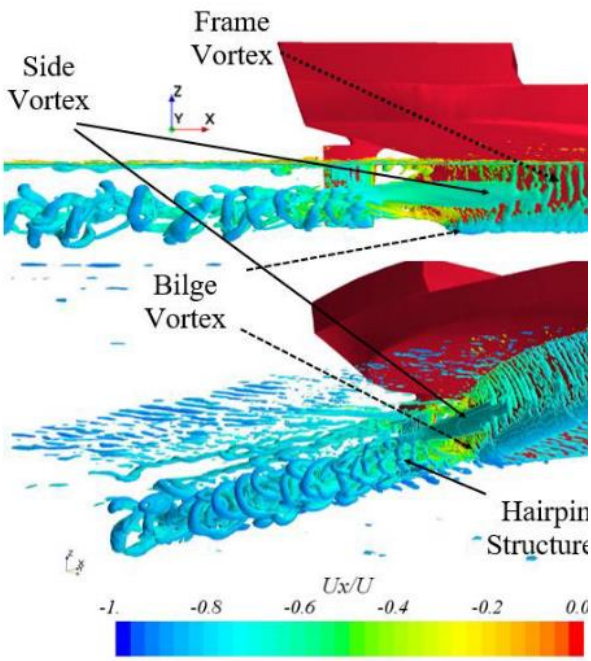

Figure 10: Iso surfaces of the Q-criterion showing the existence of different vortex systems. Adopted from (Pena et al., 2019).

1. The thickness of the boundary layer, which reduces with an increase in Reynolds number requires a fine near-wall mesh to capture well the viscous effects.
2. The unsteady nature of the ship resistance problem, which may be modelled with time-averaged approaches.
3. The neglect of surface roughness, which becomes more significant at full-scale.

The final point (3) has been investigated by numerous researchers, and is an active field of study at present. Recent contributions include K. Kim et al., (2019) and Song et al. (2019), where the authors investigated the drag penalty resulting from surface roughness, and confirmed the RANS approach is capable of modelling the thickening of the boundary layer as a result of fouling. The authors performed model- and full-scale simulations of the KCS in calm waters and assessed the effects of different levels of hull fouling on ship resistance. A review on the effect of surface roughness and fouling on ship resistance (Andersson et al., 2020), however, found disagreements in the academic community with respect to the approach to model roughness. This stems from the difficulty in relating CFD roughness parameters to a physical measure of roughness. Therefore, although modelling a rough hull condition is not challenging per se, it is difficult to know what that corresponds to in reality.

Computational studies in full- and model-scales are useful to determine flow features that may dominate at low Reynolds numbers, but are reduced in importance at high Reynolds numbers. For instance, the strength of the bilge vortex, as well as wake gradient are reduced at full-scale (Farkas et al., 2018; Zhou et al., 2019).

Niklas and Pruszko (2019) and Terziev et al. (2019) used double body and multiphase simulations to demonstrate the sensitivity of full-scale total resistance predictions on the choice of methodology. Specifically, approach taken to predicting the wave resistance, form factor, and frictional resistance can lead to a high scatter in full-scale, depending on the approach.

Full-scale experimental and combined EFD/CFD studies (Hiroi et al., 2019; Inukai, 2019; Mikkelsen et al., 2019; Niklas and Pruszko, 2019; Sakamoto et al., 2019) have become more frequent. However, a greater number of openly available full-scale trails are

required, accompanied by CFD studies into the optimal set-up to establish greater confidence in the method. For example, Sun et al. (2020) presented a set of numerical simulations which compared well with sea trial data. They compared different modelling strategies, featuring the inclusion and omission of surface roughness and its effect on the predicted power. A sample of the results reported in Sun et al. (2020) is shown in Figure 11.

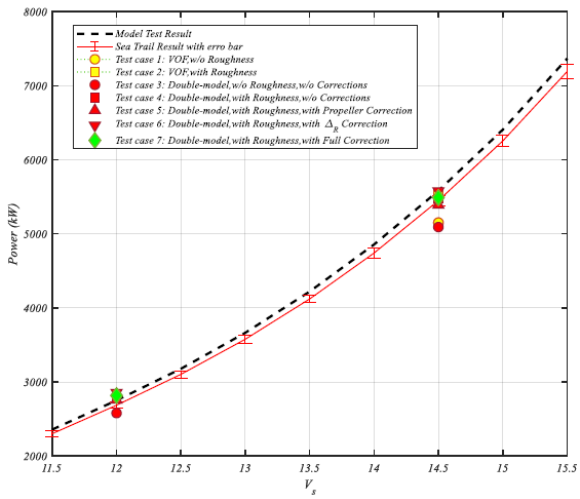

Figure 11: Power predictions compared to sea trial data. Adopted from Sun et al. (2020).

Alternatively, the study of Orihara and Tsujimoto (2017) and Tsujimoto and Orihara (2018) show a promising approach. In their studies, the authors predicted the full-scale ship performance and validated the resulting data by fitting the ship with on-board monitoring equipment. The findings of the studies include that further work is required to improve the speed-power predictions in conditions that do not closely match the scale. The authors point out that the parameters are highly affected by encountered waves. For this reason, the performance prediction technique requires that the encountered conditions are similar to the ones assumed in the computations. This may be taken as an indication that idealised conditions, necessary for validation purposes are difficult to achieve in full-scale.

3.4 CONCLUSIONS

Several trends can be identified in the field. The number of studies into the prediction of full-scale ship performance prediction have increased noticeably in the recent years. These are coupled with the increase in the availability of computational resources. However, the currently reported cell numbers are not thought sufficient to allow higher fidelity modelling (LES) of turbulent quantities in full-scale. A bridging alternative between RANS and LES has been demonstrated to be capable of providing accurate results when compared to full-scale sea trial data. One of the main issues in the accurately performing full-scale simulations, the lack of validation studies, is being addressed (Ponkratov, 2016). To further facilitate developments in the field and provide further insight, open source data for a range of hull forms and conditions are necessary to test available techniques. Such data would enable the determination of best practices in all areas examined above: near-wall grid topology, surface roughness, as well as turbulence modelling approach. It is therefore of critical importance that the number of benchmark cases increases. In this respect, contributions in the form of the JoRes project, whose completion is expected in April 2022 will undoubtedly aid the wider field. It is important to evaluate whether any lessons learned from the first round of the project (Ponkratov, 2016) can translate into a smaller scatter of predicted data. This will also assist in setting the groundwork towards pinpointing the most suitable computational approaches to predict full-scale flows. Below, the main conclusions are summarised.

- Work in the field of full-scale ship performance prediction is accelerating, based on the number of recent studies.
- Confidence in full-scale CFD simulations must be increased by demonstrating good predictive accuracy over a range of conditions, consistently.

- At present, the scatter predictions submitted to the Lloyd's register workshop suggests further work is needed to identify best practices in full-scale simulations.
- The main challenges are associated with the grid resolution, turbulence modelling, and surface roughness treatment.

4. REVIEW OF EFD/CFD COMBINATIONS FOR RELEVANT APPLICATIONS

The most frequent example of combined methods is the use of EFD to validate CFD methods. Examples of this are widespread and form part of best practice guidelines for the effective use of CFD. The topic of CFD validation is covered in more detail in Section 7 and therefore will not be discussed further here. These examples are predominantly focused on building confidence in a CFD method which is then used in isolation and therefore do not fully explore the potential of what could be achieved with combined methods. This chapter will therefore focus on how a combination of EFD and CFD has been used to provide greater insight then either could do in isolation. Two such examples are given in Wang Z-Z et al (2015a) and Eça, et al (2010) for numerical friction line and surface roughness on ship viscous resistance, respectively. These will be elaborated further below.

4.1 INVESTIGATING EMPIRICAL RELATIONSHIPS TO BE USED WITHIN THE SCALING PROCESS

Several studies have been carried out recently using CFD to investigate the dependency of skin friction coefficient with Reynolds number and compared this to empirical friction lines.

Wang Z-Z et al (2015a) derive through very careful CFD computations a numerical friction line which can be used when scaling resistance from a model test. The Reynolds number dependency of the form factor, vanish almost completely when the numerical friction line is used instead of the traditional ITTC-1957 model-ship correlation line. This is an example on where CFD has been used to improve the scaling methods. However, it should be pointed out that other empirical friction lines (Grigson and Katsui) also has this advantage over the ITTC-1957 line, and that the latter is not a pure friction line but include full scale correlation as well. A potential pit fall is the laminar to turbulent transition at the lower Reynolds numbers, which is notoriously difficult to predict with RANS computations.

Eça, et al (2010) use CFD to investigate the effect of hull roughness on the resistance. They were able to conclude that the Townsin formula, currently in the ITTC Recommended Procedures, is the most appropriate of several investigated empirical formulations. The study is a good example of how CFD can be very useful to evaluate empirical relations. Apart from that, the study also gave deeper insight into the effect of roughness on friction and viscous pressure and how that differs depending on hull shape. This may inspire to even better formulations in the future.

They find that very fine grid close to the wall is needed when analysing roughness effects. Even with careful grid convergence work, the numerical uncertainty is larger than that obtained from smooth surface computations. Another uncertainty is the conversion between equivalent sand grain roughness and the mean apparent amplitude, which is what is used in ship practice and in the ITTC equations for roughness allowance. This relation is, as the authors point out, a research topic of itself, and should be addressed in further studies.

Remolà (2014) attempt to verify the method for scaling of appendage viscous drag recommended in ITTC, the so-called beta-method. This method is in short, to estimate the

drag of appendages from resistance test with and without appendages, and reduce the drag coefficient by a factor and add it to the full scale resistance of the base hull. This is criticized to be a very crude method with large uncertainties. Using CFD to examine and perhaps refine the method would make a great contribution. Unfortunately, the CFD computations in the referenced work were not successful and no conclusions were made. However, the attempt is interesting and should be considered for further studies.

Wang et al. (2016a) develop a new method for scaling model test of CRP (contra rotating propeller) using CFD. The CFD computations reveals in detail the scale effect for the various components and this knowledge is used when the authors suggest scaling equations for the influence of the first propeller on the pod house resistance and the propulsion coefficients of the second propeller. This is a good example of where CFD has provided deep insights which would not be possible before, and how this is transferred to a scaling equation that can be used without CFD.

4.2 CFD DERIVED COMPONENTS USED WITHIN THE SCALING PROCESS

Raven et al (2008) were one of the first to explicitly suggest "replacing parts of the extrapolation procedures by CFD computations". Since then several authors have investigated the use of CFD to derive the form factor.

Raven et al (2008) suggest to use double model computations to derive the viscous resistance, and from that derive the form factor using a friction line. Since the form factor is shown to be Reynolds number dependent when the ITTC-1957 model-ship correlation line is used, they recommend using a numerically derived friction line. Wang Z-Z et al (2015a) come to the same conclusion.

Raven et al (2008) mention that care has to be taken with the CFD setup when deriving the form factor in this way. The same applies to investigating the scale effects in general using CFD. The viscous pressure resistance is especially sensitive to incomplete convergence, boundary conditions etc. Grid type, grid density, discretisation scheme and domain size also influence the result.

Wang et al (2016b) suggest deriving the form factor without a friction line by defining k=Cpv/Cf, where Cpv and Cf both come from CFD double model computations. They point out that grid type and turbulence model can affect the results. However, it is unclear how their form factor is meant to be used for full scale resistance, if no friction line is to be involved.

More recently a wider study investigating the use of CFD to obtain the form factor was initiated by this specialist committee. Seven codes and six different turbulence models were used to determine the form factor for the KCS and the KVLCC2 using double body simulations. This study further confirms the speed dependence of form factor derived using the ITTC-1957 model-ship correlation line but shows that this significantly reduces using the Katsui line and is nearly eliminated using numerical friction lines (Korkmaz et al 2021a).

The benefits of using a CFD determined form factor within the power prediction process have been investigated further by applying this method to a wide range of model scale tests and comparing the results against sea trials data Korkmaz et al 2021b. They conclude that generally powering predictions are improved by the use of CFD based form factors but crucially no deterioration was observed. The impact of a wide range of numerical settings are investigated allowing general recommendations to be made about implementing this method in the future.

The benefit of using CFD for the form factor (regardless of which friction line to use) is especially apparent for ships where the Prohaska method fails due to wave making even at low speeds. For such cases, the derivation of form factor is very problematic using the standard EFD methods.

4.3 USE OF CFD TO PROVIDE GREATER INSIGHT THAN THE ONE OBTAINABLE FROM EFD ALONE

With increased numbers of simulations of the flow around full scale ships being conducted, CFD can be used to investigate scale effects by comparing flow fields between model and ship scale.

Wang et al (2015b) used double body RANS simulations to investigate the scale effects on the nominal wake shape and mean values across a wide range of Reynolds numbers. They found that the mean nominal wake fraction reduced by almost 50% at full scale and there were significant changes in circumferential variation in nominal wake with scale, especially at inner radii. Recommendations are made regarding how similar simulations could be used to help model scale experiments in the future. A comparison of the CFD method with model scale experiments shows agreement within 10%. No validation of the method is available for the full scale simulations.

In a similar study vein, Guiard (2013) describe how the Mewis Duct is designed using both model and full scale CFD, where the model scale CFD is compared with model test data. This paper discusses the challenges associated with full scale CFD predictions and the impact of different turbulence models used.

More recently Kok et al (2020) used both model scale and full scale CFD to investigate the scale effects in self-propelled containership squat. Again the CFD method was validated at model scale with the full scale CFD compared against the model data scaled up using the ITTC1978 extrapolation method and other empirical methods. They concluded that scale effects on squat were minimal due to the strong dependency on the Bernoulli wave.

These papers highlight the potential insights that can be gained from full scale CFD, especially the detailed flow fields, but ultimately highlight the need for full scale EFD data to validate such methods to fully realise their potential.

Another area where CFD can provide increased insight is to provide detailed flow field and pressure data to complement an experiment. This can help understand the flow physics behind trends observed in the experimental data.

Tian et al (2017) present a detailed experimental study of blade vibration conducted in different wake flows within a cavitation tunnel. Wire meshes upstream are used to generate either 4 or 6 cycle wake patterns. CFD is then used to provide greater understanding of the forces acting on individual blades and explain the differences in dynamic strain observed in different test cases.

Carrica et al (2016) conducted an experimental and numerical study of a zigzag manoeuvre for the KCS in shallow water. This work provided good quality experimental results to validate numerical tools, which in turn can be used to get significant insight of the hydrodynamics occurring during the manoeuvre. The velocity, pressure fields and vortex structures obtained from the CFD are very challenging to obtain experimentally and could help to understand the detailed flow physics in these type of manoeuvres.

4.4 USE CFD TO HELP DESIGN OR CORRECT EXPERIMENTAL TEST PROCESSES

It is now often standard practice to use CFD for the design of a new hull form, with experimental tests being reserved for evaluating final designs. This process increases the efficiency of the experimental test campaigns but can also be used to identify specific areas of the design or operating conditions which need to be evaluated during the experiments.

Another example of using CFD as part of an experimental procedure is the blockage correction method proposed by Raven (2019). This approach uses numerical simulations to determine the blockage effects for shallow water model tests conducted in a basin of limited width. Such a combined approach improves the accuracy of the experimental prediction accounting for some of the limitations often present when conducting a model scale tests.

4.5 CONCLUSIONS

It can be seen from the previous publications discussed in this chapter that there are many opportunities to be gained from combined CFD and EFD methods. These can range from CFD providing greater insight to flow physics, the development of new empirical relationships that improve scaling predictions to CFD calculations becoming an integral part of the scaling or correction process. In all cases it is clear however that to adopt such combined methods a clear validation and verification process is needed to ensure the potential benefits are achieved.

5. SUGGESTED IMPROVEMENT OF CURRENT RECOMMENDED PROCEDURES BY USING CFD IN COMBINATION WITH MODEL TEST

5.1 CFD-BASED FORM FACTORS

This section describes work that was carried out in close cooperation between the Resistance and Propulsion Committee and the Specialist Committee on CFD and EFD Combined Methods.

As described in Section 2 above, there are a number of known issues with the existing scaling methodologies that could possibly be improved with CFD/EFD combined methods. One of them is the form factor used in the “1978 ITTC Performance Prediction Method” (ITTC 7.5-02-03-01.4). The possibility to use CFD instead of the Prohaska method has been suggested in literature by several authors as described in Chapter 4. The Committees decided to investigate whether a modification of the 1978 Power Prediction method regarding the possibility to use CFD for the form factor could be beneficial. The motivation for selecting this issue from the list is that it was regarded as a major error source in EEDI and contract power prediction, and it is believed to have a potential to be improved with CFD, since state-of-the-art CFD can handle model scale resistance computations well. Improving the form factor determination is to be preferred rather than returning to “2D” ITTC 1957 Power Prediction Method (where form factor is not used). It was shown in the seventies that the prediction accuracy was improved with the 1978 Performance Prediction Method and it was selected as the recommended method. Since then, the 1978 method has been the standard method and modern databases are built upon it.

Several aspects needed to be studied before the committees could submit a proposal for this modification:

1. Whether CFD-derived form factors can be shown to improve, or at least not deteriorate,

the scatter of full-scale predictions compared to sea trials
2. If any general recommendations on how to perform the CFD-simulations can be formulated.
3. Which friction line should be used to derive the form factor?

5.1.1 Comparison with sea trials

When the "1978 Performance Prediction method" was originally derived, several versions were compared and the criterion for selecting the best method was the amount of scatter of full-scale power predictions compared to a large number of sea trials. It was therefore relevant to investigate whether any organisations recently have been able to demonstrate that using CFD-derived form factors improves, or at least does not deteriorate, the scatter. Only two ITTC members reported back on this aspect. MARIN reports that it has now become standard to compute the form factor for each tank project, using the RANS code Parnassos in double-body mode. The $1+k$ obtained is well correlated with what they get from a Prohaska plot of low-speed tests, though not precisely equal. MARIN has no concrete information on whether and how the sea trial correlation improves but believes it is more solid, less subjective, and also more efficient. SSPA claims that CFD-based form factors reduce the scatter compared to the original 1978 Performance Prediction method as well as the method without the form factor ("2D-method"). As presented in Korkmaz et al. (2021b), full scale speed-power-rpm relations between 78 speed trials and the corresponding full scale predictions based on model tests carried out at SSPA were compared. The probability density functions (PDFs) of the normalized correlation factors (where the value of 1 indicates predictions and the speed trials are equal) were calculated as can be seen in **Figure 12**. The comparison of the standard deviations for the power predictions indicates that the scatter is reduced when the CFD based form factors from the EASM turbulence model are used compared to the Prohaska method. The improvements were larger when the ITTC-1957 model-ship correlation is replaced with the numerical friction line of the same turbulence model and the code used for the double body computations.

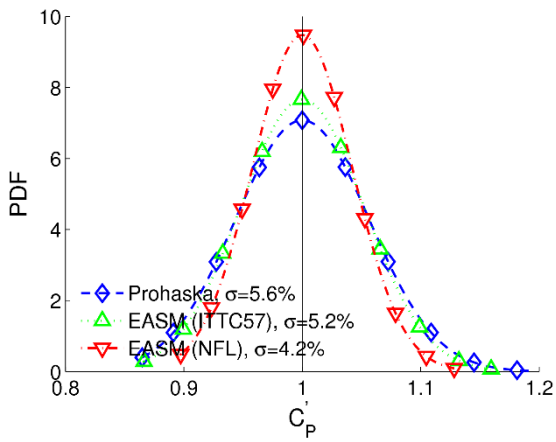

Figure 12: The probability density functions (PDFs) of the normalized correlation factor for power using the Prohaska Method, CFD based form factors with the ITTC-1957 model-ship correlation and the numerical friction lines using EASM turbulence model (Korkmaz et al., 2021b)

5.1.2 How to perform the CFD-simulations

According to ITTC 7.5-03-02-04 "Practical Guidelines for Ship Resistance CFD", a form factor can be computed as

$$(1+k) = \frac{C_T}{C_F} \tag{1}$$

where C_T is the resistance from double body RANS computation (i.e. friction and viscous pressure resistance)

C_F is the 2D flat plate friction resistance at the same Reynolds number.

CFD-simulations for the form factor can be performed with different codes, turbulence models, grid sizes and so on. In order to investigate if any general recommendations on the set-up could be given, a benchmark study for

ITTC members was launched. Initially, 4 members submitted computational results. One computation from published literature could be added. This data collection was the basis for the initial recommendations to modifications of the recommended procedures. In late 2019, the study was expanded to include 9 participants with 286 submissions. The work is published in a journal article (Korkmaz et al., 2021a), which includes more detailed results and discussions than what can be comprised here.

The test cases were the two open hull forms KVLCC2 and KCS (Van, 2011) at design draught and KVLCC2 at ballast draught (Korkmaz et al., 2021a).

CFD computations were performed using double model RANS at specified Reynolds numbers, and the form factors derived from the fraction between the CFD viscous resistance coefficient and the 2D flat plate friction resistance from the ITTC-1957 model-ship correlation line.

The participating organisations and their codes are listed in Table 1.

Over-all results summary

Summaries of the form factor predictions are shown in Figure 13. Even though there is some spread between the submissions, the mean is very close to the experimentally derived form factor. This means that if the CFD-based form factor is used in a power prediction, the correlation factors (Ca or Cp) derived from earlier model test statistics, can still be used. Additionally, majority of the CFD-based form factor predictions for KVLCC2 in ballast draught are within the experimental uncertainty of the form factor (1.9% of 1 + k for the 95% confidence interval) determined by Prohaska method (Korkmaz et al 2021a).

Code

All participating codes were well-known, established RANS codes, widely used for marine applications. No general difference could be detected between the codes except for one code, which initially gave obviously unrealistic results. The code developers were contacted and found one error in the friction integration algorithm and a bad cell distribution in the default setting (see more below). Participants that used that code re-submitted with the updated code and mesh, which resulted in comparable results. The lesson learned is that even well-established codes may have weak points and the users must carry out their own validation work for their specific task.

Table 1: Participants in form factor benchmark study

Organisation	Code	Initial study	Extended study
Centrale Nantes	ISIS-CFD	x	x
SSPA	Shipflow	x	x
University of Strathclyde	Star-CCM+	x	x
NMRI	NAGISA	x	x
MARIN	ReFresco	x	
University of Michigan	Open FOAM / Helyx		x
China Ship Scientific Research Centre	NaViiX		x
Ocean, Coastal and River Engineering, NRC-OCRE	Open FOAM		x
Shanghai Ship and Shipping Research Institute	Star-CCM+		X
Yokohama National University	SURF		x

Cell distribution

Variation in longitudinal and vertical cell distribution was studied by one participant (also reported in Korkmaz 2019). The form factor is rather robust with regards to cell distribution, even for a very coarse grid in the fore body the differences in form factor were within 0.02. The only grid that gave inaccurate result was when the cell distribution in the aft body was extremely coarse.

Grid type and wall treatment

106 submissions were carried out using wall functions and 180 using wall-resolved grids. Vast majority of the structured grids utilized wall resolved grids, while most of the unstructured grids used wall functions. The type of grid and wall treatment showed somewhat indicative trends on the form factor: form factors from wall resolved and structured grids were higher than the simulations with wall functions and unstructured grids on average.

Normalized wall distance y+

Except very few simulations, the submissions used recommended average y+ <1 for wall resolved and y+ >23 for wall functions). The identified y^+ (first cell size normal to the wall) did not show general trends but different codes indicated varying tendencies. (UofM used adaptive wall functions and provided results that spanned 1 < y+ < 100.)

Number of cells

All submissions had more than 0.4 million cells. No difference in scatter or level could be detected based on number of cells, although as the cell number increases for a given code, the results for that code converge.

Turbulence model

Five turbulence models were represented: k-ω SST, realizable k-ε, RNG k-ε, Spalart-Allmaras and EASM. Turbulence modelling is identified as one of the most influential aspect of the CFD set-up. However, no general trends are observed but different codes indicated

varying tendencies, sometimes opposite trends among to codes.

Speed (Reynolds number)

When a Prohaska plot from model test is used to derive the form factor, a straight line is extrapolated using mainly the measurements at the lowest speed practically possible. It means that the correlation factors (Ca/Cp) are derived based on these points. Ideally, it should not matter, as the form factor should be independent of speed. However, a known flaw of the ITTC-1957 model-ship correlation line is that it is too steep at the lower Reynolds numbers (see for example Korkmaz et al., 2021a). Therefore, the CFD based form factor is different when derived at the Reynolds number corresponding to the model scale design speed compared to a Reynolds number corresponding to the low speed points of a resistance test. For the test cases in the study, the differences in form factors are about 0.011 and 0.015 for KVLCC2 and KCS, respectively (Figure 13). When using CFD based form factors for power predictions in combination with the correlation factors (Ca or Cp) derived from earlier model tests, the CFD computations can be done either at the Reynolds number corresponding to the lower end of the model test speed range or to the design speed. This is because the correlation between the form factors derived from the earlier model tests and the CFD based form factors are both based on the EFD techniques (turbulence stimulation, hull openings, inclusion of appendages such as rudders) and test characteristics (such as the typical Reynolds number range) in the case of EFD, and the CFD set-up (such as the choice of the turbulence model, the type of wall treatment). Additionally, some members report numerical instabilities when attempting double model computations at low speeds for hulls with pronounced bulbous bows. For those cases, it may help to run at a higher Reynolds number, corresponding to design speed. Another option is to increase the forward trim in the computations. It can also be argued that the form factor should be derived at the most important speed, i.e. design speed. These discussions would be resolved with a friction line other than the ITTC-1957 model-ship correlation line.

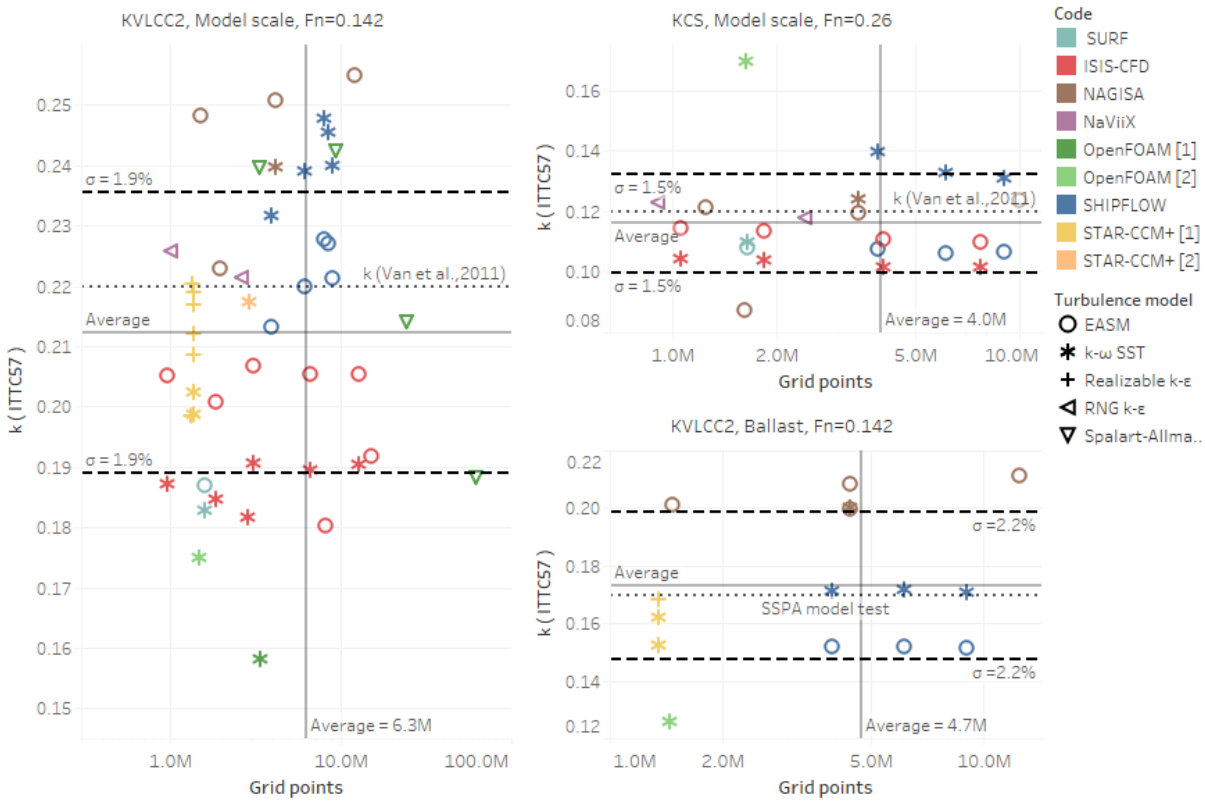

Figure 13: Form factor, k, based on ITTC-1957 model-ship correlation line versus grid size for KVLCC2 hull in design loading condition at Fn=0.142 (left), KCS hull in design loading condition at Fn=0.26 (top right) and KVLCC2 in ballast loading condition Fn=0.142 (bottom right) (Korkmaz et al., 2021a)

Draft and trim

It can be argued that the form factor should be derived at the resultant draft after dynamic sinkage and trim that the ship will have at the design speed. However, since the experimentally based form factor is derived by extrapolating to zero speed wave resistance, this also means extrapolating to the zero speed draft, which may be different from the draft at the design speed due to dynamic sinkage and trim. When using a form factor for power prediction in combination with the correlation factors derived from earlier model tests, then the form factor should be derived at the static draft. In the presence of a bulb close to or piercing the water surface, the computation may be problematic due to suppression of large waves especially at low speed. Imposing a slight forward trim so that the bulb is sub-merged may help.

Transom

A deeply submerged transom may be problematic for RANS codes. Raven 2019 suggests that adding a wedge with slip condition is a possible solution. No distinctive effect of slightly submerged transom (submerged transom area divided by maximum midship cross-section up to 0.015) were found on the correlation between the predictions and the speed trials (Korkmaz et al., 2021b). More studies are needed to be able to give general recommendations. In the meantime, each organisation should develop their own validated solution.

Flow separation

Flow separation that occurs at model scale but not at full scale is a known scaling problem that may occur on full hull forms. Raven 2019 suggests that one way to detect and possibly correct for this is to compute the CFD-based form factor at both model and full scale. The model scale form factor is used to derive the wave resistance and the full scale form factor is used to compute the full scale viscous resistance. This suggestion has been tested in Korkmaz et al. (2021b), and it has been confirmed that the prediction accuracy is increased for the hulls exhibiting separation. This is a promising option that should be investigated further by other members.

5.1.3 Which friction line that should be used to derive the form factor

As described in Section 2, the ITTC-1957 model-ship correlation line has been criticised by several authors in the literature as well as in internal discussions in the ITTC community. It is now clear that the reported scale dependency of the form factor is caused by the non-physical shape of the ITTC 1957 line, rather than the form factor concept itself. Some authors propose to overcome this by either using another friction line, for example Katsui as in Raven (2009), or by omitting the use of a friction line as in Wang et al. (2015). Korkmaz (2021b) showed that adoption of numerical friction lines can introduce improvements to the power predictions compared with a large number of sea trials. However, the main cause of the gain in the accuracy of the predictions were not due to elimination of the scale effects on form factors but another minor contributing factor. As concluded in Korkmaz (2021b), the usage of numerical friction lines led to a readjustment of the full scale viscous resistance predictions which can be obtained by modifying the correlation allowance (Ca) to a large extent. It has also been suggested that each user derive its own friction line based on CFD, using the same turbulence model and CFD method as used for the hull. If this can be shown to give higher accuracy, ITTC should formulate a Recommended Procedure for deriving such a friction line.

It has to be stressed that replacing the ITTC-1957 model-ship correlation line in the power prediction methods implies that the correlation factors (Ca or Cp) are no longer valid. It would mean a very large work effort for the individual model test institutes to derive new correlation factors, and it can only be motivated if the accuracy can be shown to be improved. For this reason, it was decided for the time being to recommend to continue using the ITTC-1957 model-ship correlation line, also for CFD based form factors.

5.2 Conclusions and recommendations

The mentioned joint committee study, as well as published papers, some of them with committee members as authors, forms the motivation for the final suggested Recommended Procedures. The following was concluded:

Since the study contains only limited number of test cases and only one organisation's comparison with a large number of sea trials, it can neither be concluded nor rejected that that CFD-based form factors should *replace* the Prohaska method.

It should be suggested that CFD-based form factors can be used to *support* the conventional Prohaska method.

ITTC should encourage the use of CFD-based form factors to support the conventional method, as it seems likely that it improves the accuracy of the predictions on average.

When more institutes gain experience with CFD-based form factors, the recommendations should be re-evaluated.

To start with, C_F should be recommended to be derived from the ITTC-1957 model-ship correlation line, in spite of its drawbacks. In this way, each organisations' correlation factors (Ca or Cp) can be kept unchanged.

The use of alternative friction lines for C_F should be investigated further:

- What are the implications of changing to a published line such as Katsui or Grigson?
- Is it more accurate to use a CFD-based friction line using the same CFD-models as for the hull?

No general recommendation on how to perform the CFD computations for form factor can be given. Suitable choice of mesh, turbulence model etc. is code dependent. Therefore to ensure the quality of CFD prediction of form factor, refer to the new "Quality assurance in Ship CFD Application", 7.5-03-01-02.

Based on the study and considerations described above, improvements of the following Recommended Procedures were suggested to the Resistance and Propulsion Committee:

ITTC 7.5-03-02-04 "Practical Guidelines for Ship Resistance CFD", Section 3.1

ITTC 7.5-02-03-01.4 "1978 ITTC Performance Prediction Method", Section 2.4.1

The committee recommends the full conference to adopt the modifications of the procedures.

6. REVIEW OF CURRENT ITTC PROCEDURES FOR POTENTIAL USE OF COMBINED EFD AND CFD

In this section, the current ITTC Procedures are reviewed for possible benefits from combined EFD and CFD in the future.

6.1 AN OVERVIEW

In the 2017 Edition of the ITTC procedures (2017), there are a total 79 procedures, among which 60 are related to EFD only, seven are related to both EFD and CFD, five are only related to CFD, and the rest of them are routine work related. Among 39 guidelines in 2017 ITTC, there are 25 that are only related to EFD, four are related to both EFD and CFD, and five are related to only CFD. Also, of the 13 work instructions, one is about the introduction of suggested formats, and the rest are about calibration of testing equipment.

6.2 RESISTANCE, PROPULSION AND POWERING PERFORMANCE

Guideline 7.5-01-03-04 is about benchmarking for PIV and SPIV setups. This guideline mentions using RANS simulation to assist in testing by calculating flow separation. Procedure 7.5-03-02-02 lists the resistance and propulsion benchmark database that can be used for CFD validation.

Guideline 7.5-02-03-02.5 mentions the method of using combined CFD (RANS) and EFD to tune a model scale wake field in a cavitation tunnel towards a full-scale wake field. Similarly, procedure 7.5-02-03-03.7 talks about how to use combined methods of simulation, as well as model tests, to predict cavitation and erosion damage on "unconventional" rudders and on rudders behind highly loaded propellers. Procedure 7.5-02-05-3.2 mentions the use of CFD and model test combination to determine the head rise across the pump, and the inlet duct loss for waterjet system performance analysis.

The phenomenon of wave breaking and the resistance in waves is currently being studied in detail with unsteady RANS.

Exact simulation is not achievable due to insufficient knowledge of the actual full-scale

flow field and simulation approximations due to Reynolds number, Froude number, and non-geosim hull representations, therefore, further research is required to understand how to use CFD at full scale for resistance, propulsion, and powering.

Also, CFD is being used to study cavitation in detail. With regards to gap cavitation, the viscous effect in the gap is currently of focus with unsteady RANS. Rigorous procedures for the numerical modelling of cavitating flows will be formed in the next 3 years.

6.3 MANOEUVRING AND SEAKEEPING

Guideline 7.5-03-04-02 introduces validation and verification of RANS solutions in the prediction of manoeuvring capabilities, using methods from QM 7.5-02-06-04 "Uncertainty Analysis for Manoeuvring Predictions based on Captive Manoeuvring Testing" and QM 7.5-02-06-05 "Uncertainty Analysis for Free Running Manoeuvring Model Test".

Procedure 7.5-02-07-02.5 addresses verification and validation of linear and weakly non-linear seakeeping computer codes. This procedure mainly discusses using experiments for CFD validation, with multiple mentions of 7.5-02-07-02.3 "Experiments on Rarely Occurring Events". One typical example of CFD/EFD combined method is mentioned in procedure 7.5-02-07-02.8, which calculates the weather factor f_w for the decrease of ship speed in wind and waves. This procedure includes methods of experiment, numerical computation, and empirical formulae.

A standard simulation procedure of free running, and the calculation of hydrodynamic coefficients in calm water, can be formed in the next 3 years. The manoeuvring hydrodynamic coefficients in waves, especially the coupling effects between different coefficients can be obtained based on unsteady RANS simulations. The general procedures may be formed in the next few years. Scale effects, including the larger model wake fraction, and the larger model resistance, can be studied based on the unsteady RANS, and the non-similar rudder inflow between model and full scale can be further studied.

The numerical procedure of sloshing can be formed in the next three years. The simulation of added resistance in head waves based on unsteady RANS has been widely carried out by many scholars, especially the cases in short waves. Based on these research results, the added resistance in oblique waves can be studied in the next three years. The numerical simulation for ship motion with green water based on CFD method has been widely used in recent years, and it can be extended to the research for the large amplitude motion with green water. Simulation of multidirectional irregular wave spectra and modelling of complex ice environment can be achieved based on unsteady RANS.

6.4 STABILITY AND HYDRODYNAMIC NOISE

The numerical simulation of large amplitude roll damping using CFD is the focus of much current research, and the numerical prediction of free rolling based on unsteady RANS has been widely accepted for many cases. However, instructions on how to calculate roll damping coefficients for different types of ship has still not been recommended by the ITTC. A procedure for the prediction of roll damping coefficients based on the free rolling should be determined in the next 3 years. At present, the simulation of large roll damping based on unsteady RANS is mostly concentrated in calm water, and more attention should be paid for the calculation process of large amplitude roll damping in waves.

The direct simulation of different failure modes based on unsteady RANS, such as parametric rolling, pure loss of stability, dead ship, excessive acceleration, surfing riding/ broaching has been attempted in recent years. More complex and accurate simulations will be possible in the next few years, and simulation procedures for parametric rolling and dead ship can also be formed in the ensuing years.

For stability in waves, the capsize boundary is an important quantity. However, the capsize boundary is difficult to quantify because of the chaotic behaviour due to nonlinearity of restoring moment. Therefore, CFD is recommended for the determination of capsize boundary. This can also help to further develop the model test procedures for the determination of the capsize boundary.

Numerical simulation based on CFD method can be used to understand of the physics and behaviour of the motion of a damaged ship and the flooding process. Air compressibility is an important factor that affects damage flooding, and the study of the influence of air compressibility through model test requires high test conditions. Therefore, the influence of air compressibility can be systematically studied based on CFD method in the next few years, and the numerical research can provide guidance for the study of this mechanism.

Besides physical tests, numerical methods for structure-borne noise will be more involved in the next years. As the excitation source, the spatial-temporal distribution of turbulent flow will be more detailed and accurately CFD predicted. These demanding requirements still require a great deal of effort on future CFD.

6.5 GENERAL RECOMMENDATIONS

6.5.1 ELIMINATION OF THE SCALE EFFECT BY COMBINED EFD AND CFD

Scale effects have been mentioned in many procedures for different phenomena, and the combination of EFD and CFD method can play an important role in the study of such problems.

Two scale effect phenomena including the larger model wake fraction and the larger model resistance have been mentioned in the procedure of manoeuvring. The scale effect can be eliminated by the combination of EFD and CFD.

Scale effects in manoeuvring have yet to be fully understood, and they are mainly due to a non-similar rudder inflow between model and full scale. Therefore, we can also use the combination of EFD and CFD for research on the role of non-similarity.

The procedure of 'Validation of Manoeuvring Simulation Models_7.5-02-06-03', describes the development of simulation models, and the ways that they are validated. This procedure is in fact a classical case for the combination of CFD and EFD. We suggest more detailed or improved validation methods.

The procedure 'Seakeeping Experiments 7.5-02-07-02.1', mentions scale effects and the key factors that can also be studied by the combination of EFD and CFD.

In the procedure 'Cavitation Induced Pressure Fluctuations: Numerical Prediction Methods 7.5-02-03-03.4', the accurate and reliable full-scale predictions of cavitation-induced pressure fluctuation should be confirmed by the combination of CFD and EFD.

For the procedure of 'Cavitation Induced Erosion on Propellers, Rudders and Appendages Model Scale Experiments 7.5-02-03-03.5', the

scale effects related to fluid effects and bubble dynamic effects in cavitation testing can be investigated by the combination of CFD and EFD.

For the procedure of 'Prediction of Cavitation Erosion Damage for Unconventional Rudders or Rudders Behind Highly-Loaded Propellers 7.5-02-03-03.7', the gap cavitation scale effect, the viscous effect within the gap, and vortex cavitation can be studied by the combination of EFD and CFD.

For the procedure of 'Modelling the Behaviour of Cavitation in Waterjets' 7.5-02-03-04.8, numerical modelling has been paid more and more attention due to the high cost required for experimental modelling. The highest quality results in modelling the behaviour of cavitation in waterjets can be obtained by combination of EFD and CFD.

6.5.2 UNCERTAINTY ANALYSIS

Almost all model tests and simulations must be accompanied by uncertainty analysis. Future work should be directed towards improved and unified uncertainty analyses.

For the guideline of 'Underwater Noise from Ships, Full Scale Measurements _7.5-04-04-01', the sources of uncertainty and variability can be studied by the combination of EFD and CFD.

For the procedure of 'Experiments on Rarely Occurring Events 7.5-02-07-02.3', the rarely occurring events can be first studied by CFD, and then further validated through the combination of CFD and EFD.

For the procedure of 'Laboratory Modelling of Multidirectional Irregular Wave Spectra 7.5-02-07-01.1', the verification and validation procedure for added resistance codes can be realized by the combination of EFD and CFD methods.

For the procedure of 'Cavitation Induced Pressure Fluctuations: Numerical Prediction Methods 7.5-02-03-03.4', there is just one rigorous verification and validation procedure. Therefore, universally-accepted V&V procedures for CFD should be established.

For the procedure of 'Floating Offshore Platform Experiments 7.5-02-07-03.1', many parameters cause uncertainties in floating offshore platform tests, and CFD can be utilized to study the influence of different factors of uncertainty.

7. UNCERTAINTY ASSESSMENT METHODS FOR CFD SIMULATIONS

In this chapter, various uncertainty assessment methods for CFD simulations are reviewed with applications to naval hydrodynamics in mind. Firstly, the ITTC Procedure and Guidelines (2017) and the American Society of Mechanical Engineers (ASME) standard procedures are compared and their differences are discussed. Yao et al. (2013) proposed verification and validation based on the orthogonal design approach and it is described in detail. Other recent approaches, such as N-version and Roy's method, are also reviewed. Finally, the ISO procedures are presented and compared with the ASME procedures.

7.1 DIFFERENCE IN ITTC AND ASME PROCEDURES

7.1.1 GRID REFINEMENT RATIO ($\boldsymbol{r_i}$)

In ITTC Procedure and Guidelines (2017), iterative and parameter convergence studies are conducted using multiple solutions, at least three, with systematic parameter refinement by varying the ith input parameter Δx_i while holding all other parameters constant. Many common input parameters are of this form, e.g., grid spacing, time step, and artificial dissipation.

Iterative errors must be accurately estimated or negligible in comparison to errors due to input parameters before accurate convergence studies can be conducted.

Careful consideration should be given to the selection of uniform parameter refinement ratio, r_i in terms of the element size, Δx_i.

$$r_i = \Delta x_{i,2}/\Delta x_{i,1} = \Delta x_{i,3}/\Delta x_{i,2} = \Delta x_{i,m}/\Delta x_{i,m-1} \quad (2)$$

The most appropriate values for industrial CFD are not yet fully established. Small values, i.e., very close to one, are undesirable since solution changes will be small and sensitivity to input parameter may be difficult to identify compared to iterative errors. Large values alleviate this problem; however, they also may be undesirable since the finest step size may be prohibitively small, i.e., require many steps, if the coarsest step size is designed for sufficient resolution such that similar physics are resolved for all solutions. Also, similarly as for small values, solution changes for the finest step size may be difficult to identify compared to iterative errors, since iterative convergence is more difficult for the small step size. Another issue is that for parameter refinement ratio other than $r_i = 2$, interpolation to a common location is required to compute solution changes, which introduces interpolation errors. However, in cases of industrial CFD, $r_i = 2$ may often be too large. A good alternative may be $r_i = \sqrt{2}$, as it provides a fairly large parameter refinement ratio and at least enables prolongation of the coarse parameter solution as an initial guess for the fine parameter solution.

In the ASME procedure, Roache (1998) defines a representative cell, mesh, or grid size, h. For example, for three-dimensional, structured, geometrically similar grids, which is not necessarily a Cartesian one,

$$\mathrm{h} = [(\Delta x_{max})(\Delta y_{max})(\Delta z_{max})]^{1/3} \quad (3)$$

For unstructured grids one can define

$$\mathrm{h} = \left[\left(\sum_{i=1}^{N} \Delta V_i\right)\Big/ N\right]^{1/3} \quad (4)$$

where N is the total number of cells used for the computations and ΔV_i is the volume of the ith cell.

It is desirable that the grid refinement factor, $\mathrm{r} = h_{coarse}/h_{fine}$, should be greater than 1.3 for most practical problems. This value of 1.3 is again based on experience and not on some formal derivation. The grid refinement should, however, be made systematically; that is, the refinement itself should be structured even if the grid is unstructured.

7.1.2 UNCERTAINTY ($\boldsymbol{U_i}$) AND ORDER OF ACCURACY ($\boldsymbol{p_i}$)

In Uncertainty Analysis in CFD Verification and Validation Methodology and Procedures 7.5-03-01-01 (ITTC, 2017), the generalized Richardson Extrapolation (RE) is used to estimate the error δ_i^* for the selection of the ith input parameter and order of accuracy p_i. The error is expanded in a power series expansion with integer powers of Δx_i as a finite sum. The accuracy of the estimates depends on how many terms are retained in the expansion, the magnitude (or importance) of the higher order terms, and the validity of the assumptions made in the RE theory.

With three solutions, only the leading term can be estimated, which provides one term estimates for error and order of accuracy.

$$\delta_{RE,1}^{*(1)} = \frac{\varepsilon_{i,21}}{r_i^{p_i} - 1} \quad (5)$$

$$p_i = \frac{\ln\left(\varepsilon_{i,32}/\varepsilon_{i,21}\right)}{\ln(r_i)} \quad (6)$$

where $\varepsilon_{i,32} = \varphi_{i,3} - \varphi_{i,2}$ is changes between coarse-medium solutions and $\varepsilon_{i,21} = \varphi_{i,2} - \varphi_{i,1}$ is changes between medium-fine solutions.

Although not proposed by Roache (1998), the factor of safety F_s approach can be used for situations where the solution is corrected with an error estimate from RE as

$$U_i = (F_s - 1)\left|\delta_{RE,1}^{*}\right| \quad (7)$$

The exact value for factor of safety is somewhat ambiguous and $F_s = 1.25$ is recommended for careful grid studies.

In the ASME procedure, let $h_1 < h_2 < h_3$ and $r_{21} = h_2/h_1$, $r_{32} = h_3/h_2$ and calculate the apparent (or observed) order, p, of the method from reference

$$\mathrm{p} = [1/\ln(r_{21})][1/\ln|\varepsilon_{32}/\varepsilon_{21}| + q(p) \quad (8)$$

$$\mathrm{q}(p) = \ln\left(\frac{r_{21}^{p} - s}{r_{32}^{p} - s}\right) \quad (9)$$

$$\mathrm{s} = 1 \cdot \sin(\varepsilon_{32}/\varepsilon_{21}) \quad (10)$$

where $\varepsilon_{32} = \varphi_3 - \varphi_2$, $\varepsilon_{21} = \varphi_2 - \varphi_1$, and φ_k denote the simulation value of the variable on the kth grid. Note that $\mathrm{q}(p) = 0$ for a constant r. This set of three equations can be solved using fixed point iteration with the initial guess equal to the first term, i.e., q = 0.

For example, suppose that we need to calculate and report the following error estimates along with the observed order of the method p. Approximate relative error may be cast as a dimensionless form or in a dimensioned form, respectively as follows:

$$e_a^{21} = \left|\frac{\varphi_1 - \varphi_2}{\varphi_1}\right| \quad (11)$$

$$e_a^{21} = |\varphi_1 - \varphi_2| \quad (12)$$

The error was estimated from the equation

$$U_i = \frac{Fs \cdot e_a^{21}}{r_{21}^{p} - 1} = F_s\left|\delta_{RE,1}^{*}\right| \quad (13)$$

For the factor of safety, F_s, Roache (1998) recommended a less conservative value for F_s = 1.25, but only when using at least three grid solutions and the observed *p*.

7.2 CFD RESULTS VERIFICATION BASED ON ORTHOGONAL DESIGN

Based on the orthogonal design and the statistical inference theory, Yao et al. (2013) developed a new verification method and the related procedures in the CFD simulation. It is shown that the new method can be used for the verification in the CFD uncertainty analysis and can reasonably and definitely judge the credibility of the simulative result. The concept of the validation process recommended by ITTC is vague. The turbulence model of the CFD

simulation should be an important source of uncertainty, which is the greatest contribution to the CFD uncertainty. However, the turbulence model's uncertainty evaluation method is not included in the recommended procedure. The interactions between the calculated factors are not considered in the validation method in the recommended procedures, and it is assumed that the calculated parameters are independent of each other. But the interactions will affect the estimation of the combined standard uncertainty and the validation process.

7.2.1 ORTHOGONAL DESIGN METHOD

The orthogonal design method refers to the method used in a physical test involving multiple elements. Provided that the numerical simulation could be regarded as a virtual physical test, this method may as well be used to design and analyse the virtual test process and the results.

Firstly, the calculation factors to be examined should be divided into the controlled calculation factors and the out-of-control calculation factors. The former are the major elements that affect the simulation result, and the latter include all minor elements other than the controlled calculation factors.

When the controlled calculation factors and their interaction and the level are set, the orthogonal array should be chosen to ensure that all controlled factors and some blank columns are included. The statement heading should be designed in a way that the controlled factors and the interaction scheduled to be examined in every column should not be overlapped in the effect.

7.2.2 VARIANCE ANALYSIS METHOD

The variance analysis refers to a method, which distinguishes the experiment results affected by different factor level (including interaction) changes or errors. The F test is the basis of the variance analysis and is mainly used to check whether there is a significant difference among levels of calculation factors.

Assume that F is the ratio of the average sum of squares of deviations caused by the factor level change and the average sum of squares of deviations caused by errors, as

$$\mathrm{F} = \frac{\frac{S_j}{f_j}}{\frac{S_e}{f_e}} \tag{14}$$

where f is the degrees of freedom and S is the sum of squares of deviations. Therefore, if the ratio of the effect on the simulation result attribution of the controlled calculation factors and the out-of-control calculation factors can be identified as F, then F can be used to check whether some major calculation factors are omitted. Meanwhile, S_j and S_e represent the influence of the controlled factors and their interactions on the simulation result and that of the out-of-control factors and their interaction on the simulation result, respectively.

7.2.3 TYPE A EVALUATION OF STANDARD UNCERTAINTY

When $\bar{y}$ is the estimated value of the simulated physical quantity y and obtained based on the statistical method, u(y) is the standard uncertainty of Type A and can be obtained through statistical analysis of y

$$\mathrm{u(y)} = \mathrm{s}(\bar{y}) = \frac{s(y)}{\sqrt{n}} = \sqrt{\frac{\sum_{i=1}^{n}(y_i - \bar{y})^2}{n(n-1)}} \tag{15}$$

In the process of the numerical simulation under a certain statistical control, if $\bar{y}$ is the arithmetic mean value and serves as the estimated value of y, n is the number of independent simulations, i.e., the number of calculations on the orthogonal table, y_i is the calculation result of independent simulations at i^{th} time, the combined standard deviation, S_p, can be used as a token and the standard uncertainty of the simulation result is

$$u(y) = \frac{s_p}{\sqrt{n}} = \sqrt{\frac{\sum_{i=1}^{n}(y_i - \bar{y})^2}{n(n-1)}} \tag{16}$$

where S_p represents the combined standard deviation, S_i the sample standard deviation, p the sampling frequency, i.e., the number of calculations at the same level, and n the total number of samples.

If the controlled calculation factor A is put on column j in the orthogonal table, its number of levels being l, the repeated number of each level being p, and the degree of freedom being $f_A = l - 1$, the sum of squares of the deviations s_A and u_A the uncertainty of Type A can be calculated and so can S_{AxB} of the interaction of the calculation Factors A and B, the out-of-control calculation factor or the random error standard deviations s_e and uncertainty u_e.

$$S_A = \sqrt{\frac{S_A}{f_A}}, u_A = \frac{S_A}{\sqrt{N}} \tag{17}$$

$$S_{AxB} = \sqrt{\frac{S_{AxB}}{f_{AxB}}}, u_{AxB} = \frac{S_{AxB}}{\sqrt{N}} \tag{18}$$

$$S_e = \sqrt{\frac{S_{blankrow}}{f_{blankrow}}}, u_e = \frac{S_e}{\sqrt{N}} \tag{19}$$

where S_j the sum of squares of deviations on any column j in the orthogonal table, which can be calculated as follows

$$S_j = \frac{I_j^2 + II_j^2 + \cdots + (l_j)^2}{p} - \frac{(\sum_{i=1}^{N} y_i)^2}{N} \tag{20}$$

In this formula, I_j, II_j, represent the sum of y numbers listed on levels “1”, “2” on column j. As to the interaction, the following formula is used

$$S_{AxB} = \sum_j S_j, \ f_{AxB} = (l-1)^2 \tag{21}$$

7.2.4 TYPE B EVALUATION OF STANDARD UNCERTAINTY

When y is the estimated value of the simulated physical quantity Y and is not obtained based on the statistical method, its estimated variance, $u^2(y)$, and $u(y)$, the uncertainty components for Type B, can be evaluated according to the methods such as those based on the historical data, the experience, the adopted error correction formula, the CFD software instruction and other information provided by other documentation.

Based on the information above, the evaluation methods of the uncertainty for Type B are to judge the probable interval (-a, a) of the simulated value, by using the confidence level (including the probability) to estimate the coverage factor k and then to calculate the uncertainty by the formula as follows:

$$u(y) = \frac{a}{k} \quad (22)$$

In the CFD simulation, the uncertainty component for Type B comes mostly from the uncertainty caused by known and correctable system errors and the imperfection in the correction method. The truncation error and the iterative error of the numerical computation can have an approximate correction and its uncertainty u_G and u_I can be calculated by k factor formula. The mathematical model error and the accumulation of the rounding error that are not clear or not possible to correct will be classified into the uncertainty components of Type A.

The formula of truncation uncertainty and iterative uncertainty are as follows:

$$u_G = \frac{\delta_{RE}}{\sqrt{3}} \quad (23)$$

$$u_I = \frac{y_U - y_L}{2\sqrt{6}} \quad (24)$$

where y_U and y_L are the upper bound and the lower bound of the simulation result that can meet the condition of convergence.

7.2.5 CALCULATION OF COMBINED STANDARD UNCERTAINTY

The u_c, combined standard uncertainty of CFD, is the sum of the variances of all standard component uncertainties $u_I(x)$. If there is a significance interaction, the covariance can be used

$$u_c = \sqrt{\sum_{i=1}^{n} u_i^2} \quad (25)$$

$$u_c = \sqrt{\sum_{i=1}^{n} u_i^2 + 2\sum_{i=1}^{n}\sum_{j=i+1}^{n} r(x_i, x_j)u(x_i)u(x_j)} \quad (26)$$

In this formula, $u(x_i)$ and $u(x_j)$ are the standard uncertainties of x_i and x_j, r is the estimated valued of the correlation coefficient of x_i and x_j.

7.2.6 EVALUATION OF EXPANDED UNCERTAINTY

For the combined uncertainty, u_c, corresponding to the standard deviation, the probability of containing the true value is 68% at the interval of the simulation results $y \pm u_c$. In some engineering applications, a high confidence probability level is required so that the simulation falls into the interval, and in the hope that the interval contains with a great probability the simulated value reasonably endowed. To meet this requirement, the expanded uncertainty, U, can be calculated by multiplying the combined uncertainty and the coverage factor k. The following formula is used

$$U = ku_c(y) \quad (27)$$

Therefore, the result is represented as $Y = y \pm u$, where y is the estimate of the simulated value, the interval $y - U \leq Y \leq y + U$ is the extent containing with a great probability the reasonably endowed y distribution. The coverage factor, k, ranges from 2 to 3 based on the confidence level required by the interval $y \pm U$. if k is 2, it means that the simulation result value, which obeys the normal distribution, will be in the range of the estimated value $\pm U$ according to 95% of probability level of that interval can reach up to 99%.

7.3 VALIDATION METHOD AND PROCESS IN CFD UNCERTAINTY ASSESSMENT

After the CFD simulation result is verified, it is usually required to be validated. The validation method proposed by Yao et al. (2013) is described in the following. The validation may be characteristic parameters of the simulation results and the experiment results by using the statistical inference theory. In fact, the results of the physical experiment or the numerical simulation are random variables, and it can be assumed that they obey the normal distribution $N(\mu,\sigma)$. The comparison of two random variables should be made by the concepts and the means of the statistical inference. Strictly speaking, only if the statistical characteristic parameters μ and σ of the two random variables are equal. No significant differences between them can be validated.

7.3.1 STATISTICAL INFERENCE METHOD FOR VALIDATION

The statistical inference is based on one or several sub-samples to infer or judge the statistical characteristics of it population. The degree of confidence is an important index to measure the reliability. Here, the problem is to use the statistical inference method to judge whether the expectation, μ_c, and the variance, σ_c^2, of the numerical simulation population inferred from the small sample are the same as the expectation, μ_T, and the variance, σ_T^2, of the population of the experiment. If so, then the numerical simulation results are validated.

7.3.2 F-TEST

In the CFD validation process, one first judges whether the variance of the population of the numerical simulation, σ_c^2, and that of the experiment, σ_T^2, in the statistical sense is the same or not, by means of the F-test of the statistical inference theory.

Define the following F variable

$$\mathrm{F} = \frac{\widehat{\sigma_c}^2}{\widehat{\sigma_T}^2} = \frac{S_C^2}{S_T^2} = \frac{\frac{S_c}{f_c}}{S_T^2} \tag{28}$$

where $\widehat{\sigma_T}$ is the estimate of the population of the experiment σ_T, S_T^2 is the experimental standard deviation, which can be obtained from the database of the benchmark test or the historical information. Suppose that it is known and its degree of freedom is ∞. $\widehat{\sigma_c}$ is the estimate of the CFD simulation results, s_c is the sum of the squares of the deviations of the simulation results. f is the degree of freedom, $f_c = N - 1$, N is the size of the numerical simulation sub-sample, and is called the program number of the orthogonal design.

The data can be obtained from the verification process of the CFD simulation based on the orthogonal design, as in Equations (26) and (27).

$$\mathrm{S_j} = \mathrm{S}_j = \frac{I_j^2 + II_j^2 + \cdots + \left(l_j\right)^2}{p} - \frac{\left(\sum_{i=1}^{N} y_i\right)^2}{N} \tag{29}$$

where l is the level of the calculation factor, p is each level's repetitive number, y is the simulation results, $\mathrm{I_j}$, $\mathrm{II_j}$, represent the sum of y numbers listed on levels "1", "2" on column j.

For the interaction, we have

$$\mathrm{S_{AxB}} = \sum \mathrm{S}_j \ , f_{A\mathrm{xB}} = (l-1)^2 \tag{30}$$

Although N cannot be very large, the full factor program information can be obtained, because it is a sample from the orthogonal design and the overall information can be obtained from a part of the implementation. So its F-test confidence is higher than the common sample. If $\mathrm{F} > \mathrm{F_a}(f_c, \infty)$, then the statistical hypothesis $\sigma_c^2 = \sigma_T^2$ is untrue, otherwise, it can be believed that $\sigma_c^2 = \sigma_T^2$, which means that the population variances of the numerical simulation and the experiment are equal.

7.3.3 T-TEST

From the law of large numbers, the best unbiased estimator of the expectation, μ, of random variables is the arithmetic mean. So in the validation process, the average of the population of two random variables, i.e., the results of the numerical simulation and the physical experiment, are compared.

If the two samples are relatively large and equal, even the variances are different, the t-test method can be approximately applied. In fact, the experiment sub-sample is assumed to be a big sub-sample from the benchmark test, and the sub-sample of the numerical simulation is an approximate large sub-sample obtained by the orthogonal design, so the requirements of a relatively large number for the two sub-sample of the same size can be approximately met.

The statistical hypothesis goes like this: "The averages of the population of the sub-samples from the numerical simulation and the experiment are equal, $\bar{X}_c = \bar{X}_T$". Here, $\bar{X}_c$ and $\bar{X}_T$ are the averages of the results from the numerical simulation and the experiment, N_c and N_T are the sizes of the sub-samples. Define the *t* variable as

$$t = \frac{\bar{X}_c - \bar{X}_T}{\sqrt{\frac{N_c \widehat{\sigma_c}^2 + N_T \widehat{\sigma_T}^2}{N_c + N_T - 2}} \sqrt{\frac{1}{N_c} + \frac{1}{N_T}}} \tag{31}$$

$$f = (N_c - 1)(N_T - 1) \tag{32}$$

With the general aspects, $N_c = N_T = N$ and N is large enough, the Equation (29) can be rewritten as

$$t = \frac{\bar{X}_c - \bar{X}_T}{\sqrt{\frac{\widehat{\sigma_c}^2 + \widehat{\sigma_T}^2}{N}}} = \frac{\bar{X}_c - \bar{X}_T}{\sqrt{\frac{s_C^2 + s_T^2}{N}}} = \frac{\bar{X}_c - \bar{X}_T}{\sqrt{u_C^2 + u_T^2}} \tag{33}$$

where u_c and u_T are the combined uncertainty of the CFD simulation and the experiment, respectively.

Considering that the current CFD simulation accuracy cannot reach the level of the experiment, so for simplicity, the term u_T can be omitted, Equation (28) can be simplified as

$$t = \frac{|\bar{X}_c - \bar{X}_T|}{u_c}, \qquad f_c = N - 1 \tag{34}$$

According to the t variable degrees of freedom f and the confidence level α, $t_a(f_c)$, the critical value of the variable t can be obtained. If $t < t_\mathrm{a}$, then $\bar{X}_c = \bar{X}_T$, the statistical hypothesis is not untrue. The simulation results can be validated.

7.3.4 VALIDATION PROCESS

For the simulation results, it is necessary to judge by the statistical inference method whether the expectation and the variance of the

population of the simulation results obtained from a small sub-sample are the same as those of the population of the experiment results. If they are equal, the simulation results are validated. The proposed validation methodology and its process of the CFD numerical simulation can be summarized as in the Figure 14.

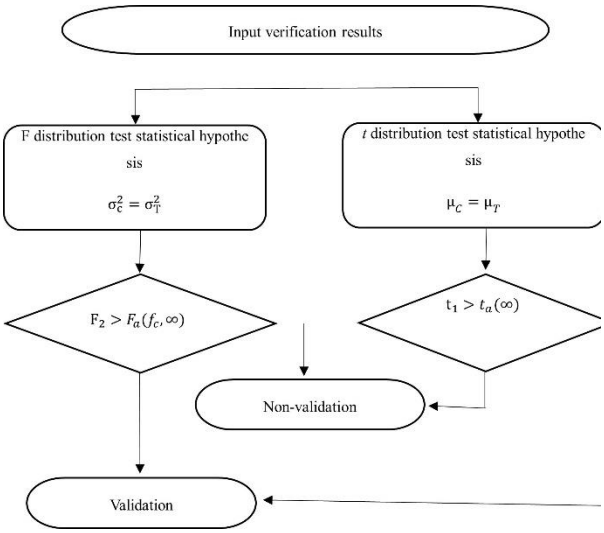

Figure 14: Flow chart of CFD simulation result's validation

7.4 METHODS FOR GRID CONVERGENCE

7.4.1 LEAST SQUARE ROOT METHOD

Where the use of unstructured grids leads to variability in the grid, the error can be estimated using a Least Squares Root (LSR) method (Eça at al., 2010; Larsson at al., 2013). This requires at least four solutions to perform a curve fit of

$$\varphi_i = \varphi_0 + \alpha {h_i}^p \tag{35}$$

where i is the grid number from 1 to the number of grids and h_i is the size ratio.

The convergence condition is determined based on the observed order of accuracy, p, such that $p > 0$ indicates monotonic convergence and $p < 0$ indicates monotonic divergence. Oscillatory convergence is defined as being when the solution is alternately above and below the exact solution.

Since p is strongly influenced by the amount of scatter in the solutions, such that it may be larger than the theoretical order of accuracy, leading to an underestimate of the error, three alternative error estimates are provided, also found by curve fitting.

$$\delta_{RE} = \varphi_i - \varphi_0 = \alpha {h_i}^p \tag{36}$$

where φ_i is the numerical solution of any local or integral scalar quantity on a given grid, φ_0 is the estimated exact solution, and α is a constant.

If results on more than three grid are available, φ_0, α and p are obtained with a Least Squares Root method that minimizes the function:

$$S(\varphi_o, \alpha, p) = \sqrt{\sum_{i=1}^{n_g} (\varphi_i - (\varphi_o - \alpha {h_i}^p))^2} \tag{37}$$

where n_g is the number of grids available. The minimum of $S(\varphi_o, \alpha, \mathrm{p})$ is found by setting its derivatives with respect to φ_o, p_j and α_j equal to zero, (Eca at al., 2007). The standard deviation of the fit, U_s, is given by

$$U_s = \sqrt{\frac{\sum_{i=1}^{n_g} (\varphi_i - (\varphi_o - \alpha {h_i}^p))^2}{n_g - 3}} \tag{38}$$

LSR method establishes the apparent order of convergence p from the least squares solution. Oscillatory convergence or divergence is identified by n_{ch}, the number of times the difference between consecutive solutions changes sign, i.e. $(\varphi_{i+1} - \varphi_i) \times (\varphi_i - \varphi_{i-1}) < 0$. The apparent convergence condition is then decided as follows:

(1) $p > 0\ for\ \varphi \rightarrow$ Monotonic convergence.

(2) $p < 0\ for\ \varphi \rightarrow$ Monotonic divergence.

(3) $n_{ch} \geq INT(n_g) \rightarrow$ Oscillatory convergence or divergence.

The only condition which allows an error estimation based on Richardson extrapolation is monotonic convergence. But even then small perturbations in the data may lead to significant changes in the estimated value of p, and thus sometimes to unsatisfactory results when the GCI in the LSR method.

In an attempt to overcome this, the maximum difference between all the solutions Δ_M is introduced.

$$\Delta_M = \max(|\varphi_i - \varphi_j|) \quad with\ 1 \leq i \leq n_g \wedge 1 \leq j \leq n_g \tag{39}$$

Two error estimators based on power series expansion with fixed exponents are:

$$\delta_{RE}^{12} = \varphi_i - \varphi_j = \alpha_1 h_i + \alpha_1 {h_i}^2 \tag{40}$$

$$\delta_{RE}^{02} = \varphi_i - \varphi_o = \lambda_1 {h_i}^2 \tag{41}$$

δ_{RE}^{12} and δ_{RE}^{02} are also calculated in the LSR method and so we will have standard deviations given by

$$U_S^{12} = \sqrt{\frac{\sum_{i=1}^{n_g}(\phi_i - (\phi_o + \alpha_1 h_i + \alpha_1 {h_i}^2))^2}{n_g - 3}} \tag{42}$$

$$U_S^{02} = \sqrt{\frac{\sum_{i=1}^{n_g}(\phi_i - (\phi_o + \lambda_1 {h_i}^2\, d))^2}{n_g - 3}} \tag{43}$$

LSR method procedure for the estimation of the numerical uncertainty, valid for a nominally second-order accurate method, is as follows:

(1) The observed order of accuracy p is estimated with the LSR method to identify the apparent convergence condition according to the definition given above.

(2) For monotonic convergence:

For $0.95 \leq p < 2.05$

$$U_\phi = 1.25(\delta_{RE} + U_s) \tag{44}$$

For $0 < p < 0.95$

$$U_\phi = \min(1.25(\delta_{RE} + U_s),\ 1.25 \min\left(1.6, \frac{2.28}{\mathrm{p}} - 1.4\right)\left({\delta_{RE}}^{12} + U_S^{12}\right)) \tag{45}$$

For $p \geq 2.05$

$$U_\phi = \max(1.25(\delta_{RE} + U_s),\ 1.25 \min(1.6, 3p - 5.15)\left({\delta_{RE}}^{02} + U_S^{02}\right)) \tag{46}$$

(3) For monotonic convergence:

$$\mathrm{U}_\phi = 3\Delta_\mathrm{M} \tag{47}$$

7.4.2 RICHARDSON EXTRAPOLATION

In Eça and Hoekstra (2014), Richardson Extrapolation (RE) is based on the assumption that discrete solutions have a power series representation in the grid spacing. RE approach requires at least three grids. Three grids are in the asymptotic range and the data have no scatter. The basic estimation equation of discretization error is:

$$\epsilon_\phi \cong \delta_{\mathrm{RE}} = \phi_i - \phi_o = \alpha h_i^p \tag{48}$$

ϕ_i stands for any integral of other functional of a local flow quantity, ϕ_o is the estimate of the exact solution, α is a constant to be determined, h_i is the typical cell size and p is the observed order of grid convergence (Roache, 1998). The estimation of ϵ_ϕ requires the determination of ϕ_o, α and p. Therefore, the minimum number of grids (n_g) required for the estimation of ϵ_ϕ is three, unless p is assumed equal to a theoretical value, which is often not justified for practical problems.

The assumptions inherent in the application of Equation (47) are:

The grids must be in the "asymptotic range" to guarantee that the leading term of the power series expansion is sufficient to estimate the error.

The density of the grids is representable by a single parameter, the typical cell size of the grids, h_i. This requires the grids to be geometrically similar, i.e. the grid refinement ratio must be constant in the complete field and grid properties like the deviation from orthogonality, skewness, etc. must remain unaffected.

With equal grid refinement ratios between medium/finest and coarsest/medium grids, i.e. $h_2/h_1 = h_3/h_2$, a grid triplet suffices to estimate the apparent grid convergence behavior based on the discriminating ratio:

$$\mathrm{R} = \frac{\phi_1 - \phi_2}{\phi_2 - \phi_3} \tag{49}$$

where the subscripts 1, 2 and 3 stand for fine, medium and coarse grid, respectively (Roache, 1998).

- Monotonic convergence for 0 < R <1.
- Monotonic divergence for R > 1.
- Oscillatory convergence for R < 0 and $|R| < 1$.
- Oscillatory divergence for R < 0 and $|R| > 1$.

In fact, the discriminating ratio R is related to the observed order of grid convergence p and the grid refinement ratios $h_2/h_1 = h_3/h_2$ by

$$\mathrm{R} = \left(\frac{h_1}{h_2}\right)^p \left(\frac{\left(\frac{h_2}{h_1}\right)^p - 1}{\left(\frac{h_3}{h_2}\right)^p - 1}\right) \mathrm{R} = \frac{\phi_1 - \phi_2}{\phi_2 - \phi_3} \tag{50}$$

which for $h_2/h_1 = h_3/h_2$ reduces to

$$\log(R) = p \log\left(\frac{h_1}{h_2}\right) \tag{51}$$

Hence, in such conditions, $\mathrm{p} > 0$ is equivalent to $0 < \mathrm{R} < 1$ and $\mathrm{p} < 0$ to $\mathrm{R} > 1$.

In order to be able to deal with the shortcomings of "practical calculations", three other error estimators can be used.

$$\epsilon_\phi \cong \delta_1 = \phi_i - \phi_o = \alpha h_i \quad (52)$$

$$\epsilon_\phi \cong \delta_2 = \phi_i - \phi_o = \alpha h_i^2 \quad (53)$$

$$\epsilon_\phi \cong \delta_2 = \phi_i - \phi_o = \alpha h_i + \alpha h_i^2 \quad (54)$$

These three alternatives are only used if the estimation with Equation (47) is impossible or not reliable, i.e. the observed order of grid convergence is either too small or too large. The first two options, Equations (51) and (52), are suitable for monotonically converging solutions only, whereas the latter can be used as well with non-monotonic convergence.

7.4.3 SQUARE ROOT EXTRAPOLATION

The error estimators presented above require three grids, using Equations (47) and (53), or two grids, using Equations (51) and (52), to estimate an error (Eça and Hoekstra, 2014). But error estimation based on three or two grids is not reliable for noisy data due to the extreme sensitivity of the determination of p to small perturbations (Eça and Hoekstra, 2002). Therefore, it is virtually impossible to decide whether or not a given set of data is in the "asymptotic range". Note that in the presence of scatter, an observed order of grid convergence equal to the formal order of grid convergence may be fortuitously obtained and is not sufficient to label the data set as being in the "asymptotic range". Furthermore, a single grid triplet gives only one instance of p, because Equation (47) has three unknowns. Redundancy, and thus the possibility of a quality check on the value of p, only occurs when the fourth grid is added. Therefore, it is highly recommendable to use at least four grids when some scatter in the data is expected, i.e. for most engineering flow problems.

In such conditions $(n_g \gg 4)$, it is possible to do the error estimation in the least-squares sense, i.e. to determine ϕ_o from the minimum of the functions:

$$S_{RE} = \sqrt{\sum_{i=1}^{n_g} w_i \left(\phi_i - \left(\phi_o + \alpha h_i^p\right)\right)^2} \quad (55)$$

$$S_1 = \sqrt{\sum_{i=1}^{n_g} w_i \left(\phi_i - \left(\phi_o + \alpha h_i^p\right)\right)^2} \quad (56)$$

$$S_2 = \sqrt{\sum_{i=1}^{n_g} w_i \left(\phi_i - \left(\phi_o + \alpha h_i\right)\right)^2} \quad (57)$$

$$S_{12} = \sqrt{\sum_{i=1}^{n_g} w_i \left(\phi_i - \left(\phi_o + \alpha h_i + \alpha h_i^2\right)\right)^2} \quad (58)$$

The least-squares minimization of Equations (58) to (61) is presented as follows, which also includes the definition of the standard deviation of the fits, σ, that will be sued as a measure of the quality of the fits (Rawlings et al., 1998).

$$w_i = \frac{1/h_i}{\sum_{i=1}^{n_g} 1/h_i} \log(R) = p \log\left(\frac{h_1}{h_2}\right) \quad (59)$$

$$\sigma_{RE} = \sqrt{\frac{\sum_{i=1}^{n_g} n_g w_i \left(\phi_i - \left(\phi_o + \alpha h_i^p\right)\right)^2}{\left(n_g - 3\right)}} \quad (60)$$

$$\sigma_1 = \sqrt{\frac{\sum_{i=1}^{n_g} n_g w_i \left(\phi_i - \left(\phi_o + \alpha h_i^p\right)\right)^2}{\left(n_g - 3\right)}} \quad (61)$$

$$\sigma_2 = \sqrt{\frac{\sum_{i=1}^{n_g} n_g w_i \left(\phi_i - \left(\phi_o + \alpha h_i\right)\right)^2}{\left(n_g - 3\right)}} \quad (62)$$

$$\sigma_{12} = \sqrt{\frac{\sum_{i=1}^{n_g} n_g w_i \left(\phi_i - (\phi_o + \alpha h_i + \alpha h_i^2)\right)^2}{(n_g - 3)}} \quad (63)$$

7.5 N-VERSION APPROACH

For ship hydrodynamics, verification usually uses either the Fs or LSR methods. The numerical uncertainties U_{SN_i} associated to individual code/simulation S_i use the root-sum square of the iterative U_{I_i} grid U_{G_i}, and time-step U_{T_i} uncertainties

$$U_{SN_i} = \sqrt{U_G^2 + U_{T_i}^2 + U_{I_i}^2} \quad (64)$$

where i indicates an individual code and S_i is the solution on the finest grid. ASME (2009) advocates adding ${U_{I_i}}^2$ with ${U_{G_i}}^2$ and ${U_{T_i}}^2$. Iterative and grid/time verification studies are difficult and unfortunately often neglected. The Fs method requires monotonic convergence and ratio of the Richardson extrapolation and theoretical order of accuracy $P = P_{RE}/P_{th} \leq 2$, due to lack of data for P > 2 used for estimation of the required factor of safety. LSR method allows for oscillatory convergence, but there are differences of opinion on some aspects of the procedures.

The comparison error E_i is

$$E_i = D - S_i \quad (65)$$

D is the experimental data. Validation compares E_i with the validation uncertainty

$$U_{V_i}^2 = U_{E_i}^2 - U_{SM_i}^2 = U_{SN_i}^2 + U_D^2 \quad (66)$$

U_{SM} and U_D are the simulation modelling and experimental data uncertainties, respectively. The simulations are validated at an interval U_{V_i} if

$$|E_i| \leq U_{V_i} \quad (67)$$

If $U_{V_i} \ll |E_i|$, the sign and magnitude of $E_i \approx \delta_{SM}$ can be used to make modelling improvements. U_{V_i} includes all estimable uncertainties in the data and the simulations, and is the key metric in the validation process, which sets the interval at which validation can be achieved and may or may not meet programmatic requirements/tolerances.

Individual code solution V&V provides metrics for both the error E_i and its uncertainty U_{V_i}, from which conclusions can be made concerning acceptability or improvement strategies. The experimental uncertainty U_D usually includes both systematic and random components, whereas the numerical uncertainty U_{SN_i} is based solely on the systematic error and uncertainty estimates. Sensitivity and UQ studies using random perturbations of CFD code input parameters fail to provide an accurate simulation random uncertainty estimate as not representative of the inherent randomness in the CFD process as applied by different codes and/or users for different applications.

N multiple solutions from different codes and/or users for specified benchmark test cases provide the necessary data for assessment of CFD SoA capability, including individual solution and man code errors and estimates for simulation and absolute error random uncertainties. The assumption is made that the scatter of the CFD results represents the reproducibility of the computations. Results from many users of the same code are similar to N-order replication level experiments (individual facility and measurement systems),

whereas results from many different codes are similar to M×N-order replication level experiments (multiple facilities and measurement systems).

7.5.1 N-VERSION VERIFICATION

At the multiple code/user level, the individual code/solution uncertainty includes both systematic/bias and random/precision components

$$U_{S_i}^2 = B_{S_i}^2 + P_{S_i}^2 = \left(B_{SM_i}^2 + B_{SN_i}^2\right) + P_{S_i}^2 \quad (68)$$

where bias uncertainties are estimated at the simulation (single realization) level and precision uncertainties at the code (N-version, multiple realization) level.

Equations (63) and (65) assume that correlated modelling and numerical errors are negligible as a first approximation. Thus, the systematic uncertainty should include correlated modelling and numerical errors at a higher order of approximation. In contrast, P_{S_i} includes all simulation random uncertainties, including those arising from modelling and numerical errors and their correlations, i.e., represents the random simulation uncertainty.

Equation (67) can be written for both an individual code S_i and the average of N-version codes (mean code)

$$\bar{S} = \frac{1}{N}\sum_{i=1}^{N} S_i \quad (69)$$

$$U_{\bar{S}}^2 = B_{\bar{S}}^2 + P_{\bar{S}}^2 \quad (70)$$

Solution V&V studies (individual code/simulation level) provide

$$B_{S_i}^2 = B_{SM_i}^2 + B_{SN_i}^2 \quad (71)$$

Usually, B_{SM_i} is not known. However, in some cases (for instance, when using fluid property data), it can be estimated and included. The mean code bias is based on the average root-sum-square for the individual codes

$$B_{\bar{S}}^2 = \frac{1}{N}\sum_{i=1}^{N} B_{S_i}^2 = B_{\overline{SM}}^2 + B_{\overline{SN}}^2 \quad (72)$$

N-version verification (code level) provides

$$P_{S_i} = 2\sigma_s \quad (73)$$

where

$$\sigma_S = \left[\frac{1}{N-1}\sum_{i=1}^{N}(S_i - \bar{S})^2\right]^{\frac{1}{2}} = \left[\frac{1}{N-1}\sum_{i=1}^{N}(E_i - \bar{E})^2\right]^{1/2} = \sigma_E \quad (74)$$

and

$$P_{\bar{S}} = \frac{2\sigma_s}{\sqrt{N}} \quad (75)$$

$\sigma_S\%\bar{S}$ provides a measure of the scatter in the multiple CFD solutions for the specified benchmark test case. U_{S_i} including P_{S_i} (similarly for $U_{\bar{S}}$ and $P_{\bar{S}}$) provides a simulation uncertainty estimate at the N-order replication

level. The mean code is a fictitious representation of the average of the N-version population. Outliers can be identified and rejected similarly as with experimental data using, e.g., Chauvenet's criterion. Herein, for simplicity, a solution is rejected if its deviation from the mean is larger than $2\sigma_S$, i.e., $N \approx 10$.

The estimated truth $\overline{S_{ET}}$ and S_{ET} lies within the confidence intervals

$$\mathrm{S_i} - U_{S_i} \leq S_{ET} \leq S_i + U_{S_i} \tag{76}$$

and

$$\bar{S} - \bar{U}_{\bar{S}} \leq \bar{S}_{ET} \leq \bar{S} + U_{\bar{S}} \tag{77}$$

The assumption that for $N \geq 10$ and codes/simulations sufficiently similar in modelling and numerical methods and code development that S_i distribution is approximately normal is reasonable; however, multiple peaks and skewed distributions are also realized and should be expected, e.g., clustering around turbulence models or grid types.

7.5.2 N-VERSION VALIDATION

The CFD SoA assessment is based on N-version validation for the specified benchmark test case. The average error and average absolute error are, respectively,

$$\bar{E} = \frac{1}{N}\sum_{i=1}^{N} E_i \tag{78}$$

$$\overline{|E|} = \frac{1}{N}\sum_{i=1}^{N} |E_i| \geq |\bar{E}| \tag{79}$$

The average absolute error is always greater than or equal to the absolute value of the signed average error. Previous certification approach used average error with the sign and $\sigma_S = \sigma_E$ for estimating simulation and error random uncertainties. Bias and precision uncertainties were estimated similarly as for solution validation, i.e., treating E_i and $\bar{E}$ as data reduction equation and using propagation of error analysis. Clearly, the average absolute error is a better indicator of CFD SoA capability, as average of large positive and negative errors leads to erroneous result that the errors are small. Herein, average absolute error and its scatter are used for the CFD SoA assessment.

The average absolute error uncertainty consists of bias and precision components

$$U_{\overline{|E|}}^2 = B_{\overline{|E|}}^2 + P_{\overline{|E|}}^2 \tag{80}$$

The bias uncertainty is evaluated using $\overline{|E|}$ as data reduction equation and propagation of error analysis, whereas precision uncertainty uses $\overline{|E|}$ as data reduction equation and end-to-end analysis in which the standard deviation is evaluated for $\overline{|E|}$ itself. Note that this is the usual practice in experimental uncertainty analysis. Thus, the bias uncertainty is comprised of contributions for both the experimental and simulation uncertainties

$$\begin{aligned} B_{\overline{|E|}}^2 &= U_D^2 + B_{\bar{S}}^2 \\ &= U_D^2 + B_{\overline{SM}}^2 + B_{\overline{SN}}^2 \end{aligned} \tag{81}$$

The precision uncertainty is approximated as

$$P_{\overline{|E|}} = \frac{2\sigma_{|E|}}{\sqrt{N}} \tag{82}$$

where average absolute error standard deviation is

$$\sigma_{|E|} = \sqrt{\frac{1}{N-1}\sum_{i=1}^{N}\left(|E_i| - \overline{|E|}\right)^2} \tag{83}$$

with the absolute value statistical property of the folded normal distribution

$$\sigma_{|E|}^2 = \sigma_E^2 + \bar{E}^2 - \overline{|E|}^2 \leq \sigma_E^2 = \sigma_S^2 \tag{84}$$

$\sigma_{|E|}\%D$ provides a measure of the scatter in the multiple solution absolute errors for the specified benchmark test case.

Following the same reasoning and approach used for solution validation, SoA uncertainty U_{SoA} is defined as:

$$\begin{aligned} U_{SoA}^2 &= U_{\overline{|E|}}^2 - B_{\overline{SM}}^2 \\ &= U_D^2 + B_{\overline{SN}}^2 + P_{\overline{|E|}}^2 \end{aligned} \tag{85}$$

U_{SoA} includes all estimable uncertainties in the data and the simulations and is the key metric in the assessment of the CFD SoA. It sets the interval at which the SoA can be achieved and may or may not meet programmatic requirements/tolerances.

$$\overline{|E|} \leq U_{SoA} \tag{86}$$

For the mean code is N-version validated at the interval of the SoA uncertainty U_{SoA}, whereas for

$$\overline{|E|} > U_{SoA} \tag{87}$$

the mean code is not N-version validated due to modelling assumptions. In theory, $\bar{E}$ can be used for modelling assumptions improvements. In particular,

$$\overline{|E|} \gg U_{SoA} \tag{88}$$

$$\bar{E} \approx \delta_{\overline{SM}} \tag{89}$$

The sign of $\bar{E}$ may be of value; however, clearly improvements are made at the individual code/simulation level.

Similar analysis can be done for the individual code/simulation

$$U_{|E_i|}^2 = B_{|E_i|}^2 + P_{|E_i|}^2 \tag{90}$$

$$\begin{aligned} B_{|E_i|}^2 &= U_D^2 + B_{S_i}^2 \\ &= U_D^2 + B_{SM_i}^2 \\ &\quad + B_{SN_i}^2 \end{aligned} \tag{91}$$

$$P_{|E_i|} = k\sigma_{|E|} \tag{92}$$

$$\begin{aligned} U_{SoA_i}^2 &= U_{|E_i|}^2 - B_{SM_i}^2 \\ &= U_D^2 + B_{SN_i}^2 + P_{|E_i|}^2 \end{aligned} \tag{93}$$

Note that the coverage factor k in Equation (91) follows the folded normal distribution quantiles and is asymmetric for lower and upper bound. Depending on the mean and standard deviation of the signed error, k ranges from 1.3 to 2 for the lower bound and from 2 to 2.4 for the upper bound. For simplicity, hereafter, the approximated value $k = 2$ is used.

$$|E_i| \leq U_{SoA_i} \tag{94}$$

For individual code/simulation is N-version validated at interval U_{SoA_i} , whereas for

$$|E_i| > U_{SoA_i} \tag{95}$$

individual code/simulation is not N-version validated due to modelling assumptions. E_i can be used for modelling assumptions improvements.

$$|E_i| \gg U_{SoA_i} \tag{96}$$

$$E_i \approx \delta_{SM_i} \tag{97}$$

The equations for N-version validation are similar to those for individual solution validation, except therein $P_{|E_i|}$ is not included

$$U_{SoA_i}^2 - P_{|E_i|}^2 = U_{V_i}^2 = U_D^2 + B_{SN_i}^2 \tag{98}$$

N-version validation provides additional confidence compared to individual solution validation, since it is additionally based on statistics of the normal distribution of N-versions. State-of-the-art uncertainty is also an improvement over simply identifying outliers based on σ_S alone, since additionally includes considerations of bias uncertainties. As with experimental uncertainty analysis, maximum confidence is achieved if both bias and precision uncertainties are considered. Subgroup analysis procedures can be used for isolating and assessing differences due to the use of different models and/or numerical methods.

Programmatic requirements/tolerances U_{req} can be considered similarly as for solution validation, but with U_V replaced by U_{SoA_i}. Since U_{SoA_i} is $\geq U_V$, it will always be a more conservative assessment. There are six possible combinations of $|E_i|$, U_{SoA_i} , and U_{req} assuming none are equal

$$\begin{aligned}
&Case\ 1\ |E_i| < U_{SoA_i} < U_{req} \\
&Case\ 2\ |E_i| < U_{req} < U_{SoA_i} \\
&Case\ 3\ U_{req} < |E_i| < U_{SoA_i} \\
&Case\ 4\ U_{SoA_i} < |E_i| < U_{req} \\
&Case\ 5\ U_{SoA_i} < U_{req} < |E_i| \\
&Case\ 6\ U_{req} < U_{SoA_i} < |E_i|
\end{aligned} \tag{99}$$

In cases 1, 2, and 3, N-version validation is achieved at the U_{SoA_i} interval, i.e., the comparison error is below the noise level. From an uncertainty perspective, modelling errors cannot be isolated. In cases 4, 5, and 6, the comparison error is larger than the noise level, i.e., $U_{SoA_i} < |E_i|$ such that from an uncertainty perspective, the sign and magnitude of E can be used to estimate δ_{SM}. If $U_{SoA_i} \ll |E_i|$, $\mathrm{E} = \delta_{SM}$. Only cases 1 and 4 meet the programmatic requirements.

Consideration of programmatic requirements/tolerances resolves two paradoxes of the Coleman and Stern (1998) solution validation approach: (1) that only when validation is not achieved it is possible to have confidence that the error equals the modelling error; and (2) validation is easier to achieve for large U_V , i.e., noisy experiments and/or simulations. These paradoxes are mentioned at the individual code/simulation level but are also true for N-version validation with U_V replaced by U_{SoA_i}.

The reason for paradox (1) is that only for $U_V = 0$ it is true that $E = \delta_{SM}$, which only can occur for cases 4 to 6. For case 4, even though validation is not achieved both $|E_i|$ and U_V are

$< U_{req}$ such that programmatic requirements are met and no action is needed. For case 5, $E = \delta_{SM}$ can be used to guide improvements in modelling in order to meet programmatic requirements. For case 6, similar as for case 5, $E = \delta_{SM}$ can be used to guide improvements in modelling and reduction in U_V, i.e., U_D and/or U_{SN} (depending on their relative magnitudes) are required in order to meet programmatic requirements.

The reason for paradox (2) is that, without U_{req}, U_V is unrestricted, whereas once restricted by U_{req}, there is no possibility for acceptance of the achievement of validation by a large U_V. For case 1, both $|E_i|$ and U_V are $< U_{req}$ such that programmatic requirements are met and no action is needed. For case 2, reduction in U_V, i.e.,U_D and/or U_{SN} (depending on their relative magnitudes), is required in order to meet programmatic requirements. For case 3, reduction in both $|E_i|$ and U_V, i.e., U_D and/or U_{SN} (depending on their relative magnitudes), is required in order to meet programmatic requirements. Thus, case 3 is the most difficult as one cannot discriminate between different models with $|E_i| < U_V$ from an uncertainty perspective.

The processes for determining U_{req} and U_V/U_{SoA_i} UV/USoAi are very different; therefore, meeting or not U_{req} should not be confused with individual code/simulation and multiple codes/N-version validation. Solution validation is a process for assessing simulation modelling errors/uncertainties. N-version validation extends this concept for multiple codes/simulations, which enables inclusion of the random absolute error uncertainty in assessing the CFD SoA. Presumably, the process for determining U_{req} is dominated by financial (beyond design testing and simulation), safety, environmental, and other concerns which may or may not take into consideration E_i andU_V/U_{SoA_i}.

7.6 ROY'S APPROACH

7.6.1 CODING VERIFICATION

Software quality assurance

In Roy (2005), Software Quality Assurance, or SQA, is a formal set of procedures developed to ensure that software is reliable. SQA utilizes analysis and testing procedures including static analysis, dynamic analysis, and regression testing. Static analysis is an analysis conducted without actually running the code and includes such activities as compiling the code (possibly with different compilers on different platforms) and running external diagnostic software to check variable initialization and consistency of argument lists for subroutines and functions. Dynamic analysis includes any activity which involves running the code. Examples of dynamic analysis include run-time compiler options (such as options for checking array bounds) and external software to find memory leaks. While numerical algorithm testing is technically a form of dynamic testing, it is such an important aspect of code verification for a computational simulation that it will be addressed in a separate section. Finally, regression tests involve the comparison of code output to the output from earlier versions of the code and are designed to find coding mistakes by detecting unintended changes in the code. It is important that the regression test suite be designed to obtain coverage of as much of the code as possible (i.e., all models and coding options). The results of SQA testing should be logged so that failures can be reported and corrected. Finally, code documentation is a critical area and includes documentation of code requirements, the software development plan, the verification, and testing plan, governing and auxiliary equations, and available coding options.

Consistency and convergence

For a numerical scheme to be consistent, the discretized equations must approach the original (continuum) partial differential equations in the limit as the element size (Dx, Dt, etc.) approaches zero. For a stable numerical scheme, the errors must not grow in the marching direction. These errors can be due to any source (round-off error, iterative error, etc.). It should be noted that typical stability analyses are valid for linear equations only. Finally, convergence addresses the issue of the solution to the discretized equations approaching the continuum solution to the partial differential equations in the limit of decreasing element size. Convergence is addressed by Lax's equivalence theorem (again valid for linear equations only) which states that given a properly-posed initial value problem and a consistent numerical scheme, stability is the necessary and sufficient condition for convergence. Thus, consistency addresses the equations, while convergence deals with the solution itself. Convergence is measured by evaluating (or estimating) the discretization error. For verification purposes, it is convenient to define the discretization error as the difference between the solution to the discretized equations f_k and the solution to the original partial differential equation f_{exact}

$$DE_k = f_k - f_{exact} \tag{100}$$

where k refers to the mesh level. For the purposes of this paper, the round-off and iterative convergence error are addressed separately, therefore their contributions to the overall discretization error are neglected.

Method of exact solutions

Code verification has traditionally been performed by using the method of exact solutions. This approach involves the comparison of a numerical solution to an exact solution to the governing partial differential equations with specified initial and boundary conditions. The main disadvantage of this approach is that there are only a limited number of exact solutions available for complex equations (i.e., those with complex geometries, physics, or nonlinearity). When exact solutions are found for complex equations, they often involve significant simplifications. For example, the flow between parallel plates separated by a small gap with one plate moving is called Couette flow and is described by the Navier–Stokes equations. In Couette flow, the velocity profiles are linear across the gap. This linearity causes the diffusion term, a second derivative of velocity, to be identically zero. In contrast to the method of manufactured solutions discussed in the next sub-section, the method of exact solutions involves the solution to the forward problem. That is given a partial differential equation, boundary conditions, and initial conditions, the goal is to find the exact solution.

Method of manufactured solutions

The method of manufactured solutions, or MMS, is a general and very powerful approach to code verification. Rather than trying to find an exact solution to a system of partial differential equations, the goal is to ''manufacture'' an exact solution to a slightly modified set of equations. For code verification purposes, it is not required (in fact, often not desirable) that the manufactured solution be related to a physically realistic problem; recall that verification deals only with the mathematics of a given problem. The general concept behind MMS is to choose the solution a priori, then operate the governing partial differential equations onto the chosen solution, thereby generating analytical source terms. The chosen (manufactured) solution is then the exact solution to the modified governing equations made up of the original equations plus the analytical source terms. Thus, MMS involves the solution to the backward problem: given an original set of equations and a chosen solution, find a modified set of equations that the chosen solution will satisfy. The initial and boundary conditions are then determined from the solution.

The use of manufactured solutions and grid convergence studies for the purpose of code verification was first proposed by Roache and Steinberg (1984). They employed symbolic manipulation software to verify a code for generating three-dimensional transformations for elliptic partial differential equations. These concepts were later extended by Roache et al. (1990). The term ‘‘manufactured solution’’ was coined by Oberkampf and Blottner (1998) and refers to the fact that the method generates (or manufactures) a related set of governing equations for a chosen analytic solution. An extensive discussion of manufactured solutions for code verification was presented by Salari and Knupp (2000) and includes both details of the method as well as application to a variety of partial differential equation sets. This report was later refined and published in book form by Knupp and Salari (2002). A recent review/tutorial was given by Roache (2002), and the application of the manufactured solutions procedure for the Euler and Navier–Stokes equations for fluid flow was presented by Roy et al. (2004).

The procedure for applying MMS with the order of accuracy verification can be summarized in the following six steps:

Step 1. Choose the form of the governing equations

Step 2. Choose the form of the manufactured solution

Step 3. Derive the modified governing equations

Step 4. Solve the discrete form of the modified governing equations on multiple meshes

Step 5. Evaluate the global discretization error in the numerical solution

Step 6. Apply the order of accuracy test to determine if the observed order of accuracy matches the formal order of accuracy

The fourth step, which includes the solution to the modified governing equations, may require code modifications to allow arbitrary source terms, initial conditions, and boundary conditions to be used. Manufactured solutions should be chosen to be smooth, analytical functions with smooth derivatives. The choice of smooth solutions will allow the formal order of accuracy to be achieved on relatively coarse meshes, and trigonometric and exponential functions are recommended. It is also important to ensure that no derivatives vanish, including cross-derivatives. Care should be taken that one term in the governing equations does not dominate the other terms. For example, when verifying a Navier–Stokes code, the manufactured solution should be chosen to give Reynolds numbers near unity so that convective and diffusive terms are of the same order of magnitude. Finally, realizable solutions should be employed, that is, if the code requires the temperature to be positive (e.g., in the evaluation of the speed of sound which involves the square root of the temperature), then the manufactured solution should be chosen as such.

MMS has been applied to the Euler equations, which govern the flow of an inviscid (frictionless) fluid (Roy, 2004). The two-dimensional, steady-state form of the Euler equations is given by

$$\frac{\partial(\rho u)}{\partial \mathrm{x}} + \frac{\partial(\rho v)}{\partial \mathrm{y}} = f_m \tag{101}$$

$$\frac{\partial(\rho u^2 + p)}{\partial \mathrm{x}} + \frac{\partial(\rho u v)}{\partial \mathrm{y}} = f_x \tag{102}$$

$$\frac{\partial(\rho u v)}{\partial \mathrm{x}} + \frac{\partial(\rho v^2 + p)}{\partial \mathrm{y}} = f_y \tag{103}$$

$$\frac{\partial(\rho u e_t + p u)}{\partial \mathrm{x}} + \frac{\partial(\rho v e_t + p v)}{\partial \mathrm{y}} = f_e \tag{104}$$

where arbitrary source terms f are included on the right-hand side, and e_t is the specific total energy, which for a calorically perfect gas is given by

$$e_t = \frac{1}{\gamma - 1} RT + \frac{u^2 + v^2}{2} \tag{105}$$

The final relation needed to close the set of equations is the equation of state for a calorically perfect gas

$$\mathrm{p} = \rho \mathrm{RT} \tag{106}$$

The manufactured solution for this case is chosen as

$$\rho(x,y) = \rho_0 + \rho_x sin\left(\frac{a_{\rho x}\pi x}{L}\right) + \rho_y cos\left(\frac{a_{\rho y}\pi y}{L}\right) \tag{107}$$

$$u(x,y) = u_0 + u_x sin\left(\frac{a_{ux}\pi x}{L}\right) + u_y cos\left(\frac{a_{uy}\pi y}{L}\right) \tag{108}$$

$$\mathrm{v}(x,y) = v_0 + v_x sin\left(\frac{a_{vx}\pi x}{L}\right) + v_y cos\left(\frac{a_{vy}\pi y}{L}\right) \tag{109}$$

$$\mathrm{w}(x,y) = w_0 + w_x sin\left(\frac{a_{wx}\pi x}{L}\right) + w_y cos\left(\frac{a_{wy}\pi y}{L}\right) \tag{110}$$

The subscripts here refer to constants (not differentiation) with the same units as the variable, and the dimensionless constants generally vary between 0.5 and 1.5 to provide smooth solutions over an L × L square domain. For this case, the constants were chosen to give supersonic flow in both the positive x and positive y directions. While not necessary, this choice simplifies the inflow boundary conditions to Dirichlet values at the inflow and Neumann (gradient) values at the outflow. The inflow boundary conditions are determined from the manufactured solution.

7.6.2 SOLUTION VERIFICATION

Sources of numerical error

The three main sources of numerical error in a computational simulation are round-off error, iterative convergence error, and discretization error. The latter error source includes both errors in the interior discretization scheme as well as errors in the discretization of the boundary conditions. These error sources are discussed in detail in the following sub-sections.

Round-off error

Round-off errors occur due to the use of finite arithmetic on digital computers. For example, in a single-precision digital computation, the following result is often obtained

$$3.0 * \left(\frac{1.0}{3.0}\right) = 0.999999 \tag{111}$$

while the true answer is of course 1.0. Round-off error can be important for both ill-conditioned systems of equations as well as time-accurate simulations. The adverse effects of round-off error can be mitigated by using more significant digits in the computation. Standard computers employ 32 bits of memory for each storage location. In a double-precision calculation, two storage locations are allocated for each number, thus providing 64 bits of memory. Higher-precision storage can be accessed through variable declarations, by using appropriate compiler flags, or by employing one

of the recently developed 64-bit computer architectures.

Iterative convergence error

Iterative convergence error arises due to incomplete iterative convergence of a discrete system. Iterative methods are generally required for complex nonlinear systems of equations, but are also the most efficient approach for large, sparse linear systems. The two classes of iterative approaches for linear systems are stationary iterative methods (Jacobi, Gauss–Seidel, line relaxation, multigrid, etc.) and Krylov subspace methods (GMRES, conjugate gradient, Bi-CGSTAB, etc.). Nonlinear systems of equations also employ the above iterative methods, but generally in conjunction with a linearization procedure (e.g., Picard iteration, Newton's method).

Discretization error

The discretization error was defined in Equation (99) as the difference between a numerical solution and the exact solution to the continuum partial differential equations. It arises due to the conversion of the differential equations into an algebraic system of equations (i.e., the discretization process). This process necessarily introduces discretization parameters such as the element size ($\Delta x, \Delta y$ and Δz) and/or the time step(Δt). The discretization error can be clearly related to the truncation error for linear problems; however, for nonlinear problems, this relationship is not straightforward. There are two main reasons for evaluating the discretization error. The first reason is to obtain an assessment of the discretization error associated with a given solution, which might be needed during an analysis of simulation results or for a model validation study. This error assessment can take three distinct forms: an error estimate (e.g., the most likely value for the error is -5%), an error band (e.g., a confidence level of 95% that the error is within ±8%), or an error bound (e.g., the error is guaranteed to be within ±8%). The second reason for evaluating the discretization error is to drive a grid adaptation process. Grid adaptation can involve locally adding more elements (h-adaptation), moving points from a region of the low error to a region of high error (r-adaptation), or locally increasing the formal order of accuracy (p-adaptation).

<u>Discretization error estimation</u>

There are several methods available for estimating discretization error. These methods can be broadly categorized as a priori methods and posteriori methods. The a priori methods are those that allow a limit to be placed on the discretization error before the numerical solution is calculated, i.e., find C and p such that DE $< Ch^p$. Here p is simply the formal order of accuracy and can be determined by the methods discussed earlier. The determination of the constant C is challenging and generally problem-dependent, and can be very large (and thus not useful) for complex problems. The majority of research today is focused on posteriori methods for estimating the discretization error. These methods provide an error estimate only after the numerical solution is computed. The posteriori methods can be further sub-divided into finite-element-based error estimators and extrapolation-based error estimators. Although a brief overview of the former is given in the next sub-section, this paper focuses on the latter approach since it is equally applicable to finite-difference, finite-volume, and finite-element methods.

In general, the level of maturity for all of the posteriori error estimation methods is heavily problem-dependent (Stewart, 2003). As a whole, they tend to work well for elliptic problems, but are not as well-developed for parabolic and hyperbolic problems. The level of complexity of the problem is also an important issue. The error estimators work well for smooth, linear problems with simple physics and geometries; however, strong nonlinearities, discontinuities,

singularities, and physical and geometric complexity can significantly reduce the reliability and applicability of these methods.

Finite-element-based error estimator

Two fundamentally different types of discretization error estimators have been developed from the finite-element method (Stewart, 2003). The most widely-used are recovery methods, which involve post-processing of the solution gradients (Zienkiewicz and Zhu, 1992) or nodal values (Zhang et al., 2002) on patches of neighbouring elements. The former approach is often referred to as the ZZ error estimator, while the latter as polynomial preserving recovery (PPR). The basic formulations provide error estimates only in the global energy norm; extensions to quantities of interest must generally be done heuristically (e.g., a 5% error in the global energy norm may correspond to a 10% error in heat flux for a given class of problems). Although difficult to analyse mathematically, recovery-based error estimators do provide ordered error estimates. That is, the error estimate gets better with mesh refinement. Recovery-based methods can be extended to finite-difference and finite-volume schemes, but this process generally requires additional effort.

The second class of error estimators that have arisen from finite elements are residual-based methods. These methods take the form of either explicit residual method (Eriksson and Johnson, 1987) or implicit residual methods (Babuska and Miller, 1984). These methods were originally formulated to provide error estimates in the global energy norm. Extension of both the explicit and implicit residual methods to provide error estimates in quantities of interest generally requires the solution to the adjoin system (i.e., the dual problem). The explicit method has been extended to finite-volume schemes by Barth and Larson (2002). For more information on residual-based posteriori error estimators for finite-elements (Ainsworth and Oden, 2000; Babuska, 1986).

Extrapolation-based error estimators

The extrapolation-based error estimators come in two different forms. The most popular approach is based on Richardson extrapolation (Richardson, 1910; Richardson, 1927) and requires numerical solutions on two or more meshes with different levels of refinement. The numerical solutions are then used to obtain a higher-order estimate of the exact solution. This estimate of the exact solution can then be used to estimate the error in the numerical solutions. The second type of extrapolation-based error estimator is order extrapolation (p-extrapolation). In this approach, solutions on the same mesh, but with two different formal orders of accuracy, are used to obtain a higher-order accurate solution, which can again be used to estimate the error. The drawback to order-extrapolation is that it requires advanced solution algorithms to obtain higher-order numerical schemes, which can be difficult to code and expensive to run. The main advantage of the extrapolation-based error estimators is that they can be applied as a post-processing step to any type of discretization, whether it be a finite-difference, finite-volume, or finite-element method.

<u>Richardson extrapolation</u>

Richardson extrapolation is based on the series expansion of the discretization error which can be rewritten as

$$\begin{aligned} \mathrm{DE_k} &= f_k - f_{exact} \\ &= g_1 h_k + g_2 h_k^2 + g_3 h_k^3 \\ &\quad + g_4 h_k^4 + HOT \end{aligned} \tag{112}$$

where g_i is the coefficient of the ith order error term and the exact solution f_{exact} is

generally not known. The assumptions that are required for using Richardson extrapolation are that (1) the solutions are smooth, (2) the higher-order terms in the discretization error series expansion are small, and (3) uniform meshes are used. The second assumption regarding the higher-order terms is true in the asymptotic range, where his sufficiently small that the lower-order terms in the expansion dominate. While the last assumption regarding uniform meshes appears to be quite restrictive, transformations (either local or global) can be used if the order of accuracy of the transformation is equal to (or higher than) the order of the numerical scheme. Transformations will be discussed in detail in a later subsection.

Standard Richardson extrapolation

The standard Richardson extrapolation procedure assumes that the numerical scheme is second-order accurate, and that the mesh is refined or coarsened by a factor of two. Consider a second-order discretization scheme which is used to produce numerical solutions on two meshes: a fine mesh ($\mathrm{h}_1 = h$), and a coarse mesh ($\mathrm{h}_2 = 2h$). Since the scheme is second-order accurate, the $\mathrm{g}_1$coefficient is zero, and the discretization error equations on the fine and coarse meshes can be rewritten as

$$\begin{aligned} \mathrm{f}_1 &= f_{exact} + g_2 h^2 + O(h^3) \\ \mathrm{f}_2 &= f_{exact} + g_2 (2h)^2 \\ &\quad + O((2h)^3) \end{aligned} \tag{113}$$

Neglecting higher-order terms, these two equations can be rewritten as

$$\begin{aligned} \mathrm{f}_1 &= f_{exact} + g_2 h^2 \\ \mathrm{f}_2 &= f_{exact} + g_2 (2h)^2 \end{aligned} \tag{114}$$

Solving the first equation for g_2 yields

$$\mathrm{g}_2 = \frac{f_1 - f_{exact}}{h^2} \tag{115}$$

and solving the second equation for $\mathrm{f}_{\mathrm{exact}}$ gives

$$\mathrm{f}_{\mathrm{exact}} = f_2 - g_2 (2h)^2 \tag{116}$$

Substituting Equation (115) into Equation (116) gives

$$\begin{aligned} \mathrm{f}_{\mathrm{exact}} &= f_2 - \left[\frac{f_1 - f_{exact}}{h^2}\right](2h)^2 \\ &= f_2 - 4f_1 + 4f_{exact}\mathrm{f}_{\mathrm{exact}} \\ &= f_2 - g_2 (2h)^2 \end{aligned} \tag{117}$$

Or simply

$$\mathrm{f}_{\mathrm{exact}} = f_1 + \frac{f_1 - f_2}{3} \tag{118}$$

Standard Richardson extrapolation thus provides a ‘‘correction’’ to the fine grid solution. This expression for the estimated exact solution $\mathrm{f}_{\mathrm{exact}}$ is generally third-order accurate. This expression for the estimated exact solution $\mathrm{f}_{\mathrm{exact}}$ is generally third-order accurate. In Richardson’s original work (Richardson, 1910), he used this extrapolation procedure to obtain a higher-order accurate solution for the stresses in a masonry dam based on two second-order accurate numerical solutions. In Richardson’s case, he employed central differences which cancelled out the odd powers in the truncation error. His estimate for the exact solution was thus fourth-order accurate.

Generalized Richardson extrapolation

Richardson extrapolation can be generalized to pth-order accurate schemes with solutions on a fine mesh (spacing h_1) and a coarse mesh (spacing h_2), which are not necessarily different by a factor of two. Introducing the general grid refinement factor

$$\mathrm{r} = \mathrm{h}_2/h_1 \tag{119}$$

and setting $\mathrm{h}_1 = h$, the discretization error equations can be written as

$$\mathrm{f}_1 = f_{exact} + g_p h^p + O(h^{p+1}) \tag{120}$$

$$\mathrm{f}_2 = f_{exact} + g_p (rh)^p + O((rh)^{p+1}) \tag{121}$$

Neglecting the higher-order terms, these two equations can be solved for $\mathrm{f}_{\mathrm{exact}}$ to give

$$\mathrm{f}_{\mathrm{exact}} = f_1 + \frac{f_1 - f_2}{r^p - 1} \tag{122}$$

which is generally a (p+1)th order accurate estimate. Again, it should be emphasized that Richardson extrapolation relies on the assumption that the solutions are asymptotic (i.e., the observed order of accuracy matches the formal order).

Observed order of accuracy

When the exact solution is not known (which is generally the case for solution verification), three numerical solutions on different meshes are required in order to calculate the observed order of accuracy. Consider a pth-order accurate scheme with numerical solutions on a fine mesh (h_1), a medium mesh (h_2), and a coarse mesh (h_3). For the case of a constant grid refinement factor

$$\mathrm{r} = \mathrm{h}_2/h_1 = \mathrm{h}_3/h_2 \tag{123}$$

we can thus write

$$\mathrm{h}_1 = h, h_2 = rh, h_3 = r^2 h \tag{124}$$

The three discretization error equations can be written as

$$\mathrm{f}_1 = f_{exact} + g_p h^p + O(h^{p+1}) \tag{125}$$

$$\mathrm{f}_2 = f_{exact} + g_p (rh)^p + O((rh)^{p+1}) \tag{126}$$

$$\mathrm{f}_3 = f_{exact} + g_p (r^2 h)^p + O((r^2 h)^{p+1}) \mathrm{h}_1 = h, h_2 = rh, h_3 = r^2 h \tag{127}$$

Neglecting the higher-order terms, these three equations can be used to solve for the observed order of accuracy p to give

$$\mathrm{p} = \frac{\ln\left(\frac{f_3 - f_2}{f_2 - f_1}\right)}{\ln(r)} \tag{128}$$

Note that here the observed order of accuracy is calculated and does not need to be assumed (as with Richardson extrapolation).

For the case of non-constant grid refinement factors

$$\mathrm{r}_{12} = \frac{h_2}{h_1}, r_{23} = \frac{h_3}{h_2} \tag{129}$$

where $\mathrm{r}_{12} \neq r_{23}$, the determination of the observed order of accuracy p is more

complicated. For this case, the following transcendental equation (Roache, 1998) must be solved

$$\frac{f_3 - f_2}{r_{23}^p - 1} = \mathrm{r}_{12}^p \left(\frac{f_2 - f_1}{r_{12}^p - 1} \right) \tag{130}$$

This equation can be easily solved using a simple Picard-type iterative procedure.

Richardson extrapolation as an error estimator

In some cases, researchers mistakenly report discretization error estimates by giving the relative difference between two numerical solutions computed on different meshes, i.e.,

$$\text{Diff} = \frac{f_2 - f_1}{f_1} \tag{131}$$

This relative difference can be extremely misleading when used as an error estimate. To see why, let us first develop a discretization error estimator using generalized Richardson extrapolation. The relative discretization error (RDE) is simply the difference between the numerical solution and the exact solution, normalized by the exact solution, which for the fine grid (k = 1) can be written as

$$RDE_1 = \frac{f_1 - f_{exact}}{f_{exact}} \tag{132}$$

Substituting the generalized Richardson extrapolation result from Equation (115) into the numerator gives

$$RDE_1 = \frac{f_1 - f_{exact}}{f_{exact}} \tag{133}$$

$$= \frac{f_1 - \left[f_1 + \frac{f_1 - f_2}{r^p - 1} \right]}{f_{exact}}$$

$$= \frac{f_2 - f_1}{f_{exact}(r^p - 1)}$$

The reason for leaving f_{exact} in the denominator will be apparent shortly. Consider two numerical solutions where some quantity of interest has a relative difference (from Equation (130)) of 5%. For a third-order accurate scheme with r = 2, the error estimate based on Richardson extrapolation (Equation (132)) is 0.71%. However, for a first-order accurate numerical scheme with a grid refinement factor of 1.5, the error estimate based on Richardson extrapolation is 9.1%. Thus, a 5% relative difference in the two solutions can mean very different values for the relative discretization error, depending on the order of accuracy of the scheme and the grid refinement factor. This example illustrates the importance of accounting for the $(r^p - 1)$ factor for obtaining accurate error estimates. This understanding led to the development of Roache's Grid Convergence Index, to be discussed in a later sub-section.

<u>Roache's grid convergence</u>

Roache (1994) proposed the Grid Convergence Index, or GCI, as a method for uniform reporting of grid refinement studies. The GCI combines the often reported relative difference between solutions (Equation (130)) with the $(\mathrm{r}^\mathrm{p} - 1)$ factor from the Richardson extrapolation-based error estimator (Equation (132)). The GCI also provides an error band rather than an error estimate.

Definition of GCI

The GCI for the fine grid numerical solution is defined as

$$\mathrm{GCI} = \frac{F_s}{r^p - 1}\left|\frac{f_2 - f_1}{f_1}\right| \quad (134)$$

where F_s is a factor of safety that is usually set to three (F_s= 3). Comparing the GCI to the extrapolation-based RDE estimator given in Equation (132), we see that the GCI uses a factor of safety F_s, it employs absolute values to provide an error band, and it replaces f_{exact} in the denominator of Equation (132) with f_1. Most importantly, the GCI correctly accounts for the (assumed) order of accuracy p and the grid refinement factor r.

Relation between of GCI and a Richardson extrapolation-based error band

The relative discretization error estimate from Equation (132) can easily be converted to an error band (RDE_band) by taking the absolute value and multiplying by a factor of safety F_s, resulting in

$$RDE_{band} = \frac{F_s}{r^p - 1}\left|\frac{f_2 - f_1}{f_1}\right| \quad (135)$$

Now, the only difference between the Richardson extrapolation-based error band ($\mathrm{RDE_{band}}$) and the GCI is the use of f_{exact} in the denominator rather than f_1. Will this make a significant difference? It was shown by Roy (2001) that the error in the GCI relative to the $\mathrm{RDE_{band}}$ is given by

$$\left|\frac{\mathrm{GCI} - \mathrm{RDE_{band}}}{\mathrm{RDE_{band}}}\right| = \frac{F_s}{r^p - 1}\left(\frac{f_2 - f_1}{f_1}\right) = \frac{GCI}{F_s} \quad (136)$$

The error in the GCI relative to the $\mathrm{RDE_{band}}$ is thus an ordered error, meaning that it is reduced with mesh refinement (i.e., as $h \to 0$).

Factor of safety in the GCI

It is important to include the factor of safety in the GCI and the $\mathrm{RDE_{band}}$. Both of these error bands are based on Richardson extrapolation, and we do not know a priori whether the estimated exact solution is above or below the true exact solution to the continuum partial differential equations. In general, there is an equal chance that the true exact solution is above or below the estimated value. Thus a factor of safety of F_s= 1 centred on the fine grid numerical solutionf1will only provide 50% confidence that the true error (f_{exact}) is within the error band. Increasing the factor of safety should increase the confidence that the true error is within the error band. The value for the factor of safety that would provide a 95% confidence band is currently a subject of debate. When only two numerical solutions are performed, the observed order of accuracy cannot be calculated and must be assumed. For this case, Roache (1998) recommends F_s= 3. When three solutions are per-formed, the observed order of accuracy can be calculated. If the observed order matches the formal order of accuracy, Roache (1995) recommends a smaller factor of safety of F_s= 1.25. However, when the solutions are far outside the asymptotic range, the accuracy of the extrapolation procedure is unpredictable and possibly random. In this case, no choice for the factor of safety is sure to be conservative.

<u>Practical aspects of grid refinement</u>

Grid refinement versus grid coarsening for structured meshes

In theory, it should not make a difference whether we start with the coarse mesh or the fine mesh. However, in practice, grid coarsening on structured meshes is often easier than grid refinement, especially for complex meshes.

Here, complex meshes are defined as those with complex geometries and/or significant grid clustering. For uniform meshes, refinement can be performed by simply averaging neighbouring spatial locations. For stretched meshes, this type of refinement will lead to discontinuities in the ratio of neighbouring element sizes near the original coarse grid nodes. A better strategy for stretched meshes is to use higher-order interpolation to obtain smooth stretching distributions; however, this process can be challenging on highly complex grids. The primary problems that arise during mesh refinement are due to a loss of geometric definition at object surfaces, especially at sharp corners. Furthermore, for structured grid approaches requiring point-to-point match-up at inter-zone boundaries, the refinement strategy must ensure that these points are co-located. Thus for complex, structured meshes, it is often easier to simply start with the fine mesh and successively remove every other point in each of the coordinate directions.

Grid refinement versus grid coarsening for unstructured meshes

For unstructured meshes, it is generally easier to start with the coarse mesh, then refine by sub-dividing the elements. This is due to the difficulties of merging elements in a manner that preserves the element type while enforcing the requirement of a constant grid refinement factor over the entire domain. While refinement for unstructured grid approaches inherits all of the drawbacks of refinement for structured grids dis-cussed in the previous section, there are currently efforts underway to make surface geometry information directly available to mesh refinement routines (Tautges, 2001).

The choice of methods for refining the elements will determine the effective grid refinement factor. In two dimensions, triangular elements can easily be refined by connecting the midpoints of the edges, thereby creating four new triangular elements.

Non-integer grid refinement

It is not necessary to use grid refinement factors of two, a process referred to as grid doubling or grid halving (depending on whether one starts with the fine mesh or the coarse mesh). For simple meshes, grid refinement factors as small as r = 1.1 can be employed (Roache, 1998). Using non-integer grid refinement factors may increase the chance of getting all mesh solutions into the asymptotic grid convergence range. However, non-integer grid refinement factors are difficult to apply to complex meshes, especially those involving significant mesh stretching. For simulations on complex, structured meshes, the grid generation can sometimes make up the majority of the overall analysis time. Thus, relying on the original grid generation procedure for grid refinement can be expensive; furthermore, it is difficult to enforce a constant grid refinement factor over the entire domain. Higher-order interpolation can be used for non-integer grid refinement. Here it is again better to start with the fine mesh and then coarsen (at least for structured meshes); however, the same geometry definition problems discussed earlier still exist. When a grid refinement factor of two is employed, there is only significant effort involved in generating the fine mesh; the coarser meshes are found by simply removing every other point. The drawback is not only that the fine mesh may be unnecessarily expensive, but there is also an increased chance that the coarse mesh will be outside the asymptotic grid convergence range.

Independent coordinate refinement

It is sometimes the case that the discretization errors come primarily from just one of the coordinate directions. In such cases, it can be helpful to perform independent refinement in the coordinate directions to determine which one is the primary contributor to the overall discretization error. For independent refinement in x and y, we can write

$$f_k = f_{exact} + g_x(\Delta x_k)^p + g_y(\Delta y_k)^q + HOT \quad (137)$$

where the error terms for each direction are included. In order to keep the analysis general, the order of accuracy in the x direction is p and the order of accuracy in the y direction is q, where the two may or may not be equal. Note that for some numerical schemes, a cross term (e.g., $g_{xy}(\Delta x)^s(\Delta y)^t$)) may also bepresent. As in Richardson extrapolation, assume that p and q are equal to the formal order of accuracy. Consider the case of two solutions ($k = 1$ and $k = 2$) with refinement only in the x direction by a factor of r_x. As the Δx element size is refined, the term $g_y(\Delta y_k)^q$ will be constant. We are now unable to solve for the exact solution fexact, but instead must solve for the quantity

$$f_{exact,x} = f_{exact} + g_y(\Delta y_k)^q \quad (138)$$

which includes the error term due to the Δy discretization. Neglecting higher-order terms, the following two equations

$$f_1 = f_{exact,x} + g_x(\Delta x)^p \quad (139)$$

$$f_2 = f_{exact,x} + g_x(r_x \Delta x)^p \quad (140)$$

can be solved for $f_{exact,x}$

$$f_{exact,x} = f_1 + \frac{f_1 - f_2}{r_x^p - 1} \quad (141)$$

and the leading x-direction error term

$$g_x(\Delta_x)^p = \frac{f_2 - f_1}{r_x^p - 1} \quad (142)$$

Similarly, introducing a third solution ($k = 3$) with coarsening only in the y direction allows us to solve for the y-direction error term

$$g_y(\Delta y)^q = \frac{f_3 - f_1}{r_y^q - 1} \quad (143)$$

The size of the two error terms from Equations (141) and (142) can then be compared to determine the appropriate direction for further mesh refinement.

7.7 COMPARISON OF ASME AND ISO PROCEDURES

In Oberkampf and Roy (2010), the definitions accepted by AIAA (1998) and ASME (2006) for verification and validation as applied to scientific computing address the mathematical accuracy of a numerical solution (verification) and the physical accuracy of a given model (validation); however, the definitions used by the software engineering community (e.g., ISO, 1991; IEEE, 1991) are different. In software engineering, verification is defined as ensuring that software conforms to its specifications (i.e., requirements), and validation is defined as ensuring that software actually meets the customer's needs. Some argue that these definitions are really the same; however, upon closer examination, they are in fact different.

The key differences in these definitions for verification and validation are since, in scientific computing, we begin with a governing partial differential or integral equation, which we will refer to as our mathematical model. For problems that we are interested in solving, there is generally no known exact solution to this model. It is for this reason that we must develop

numerical approximations to the model (i.e., the numerical algorithm) and then implement that numerical algorithm within scientific computing software. Thus the two striking differences between how the scientific computing community and the software engineering community define verification and validation are as follows. First, in scientific computing, validation requires a comparison to experimental data. The software engineering community defines validation of the software as meeting the customer's needs, which is, in our opinion, too vague to tie it back to experimental observations. Second, in scientific computing, there is generally no true system-level software test (i.e., a test for correct code output given some code inputs) for real problems of interest. The "correct" output from the scientific software depends on the number of significant figures used in the computation, the computational mesh resolution and quality, the time step (for unsteady problems), and the level of iterative convergence.

7.7.1 ASME PROCEDURE

ASME procedure (2009) follows a five-step procedure proposed by Knupp & Salari (2002).

Step 1: Define a representative cell, mesh, or grid size, h. For example, for three-dimensional, structured, geometrically similar grids (not necessarily Cartesian),

$$h = [(\Delta x_{max})(\Delta y_{max})(\Delta z_{max})]^{1/3} \quad (144)$$

For unstructured grids one can define

$$h = \left[\left(\sum_{i=1}^{N} \Delta V_i\right)\Big/N\right]^{1/3} \quad (145)$$

where N=total number of cells used for the computations and ΔV_i=volume of the ith cell.

Step 2: It is desirable that the grid refinement factor, $r = h_{coarse}/h_{fine}$, should be greater than 1.3 for most practical problems. This value of 1.3 is again based on experience and not on some formal derivation. This value of 1.3 is again based on experience and not on some formal derivation. The grid refinement should, however, be made systematically; that is, the refinement itself should be structured even if the grid is unstructured.

Step 3: Let $h_1 < h_2 < h_3$ and $r_{21} = h_2/h_1$, $r_{32} = h_3/h_2$ and calculate the apparent (or observed) order, p, of the method from reference

$$p = [1/\ln(r_{21})][1/\ln|\varepsilon_{32}/\varepsilon_{21}| + q(p)] \quad (146)$$

$$q(p) = \ln\left(\frac{r_{21}^p - s}{r_{32}^p - s}\right) \quad (147)$$

$$s = 1 \cdot \sin(\varepsilon_{32}/\varepsilon_{21}) \quad (148)$$

where $\varepsilon_{32} = \varphi_3 - \varphi_2$, $\varepsilon_{21} = \varphi_2 - \varphi_1$, and φ_k denotes the simulation value of the variable on the kth grid. Note that $q(p) = 0$ for r = constant. This set of three equations can be solved using fixed point iteration with the initial guess equal to the first term (i.e., q = 0).

Step 4: Calculate the extrapolated values from the equation

$$\varphi_{ext}^{21} = \left(r_{21}^p \varphi_1 - \varphi_2\right)/\left(r_{21}^p - 1\right) \quad (149)$$

Step 5: Calculate and report the following error estimates along with the observed order of the method p. Approximate relative error may

be cast as a dimensionless form or in a dimensioned form, respectively as follows:

$$e_a^{21} = \left|\frac{\varphi_1 - \varphi_2}{\varphi_1}\right| \quad (150)$$

$$e_a^{21} = |\varphi_1 - \varphi_2| \quad (151)$$

The error was estimated from the equation

$$U_i = \frac{Fs \cdot e_a^{21}}{r_{21}^p - 1} = F_s\left|\delta_{RE,1}^*\right| \quad (152)$$

For the Factor of Safety, Fs, Roache (1998) recommended a less conservative value for F_s = 1.25, but only when using at least three grid solutions and the observed p.

7.7.2 ISO PROCEDURE

ISO 16730 (2008) provides a framework for assessment, verification, and validation of all types of calculation methods. It does not address specific models, but is intended to apply to both analytical models and complex numerical models that are addressed as calculation methods in the context of these international standards. It is not a step-by-step procedure, but does describe techniques for detecting errors and finding limitations in a calculation method. the standards include the following:

-A process to ensure that the equations and calculation methods are implemented correctly (verification) and that the calculation method being considered in solving the appropriate problem (validation);

-Requirements for documentation to demonstrate the adequacy of the scientific and technical basis of a calculation method;

-Requirements for data against which a calculation method's predicted results shall be checked

The example in ISO/TR 16730-3 (2013) describes the application of procedures given in ISO 16730-1 for a computational fluid dynamics (CFD) model (ISIS). The main objective of the specific model treated in ISO/TR 16730-3:2013 is the simulation of a fire in an open environment or confined compartments with a natural or forced ventilation system.

8. SUGGESTED PROCEDURES TO ENSURE THE QUALITY OF CFD/EFD COMBINED PREDICTIONS

This section describes work that was carried out mainly by a joint working group with members from the Resistance and Propulsion Committee and the Specialist Committee on CFD and EFD Combined Methods.

8.1 General considerations

ITTC's recommended procedures for model tests are sometimes referenced in legal texts such as the EEDI regulations and in commercial contexts such as building contracts. Similar references for CFD computations have up to now not been requested. The introduction of CFD/EFD combined methods in, for example power predictions, will call for adequate procedures in order to ensure that accurate results are delivered.

A number of possible measures to take to ensure accurate results were discussed in the Joint Working Group:

1. Formulate detailed Recommended Procedures on how to perform the CFD simulations

2. Introduce a certification of CFD codes or certification of organisations conducting CFD simulations
3. Require that code vendors provide locked settings for certain type of computations.
4. Require that each organisation carries out quality control of their own CFD process

Option 1-3 were rejected with the following motivations:

A detailed prescribed procedure how to perform CFD simulations is not feasible. A definition of a "correct" procedure depends on the code, the type of grid, the type of case and so on. It would be a tremendous work to formulate recommended procedures that cover even the most common codes and cases. Moreover, since the technology is developing rapidly, such recommended procedures would soon be outdated. Some general *guidelines* could be given based on the outcome of international benchmark studies. However, these alone cannot ensure that the results are accurate.

Certification of CFD-codes would not be a sufficient requirement, as the uncertainty mainly stems from the users, not the codes. The available codes must be assumed to be verified by the vendors. Certification of the users would require an independent authority and we cannot see who that would be. Certification is not in line with ITTC praxis for model test. However, the committees can formulate a set of Competency Guidelines to assist customers of CFD-work when selecting the provider. See Section 8.4.

To require the CFD code vendors to provide locked standard settings for certain tasks would again require an independent authority that formulate test criterion. Very few commercial code vendors would probably spend effort on producing such settings.

The only option that the Joint Working Group deemed feasible for ITTC is to prescribe how each organisation should carry out quality control of their own CFD process, and how to demonstrate it. Currently there is no ITTC Guideline or Recommended Procedures describing this and therefore the Joint Working Groups decided to cover this gap. The following section describes the consideration behind the new suggested procedure.

8.2 A new procedure for Quality Assurance in Ship CFD Solutions

The existing ITTC Recommended Procedures 7.5-03-01-01 "Uncertainty Analysis in CFD Verification and Validation Methodology and Procedures" describes the CFD verification and validation process thoroughly. Such a process is useful for code developers and researchers when demonstrating the uncertainty of a solution or a methodology. It is however not very useful for the daily work such as performance evaluation in the design process. The *verification* process requires that computations are carried out for multiple refined grids. This is often regarded as not feasible for commercial reasons and it is often assumed not necessary for routine work, when it has been done once for a similar case. The *validation* process assumes that benchmark data is available, which is normally not the case during consultant or design work. For these reasons, it is unclear how the existing procedure should be applied in the daily work for clients. Instead, the Joint Working Group decided to formulate a new procedure that is useful for consultant or design work for clients especially when organizations regularly carry out CFD predictions of cases that are similar to each other. The procedure could be used by organizations that wish to demonstrate their ability to carry out CFD. It could also be used as purchase condition by clients who order CFD work. Finally, such procedure can be referenced within the ITTC framework.

The principle for the suggested process is that each organisation:

1. develops their own Best Practice Guideline (BPG)
2. assesses that it gives acceptable uncertainties
3. follows the BPG in consultancy services to clients

8.2.1 Best Practice Guideline

The BPG is a detailed description of how to set-up, run and interpret a CFD simulation for a specific type of prediction and for a required uncertainty. The new procedure lists the minimum content of a BPG.

The BPG should give differentiated instructions depending on the type of case and required uncertainty. As an example, BPG for wave resistance computations cannot be used for form factor computations, planing hulls must be treated differently from displacement hull etc. In the new procedure we define the term "case type" as:

- Type of prediction; resistance, propulsion power, nominal wake, detailed flow, performance in waves etc.
- Ship type and condition; determining factors are e.g. relative size of resistance components (related to *CB*, *Fr*, *Re*), propulsion type, unusual hull forms and hull features

The definition of a "case type" at each organisation is in their responsibility and should follow the findings of state of the art experimental and computational maritime fluid dynamics. To define a case type, an organisation can follow the above mentioned criteria but is not limited to them.

8.2.2 Quality assessment

The organization should assure that the BPG is formulated such that it gives the requested uncertainty level *for the specified case type* by the following steps.

<u>Numerical and modelling uncertainty</u>

Verification and validation against measured data can be carried out for a few typical cases of the actual case type according to ITTC 7.5-03-01-01. This gives important knowledge to the organization which grid and solver settings have to be used for a defined case type with respect to a desired uncertainty level.

<u>Total uncertainty</u>

The Verification and Validation process, according to the existing ITTC Recommended Procedure Uncertainty Analysis in CFD, Verification and Validation Methodology and *Procedures* 7.5-03-01-01, is strictly speaking only valid for the investigated case, to which we already have a measured result. Can this be valid for the other cases in our daily work? The Recommended Procedure 7.5-03-01-01 leaves the question open: "*Whether to and how to associate an uncertainty level at a validated condition with a prediction at a neighbouring condition is very much unresolved and is justifiably the subject of much debate at this time*".

The solution that was selected for the new procedure is a so called "big sample approach", as for example demonstrated in Zhao et al 2017. This gives an indication of the "uncertainty of applying at a neighbouring condition". It can also be seen as a way to capture the random part of the uncertainty due to difference in the CFD set-up. In the model test world, the repeated test with a standard model, which is common practice in ITTC community, is used to capture the random part of the uncertainty. The new procedure hence requires that the BPG is

assessed using a large number of samples of similar type and preferably by different users in the organization.

The result should be presented in the form of statistics of the comparison error, E, given by the difference between the measured data, D, and simulation, S:

$$E = D - S \tag{153}$$

Note that E contains uncertainty of the simulation as well as the measured data.

The comparison error should be based on the same variable and same condition, including scale, as the CFD-simulation aims to predict, i.e. for full scale CFD-predictions, full scale measurements are needed.

The data for comparison can be provided by the same organisation that performs the CFD simulations. Due to the larger number of samples, the precision of each measurement may be less than for benchmark cases. For full scale measurements the precision is often very low. This needs to be considered in the comparison.

The number of cases that are required depends on the scatter of the result and the required accuracy. In practice, it is likely to be limited to the number of available measured data points. The more cases that an organization can include, the higher the confidence they can claim to have in their predictions.

8.2.3 Demonstration

The new ITTC Recommended Guidelines 7.5-03-01-02 Uncertainty Analysis in CFD, Guidelines for RANS Codes also provides guidelines for implementation of Quality Management procedure 7.5-03-01-01. This includes presenting the comparison error in a statistical way, for example as in Figure 15. If the number of data points permits, the probability for an error within the required level can be given.

The case type, for what that comparison is valid for, needs to be included in the quality assessment demonstration, as well as the number of cases that is used for the statistics.

8.3 Suggested new Recommended Procedure

Based on the work and considerations described above, a new Recommended Procedure was suggested, which is expected to replace the existing recommended guideline Uncertainty Analysis in CFD, Guidelines for RANS Codes 7.5-03-01-02:

7.5-03-01-02 “Quality Assurance in Ship CFD Applications”

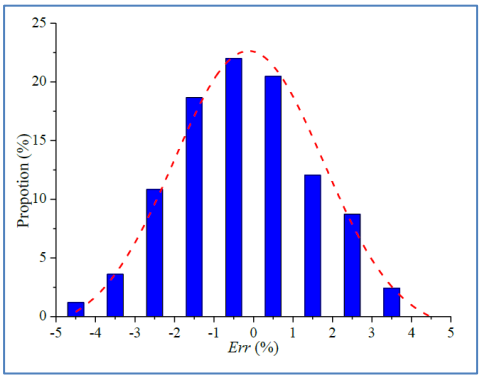

Figure 15. Example of quality assessment demonstration. Distribution of comparison error (Zhao et al 2017)

8.4 Advice to customers of CFD services

The following advice is directed to parties who are in the process of contracting for CFD consultancy services.

It is advisable to choose a CFD-service provider that:

1. follows either the existing ITTC Recommended Guidelines 7.5-03-01-02

"Uncertainty Analysis in CFD, Guidelines for RANS Codes" or when approved the new ITTC Recommended Guideline 7.5-03-01-02 "Quality Assurance in Ship CFD Applications"
2. uses a CFD-code that is considered to be established and state-of-the-art for hydrodynamics; with documented verification and validation, preferable demonstrated by participation in international benchmark studies
3. has a validation and correlation strategy against measured data, (including feedback from full scale data if full scale predictions are delivered)
4. has demonstrated expertise in maritime hydrodynamics

8.5 Conclusions

The introduction of CFD/EFD combined methods in, for example power predictions, will call for adequate procedures in order to ensure that accurate results are delivered.

A procedure that is useful for the daily work such as performance evaluation in the design process is needed.

To write a detailed description how to carry out CFD simulations is not a feasible option.

The committee has together with the Resistance and Propulsion Committee suggested a new Recommended Guideline "Quality Assurance in Ship CFD Applications". The principle is that each organization derive their own Best Practice Guidelines and demonstrate their ability using multiple comparisons with measured values.

It is recommended that the full conference to adopt the new guideline.

8.6 Recommendations for further work

It is recommended that statistical techniques be used to assess the quality and accuracy of CFD analysis. Does the errors in general fit to the normal distribution as in Figure 15? How many cases are required? In case that no known distributions can be fit to the data, what is the alternative way? Can the mean error be an alternative way to assess?

ITTC can assist by providing a commonly agreed list of what different simulation "cases types" are and what the main parameters for BPG definition could be. An evaluation of CFD work as well as CFD benchmark workshops is required.

9. LIAISON WITH THE ITTC TC OF RELATED TECHNICAL AREAS

The committee collaborated with the Resistance and Propulsion Committee in two matters:

1. The proposed application of combined methods for form factor, which resulted in modifications to several procedures. (See Section 5)
2. Methods for CFD quality assurance, which was discussed in a joint working group between the two committees and resulted in a new proposed guideline for Quality Assurance and Ship CFD (see Section 8)

To complete TOR 5, all committee members were in contact with representatives from most of the other Technical Committees (see Section 6).

One of the committee members attended the meeting of the Specialist Committee on Ships in Operation at Sea in September 2018. Discussions and suggestions were made on the benchmark study for the evaluation of CFD

applicability to determine the wind resistance.

As a Specialist committee, we have also reviewed the ITTC Manoeuvring Committee's revisions to the following guidelines and procedures:

- The Recommended Guideline 7.5-03-04-01 "Guideline on Use of RANS Tools for Manoeuvring Prediction"
- The Recommended Procedure 7.5-02-06-03 "Validation of Manoeuvring Simulation Models"
- The Recommended Guideline 7.5-03-04-02 "Validation and Verification of RANS Solutions in the Prediction of Manoeuvring Capabilities"

10. LIAISON WITH OTHER GROUPS OUTSIDE ITTC

10.1 CFD WORKSHOP COMMITTEE

Since the first CFD Workshops in ship hydrodynamics held in 1980 at Gothenburg, Sweden (Larsson, 1981), the subsequent Workshops have been organized at approximately five year intervals at Gothenburg and Tokyo, Japan, alternately. The common objective of these Workshops was the assessment of up-to-date numerical methods for ship hydrodynamics to aid code development, establish best practices and guide industry. Currently the CFD Workshops are being organized by the Steering Committee which consists of the hosts of the previous and next workshops and the area representatives in America, Europe and Asia. The committee summarised the evaluations of the last CFD Workshop, "Tokyo 2015" (Hino, 2015), and published the book (Hino, 2020). Also, the committee is working of the planning of the next Workshop, "Wageningen 202X" which was initially planned to be held in 2021 at Wageningen, Netherland hosted by MARIN but postponed to the later year due to the delay of SIMMAN Workshop and the circumstances related to COVID-19.

The present Specialist Committee on CFD and EFD Combined Methods was in contact with the Steering Committee of CFD Workshop through the common committee member.

Test cases for the "Wageningen 2021" Workshop are being discussed in the Steering Committee and Japan Bulk Carrier (JBC), KRISO Container Ship (KCS), ONR Tumblehome (ONRT) and a full-scale ship (not decided yet) have been selected as ship hulls. During the process, several suggestions were made from the Specialist Committee. In particular, the Specialist Committee proposed a blind test for which two members of Specialist Committee offered to provide tank test data. Unfortunately, the detailed local flow data demanded by the CFD workshop could not be offered and this suggestion was abandoned.

The information exchange on the benchmark data for full-scale ships between two committees was extremely useful. The communication between ITTC and the CFD Workshop Committee should continue in the future.

11. TOR 10

"Act as a research coordinator for other researchers who wish to contribute: Suggest research topics that lead towards the given committee goals, assembly and review of ongoing work."

11.1 LIST OF POTENTIAL RESEARCH TOPICS

The CFD/EFD committee has been working as a research coordinator among the committee members, their respective institutions, and the greater international ship hydrodynamics

community. The committee has initiated a form-factor study in which it is investigating the possibility of calculating the form factor for a ship hull using double-body CFD that can be used in tandem with EFD measurements at model scale of ship resistance and powering. The numerically-determined form factor may be superior to the current practice of an experimentally-determined form factor.

In addition to the form-factor study, the committee has compiled a list of research areas that utilize combined CFD/EFD.

- Experimental program for smooth body separation at full scale Reynolds numbers.
- Full scale field measurements of boundary layer and viscous wake.
- Use database of model scale EFD/CFD, full scale CFD, and sea trials to develop more accurate correlation allowance for extrapolation. The world-wide community collectively has an extensive database that could be studied to derive a better correlation allowance.
- Ability of CFD to predict wind resistance corrections for full scale speed trial corrections. A benchmark-study is ongoing and we encourage researchers and students to participate.
- Shallow water correction based on CFD simulations.
- Scale effects and ability of different CFD methods to predict effect of ESD and local inflow to propeller.
- Skin friction reduction methods with CFD.
- Ability of CFD to predict added resistance in waves and calm water.
- Importance of scale effects on wake and rudder force for seakeeping and manoeuvring tests.
- Using CFD to plan model test campaign for example selecting most important cases in a seakeeping program.
- Numerical models for ice loads.
- Scale effects and the ability of CFD methods to predict local propeller induced noise.
- Use EFD to tune CFD methods for roll damping, investigate scale effects for roll damping fins.
- Scale effects on appendage drag for calm water speed power predictions.
- Investigate scale effects on manoeuvring performance, e.g., propeller hull interactions. Design model scale propeller that creates correct propeller loads at model scale?
- Modelling of environmental conditions. Could CFD help understand physics involved in interactions when generating model scale waves, wind and current?
- Free surface effects on the boundary layer at full scale.

12. CONCLUSIONS AND RECOMMENDATIONS

SUMMARY

In the maritime hydrodynamic field, EFD and CFD have up to now been seen as two separate, almost competing tools. This is reflected in ITTC's procedures, which clearly separate CFD and model tests. Within ITTC, most organisations have the knowledge and resources to apply both EFD and CFD. This could be used to our advantage to a higher extent. Therefore, the "Specialist Committee on CFD and EFD Combined Methods" was formed in 2017 with the purpose to "initiate and support the process of introducing combined EFD/CFD methods in ITTC's procedures".

During these first three years, the Committee has supported the introduction of combined CFD/EFD methods in ITTC's procedures by performing a study on CFD based form factors to back up a proposed modification of the power prediction procedure. Furthermore, other possible improvements of the procedures using combined methods have been suggested and

good examples of combined methods in the literature have been highlighted. The potential hesitation towards CFD methods in terms of uncertainty and trustworthiness have been addressed by proposing a new procedure for CFD Quality assurance.

It is concluded that the Committee has served its purpose and completed its tasks.

The Committee recommends that for the next ITTC period each committee should be requested to consider applications of combined methods in their respective fields. Each committee should also monitor and report on the uncertainty of CFD versus EFD for their relevant applications. This could be stressed by modifying The General Terms, as well as be included in each committee TOR.

Even if each committee will work with CFD and CFD/EFD combined methods in their respective fields, it would be useful to have one committee responsible for general issues of CFD and CFD/EFD and oversee that the idea of combinations is continuously developed and promoted. The Committee therefore recommends that in the next period one committee is appointed to be responsible for the CFD/EFD combined methods including CFD issues on an overview level. This includes the procedures for uncertainty assessment and quality assurance of CFD, review and highlight good examples of combined methods, suggest and initiate new applications of combined methods.

It is a common misconception in the maritime industry that the ITTC community favour experimental methods against computational. The truth is that ITTC members perform *hydrodynamic* predictions to the maritime industry with the most suitable tool available - numerical or experimental. Having access to both EFD, CFD and full scale trials, we are in the best position to distinguish and be aware of the accuracy and capability of the different methods. ITTC could be more active in communicating this to all stakeholders. It could therefore be the task of the appointed committee to spread information in an understandable way to the maritime world outside ITTC on uncertainty of CFD versus EFD and combined methods, for example by compiling such information from the other committees.

12.1 REVIEW OF RECENT STUDIES ON CLAIMED ISSUES OF MODEL TEST PREDICTION METHODS, FOR EXAMPLE SCALE EFFECTS

Model tests are still an accurate reliable way of prediction the speed power for ships. Nevertheless the computational methods can truly assist to improve the applied methods during the general scaling process by assisting and improving an individual scaling problem.

To identify which of the scaling problems would be the most suitable to be used for applying a CFD method for their improvement, the problems were listed and ranked them on different aspects. Different individual scaling problems for the calm water speed power prediction have been identified and their general uncertainty has been assessed to the level of impact on the prediction of correct trends in design as well as on the absolute powering level. The scaling problems have been rated on their frequency of occurrence in the typical business of towing tank facilities. The CFD method, which could be used in a certain scaling problem, has been assessed if it is easy to be used and state of the art for industrial CFD application. The possible improvement of the accuracy of a certain scaling problem by using CFD methods was judged as well.

All these aspects have been collected in a matrix-like overview. The determination of the form factor was addressed to be the most valuable one for further investigation to be used in combination with CFD methods.

It has to be noted here, that scaling effects and their possible assistance by CFD methods have been investigated separately here and not the combination of different scaling processes. It is known that scale effects have impact on the ranking: some scale effects are over predicting and some are under predicting. Effects are mixed and can interact in the end of a complete speed power prediction process and CFD methods could help to become aware of these effects. Picking out one scale effect and make it more robust by insights from CFD methods can result in that the final speed power prediction is not even more correct, because all scaling effects are mixed and working together hand in hand. The use of a correlation allowance finally corrects it. You have to be very careful by changing single scaling methods without checking the overall accordance with a modified correlation allowance value. Methods for checking and adapting the correlation allowance have to be available when changing individual parts of the scaling process.

The committee identified further scaling processes to be addressed in future for the consideration if CFD methods to be used in assistance for a more precise speed power prediction. The most important problems are: propeller-open-water scaling, effective wake scaling, scaling problems of immersed transoms and scaling of energy saving devices. Besides the scaling problems in the calm water speed power prediction, scaling problems in fields of manoeuvring, sea keeping and cavitation are also worth to look into them more in detail.

12.2 REVIEW OF BENCHMARK STUDIES, ACCURACY, ACHIEVEMENTS AND CHALLENGES OF FULL-SCALE SHIP CFD

- Work in the field of full-scale ship performance prediction is accelerating, based on the number of recent studies.
- Confidence in full-scale CFD simulations must be increased by demonstrating good predictive accuracy for large number of cases and over a range of conditions, consistently.
- At present, the scatter of predictions submitted to the Lloyd's Register workshop in 2016 suggests that the accuracy in power predictions with full scale CFD is still much lower than extrapolated towing tank tests. This cannot be expected to be improved simply by adding more computational power. Further work is needed to improve the computational models in full-scale simulations.
- The main challenges in full-scale CFD are identified as follows.
  - The accuracy and the resolution of the flow within a viscous and turbulent boundary layer.
  - Turbulence modelling.
  - Prohibitively large number of cells.
  - Modelling of flow separation.
- The largest barrier to improving the accuracy of full-scale CFD predictions is the lack of sea trials' data available in open literature.

The Committee recommends ITTC to continue monitoring the advances within full-scale CFD of maritime applications. Furthermore, to initiate or promote measurement campaigns of high Reynolds number flow cases.

12.3 REVIEW OF EFD/CFD COMBINATIONS FOR RELEVANT APPLICATIONS

The term CFD/EFD Combined Method could mean many different things. The Committee has categorised possible applications into the following areas:

1) Using CFD to derive new "empirical" relations to be used in an EFD scaling

process, or verify existing ones. Examples found in literature are shallow water corrections, propeller open water scaling, and roughness allowances.

2) Using CFD to derive one component in a model test scaling procedure for the actual ship. An example is CFD-based form factor within the power prediction procedure. Another example is wind resistance in speed trial evaluation.
3) Using CFD to design model test set-ups in order to conduct more efficient or accurate model tests. Not much is described in the literature. However, this has potential to be beneficial to ITTC members. Therefore, more attempts to collect good examples on this should be made and shared, in order to inspire other members. Examples could be:
   a) Turbulence stimulation location
   b) Plan calm water test by selecting most appropriate speed.
   c) Plan seakeeping test programs (decide wave lengths, position in tank, timing of test, etc).
   d) Pre-EFD prediction in order to give the test manager a warning if some measurement goes wrong.
   e) Blockage correction.
   f) Design of cavitation hull that correctly generates the scaled full-scale-wake
4) Tuning and validating CFD in model-scale for a specific case and use that to increase the confidence in the full scale modelling of the same case. This provides greater insight into scale effects and higher confidence in the full-scale predictions. A number of authors discuss various scale effects in the literature, especially of energy saving devices. Regarding possible tuning of CFD using EFD, one example is transition models applied to propeller blades, where the inflow turbulence level is tuned using EFD in order to get the correct transition point. There are also commercial providers of energy saving devices who claim greater confidence in the full-scale CFD prediction based on model test comparison. However, the question whether a CFD set-up that is validated at model-scale is also tuned for full-scale is not frequently discussed. This is an important knowledge gap. More full-scale validation cases are needed, not only speed trials but also details of the flow.
5) Using EFD to improve CFD models in general. Turbulence models and roughness models are examples of this.

It is concluded that a great deal of combined methods are already in use in the community for some years. The exact term “CFD/EFD Combined Methods” has appeared in at least two publications after the formation of our committee, but not connected to any of its committee members. Hence we believe that the committee has already had an effect to establish combined methods as a named concept and that in itself can stimulate its usage.

The Committee recommends that ITTC continues to monitor and suggest examples of CFD/EFD Combined Methods in order to inspire the community. It is suggested to continue using the categories given above when describing applications.

12.4 SUGGEST IMPROVEMENT OF CURRENT RECOMMENDED PROCEDURES BY USING CFD IN COMBINATION WITH MODEL TEST

The committee carried out a joint study with members form the Resistance and Propulsion committee on CFD form factors. The group was expanded with other external participants and included in total 9 organisations with 8 different CFD codes. The work is currently being documented in a journal paper, to be submitted in February 2020.

The following was concluded:

- Since the study contains only a limited number of test cases and only one

organisation compared with a large number of sea trials, it can neither be affirmed nor rejected that that CFD-based form factors should replace the Prohaska method.

- It should be suggested that CFD-based form factors can be used to support the conventional Prohaska method.
- ITTC should encourage the use of CFD-based form factors to support the conventional method, as it seems likely that it improves the accuracy of the predictions on average.
- When more institutes gain experience with CFD-based form factors, the recommendations should be re-evaluated.
- The 1957 ship model correlation line caused the form factor to be Reynolds number dependent, which it should not be in principle. The main reason for this seems to be the too steep gradient towards lower Reynolds numbers. In practise this has minor influence on the power predictions thanks to the correlation factors, which are calibrated for each tank's individual data set. However, when using models of different size (Reynolds number) than the data set, especially for small towing tanks, this may be larger problem. The use of alternative lines should be investigated.
- To start with, C_F should be recommended to be derived from the ITTC-1957 model-ship correlation line, in spite of its drawbacks. In this way, each organisations' correlation factors (CA or CP) can be kept unchanged. The use of alternative friction lines for C_F should be investigated further.
- Ensure the quality of CFD prediction of form factor by referring to the new "Quality Assurance in Ship CFD Application", 7.5-03-01-02

Based on this study, as well as other publications, the committee proposed modifications to the Recommended Procedures:

- ITTC 7.5-03-02-04 "Practical Guidelines for Ship Resistance CFD", Section 3.1
- ITTC 7.5-02-03-01.4 "1978 ITTC Performance Prediction Method" , Section 2.4.1

The proposals were implemented by the Resistance and Propulsion Committee.

The Committee recommends that ITTC adopt the modifications.

12.5 SUGGESTION TO WHAT PARTS OF THE ITTC PROCEDURES THAT COULD BENEFIT FROM COMBINED METHODS IN FUTURE WORK

Based on discussions with members from the other committees some ideas for application of combined methods have been put forward. It is concluded that there is potential of promoting combined methods in most fields within ITTC. However, the experts in each committee are better suited to come up with the ideas, initiate and investigate them further. The Committee recommends ITTC to request each committee to consider CFD/EFD Combined Methods within their respective field.

- Ice
  - Numerical model for ice loads including accurate ice models
  - Ice paths under the hull
- Noise
  - Greater understanding of local noise sources from CFD
  - Scale effects on propeller flow fields
- Stability in Waves
  - Currently writing procedures on prediction of ship roll damping using CFD
  - Tune models based on experimental data.
- Operation of ships at sea
  - Wind resistance corrections:

  - New air resistance benchmark test cases available
  - Shallow water correction based on CFD simulations.
  - Added resistance in waves is challenging to do at this time.
- ESD
  - Local flow features at full scale
  - Scale effects on flow into the propeller
  - Skin friction reduction methods in CFD
  - Independent provider/assessor of full scale CFD
- Manoeuvring, Ocean Engineering
  - Investigate scale effects
  - Efficient planning of test
  - Propeller hull interactions, design model scale propeller that creates correct propeller loads at model scale
- Sea keeping
  - Scale effects on wake and rudder force
  - Calculation of Cw using CFD
  - Use CFD to plan model test campaign (select most important cases)
  - Use EFD to tune CFD for roll damping
    - Scale effects for roll damping fins
- R&P:
  - Scale effects on appendage drag
  - Effective wake scaling
  - POW scaling
  - Numerical Friction line
  - Transom resistance scaling
  - Wave resistance scaling
  - Roughness effect
  - Pre-test prediction and planning of test
- Manoeuvring in Waves
  - Scale effects
  - Plan tests
- Marine Renewable Energy Devices
  - Scale effects, plan tests
- Modelling of Environmental Conditions
  - Produce guidelines for generating model scale waves, wind and current
  - Use CFD to help understand physics involved in interactions

12.6 REVIEW OF PAST WORK AND PROCEDURES, WITHIN AND OUTSIDE ITTC, ON CFD UNCERTAINTY, VALIDATION & VERIFICATION (V&V), APPLIED TO THE MARINE AND OTHER BUSINESS SECTORS

The credibility of CFD simulations requires the estimation of numerical uncertainties to avoid the risk of making erroneous conclusions. To assess the reliability and accuracy of the CFD results, there are various procedures used for verification and validation.

- CFD results can be verified by performing grid and time-step convergence studies to assess numerical uncertainty.
- CFD results can be validated by comparing them with theoretical solutions and experimental data.
- The validation and verification (V&V) standard proposed by American Society of Mechanical Engineers (ASME) or the ITTC Recommended Procedure 7.5-03-01-01 can be used to quantify numerical uncertainties and to validate CFD results for a single solution when a corresponding experimental value exists.
- How to transfer the uncertainty level to a prediction at a neighbouring condition is unresolved.
- The established procedures for verification and validation are applied in some but not all scientific publications.
- A guidance of how to deal with uncertainty assessments of CFD in routine work, such as predictions to clients, is lacking. This means that clients cannot request quality assurance in the same way as for model test. The main question marks are
  - How to deal with validation when experimental data does not exist, i.e. how to transfer the uncertainty level to a neighbouring condition.

- Whether a grid convergence study needs to be performed for every case in routine work, or can the uncertainty level be assumed from a similar case.

12.7 SUGGEST PROCEDURES TO ENSURE THE QUALITY OF CFD/EFD COMBINED PREDICTIONS

The introduction of CFD/EFD combined methods in for example power predictions will call for adequate procedures in order to ensure that accurate results are delivered. The review in TOR 6 concludes that a procedure useful for the daily work, such as performance evaluation in the design process, is lacking. The committee has together with the Resistance and Propulsion Committee carried out a joint study with the purpose of proposing ways to deal with this.

To write a detailed description how to carry out CFD simulations is not a feasible option. It is proposed that each organisation derive their own Best Practice Guidelines and demonstrate their ability using multiple comparisons with measured values. This is described in a new proposed Recommended Procedure:

7.5-03-01-02 "Quality Assurance in CFD Ship Applications"

The Committee recommends to the Full conference:

- To adopt the new procedure.
- To monitor the use of the new procedure and update the Recommended Procedure if needed, especially the proposed way of presenting the comparison error.
- To continue maintaining and improving the existing Recommended Procedure 7.5-03-01-01, "Uncertainty Analysis in CFD", which describes several options. The Full conference should consider narrowing this down, as it has to follow the development of new CFD techniques.

12.8 LIAISON WITH THE ITTC TC OF RELATED TECHNICAL AREAS

The committee carried out joint work with the Resistance and Propulsion committee with excellent cooperation.

12.9 LIAISON WITH OTHER GROUPS OUTSIDE ITTC

The present Specialist Committee kept in touch with the Steering Committee of the next CFD Workshop "Wageningen 2020" through the common committee member. Some discussions have been made between two committees regarding the test cases of the workshop including full-scale benchmark data and the possibilities of the blind test cases etc. Several committee members are also members of the JoRes project for full-scale CFD.

The communication was a very useful opportunity for information exchange, and it is recommended to continue the contact with the CFD Workshop committee and JoRes, and to establish the connection with other possible groups outside ITTC.

12.10 SUGGEST RESEARCH TOPICS THAT CONTRIBUTE TO THE COMMITTEE GOALS

The committee compiled a list of suggested research topics and unresolved questions. It was published on a committee member's webpage and spread in social media.

It was concluded that it is easy to formulate interesting research suggestions but more difficult to disseminate them. The committee recommends ITTC to open a new page on ITTC webpage where suggested research topics from all committees can be listed. This could be very useful and inspiring for PhD students and researchers in the community. It could be the task of each committee to add to the list.

12.11 PRESENT COMMITTEE RESULTS IN A PUBLIC PAPER

The committee is requested to present the results "in a format directed towards the typical receiver of ship predictions including both ship owners and authorities." This has been interpreted as an article in industry-involved journals and conferences.

The AC requested that the material should first be presented in the committee report to the next conference, and thereafter in a publication. The latter should be in ITTC name (actual authors may be identified) and needs the approval of the Executive Committee (which may delegate it to the AC).

It is challenging to comply with AC's request, since the Committee will no longer exist after the next conference. The Committee will solve this by preparing as much as possible before the conference. Contribution to the articles will be done by some committee members on a voluntary basis, not by the full committee.

It is a good idea to increase the communication with the world outside ITTC, for example to explain issues like CFD versus EFD uncertainty to the stakeholders who actually *use* the results.

It is recommended that AC indicate a timeline for the approval and submission process if the next committee is given a similar task.

13. References

Amadeo M-G., Gonzalez-Adalid J., Perez-Sobrino M., Gonzalez-Gutierrez L., 2017, "Open Water results comparison for three propellers with transition model, applying crossflow effect, and its comparison with experimental results", SMP 2017.

American Institute of Aeronautics and Astronautics., 1998, "AIAA guide for the verification and validation of computational fluid dynamics simulations", American Institute of aeronautics and astronautics.

Andersson, J., Oliveira, D.R., Yeginbayeva, I., Leer-Andersen, M., Bensow, R.E., 2020, "Review and comparison of methods to model ship hull roughness". Applied Ocean Research Vol. 99, pp. 102119. https://doi.org/10.1016/j.apor.2020.102119

ASME, 2009, "Standard for Verification and Validation in Computational Fluid Dynamics and Heat Transfer", American Society of Mechanical Engineers, New York, Standard No. V&V 20-2009.

ASME V&V 10-2006., 2006, "Guide for verification and validation in computational solid mechanics", American Society of Mechanical Engineers.

Baltazar J., Rijpkema D., Falcao de Campos J.A.C. , 2017, "On the Use of the gamma RE_theta Transition Model for the Prediction of the Propeller Performance at Model-Scale", SMP 2017.

Bhattacharyya A., Neitzel J.C., Stehen S. , Abdel-Maksoud M., Krasilnikov V., 2015a, "Influence of Flow Transition on Open and Ducted Propeller Characteristics", SMP 2015.

Bhattacharyya A., Krasilnikov V., Steen S., 2015b, "Scale Effects on a 4-Bladed Propeller Operating in Ducts of Different Design in Open Water", SMP 2015.

Bhushan, S., Xing, T., Carrica, P., Stern, F., 2009, "Model- and Full-Scale URANS Simulations of Athena Resistance, Powering, Seakeeping, and 5415 Manoeuvring". Journal of Ship Research Vol. 53, pp. 179–198.

Bhushan, S., Xing, T., Carrica, P., Stern, F., Des, U., 2007, "Model- and Full-Scale URANS / DES Simulations for Athena R / V Resistance , Powering , and Motions", in: 9th International Conference on Numerical Ship Hydrodynamics Ann Arbor, Michigan. pp. 5–8.

Bonfiglio L., Brizzolara S., 2015, "Effect of turbulence models on RANSE predictions of transient flow over blade sections", SMP 2015.

Bulten, N., Nijland M., 2011, "On the development of a full-scale numerical towing tank Reynolds scaling effects on ducted propellers and wakefields", Second International Symposium on Marine Propulsors, SMP 2011.

Bulten N., Stoltenkamp P., 2017, "Full-scale CFD: the end of the Froude-Reynolds battle", SMP 2017.

Carrica, P.M., Mofidi, A., Eloot, K. and Delefortrie, G., 2016. "Direct simulation and experimental study of zigzag maneuver of KCS in shallow water". Ocean engineering, 112, pp.117-133.

Choi J-K., Park H-G. and Kim H-T., 2014, "A numerical study of scale effects on performance of a tractor type podded propeller", IJNAOE 2014.

Coleman, H., Stern, F., 1998, "Closure to 'Discussion of. Uncertainties and CFD Code Validation'(1998, ASME J. Fluids Eng., 120, p. 635)", Journal of Verification, Validation and Uncertainty Quantification, Vol. 120(3), pp 635-636.

Demirel Y.K., Khorasanchi M., Turan O., Incecik A., Schultz M.P., 2014, "A CFD model for the frictional resistance prediction of antifouling coatings", Ocean Engineering.

Demirel Y.K., Turan O., Incecik A., 2017, "Predicting the effect of biofouling on ship resistance using CFD", Applied Ocean Research, Vol. 62, pages 100-118, https://doi.org/10.1016/j.apor.2016.12.003.

Dong X-Q., Li W., Yang C-J., Noblesse F., 2017, "RANSE-based Simulation and Analysis of Scale Effects on Open-Water Performance of the PPTC-II Benchmark Propeller", SMP 2017.

Duvigneau, R., Visonneau, M., Deng, G.B., 2003, "On the role played by turbulence closures in hull shape optimization at model and full scale". Journal of Marine Science and Technology Vol. 8, pp. 11–25. https://doi.org/10.1007/s10773-003-0153-8

Duy T-N., Hino T., Suzuki K., 2017, "Numerical study on stern flow fields of ship hulls with different transom configurations", Ocean Engineering.

Eça, L., Hoekstra, M., 2002, "An evaluation of verification procedures for CFD applications", In 24th Symposium on Naval Hydrodynamics, Fukuoka, Japan, July, pp 568-587.

Eça L., Hoekstra M., 2005, "On the accuracy of the numerical prediction of scale effects on ship viscous resistance", MARINE 2015.

Eça, L., Hoekstra, M., 2006, "Discretization uncertainty estimation based on a least squares version of the grid convergence index", In 2nd workshop on CFD uncertainty analysis. Lisbon, Portugal.

Eça L., Hoekstra M., 2008, "The numerical friction line", Journal of Marine Science and Technology, 13, pp. 328–345, https://doi.org/10.1007/s00773-008-0018-1

Eça, L., Hoekstra, M., 2014, "A procedure for the estimation of the numerical uncertainty of CFD calculations based on grid

refinement studies", Journal of Computational Physics, Vol. 262, pp 104-130.

Eça, L., Hoekstra, M., Hay, A., Pelletier, D., 2007, "A manufactured solution for a two-dimensional steady wall-bounded incompressible turbulent flow", International Journal of Computational Fluid Dynamics, Vol. 21(3-4), pp 175-188.

Eça L., Hoekstra M. and Raven H.C., 2010, "Quantifying Roughness Effects by Ship Viscous Flow Calculations", 28th Symposium on Naval Hydrodynamics, Pasadena, California.

Eça, L. S., Vaz, G., Hoekstra, M., 2010, "Code verification, solution verification and validation In RANS solvers", In International Conference on Offshore Mechanics and Arctic Engineering, Vol. 49149, pp 597-605.

Farkas, A., Degiuli, N. and Martić, I., 2017, "Numerical simulation of viscous flow around a tanker model", Brodogradnja, 68 (2), 109-125. https://doi.org/10.21278/brod68208

Farkas, A., Degiuli, N., Martić, I., 2018, "Assessment of hydrodynamic characteristics of a full-scale ship at different draughts". Ocean Engineering Vol. 156, pp. 135–152. https://doi.org/10.1016/j.oceaneng.2018.03.002

Fujisawa, T., Tsubokura, M., Tanaka, H., 2020, "Study on Estimation of Flow Around Marine Propeller by Large-Scale LES and Affection of Grid Resolution and Reynolds Number", in: Proceedings of the ASME 2020 39th International Conference on Ocean, Offshore and Arctic Engineering, OMAE2020, August. Florida, US, pp. 1–8.

Garcia-Gomez, 2000, Garcia-Gomez, A., 2000, "On the form factor scale effect", Ocean Engineering, (26).

Garenaux, M., de Jager, A., Raven, H.C., Veldhuis, C., 2019, "Shallow-Water Performance Prediction: Hybrid Approach of Model Testing and CFD Calculations", in: Practical Design of Ships and Other Floating Structures. Springer, Singapore, pp. 63–82. https://doi.org/10.1007/978-981-15-4624-2_4

Giannoulis, 2019, Giannoulis A., Halse K.H., 2019, "Evaluation of a practical approach for numerical propulsion tests", OMAE 2019

Gornicz, T., van det Ploeg, A., Scholcz, T., 2016, "Trim wedge optimisation with viscous free surface computations", PRADS 2016.

Grigson C.W.B., 1999, "A planar friction Algorithm and ist use analysing hull resistance", RINA.

Gudla, A.S.T., Kalyanam, S.S., Bhattacharyya, A., Sha, O.P., 2019, "Asymmetric Stern Modifications for KVLCC2", in: Practical Design of Ships and Other Floating Structures. Springer, Singapore, pp. 258–268. https://doi.org/10.1007/978-981-15-4624-2_15

Guiard T., 2017, "Full-Scale Self-Propulsion Calculations Including Roughness Effects and Validation with Sea Trial Data", Star Global conference.

Guiard, T., Leonard, S., Mewis, F., 2013, "The Becker Mewis Duct® - Challenges in Full-Scale Design and new Developments for Fast Ships", Third International Symposium on Marine Propulsors smp'13, Launceston, Tasmania, Australia.

Guilmineau E., Deng G.B., Leroyer A., Queutey P., Visonneau M., Wackers J., 2015, "Influence of the Turbulence Closures for

the Wake Prediction of a Marine Propeller", SMP 2015.

Haase, M., Zurcher, K., Davidson, G., Binns, J.R., Thomas, G., Bose, N., 2016, "Novel CFD-based full-scale resistance prediction for large medium-speed catamarans". Ocean Engineering Vol. 111, pp. 198–208. https://doi.org/10.1016/j.oceaneng.2015.10.018

Hafermann D., Schneider M., Richards J., Chao K.Y., Takai M., 2010, "Investigation of Propulsion Improving Devices with CFD", PRADS 2010.

Hally D., 2017, "A RANS-BEM coupling procedure for calculating the effective wakes of ships and submarines", SMP 2017.

Hasuike N., Okazaki M., Okazaki A. and Fujiyama K., 2017, "Scale effects of marine propellers in POT and self propulsion test conditions", SMP 2017.

Heinke H-J., Hellwig-Rieck K., 2011, "Investigation of Scale Effects on Ships with a Wake Equalizing Duct or with Vortex Generator Finns", Second International Symposium on Marine Propulsors, SMP11.

Heinke H.-J., Hellwig-Rieck K., Lübke L., 2019, "Influence of the Reynolds Number on the Open Water Characteristics of Propellers with Short Chord Lengths", SMP 2019.

Helma S., 2015, "An Extrapolation Method Suitable for Scaling of Propellers of any Design", SMP 2015.

Helma S., Streckwall H., Richter J., 2017, "The effect of propeller scaling methodology on the performance prediction", SMP 2017.

Hino, T. (Ed.), 2015, "Tokyo 2015: A Workshop on CFD in Ship Hydrodynamics," Workshop Proceedings, Tokyo, Dec. 2–4.

Hino, T. et al. (Ed.), 2020, "Numerical Ship Hydrodynamics: an assessment of the Tokyo 2015 Workshop, Springer.

Hino T., Stern, F., Larsson, L., Visonneau, M., Hirata, N., Kim J., 2021, "Numerical Ship Hydrodynamics - An Assessment of the Tokyo 2015 Workshop", Springer 2021.

Hiroi, T., Windén, B., Kleinwächter, A., Ebert, E., Fujisawa, J., Kamiirisa, H., Damaschke, N., Kawakita, C., 2019, "Full-Scale On-board Measurements of Wake Velocity Profiles , Underwater Noise and Propeller Induced Pressure Fluctuations". Conference Proceedings The Japan Society of Naval Architects and Ocean Engineers Vol. 29, pp. 193–198.

Hollenbach U., 2009, "Pro's and Con's of the form-factor using Prohaska's method when extrapolating the model resistance", STG Annual Meeting.

Huang, Y.T., Lin, B.C., 2019, "Design and development of the energy saving rudder-bulb-fin combination by using computational fluid dynamics technique", in: Practical Design of Ships and Other Floating Structures. Springer, Singapore, pp. 290–302.

IEEE Standards Coordinating Committee., 1991, "IEEE Standard Glossary of Software Engineering Terminology (IEEE Std 610.12-1990)", Los Alamitos. CA: IEEE Computer Society, Vol. 169.

Inukai, Y., 2019, "Full Scale Measurement of The Flow Field at The Stern by Using Multi - Layered Doppler Sonar (MLDS)", in: Sixth International Symposium on Marine Propulsors Smp'19, Rome, Italy.

ISO, 1991, "9000-3: Quality Management and Quality Assurance Standards-Part 3: Guidelines for the Application of ISO 9001 to the Development, Supply and

Maintenance of Software", International Standards Organization, Geneva, Switzerland.

ISO., 2008, "ISO 16730-1, Fire Safety Engineering - Assessment, Verification and Validation of Calculation Methods - Part 1: General", International Organization for Standardization, Geneva.

ISO., 2013, "ISO/TR 16730-3, Fire Safety Engineering - Assessment, Verification and Validation of Calculation Methods - Part 3: Example of a CFD model", International Organization for Standardization, Geneva.

ITTC, 1957, "Subjects 2 and 4 - Skin Friction and Turbulence Stimulation", 8th International Towing Tank Conference, (https://ittc.info/media/3107/subjects-2-4-skin-friction-and-turbulence.pdf)

ITTC, 1978, "Report of Resistance Committee", 15th International Towing Tank Conference , (https://ittc.info/media/2865/report-of-resistance-committee.pdf)

ITTC, 1990, "Report of the powering performance committee", 19th International Towing Tank Conference , (https://ittc.info/media/2304/report-of-the-power-performance-committee.pdf)

ITTC, 1999, "The Specialist Committee onUnconventional Propulsors", 22nd International Towing Tank Conference, (https://ittc.info/media/1516/specialist-committee-on-unconventional-propulsion.pdf)

ITTC, 2005, "The Specialist Committee on Azimuthing Podded Propulsion", 24th International Towing Tank Conference, (https://ittc.info/media/5864/volume-ii-specialist-committee-on-app.pdf)

ITTC, 2008, "The Specialist Committee on Azimuthing Podded Propulsion", 25th International Towing Tank Conference, (https://ittc.info/media/3493/volume2_5azimuthingpoddedpropulsion.pdf)

ITTC, 2011, "The Specialist Committee on Scaling of Wake Field", ITTC 2011, 2011(https://ittc.info/media/5530/10.pdf)

ITTC, 2017a, "7.5-02-02-01 Resistance Test", ITTC –Recommended Procedures and Guidelines, (https://www.ittc.info/media/8001/75-02-02-01.pdf)

ITTC, 2017b, "7.5-02-03-01.4 1978 ITTC Performance Prediction Method", ITTC – Recommended Procedures and Guidelines, (https://www.ittc.info/media/8017/75-02-03-014.pdf)

ITTC, 2017c, "7.5-02-03-01.3 Podded Propulsion Tests and Extrapolation", ITTC – Recommended Procedures and Guidelines, (https://www.ittc.info/media/8015/75-02-03-013.pdf)

ITTC, 2017d, "7.5-02-03-01.6 Hybrid Contra-Rotating Shaft Pod Propulsors Model Test", ITTC –Recommended Procedures and Guidelines, (https://www.ittc.info/media/8021/75-02-03-016.pdf)

ITTC, 2017e, "7.5-02-03-01.1 Propulsion/ Bollard Pull Test", ITTC –Recommended Procedures and Guidelines, (https://www.ittc.info/media/8011/75-02-03-011.pdf)

ITTC, 2017f, "7.5-04-05-01 Guideline on the determination of model-ship correlation factors", ITTC –Recommended Procedures and Guidelines, (https://www.ittc.info/media/8185/75-04-05-01.pdf)

ITTC Procedures and Guidelines, 2017, "7.5-03-01-01 Uncertainty Analysis in CFD

Verification and Validation, Methodology and Procedures", ITTC –Recommended Procedures and Guidelines, (https://www.ittc.info/media/).

Kim H-T., Kim H-T., Kim J-J. and Lee D-Y., 2019b, "Study on the skin-friction drag reduction by air injection using computational fluid dynamics-based simulations", PRADS 2019.

Kim M-C., Shin Y-J. , Lee W-J., Lee J-H., 2017, "Study on Extrapolation Method for Self-Propulsion Test with Pre-Swirl Device", SMP 2017.

Kim, K., Leer-Andersen, M. and Werner, S., 2019, "Roughness Effects on Ship Design and Operation", in: Practical Design of Ships and Other Floating Structures. Springer, Singapore, pp. 186–204.

Kim, K., Leer-Andersen, M., Werner, S., Orych, M., Choi, Y., 2012, "Hydrodynamic Optimization of Pre-swirl Stator by CFD and Model Testing", 29th Symposium on Naval Hydrodynamics Gothenburg, Sweden, 26-31 August.

Kim, K.S., Kim, Y.C., Yang, K.K., Kim, J., Hwang, S., Kim, M.S., Lee, Y.Y., Ahn, H., 2019, "Full Scale Computations for Resistance and Self-propulsion Performances of Commercial Ship by RANS Simulations", in: Practical Design of Ships and Other Floating Structures. Springer, Singapore, pp. 28–43. https://doi.org/10.1007/978-981-15-4624-2_2

Kim, W., Jang, Y., Kim, M., 2016, "Performance analysis for DSME Cap Fin in model and full-scale", PRADS 2016.

Kinaci O.C., Sukas O.F., Bal S., 2016, "Prediction of wave resistance by a Reynolds-averaged Navier–Stokes equation–based computational fluid dynamics approach", Journal of Enginering for the Maritime Enviroment, 3 (230).

Klose R., Schulze R., Hellwig-Rieck K., 2017, "Investigation of Prediction Methods for Tip Rake Propellers", SMP 2017.

Knupp, P., Salari, K., 2002, "Verification of computer codes in computational science and engineering. CRC Press.

Kok, Z., Duffy, J., Chai, S. and Jin, Y., 2020, "Benchmark case study of scale effect in self-propelled container ship squat". ASME 2020 39th International Conference on Ocean, Offshore and Arctic Engineering. American Society of Mechanical Engineers Digital Collection.

Korkmaz, K.B., Werner, S. and Bensow, R., 2019a, "Investigations for CFD Based Form Factor Methods" In Proceedings of the Numerical Towing Tank Symposium (NuTTS 2019), Tomar, Portugal, 29 September–1 October 2019.

Korkmaz K.B., Werner S., Bensow R., 2019b, "Numerical friction lines for cfd based form factor determination", MARINE 2019.

Korkmaz K.B., Werner S., Sakamoto N., Queutey P., Deng G., Yuling G., Guoxiang D., Maki K., Ye H., Akinturk A., Sayeed T., Hino T., Zhao F., Tezdogan T., Demirel Y.K. and Bensow R., 2021a, "CFD Based Form Factor Determination Method", Ocean Engineering, Vol. 220, 108451, https://doi.org/10.1016/j.oceaneng.2020.108451.

Korkmaz, K. B., Werner S., Bensow R., 2021b, "Verification and Validation of CFD Based Form Factors as a Combined CFD/EFD Method", J. Mar. Sci. Eng., 9(1), 75; https://doi.org/10.3390/jmse9010075.

Kouh, J-S., Chen, Y-J., Chau, S-W., 2009, "Numerical study on scale effect of form

factor", Ocean Engineering, Vol. 36, Issue 5, pp 403-413.

Krasilnikov V., 2013, "Self-Propulsion RANS Computations with a Single-Screw Container Ship", SMP 2013.

Krasilnikov V., Sileo L. and Steinsvik K., 2017, "Numerical investigation into scale effect on the performance characteristics of twin-screw offshore vessels", SMP 2017.

Krasilnikov V., Koushan K., Nataletti M., Sileo L. and Spence S., 2019, "Design and Numerical and Experimental Investigation of Pre-Swirl Stators PSS", SMP 2019.

Larsson, L. (Ed.), 1981, "SSPA-ITTC Workshop on Ship Boundary Layers", SSPA Report 90, Gothenburg, Sweden.

Larsson, L., Stern, F., Visonneau, M., 2013, "Numerical ship hydrodynamics: an assessment of the Gothenburg 2010 workshop", Springer Science & Business Media.

Lee J-H., Kim M-C., Shin Y-J., Kang J-G., 2017, "Study on Performance of Combined Energy Saving Devices For Container Ship by Experiments", SMP 2017.

Lee Y-G., Ha Y-J., Lee S-H., Kim S-H., 2018, "A study on the estimation method of the form factor for a full-scale ship", Brodogradnja, 69 (1).

Liefvendahl, M., Fureby, C., 2017, "Grid requirements for LES of ship hydrodynamics in model and full scale". Ocean Engineering Vol. 143, pp. 259–268. https://doi.org/10.1016/j.oceaneng.2017.07.055

Li D-Q., Lindell P., Werner S., 2019, "Transitional flow on model-scale propellers and their likely influence on performance prediction", SMP 2019.

Lin T-Y. and Kouh J-S., 2015, "On the Scale Effect of Thrust Deduction in a Judicious Self-Propulsion Procedure for a Moderate-Speed Containership", J Mar Sci Technology, Vol. 20, pp 373–391, https://doi.org/10.1007/s00773-014-0289-7

Lücke T., Streckwall H., 2017, "Experience with Small Blade Area Propeller Performance", SMP 2017.

Mikkelsen, H., Steffensen, M.L., Ciortan, C., Walther, J.H., 2019, "Ship scale validation of CFD model of self-propelled ship". MARINE 2019 Computational Methods in Marine Engineering VIII pp. 718–729.

Mikkelsen H., Walther J.H., 2020, "Effect of roughness in full-scale validation of a CFD model of self-propelled ships", Applied Ocean Research, Vol. 99, 102162.

Müller S-B., Abdel-Maksoud M, Hilbert G., 2009, "Scale effects on propellers for large container vessel", First International Symposium on Marine Propulsors, 2009.

Nguyen, T.V., Ikeda, Y., 2016, "Reynolds Number and Propeller effects on lift and drag forces on a high lift rudder with wedge tail", PRADS 2016.

Niklas, K., Pruszko, H., 2019, "Full-scale CFD simulations for the determination of ship resistance as a rational, alternative method to towing tank experiments". Ocean Engineering Vol. 190, pp. 106435. https://doi.org/10.1016/j.oceaneng.2019.106435

Oberkampf, W. L., Blottner, F. G., 1998," Issues in computational fluid dynamics code verification and validation", American Institute of Aeronautics and Astronautics (AIAA) Journal, Vol.36(5), pp 687-695.

Oberkampf, W. L., Roy, C. J., 2010, “Verification and validation in scientific computing”, Cambridge University Press.

Okada Y., Katayama K., Okazaki A., Okazaki M., Fukuda K., Kobayashi Y., Kajino T., 2017, "The Battle Royal of Energy Saving Devices for a Ship", SMP 2017.

Okazaki A., Yamasaki S., Kawanami Y., Ukon Y. and Ando J., 2015, "The Effect of Tip Rake on Propeller Open Water Efficiency and Propulsive Efficiency", SMP 2015.

Oliva-Remolà, A., Rojas, L.P., Arribas, F.P., 2014, "A contribution to appendage drag extrapolation using computational tools", Developments in Maritime Transportation and Exploitation of Sea Resources - Proceedings of IMAM 2013, 15th International Congress of the International Maritime Association of the Mediterranean, 1, pp. 67-72

Oliva-Remolà, Adriana & Rojas, Luis & Arribas, F.P.. (2013). “A contribution to appendage drag extrapolation using computational tools.”, Developments in Maritime Transportation and Exploitation of Sea Resources, pp. 67-72, DOI:10.1201/b15813-10, Corpus ID: 53547412

Oliveira D., Larsson A.I., Granhag L., 2018, "Effect of ship hull form on the resistance penalty from biofouling", The Journal of Bioadhesion and Biofilm Research, 34(3).

Orihara, H., Tsujimoto, M., 2017, "Performance prediction of full-scale ship and analysis by means of on-board monitoring . Part 2 : Validation of full-scale performance predictions in actual seas". Journal of Marine Science and Technology Vol. 0, pp. 0. https://doi.org/10.1007/s00773-017-0511-5

Park H-G., Choi J-K. and Kim H-T., 2014, "An estimation method of full-scale performance for pulling type podded propellers", IJNAOE, Vol. 6, Issue 4, pp 965-980.

Park, D-W., 2015, "A study on the effect of flat plate frition resistance on speed performance prediction of full-scale", International Journal of Naval Architecture and Ocean Engineering, 2015(7).

Pecoraro A., Di Felice F., Felli M., Salvatore F., Viviani M., 2013, "Propeller-hull interaction in a single-screw vessel", SMP 2013.

Pena, B., Muk-Pavic, E., Ponkratov, D., 2019, "Achieving a high accuracy numerical simulations of the flow around a full scale ship", in: Proceedings of the International Conference on Offshore Mechanics and Arctic Engineering - OMAE. pp. 1–10. https://doi.org/10.1115/OMAE2019-95769

Peravali S. K., Bensow R., Gyllenram W. and Shiri A., 2016, "An investigation on ittc 78 scaling method for unconventional propellers", ICHD 2016.

Pereira, F.S., Eca, L., Vaz, G., 2017, "Verification and Validation exercises for the flow around the KVLCC2 tanker at model and full-scale Reynolds numbers". Ocean Engineering Vol. 129, pp. 133–148. https://doi.org/10.1016/j.oceaneng.2016.11.005

Peric, M., 2019, "White paper: Full-scale simulation for marine design". Siemens White Paper.

Ponkratov, D., 2016, "Lloyd’s Register workshop on ship scale hydrodynamics", in: Ponkratov, D. (Ed.), 2016 Workshop on Ship Scale Hydrodynamic Computer Simulation. p. 2016. https://doi.org/10.1002/ejoc.201200111

Ponkratov D., 2021, "Jores - Development of an industry recognised benchmark for Ship

Energy Efficiency Solutions https://jores.net/".

Quereda R., Bernal L., Pérez-Sobrino M., González-Adalid J., 2019, "Critical values of Rn defining transitional flow", SMP 2019.

Quereda R., Pérez-Sobrino M., González-Adalid J. , Soriano C., 2017, "Conventional propellers in CRP-POD configuration. Tests and extrapolation", SMP 2017.

Raven H., van der Ploeg A., Starke B., 2004, "Computation of free-surface viscous flows at model and full-scale by a steady iterative approach", 25th Symposium on Naval Hydrodynamics.

Raven, C.H., Ploeg, A., Starke, A.R., 2008, "Towards a CFD-based prediction of ship performance - Progress in predicting full-scale resistance and scale effects", RINA - International Conference - Marine CFD 2008.

Raven, H., van der Ploeg, A., Starke, A.R., Eça, L., H. 2009 "Towards a CFD-Based Prediction of Ship Performance --- Progress in Predicting Full-Scale Resistance and Scale Effects." International Journal of Maritime Engineering 135: 12

Raven H.C., 2017, "Combined CFD/EFD Methods-Exploiting CFD for Improving Performance Predictions", ITTC 2017.

Raven H., Private communication, 2019

Rawlings, J. O., Pantula, S. G., Dickey, D. A., 2001, "Applied regression analysis: a research tool", Springer Science & Business Media.

Regener, P. B. , Mirsadraee Y., and Andersen P., 2017, "Nominal vs. Effective Wake Fields and their Influence on Propeller Cavitation Performance", SMP 2017.

Rijpkema, D., Vaz, G., 2011, "Accurate model and full-scale viscous flow computations on propulsors", The Naval Architect, Issue (JULY-AUGUST), pp. 52-55

Rijpkema D., Baltazar J., de Campos J.F., 2015, "Viscous flow simulations of propellers in different Reynolds number regimes ", SMP 2015.

Roache, P.J., 1998, "Verification and Validation in Computational Science and Engineering", Hermosa publishers, Albuquerque, New Mexico.

Roache, P. J., 2002, "Code verification by the method of manufactured solutions", Journal of Fluids Engineering, Vol. 124(1), pp 4-10.

Roache, P. J., Knupp, P. M., Steinberg, S., Blaine, R. L., 1990, "Experience with benchmark test cases for groundwater flow", In 1990 Spring Meeting of the Fluids Engineering Division, Toronto, Ont, Can, 06/04-07/90, 49-56.

Roache, P. J., Steinberg, S., 1984, "Symbolic manipulation and computational fluid dynamics", American Institute of Aeronautics and Astronautics (AIAA) Journal, Vol. 22(10), pp 1390-1394.

Roy, C. J., Nelson, C. C., Smith, T. M., Ober, C. C., 2004, "Verification of Euler/Navier–Stokes codes using the method of manufactured solutions", International Journal for Numerical Methods in Fluids, Vol. 44(6), pp 599-620.

Sakamoto, N., Ohashi, K., Kobayashi, H., 2019, "Overset RaNS Computation of Flow around Bulk Carrier with ESD in Full Scale and its Validation". Conference Proceedings The Japan Society of Naval Architects and Ocean Engineers Vol. 29, pp. 199–204.

Salari, K., Knupp, P., 2000, "Code verification by the method of manufactured solutions

(No. SAND2000-1444)", Sandia National Labs., Albuquerque, NM (US); Sandia National Labs., Livermore, CA (US).

Sánchez-Caja A., Ory E., Salminen E., Pylkkänen J., Siikonen, T., 2003, "Simulation of Incompressible Viscous Flow Around a Tractor Thruster in Model and Full Scale. ", The 8th International Conference on Numerical Ship Hydrodynamics.

Sasajima, H. and Tanaka, I., 1966, "On the estimation of wakes of ships", XI ITTC, Tokyo.

Sasaki N., Atlar M., 2019, "Scale Effect of Gate Rudder", SMP 2019.

Sezen, S., Cakici, F., 2019, "Numerical Prediction of Total Resistance Using Full Similarity Technique". China Ocean Engineering Vol. 33, pp. 493–502. https://doi.org/10.1007/s13344-019-0047-z

Shin K-W., Andersen P., 2017, "CFD Analysis of Scale Effects on Conventional and Tip-Modified Propellers", SMP 2017.

Song K-W., Guo C-Y., Wang C., Sun C., Li P., Zhong R-F., 2019, "Experimental and numerical study on the scale effect of stern flap on ship resistance and flow field", Ships and Offshore Structures, Vol. 15, Issue 9, pp 981-997.

Song, S., Demirel, Y.K., Atlar, M., 2019, "An investigation into the effect of biofouling on the ship hydrodynamic characteristics using CFD". Ocean Engineering Vol. 175, pp. 122–137. https://doi.org/10.1016/j.oceaneng.2019.01.056

Starke B., Raven H.C., van der Ploeg A., 2007, "Computation of transom-stern flows using a steady free-surface fitting RANS method", 9th International Conference on Numerical Ship Hydrodynamics.

Starke, A.R., Drakopoulos, K., Toxopeus, S.L., Turnock, S.R., 2017, "RANS-based full-scale power predictions for a general cargo vessel, and comparison with sea-trial results". 7th International Conference on Computational Methods in Marine Engineering, MARINE 2017 Vol. 2017-May, pp. 353–364.

Stewart J.R., 2003, "A posteriori error estimation for predictive models", Presentation at the Workshop on the Elements of Predictability, Johns Hopkins University, Baltimore, Maryland, November 13–14.

Strasser G., 2018, "QSG Note on Model-Ship Extrapolation Process", Private communications

Streckwall H., Greitsch L., Scharf M., 2013, "An advanced Scaling Procedure for Marine Propellers", SMP 2013.

Sun, W., Hu, Q., Hu, S., Su, J., Xu, J., Wei, J., 2020, "Numerical Analysis of Full-Scale Ship Self-Propulsion Performance with Direct Comparison to Statistical Sea Trail Results". Journal of Marine Science and Engineering Vol. 8, pp. 1–22.

Sun W., Hu S., Su J., Wei J., Huang G., 2019, "Numerical Analysis of Hull- Propeller and Free Surface Interaction at Model- and Full-Scale", SMP 2019.

Tacar Z., Sasaki N., Atlar M., Korkut E., 2019, "Investigation of scale effects on gate rudder® performance", AMT 2019.

Tahara Y., Himeno Y., Katsui T., 2003, "Computation of ship viscous flow at full-scale Reynolds number: consideration of near-wall flow model including surface

roughness effect", Journal of The Society of Naval Architects of Japan, (192).

Tamura, K. and Sasajima, T., 1977, "Some Investigation on Propeller Open-Water Characteristics for Analysis of Self-Propulsion Factors", Mitsubishi Technical Bulletin, No. 119, pp 1-12.

Tautges, T. J., 2001, "CGM: A geometry interface for mesh generation, analysis and other applications", Engineering with Computers, Vol. 17(3), pp 299-314.

Terziev, M., Tezdogan, T., Incecik, A., 2019, "A geosim analysis of ship resistance decomposition and scale effects with the aid of CFD". Applied Ocean Research Vol. 92. https://doi.org/10.1016/j.apor.2019.101930

Terziev, M., Tezdogan, T., Incecik, A., 2020, "A posteriori error and uncertainty estimation in computational ship hydrodynamics". Ocean Engineering Vol. 208, pp. 107434. https://doi.org/10.1016/j.oceaneng.2020.107434

Tezdogan, T., Incecik, A., Turan, O., 2016, "Full-scale unsteady RANS simulations of vertical ship motions in shallow water". Ocean Engineering Vol. 123, pp. 131–145. https://doi.org/10.1016/j.oceaneng.2016.06.047

Toki N., 2008, "Investigations on Correlation Lines through the analysis of Geosim Model test results", Journal of the Japan Society of Naval Architects and Ocean Engineers.

Townsin R. L., Medhurst J. S., Hamlin N. A., Sedat B. S, 1984, "Progress in Calculating the Resistance of Ships with Homogeneous or Distributed Roughness ", NECIES Centenary Conference on Marine Propulsion.

Tsujimoto, M., Orihara, H., 2018, "Performance prediction of full-scale ship and analysis by means of on- board monitoring (Part 1 ship performance prediction in actual seas)". Journal of Marine Science and Technology Vol. 0, pp. 0. https://doi.org/10.1007/s00773-017-0523-1

van der Ploeg A., Starke B., 2011, "Prediction of the transom flow regime with viscous free surface computations", MARINE 2011, (29).

Van Hoydonck W., Delefortrie G., De Maerschalck B. and Vantorre M., 2018, "Open-Water Rudder Tests using CFD", SNH 2018.

Van S.-H, Ahn H., Lee Y.-Y., Kim C., Hwang S., Kim J., Kim K.-S., Park I.-R., 2011, "Resistance characteristics and form factor evaluation for geosim models of kvlcc2 and kcs", Advanced Model Measurement Technology for EU Maritime Industry - AMT'11.

Veikonheimo T., Miettinen P., Huisman J., 2017, "On the advanced extrapolation method for a new type of podded propulsor via CFD simulations and model measurements", SMP 2017.

Visonneau M., Queutey P. and Deng G.B., 2006, "Model and full-scale free-surface viscous flows around fully-appended ships", ECCOMAS CFD.

Visonneau, M., G.B. Deng, E. Guilmineau, P. Queutey & J. Wackers, 2016, "Local and Global Assessment of the Flow around the Japan Bulk Carrier with and without Energy Saving Devices at Model and Full Scale", 31th Symposium on Naval Hydrodynamics.

Wageningen 2021: a Workshop on CFD in Ship Hydrodynamics", https://w2020.marin.nl/

Wang, J., Yu, H. and Feng, Y. 2019 "Feasible study on full-scale delivered power prediction using CFD/EFD combination method" J Hydrodyn Vol 31, pp 1250–1254 (2019).

Wang J., Yu H., Zhang Y. and Xiong X., 2016, "CFD-Based Method of Determining Form Factor k for Different Ship Types and Different Drafts", Journal of Marine Science Applications, Vol. 15, pp 236–241.

Wang W.-H, Gu M.-Y. and Wang Y.-Y., 2015, "Calculation method of form factor based on energy conservation of ship wave-making. ", Journal of Ship Mechanics, Vol. 19.

Wang, Z-Z., Xiong, Y., Shi, L. and Liu, Z., 2015, "A numerical flat plate friction line and its application", Journal of Hydrodynamics 23, pp 383–393.

Wang, Z-Z., Xiong, Y., Wang, R., Shen, X-R. and Zhong, C-H., 2015, "Numerical study on scale effect of nominal wake of single screw ship", Ocean Engineering, Vol. 104.

Wang, Z-Z., Xiong Y., Wang R., Zhong C-H., 2016, "Numerical investigation of the scale effect of hydrodynamicperformance of the hybrid CRP pod propulsion system", Applied Ocean Research, Vol. 54.

Wawrzusiszyn M., Kraskowski M., Król P., Bugalski T., 2018, "Experimental and Numerical Hydrodynamic Analysis of Propulsion Factors On R/V Nawigator XXI with a Pre-Swirl Stator Device", NUTTS 2018.

Werner S., Gustafsson L., "Uncertainty of Speed Trials", In the proceedings of Hull PIC 2020, Hamburg, Germany.

Xia, L., Lundberg J., Bensow R., 2012, "Performance Prediction of a Nozzle Propeller", 29th Symposium on Naval Hydrodynamics.

Xing-Kaeding Y., Gatchell S. and Streckwall H., 2015, "Towards Practical Design Optimization of Pre-Swirl Device and its Life Cycle Assessment", SMP 2015

Yamano T., Kusunoki Y., Kuratani F., Ikebuchi T. and Funeno I., 2001, "On Scale effect of the resistance due to stern waves including forward-oriented wave breaking just behind a transom stern", PRADS 2001.

Yazaki A., 1969, "A Diagram to Estimate the Wake Fraction for a Actual Ship from a Model Tank Test", 12th ITTC, Rome.

Yao, Z. Q., Shen, H. C., Hui, G. A. O., 2013, "A new methodology for the CFD uncertainty analysis", Journal of Hydrodynamics, Ser. B, 25(1), pp 131-147.

Zhang, H., Wang, X., Chen, X., 2018, "Scale Effect Studies on Hydrodynamic Performance for DTMB 5415 Using CFD", in: Proceedings of the ASME 2018 37th International Conference on Ocean, Offshore and Arctic Engineering, June. pp. 1–7.

Zhao et al 2017, "An Innovative Methodology of Confidence Level Assessment for Virtual Test of Ship Hydrodynamics", The 30th American Towing Tank Conference

Zhou, Y., Liu, L., Cai, X., Feng, D., Guo, B., 2019, "Numerical study on scale effect of KCS", in: Proceedings of the ASME 2019 38th International Conference on Ocean, Offshore and Arctic Engineering OMAE2019 June 9-14, 2019, Glasgow, Scotland, UK. pp. 1–7. https://doi.org/10.3390/app9204442

Zondervan G-J., de Jager A., Veldhuis C., Garenaux M., Bosschers J., Janse G., 2019, "Advances in Design and Analysis of Ducted Propellers for Dredging Vessels", PRADS 2019.

Appendix A. level of impact for different issues affecting the scaling and performance prediction

Table 2 Determination of the level of impact for different issues affecting the scaling and performance prediction procedure of vessels. Rank 0-1-2 (2 is highest).

Item	Impact on trend and design	Impact on absolute power	Frequency of occurrence	Total impact	Possibility to improve with CFD
Hull friction determination using alternative friction or correlation line	1	0	2	3	1
Determination of the form factor	2	2	2	6	2
Wave resistance	1	0	1	2	2
Transom drag	2	1	1	4	2
Roughness allowance	0	1	2	3	1
Appendage resistance	2	1	1	4	2
Flow separation or vortex on the hull	2	1	1	4	0
Propeller open water scaling	2	0	2	4	1
Nominal wake field scaling	2	1	1	4	2
Effective wake scaling	2	1	2	5	2
Energy Saving Device	2	2	1	5	1
Ducted propeller	2	2	0	4	1

The Specialist Committee on Energy Saving Methods

Final Report and Recommendations to the 29th ITTC

1. INTRODUCTION

1.1 MEMBERSHIP AND MEETINGS

The Specialist Committee on Energy Saving Methods (SC-ESM) was appointed by the 28th ITTC in Wuxi, China, 2017, and it consists of the following members (see picture in Figure 1):

- Professor Inwon Lee, Pusan National University, Korea (Chairperson)
- Dr. James Gose, University of Michigan, USA (Secretary)
- Dr. Andrea Coraddu, University of Strathclyde, UK
- Professor Jianting Chen, Shanghai Ship and Shipping Research Institute, China
- Professor Munehiko Hinatsu, Osaka University, Japan
- Dr. Ramon Quereda, CEHIPAR (Canal de Experiencias Hidrodinámicas del Pardo), Spain
- Professor Tie Li, Shanghai Jiao Tong University, China

Figure 16: Photograph of ESM attendees at CEHIPAR

Four Committee meetings were held as follows:

- Pusan National University, Korea, 15-16 March 2018
- CEHIPAR, Spain, 5-6 November 2018

- University of Michigan, USA, 17-18 June 2019
- University of Strathclyde, UK, 6-7 February, 2020

1.2 TERMS OF REFERENCE OF THE 28TH ITTC

In its Terms of Reference (ToR) document, the 28th ITTC mandated the ESMC to perform the following Tasks:

1. Continue a systematic survey of energy saving methods (excluding machinery), devices, applications and possible savings, including the influence on the EEDI formula. Identify the effect of energy saving methods on different sea trial and EEDI drafts. Consider a complementary metric to EEDI to represent power savings.
2. Continue identifying and update the physical mechanisms for the newly introduced energy saving methods.
3. Update a survey on frictional drag reduction methods, including air lubrication and surface treatment.
4. Update a survey on energy savings based on the use of wind energy.
5. Develop guidelines for: CFD methods, model tests, scaling, for energy saving devices, taking into account Tokyo 2015 CFD workshop results investigating the influence of ESD. Continue to identify the needs for new model test procedures (resistance and propulsion, extrapolation methods) to investigate the effect of energy saving methods.
6. Collect and discuss the full scale data obtained through relevant benchmark tests on the effect of energy saving methods. Review relevant issues to be solved to develop a procedure to conduct in-service performance evaluation for ESM and define the way of using full scale data for validating the effect of ESM.
7. Identify and recommend the tasks related to energy saving methods and devices that should be undertaken during the 30th ITTC by general committees.

1.3 LIAISON WITH OTHER COMMITTEES AND OVERLAP ON TORS

We have been in contact with the Resistance and Propulsion (R&P) committee both by email and by joint meetings as follows;

- Attendance of chair (Inwon Lee) at the 4th meeting of R&P, KRISO, Daejon, 14 January 2020.

This was to clarify areas of overlap, decide who will move such areas forward and to discuss areas of common interest. Considering the termination of the committee after the 29th ITTC, the items of ToR which needs to be transferred to general committee were discussed.

1.4 GENERAL REMARKS

As the first item of our ToR implies, there exist various approaches to save energy for marine vessels. Although there has been recent progress in retrofit devices to enhance propulsion efficiency, which are commonly described as “energy saving devices”, it is also important to remember that the potential scope of energy saving methods are quite extensive including aspects of initial design and ship operation.

Good initial design for hull form and propeller with less power demand should always be addressed as a relevant energy saving method. It must be emphasized that design is aimed at good performance not only for the model test/trial condition in ‘calm seas’ but also for the

service conditions with wind and waves. Optimised hull forms to minimise added resistance in waves is a good example of a design approach to energy saving.

Many energy saving methods can be characterised as suitable for retrofit with the aim of reducing drag or the propulsive losses for an existing design. In addition, these measures are often applicable to the initial design phase. Examples would include air lubrication and low frictional coatings for reducing skin frictional resistance. On the other hand, there are devices designed to control the flow around the propeller to reduce propulsive losses. Use of renewable energy, such as wind and solar, also falls in this category.

The final category would correspond to the optimal operation. Being free from additional investment, this is often regarded as the most effective approach by ship operators. Examples of this category include slow steaming, hull/propeller cleaning, weather routing and trim optimization, etc.

2. SURVEY OF ENERGY SAVING METHODS

2.1 CATEGORIZATION OF ENERGY SAVING METHODS

In the 28th ITTC, we proposed the categorization of energy saving methods. Although some different categorization may exist, drastic changes in Energy Saving Technologies would not be found and this categorization keeps in the present committee (see Table 1). However, some newly ideas are proposed and we add these in this category table. An idea called "Gate Rudder" is newly introduced by Sasaki et al. (2019), and this is put in the category of the Technique of Inflow Management at Axial Efficiency of Reducing propulsive losses. An idea of "Ducted Contra-Rotating Propeller (DCRP)" is introduced by Cai et al. (2019), this is set in the two categories the Technology of Inflow Management at Axial Efficiency of Reducing propulsive losses and the Technology of Reduce rotational energy in the propeller wake at Rotational efficiency of Reducing propulsive losses.

Table 3: Categories of Energy Saving Methods

Principle	Mechanism	Technique	Methodology
Direct drag reduction	frictional resistance	less wetted sueface area less sheer force	air lubrication
			low friction paint
	viscous pressure resistance	boundary layer control	generate local vortex by fins
			hull form optimisation
	wave-making resistance	bow shaping	bulbous bow
			hull form optimisation
	wind drag reduction	shaping of upper structures	corner rounding
			downsizing of upper structure
	added wave resistance	incident wave reflection	bow shaping
		ship motion	hull shape
Reducing Propulsive losses	relative rotative efficiency	bilge vortex energy recovery	pre swirl stators
			vortex generators
	hull efficiency	hull-propeller interaction	vortex generators
			hull-propeller optimisation
	rotational efficiency	reduce rotational energy in the propeller wake	pre swirl stators
			contra-rotating propeller
			reaction rudder
			rudder fin
			hub fins
			overlapping propeller
	axial efficiency	hub vortex recovering	hub fins
			rudder bulb
		reduce tip vortex	tip-fin propeller
			tip-rake propeller
			CLT propeller
		inflow management	ducts
			overlapping propeller
	frictional efficiency	coatings	low friction paint
		injection	
	propeller design	blade design	area, thickness, section, tip loaded propeller
		CFD, optimization	
Use of renewable energy	wave	wing theory in waves	forebody fin
	wind energy	thrusut by wing lift	sail
			kite
			flettner rotor
	solar energy	energy change	photovoltaic panels
Operation	optimisation in operation	ICT	weather routing
			slow steaming
	aging	maintenance	docking
			roughness treatment

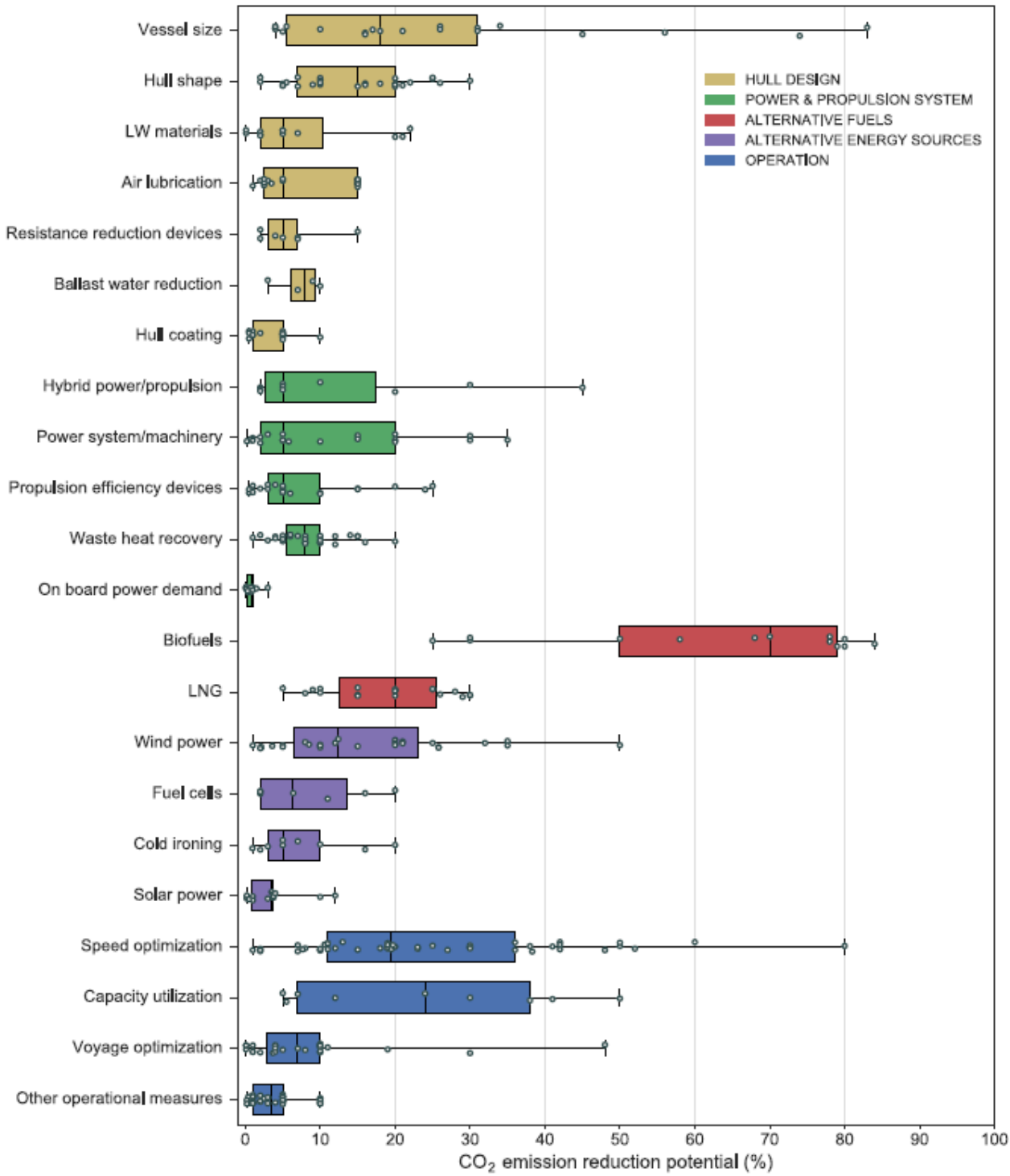

Figure 17: CO_2 emission reduction potential from individual measures, classified in 5 main categories of measures, Bouman et al., (2017)

Bouman et al., (2017) reviewed a lot of literatures, mainly issued in between 2009 and 2016, related to the energy saving and showed a very interesting chart (see Figure 2). They summarized the potential of the reduction of CO_2 emission from individual measures. Although the potential of the reduction of CO_2 emission spans widely for each measures, it may be useful for us to roughly understand the tendency of energy saving potential for each measure.

2.2 REVIEW OF RECENT RESEARCH ON ESM

In this section, recent work related to the energy saving methods are reviewed. The conferences we reviewed over the period 2017-2020 were:

- Applied Ocean Research (AOR)
- China Ocean Engineering (COE)
- International Shipbuilding Progress (ISP)
- International Journal of Naval Architecture and Ocean Engineering (IJNAOE)
- Journal of Hydrodynamics (JHD)
- Journal of Marine Science and Technology (JMST)
- Journal of Ship Research (JSR)
- Ocean Engineering (OE)
- Advanced Model Measurement Technology for the Marine Industry (AMT)
  - 11-13 October (2017), Glasgow, UK
  - 9-11 October (2019), Rome, Italy
- Computer and IT Application in the Marine Industries (COMPIT)
  - 15-17 May (2017), Cardiff, UK
  - 14-16 May (2018) Pavone, Italy
  - 25-27 May (2019) Tullamore, Ireland
  - 17-19 August (2020), Pontignano, Italy
- Symposium on High-Performance Marine Vehicle (HIPER)
  - 17-19 October (2016), Cortona, Italy
  - 11-13 September (2017), Zevenwacht, South Africa
- Hull Performance & Insight Conference (HullPIC)
  - 27-29 March (2017), Ulrichshusen, Germany
  - 12-14 May (2018) Redworth, UK
  - 6-8 May (2019) Gubbio, Italy
  - 26-28 October (2020) Hamburg, Germany
- International Naval Architecture and Maritime Symposium (INT NAM)
  - 24-25 April (2018), Istanbul, Turkey
- International Ocean and Polar Engineering Conference (ISOPE)
  - 25-30 June (2017), San Francisco, USA
  - 10-15 June (2018), Sapporo, Japan
  - 16-21 June (2019), Honolulu, USA
  - 11-16 October (2020), Shanghai, China
- International Conference on Computational Methods in Marine Engineering (MARINE)
  - 15-17 May (2017), Nante, France
  - 13-15 May (2019), Gothenburg, Sweden
- Technology and Science for the Ships of the Future, 19th International Conference on Ship & Maritime Research (NAV 2018): 20-22 June (2018), Torieste, Italy
- Numerical Towing Tank (NuTTS)
  - 1-3 October (2017), Wageningen, The Netherlands
  - 30 September-3 October (2018), Cortna, Italy
  - 29 September-1 October (2019), Tomar, Portugal
- International Conference on Ocean, Offshore and Arctic Engineering (OMAE)
  - 25-30 June (2017), Tronheim, Norway
  - 17-22 June (2018), Madrid, Spain
  - 9-14 June (2019), Glasgow, UK
- International Symposium on Practical Design of Ships and Other Floating Structures (PRADS): 22-26 September (2019), Yokohama, Japan

- International Symposium on Marine Propulsors (SMP)
  - 12 - 15 June (2017), Espoo, Finland
  - 26 - 30 May (2019), Rome, Italy
- Symposium on Naval Hydrodynamics (SNH)
  - 5-10 August (2018), Hamburg, Germany
  - 18-23 October (2020), Osaka, Japan

2.3 DIRECT DRAG REDUCTION

2.3.1 FRICTIONAL RESISTANCE

FRICTIONAL RESISTANCE

Air lubrication is one of the typical direct frictional reduction methods and still many researchers have been working on this theme. As the development of computers, the research using CFD increases in number.

Rotte et al. (2018) carried out numerical simulation of the flat bottom boundary layer flow with air cavity and the results are compared with PIV data. Arakawa et al. (2018) carried out CFD simulation of ship flows in the air lubricated condition. They also simulated self-propelled condition at the air lubrication with/without pre-swirl duct, WAD.

Wang et al. (2017) showed the experiment using 5m-long flat bottom shallow draft vessel. In the experiment the injection position was changed and obtained up to 15.5% drag reduction in the model test. Wang et al. (2018), the same group, evaluated about 10-15% energy saving for the full scale ship without considering air supply power. In addition, Yang et al. (2018) analysed the Wang's same model test by CFD.

Kawakita (2018) summarized the air lubrication technology widely from the view point of actual ship design.

Mäkiharju & Ceccio (2018) investigated experimentally the behaviour of injected air on a flat bottom of ship with differing the number of injection point. Ikeda (2018) introduced his research on the bottom air cavity to reduce the bottom frictional resistance experimentally and numerically.

Ravina & Guidomei (2018) introduced the activity of drag reduction by use of air injection at Genova University, in which two types of simple flat plates and 1.8m-long ship model are used for the experiment. Park & Lee (2018) investigated the spread of air injection pattern experimentally and derived an empirical formula to evaluate the spread angle of air injected area with air rate and ship speed. Kim et al. (2018) carried out the CFD simulation of air injection at the bottom of bulk carrier for model and full scale in order to verify methods to extrapolate the drag reduction from model test to full-scale. Kim et al. (2019) carried out numerical simulation of two-phase flow to evaluate the frictional resistance due to air injection. They also evaluated the drag reduction for LNG carrier and compared with sea trial data.

Zhao et al. (2020) numerically simulated micro air bubble flows over axisymmetric body and studied the drag reduction rate vs. bubble size, body speed as well as air injection rate. Charruault et al. (2019) studied the free surface deformation of air cavity as well as drag reduction.

When the application of the air lubrication method to an actual ship is considered, a use of scavenging gas of main engine for the air injection to a ship bottom is one of promising methods, especially for a deep draft ship. Bondarenko & Fukuda (2018) analysed the main engine plant system under scavenging bypass condition.

Yehia et al. (2019) investigated the drag reduction due to the air lubrication by CFD analysis using Series 60 ship hull and evaluated the drag reduction rate at the full load and ballast conditions. Furthermore, trim optimization is combined under the air lubricated condition. They showed the drag reduction rate increases at optimized trim condition quantitatively.

Super-hydrophobic surface (SHS) is often employed as the measure of drag reduction. Many works on this theme are to clarify the physical mechanism by use of numerical simulation. Here, we review the works focused on marine engineering. Peifer et al. (2020) studied the air injection method with super-hydrophobic surface. This is a kind of basic research to use a flat plate in a wind tunnel. They showed that the lower air injection rate for SHS can achieve the same drag reduction for non-SHS. Katsuno et al. (2018) carried out CFD simulation of flows with super-hydrophobic coating for 2D wing section and marine propeller. They solve RANS equations with k-ω SST with modified velocity boundary condition to aim at considering SHS effect.

Riblet is one of the well-known measures to reduce the frictional drag and once many researchers have studied. Zhan et al. (2017) carried out the numerical simulation of flows with riblet surface and discussed the mechanism of the drag reduction. Chen et al. (2017) studied the three dimensional scalloped riblet by CFD.

For the compliant coating, Delfos et al. (2017) reported their research, however, they could not find out the drag-reduced coating in their research. Very precise measurement of flows around compliant coating is reported by the same group, Greidanus et al. (2017). Schrader (2019) showed that about 3% drag reduction has been predicted in the boundary layer along the hull model of small search-and-rescue boat.

Low frictional hull coating is also another important method to save energy. This method has an advantage of no further installation work for setting appendages to the ship hull. Lee & Park (2017, 2018) showed about 10% decrease of ship speed by use of the frictional drag reduction self-polishing co-polymer (FDR-SPC), applied on 176k bulk carrier. Being annual conference dedicated to the effect of hull coating on ship performance, the HullPIC is worth being paid continued attention. Among many literature, Demirel (2018) gave a notable review on the antifouling marine coating. Goler et al. (2017) gave a notable report on the full-scale energy saving effect of hull coating in this conference.

Frictional drag reduction by active control of micro-objects on the surface is another method. Ge et al. (2017) carried out a numerical simulation of turbulent boundary flows controlled by dimples/pimples distributed on the surfaces and demonstrated the decrease of frictional and total drag reduction and increase of slight pressure drag.

VISCOUS PRESSURE RESISTANCE/HULL FORM OPTIMIZATION

Owing to the rapid development of computers and CFD softwares, researches related to the hull form optimization has been increasing in number. More than 20 works are reported in the present survey of literatures. Many works are on the methodology of hull optimization. Wackers et al. (2018) showed the effectiveness of a multi-fidelity meta-modelling and adaptive local grid refinement method to refine a ship hull form. Scholcz & Veldhuis (2017) demonstrated a $C_b = 0.786$ tanker hull optimization using a surrogate based global optimization to reduce computational time.

Tahara et al. (2019) presented their work on the hull optimization including pre-swirl duct or stator to minimize ship power using multi-objective optimization.

WAVE MAKING RESISTANCE/HULL FORM OPTIMIZATION

Huang et al. (2017) studied a new vortex search algorithm, aiming at avoiding trap in the local optimum solution, and by use of this method, they modified the fore part of KCS hull for the decrease of wave resistance. Liu et al. (2017) also carried out the optimization of the fore part of KCS hull using variance-based sensitivity analysis, Sobol and kriging model-based tensor-product basis function methods. Goren & Calisal (2017) studied to rationalize the design concept of wave resistance reduction and developed a mathematical programming procedure based on Wolfe's algorithm. Guo et al. (2017) modified the ship bow part by adding a retrofitted structure to reduce the ship resistance in waves and carried out CFD simulation to show its effectiveness. Yu et al. (2017) carried out a ship bow form optimization at calm and irregular head waves to achieve 13.2% reduction in the wave-making resistance and 9.5% reduction in the mean added resistance at sea state 5. Yang & Kim (2017) carried out CFD simulation of added wave resistance for VLCC with different type of bow form especially in shot waves and compared with experiment data.

Demo et al. (2018a) investigated a shape parametrization to refine the shape of sonar dome of combatant ship. His group also presented their work on the bulbous bow form optimization (Demo et al., 2018b). Yang et al. (2018) investigated a hull form optimization in order to reduce ship resistance at two different speeds using 3000 ton fishing boat. Raven (2018) showed the aft-body optimization to minimize wave resistance using multi-fidelity technique with a parametric blending of basis hull forms. Raven & Scholcz (2019) also summarized their optimization method. Zhang et al. (2017) investigated an optimization of sonar dome form of DTMB5415 using an improved particle swarm optimization (IPSO). Zhang et al. (2018) also studied the similar problem by use of a non-linear programming method to reduce wave making resistance.

Coppedè et al. (2017, 2018) demonstrated KCS hull form optimization based on a response surface approach. Their group also presented a surrogate model based approach for hull form sensitivity analysis. Wei et al. (2019) optimized the fore part of KCS using reliability-based robust design optimization. Heo et al. (2019) optimized the bow part of KVLCC2 hull form to reduce added wave resistance.

Park et al. (2020) carried out an optimization of hull form design parameters of a small LNG bunkering vessel (SLBV) such as longitudinal centre of buoyancy (LCB), fore-body shape and after-body shape to achieve 9.5% reduction of effective power.

Niklas & Pruszko (2019) demonstrated out a full scale CFD simulation for their newly proposed X-bow form. Another researches applying bow fin (Bøckmann et al. (2018)) or bow flat plate (Liu et al. (2018)) are also reported.

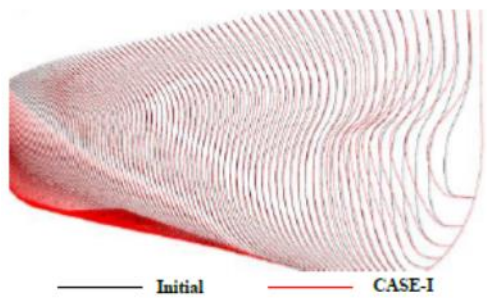

Figure 18: Deformation of invisible bow

Ouyang et al. (2020) worked out the optimization of the bow lines and stern shape of bulk carrier to minimize the wave resistance. The shape of bulbous bow is called invisible bow. The optimized bulk carrier led to about 18% decrease of the residual resistance, 2.3% increase of the frictional resistance and 2.9% decrease of the total resistance.

AIR RESISTANCE REDUCTION

Nguyen et al. (2017) performed the numerical simulation to show the effectiveness of covering loaded containers on a container ship. The containers are fully/partially covered on their side. The numerical results showed up to 50% of air drag reduction is obtained for 30° oblique wind. Majidian & Azarsina (2018) also carried out a numerical simulation of air drag evaluation for 9000TEU container ship. They obtained approximately 25% wind drag reduction at optimal container stack configuration. They also mentioned the relation between the stack configuration of containers and the air drag.

2.3.2 REDUCING PROPULSIVE LOSSES

RELATIVE ROTATIVE EFFICIENCY

Here, the ESDs are categorized into vortex generator, appendages or the hull form modification. Inoue & Saito (2017) investigated the combination of fins separately set around the stern of tanker hull to aiming at getting the target wake pattern at the propeller plane. Furthermore, they combined these fins with pre-swirl duct to enhance the propulsive efficiency. Schrader & Marzi (2017) investigated their special appendages which are set on both side of ship stern aiming to deflect the outer streamlines in the after-body flow field towards the hull surface. Suryateja et al. (2019) studied an asymmetric stern form without adding any appendages using KVLCC2 for model and full scale ship to improve the propulsive efficiency.

ROTATIONAL EFFICIENCY

This category includes pre-swirl stators/duct, rudder bulb, rudder fin, PBCF, CRP and so forth. Quite a lot of researches categorized herein have been carried out. EU performed the project to study ESDs intensively in FP7 project GRIP (Green Retrofitting through Improved Propulsion) project from 2011 to 2015. In this project, pre-swirl stator, duct, rudder bulb and propeller boss cap fin are mainly focused to study. These results are issued in *International Shipbuilding Progress Vol.63, Iss.3-4* as a special issue. In this volume, researches widely spanned in the above ESDs are reported. For instance, the working principle of pre-swirl stator is summarized by Streckwall & Yan (2017), and Schuilling & van Terwigsa (2017). The research of the strength of pre-swirl stator is presented by Paboeuf & Cassez (2017) and Hübler et al. (2017) introduced the retrofitting process of pre-swirl stator. The research of rudder bulb is reported by Coache & Meis Fernández (2017). Hasselaar & Yan (2017) reported the sea trial result with/without the pre-swirl stator and compared with full-scale simulation result. This gives very interesting and important information since the trial result of ESDs is scarcely published in open literature. Hence this issue worth being paid attention.

Besides this project, still many researches in a variety of organizations have been conducted study in relation to ESD. Most researches are involved in pre-swirl duct. Tacar & Korkut (2017) investigated the performance of the pre-swirl duct using 9 geometrically different ducts and showed the most effective duct under equipped on 7000 DWT tanker. Furcas et al (2019) proposed a simulation-based design optimization, SBDO, approach for the design of a pre-duct type energy saving device. Pre-ducts

reduce the wake losses, contribute to a better interaction between the propeller and the hull, and generate an additional thrust.

Wake Equalizing Duct (WED) maximizes the thrust delivered. Results from the design activity show sensible improvement of the overall propulsive efficiency. A Japan bulk carrier has been used to validate. Katayama et al. (2017), Kobayashi et al. (2017) carried out the investigation of the pre-swirl duct, named "Neighbor Duct", whose shape is vertically elongated oval. The experiment and CFD simulation are performed and about 4.4% energy saving in full scale ship is predicted.

Go et al. (2017) numerically simulated the pre-swirl duct and propeller combination in open water condition. Kume et al. (2018) performed to measure the pressure distribution around a pre-swirl duct in self-propelled condition in calm water. In order to do the measurement, they made the special duct model by use of 3D printer in which many built-in pressure holes and built-in pressure-lead small pipes are contained. They showed the difference of pressure on the duct due to the variation of propeller load. In order to develop the design method to obtain the optimal Mewis duct, Chang et al. (2019) carried out the numerical simulation of propulsive performance with the systematic variation of fan shape of Mewis duct and with systematic variation of duct location.

Kim et al. (2020) carried out a very interesting work. They investigated the roughness effect in full scale ship equipped a combined ESD of pre-swirl fin and duct. They show that the ESD performance decreases as Reynolds number increases, in other words, ESD performance at full scale ship decreases from that at model scale. However, if we consider the effect of roughness at full scale, ESD performance increases. This means that the effect of the roughness is very important to estimate the ESD performance at full scale ship.

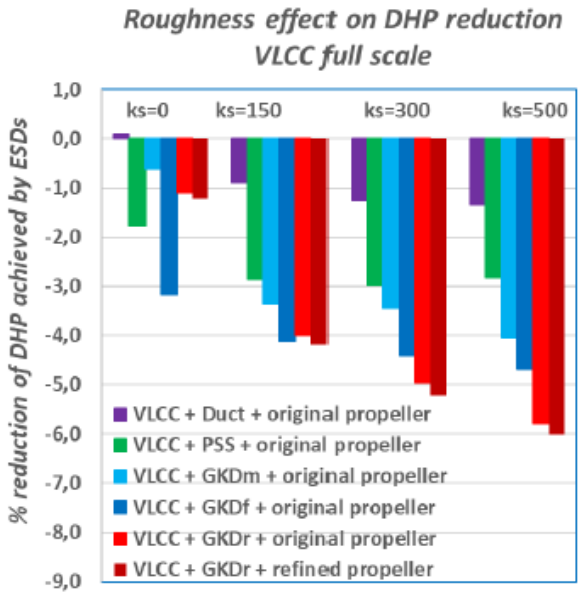

Figure 19: Possible DHP reduction predicted for different ESDs at varying rough surface conditions

Ikenoue et al. (2020) investigated the scale-up method for a pre-swirl duct. They compare the results from traditional scale-up method with those from direct full scale CFD method and show that the importance of the CFD simulation to evaluate ESD for the full-scale ship.

Next topic is the pre-swirl stator. Kim et al. (2017) proposed an extrapolation method for the analysis of self-propulsion test with a pre-swirl device. Due to the concerns on global warming and the establishment of the EEDI, energy saving devices are now widely employed. It was stated that the ITTC 1978 scaling method is not adequate for the prediction of ship performance for pre-swirl device because the counter swirl component results from inviscid mechanism. In this paper, an alternative scaling method to consider separately viscous axial wake and inviscid tangential wake is proposed.

Voermans (2017) analysed an energy saving device, pre-swirl stator, commercially known as Wärtsilä Energy Flow, which gives sufficient power reduction and fulfils structural requirements. Ease in the installation will lead

to a wider utilization. The results of CFD analysis show that the generated pre-swirl considerably increases the propeller blade efficiency in the quadrant of the upcoming blade.

Figure 20: An example of Pre-swirl stator, Voermans (2017)

Król et al. (2017) introduced a design system for the pre-swirl stators and propeller developed at Ship Design and Research Centre (CTO). Zhou et al. (2018), and the same group (Nian et al., 2019) carried out the experiment and CFD simulation for the pre-swirl stator, named Y-Fin, in the condition of calm water and waves and showed the features of ESD in waves. Krasilnikov et al. (2019) carried out the full-scale CFD simulation for different type of three pre-swirl stators and considered the mechanism of the performance difference.

Nielsen & Wei (2019) presented a novel device named as controllable pre-swirl Fins (CPSF), placed in front of the propeller and arranged in such a way that they can be adapted to different operating conditions by optimizing their pitch and flaps settings. In order to analyse the kinetic energy in the hull wake, four sections across the hull are selected. The CFD model scale optimization results were then validated against an extensive and dedicated series of model tests in a towing tank. The subsequent tests were used to determine the optimum flaps angles. CPSF could lead to savings of the delivered shaft power by about 3-4% in case of the selected bulk carrier used for validation. Jin & Nielsen (2020) also studied the energy saving for CPSF experimentally and numerically. They further designed propellers with different propeller rake and obtained up to 4% energy saving with CPSF and newly designed propeller.

Contra-Rotating Propeller (CRP) is one of well-known energy saving methods by recovering propeller rotational wake. A pod type CRP (POD with each propeller is equipped on both end side of POD) is studied numerically by Su et al. (2017), Hou & Hu (2018), Hou et al. (2019). Sánchez-Caja et al. (2017) carried out the numerical investigation for Tri-CRP-POD (POD with one propeller is equipped on one side of POD and tandem two propellers are equipped on the opposite side) system. These works are conducted in the open water condition. Güngör (2017) presented a design process of CRP equipped after torpedo-like body of revolution. Quereda et al. (2017) explained a CRP-POD propulsion system concept and the challenges related to testing at model scale. The full power is divided in two parts with different percentage of the total power. The methods to carry out resistance, open water and self-propulsion tests were elaborated. Energy saving with the configuration were compared with conventional propeller for an 8,500 TEU container ship with 8% to 10% power saving being attained.

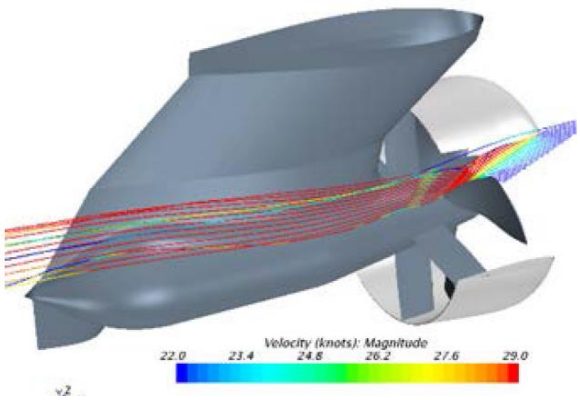

Figure 21: Ducted POD propulsor, Veikonheimo et al. (2017)

Veikonheimo et al. (2017) presented a method for the full-scale extrapolation of model

scale measurements on a multi component podded propulsor. The scaling is based on model tests in which nozzle and stator propeller and the unit forces were measured. Those can be extrapolated separately with the aid of actuator disk theory and CFD computations.

Quereda et al. (2019a) reported the advantages of the CRP-POD propulsion system in comparison with the traditional propulsion, based on the analysis of the results of the tests carried out with models in the CEHIPAR facilities. In recent years, the incorporation of the aft propeller in a POD unit not only avoids mechanical problems related to co-axial shafts but also allows the POD housing to act as a rudder. The traditional rudder has disappeared, the efficiency has increased and better manoeuvrability has been obtained in both azimutal-POD and rudder-POD configurations. Advanced propellers design methods, based on numerical calculations, permit to obtain high efficiency propellers, as tip rake, CLT propeller among others. Future merchant ships, provided with CRP-POD propulsion system, will produce low CO_2 emissions to the environment.

Krasilnikov et al. (2017) investigated, by means of CFD, the problem of scale effect for the two offshore vessels equipped with twin pod propulsion systems, featuring dual-end propellers which operate in counter-rotating (CRP) and co-rotating (TANDEM) modes. The effect of Reynolds number on vessel towing resistance, propulsor open water characteristics and vessel propulsive performance was investigated.

Inukai & Ando (2017) presented a new performance prediction method for a ship with contra-Rotating propellers (CRP). The main features were to treat CRP as a combination of two single propellers and to consider the mutual interaction between the aft and forward propeller adequately. To verify a validity of the method, self-propulsion factors of propeller working in a simplified flow were analysed at first. Full scale delivered power was estimated for a VLCC with various methods and the difference was analysed. The estimated power-speed curves with those obtained by sea trials were compared to show a satisfactory agreement.

Chen et al. (2020) carried out the CFD simulation for the vane wheel propeller with different blade numbers and showed the dependence of blade number on the propeller performance and the vortical flow field.

Cai, H-P et al. (2019) proposed a general numerical method of predicting hydrodynamic performance of ducted contra-rotating propeller, DCRP. This method was based on the solution of unsteady RANS equation with the SST, k-ω turbulence model, employing the sliding mesh model to simulate the unsteady interaction between the two blade rows of the CRP and in the gap between the CRP and surrounding duct. Numerical predictions were carried out for a DCRP and results were compared with experimental data.

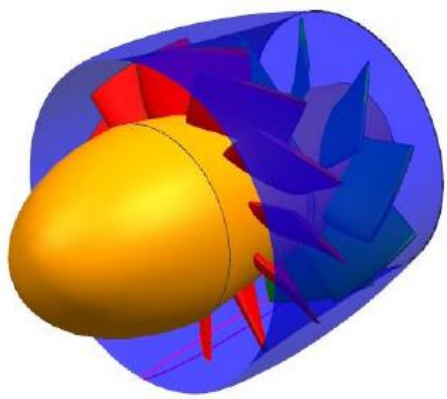

Figure 22: DCRP, Cai et al. (2019)

PBCF also has been often studied as an energy saving device for many years. Mizzi et al. (2017) demonstrated an approach to design PBCF in the open water condition by use of CFD analysis in both model scale and full scale. Xu & Wan (2018) also analysed PBCF in full

scale condition. Zhang et al. (2019) analysed PBCF under different section geometries. Gaggero (2018) and Gaggero & Villa (2018) presented an optimization method for PBCF. These works were all performed under open water condition. Kimura et al. (2019) studied the test method for the propeller with PBCF in order to evaluate full-scale performance of PBCF correctly. They also showed the enhancement of energy saving effect by means of suitable combination of PBCF and other ESDs.

Rudder bulb fin is another popular ESD which converts the rotational propeller wake to thrust. Many works have been reported on this topic. Truong et al. (2017) carried out PIV measurement and CFD simulation to investigate the energy saving of rudder bulb fin equipped on KVLCC2. Truong et al. (2018) subsequently reported the result of an improved rudder-bulb fin, an asymmetric fin. Similar work was done by Huang et al. (2019), however, they also investigated the strength of bulb-fin for its design. Hori et al. (2017) studied the improvement of propulsive performance by the combination of pre-swirl duct, the rudder bulb fin and twisted rudder, by numerically and experimentally. Wang et al. (2017) numerically studied the performance of rudder bulb-turbine in open water condition.

Ship owners have come to seek a more fuel-efficient ship operation at lower cost. With the advent of EEDI regulations, ships are installed with several energy saving devices but the amounts of the fuel consumption from synergistic effects are sometimes unclear at the design stage. Okada et al. (2017) and Tachikawa et al. (2019) presented the experimental work for the improvement of propulsive efficiency by combination of Ultimate rudder, propeller boss cap and pre-swirl duct, here Ultimate rudder is a kind of rudder bulb whose top almost touches to the propeller boss cap. They reported up to 8.7% energy saving in the model test. They also investigated the reduction of radiated noise with the combination of ESDs. Htay et al. (2020) worked out CFD simulation to investigate the feature of propulsive performance of KVLLC2 equipped with rudder-bulb fins (RBFS) in waves. They showed the self-propulsion factors at different incident wave length and obtained that the propulsive efficiency increases with RBFS at longer incident waves.

Klose et al. (2017) analysed different prediction method for tip raked propellers. Effect of Reynolds number was taken into account because it is necessary to ensure a fair comparison with different propeller designs. As a consequence of the analysis they developed an improved Reynolds number correcting method. Shin et al. (2017) compared the open water characteristics of tip modified propeller and conventional propeller designed for the same operating condition, by means of CFD. Model scale computations were performed using a larminar-turbulence transition model. Fully turbulent flow is considered for full scale computations. They concluded that the effects of the transition model show that laminar and transitional flow modelling is crucial in model scale computations. Lee et al. (2017) also studied the improvement of energy saving effect by combining several kinds of ESDs, such as twisted ruder, wavy twisted rudder, tip rake propeller and pre-swirl stator equipped on a container ship. Their test result showed up to 5.4% energy saving.

Pérez-Sobrino et al. (2016a) presented the so called SISTEMAR strip method in detail. The summary of the method is to obtain the OWT corrections by integration of the corrections obtained at each blade and eventually end plate sections. Taking into account the Reynolds number values on each section, the influence of the flow around the propeller sections was considered to analyse the corrections on different flows, laminar, turbulent and transitional zone on the blade surface. Quereda

et al. (2019b) published a paper related to the validation of the strip method procedure by analysing a comprehensive set of OWT results, both for conventional and Contracted and Loaded Tip (CLT) propeller. They addressed that the strip method is practically equivalent to the application of ITTC'78-PPM for calculation of OWT scale effects of conventional propellers.

Kanemaru et al. (2017) proposed new types of rudder to aim at enhancing the propulsive performance. Two types of rudders were considered; one is the swept back rudder and the other is the high thrust rudder which has U-shaped notch at the leading edge of rudder at propeller boss positon.

Rear stator is the device to recover the propeller rotational wake to the thrust. Feng et al. (2019) performed the CFD simulation of the rear stator just behind the ducted propeller working in the open water and evaluated the propulsive performance of this combined propulsor.

AXIAL EFFICIENCY

Shin & Andersen (2017) numerically investigated the scale effect of tip modified propeller in the open water condition and compared with the performance of a conventional propeller. For the podded propeller, Zhai et al. (2017) studied the optimization of casing form to increase the propulsive performance. González-Adalid et al. (2018) investigated the full-scale propulsive performance of Contracted and Loaded Tip (CLT) propeller retrofitted on 175,000 m^3 LNG tanker and reported about 8% power saving compared with conventional propeller.

Researches on the ducted propeller can be found in SMP'17, NuTTS'19 and Ocean Engineering. Among others, Gaggero et al. (2017) and Remaud et al. (2019) are worth being mentioned, in which the relation between the propulsive performance and the sectional shape of duct is investigated.

Recently, Sasaki et al. (2016) carried out the research on "Gate Rudder", which is twin rudder system located aside propeller. Although a 6-8% energy saving from the tank test was reported, the raw results of tank test itself is not shown in the paper. Sasaki et al. (2018) demonstrated the effectiveness of Gate rudder by showing the sea trial result with sister ships, one is equipped with a conventional rudder and the other equipped with the Gate rudder. They stated 14% energy saving at Gate rudder. Sasaki et al. (2019) subsequently showed the voyage data of the sister ships to demonstrate the effectiveness of Gate rudder. They tried to clarify the reason of discrepancy and mentioned that the discrepancy would be due to the scale effect. Tacar et al. (2019), carried out the full-scale CFD simulation for Gate rudder. According to their computation, the propeller efficiency is not improved itself by setting Gate rudder, but, large energy saving at Gate rudder equipped on the ship is obtained by comparing the numerically simulated power curves. The 14% energy saving for the actual ship is a tremendous value, but seems to be still too large since the model ship gain shows up to 8% energy saving. Much more disclosed data and discussion seems to be necessary and at the same time, the research at other organizations would be expected.

2.3.3 PROPELLER DESIGN

The search for increasing propulsive efficiency of ship propellers leads to the criterion of propeller blades with unconventional geometries like CLT and Tip Rake propellers. Sánchez et al. (2019) examines the effect of different tip configuration on the performance of the propellers. The tip region cannot be described with the traditional profiles' sections. Cylindrical surfaces have used to define it. Viscous flow simulation such RANS

and Detached Eddy Simulation (DES) were used to asses a generic test case. In order to reduce the frictional resistance acting on the propeller blade, a small area blade propeller is proposed as an effective measure. Lücke et al. (2017) summarized the test method and CFD simulation for a small area blade propeller. Tip modified propeller was also developed aiming at the increase of propulsive efficiency. Segawa et al. (2019) showed the method of optimum design of propeller which acts behind a pre-swirl duct as well as uniform flow. Kang et al (2019) employed a Kappel propeller, CLT propeller and Tip Rake propeller for the analysis. The parametric study for the optimum rake shape was conducted and the performance of the final design was verified by CFD and model tests. Zhang et al. (2020) also carried out the numerical simulation to investigate the propeller performance and propeller flow field for CLT propeller and Kappel propeller.

2.3.4 USE OF RENEWABLE ENERGY

As one of energy saving methods using wind energy, here, a couple of works for a kite and Flettner Rotor are briefly introduced. More detailed review can be found in chapter 4. Duport et al. (2017) investigated the aerodynamic performance of kite using lifting line theory and RANS simulation. Turan et al. (2018) investigated the methodology of the optimal weather routing of the ship equipped Flettner Rotor.

The use of wave energy is another method. Matusiak & Rautaheimo (2017) carried out a feasibility study to use hull fins which convert wave energy to thrust. Chiu e al. (2018) studied on the active controlled bow fin on the ship going in irregular waves to augment the ship propulsion by converting the wave energy to the propulsive power.

2.3.5 OPERATION

Pertaining to the research of weather routing, review papers are mainly deal with the evaluation of methods of route optimization. Wang et al. (2017) compared Isochrone/Isopone algorithm, 2D/3D dynamic programing and Dijkstra algorithm for a North Atlantic route. Wang et al. (2018) also reported a study of route optimization using genetic algorithm. Zaccone et al. (2018a) investigated a voyage route optimization between near Denia, Spain and Geneva, Italy in consideration of the ship propulsive performance under real weather condition. Zaccone et al. (2018b) also studied a route optimization at North Atlantic route. Lin et al. (2018) showed the particle swarm optimization for a voyage route optimization. They applied this method to the route between Keelung and San Francisco. Orlandi et al. (2018) introduced PROFUME Demonstrator developed under ESA ARTES Integrated Applications Promotion (IAP) Project, which optimize a voyage route to minimize fuel consumption using on-board collected data. Mannarini et al. (2018) demonstrated a route optimization by refereeing EEOI for a North Atlantic route.

As another optimization of the operation, recently the study of trim optimization has been increasing in number. Liarokapis et al. (2017) carried out the experiment under several conditions combined by different displacement and trim angle. They used a model of high-speed small passenger vessel with chain. Drouet et al. (2017) investigated the trim optimization for a container ship at different sea state conditions as well as at calm water condition and showed that the optimal trim mainly depends on the draft and the sea-state. Braidotti et al. (2018) studied an optimal ballast water allocation system for the reduction of fuel consumption and demonstrated its effectiveness. Sogihara et al. (2018) evaluated the energy saving by taking the optimal trim in a sample voyage. Duan et al.

(2019) carried out CFD simulation to show the relation between the ship resistance and trim for VLCC at design and ballast conditions. Wang et al. (2020) investigated numerically the flow field and propeller forces at several different trim conditions for ONR tumblehome ship model 5613. Fan et al. (2020) investigated numerically the difference of ship resistance at the different trim conditions for a bulk carrier.

As a unique method, Makino et al. (2017) proposed to control the propeller pitch angle optimally when the ship goes in waves to reduce total propeller power.

2.3.6 OTHERS/DESIGN

Simulation based design system has been continuously studied at several organizations. Huang et al. (2017) investigated a homotopy method to optimize a container ship hull form in order to get a target wave resistance. Van der Ploeg et al. (2018) showed a method to deform the stern shape of container ship equipped a large area propeller, then the original stern has a tunnel stern, by adopting stern asymmetry concept. Wei et al. (2019) studied the resistance of four hull forms for high speed wave-piercing mono-hull ship at calm and incident wave conditions using CFD simulation. Ichinose et al. (2019) summarized a design system to optimize ship propulsive performance and cargo capacity by showing the sample simulation using 62k bulk carrier. Ichinose & Tahara (2019) also introduced a hull form design system based on a database utilization to obtain a target wake. Xiong et al. (2019) applied a tunnel stern form with edge to a cruise ship and 2.6% of power reduction at design speed can be expected.

Krieg & Mohseni (2017) investigated a new concept of an underwater vehicle which utilizes a set of novel cephalopods inspired pulsed jet thruster. They suggest that the efficiency of this type of propulsor may be significantly higher than previously. There are many works to do, due to viscous dissipation of kinetic energy prior to measurement of the wake energy.

3. USE OF WIND ENERGY

3.1 BACKGROUND

According to recent estimates, global shipping emits on average about 1 billion tonnes of carbon dioxide (CO_2) on an annual basis, equivalent to over 3% of the global anthropogenic CO_2 emissions. These figures are expected to increase significantly in the future despite market-driven and regulatory efficiency improvements, just due to the growth of the sector. Measures that can significantly reduce the CO_2 emissions of the shipping sector will, therefore, have a crucial role in the future.

Several measures have been identified, or even applied, with the potential to achieve substantial emission reductions, like slow-steaming, bio-fuels, and alternative propulsion technologies. Slow steaming has been already analysed to a great extent, whereas bio-fuels have raised concerns about environmental impact and availability. Among alternative propulsion technologies, a resurgence on wind-assisted propulsion is observed in recent years, primarily due to its high-potential for fuel consumption and emission reduction.

Wind power is currently being developed through both conventional sails and modern alternatives. These include Flettner rotors, kites or spinnakers, soft sails, wing sails and wind turbines (Parker, 2013). The compatibility of different designs varies between ship classes due to potential interference with cargo handling (Parker, 2013; Traut et al., 2014). However it is known that any current design alone cannot provide the typical ships propulsive power demand, but high wind speeds typically encountered in high seas (Staffell & Pfenninger, 2016) can allow for significant fuel savings,

whilst maintaining full speed (Halim et al., 2018; Hirdaris & Cheng, 2012). Furthermore, research has shown that wind propulsion is most effective at slower speeds (e.g. less than 16 knots), and on smaller ships (3,000 - 10,000 tonnes) (Smith et al., 2016), which account for one-fifth of global cargo ships.

Various studies have estimated fuel savings across a wide range: 2-24% for a single Flettner rotor, 1-32% for a towing kite (Traut et al., 2014), up to 25% for the eConowind sails (which pack into a single container) (Traut et al., 2014) and some estimate savings from 10 to 60% at slow speeds (Smith et al., 2016). These results prompted several shipping companies to add sails to cargo vessels (Smith et al., 2016), however gradual uptake is not predicted until 2025, due to their relative immaturity of the market (Parker, 2013). Additional barriers for the wide adoption of these solutions in the industry have been identified by the scientific community, such as unfamiliarity with technology, safety and reliability concerns, and lack of demonstration (Rehmatulla et al., 2017). Of equal importance is the fact that no data on capital costs were found for the installation of wind assistance systems as they are at an early stage of development, but the potential fuel savings are large and further research is required to determine cost-effectiveness under different operational conditions and ship types.

3.2 WING SAILS

Jo et al. (2013) investigated the performance of multiple wing sails to enhance ship thrust. They solve the flow around the wings using Computational Fluid Dynamics (CFD) to evaluate the generated thrust. (Ouchi et al., 2013) introduced a new concept of wind sail ship ”Wind challenger”, in which the motor-assisted auxiliary system is applied, and they carried out a voyage simulation and evaluated the energy-saving rate of ”Wind Challenger”. Viola et al. (2015) developed a velocity prediction program for ships with propulsion assisted by wing sails. They used the ratio between the propeller thrust of a ship with and without wings as a measure of the energy efficiency and showed the possibility to reduce the propeller thrust of a KVLCC2 by up to 10% in cross winds. They concluded that the efficiency of the wing sails is crucial to achieving minimum savings with high aspect ratio wings performing best.

3.3 TOWING KITES

Naaijen & Koster (2007) performed a theoretical analysis of potential fuel savings for a kite propulsion system. The study included the effect of the propeller running in an off-design condition, and concluded that the additional resistance due to leeway angle is small. Dadd et al. (2011) assessed different kite trajectories, and they produced performance polar diagrams for a 300 m^2 kite, assessing various operational parameters, such as aspect ratio and flight angle. Fagiano et al. (2012) investigated a high altitude kite system (200-600m) which is designed to generate electricity as the line is pulled as well as produce thrust, which can then be winched in during a de-powered condition producing a net energy production. Leloup et al., (2016) developed a performance prediction program, dedicated to merchant ships, in order to assess the fuel savings abilities of a kite. They concluded that using a 320 m^2 kite on a 50,000 DWT tanker, the fuel savings predicted were about 10% for a Beaufort 5 sea state, and could reach values of 50% for wind velocities corresponding to a Beaufort 7 sea state. Leloup et al. (2014) developed a 6 degree of freedom sailboat dynamic simulation model, to evaluate kite performance in comparison with classical rig sailing. Their comparative results indicated that the boat towed by kite could achieve a significantly superior sailing performance.

3.4 FLETTNER ROTORS

The most studied technology on wind-assisted propulsion is Flettner rotors. Pearson (2014) developed a model for assessing the performance gains from Flettner rotors and performed an initial assessment of the viability of retrofitting them to a specific ship. Craft et al. (2014) assessed Flettner-Thom rotors using RANS and LES with comparison to experimental data. They concluded that the Thoms multiple drums affected the boundary layer at low Reynolds numbers to improve the lift coefficients achieved. Lu & Ringsberg (2020) developed a four degree-of-freedom ship performance prediction model, to perform a parametric study of the Flettner rotor technology. The results showed that fuel savings ranging between 5.6% and 8.9% were achievable. The authors also underlined the sensitivity of the results with respect to vessel speed, voyage routes and weather conditions. Other effects on the performance of Flettner rotors were identified in the work of Bordogna et al. (2020). The study indicated that the aerodynamic performance of the two Flettner rotors was affected by their interaction, and generally, the effect is more noticeable when the devices are set closer to each other and are in alignment with the wind direction. Copuroglu & Pesman (2018) investigated the effects of Flettner rotors on the roll motion of ships and, subsequently the effects of roll motion on the performance of the rotors themselves.

3.5 IN-SERVICE GAINS

Cui et al. (2016) developed performance prediction software that allows different wind assistance devices to be assessed. They assessed modern square rigged sails (DynaRig), rotors and kites on one coastal and one ocean route. They results showed that sails and kites delivered between 9-10 % fuel savings whereas Flettner rotors provided 23%. Little difference was observed between the two routes. However, both had similar mean true wind speeds. Traut et al. (2014) used numerical models of a Flettner rotor and a towing kite to assess their performance over five different trade routes concluding that different technologies performed better on different routes. Bentin et al. (2016) assessed the optimal routing of a conventional multipurpose cargo ship with Flettner rotors operating in the north Atlantic and predicted energy saving between 20-50% depending on ship speed and wind conditions. Argyros (2017) provides a review of wind assisted shipping, summarising quoted energy saving potential of different technologies and a cost analysis of payback periods for different fuel prices, fuels savings and capital investment required. They concluded that wind assistance is one of the few technologies that has the potential to provide double digit fuel savings. Caughlan (2016) also provided a summary of wind assisted technologies concluded that a mean energy saving potential of 20% might be achievable.

3.6 CONCLUSIONS AND FUTURE TRENDS

The sustainability of the shipping industry, like any other industry, largely depends on the elasticity of demand for the service and the profitability through the minimisation of the operating costs. These costs in the past have largely depended on the price of marine fuels, but with environmental concerns now being in the forefront, this is subject to change. The assessment and understanding of the interdependencies and effects of environmentally optimised solutions and emission mitigation policies, along with the adaptation of more fuel efficient solutions will be paramount.

As a consequence, research on environmentally sustainable marine propulsion

solutions in recent years has been intensified, to address precisely these issues. Wind energy was one of the key sources of propulsive power on ships in ancient times. However as a renewable, abundant and free source of energy, it has not been adequately exploited by the shipping industry in recent times. Wind-assisted propulsion for the marine sector has the potential of being the ”old but beneficial” technology that could allow significant fuel and emission reduction (Talluri et al., 2016). As research studies suggest, compared to other renewable solutions, it has the advantage of being always available in the open sea, and it may be retrofitted on an already existing ship, as an alternative source of power.

The research community is in agreement that wind-assisted propulsion technologies can have a positive impact on the fuel consumption and emissions of commercial ships, however the fuel savings achieved are hard to quantify, as they are sensitive to a number of factors: Ship type and dimensions, operating speed, voyage route and corresponding weather conditions. Scientists and research engineers are actively advancing the related technologies and are developing the necessary computational frameworks to assess the technical, environmental, and economic feasibility. However, ship owners and operators are mostly concerned with the technical risks involved, and the hidden costs of a not yet matured technology (Rehmatulla & Smith, 2015). As such, the demand for, and importance of, holistic analyses that quantitatively establish the benefits of these solutions, and de-risk the technology at a preliminary design phase, is higher than ever, and is not expected to decrease in the future.

4. CFD, EFD AND SCALING METHODS

4.1 CFD METHODS FOR ESD

4.1.1 REVIEW OF TOKYO 2015 CFD WORKSHOP

The Tokyo 2015 Workshop on CFD in Ship Hydrodynamics was held at National Maritime Research Institute (NMRI) in Tokyo on 2-4 December, 2015. The purpose of the workshop was the same as the preceding workshops and it was to assess state-of-the arts of the contemporary CFD codes for ship hydrodynamics. In the workshop, three ship hulls were selected and a total of 17 test cases were specified by the organizers. 30 groups submitted their computed results for one or more cases.

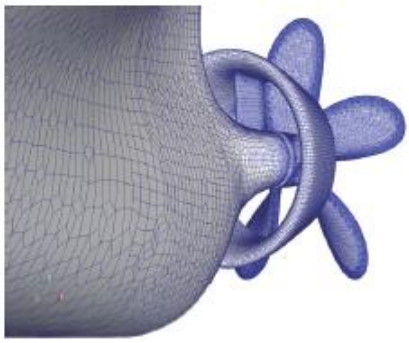

Figure 23: Surface mesh of the ESD considered for JBC in Tokyo 2015 CFD workshop (Shen and Korpus, 2015)

Among three ship hulls under consideration, the Japan bulk carrier (JBC) was associated with ESD (see Figure 8). CFD simulation on resistance and self-propulsion performance were carried out either with ESD and without ESD. The validation and verification (V&V) results drew attention of the committee, because they can shed some lights on the overall level of accuracy of CFD simulation. Comparison of numerical errors between the case with ESD and without ESD would imply how adequately the

state of the art CFD simulation deal with the propulsive performance of ESD. In this regard, the V&V results for the JBC case 1.5a (without ESD) and the JBC case 1.6a (with ESD) are compared.

The first comparison is made in Figure 9, which plots the values of comparison error $E\%D = (D - S)/D \times 100$ of the thrust coefficient K_T in the self-propulsion condition for without ESD and with ESD. Here, D and S refer to EFD and simulation value, respectively. Figure 10 plots the grid uncertainty U_G involved in the prediction of thrust coefficient K_T in the self-propulsion condition for without ESD and with ESD. In both figures, the relative magnitude of numerical error and the grid uncertainty between with and without ESD vary depending on simulation cases, *i.e.*, in some cases errors without ESD is larger, but in other cases, *vice versa*. This means that the presence of ESD does not affect significantly the simulation accuracy and the uncertainty. Depending on the CFD code considered, there appears a large variance in the accuracy and the uncertainty. Similar behaviour is found for the total resistance coefficient C_T and the torque coefficient K_Q as well. If the cases with ESD had presented unambiguous increase in the level of CFD error and uncertainty over the counterpart cases without ESD, then it would have been reasonable to conclude that the state of the art CFD technique was inadequate for the ESD, which would necessitate a particular, dedicated CFD procedure for ESD. The results, however, indicate that there is no such inadequacy.

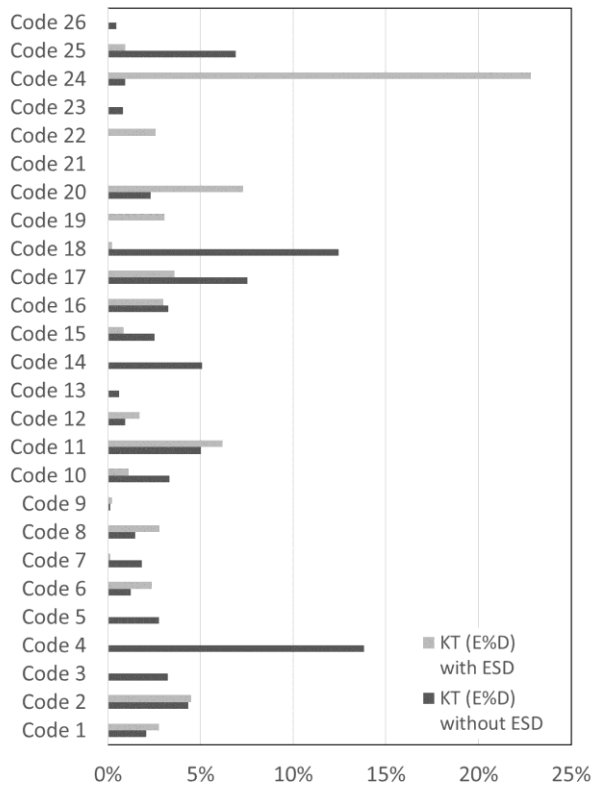

Figure 24: Comparison of % error in thrust coefficient K_T in Tokyo 2015 Workshop

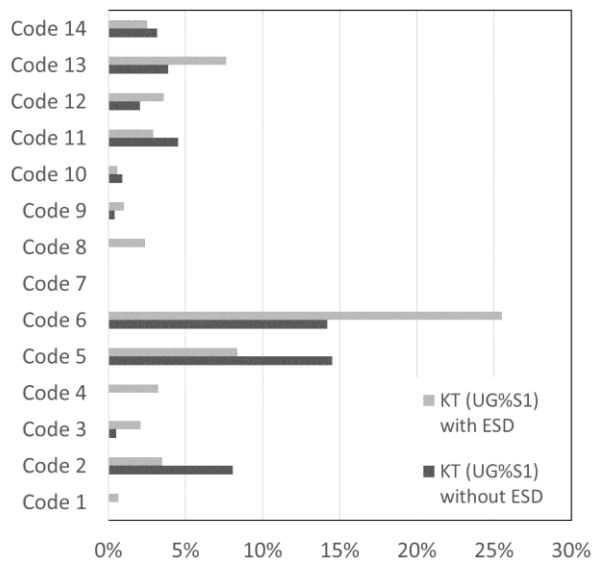

Figure 25: Comparison of the grid uncertainty associated with thrust coefficient K_T in Tokyo 2015 Workshop

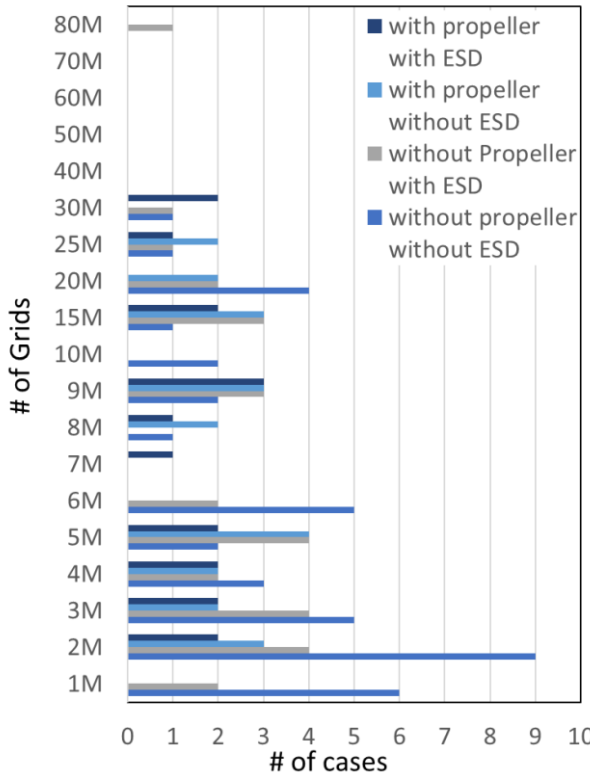

Figure 26: Distribution of the number of grids in Tokyo 2015 Workshop

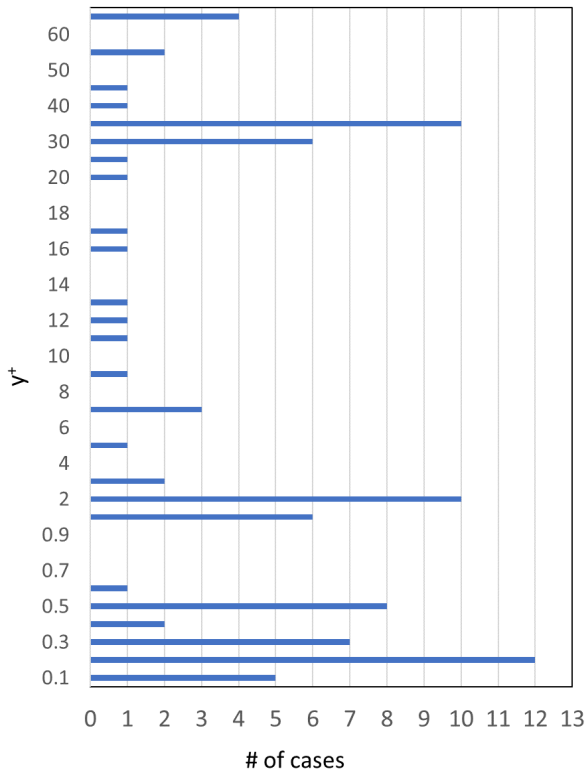

Figure 27: Distribution of the values of y^+ in Tokyo 2015 Workshop

The next review topic of Tokyo 2015 Workshop is the statistics of CFD parameters, which can give an idea on the best practice of CFD. The parameters under considerations are; the number of grids, the wall-normal coordinate of wall function y^+, the minimum and maximum location of the computational domain. Values for those parameters in all cases were compiled through questionnaire by the organizer of the Tokyo 2015 Workshop on CFD and the statistics of such parameters are plotted in Figures 11 through 14.

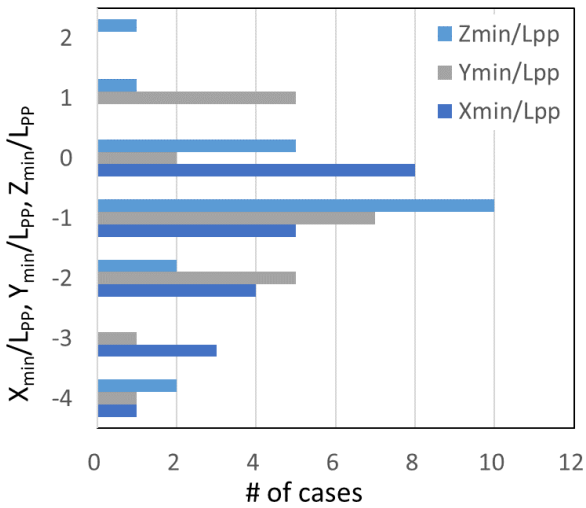

Figure 28: Distribution of minimum values of computational domain

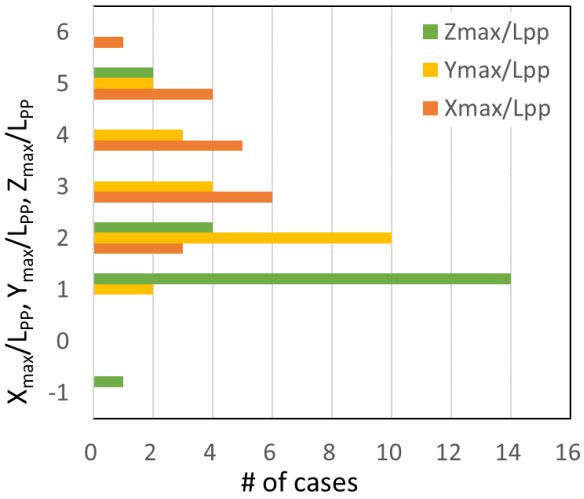

Figure 29: Distribution of maximum values of computational domain

4.1.2 REVIEW OF THE PROPOSED CFD GUIDELINE FROM PRADS 2016

Hino et al. (2016) presented a benchmark data for the validation of CFD simulation results for a Japan bulk carrier (JBC) equipped with an energy saving circular duct. As a matter of fact, this case coincides with the JBC case with ESD in Tokyo 2015 Workshop on CFD. In addition to the benchmark data based on a stereoscopic particle image velocimetry (SPIV) measurement, they proposed a "Guideline for CFD Analysis of a Ship with ESD".

Aimed at identifying the necessity to setup a separate guideline dedicated to ESD simulation, the committee had it reviewed by CFD experts in academia and industry. The guideline section in Hino et al. (2016) was compared with the following ITTC guidelines related to CFD;

- ITTC (2014a) 7.5-03-02-03 Practical Guidelines for Ship CFD Applications.
- ITTC (2014b) 7.5-03-02-04 Practical Guidelines for Ship Resistance CFD.
- ITTC (2014c) 7.5-03-03-01 Practical Guidelines for Ship Self-propulsion CFD.

It was found that some of the statements in the proposed guideline are not included in the existing guidelines. On the other hand, it also can be said true that those suggestions are largely well-known in the CFD community. In addition, it is hard to ascertain that the guideline by Hino et al. (2016) took into considerations for the relevant aspects of diverse types of ESDs, because only the circular duct was dealt with. Considering these points, the committee concludes that it is premature to setup a CFD guideline dedicated to ESD in the absence of reliable database of CFD as well as EFD results for various kinds of ESD.

4.2 EXPERIMENTAL METHODS FOR ENERGY SAVING METHOD

4.2.1 SUMMARY ON LITERATURE ON MODEL TESTS PROCEDURE

In order to reduce greenhouse gas emissions, various energy-saving devices are used on ships. Due to the influence of various factors such as technology and economy, there are many market applications, such as pre-swirl with duct (e.g. Becker Mewis Duct[○,R]), Pre-Swirl Stators, propeller boss cap fin (PBCF), rudder ball, etc. In the design of these energy-saving devices, CFD technology is widely used to evaluate the energy-saving effect and optimize the design scheme. However, in order to prove the energy-saving effect of the above-mentioned energy-saving devices (ESD) in the use of commercial ships, it is generally required to carry out model test verification. At the same time, when the classification society certifies the EEDI certificate, it will ask for the supporting documents for ESD's effect. Therefore, in the foreseeable future, model tests verification or other type of experimental is an indispensable way of EEDI index certification, especially for ESD with complex flow field.

PRE-SWIRL STATORS AND PRE-SWIRL WITH DUCT

Although the research on ESD has researched for decades, the test procedures and extrapolation methods for ESD are still in constant updating. At present, the method proposed by The Specialist Committee on Unconventional Propulsors in 1999 (22nd ITTC) is widely used for the Pre-Swirl Stators and pre-swirl with duct, the ESD in front of the propeller. This method needs to conduct model tests with and without ESD respectively, but in order to save cost in actual commercial projects, sometimes only one design draft condition can complete the both tests with and without ESD. The prediction in other draft conditions refer to the design draft for wake correction. According to the relevant literature, the difference of effect in different draughts is not so much.

PBCF & RUDDER BULBOUS FIN

Another controversial issue is the scale effect of PBCF. At present, the common practice is to conduct the propeller open water test with and without PBCF in the cavitation tunnel respectively or do the normal POT and reverse POT in the tank.

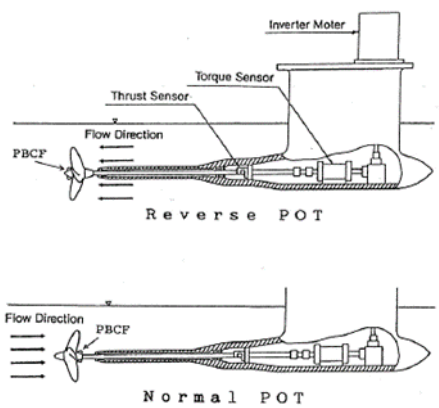

Figure 30: Arrangements of Normal POT and Reverse POT (Hansen et al., 2011)

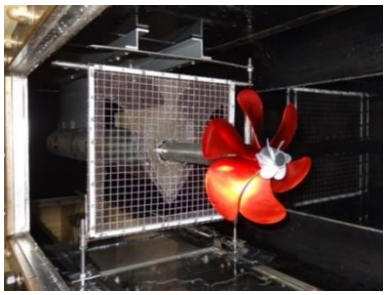

Figure 31: Arrangement of Wire mesh screen (Kimura et al., 2019)

Different from the general method in uniform wake test, Kimura et al. (2019) evaluated the full scale energy saving effect of PBCF by reversed POT with wire-mesh screen method and took account to simulate the ship wake.

The PBCF efficiency in full scale will be verified by the full scale ship monitoring data. According to the relevant literature (Ouchi & Tamashima.,1989), full-scale will be 2 to 3 times greater than the model scale predictions.

At present, 3D printing technology has been widely used in the manufacture of ESD. It is not only reducing the cost of model manufacture, but also saving much time compared with the traditional NC drilling method. However, the material for 3D model manufacture needs to consider that which be less water absorption and expansion. In addition, the model with fin, such as PBCF and pre-swirl stator, should be paid attention to the thickness at the edges to ensure that there is no deformation.

Figure 32: Various hub caps with fins (Müller et al., 2017)

Based on KVLCC2 Tanker, Truong et al. (2017) studied the rudder bulbous fin system with EFD and CFD methods. After optimizing the angle of attack for fin, the energy saving effect can get more than 2%.

Figure 33: Rudder bulbous fin system (Truong et al., 2017)

CRP-POD PROPULSION SYSTEM

Various forms of counter rotating propulsion systems are effective energy-saving propulsion systems. The CRP-POD propulsion system configuration including two different propellers arranged in the same geometrical shaft with a short distance in between them and rotating in opposite sense but with a specific driven system. Hull resistance test is carried out in the same as any other propulsion configuration because this propulsion system is considered as a unit. The extrapolation method for this CRP-POD system based on the guidelines of the existing ITTC standard procedures has been proposed by Quereda et al. (2017).

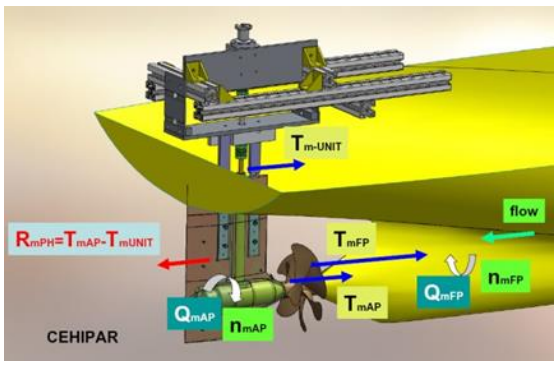

Figure 34: Arrangement to carry out self propulsion test (Quereda et al., 2017)

AIR LUBRICATION

Air lubrication is resistance reduction is also a hopeful method to save energy. There are three options of air application to reduce ship resistance: thin air layer, air bubbles and artificial air cavity system. The air bubble and air cavity techniques have been tested in full-scale conditions. Silberschmidt et al. presented that the Silverstream® System with air bubbles through the use of tank testing, full scale sea trials and long term performance monitoring has led to proven net savings in excess of 4%, commercial contracts and projected savings of 8% across vessel types. Borusevich et al. (Krylov State Research Centre, Russia) developed a method called Air Cavity Technology greatly improved the effect of resistance reduction up to 15-25%.

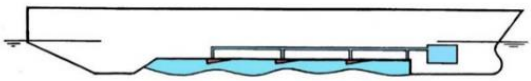

Figure 35: Bottom configuration for air cavity generation by KSRC method (Borusevich et al., 2016)

Figure 36: Photo of tanker model with recess (Borusevich et al., 2016)

Ravina & Guidomei (2018) conduct an experimental application of air-bubbling techniques on flat plates and hull models. Wang et al. (2018) conducted a model test for a 20,000 DWT bulk carrier in different injection position combinations, different towing velocities and

different injection flow rates. The results show that the best drag reduction can reach 15.5% at design speed.

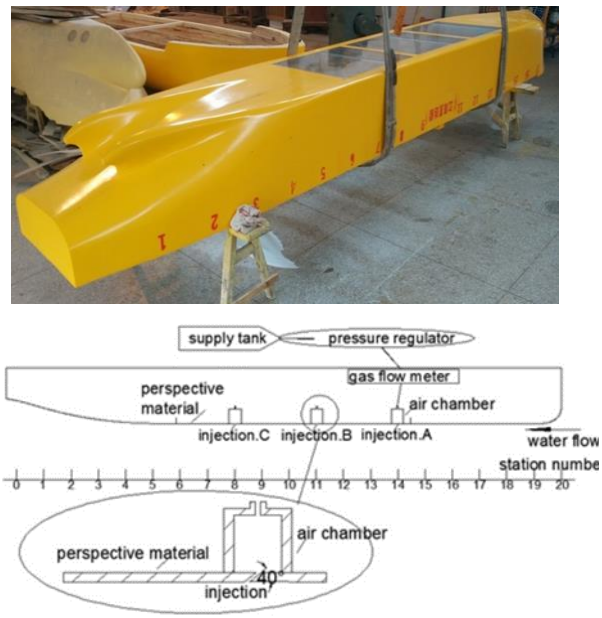

Figure 37: Photo of model and the schematic diagram of air injection system (Wang et al., 2018)

COATING DRAG REDUCTION

The development of coating drag reduction technology similar to air lubrication is also very popular. There are various test methods for how to measure the drag reduction effect. Lee & Chun (2013) conducted the flat plates measurement in towing tank to evaluate the low frictional AF(Anti-Fouling) paints.

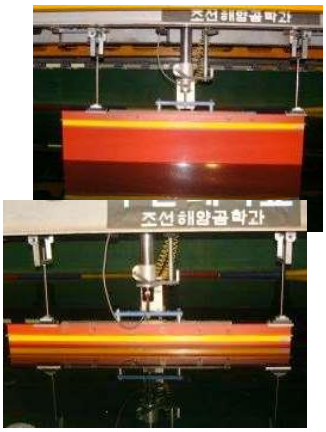

Figure 38: Flat plate assembly installed on towing carriage (Lee et al., 2013)

Klijnstra & Bakker (2017) put forward a new methodology which is measurement of friction drag properties of hull coatings that have been exposed to different types of static or dynamic ageing regimes. Schulze & Klose (2017) conducted friction measurements of different coatings in a Friction Tunnel. The friction tunnel provides reliable and quick friction measurements of different surfaces. The field of application is wide.

Figure 39: Friction tunnel (Schulze & Klose, 2017)

BIONIC TECHNOLOGY

Bionic technology is also a research direction of ship energy saving in future. Schrader (2018) conducted the coating tests in the Hydrodynamics and Cavitation Tunnel. The coatings similar to dolphin was made from polymeric materials with compliant coating.

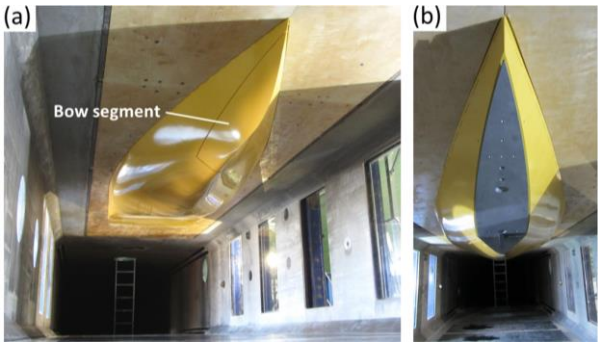

Figure 40: Experimental setup: (a) Wetted-hull model with painted reference bow segment (rigid surface) in the water-tunnel test section. (b) Base plate of load cell with bow segment removed (Schrader, 2018)

ENERGY SAVING IN WAVES

Many researches focus on the energy-saving effect in still water, while the actual ship is sailing in waves condition, and the drag reduction technology in waves has much practicability

Chiu et al. (2018) installed the pitch collapsing bow fin energy-saving device on a container ship model, and verified the energy-saving effect of about 4.29% by model test in waves

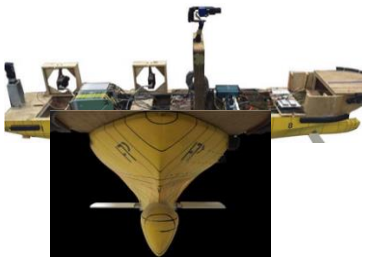

Figure 41: Ship model with active pitch oscillating bow fin (Chiu et al., 2018)

Yasukawa & Ishikawa (2017) studied a Catamaran in Waves by a biologically inspired hydrofoil plate. The spring was put inside the foil model to produce a restoring force for roughly keeping the initial angle of attack of the wing. The tests were carried out in calm water and regular head wave conditions and the maximum EHP reduction ratio by the hydrofoil was about 10%-15%.

Figure 42: Models (left: catamaran, right: hydrofoil) by Yasukawa & Ishikawa (2017)

4.2.2 SURVEY ON THE BEST PRACTICE OF MODEL TESTS FOR AIR-LAYER INJECTION

Skin friction reduction is one of promising techniques of ship energy saving and air lubrication has been implemented in several tens of vessels so far. In 2017, the 28th ITTC adopted a recommended guideline "7.5-02-02-03 Resistance and Propulsion Test and Performance Prediction with Skin Frictional Drag Reduction Techniques" as a guideline to extrapolate model test results to a full-scale performance prediction. The model test procedure for air lubrication, however, has not

been standardized yet, which may cause a significant deviation in the model test results among model test organizations.

In this regard, the committee was asked by AC to give more detailed description of model test procedure on the air lubrication techniques such as test condition (e.g. model scale pressure and air flow rate corresponding to full scale). In line with this suggestion, the committee carried out a survey to investigate the current status of model test practices involved with air lubrication among organizations. A 12-item questionnaire was distributed among relevant organizations worldwide, among which 11 organizations replied it. The following summarizes the replies.

1. **(Area info)** In which ITTC geographic area list below does your organization belong to?

Choice	Area	# of choices (%)
1	Americas	0 (0.0)
2	Central Europe	0 (0.0)
3	East Asia	8 (72.7)
4	Northern Europe	0 (0.0)
5	Pacific Islands	3 (27.3)
6	Southern Europe	0 (0.0)

2. **(Category of organization)** Which category listed below does your organization fall into?

Choice	Type	# of choices (%)
1	Academia (University)	4 (36.4)
2	Research Institute	4 (36.4)
3	Private Company	3 (27.3)
4	None of the Above	0 (0.0)

3. **(Test experience)** How many times has your organization conducted model tests involved with air lubrication so far? (times referring to the number of independent test campaign)

Choice	Type	# of choices (%)
1	Never	1 (9.1)
2	1~4 times	5 (45.5)
3	5~10 times	0 (0.0)
4	More than 10 times	5 (45.5)
5	No idea	0 (0.0)

4. **(Ship types considered)** Mark all relevant ship types which have been involved with air lubrication mode tests. (multiple answers allowed)

Choice	Type	# of choices (%)
1	Oil/Chemical Tanker	4 (19.0)
2	Bulk/Cargo Carrier	6 (28.6)
3	Containership	3 (14.3)
4	LNG/LPG carrier	2 (9.5)
5	Passenger/RORO/Cruise	2 (9.5)
6	Other types	3 (14.3)
7	No idea	1 (4.8)

5. **(Distribution of scale factor)** Mark all relevant ranges of scale factor λ which your past model tests fall into. (multiple answers allowed)

Choice	Type	# of choices (%)
1	$\lambda = 1.0$ (Full scale)	1 (6.3)
2	$1.0 < \lambda \leq 10.0$	3 (18.8)
3	$10.0 < \lambda \leq 50.0$	4 (50.0)
4	$50.0 < \lambda \leq 100.0$	1 (6.3)
5	$\lambda > 100.0$	1 (6.3)
6	No idea / None of the above	2 (12.5)

6. **(Location of air injector)** In which part of the model ship was/were the injector hole(s) placed?

Choice	Type	# of choices (%)
1	Flat bottom	9 (64.3)
2	Side bottom	1 (7.1)
3	Both	3 (21.4)
4	No idea	1 (7.1)

7. **(Injection pressure)** How high was the air pressure set just before the injection hole(s) in the model test? (pressure in the settling chamber/regulator before injection hole(s); multiple answers allowed)

Choice	Type	# of choices (%)
1	Atmospheric pressure	1 (8.3)
2	Full scale (hydrostatic pressure in full scale)	0 (0.0)
3	Model scale (hydrostatic pressure in model scale)	6 (50.0)
4	Polytropic expansion considered at injection hole $pv^n = C$	0 (0.0)
5	Arbitrary pressure	2 (16.7)
6	None of the above	0 (0.0)
7	No idea	3 (25.0)

8. **(Injection flow rate)** How large was the air flow rate set in the model test? (multiple answers allowed)

Choice	Type	# of choices (%)
1	Full scale (same as full scale flow rate)	1 (7.1)
2	Same as the critical value of film thickness $t_f = Q_a/B \cdot U$ in full scale (B = ship breadth; U = ship speed)	8 (57.1)
3	Geometric scale of the critical value of film thickness $t_{f.model} = \frac{t_{f.full\,scale}}{\lambda}$	1 (7.1)
4	Arbitrary flow rate	2 (14.3)
5	None of the above $t_a = Q_a/B_a \cdot U$ (B_a = breadth of air covered area) or $t_b = Q_a/B_i \cdot U$ (B_i = air injector breadth)	1 (7.1)
6	No idea	1 (7.1)

9. **(Extrapolation method)** What kind of extrapolation method was used for extrapolation to full scale?

Choice	Type	# of choices (%)
1	Never (only model scale performance was measured)	3 (27.3)
2	ITTC recommended guideline 7.5-02-02-03	0 (0.0)
3	ITTC 1978 7.5-02-03-01.4 Performance Prediction Method	4 (36.4)
4	Own guideline	3 (27.3)
5	No idea	1 (9.1)

10. **(R_{TM} reduction ratio for model)** How large was the reduction ratio of total resistance of model $r_M = 1 - R_{TM,air\,injection}/R_{TM,baseline}$ upon air lubrication? (multiple answers allowed)

Choice	Type	# of choices (%)
1	$0\% < r_M \leq 5\%$	5 (26.3)
2	$5\% < r_M \leq 10\%$	2 (10.5)
3	$10\% < r_M \leq 15\%$	1 (5.3)
4	$15\% < r_M \leq 20\%$	5 (26.3)
5	$r_M > 20\%$	5 (26.3)
6	No idea	1 (5.3)

11. **(R_{TS} reduction ratio for full scale)** How large was the predicted reduction

ratio of total resistance of full scale $r_S = 1 - R_{TS,air\ injection}/R_{TS,baseline}$ upon air lubrication ? (this does not include the deduction of air injection power; multiple answers allowed if necessary)

Choice	Type	# of choices (%)
1	0% < r_S ≤ 5%	2 (10.5)
2	5% < r_S ≤ 10%	5 (26.3)
3	10% < r_S ≤ 15%	6 (31.6)
4	15% < r_S ≤ 20%	2 (10.5)
5	r_S > 20%	2 (10.5)
6	No idea	2 (10.5)

12. **(Suggestions)** Propose freely what needs to be included in the recommended procedure/guideline of air lubrication model test.

- The performance at full scale of air lubrication system can hardly be evaluated from the model scale tests, due to the difference of air bubbles behaviours according the difference of scale. In addition, the size of bubble is relatively much large in comparison with the scale.
- CFD analysis is believed to be more valuable that mode scale ship tests. Instead, localized large scaled model test could give us information on the behaviors of air bubbles and friction reduction.
- In order to extrapolate the model test results of the air lubrication system, it is necessary to introduce a model-ship correlation factor for the frictional reduction rate because the air behaviour (size and trajectory) of the model and full scale are different.
- The CFD analysis can be fully utilized to understand this model-ship relationship.
- Since the bubble size cannot be controlled similar between model scale and full scale, it is difficult to predict the effect of air lubrication in full scale directly from model scale. So the importance of feedback from full scale and/or combination with two-phase (i.e. air-water) flow CFD should be pointed out.
- It might be important to discuss prediction of the influence of air bubble not only on reduction of frictional drag but also on self-propulsion factors, propeller open water characteristics, cavitation performance.

4.3 CONSIDERATIONS ON SCALING METHOD FOR ESD

OWT (Open Water Tests) corrections used in ITTC'78-PPM are based in the approach of the equivalent profile that identifies the behaviour of the blade with the blade cylindrical section at 0.75R. With this approach it is impossible to distinguish advanced forms of blade propellers like end plate, tip raked, etc. Propeller open water parameters K_T and K_Q measured at model scale must be corrected to obtain appropriated values to be used for predictions at full scale, Streckwall et al. (2013).

Pérez-Sobrino et al. (2016a) presented the so called SISTEMAR strip method in detail. The summary of the method is to obtain the OWT corrections by integration of the corrections obtained at each blade and eventually end plate sections, by using the following expressions:

$$\delta K_T = -\frac{z}{2}\int_{x_{hub}}^{x_{tip}} \delta(C_D)\cdot[J^2+(\pi x)^2]\cdot\frac{c}{D}\cdot sen\varphi\cdot dx \quad (1)$$

$$\delta K_Q = \frac{z}{4}\int_{x_{hub}}^{x_{tip}} \delta(C_D)\cdot[J^2+(\pi x)^2]\cdot\frac{c}{D}\cdot cos\varphi\cdot x\cdot dx \quad (2)$$

The differences in the viscous drag coefficient will be calculated from the respective frictional coefficients of the blade sections at model and ship scales:

$$\delta(C_D) = C_{Dm} - C_{Ds} \quad (3)$$

$$C_{Dm} = 2 \cdot \left(1 + 2\frac{t}{c}\right) \cdot C_{Fm} \quad (4)$$

$$C_{Ds} = 2 \cdot \left(1 + 2\frac{t}{c}\right) \cdot C_{Fs} \quad (5)$$

As the R_n is very different during model tests compared to full scale, the main question of these methods is how to compute the frictional coefficient, C_F, as a function of the type of flow developed over each blade section. Figure 8 presents the scheme of how different types of flow can be developed over a blade section as R_n increases.

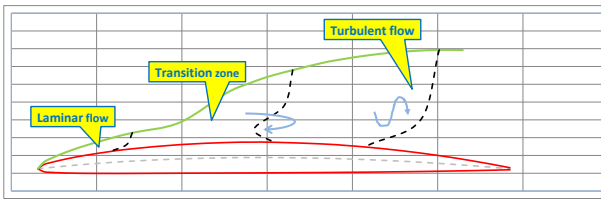

Figure 43: Scheme of flow developed over the blade sections

When flow can be considered as laminar, the proposed formula to be used is the well-known expression due to Blasius for laminar boundary layers on smooth surfaces:

$$C_{Fm} = \frac{1{,}3282}{\sqrt{R_n}} \quad (6)$$

For fully turbulent flow the well-known formula due to Prandtl and Schlichting for smooth plates can be used both for model and for full scale.

$$C_{Fs} = \frac{0{,}455}{(\log R_n)^{2{,}58}} \quad (7)$$

In the already mentioned reference Pérez-Sobrino et al (2016a) it is explained that flow can be considered turbulent if the section R_n is larger than this critical number: von Doenhoff and Horton (1956)

$$R_{n\ critical\ turbulent} = 415\frac{c}{k_p} \quad (8)$$

It has been considered that flow will be laminar at ship scale until the value of $R_n = 2 \times 10^5$ which is a limit value generally accepted for the laminar flow in profiles.

$$R_{n\ crit\ lam-trans\ (ship)} = 2.0 \times 10^5 \quad (9)$$

But at model scale both paint tests and CFD calculations have shown that flow developed over the blades is quite different mainly in the upper part of the blade, Figure 16, for conventional and unconventional propellers.

CONVENTIONAL

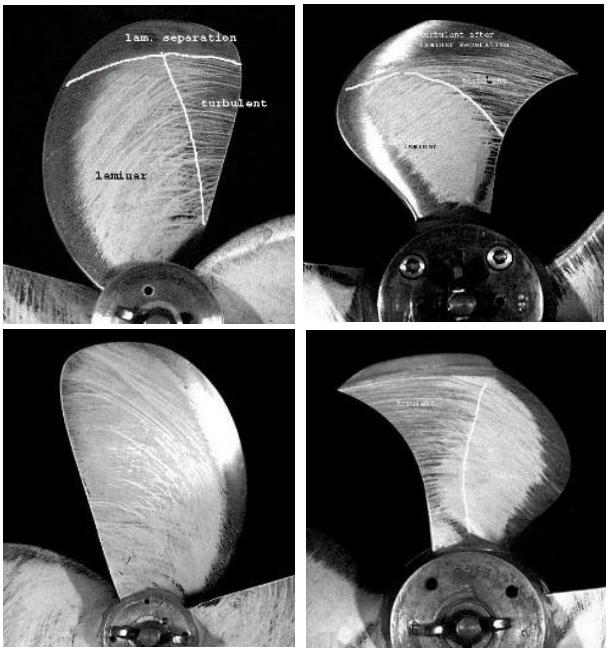

Figure 44: Paint tests results.
Taken from R&D Project "LEADING EDGE".

UNCONVENTIONAL(CLT)

In order to take also into account, the differences in diameter, rps of the OWT and the roughness of the blades, similar expressions to equation 8 have been derived for conventional and unconventional blades.

For conventional blades:

$$R_{n\ crit\ lam-trans\ (model-CONV)} = K_1 \cdot \frac{c}{k_p} \quad (10)$$

For unconventional blades:

$$R_{n\ crit\ lam-trans(model-UNCONV)} = K_2 \cdot \frac{c}{k_p} \quad (11)$$

Values of $K_1 = 42$ and $K_2 = 30$ have been deduced from model paint tests and CFD calculations that the extension of laminar zone in unconventional (CLT) propellers is smaller than in the case of conventional propellers, so critical R_n, to define laminar zone, must be smaller for unconventional (CLT) propellers. In the middle of these two sectional critical R_n numbers (so for R_n larger than $R_{n\ crit\ lam-trans}$ but smaller than $R_{n\ crit\ turbulent}$) the flow over the blade profiles is in a so-called transition zone, where there exists some uncertainty about the value of C_F.

This method proposes to interpolate with actual R_n of the section between the C_F values corresponding to laminar and turbulent limits. In this way the proposal does not include any specific friction line for transition zone but values of C_F in transition zone depend on each specific case and section data. The procedure has been validated by analysing a comprehensive set of OWT results, both for conventional and end plate tip loaded (CLT) propellers (Quereda et al., 2019b) This validation has confirmed that the strip method is practically equivalent to the application of ITTC'78-PPM for calculation of OWT scale effects of conventional propellers.

5. RECOMMENDED GUIDELINE

The 29th ITTC has decided to publish a new guideline titled "Scaling Method for ship wake fraction with pre-swirl devices". The purpose of the guideline is to complement the ITTC 1978 procedure for the prediction of the delivered power and rate of revolutions for single and twin screw ships with either Pre-Swirl Stator (PSS) or Pre-Swirl Duct (PSD) being installed.

5.1 SCALING METHOD FOR SHIP WAKE FRACTION WITH PRE-SWIRL DEVICES

5.1.1 FLOW CHARACTERISTICS AROUND PRE-SWIRL DEVICE AND PROPELLER

Pre-swirl device generates a counter swirl flow to save rotational energy from propeller. For the prediction of powering performance, ITTC 1978 method adopts the thrust identity method to find out the effective mean wake fraction. As shown in Figure 30, the angle of attack α depends on the inflow velocity on propeller plane (U_A) and the rotational velocity ($2\pi nr$) if the induced velocity is neglected. If the rotational velocity (speed of revolution) is kept same as in the POW (Propeller Open Water) condition and in the propeller behind ship condition, the inflow velocity is therefore colinear to the thrust. The counter swirl flow generated will be of potential nature rather than viscous.

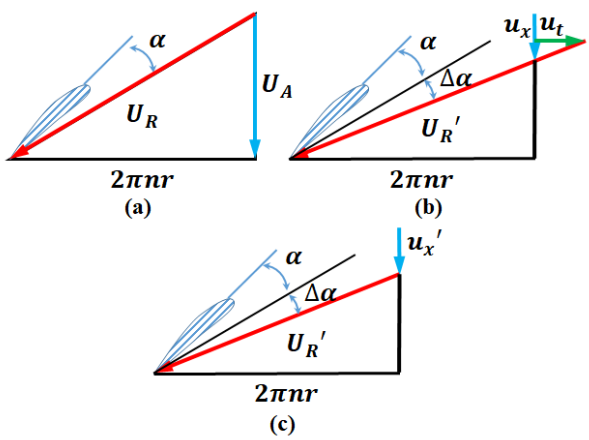

Figure 45: Change of inflow angle at the propeller blade section due to the induced velocity of the ESD

The difficulty in scaling arises from the point that the pre-swirl device makes not only a counter swirl but also axial flow retardation. It is therefore necessary to decompose the axial and tangential components separately. As shown in Figure 30 (b), the presence of pre-swirl device causes the relative velocity to propeller blade to change as U_R' with increased angle of attack $\alpha + \Delta\alpha$, thereby increasing thrust. Therefore, the open water characteristics of the compound propulsor (propeller & pre-swirl device) become different from that of propeller only. If the scaling is applied to the total amount of model wake based on the thrust identity defined in the ITTC 1978, this might result in overestimating axial induced velocity u_x', as depicted in Figure 30 (c). Thus, the increase in thrust due to both axial and tangential induced velocity might be misinterpreted solely by the axial induced velocity by ITTC 1978 method.

5.1.2 ITTC 1999 METHOD: BACKGROUND AND LIMITATION

This so-called "ITTC 1999 method" does not actually belong to the ITTC recommended procedures and guidelines. This was introduced in the 22nd ITTC final report of the Specialist Committee on Unconventional Propulsors (ITTC 1999).

The combined propulsor, such as PSS – propeller system, can be analysed with two kinds of method shown in Figure 31. In method A, the pre-device is considered as a combined propulsor, which means the pre-device and propeller are treated as a whole propulsor. This assumption implies that in both open water and self-propulsion tests, the thrusts of propeller and stator are measured simultaneously and their sum is used as the thrust of the propulsion system. The report addressed that the ITTC 1978 procedure fails to scale the performance of unconventional propulsion systems correctly, and this is due to two main causes. The first one is the laminar flow generated around the devices in the model test environment (scale); the second is that the model hull has a boundary layer that differs from the full scale one both in thickness and in velocity distribution.

Figure 46: ITTC 1999 Method

In method B, which is commonly referred to as ITTC 1999, the pre-device is considered as a part of hull, therefore the resistance test is carried out with pre-device while the POW test is executed with propeller alone. This procedure does not require the joint test of the stator and the propeller because the stator is tested being considered as the part of the hull. On the other hand, it requires a double set of resistance and self-propulsion tests are done: with and without the stator.

The scaling process is again the two dimensional approach of the ITTC 1957 method with an exception made for the determination of the full-scale wake, which is performed by means of the following formula that closely resembles that suggested by the ITTC 1978 correlation procedure:

$$w_S = (t_{MO} + 0.04) + (w_{MO} - t_{MO} - 0.04) \times \frac{C_{FS}+C_A}{C_{FM}} + (w_{MS} - w_{MO}) \quad (12)$$

While the standard ITTC 1978 ship wake is:

$$w_S = (t + 0.04) + (w_M - t - 0.04)\frac{(1+k)C_{FS}+\Delta C_F}{(1+k)C_{FM}} \quad (13)$$

The major difference compared with the ITTC 1978 formulation is the term $(w_{MS} - w_{MO})$. Since in the opinion of Van et al. (1993) the main effect of the stator is the increase of the angles of attack of the propeller blade sections, the stator action can be considered as mainly potential phenomenon. Thus, the difference in wakes with and without stator can be directly transferred to full scale.

5.1.3 SCALING METHOD FOR PRE SWIRL DEVICES

Lee (2015) carried out a comparative full-scale performance prediction for the pre-swirl devices based on the ITTC 1978 method and the ITTC 1999 method. It was addressed that the ITTC 1978 method has a limitation for extrapolating such a pre-swirl device. The ITTC 1999, a newer procedure which adopts different scaling for the axial and tangential component of wake, does not appear to clarify the flow mechanism around the propeller section. It was then proposed a new extrapolation method which leads to a more reasonable estimate for the angle of attack to the propeller. This approach has been presented by Kim *et al.* (2017) at the 5th International Symposium on Marine Propulsion and the corresponding extrapolation formula is given as follows:

$$w_S = (t_{MS} + 0.04) + \left(w_{MS,axial} - t_{MS} - 0.04\right)\frac{C_{FS} + C_A}{C_{FM}} + w_{MS,tangential} \quad (14)$$

$$w_{MS,axial} = w_{MO} + (w_{MS} - w_{MO}) \cdot Factor_{axial}$$

$$w_{MS,tangential} = (w_{MS} - w_{MO}) \cdot Factor_{tangential}$$

This is a compromise between ITTC 1978 and ITTC 1999 in that the axial velocity component and tangential velocity component are scaled separately. The axial wake, being of viscous nature, is scaled following ITTC 1978. On the contrary, the tangential wake, considered as potential flow phenomenon, is not scaled after the assumption of ITTC 1999. In addition, the thrust deduction factor is changed from that without a pre-swirl device in the ITTC 1999 method to that with a pre-swirl device.

It was found that the portions of tangential and axial velocity vary according to the vessel type as well as the device type. As shown in Table 2, Kim et al. (2017) proposed the factors of axial and tangential portion to be 0.3 and 0.7 in PSS case and 0.8 and 0.2 in PSD case, respectively. It is worthwhile to mention that the factors in Table 2 have been derived from limited ship types, i.e., KCS for PSS and KVLCC for PSD. Therefore, a generalization toward identifying a reasonable value range for each factor based on case studies with more ship types is necessary.

Table 4: Factors of axial and tangential portion

ESD Type	$Factor_{axial}$	$Factor_{tangential}$
PSS	0.3	0.7
PSD	0.8	0.2

6. FULL SCALE DATA

6.1 BACKGROUND

Very little full scale data have been found, this in light of the fact that full scale measurement is not easy. It requires special skill to obtain quality measurements. In addition, for merchant ships it is difficult to get time to conduct measurements.

One of the aims of full scale data for ESM is to compare the ESD/ESM effects in actual ships

to model tests. The mechanism is not always the same between model and full scale. While CFD researchers are attempting to solve this, data for validation are scarce.

6.2 SURVEY OF LITERATURE

6.2.1 ENERGY SAVING DEVICES

The most notable literature regarding the full-scale performance in this category is Hasselaar & Yan (2017), who reported the sea trial result with/without the pre-swirl stator and compared with full-scale simulation result. This study was carried out as a part of EU's FP7 project GRIP (Green Retrofitting through Improved Propulsion) project from 2011 to 2015.

Wienke (2017) showed four examples (three examples are related to duct and one is PBCF) of the comparison of the speed-power curve from model test with sea trial data. In three out of four cases, the power saving effect predicted by the model test appeared to be greater than that obtained sea trial. In two cases, the power saving effect was not confirmed from sea trial results. For the case when the sea trial was carried out two different drafts (ballast and scantling), the model test prognosis turned out to be more optimistic for the scantling draft. In other words, the power saving effect was overestimated by a larger amount for the scantling draft. The model test accuracy was found to be dependent upon the extrapolation method. In addition, it was emphasized that the hull cleaning effect and the ESD effect should be separated for the retrofit case.

Themelis et al. (2019) utilized a performance monitoring system in order to examine the fuel savings for an oil tanker in which a pre-swirl duct (also known as Mewis duct) had installed during dry-dock. Three years of operational data utilizing the LAROS platform for the signal processing, data collection and analysis have been used, covering a period before and after the installation of the duct. Through comparison with a sister vessel without such ESD but with similar hull and propeller cleaning history, they concluded that the ESD led to saving of fuel oil consumption by 3.5 – 5%.

Sakamoto et al. (2020) compared the full-scale measured wake and CFD results for two different ships, one is the 1600TEU container ship "Sydney Express" and the other is the 63,000DWT bulk carrier equipped with pre-swirl duct. This paper is notable in that the validation of full-scale CFD simulation based on full-scale experimental data was carried out. This is attributable to the development of PIV and CFD techniques.

6.2.2 AIR LUBRICATION

De Freitas et al. (2019) introduced a full scale data of air lubricated 40,000 DWT chemical tanker and showed about 5% energy saving on the average. In addition, they emphasized the complex nature of performance assessment due to various uncertainties resulting from disturbances such as varying draft, inaccurate measurement of speed through water (STW), lack of data at certain speed range, changing environmental conditions and inaccurate wind speed, etc. They stated that the ISO19030 and basis of data filtering is currently the only viable means of executing analysis performance of the ESM under consideration.

6.2.3 LOW FRICTION ANTI-FOULING (AF) COATING

Goler et al. (2017) presented the fuel consumption for alternative hull coating using 8 sister high speed Ro-Ro vessels, built at the same shipyard and showed the significant fuel savings for the foul release silicone coatings.

Cho et al. (2021) carried out the evaluation of the performance of frictional drag reducing anti-fouling (FDR-AF) marine coating based on the ISO19030 standard. In-service navigation data collected from the 176k DWT bulk carrier during five years were analysed to assess the speed improvement performance of the coating. It is notable that they were able to isolate the effect of drag reducing coating by comparing two identical freshly-coated vessel condition just after re-docking with only coatings being changed. They indicated that the coating leads to a speed increase of 3.72% over the conventional AF coating, which is equivalent to power (fuel) saving of 11.7%.

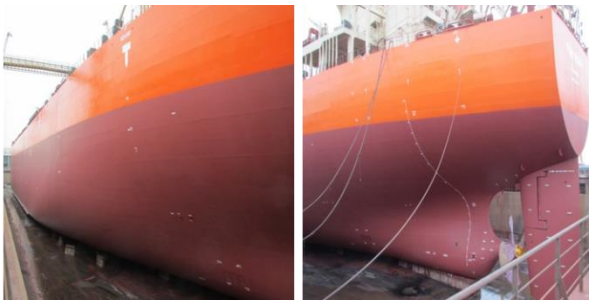

Figure 47: Photographs of the 176k DWT bulk carrier with FDR-AF marine coating

6.2.4 DETAILED FLOW MEASUREMENT IN FULL SCALE

Although the full-scale measurement itself does not belong to the ToR, it is worthwhile to notice new techniques of instrumentation of full-scale flow field measurement, because it can provide a reliable basis to validate full-scale CFD prediction. Also it can shed some lights on understanding how the speed on ground (SOG) and the speed through water (STW) are related, which remains unsolved especially for the evaluation of in-service performance of ESM. In that account, Inukai et al. (2018, 2020) shows an exemplary result of full-scale flow measurement around propeller of a 14,000-TEU containership using Multi-Layered Doppler Sonar (MLDS). Furthermore, they are continuing their measurement campaign to widen the application to VLCC. Their forthcoming report is worthy of particular attention.

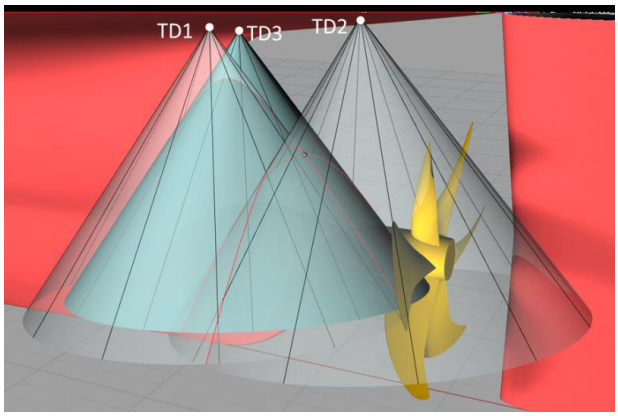

Figure 48: Measurement range with three Multi-Layered Doppler Sonar (MLDS) in Inukai et al. (2020)

7. CONCLUSIONS

A brief summary of each of the substantive chapters of this report is presented highlighting them. Additionally, potential tasks for the next committee are provided.

Chapter 2 categorises and discusses the ESMs available at the time of this publication. Furthermore, it provides references from the recent literature and then discusses each of them in turn. It provides background for the subsequent sections as well as a general review of each of the energy saving methods.

In chapter 3 the recent literature on wind-assisted propulsion is assessed. This remains one of the few possibilities for realising double digit energy savings for commercial ships however issues associated with capital cost, crewing requirements and unpredictability of weather conditions remain as challenges to uptake.

Chapter 4 is an in-depth discussion of computational fluid dynamics, experimental fluid dynamics, and scaling methods as each relates to energy saving methods and devices. In section 4.1, the necessity of CFD guideline is reviewed in two aspects; first, "Guidelines for CFD analysis of a ship with ESD" described in the PRADS 2016 paper (Hino *et al.* 2016) was reviewed and compared with the existing CFD guidelines by CFD experts. second, the influence of ESD on the CFD results reported in the Tokyo 2015 CFD workshop is described in detail. In section 4.2, the new or specially proposed experimental methods or test schemes for ESD were shown to be largely absent since 2016. In addition, the best practice of the test condition for air lubrication is summarized.

Chapter 5 presents a new guideline on scaling method for ship wake fraction with pre-swirl devices.

Full scale data were to be the subject of section 6; however these datasets were found to be severely deficient. It was concluded that we need more full scale data, not only power saving data, but also detailed data such as velocity and/or pressure distributions as changed by ESMs. To obtain detailed data, a comprehensive research project might be effective. The intellectual property issue also needs to be solved.

7.1 POTENTIAL TASKS FOR THE NEXT COMMITTEE

A) Continue to monitor the development of relevant techniques for ship energy saving and identify the needs to complement the present EEDI framework in response to the adoption of alternative fuels and the receptivity of innovative technologies. Consider, if necessary, a complementary metric to EEDI to represent power savings.

B) Identify the necessity of guidelines for CFD methods, model tests and scaling for energy saving devices.

C) Collect full scale data obtained through relevant benchmark tests on the effect of energy saving methods. Use the full scale data for validating the effect of ESM. Develop a guideline to conduct in-service performance evaluation for ESM.

7.2 RECOMMENDATIONS TO THE CONFERENCE

The 29th ITTC Specialist Committee on Energy Saving Methods recommends adopting the new guideline on 'Scaling Method for ship wake fraction with pre-swirl devices'.

8. REFERENCES

Arakawa, D., Kawasima, H., Kawakita, C., 2018, "Numerical Estimation of Self-propulsion Factors for Ship with Air Lubrication " ISOPE 2018, Sapporo, Japan, pp.855-862

Argyros. D., 2017, "Wind-powered shipping: A review of the commercial, regulatory and technical factors affecting uptake of wind-assisted propulsion." Lloyd's Register Marine, pp.1–5.

Bentin, M., Zastrau, D., Schlaak, M., Freye, D., Elsner, R., Kotzur, S., 2016, "A new routing optimization tool-influence of wind and waves on fuel consumption of ships with and without wind assisted ship propulsion systems", Transportation Research Procedia, Vol. 14 pp.153-162

Bøckmann, E., Yrke, A., Steen, S., 2018, "Fuel savings for a general cargo ship employing retractable bow foils" Applied Ocean Research, Vol. 76, pp.1-10

Bondarenko, O., Fukuda, T., 2018, "The Advantage of Air Lubrication System Integration into the Propulsion Plant" 8th PAAMES AMEC, Busan, Korea, pp.124-132

Bordogna, G., Muggiasca, S., Giappino, S., Belloli, M., Keuning, J. A., Huijsmans, R. H. M., 2020, "The effects of the aerodynamic interaction on the performance of two Flettner rotors." Journal of Wind Engineering and Industrial Aerodynamics, Vol. 196, 104024

Borusevich, V.O., Pustoshny, A.V., Sverchkov, A.V., Trincas, G., 2016, "Impact of Air Cavity Technology on Ship Drag Reduction: Experience from Research Studies", 10th Symposium on High-Performance Marine Vehicles, HIPER'16, Cortona, Germany, 17-19 October 2016, pp. 94-107

Bouman, E., Lindstad, E., Rialland, A.I., Strømman, A. H., 2017, "State-of-the-art technologies, measures, and potential for reducing GHG emission from shipping –A review", Transportation Research Part D pp.408-421

Braidotti, L., Mauro, F., Sebastiani, L., Bisiani, S., Bucci, V., 2018, "A Ballast Allocation Technique to Minimize Fuel Consumption" NAV 2018, Trieste, Italy, pp.97-104

Cai, H.P., Hao, C.P., Zhang, H. et. al., 2019, "Hydrodynamic Performance Prediction Method for the Ducted Contra-Rotating Propeller". 6th International Symposium on Marine Propulsors (SMP'19), Rome, Italy, May 2019

Carlton, J., Aldwinkle, J., Anderson, J., 2013, "Future ship powering options: exploring alternative methods of ship propulsion", Royal Academy of Engineering, London

Caughlan, S.A., 2016, Energy efficiency white paper, pp.1-115

Chang, X., Sun, S., Zhi, Y., Yuan, Y., 2019, "Investigation of the effects of a fan-shaped Mewis duct before a propeller on propulsion performance" Journal of Marine Sscience and Technology, Vol. 24, pp. 46–59

Charruault, F., Westerweel, J., van Terwisga, T., Breugem, W-P., 2017, "On the Drag Reduction Induced by an Air Cavity and Characterisation of Its Free Surface" AMT'17, Glasgow, UK, October 2017, pp.172-185

Chen, C. G., Hu, J., Zhang, W. P., Wang, Y. Z., 2020, "The Effects of Number of Blades of Free Vane Wheel on Energy-saving" ISOPE 2020, Shanghai, China, pp.2048-2054

Chen, W., Zhang, H., Wang, L., Leng, W., Hou, G., 2017, "Drag Calculation of Macroscopic Objects with Riblet Microstructure" ISOPE 2017, San Francisco, USA, pp.858-864

Chiu, F. C., Huang, S. W., Wu, T. L., Guo, J. H., Tsai, J.F., 2018, "Ship Propulsion in Irregular Waves Augmented by an Active Pitch Oscillating Bow Fin" 8th PAAMES AMEC, Busan, Korea, pp.4-12

Cho, Y., Jeon, K. H., Lee, S. B., Park, H., Lee, I., 2021, "Evaluation of In-service Speed Performance Improvement by means of FDR-AF (Frictional Drag Reducing Anti-Fouling) marine coating based on ISO19030 standard" Scientific Reports, Vol. 11, article no. 1062

Coppedè, A., Gaggero, S., Vernengo, G., Villa, D., 2018, "Surrogate Model for Ship Resistance: A Sensitivity Analysis of Shape Deformation" NuTTS2018, Cortna, Italy

Coppedè, A., Gaggero, S., Vernengo, G., Villa, D., 2019, "Hydrodynamic shape optimization by high fidelity CFD solver and Gaussian process based response surface method" Applied Ocean Research, Vol. 90, pp.1-12

Copuroglu, H. I., Pesman, E., 2018, "Analysis of flettner rotor ships in beam waves", Ocean Engineering, Vol. 150, pp.352-362

Coache, S., Meis Fernández, M., 2017, "ESD design for a validation bulk carrier", International Shipbuilding Progress, Vol. 63, Iss. 3-4, pp. 211-226

Craft, T., Johnson, N., Launder, B., 2014, "Back to the future- a re-examination of the aerodynamics of flettner-thom rotors for maritime propulsion", Flow, turbulence and combustion, Vol. 92 (1-2) pp.413-427

Cui, T., Howett, B., Lu, R., Kim, M. Y., Demirel, Y. K., Turan. O., Day. S., Incecik. A., 2016, "Voyage Optimisation towards Energy Efficient Ship Operations." SCC2016: Shipping in Changing Climates Conference

Dadd, G. M., Hudson, D. A., Shenoi, R., 2011, "Determination of kite forces using three-dimensional flight trajectories for ship propulsion", Renewable Energy Vol. 36, Iss. 10, pp.2667-2678

De Freitas, L., Silberschmidt, N., Pappas, T., Connolly, D., 2019, "Full-Scale Performance Measurement and Analysis of the Silverstream Air Lubrication System" HullPIC'19, Gubbio, Italy, pp.201-210

Delfos, R., Greidanus, A., Charruault, F., Westerweel, J., 2017, "Wave Characteristics of a Compliant Coating under a Turbulent Flow" AMT'17, Glasgow, UK, October 2017, pp.141-156

Demirel, Y. K., 2018, "New Horizons in Marine Coatings" INT NAM 2018, Istanbul, Turkey, April 2018, pp.565-582

Demo, N., Tezzele, M., Gustin, G., Lavini, G., Rozza G., 2018a, "Shape Optimization by means of Proper Orthogonal Decomposition and Dynamic Mode Decomposition" NAV 2018, Trieste, Italy, June 2018, pp.212-219

Demo, N., Tezzele, M., Mola, A., Rozza, G., 2018b, "An efficient shape parametrisation by free-form deformation enhanced by active subspace for hull hydrodynamic ship design problems in open source environment" ISOPE 2018, Sapporo, Japan, pp.565-190

Drouet, A., Sergent, P., Causeur, D., Corrignan, P., 2017, "Trim optimisation in waves" MARINE 2017, Nante, France, May 2017, pp.592-603,

Duan, W., Zhang, H., Huang, L., Liu, J., Shao, W., Cao, G., Shi, Z., 2019, "Numerical Simulation of Trim Optimization on Resistance Performance Based on CFD Method" OMAE2019-96181, Glasgow, UK

Duport, C., Deberque, M., Leroux, J-B., Roncin, K., Jochum, C., 2017, "Local Results Verification of a 3D Non-Linear Lifting Line Method for Fluid-Structure Interactions Simulation on a Towing Kite for Vessels" HIPER'17, Zevenwacht, S.Africa, pp.192-201

Fagiano, L., Milanese, M., Razza, V., Bonansone, M., 2012, "High-altitude wind energy for sustainable marine transportation", IEEE Transactions on Intelligent Transportation Systems, Vol. 13, Iss. 2, pp.781-791

Fan, X., Sun, H., Xiang, X., 2020, "Investigation on Trim Optimization of a Bulk Carrier

Based on CFD Method" ISOPE 2020, Shanghai, China, pp.3845-3849

Feng, D., Zhang, H., Sun, Y., Wang, Q., Hu, X., 2019, "Studies about Design of Rear Stator of Ducted Propeller using CFD" OMAE2019-96020, Glasgow, UK

Furcas, F., Gaggero, S., Villa, D., 2019, "Duct-type ESD: a design application using RANSE-based SBDO" smp'19, Rome, Italy, May 2019

Gaggero, S., Villa, D., Tani, G., Viviani, M., Bertetta, D., 2017, "Design of ducted propeller nozzles through a RANSE-based optimization approach" Ocean Eng., Vol. 145, pp.444-463

Gaggero, S., 2018, "Design of PBCF energy saving devices using optimization strategies: A step towards a complete viscous design approach" Ocean Eng., Vol. 159 pp.517-538

Gaggero, S., Villa, D., 2018, "An Optimization Framework for PBCF Energy Saving Devices" OMAE2018-77921, Madrid, Spain

Ge, M. W., Fang, L., Liu, Y. Q., 2017, "Drag reduction of wall bounded incompressible turbulent flow based on active dimples/pimples" Journal of Hydrodynamics, Vol. 29, Iss. 2, pp.261-271

Go, J. S., Yoon, H. S., Jung, J. H., 2017, "Effects of a duct before a propeller on propulsion performance" Ocean Eng., Vol. 136, pp.54-66

Goler, H., Bozkurt, K., 2017, "Speed Loss Analysis of High-Speed Ro-Ro Vessels Coated with New Antifoulıng Technologies" HullPIC'17, Ulrichshusen, Germany, pp.173-193

González-Adalid, J., Pérez Sobrino, M., Gennaro, G., 2018, "Retrofitting a High Efficiency CLT® Propeller on a 175K m³ LNG Tanker: Comparative Service Performance Before and After" 8th PAAMES AMEC, Busan, Korea, pp.191-197

Goren, O., Calisal, S.M., 2017, "Mathematical programming basis for ship resistance reduction through the optimization of design waterline" Journal of Marine Sscience and Technology, Vol. 22, Iss. 4, pp.772-783

Greidanus, A., Delfos, R., Westerweel, J., 2017, "Fluid-Structure Interaction of Compliant Coatings under Turbulent Flow Conditions: Force and PIV Analysis" AMT'17, October 2017, pp.157-171

Güngör, E., 2017, "Hybrid Design Method for a Generic Counter-Rotating Propeller" smp'17, Espoo, Finland, June 2017

Guo, B., Vartdal, B.J., Steen, S., 2017, "A Novel Measure to Reduce Ship Resistance in Waves" OMAE2017-61949, Trondheim, Norway

Halim, R., Kirstein, L., Merk, O., Martinez, L., 2018, "Decarbonization pathways for international maritime transport: A model-based policy impact assessment", Sustainability, Vol. 10, Iss. 7, p.2243

Hartenberger, J., Gose, J., Ceccio, S., Perlin, M., 2018, "Flow and Drag Measurements over Soft Biofilm", 32nd Symposium on Naval Hydrodynamics, Hamburg, Germany 5-10 August 2018

Hasselaar, T. W. F., Yan, X. K., 2017, "Evaluation of an energy saving device via validation speed/power trials and full scale CFD investigation" International Shipbuilding Progress., Vol. 63, Iss. 3-4, pp.169-195

Heo, J., Park, D., Berg-Jensen, J. H., Pan., Z., Vada, T. K., 2019, "Hull form Optimization to Fulfil Minimum Propulsion Power by Using Frequency and Time Domain Potential Flow Solvers" PRADS'19, Yokohama, Japan

Hino, T., Hirata, N., Ohashi, K., Toda, Y., Zhu, T., Makino, K., Takai, M., Nishigaki, M., Kimura, K., Anda, M., Shingo, S., 2016, Hull Form Design and Flow Measurements of a Bulk Carrier with an Energy-Saving Device for CFD Validations, PRADS2016, Copenhagen, Denmark

Hirdaris, S., Cheng, F., 2012, "The role of technology in green ship design", 11th International Marine Design Conference, pp.67-78

Hori, M., Kadowaki, T., Hinatsu, M., Toda, Y., 2017, "Development of Design procedure of Energy Saving Rudders Using Various Numerical Codes" ISOPE 2017, San Francisco, USA, pp.867-874

Hou, L. X., Hu, A.K., 2018, "Energy saving performance analysis of contra-rotating azimuth propulsor" Applied Ocean Research, Vol. 72, pp.12-22

Hou, L.X., Hu, A. K., Wang, S., 2019, "Energy saving performance analysis of contra-rotating azimuth propulsor. Part 2: Optimal matching investigation in model scale" Applied Ocean Research, Vol. 88, pp.29-36

Howett, B., Turan, O., Day, S., 2015, "The use of wind assist technology on two contrasting route case studies", Shipping in Changing Climates Conference, pp.75-83

Htay, W. N., Truang, T. Q., Toda, Y., 2020, "A CFD based Comparison Study of Conventional Rudder and Rudder with Bulb-Fins System of KVLCC2 in Waves", ISOPE 2020, Shanghai, China, pp.3377-3384

Huang, Y., Hou, G., Cheng, X., Feng, B., Gao, L., Xiao, M., 2017, "A new vortex search algorithm with gradient-based approximation for optimization of the fore part of KCS container ship" Journal of Marine Science and Technology, Vol. 22, Iss. 3, pp 403–413

Huang, Y. J., Feng, B. W., Hou, G. X., Gao, L., Xiao, M., 2017, "Homotopy Method for Inverse Design of the Bulbous Bow of A Container Ship" China Ocean Eng., Vol. 31, No. 1, pp. 98–102

Huang, Y. T., Lin, B. C., 2019, "Design and Development of the Energy Saving Rudder-Bulb-Fin Combination by Using Computational Fluid Dynamics Technique" PRADS'19, Yokohama, Japan

Hübbler, M., Narayanan, D., Müller, M., 2017, “Efficient retrofitting of vessels by using simulation tools and reverse engineering technologies”, International Shipbuilding Progress, Vol. 63, Iss. 3-4, pp. 109-136

Ichinose, Y., Tahara, Y., 2019, "A wake field design system utilizing a database analysis to enhance the performance of energy saving devices and propeller" Journal of Marine Science and Technology, Vol. 24, Iss. 4, pp. 1119–1133

Ichinose, Y., Tahara, Y., Takami, T., Kaneko, A., Masui T., Arai D., 2019, "A Study of Multi-objective Optimization for Propulsion Performance and Cargo Capacity" PRADS'19, Yokohama, Japan

Ikeda, Y., 2018, "Development of an Air Circulating Tank Installed in the Double Bottom of a Ship to Reduce Frictional

Resistance" INT NAM 2018, Istanbul, Turkey, April 2018, pp.109-122

Ikenoue, H., Hino, T., Takagi, Y., 2020, "Hydrodynamic Design of Energy Saving Device for Ship Scale Performance Improvement", 33rd SNH, Osaka, Japan, October 2020

Inoue, T., Saito, Y., 2017, "A Study on the Principle and Energy Saving Effect of Multi ALV-Fin" HullPIC'17, Ulrichshusen, Germany, pp.109-117

Inukai, Y., Ando J., 2017, "Full Scale Performance Prediction Method for a Ship with ContraRotating Propellers" smp'17, Espoo, Finland, June 2017

Inukai, Y., Sudo, Y., Osaki, H., Yanagida, T., Mushiake, M., Kawanami, S., 2018, "Extensive Full-Scale Measurement on Propeller Performance of 14000 TEU Container Ship" HullPIC'18, pp.27–35, Redworth, UK

Inukai, Y., Igarashi, N., Mushiake, M., Kawanami, S., 2020, "Summary of Full-Scale Measurement about Propeller Performance of 14k Container Ship" HullPIC'20, pp.126–135, Hamburg, Germany

ITTC, 1999, "Final report of the specialist committee on unconventional propulsors", 22nd International Towing Tank Conference, Seoul Korea and Shanghai, China.

ITTC, 2014a, 7.5-03-02-03 Practical Guidelines for Ship CFD Applications. 27th International Towing Tank Conference, Copenhagen, Denmark

ITTC, 2014b, 7.5-03-02-04 Practical Guidelines for Ship Resistance CFD. 27th International Towing Tank Conference, Copenhagen, Denmark

ITTC, 2014c, 7.5-03-03-01 Practical Guidelines for Ship Self-propulsion CFD. 27th International Towing Tank Conference, Copenhagen, Denmark

Jin, W., Nielsen, J. R., 2020, "Development of Controllable Pre-Swirl Fins Adapted to Different Operation Conditions", ISOPE 2020, Shanghai, China, pp.87-93

Jo, Y., Lee, H., Choi, S., Kwon, J., Ahn, S., 2013, "Aerodynamic design optimization of wing-sails", 31st AIAA Applied Aerodynamics Conference, pp. 1-24

Kang, J. G., Kim, M. C., Kim, H. U., Shin, I. R., 2019, "Study on Propulsion Performance according to Variation of Rake Distribution at Propeller Tip" smp'19, Rome, Italy, May 2019

Kanemaru, T., Yoshitake, A., Ando, J., 2017, "Development of New Type Low Drag Rudders in Propeller Slipstream" smp'17, Espoo, Finland, June 2017

Katayama, K., Okada, Y., Ichinose, Y., Fukasawa, R., 2017, "Propulsion Performance Optimization of "Neighbour Duct" by CFD" MARINE 2017, Nante, France, May 2017, pp.529-537

Katsuno, E. T., Dozzi Dantas, J. L., Nelli Silva, E. C., 2018, "Analysis of Hydrophobic Painting in Model-Scale Marine Propeller" OMAE2018-78209, Madrid, Spain

Kawakita, C., 2018, "A Hydrodynamic Design Method of Ship Applying the Air Lubrication System" ISOPE 2018, Sapporo, Japan, pp.169-176

Kim, K., Leer-Andersen, M., Werner, S., 2020, "Hydrodynamic Design of Propulsion

Devices taking into account Full Scale Roughness Effects", 33rd SNH, Osaka, Japan, October 2020

Kim, M. C., Shin, Y. J., Lee, W. J., Lee, J. H., 2017, "Study on Extrapolation Method for Self-Propulsion Test with Pre-Swirl Device," 5th International Symposium on Marine Propellers (SMP'17), Espoo, Finland, June 2017

Kim, D. Y., Lee, S. H., Paik, K. J., 2018, "Numerical Study on the Behavior of Air Layer for the Reduction of Frictional Resistance in a Model Ship" 8th PAAMES AMEC, Busan, Korea, pp.115-123

Kim, H. T., Kim, H. T., Kim, J. J., Lee, D. Y., 2019, "Study on the Skin-Friction Drag Reduction by Air Injection Using Computational Fluid Dynamics-Based Simulations" PRADS'19, Yokohama, Japan

Kimura, K., Ando, S., Ono, S., Tanaka, Y., 2019, "A Method to Predict Full Scale Performance of the Propeller Boss Cap Fins (PBCF)" smp'19, Rome, Italy, May 2019

Klijnstra, J., Bakker, M., 2017, "Drag Performance Testing in Selection of Fuel Saving Hull Coatings", 2nd Hull Performance & Insight Conference, HullPIC'17, Ulrichshusen, Germany, 27-29 March 2017

Klose, R., Schulze, R., Hellwig-Rieck, K., 2017, "Investgation of Prediction Methods for Tip Rake Propellers". smp'17, Espoo, Finland, June 2017

Kobayashi, Y., Okadak, Y., Katayama, K., Ichinose, Y., Fukasawa, R., 2017, "Optimization and Numerical Analysis of "Neighbor Duct" by CFD" NuTTS 2017, pp.115-120

Krasilnikov, V., Sileo, L., Steinsvik, K., 2017, "Numerical investigation into scale effect on the performance characteristics of twin-screw offshore vessels" smp'17, Espoo, Finland, June 2017

Krasilnikov, V., Koushan, K., Nataletti, M., Sileo, L., Spence, S., 2019, "Design and Numerical and Experimental Investigation of Pre-Swirl Stators PSS" smp'19, Rome, Italy, May 2019

Krieg, M., Mohseni, K., 2017, "Comparison of Different Methods for Estimating Energetics Related to Efficiency on an UUV with Cephalopod Inspired Propulsion". smp'17, Espoo, Finland, June 2017

Król, P., Bugalski, T., Wawrzusiszyn, M., 2017, "Development of numerical methods for marine propeller - pre-swirl stator system design and analysis" smp'17, Espoo, Finland, June 2017

Kume, K., Fukasawa, R., 2018, "Experimental Investigation of Surface Pressure Distribution of the Duct-Type Energy Saving Device for Ships both in Calm Water and in Wave Conditions" ISOPE 2018, Sapporo, Japan, pp.177-183

Lee, I., Chun, H. H., 2013, "Experimental Procedures toward the Performance Assessment for Low Frictional Marine Paints", The 3rd International Conference on Advanced Model Measurement Technology for the EU Maritime Industry, Gdansk, Poland, 17-18 September 2013

Lee, I., Park, H., 2017, "In-Service Performance Evaluation of Low Frictional AF Marine Coating" ISOPE 2017, San Francisco, USA, pp.844-850

Lee, I., Park, H., 2018, "Prediction and Verification of Full-Scale Ship Performance

of Low Frictional Marine Coating based on FDR-SPC" 32nd SNH, #35, Hamburg, Germany, August 2018

Lee, W. J., 2015, "Study on Full-Scale Performance Prediction for Pre-Swirl Device Model Test Results," Ph. D. thesis, Pusan National University

Lee, J. H., Kim, M. C., Shin, Y. J., Kang, J. G., 2017, "Study on Performance of Combined Energy Saving Devices For Container Ship by Experiments" smp'17, Espoo, Finland, June 2017

Leloup, R., Roncin, K., Bles, G., Leroux, J-B., Jochum, C., Parlier, Y., 2014, "Kite and classical rig sailing performance comparison on a one design keel boat", Ocean Engineering, Vol. 90, pp.39-48

Leloup, R., Roncin, K., Behrel, M., Bles, G., Leroux, J-B., Jochum, C., Parlier, Y., 2016, "A continuous and analytical modeling for kites as auxiliary propulsion devoted to merchant ships, including fuel saving estimation", Renewable Energy, Vol. 86, pp.483-496

Li, D. Q., Lindell, P., Werner, S., 2019, "Transitional flow on model scale propellers and their likely influence on performance prediction" smp'19, Rome, Italy, May 2019

Liarokapis, D. E., Kozadinos, G. E., Trachanas J. P., Tzabiras, G. D., 2017, "Experimental Investigation of the Trim Influence on the Resistance Characteristics of a Passenger Ship Model" AMT'17, 536 Glasgow, UK, October 2017, pp.526-536

Lin, Y. H., 2018, "The Routing Optimization of Transoceanic Voyages by Incorporating Particle Swarm Optimization Algorithm Into Weather Routing System" OMAE2018-78280, Madrid, Spain

Liu, Q., Feng, B., Liu, Z., Zhang, H., 2017, "The improvement of a variance-based sensitivity analysis method and its application to a ship hull optimization model" Journal of Marine Sscience and Technology, Vol. 22, Iss. 4, pp. 694-709

Lloyd's Register, 2015, "Wind-powered shipping: A review of the commercial, regulatory and technical factors affecting uptake of wind-assisted propulsion", London

Lu, R., Ringsberg, J. W., 2019, "Ship energy performance study of three wind-assisted ship propulsion technologies including a parametric study of the flettner rotor technology", Ships and Offshore Structures Vol. 15, No. 3, pp.249-258

Lücke, T., Streckwall, H., 2017, "Experience with Small Blade Area Propeller Performance" smp'17, Espoo, Finland, June 2017

Majidian, H., Azarsina, F., 2018, "Aerodynamic Simulation of A Containership to Evaluate Cargo Configuration Effect on Frontal Wind Loads" China Ocean Eng., Vol. 32, Iss. 2, pp.196-205

Mäkiharju, S. A., Ceccio, S. L., 2018, "On multi-point gas injection to form an air layer for frictional drag reduction" Ocean Eng., Vol. 147, pp.206-214

Makino, H., Umeda, N., Ohtsuka, T., Ikejima, G., Sekiguchi, H., Tanizawa, K., Suzuki, J., Fukazawa, M., 2017, "Energy savings for ship propulsion in waves based on real-time optimal control of propeller pitch and electric propulsion" Journal of Marine Sscience and Technology, Vol. 22, Iss. 3, pp 546 – 558

Mannarini, G., Pinardi, N., Coppini, G., 2018, "Low Carbon Intensity Routes via Ocean Currents and Waves" NAV 2018, Trieste, Italy, June 2018, pp.340-347

Matusiak, J. F., Rautaheimo, P. P., 2017, "Feasibility Study on Thrust Produced by Stabilizing Fins in Waves" ISOPE 2017, San Francisco, USA, pp.1099-1103

Mizzi, K., Demirel, Y. K., Banks, C., Turan, O., Kaklis, P., Atlar, M., 2017, "Design optimisation of Propeller Boss Cap Fins for enhanced propeller performance" Applied Ocean Research, Vol. 62, pp.210-222

Müller, J., 2017, "'HYTES' – HYKAT TESTED ENERGY SAVING DEVICES", The 5th International Conference on Advanced Model Measurement Technology for the Maritime Industry (AMT'17), pp. 347-357

Naaijen, P., Koster V., 2007, "Performance of auxiliary wind propulsion for merchant ships using a kite", 2nd International Conference on Marine Research and Transportation, pp.45-53

Nguyen, T. V., Shimizu, N., Kinugawa, A., Tai, Y., Ikeda, Y., 2017, "Numerical studies on air drag reduction methods for a large container ship with fully loaded deck-containers in oblique winds" MARINE 2017, Nante, France, May 2017, pp.1040-1051

Nian, Y. J., Hsin, C. Y., Zhou, C. S., Wu, Y. H., Shieh S-A., 2019, "Investigations of the Propeller/Pre-swirl Stator Interactions in Calm Water and in Waves" PRADS'19, Yokohama, Japan

Nielsen, J. R., Wei, J., 2019, "Pre-Swirl Fins Adapted to Different Operation Conditions" smp'19, Rome, Italy, May 2019

Niklas, K., Pruszko, H., 2019, "Full scale CFD seakeeping simulations for case study ship redesigned from V-shaped bulbous bow to X-bow hull form" Applied Ocean Research, Vol. 89, pp.188-201

Okada, Y., Katayama, K., Okazaki, A., Okazak, M., Fukuda, K., Kobayashi, Y., Kajino, T., 2017, "The Battle Royal of Energy Saving Devices for a Ship" smp'17, Espoo, Finland, June 2017

Orlandi, A., Benedetti, R., Capecchi, V., Ortolani, A., Costalli, L., 2018, "Preliminary Assessment of Route Optimisation for Fuel Minimisation and Safety of Navigation by the Use of Cooperatively Collected Data at Sea" NAV 2018, Trieste, Italy, June 2018 pp.462-471

Ouchi, K., Uzawa, K., Kanai, A., Katori, M., 2013, ""Wind challenger" the next generation hybrid sailing vessel", 3rd International Symposiums on Marine Propulsors, pp.562-567

Ouyang, X., Chang, H., Yi, Y., Feng, B., Zhan, C., Zheng, Q., 2020, "Research on Hull Form Optimization of Invisible Bulbous Ship" ISOPE 2020, Shanghai, China, pp.3858-3865

Paboeuf, S., Cassez, A., 2017, "ESD syructural issue – Upstream device", International Shipbuilding Progress, Vol. 63, Iss. 3-4, pp. 291-314

Park, S. H., Lee, I., 2018, "Optimization of Drag Reduction Effect of Air Lubrication for a Tanker Model" International Journal of Naval Architecture and Ocean Engineering, Vol. 10, No. 4, pp.427-438

Park, S. H., Park, S. C., Lee, I., 2018, "Air Lubrication Sweep Angle Estimation Based on Air Injection Condition Using Model

Experimental Image Analysis" 8th PAAMES AMEC, Busan, Korea, pp.105-114

Park, K-R, Song, G-S., Kim, H-J., Son, H-J., Park, H-G., 2020, "Hull form design for resistance minimization of small-scale LNG bunkering vessels using numerical simulation", International Journal of Naval Architecture and Ocean Engineering, Vol. 12, pp.856-857

Parker, J., 2013, "Future ship powering options. Exploring alternative methods of ship propulsion." Royal Academy of Engineering, pp.1–94.

Pearson, D. R., 2014, "The use of Flettner rotors in efficient ship design." RINA, Royal Institution of Naval Architects - Influence of EEDI on Ship Design 2014, June 2014, 162–169.

Peifer, B. C., Callahan-Dudley, C., Mäkiharju, S. A., 2020, "Air Layer on Superhydrophobic Surface for Frictional Drag Reduction" Journal of Ship Research, Vol. 64, No. 2, pp. 118-126

Pérez-Sobrino, M., González-Adalid, J., Quereda, R., Soriano, C., Morán, A., Gennaro, G., 2016a, "Scale effects in open water test results for performance prediction of conventional and unconventional propellers" Ingeniería Naval Académica. 2016. (Nº 5). Download available in web: "http://sectormaritimo.es/numero-5-abril2016". ISSN: 2340-4779.

Pérez-Sobrino, M., González-Adalid, J., Soriano, C., Morán, A., Gennaro, G., 2016b, "A New Performance Prediction Procedure for Propellers with Unconventional Tip Shape" 12th International Conference on Hydrodynamics, Paper ID: 73, Delft, The Netherlands, September 2016

Quereda, R., Sobrino, M. P., Gonzalez-Adalid, J., Soriano, C., 2017, "Conventional propellers in CRP-POD configuration. Tests and extrapolation" smp'17, Espoo, Finland, June 2017

Quereda, R., Pérez-Sobrino, M., González-Adalid, J., Soriano, C., 2019a, "CRP propulsion system for merchant ships. Past, present and future" smp'19, Rome, Italy, May 2019

Quereda, R., Bernal, L., Pérez-Sobrino, M., González-Adalid, J., 2019b, "Critical values of Rn defining transitional flow to be applied in the extrapolation of Open Water Tests (OWT) of unconventional tip shaped propellers" smp'19, Rome, Italy, May 2019

Raven, H. C., 2018, "Minimising Ship Afterbody Wave Making using Multifidelity Techniques" 32nd SNH, #84, Hamburg, Germany, August 2018

Raven, H. C., Scholcz, T. P., 2019, "An Assessment of Multifidelity Procedures for Ship Hull Form Optimisation" MARINE 2019, Gothenburg, Sweden, May 2019, pp.189-200

Ravina, E., Guidomei, S., 2018, "Experimental Investigation on Resistance Reduction by Means of Air-Bubbling Technique" OMAE2018-77980, Madrid, Spain

Rehmatulla, N., Smith, T., 2015, "Barriers to energy efficient and low carbon shipping." Ocean Engineering, Vol. 110, pp.102–112.

Rehmatulla N., Parker S., Smith T., Stulgis V., 2017, "Wind technologies: Opportunities and barriers to a low carbon shipping industry", Marine Policy, Vol. 75, pp.217-226

Remaud, R., Guilcher, P. M., Leroux, J. B. Laurens, J. M., 2019, "Design of Ducted Propellers" NuTTS 2019, Tomar, Portgal

Rotte, G., Kerkvliet, M., van Terwisga, T., 2018, "An Investigation of Air Cavity Closure Mechanisms using Scale Resolving Simulations" NuTTS2018, Cortna, Italy

Sakamoto, N., Kobayashi, H., Ohashi, K., Kawanami, Y., Windén, B., Kamiirisa, H., 2020, "An overset RANS prediction and validation of fullscale stern wake for 1,600TEU container ship and 63,000 DWT bulk carrier with an energy saving device", Applied Ocean Research, Vol. 105, 102417

Sánchez-Caja, A. González-Adalid, J., Pérez-Sobrino M., Sipilä T., 2014, "Scale effects on tip loaded propeller performance using a RANSE solver", Ocean Engineering, Vol. 88, pp. 607-617

Sánchez-Caja, A., Rauti, T., Ramstedt, K., Sipilä, T., 2017, "Numerical Investigation of Multi-Component Podded Propulsor Performance in Straight Flow" smp'17, Espoo, Finland, June 2017

Sánchez Castro, L. F., von Zadow, H., Vesting, F., 2019, "Tip Geometry Effects on Performance and Erosion for Tip Rake Propellers" smp'19, Rome, Italy, May 2019

Sasaki N., Atlar M., Kuribayashi S., 2016, " Advantages of twin rudder system with asymmetric wing section aside a propeller" Journal of Marine Sscience and Technology, Vol.21, pp.297-308

Sasaki, N., Kuribayashi, S., Atlar, M., 2018, "Gate Rudder" INT NAM 2018, Istanbul, Turkey, April 2018, pp.89-108

Sasaki, N., Atlar, M., 2019, "Scale Effect of Gate Rudder" smp'19, Rome, Italy, May 2019

Sasaki, N., Kuribayashi, S., Fukazawa, M., Atlar, M., 2019, "Gate Rudder Performance" AMT'19, Glasgow, October 2019

Scholcz, T. P., Veldhuis, C. H. J., 2017, "Multi-objective surrogate based hull-form optimization using high-fidelity RANS computations" MARINE 2017, Nante, France, May 2017, pp.231-242

Schrader, L. U., 2018, "Passive Drag Reduction via Bionic Hull Coatings", 32nd Symposium on Naval Hydrodynamics Hamburg, Germany, 5-10 August 2018

Schrader, L.U., 2019, "Passive Drag Reduction via Bionic Hull Coatings" Journal of Ship Research, Vol. 63, Issue 3, September 2019, pp.206-218

Schrader, L. U., Marzi J., 2017, "A Novel Power-Saving Device for Full-Block Vessels" NuTTS 2017, pp.205-210

Schuilling, B., van Terwigsa, T., 2017, "Hydrodynamic working principles of Energy Saving Devices in ship propulsion systems", International Shipbuilding Progress, Vol. 63, Iss. 3-4, pp. 255-290

Schulze, R., Klose, R., 2017, "Friction Measurements of Different Coatings in a Friction Tunnel", 2nd Hull Performance & Insight Conference, HullPIC'17, Ulrichshusen, Germany, 27-29 March 2017

Segawa, K., Ikeda, T., Ando, S., Kimura, K., 2019, "Marine Propeller Optimum Design in Wake Flow of Energy Saving Devices" PRADS'19, Yokohama, Japan

Shin, K. W., Andersen, P., 2017, "CFD Analysis of Scale Effects on Conventional and Tip-Modified Propellers" smp'17, Espoo, Finland, June 2017

Silberschmidt, N., Tasker, D., Pappas, T., 2016, "Silverstream® System – Air Lubrication Performance Verification and Design Development",10th Symposium on High-Performance Marine Vehicles, HIPER'16, Cortona, Italy, 17-19 October 2016, pp. 236-246

Smith, T., Raucci, C., Hosseinloo, S.H., Rojon, I., Calleya, J., De La Fuente, S., Wu, P., Palmer, K., "CO2 emissions from international shipping. possible reduction targets and their associated pathways", UMAS, London, UK

Sogihara, N., Tsujimoto, M., Fukasawa, R., Ohba, H., 2018, "Trim Optimization for Ship Performance in Actual Seas" INT NAM 2018, Istanbul, Turkey, April 2018, pp.551-564

Staffell I., Pfenninger S., 2016, "Using bias-corrected reanalysis to simulate current and future wind power output", Energy, Vol. 114 pp.1224-1239

Streckwall, H., Yan, X-K., 2017, "On the working principle of pre-swirl stators and on their application benefit and design targets", International Shipbuilding Progress, Vol. 63, Iss. 3-4, pp. 87-107

Streckwall, H., Greitsch L., Müller, J., Scharf, M., Bugalski, T., 2013, "Development of a strip method proposed to serve as a new standard for propeller performance scaling", Ship Technology Research, May 2013.

Su, Y., Kinnas, S.A., Jukola, H., 2017, "Application of a BEM/RANS Interactive Method to Contra-Rotating Propellers" smp'17, Espoo, Finland, June 2017

Suryateja, A., Srinivas, K. S., Bhattacharyya A., Sha O.P., 2019, "Asymmetric Stern Modifications for KVLCC2G" PRADS'19, Yokohama, Japan

Tacar, Z., Korkut, E., 2017, "Inflow Optmization with an Energy Saving Duct" AMT'17, Glasgow, October 2017

Tacar, Z., Sasaki, N., Atlar, M., Korkut, E., 2019, "Investigation of Scale Effects on Gate Rudder Performance" AMT'19, Glasgow, October 2019

Tachikawa, T., Okada, Y., Katayama, K., Okazaki, A., Okazaki, M., Fukuda, K., Kobayashi, Y., Kajino, T., 2019, "Efficiency improvement effect and water noise reduction by energy saving devices" MARINE 2019, Gothenburg, Sweden, May 2019, pp.603-612

Tahara, Y., Ichinose, Y., Kaneko., A., Kasahara Y., 2019, "Variable decomposition approach applied to multi-objective optimization for minimum powering of commercial ships" Journal of Marine Sscience and Technology, Vol. 24, Iss. 1, pp 46–59

Talluri, L., Nalianda, D., Kyprianidis, K., Nikolaidis, T., Pilidis, P., 2016, "Techno economic and environmental assessment of wind assisted marine propulsion systems", Ocean Engineering, Vol. 121, pp.301-311

Themelis, N., Spandonidis, C., Giordamlis, C., 2019, "Evaluating the Efficiency of an Energy-Saving Device by Performance Monitoring" HullPIC'19, Gubbio, Italy, pp.56-64

Traut, M., Gilbert, P., Walsh, C., Bows, A., Filippone, A., Stansby, P., Wood, R., 2014,

"Propulsive power contribution of a kite and a flettner rotor on selected shipping routes", Applied Energy, Vol. 113, pp.362-372

Truong, T. Q, Wu, P. C., Aoyagi, K., Koike, K., Akiyama Y., Toda Y., 2017, "The EFD and CFD Study of Rudder-Bulb-Fin System in Ship and Propeller Wake Field of KVLCC2 Tanker in Calm Water" ISOPE 2017, San Francisco, USA, pp.823-830

Truong, T. Q., Wu, P. C., Kishi, J., Toda, Y., 2018, "Improvement of Rudder-Bulb-Fin System in Ship and Propeller Wake Field of KVLCC2 Tanker in Calm Water" ISOPE 2018, Sapporo, Japan, pp.184-190

Turan, O., Cui, T., Howett, B., Day, S., 2018, "Assessing the Performance of Ships Fitted with Wind Assist Technologies: Flettner Rotor Case Study" INT NAM 2018, Istanbul, Turkey, April 2018, pp.217-230

van der Ploeg, A., Schuiling B., 2018, "Improving an Already Optimized Ship by Making its Stern Asymmetric" COMPIT'18, Pavone, Italy, pp.84-97

von Doenhoff, A. E., Horton, E. A., 1956, "A low-speed experimental investigation of the effect of a sandpaper type of roughness on boundary layer transition", NACA Report 1349, August 1956.

Van, S. H., Kim, M. C., and Lee, J. T., 1993, "Some remarks on the powering performance prediction method for a ship equipped with a pre-swirl stator-propeller system" ITTC 1993, Vol. 2.

Viola, I. M., Sacher, M., Xu, J., Wang F., 2015, "A numerical method for the design of ships with wind-assisted propulsion", Ocean Engineering, Vol. 105 pp.33-42

Voermans, A., 2017, "Development of the Wärtsilä EnergoFlow: An innovative energy saving device" smp'17, Espoo, Finland, June 2017

Wackers, J., Jeanson, C-E., Queutey, P., Visonneau M., Pellegrini R., Serani A., Diez M., 2018, "Hull shape optimisation using multi-fidelity metamodels and adaptive grid refinement" NuTTS2018, Cortna, Italy

Wang, C., Han, F., Hu, A., 2017, "Design and Performance Investigation of the Energy Recovering Rudder Bulb-turbine Device" OMAE2017-62485, Trondheim, Norway

Wang, L., He, S., Wang, J., Chen, S., Jin, Y., Li, Q., 2017, "Model Test Research of Low-speed Vessel on Gas Film Drag Reduction", ISOPE 2017, San Francisco, USA, 25-30 June 2017, pp. 835-838

Wang, H., Chen, S., Wang, L., 2018, "Experimental Research on the Influence of Air film on Propulsion Performance and Power Forecast of Low-Speed ship" ISOPE 2018, Sapporo, Japan, pp.832-838

Wang, H., Mao, W., Eriksson, L., 2018, "MetOcean Data Drived Voyage Optimization Using Genetic Algorithm" ISOPE 2018, Sapporo, Japan, pp.697-705

Wang, H., Mao, W., Eriksson, L., 2017, "Benchmark Study of Five Optimisation Algorithms for Weather Routing" OMAE2017-61022, Trondheim, Norway

Wang, L., He, S., Wang, J., Chen, S., Jin Y., Li Q., 2017, "Model Test Research of Low-speed Vessel on Gas Film Drag Reduction" ISOPE 2017, San Francisco, USA, pp.835-838

Wang, H., Chen, S., Wang, L., 2018, "Experimental Research on the Influence of

Air film on Propulsion Performance and Power Forecast of Low-Speed ship" ISOPE 2018, Sapporo, Japan, pp.832-838

Wei, C. Z., Li, Y. H., Liang, X. F., Yi, H., 2019, "Hull forms of small high-speed wave-piercing monohull crafts and hydrodynamics study" Journal of Hydrodynamics, Vol.31, pp.814-826

Wei, X., Chang, H., Feng, B., Liu, Z., Huang, C., 2019, "Hull form reliability-based robust design optimization combining polynomial chaos expansion and maximum entropy method" Applied Ocean Research, Vol. 90, pp.1-12

Wienke, J., 2017, "Verification of the Effectiveness of Energy Saving Devices" HullPIC'17, Ulrichshusen, Germany, pp.102-108

Xiong, X., Chen, H., Yu, H., He, J., Feng, Y., 2019, "Optimization Design of Novel Afterbody Shape for a Cruise Ship" PRADS'19, Yokohama, Japan

Xu, L., Wan, D., 2018, "Numerical Investigation of Scale Effect for Propeller Boss Cap Fins" ISOPE 2018, Sapporo, Japan, pp.805-811

Yang, F., Wang, L., Wang, J., Chen, S., Luo, L., Wang, M., 2017, "Numerical Simulation on Drag Reduction of River-sea Bulk Cargo by Gas Film" ISOPE 2017, San Francisco, USA, pp.839-843

Yang, K. K., Kim, Y., 2017, "Numerical analysis of added resistance on blunt ships with different bow shapes in short waves" Journal of Marine Sscience and Technology, Vol. 22, Iss. 2, pp 245–258

Yang, L., Li, S. Z., Zhao, F., Ni, Q. J., 2018, "An integrated optimization design of a fishing ship hullform at different speeds" Journal of Hydrodynamics, Vol. 30, Iss. 6, pp.1174-1181

Yasukawa, H., Ishikawa, T., 2017, “Improvement of Propulsive Performance of a Catamaran in Waves by a Biologically Inspired Hydrofoil”, 11th Symposium on High-Performance Marine Vehicles, HIPER’17, Zevenwacht, South Africa, 11-13 September 2017

Yehia, W., Moustafa, M. M., Tawfik, A. A., Nasef A., 2019, "Shipboard Fuel Consumption Reduction by Air Lubrication and Trim Optimization" OMAE2019-96770, Glasgow, UK

Yu, J. W., Lee, C. M., Lee, I., Choi, J. E., 2017, "Bow hull-form optimization in waves of a 66,000 DWT bulk carrier" International Journal of Naval Architecture and Ocean Engineering, vol. 9, pp.499-508

Zaccone, R., Figari, M., Martelli, M., 2018a, "An Optimization Tool For Ship Route Planning In Real Weather Scenarios" ISOPE 2018, Sapporo, Japan, pp.738-744

Zaccone, R., Ottaviani, E., Figari, M., Altosole, M., 2018b, "Ship voyage optimization for safe and energy-efficient navigation: A dynamic programming approach" Ocean Eng., Vol. 153, pp.215-224

Zhang, B. J., Zhang, S. L., Zhang, H., 2018, "Optimization Design of Minimum Total Resistance Hull Form Based on CFD Method " China Ocean Eng., Vol. 32, Iss. 3, pp.323-330

Zhang, D., He, W., Li, Z., 2020, "Analysis of Hydrodynamic Performance of Tip Loaded Propellers" ISOPE 2020, Shanghai, China, pp.3789-3796

Zhang, H., Dong, X. Q., Li, W., Yang, C. J., Noblesse, F., 2019, "Effects of Section Geometry on the Energy-saving Rate of PBCF and Model/full-scale Correlation - A CFD Study" MARINE 2019, Gothenburg, Sweden, May 2019, pp.670-681

Zhang, S. L., Zhang, B. J., Tahsin, T., Xu, L. P., Lai, Y. Y., 2017, "Research on Bulbous Bow Optimization Based on the Improved PSO Algorithm" China Ocean Eng., Vol. 31, Iss. 4, pp.487-494

Zhang, Y., Turan, O., 2017, "Numerical investigation of shark skin inspired riblet drag reduction structure" ISOPE 2017, San Francisco, USA, pp.851-856

Zhao, X. J., Zong, Z., Jiang, Y. C., Pan, Y., 2019, "Numerical simulation of micro-bubble drag reduction of an axisymmetric body using OpenFOAM" Journal of Hydrodynamics, Vol.31, pp.900-910

Zhao, X., Zong, Z., Jiang, Y., Sun, T., 2020, "A numerical investigation of the mechanism of air-injection drag reduction" Applied Ocean Research Vol. 94, 101978

Zhou, C. S., Mao, Y. T., Nian, Y. J., Hsin, C. Y., Shih M.M., Shieh S.A., 2018, "Analysis of the Pre-Swirl Stator Effects in Waves" 8th PAAMES AMEC, Busan, Korea, pp.13-21

Zhao, X-J., Zong, Z., Jiang, Y-C., Pan, Y., 2019, "Numerical simulation of micro-bubble drag reduction of an axisymmetric body using OpenFOAM" Journal of Hydrodynamics, Vol.31, pp.900-910

Zhao, X., Zong, Z., Jiang, Y., Sun, T., 2020, "A numerical investigation of the mechanism of air-injection drag reduction" Applied Ocean Research, Vol. 94, 101978

Zhou, C-S., Mao, Y-T., Nian, Y-J., Hsin, C-Y., Shih M-M., Shieh S-A., "Analysis of the Pre-Swirl Stator Effects in Waves" 8th PAAMES AMEC, Busan, Korea, pp.13-21

The Specialist Committee on Hydrodynamic Noise

Final Report and Recommendations to the 29th ITTC

1. OVERVIEW

This report summarizes the work of the Specialist Committee on Hydrodynamic Noise for the 29th ITTC.

1.1 MEMBERSHIP AND MEETINGS

The 28th ITTC appointed the following members to serve on the Specialist Committee on Hydrodynamic Noise:

- Johan Bosschers (chair), MARIN, Netherlands
- Romuald Boucheron, DGA/H, France
- Yezhen Pang, CSSRC, China
- Cheolsoo Park, KRISO, Korea
- Bryce Pearce (secretary), AMC, Australia
- Kei Sato, MHI, Japan
- Tuomas Sipilä, VTT, Finland, (resigned in February 2020 due to job change).
- Claudio Testa, CNR/INM, Italy
- Michele Viviani, UNIGE, Italy

The committee held three face-to-face meetings at the following locations:

- Wageningen, Netherlands, at MARIN on February 7-8, 2018
- Launceston, Australia, at AMC, on March 27-28, 2019
- Rome, Italy, at CNR/INM on February 30-31, 2020

Figure 49. Photograph of the Specialist Committee on Hydrodynamic Noise at its first meeting.

Video conferences were held on June 27, 2018; August 1, 2019; July 30, 2020; September 24, 2020; October 29, 2020; and January 27+28, 2021.

1.2 RECOMMENDATIONS OF THE 28TH ITTC

The 28th ITTC recommended the Specialist Committee on Hydrodynamic Noise for the 29th ITTC to address the following activities:

13. Present ITTC procedures and our community's capabilities to predict emitted noise from ships to the IMO. Specifically, an informative submission shall be made to MEPC 72 (Spring, 2018) of Guideline 7.5-02-01-05 Model-scale propeller cavitation noise measurements.
14. Monitor progress on shipping noise measurement procedures for shallow water and regulations as developed by ISO, classification societies and regulatory agencies.
15. Monitor progress on model-scale noise measurements with emphasis on facility reverberation and scaling of vortex cavitation noise.
16. Monitor progress on computational prediction of propeller noise with emphasis on methods using the acoustic analogy such as coupling CFD with FWHE.
17. Identify a benchmarking case for model-scale noise measurements that has,
    a) full-scale underwater radiated noise measurements available,
    b) that is a representative merchant vessel.
    c) of which geometry and measurement data can be shared with the ITTC community.
18. Maintain and update ITTC guideline 7.5-02- 01-05: Model-Scale Propeller Cavitation Noise Measurements and guideline 7.5-04-04-01: Underwater Noise from Ships, Full-Scale Measurements.

For various reasons, the Specialist Committee decided to not prepare an informative submission to the IMO MEPC 72 to be held in Spring 2018. However, an informative document was submitted by the Secretary of the ITTC without input from the Specialist Committee. For that reason, term of reference no. 1 is not further addressed in this report.

2. INTRODUCTION

Noise is described as unwanted sound which interferes with the normal functioning of a system. The noise that is described in this report is the underwater radiated noise of ships in general and of the cavitating propeller in particular. Ship noise is considered as unwanted sound as it increases the signature of naval vessels in relation to threats such as submarines, mines, and torpedoes. It may also interfere with the ability of marine mammals (Southall *et al.*, 2008) and fish (Popper & Hastings, 2009) to hear a sound of interest (masking). A significant number of studies have been and are being performed on the impact of shipping noise on marine life as shown in Figure 50. An extensive

review of these studies has been given by Duarte *et al*. (2021).

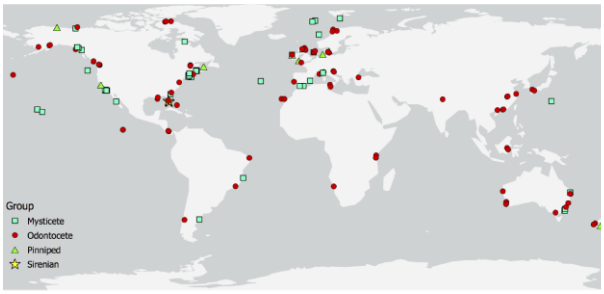

Figure 50. Map showing locations where the effect of ship noise on marine mammals has been or is being studied (Erbe, 2019).

In response to the concern of the effect of underwater noise by shipping on aquatic life, the IMO, class societies, governmental bodies and other organizations have addressed the underwater radiated noise (URN) of merchant vessels as further reviewed in this report.

The various mechanisms that contribute to the URN of ships are discussed by Ross (1976), Urick (1983), and the reports of the 27th and 28th ITTC Specialist Committee on Hydrodynamic Noise. The most important noise sources are machinery noise comprising propulsion and auxiliary components, and propeller cavitation noise. Machinery noise is typically emitted up to a frequency of about 1 kHz whereas propeller cavitation noise is emitted in the frequency range of the blade passage frequency (say 10 Hz) up to 20 kHz and above. An example of the URN spectrum of a merchant vessel is shown in Figure 51. At and below the cavitation inception speed of 10 knots, the noise is caused by machinery equipment. At higher speeds, the high-frequency noise is fully determined by propeller cavitation while the low-frequency noise is due to both machinery equipment and cavitation, with cavitation fully dominant at 16 knots.

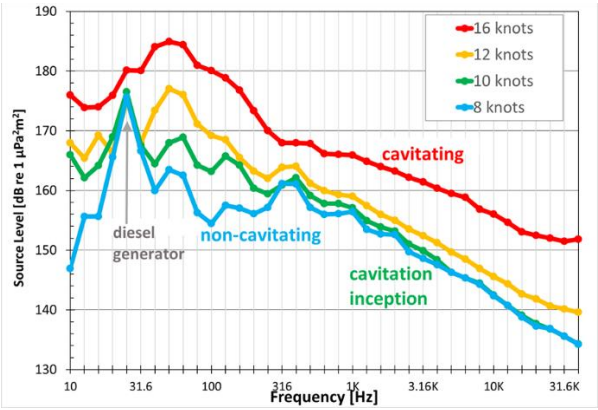

Figure 51. Underwater radiated noise spectrum of a 173 m merchant vessel, data taken from Arveson & Vendittis (2000). Cavitation inception speed is about 10 knots.

Almost all merchant vessels operate with a cavitating propeller at service speed, showing the importance of cavitation noise, with the URN levels decreasing with lower ship speed until the propeller is free from cavitation at shown in Figure 51. However, controllable pitch propellers are known to cavitate at both low and high speed and can be free from cavitation at an intermediate speed.

The interest in the URN of merchant vessels has led to several review studies on URN mitigation measures, such as Renilson (2009), Aquo-Sonic Guidelines for regulation on UW noise from commercial shipping (2015), Chmelnitsky & Gilbert (2016), McHorney *et al*. (2018), and Kendrick & Terweij (2019). In general, mitigation measures to reduce the source level of the cavitating propeller aim to either reduce ship resistance thereby reducing propeller loading, improving the homogeneity of the ship wake field in which the propeller operates, improved propeller or propulsor design with respect to cavitation extents, or using air bubbles to alleviate the cavity collapse and rebound. Measures such as ship speed reduction and rerouting have also been proposed and investigated, as well as improved manufacturing and maintenance of the propeller.

3. REGULATION

This chapter reviews the recent developments on the regulation of shipping noise at an international and national level. A more extensive review on this topic is provided by Colbert (2020). The rules of classification societies on URN are also discussed.

3.1 INTERNATIONAL LEVEL

The IMO has released non-mandatory 'Guidelines for the Reduction of Underwater Noise from Commercial Shipping' in 2014, but the topic of URN has not been on the agenda of the MEPC since. For the 75th session of the MEPC, scheduled for April 2020, proposal MEPC/75/14 was submitted by Australia, Canada and the United States with as proposed action to review the IMO guidelines and to identify next steps. The proposal was supported by a large number of countries of the EU (document MEPC/75/14/2) in which it was also proposed to address URN on the agenda of MEPC76. However, the 75th session was cancelled due to COVID-19, and was organized as a virtual meeting in November 2020. In that meeting, proposal MEPC/75/14 could not be discussed due to time restrictions and the discussion has been postponed to MEPC76.

Meetings to discuss the impact of underwater anthropogenic noise were also organized by the UN Food and Agriculture Organization (FAO, 2019) and the United Nation Convention of Law of the Sea (UNCLOS, 2018).

The International Quiet Ocean Project [1] (IQOE) aims to promote research, observations, and modelling to improve understanding of ocean soundscapes and effects of sound on marine organisms. The IQOE was founded by the Scientific Committee on Oceanic Research (SCOR) and the Partnership for Observation of the Global Oceans (POGO). The website contains a large number of links to related projects.

3.2 NATIONAL LEVEL

Australia is closely following and endorsing the developments at IMO on URN by shipping and its impact on marine life, largely due to their concern regarding the Great Barrier Reef (GBR). Legislation for Particular Sensitive Sea Areas (such as GBR) allows for speed limits to be set.

The EU has defined the Marine Strategy Frameword Directive 2008/56/EC which aims to achieve good environmental status, including underwater noise, in the European marine waters by 2020. At present, various monitoring campaigns of ambient underwater noise (sound scaping), which includes the noise of shipping, have started on a regional level, being among others the JOMOPANS [2] project in the North Sea, the QuietMED2 [3] project in the Mediterranean Sea, and the JONAS[4] project in the Atlantic Seas. The TANGO project investigates the effect of rerouting shipping lanes in the Kattegat on the soundscape and ecosystem.

Whereas the assessment of the present levels of ambient underwater noise in the European marine waters is well on its way, the critical levels have not yet been determined. The EU Technical Group on Underwater Noise (TG

[1] https://www.iqoe.org

[2] https://www.northsearegion.eu/jomopans/

[3] https://www.quietmed2.eu

[4] https://www.jonasproject.eu

Noise) provides guidance on noise monitoring and an assessment of framework and thresholds for good environmental status for impulsive and continuous noise.

Canada has a number of major shipping routes that overlap with the habitat of endangered animals like the North Atlantic right whale, the beluga whale, and the Southern Resident killer whale. Canada has regulatory mechanisms for the protection of imperilled animals through the Species at Risk Act (SARA). In 2019, measures to reduce underwater noise levels in British Columbia were introduced by the Fisheries and Oceans Canada (DFO) consisting of among others introducing no-go zones for vessels and voluntary guidelines to reduce ship speed to 7 knots or less when within 1000m of killer whales. Also, various noise monitoring programs were initiated by DFO.

Transport Canada has taken several initiatives to reduce shipping noise, such as funding a literature review on ship noise mitigation measures (Kendrick & Terweij, 2019) and organizing an international workshop on 'Quieting ships to protect the marine environment' in London (Bahtiarian, 2019). Both short-term and long-term recommendations for action and future work were defined, such as development of an improved quiet ship design guide, harmonizing the URN limits and measurement methodologies used by class societies, and improving prediction methods for hull and propeller URN prediction.

The Port of Vancouver has introduced in 2017 a discount system, EcoAction, to encourage URN mitigation measures on ships. In 2019, the program was expanded by incorporating rules of more class societies. In 2017, the Port of Prince Rupert has introduced a similar discount system, called Green Wave.

In the US, NOAA has published a roadmap to address ocean noise for a period of 10 years (Gedamke *et al.*, 2016). Marine mammals are protected in the U.S. by the Marine Mammal Protection Act and the Endangered Species Act. NOAA and other organizations are working to better understand underwater sound within the National Marine Sanctuary System[5], see Figure 52 for an example. Sound within seven national marine sanctuaries and one marine national monument will be studied. Standardized measurements will assess sounds produced by marine animals, physical processes (e.g., wind and waves), and human activities, and some results have been published by Haver *et al.* (2019)

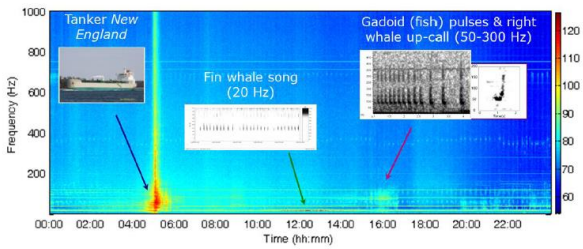

Figure 52. Example of 24-hour soundscape at Stellwagen Bank National Marine Sanctuary (Gedamke *et al.*, 2016).

The Green Marine voluntary certification program for the North American marine industry has also renewed its criteria in 2020 for ports and for ship owners on underwater radiated noise.

5 https://sanctuaries.noaa.gov/science/monitoring/sound/ , https://www.pmel.noaa.gov/acoustics/

3.3 Noise criteria

The first public noise criteria issued for non-military ships is probably the ICES[6] CR209 rule for the URN of fishery research vessels (Mitson, 1995). These noise criteria have also been adopted by classification societies, although sometimes small changes are applied in the lower frequency range.

The first classification society to issue URN rules was DNV through its Silent class in 2010, with its latest version issued in 2019. A distinction was made between five different classes of ships, each with a different criterion, being: *i)* Acoustic (ships involved in hydro-acoustic measures); *ii)* Seismic (ships involved in seismic surveys); *iii)* Fishery; *iv)* Research; and *v)* Environmental (any vessel which require controlled environmental noise emission). Other class societies followed with BV releasing rule NR614 on underwater radiated noise in 2014 (with an update in 2017) which specifies noise limits for a "URN – controlled vessel" and a "URN – advanced vessel". Ship speeds or engine load is not specified by BV. The noise limits for a "URN – specified vessel" are specified on a case-by-case study but may for instance consist of the ICES 209 norm. LR issued its noise criteria in 2017 making a distinction between Transit, Quiet and Research levels. The ship speed or engine load at which the criteria is to be met depends on ship type. RINA has released the DOLPHIN class in 2017 in which underwater radiated noise limits are defined for a "Quiet Ship" and for a "Transit Ship" while noise limits are also given for yachts and pleasure yachts. ABS issued its rules for underwater noise (UWN) in 2018 making a distinction between Commercial Vessels (either Transit or Quiet), Research Vessels, and UWN+ requirements for Commercial Vessels (either Transit or Quiet), with noise limits that are 5 dB below those of 'regular' Commercial Vessels. The ship speed for the Quiet condition depends on ship length. CCS issued its criteria in 2018 and also distinguishes three noise levels, designated Underwater Noise 1, Underwater Noise 2, and Underwater Noise 3. The ship speeds are not specified. The list of class rules on URN is given in Table 1.

The noise criteria for commercial vessels corresponding to Quiet and Transit, or similar criteria, of these class societies are presented in Figure 53 and Figure 54. Note that there are small differences in ship speeds for the Quiet condition and the engine load for the Transit condition, and that some classes do not prescribe the ship condition. LR is the only class society that prescribes the noise levels as source levels which explains the higher noise limits at low frequencies, all other class societies use radiated noise levels. BV is the only class society that prescribes the noise levels in spectrum level (i.e., dB re 1 $\mu Pa^2m^2/Hz$), all other class societies use one-third-octave levels. The noise limits by BV have been converted to one-third-octave levels in the figures. The noise limits by ABS correspond to their UWN+ class. The most stringent noise limits are by CCS.

[6] International Council for the Exploration of the Sea

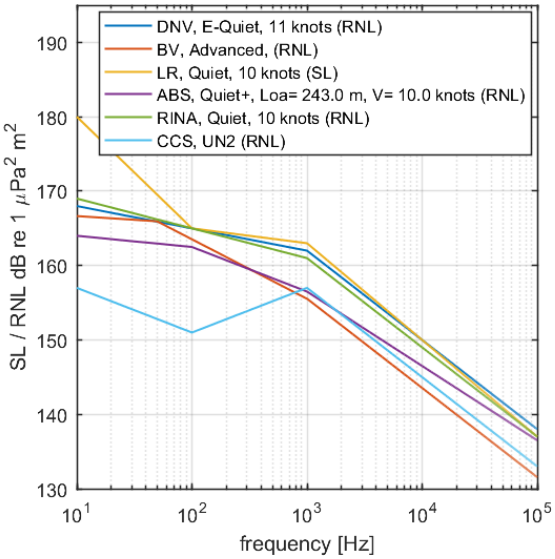

Figure 53. Noise criteria for 'Quiet' condition of commercial ships of various classification societies.

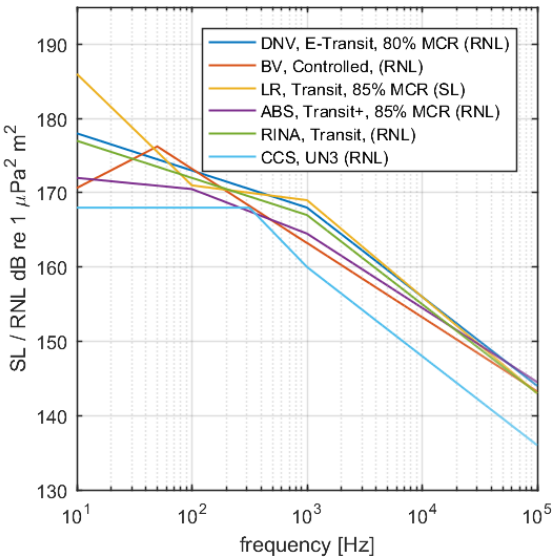

Figure 54. Noise criteria for 'Transit' condition of commercial ships of various classification societies.

Table 5. Standards for the measurement of the underwater radiated noise from ships.

National/International Standards
• ANSI/ASA, 2009, Quantities and procedures for description and measurement of underwater sound from ships, Part 1: General requirements, ANSI/ASA S12.64-2009/Part 1
• ISO 17208-1:2016 Underwater acoustics – Quantities and procedures for description and measurement of underwater sound from ships – Part 1: Requirements for precision measurements in deep water used for comparison purposes
• ISO 17208-2:2019. Underwater acoustics – Quantities and procedures for description and measurement of underwater sound from ships – Part 2: Determination of source level from deep water measurements.
• ISO/NP 17208-3:2017. Underwater acoustics – Quantities and procedures for description and measurement of underwater noise from ships – Part 3: Requirements for measurements in shallow water (under development in ISO/TC43/SC3)
• ISO 18405:2017 Underwater acoustics – Terminology.
Rules of Classification Societies
• DNV-GL (2020), Rules for classification – Ships – DNVGL-RU-Ship Pt.6 Ch.7, Section 6 Underwater Noise Emission - Silent • DNV-GL (2019), Class Guideline DNVGL-CG-0313, Edition July 2019, Measurement procedures for noise emission
• BV (2018), Underwater Radiated Noise (URN), Bureau Veritas Rule Note NR614
• RINA (2017), Amendments to Part A and Part F of "Rules for the Classification of Ships" - New additional class notation: "DOLPHIN QUIET SHIP" and "DOLPHIN TRANSIT SHIP"
• ABS (2018), Guide for the classification notation
• LR (2018), ShipRight - Design and Construction - Additional Design and Construction Procedure for the Determination of a Vessel's Underwater Radiated Noise
• CCS (2018), Guideline for ship underwater radiated noise

4. FULL-SCALE MEASUREMENT

4.1 REVIEW OF STANDARDS AND PROCEDURES

4.1.1 General review

The measured URN of a ship is affected by many factors such as ship operating condition, distance between hydrophone and ship, depth of hydrophone, measurement time, water depth, etc. As the measurement result should not depend on measurement procedures, ANSI/ASA and ISO standards have been developed for the full-scale measurement of the URN of ships. These standards are listed in Table 1. Standards have been released for deep water (from an acoustic point of view) while a standard for shallow water is still in development. Reviews and discussions of aspects relevant for the URN measurements can be found in Moreno (2014), Robinson *et al.* (2014), and the ITTC guideline 7.5-04-04-01 on Underwater Noise from Ships, Full Scale Measurements (ITTC, 2017b).

Six classification societies, such as CCS (China Classification Society), RINA (Italian Classification Society), DNV-GL (Det Norske Veritas - Germanischer Lloyd), BV (Bureau Veritas), ABS (American Bureau of Shipping) and LR (UK Lloyd's Register) have issued rules for underwater noise testing of ships. Here the differences in test requirements, test procedure and underwater noise criteria are reviewed together with ISO standards. An overview of the rules are provided in Appendix A of this report.

Hannay *et al.* (2019) reviewed the methods implemented by five Quiet Ship Certification Procedures considered. Each of the classification societies has defined one or more notations, indicating vessels meet corresponding specified noise emission criteria. In all cases the criteria are a set of 1/3-octave band (or in one case the spectral density distribution) of maximum noise emission levels. Each society also defines a measurement procedure, that includes site/depth requirements, hydrophone geometry, ship track layout, and sound level calculation instructions. Differences in the measurement procedures leads to numeric differences in measured levels between class notations. If measurement configurations are well documented, then it is possible to adjust measurements from one class notation to compare with those of another.

DNV-GL also allows for the measurement of URN using onboard pressure sensors mounted on the hull above the propeller, Figure 55 (see class guideline DNVGL-CG-0313, July 2019). The simplified measurement method is based on pressure measurements in the vicinity of the vessel's propeller(s). The method is not applicable for testing of the Silent(R) requirements or for the thruster condition of Silent(A). Additionally, the method is only applicable for vessels equipped with diesel electric propulsion systems with resiliently mounted diesel generators.

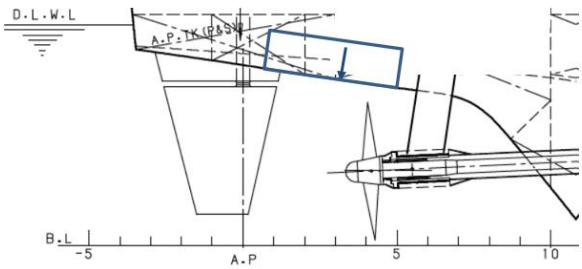

Figure 55. Pressure device locations of DNV's simplified method.

4.1.2 Hydrophone deployment

There are 2 kinds of potential deployment approaches to position the hydrophone: surface-based deployment and bottom based deployment. Practically, it is easier to deploy the hydrophones from an assistant ship or a surface buoy rather than using a bottom anchor. However, bottom anchor deployment may

effectively mitigate the effects of cable strum and sea surface effects, which leads to more accurate measurement results especially for low frequencies.

One hydrophone, three hydrophones or more than three hydrophones are used depending on the test method. DNV and CCS use the traditional one hydrophone method for shallow water test. ISO 17208-1 (ISO, 2016) and other classification societies promote three hydrophone methods both in shallow water and deep water. ISO 17208-2 (ISO, 2019a) suggests using more than three hydrophones to improve accuracy. The measurement method with three hydrophones or more reduces the variability caused by Lloyd's mirror surface image coherence and bottom reflections.

The recommendation of ISO 17208-1 standard for the deployment of three hydrophones is that the hydrophones are located at angles of 15°, 30° and 45° to the ship as measured from the sea surface.

In general, it is useful to have more than one hydrophone to create some redundancy in the measurement. If a hydrophone array with more than three hydrophones is used with a specific geometry to get more adequate and accurate measurement data, the hydrophones shall be in line as shown in Figure 56.

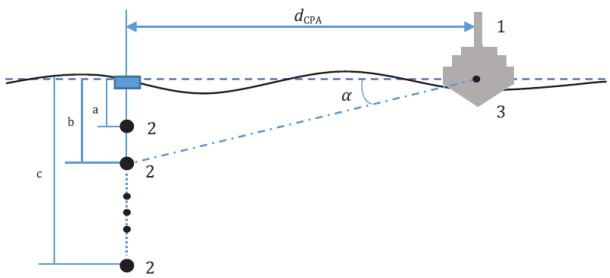

Figure 56. An example of multi-hydrophone deployment.

4.1.3 CPA distance

In ISO 17208-1, the distance for CPA (closest point of approach) is defined as the greater of either 100 m or the ship length. In practical situations, this distance cannot always be strictly controlled. The tolerance of the actual distance at CPA shall no less than -10 % and no greater than +25 % (-10 %/+25 %).

Recommendations from the AQUO project, adopted in the BV rule, specifies an expanded series of such runs past the array to acquire data at multiple CPA to aid in accounting for propagation losses. Six runs are recommended as depicted in Figure 57. Test runs are made for both port and starboard aspect at three different CPA; i) 200 m or distance of 1 ship length, ii) 400 m or distance of 1.5 ship length, iii) 500 m or distance of 2 ship length. Results from these varying CPA aid in assessing source-to-receiver propagation characteristics. Recognition is given of possible issues with low signal-to-noise for quieter ships at the greater CPA. Repeat runs at the closer CPA are recommended to help determine repeatability. Accuracy of CPA distance is specified to be +/- 10 m.

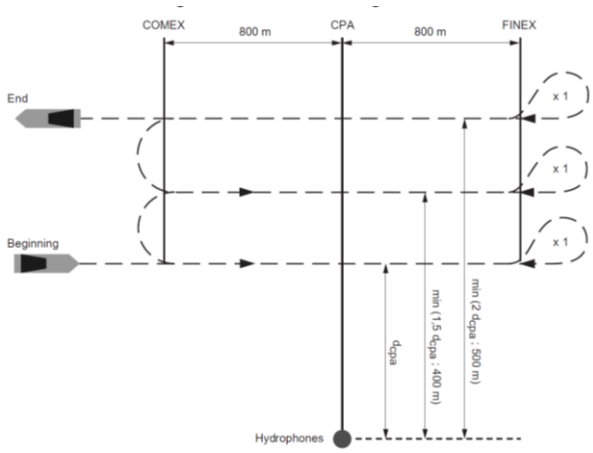

Figure 57. AQUO/BV rule multi-CPA test course configuration (AQUO-SONIC, 2015).

4.1.4 Source Level Correction

Normally, underwater radiated noise level is calculated from measured noise pressure level based on spherical spreading, for which the propagation loss is given by $20\log_{10}R/r_0$, with R the distance between hydrophone and ship, and r_0 the reference distance of 1 m. Some rules take the propagation loss in shallow water as in-between spherical spreading and cylindrical spreading, with the propagation loss given by $18\log_{10}R/r_0$ (DNV) or $19\log_{10}R/r_0$ (BV and CCS).

Since the underwater sound pressure levels are affected by the presence of the free surface (and sometimes the bottom), such quantities are considered "affected source levels" (ANSI/ASA S12.64). To evaluate the source level in the free field, i.e., without the effect of surface reflection and bottom reflection, the term "monopole source level" is introduced in ISO 17208-2. In deep water, the effect of bottom reflection is negligible, and only the Lloyd mirror effect is taken into account.

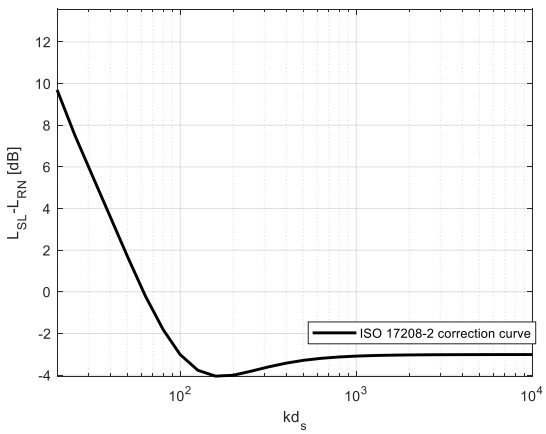

Figure 58. Correction for Lloyd-mirror effect as given by Eq. (1).

For sea trials, where sea surface scattering is influenced by sea state and bubbles, the Lloyd mirror interference pattern is only observed at low frequencies while at high frequencies an incoherent mirror image is assumed leading to a 3 dB correction. The following formulation, as shown in Figure 58, is one of the simplified formulations proposed by ISO 17208-2 for the propagation loss by Lloyd mirror (PL_{LM}) for a single hydrophone:

$$PL_{LM}\,[dB] = \begin{cases} -10log_{10}[4\sin^2(kd_s\sin\theta)] & kd_s\sin\theta \le 3\pi/ \\ -10log_{10}\,2 & kd_s\sin\theta > 3\pi/ \end{cases} \quad (1)$$

where θ corresponds to the depression angle of the hydrophone, k to the acoustic wave number, and d_s to the depth of the source. For wind speeds above approximately 5 m/s, the effect of Lloyd mirror almost disappears for frequencies above 5 kHz and PL_{LM} is close to 0 dB (Audoly & Meyer 2017; He *et al.*, 2020), see Figure 59.

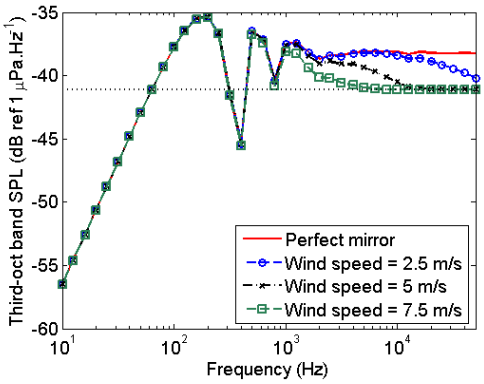

Figure 59. SPL at 100 m distance and 30° slant angle for different wind speed using Kuo's models (Audoly & Meyer, 2017).

Note that as the ship traverses the measurement track, the geometry between the ship and fixed hydrophone(s) continuously changes and hence there are continuous changes in the relative contribution (constructive or destructive) from the surface reflections to the measurements.

If the three-hydrophone geometry is strictly according to ISO 17208-1, the following correction can be applied to the average noise level as published by ISO 17208-2:

$$PL_{LM}\left[dB\right] = -10\log_{10}\left(\frac{2\left(kd_s\right)^4 + 14\left(kd_s\right)^2}{14 + 2\left(kd_s\right)^2 + \left(kd_s\right)^4}\right) \quad (2)$$

For the source depth d_S, ISO 17208-2 proposes a value of 0.7 times the ship draft, but other depths are in use as well depending on whether machinery noise or cavitation noise is dominant. This formulation is an improvement over those previously used.

4.2 Effect of shallow water

4.2.1 INTRODUCTION

In deep water, the effect of sea-surface reflection on sound propagation is much larger than the effect of bottom reflection. The definition of "deep water" is based on the assumption that the effect of bottom reflection could be negligible. In ISO 17208-1, the definition of deep water is "The minimum water depth shall be 150 m or one and one-half times (1.5x) the overall ship length, whichever is greater". DNV GL, LR, RINA and ABS follow this definition of "deep water", while BV's "minimum water depth" is 200m, and CCS has not provided a definition.

However, the depth of the "shallow water" regime for underwater radiated noise tests of ships also has a lower limit. The minimum depth in DNV's rule is at least 30 m under keel, and depth should be larger than 0.64 times ship speed squared (in m/s), while for CCS it is 40 m. Other classification societies follow ISO's requirement in which the minimum depth is defined as 60 m.

Pang *et al.* (2020b) simulated the effect of bottom reflection for various water depths. The maximum variability in sound pressure levels caused by bottom reflection (see Figure 60) is about 28.7 dB for 60 m depth，5.2 dB for 150 m depth，3.2 dB for 300 m depth，3.3 dB for 450 m depth，2.9 dB for 1000 m depth and 0.35dB for 5000 m depth. Most of rules and guidelines define 150 m as the boundary of shallow water and deep water. ANSI/ASA rules define the minimum water depth as 450 m for the class A precise measurement procedure.

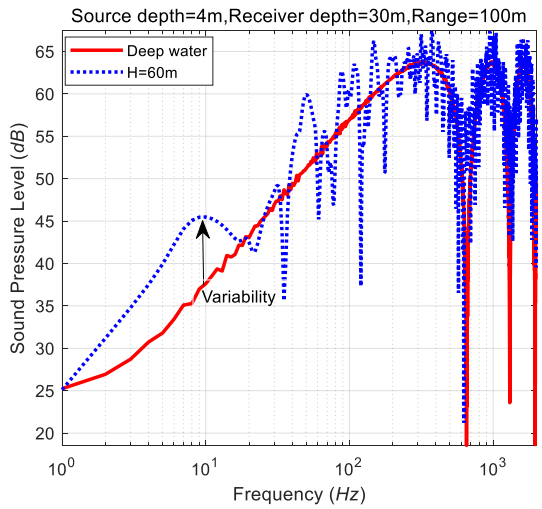

Figure 60. Received sound pressure level of monopole source in deep water and shallow water (data from Pang *et al.* (2020b).

Most of the offshore regions have a water depth less than 150 m, showing the importance of procedures for shallow water. ISO working group "17208-3" aims to develop procedures for URN measurement in shallow water.

4.2.2 OPERATIONS IN RULES AND GUIDELINES FOR SHALLOW WATER

Alternatively, the propagation loss due to free surface and bottom effects can be calculated by numerical models. BV recommends the use of the range dependent parabolic wave equation model RAM (Collins 1994; Collins *et al.* 1996), or a wave integration model, namely the Scooter/Fields model for low frequencies below 1,000 Hz (Etter 2013), and ray trace-based models, namely Bounce or Bellhop models

(Jensen *et al.* 2011), for higher frequencies. Other well validated models such as Weston's intensity model (Weston 1971) can also be used. The propagation models need as inputs the sound velocity profile as a function of depth, noise source depth, hydrophone depth, and sea bottom characteristics. A numerical model that includes near field effects may be needed when ship underwater noise measurements are made for short source-receiver configurations.

According to the BV rule, a noise test with multiple CPA distances is a practical method to analyse the field propagation loss. Pang *et al.* (2020a) have verified this procedure in the China East Sea by measuring the underwater noise of an icebreaker at eight CPA distances. Similar tests have been reported by Sipilä *et al.* (2019), where the underwater noise of another icebreaker is measured at four CPA distances varying between 136 to 174 m.

An empirical formula has been defined to correct for the influence of the environment (Meyer & Audoly, 2019). It has been determined using numerical simulations and depends on water depth and measurement distance. However, this empirical formula is only valid for a sandy sea floor. Additional work aims at extending its validity to other types of sea floor, including hard materials such as basalt (Meyer & Audoly, 2020).

Pang *et al.* (2020b) gives another empirical formula to estimate the source level based on empirical regressed propagation loss factor. Corrections for surface reflection are also taken into account in this formula. Acceptable source-level results can be obtained by simply knowing the type of seafloor and by using typical parameters in these formulas. Validation experiments conducted in a lake show that the deviation between the derived source level and the measured sound pressure level of the reference hydrophone at 1m distance from the projector is less than 3 dB.

4.3 Ship noise monitoring

As discussed in Section 3.2, a large number of programs are dedicated to measuring ambient noise in the sea and the impact of shipping noise on marine mammals, fish and invertebrates. This section presents some of the results presented in recent scientific literature.

Detailed measurements including directivity of the URN from two container ships were reported by Gassman *et al.* (2017b). They show that, for frequencies below 1 kHz, surface reflections cause large variation in measured noise levels depending on hydrophone inclination angle and should be accounted for. The effective source depth required for the correction was estimated from measurements at two separate inclination angles.

As part of a large retrofitting program of MAERSK line, the underwater radiated noise of five container vessels was measured before and after the retrofit (Gassman *et al.*, 2017a). The retrofit included replacing the bulbous bow, derating the engines for low steaming, installing propeller boss cap fins and installing a redesigned propeller. The retrofit resulted in a 6 dB lower source level for frequencies below 100 Hz and 8 dB lower source level for frequencies between 100 Hz and 1 kHz. However, the draft of the ship for the sea trials after the retrofit was 12 to 15 m which is significantly higher than for the sea trials before the retrofit where the draft was in between 9 and 12 m. This effect of this change in draft on propeller cavitation was not further investigated.

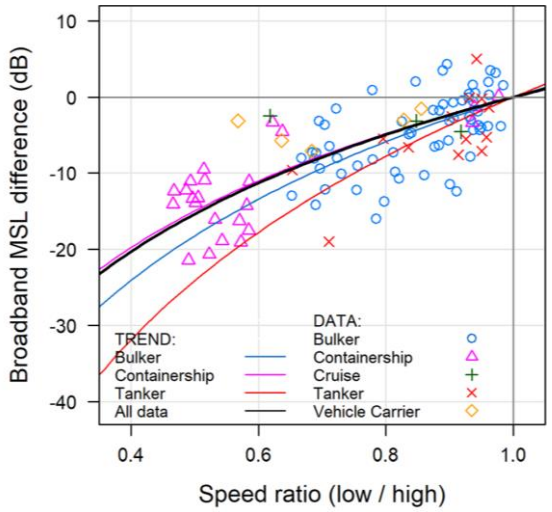

Figure 61. Effect of speed reduction on monopole source levels (MSL), MacGillivray *et al.* (2019).

The Port of Vancouver has set-up the ECHO program in which the effect of voluntary vessel speed slowdown to 11 knots on the underwater radiated noise in the Haro Strait was investigated (MacGillivray *et al.*, 2019). Noise measurements were performed at three hydrophone stations and were combined with AIS data. Measurements were performed during the slowdown trial and pre-trial and post-trial control periods. Results of five categories of piloted vessels have been published, showing a significant reduction of the source levels as shown in Figure 61. The combination of reduced source levels and longer ship passing time leads to a measured median broadband noise reduction of 1.2 dB. The reduction was 2.5 dB when filtering for periods in which the vessels were within 6 km radius of the hydrophone station (Joy *et al.*, 2019).

The reduction in shipping traffic due to COVID19 has resulted in a 1.5 dB reduction in year-over-year mean weekly noise power spectra at a hydrophone station located in the Pacific on the Juan de Fica Ridge in Canada, 60 km from a major shipping lane (Thomson & Barclay, 2020). At other hydrophone locations the reduction was 0.59 dB/week and 0.25 dB/week, whereas no significant changes were reported for another location.

4.4 Typical ship noise levels

The RANDI-3 model (Research Ambient Noise Directionality noise model) was developed based on regression analysis of a large number of measured ship noise levels (Breeding *et al.* 1996). The source level of a ship is defined as

$$L_s(f,v,l) = L_{s0}(f) + c_v \times 10log_{10}(v/v_0) + c_L \times 10log_{10}(l/l_0) + g(f,l) \quad (3)$$

In this formula, c_v and c_L are power-law coefficients for speed and length (taken to be 6 and 2, respectively), v_0 is the reference speed (12 knots), l_0 is the reference length (300 ft), $L_{s0}(f)$ is a mean reference spectrum, and $g(f,l)$ is an additional length-dependent correction to the Ross model (Breeding *et al.*, 1996).

The Institute of Acoustics (IOA) of the Chines Academy of Sciences (CAS) has performed a noise monitoring campaign in the China Yellow Sea from 2015 to 2016 (Jiang *et al.*, 2020). The hydrophone is bottom-mounted and deployed near a shipping lane. A total of 9 cargo ships, 13 container ships and 4 tankers are analyzed. The ship lengths range from 80 to 399 m, and overall source levels (20 Hz～1 kHz) varied between 171.2 dB and 188.3 dB. For the ships whose length is more than 200 m, the calculated results from the RANDI-3 model are generally higher than the measured results and the maximum difference can reach almost 20 dB. For the ships whose length is less than 200 m, there is little gap between the levels given by the RANDI-3 model and by the measured data. The results for all ships are presented in Figure 62.

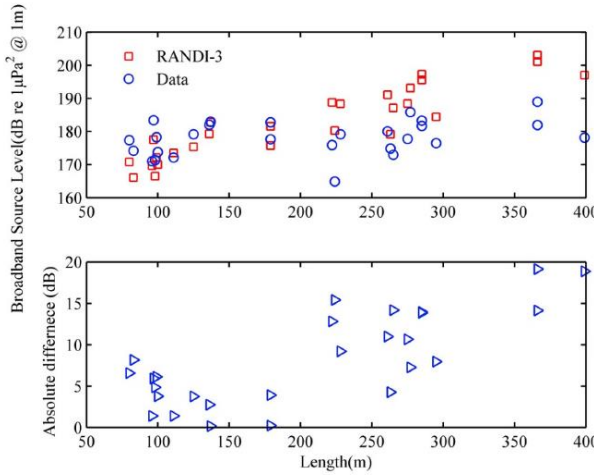

Figure 62. Broadband overall source level and absolute difference between measured data and RANDI-3 versus ship length (Jiang *et al.*, 2020).

5. MODEL-SCALE MEASUREMENT

5.1 INTRODUCTION

Performing consistent and reliable noise measurements of cavitating propellers in model-scale test facilities involves many aspects that need to be taken into account, as reviewed in the updated ITTC guideline [7] 7.5-02-03-03.9 on Model-Scale Propeller Cavitation Noise Measurements. This guideline was updated with, among others, the latest knowledge on facility reverberation and Reynolds number scaling of tip-vortex cavitation noise. These topics are discussed in this section in more detail, combined with a discussion on measurement techniques and uncertainty, and a review of water quality measurements. Results of a benchmarking exercise and comparison between model-scale predictions and full-scale data are also presented.

5.2 MEASUREMENT TECHNIQUES

The calibration step is obviously an important measurement that must be performed carefully. The estimate of the sensitivity of a hydrophone is generally given at a distance of 1m in free field environment. This value could be estimated in an anechoic chamber using gated signals to avoid the effect of reflections, or in a lake (or at sea) for very low frequencies. The latter may be costly and difficult to obtain these measurements. Recently, a novel method for calibration has been proposed by Ward & Robinson (2019) to calibrate devices at low frequencies using a small chamber and a Laser interferometer device, as presented in Figure 63. It appears as another solution for measuring the sensitivity with a relative low-cost apparatus and it is able to calibrate the hydrophone system down to 20 Hz as illustrated by Figure 64.

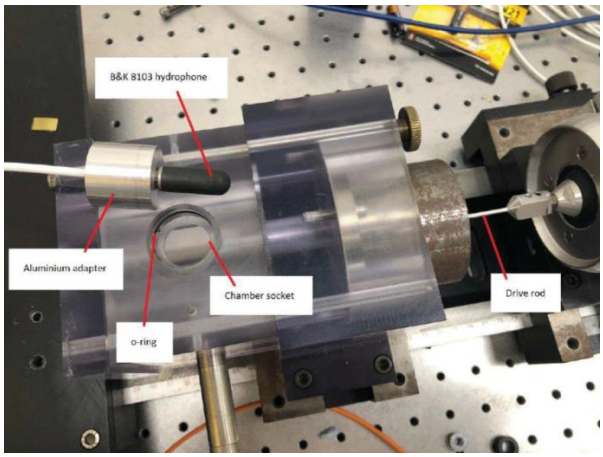

Figure 63. Device for low frequency (20-250 Hz) calibration measurement developed by Ward & Robinson (2019), here with a B&K 8103 hydrophone.

Calibration performed in a free field domain requires the "perfect" knowledge of the distance between the acoustic source and the hydrophone. The determination of the acoustic centre is an

[7] Note that the previous, obsolete, guideline was numbered as 7.5-02-01-5.

important parameter that could be estimated by the time delay of the signal between the source and the hydrophone. This estimate could be done by correlating the two signals (sine burst or sweep as used by Tani *et al.*, 2016a). A dedicated set up with particular signals (based on acoustic Barker codes or Schroeder codes) may also be used (Boucheron, 2017). These techniques permit for example, easier measurement of directivity by refining the real position of the source compared to the sensor.

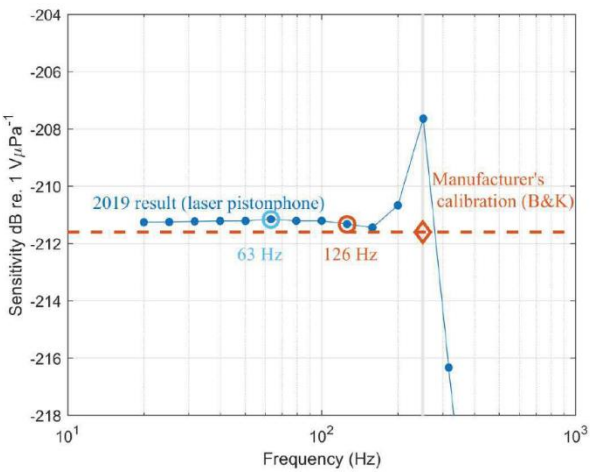

Figure 64. Calibration results obtained by Ward & Robinson (2019). Measurements with the developed technique in blue compared with manufacturer's calibration in orange.

5.2.1 MULTIPLE SENSORS TECHNIQUES

Recently, the use of several hydrophones to perform measurements has been investigated by several institutes. The aim of such measurement is not to perform redundant measurements to check the quality of the measurement but to improve the quality by combining the different signals acquired by the sensors and to enhance the estimation.

Among the techniques found in the literature, the array signal processing has been used recently by Park *et al* (2016) with a 45-hydrophone array, localized below the test section, in an application in the Large Cavitation tunnel at KRISO. Figure 65 presents a result obtained by Park *et al.* for localization of acoustic sources in a case of a propeller with cavitation. ISO committee proposes a standard for the array signal processing to localize the noise source (ISO, 2019b).

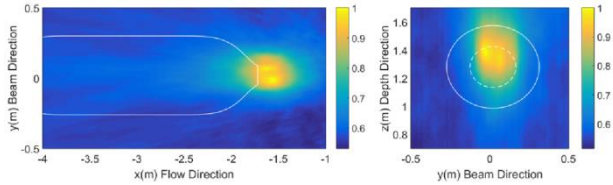

Figure 65. Localization of acoustic sources close to propeller in a cavitation case performed by Park *et al.* (2016).

Figure 66. Flush-mounted transducer set up used by Foerth & Bosschers (2016).

Localization of sources may also be performed with a flush-mounted pressure transducer embedded on the model. Figure 66 presents such a configuration performed by Foeth & Bosschers (2016).

A few transducers located in the hull directly above the propeller can also be used to localize incipient tip vortex cavitation noise in the propeller disc. Kim *et al.* (2015) used a broad-band matched field inversion technique to process these measurements.

It has to be mentioned also that several developments have been recently published in the airborne domain with rotating sources using microphones arrays. As an example, Alexander *et al.* (2020) presented a study on the ingestion of turbulence by a rotor and its consequences in terms of noise radiation and directivity pattern.

5.2.2 DENOISING

When the measurement is disturbed by pseudo-noise generated by a boundary layer (typically when the hydrophone is flush mounted in a wall or downstream on a model), different authors have developed techniques to correct the measurement from noise. All these methods are based on measurements with several hydrophones. The cross-spectral matrix is then computed and may be "denoised" with these techniques. Among all the techniques proposed, the recent works from Hald (2017), Gao *et al.* (2019), and Hald (2019) are promising. An application in a hydrodynamic domain has been recently performed by Amailland *et al.* (2018). Figure 67 presents the experimental results obtained in this study. A known source is introduced in the flow inside the test section of the facility. From the raw measurement (acoustic source + flow noise – in blue in Figure 67), the two denoising techniques tested give the curves in grey and black for the estimation of the source level (the reality being the red curve).

A recent study by Dinsenmeyer *et al.* (2020) presents the development of a new technique and a comparison with other denoising methods.

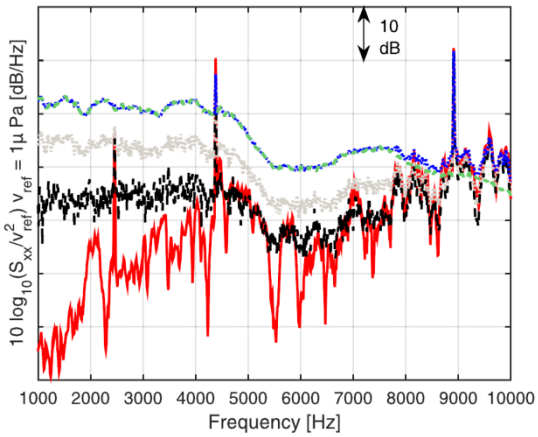

Figure 67. Denoising results from Amailland *et al* (2018). Raw measurement in blue, background noise in flow in green, source level in red. Two denoising techniques results (are given in grey and black).

5.2.3 DOPPLER EFFECT

When a given frequency emerges from the spectra, the power measured is disturbed by the Doppler Effect due to the rotation of the source compared to the fixed hydrophone (Morse & Ingard, 1968). Some features of this phenomena have been more recently investigated by Boucheron (2016). The position of the hydrophone is an important parameter as well as the nature of the source. Signal processing techniques may be implemented to remove the Doppler Effect. It is generally required if array processing is intended to be used because the frequency and phase are very important during the combination. The use of a warping time function[8] to perform the "dedopplerization" has been investigated theoretically. A comprehensive knowledge of the environment seems to

[8] A warping time function is a relationship that modifies the reception time to mimic a situation with a source and a sensor that do not move. See Baraniuk & Jones (1995) or Feltane *et al* (2018).

be required to remove the Doppler effect (Boucheron, 2020c).

5.2.4 COMBINED METHODS

In the last decade, several promising approaches have been investigated by Felli *et al* (2014, 2015). One method consists of combining direct pressure fluctuations measurements with flow measurements. Another method combines experimental measurements of the 3D velocity field (obtained with the Tomographic Particle Image Velocimetry technique) and an acoustic analogy as performed in an aeronautical domain, as depicted by Figure 68.

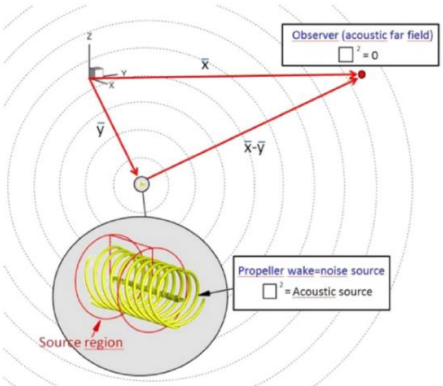

Figure 68. Principle of the acoustic analogy use described by Felli *et al.* (2015).

5.3 PRESSURE MEASUREMENTS

In the prospect of future comparisons between experimental and numerical studies (or also with theoretical results), the measurement of the overall pressure is important. This aspect is particularly relevant when the aim of the investigation is to measure the pressure field on a body-surface, like a hull-plate, when impinged by acoustic waves radiated by propellers. The question is: "are pressure transducers able to capture the overall pressure that includes scattering effects too?". In the attempt to answer to this question, a particular focus on both related and main effects is addressed in the following. As shown throughout the paragraph, this measurement must be performed jointly with a calibration step and the control of each step is important. The different steps required and discussed hereafter are,

- Calibration of an acoustic device (source or hydrophone)
- Measurement in free field
- Flush-mounted measurement (wall configuration)
- Transfer function measurement
- Measurement of an unknown source.

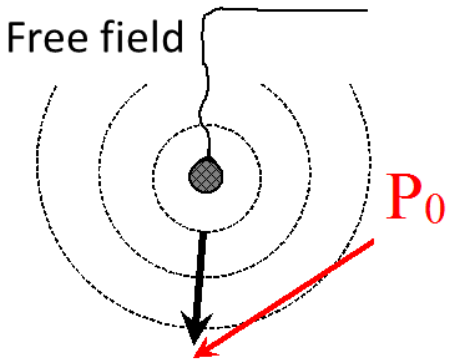

Figure 69. Free field configuration.

The absolute "acoustic" pressure (i.e., the pressure variation around the average pressure) generated at a given distance d from the source is assumed to be P_0 (Figure 21). This pressure wave comes from the source and propagates in a spherical way allowing the use of the following equation available in free field:

$$L_p = L_w - 20\, log_{10}(d) + \mathrm{C} \quad (4)$$

with L_p the sound pressure level, L_w the Acoustic Power Level of the source and C a constant depending on the different propagation medium characteristics and the reference chosen for pressure p_{ref} and power W_{ref}. It could be computed by (see Morse & Ingard, 1968)

$$\mathrm{C} = 10\, log_{10}\left(\frac{\rho\, c\, W_{ref}}{4\,\pi\, p_{ref}^2}\right). \quad (5)$$

With the classical references [9] used in underwater domain, C equals -11 dB.

In the presence of a wall, as described by Figure 70, the incident acoustic wave is reflected by the wall and generates another wave, superimposed to the incident one.

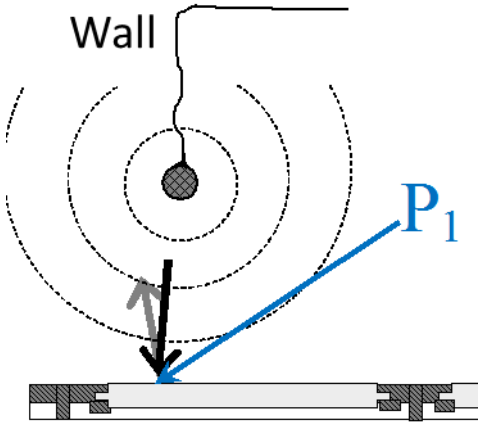

Figure 70. Wall configuration.

At the wall, the pressure P_1 that could be measured is different from P_0. The magnitude of the reflected wave depends mainly on the impedance and curvature of the wall. For the case of infinite impedance and flat wall, the total pressure is roughly twice the incidence amplitude, $P_1 \approx 2\ P_0$.

The calibration set up is described by Figure 71.

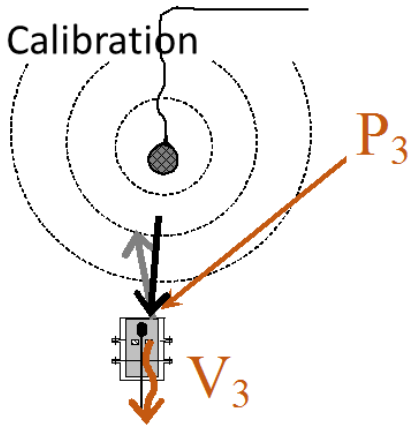

Figure 71. Calibration configuration.

The introduction of the transducer in the acoustic field disturbs the free field propagation. Locally, at the position of the transducer, a reflexion wave is present and the same effect as the one described in Figure 23 appears. The pressure acquired by the transducer, P_3 is then different from P_0. But the aim of such measurement is precisely to adjust the whole acquisition system to estimate the real acoustic pressure that should be at the position of the transducer without it. The output voltage measured by the sensor, denoted V_3 here, allows computing the sensitivity of the sensor M (expressed in Volt by Pascal) by

$$M = \frac{V_3}{P_0} \qquad (6)$$

It is worth noticing that the pressure in the last equation is the pressure in free field (because the calibration assumes that the aim of the sensor is measuring the free field, without the presence of the sensor).

After this step of calibration, it is possible to use the sensitivity of the sensor in the same

[9] These are p_{ref} = 1x10^{-6} Pa and W_{ref} = 6.67x10^{-19} W. Note that the constant C for airborne noise is computed using p_{ref} = 20x10^{-6} Pa and W_{ref} = 1x10^{-12} W. The value for W_{ref} for underwater noise has been computed so as to preserve the same value of the constant C as in air.

conditions to correct the measurement. The correction step consists of dividing the voltage measurement by the sensitivity to recover the pressure, like described by the following equation,

$$P_3^C = \frac{V_3}{M} = P_0 \quad (7)$$

This correction step, namely known as calibration, allows measuring the real free field acoustic pressure in such environment. However, it is generally not enough to correct a measurement in a hydrodynamic facility because the facility response (or the body-wall in general) is not considered. To overcome this problem, a last step is required inside the environment. This is termed a transfer function and is described by Figure 72 (see also Section 5.4 for a more detailed discussion on transfer function). Let us assume for simplicity the sensing membrane located directly on the surface where pressure has to be measured.

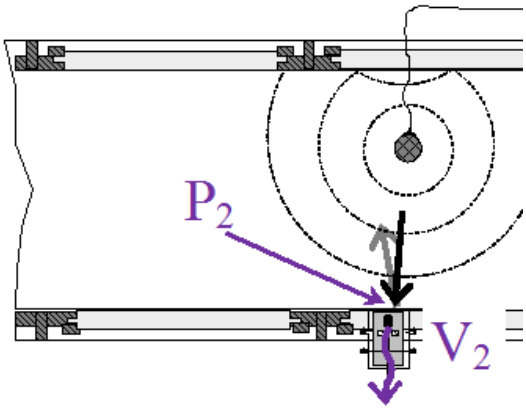

Figure 72. Transfer function configuration

The transfer function uses a calibrated source at a given position inside the environment. The measurement given by the hydrophone P_2 is different from P_0 and P_1. The difference between P_0 and P_2 represents the transfer function *TF*.

$$TF = \frac{V_2}{P_0} \quad (8)$$

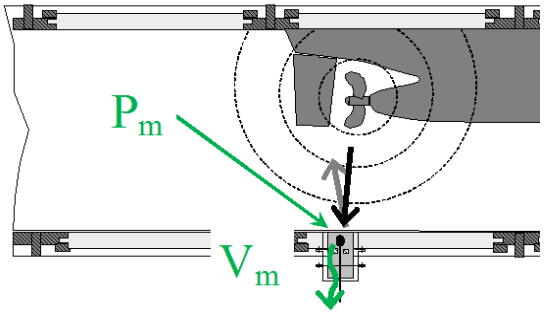

Figure 73. Measurement configuration.

Figure 73 describes the measurement configuration. The measured "raw" pressure P_m does not equal nor P_0 neither P_1 because the pressure at the wall is the superposition of both incident and reflection waves but it is also disturbed by the acoustic response of the facility (reverberation, modal behaviour, etc.). Consequently, it takes account on distance and all the environmental effects. Using this transfer function corrects the measurement V_m, as long as the location of the sources is the same in both configuration (Transfer function and measurement set up).

$$P_m^C = \frac{V_m}{TF} \quad (9)$$

Note that most calibration data are evaluated (or given by manufacturer) at a distance of one meter. This implies that all the estimations made are referenced to 1 meter. The distance plays an important role in the free field and calibration set-ups. The use of a transfer function as described in Figure 72 corrects the measurements and makes the estimation directly at one meter when it is used (because the calibration source data are given at one meter). Fortunately, experimental campaigns to measure the noise emitted by a propeller for example, has the objective to measure the power

spectral density (referred to 1 meter) and to estimate this noise at full-scale (also referred to 1 meter). All these equations may also be expressed in the decibel scale, which is generally the most common way of use. The last remark concerns the value of the absolute pressure at the wall during a measurement *Pm*. This real value is never estimated in the tests. It requires the knowledge of both the calibration data of the hydrophone and the measurement of the transfer function.

5.4 FACILITY REVERBERATION

The problem of facility reverberation was already dealt with by the previous Hydrodynamic Noise Committee, which pointed out the importance of considering this effect. In particular, as indicated in the latest release of the guidelines, when noise is measured in model-scale test facilities, it has to be kept in mind that the test sections do not resemble a free-field environment. The reflections by the walls cause interference between pressure waves which depend on wavelength (and therefore frequency) and lead to acoustic modes in the test section at low frequencies (see e.g., Boucheron *et al.*, 2017; and Hynninen *et al*., 2017). The frequency range of this effect depends on the size of the test section and is larger for the smaller size cavitation tunnels, but the effect is clearly visible for larger size facilities at low frequencies also. The so-called Schroeder cut-off frequency represents the limit below which the measured noise is influenced mainly by the acoustic modes of the facility while for higher frequencies the diffuse domain exists where statistical properties of the acoustic field hold. A formulation for an acoustic measurement in a tank, was given in Kuttruff (2009), while for cavitation tunnel applications a formulation for this cut-off frequency of a test section of infinite length, with source and hydrophone located in the test section, has been derived by Boucheron (2019a, 2020a).

Demodulation techniques can be employed to estimate the magnitude of each mode in the bandwidth where the first modes appear (Boucheron, 2019b). Due to the high number of sensors required when the number of modes increase, the technique is only practicable in a small frequency bandwidth (typically just beyond the first cut-off frequency). The addition of the amplitude of all modes allows the estimate of the whole acoustic field and the acoustic power at each frequency. Figure 74 presents an example of the reconstructed acoustic field estimated experimentally by this technique at each of the three walls of the test section of a cavitation tunnel. However, it is shown that the boundary conditions are one of the key points to ensure good performance of these techniques. A method for the estimate of the impedance of the test section walls has recently been developed (Boucheron, 2020b) and is promising.

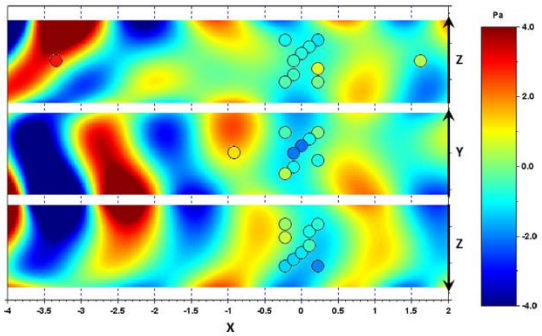

Figure 74. Acoustic field reconstruction by demodulation technique in a test section (Boucheron, 2020b).

The effect of the reflections (or reverberation) can be determined through acoustic transfer function measurements using for example, a sound source with known characteristics put at specific relevant locations in the test section (see Figure 75).

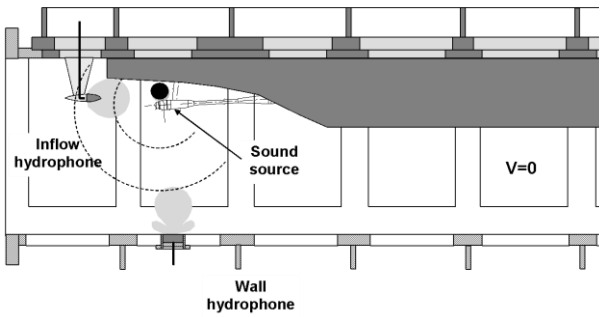

Figure 75. Transfer function measurement set-up in cavitation tunnel.

Examples of measuring the transfer function can be found in Briançon *et al.* (2013), Lafeber *et al.* (2015), Park *et al*. (2016,2018), Tani *et al.* (2016a,b) and Tani *et al.* (2019b).

According to the experiences gained during the period of activity of the Specialist Committee, the Model-Scale Measurements Guidelines have been updated for what regards the effects of facility reverberation; Many different aspects are dealt with, such as:

- Characterisation of transmitting chain, including TVR
- Type of sound projector
- Type of signal
- Position of projector
- Testing conditions, including air content
- Free surface effects
- Further general considerations

Details about these aspects may be found directly in the guidelines and in the above-mentioned references, while in this section some further information is presented about some specific topics.

For what regards the types of signal to be used for the transfer function measurement, many options have been suggested by various authors and have been used in different facilities:

- Pure tones
- White or pink noise
- Chirps
- Sweeps
- Maximum length sequences (MLS)

Basically, the choice is related to the capability of covering large frequency ranges with a single measurement (thus preferring wideband signals) and, in parallel to the need for high signal-to-noise ratio (SNR). Considering the latter, pure tones result in higher SNR, even if they may tend to amplify the waviness of the transfer function, amplifying local singularities.

Different post-processing techniques may be applied to different signals. In Tani *et al.* (2019b), the sweep signal is convolved with an inverse filter to enhance SNR and to separate the linear response of the system from the non-linear distortions that stem from the use of electronic transducers. This procedure may be successfully used to extend the TF also to low frequency ranges where SNR is very low. In Figure 76 the resulting TF using pink noise and a sine sweep (plus convolution with inverse filter) are compared, showing differences at lower frequencies, where the SNR is considerably different, as shown in Figure 77.

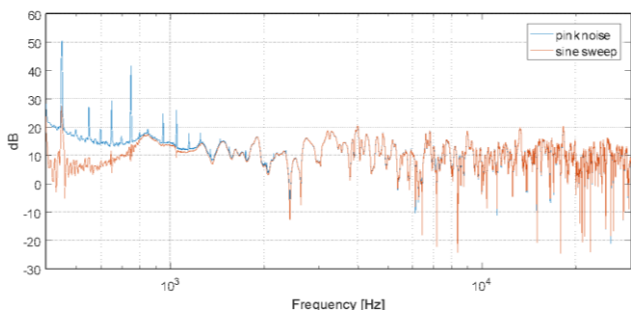

Figure 76. Comparison of transfer function obtained with pink noise and sine sweep with linear deconvolution (Tani *et al.*, 2019a).

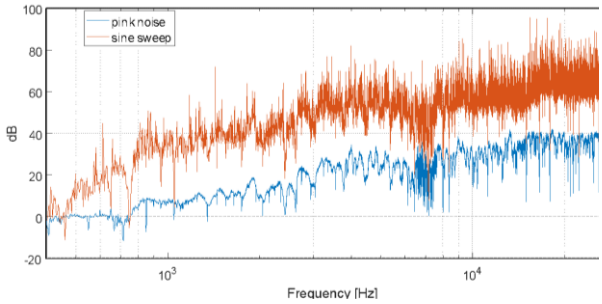

Figure 77. Signal to noise ratio (SNR) in transfer function measurements: pink noise vs sweep with linear deconvolution (Tani *et al.*, 2019b)

Further considerations may arise in the case of a twin-screw ship. This specific topic is discussed in Park *et al.* (2018), where different approaches for the measurement of the transfer function are reported, including the use of single or twin projectors and the signal adopted. Results reported are in favour of the use of a non-deterministic signal (white noise, in the specific case) in order to obtain more accurate results. Although, differences with respect to deterministic signals are anyway rather limited (about 1 dB). In Figure 78 and Figure 79 the effect of using either a non-deterministic or a deterministic signal is shown, comparing the transfer functions obtained with two different ways for evaluating the transfer function (Type 1 and Type 2 in the figures). In Figure 79 a larger (even if still limited) discrepancy between the transfer functions is evident.

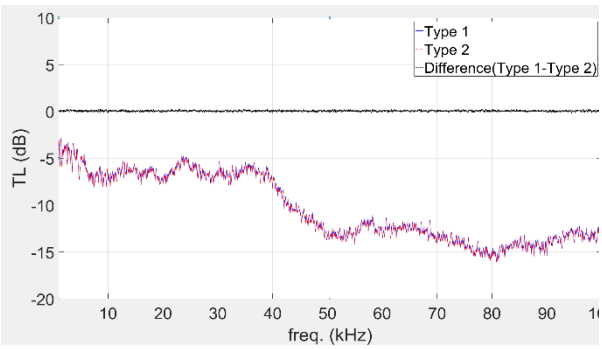

Figure 78. Transfer function comparison with white noise input (Park *et al.*, 2018).

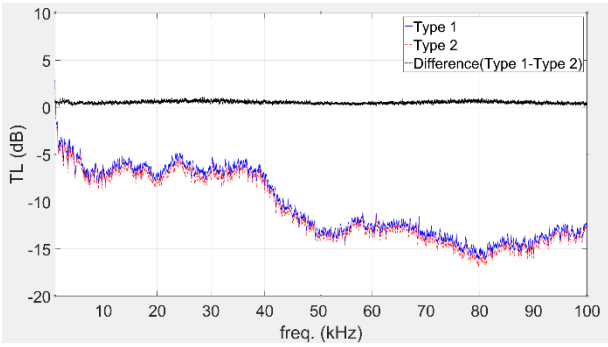

Figure 79. Transfer function comparison with Linear Frequency Modulation (LFM) input (Park *et al.*, 2018).

Additionally, the transducer position is important since it affects the transfer function. Since cavitation is not generally present at a unique position and the characteristics of the transfer function may vary with position, it is preferable to measure the transfer function using multiple transducer positions and averaging the results (Briançon *et al.*, 2013; Tani *et al.*, 2019b). As a possible alternative to the use of multiple positions, in Tani *et al.* (2019b) results obtained with a rotating source are compared with results at different positions of the transducer, as shown in Figure 80.

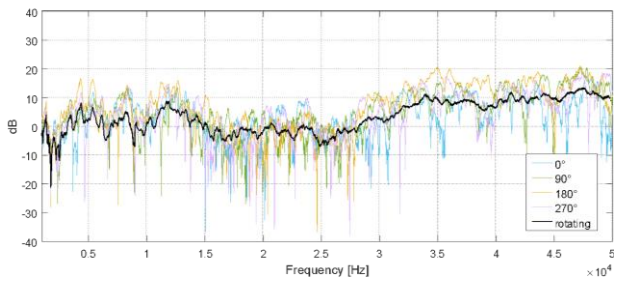

Figure 80. Measured transfer function with fixed and rotating source, narrowband representation (Tani *et al.*, 2019b).

This approach seems promising; however, it may pose practical problems and is more complex, especially in the case where the signal has to be emitted only in correspondence to a specific range of angular positions if cavitation phenomena are not present in the whole propeller revolution. In this second case, the

relevant angular positions may arise from visual observations or from source localisation techniques.

The use of multiple positions and averaging may also have the advantage of smoothening the transfer function which otherwise tends to present rather large hump and hollows. As an example, this feature is evident in Figure 81 (Tani *et al*., 2019b). Humps and hollows appear to be present in both the transfer function and in the propeller radiated noise levels, which present similar patterns, as expected. However, they seem to be more pronounced in the first case. This suggests that the frequency response of the facility to the cavitation noise, even if presenting similar features, is likely different from the one measured with the electronic noise source, in which the humps and hollows may be amplified. The problem of smoothing is well known in ocean acoustics (Harrison & Harrison, 1995); this is further discussed, for the case of model testing facilities, in Briançon *et al*. (2013).

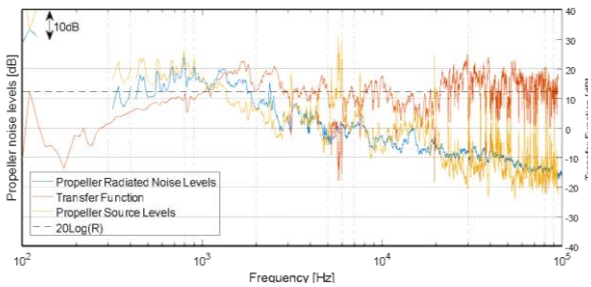

Figure 81. Example of radiated noise levels, transfer function and source levels (Tani *et al*., 2019b).

5.5 TIP-VORTEX SCALING

Various publications have addressed the effect of Reynolds number on the URN of tip-vortex cavitation when performing model tests. Scaling rules for the URN have been proposed by Strasberg (1977), Baiter (1989), and Blake (2017), where various functions of the cavitation number σ and cavitation number at inception σ_i are proposed. Oshima (1990, 1994) shows that high-frequency hull-pressure levels caused by a propeller with a cavitating vortex arising at the face of the propeller are well predicted if the cavitation number in the cavitation tunnel is selected smaller than the cavitation number at full-scale. The ratio of the model-scale and full-scale cavitation number is written as the ratio of the corresponding Reynolds number, *Re*, similar to the scaling rule for cavitation inception by McCormick (1962),

$$\frac{\sigma_m}{\sigma_s} = \left(\frac{\mathrm{Re}_m}{\mathrm{Re}_s}\right)^n \tag{10}$$

where subscript *m* corresponds to the model-scale condition and *s* the full-scale condition. Oshima (1990) shows that good agreement between model-scale and full-scale noise levels are obtained for n = 0.15 while near cavitation inception a value n = 0.35 should be used. Park & Seong (2017) present a relation to scale model-test URN levels to full-scale that includes a correction for the dissimilarity in Reynolds number using the ratio of full-scale and model-scale Reynolds number raised to a power 2.5 n using n = 0.32. A similar correction was also applied to frequencies. This correction method was used by Park *et al*. (2019) who showed that a value of n = 0.1 gives best agreement between sea trial data and model test results.

An alternative approach is proposed by Bosschers (2018a, 2020). The similarity of vortex cavity diameter is investigated using an analytical formulation for the azimuthal velocity distribution of a 2-D vortex, providing a function, f, between ratio of vortex-cavity size, r_c, and viscous core size, r_v, and the ratio of the cavitation number and the cavitation inception number:

$$\frac{r_c}{r_v} = f\left(\frac{\sigma}{\sigma_i}\right). \quad (11)$$

It was shown that the function f is independent of the vortex strength when the Lamb-Oseen vortex is used. Applying the function to model-scale and full-scale conditions, and using the relation between viscous core size and cavitation inception for the Lamb-Oseen vortex, results into

$$\left(\frac{r_c}{D}\right)_m = \left(\frac{r_c}{D}\right)_s \left(\frac{\sigma_{i,s}}{\sigma_{i,m}}\right)^{1/2} \frac{f\left[\left(\sigma/\sigma_i\right)_m\right]}{f\left[\left(\sigma/\sigma_i\right)_s\right]}. \quad (12)$$

Through this relation, a cavitation number at model-scale can be obtained from which the non-dimensional cavity size at model-scale is identical that at full-scale. It is then assumed that the resulting URN levels are also similar. Analysis of limiting situations show that near inception, the cavitation number should be adjusted according to the classical McCormick scaling rule while for fully developed cavitation the cavitation number at model-scale should be identical to that at full-scale. If the required change in cavitation number cannot be obtained at model-scale, a semi-empirical correction is applied to the URN levels that makes use of the difference in relative vortex cavity size between model-scale and full-scale. The result of applying this correction procedure to the experimental data of Oshima (1990) is shown in Figure 82.

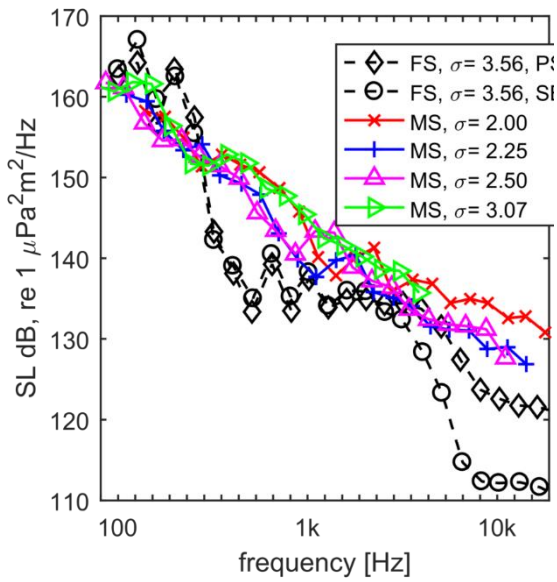

Figure 82. Data of Oshima (1990) corrected by the tip-vortex scaling method of Bosschers (2020).

5.6 WATER QUALITY

The influence of water quality, quantified indirectly by dissolved gas level or directly as a microbubble/nuclei population measurement, has long been considered for its impact on the inception and development of cavitation and its scaling, and the associated flow/hull pressure fluctuations and propagation of noise into the surrounding environment (see for example, Arndt & Keller, 1976; Lovik, 1981; Weiten-dorf, 1981; Bark, 1985). It has been found that nuclei populations can differ between facilities for comparable dissolved gas levels and vary in time within a particular facility (Weitendorf & Tanger, 1999; Heinke *et al.*, 2012). Some water tunnels have been designed to control the nuclei population independent of the dissolved gas level (e.g., Briancon-Marjollet & Michel, 1990; Khoo *et al.,* 2020a) but in general this is not the case.

With respect to hull pressure fluctuations Johannsen (1998) reported that in the large HYKAT facility a high dissolved oxygen content (80% saturation) was required for good

agreement between model and full-scale results. At a lower content of 40% the first peak of the model hull pressure signal was substantially higher due to the absence of damping provided by the free bubble population present at the higher saturation level. Similarly, Heinke (2003) and Bosschers & van Wijngaarden (2012) have reported an improved full-scale correlation of high harmonics with a greater gas content (60% saturation rather than 30%).

Little has been published on the effect of water quality on noise propagation in facilities since the 80's (e.g., Blake & Sevik, 1982). Kamiriisa (2001) reported a very significant reduction in sound level from a cavitating propellor above 5 kHz with a variation in dissolved gas level from 70-100%, but no difference below 70%. The main/sole source of recent work assessing the effect of water quality on noise measurement at model-scale is that undertaken by the group at the University of Genoa (Tani *et al*., 2019b). In particular, a possible method for qualitatively assessing the presence of scattering effects is described, despite only giving a rough indication. Possible significant reductions in the sound level (up to 30 dB at most influenced frequencies) are reported in correspondence to worst conditions, showing that this problem has to be considered carefully, especially in facility where presence of free traveling bubbles is more likely to occur. Other than this work, when reported, studies only typically indicate that ITTC recommendations are followed for dissolved gas level and little other comment about water quality is generally made.

Some recent works examining measurement techniques and the influence of nuclei on cavitation inception and nuclei dynamics in test facilities is discussed in further detail below.

5.6.1 ABOUT MEASUREMENTS OF WATER QUALITY

Nuclei measurements, or as reported by many authors, the measurement of the quality of water is a crucial aspect regarding cavitation inception. The objective of this measurement is not to have a global overview of the water quality in the whole facility but more to estimate the quality of water that is just upstream of a test model, e.g., a propeller. Both the position and the size of a nucleus has an important influence on cavitation inception and development (Chen *et al.*, 2019; Rijsbergen & Beelen, 2019).

Different techniques have been developed in the past that may be adapted to perform bubble size and concentration measurements. We can cite the cavitation susceptibility meter (see e.g., Lecoffre, 1987; Khoo *et al.*, 2016; Khoo *et al*., 2020a) that make the microbubble cavitate in a Venturi device (see Figure 83). The relationship between the critical radius of a bubble and the pressure allow to compute a cumulative distribution of a microbubble population by modifying the flow rate in the Venturi.

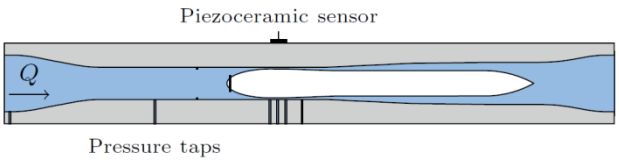

Figure 83. Centerbody Susceptibility Meter schematic principle (adapted from Khoo *et al.*, 2020a).

This technique can measure very low concentration and very small microbubbles but is highly intrusive. It is not suitable for an embedded technique on a whole model dedicated to noise measurements but could be used prior to the noise tests if the water quality conditions are controlled in the facility.

To perform synchronous measurements with noise, only optical techniques are currently available:

- Shadowgraphy: this technique requires the alignment between the light, the measurement volume, and the camera. Particular attention must be paid to the design of the optic and the image processing (see Boucheron *et al*., 2018).

- Phase Doppler Anemometry: this technique could be efficient but requires an optical design at fixed angles (Boucheron *et al.*, 2018). These angles are given by the refractive index of air and water and could not be changed. If the facility provides such angles, this technique could be used efficiently.

- Holography: In-line holography (see Lebrun *et al.*, 2011) may also be used in a small environment. The measurement volume of this technique is very small and the distance between the laser probe and camera must be small.

- Defocus technique: this technique is based on the light scattered by the microbubble and measured with an out-of-focus camera (see the principle described in Figure 84). Note that there is a range of differing acronyms[10] used for this same technique, but all are based on the principle of obtaining an interference pattern from a defocussed optical path (Russell *et al.*, 2020a).

  Birvalski & Rijsbergen (2018a,b) used this technique in a basin with the estimation of both the size distribution and the concentration. The latter is difficult to obtain accurately because it is highly dependent on the measurement of the light power profile of the laser beam. A recent study by Russell *et al.* (2020a,b) details the calibration of the defocus technique for both size and concentration measurements and the application in their tunnel. Ebert *et al.* (2018) have presented an application of such technique at full-scale in the North Sea off Scotland.

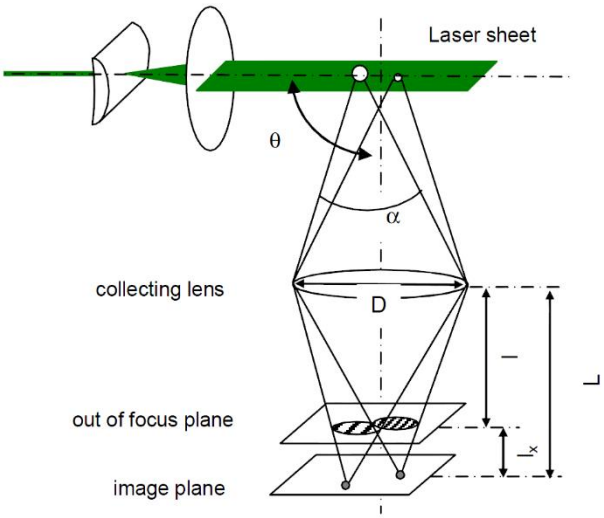

Figure 84. Principle of the defocus technique (from Méès *et al.*, 2010).

The accuracy of these techniques depends on the optical arrangement and on the image processing used. A comparative study for 3 of them has been made in Boucheron *et al.* (2018) exhibiting the spread of results obtained with the same bubbles.

[10] Differing acronyms in use include:

IMI - Interferometric Mie Imaging, MSI - Mie Scattering Imaging, GPD - Global Phase Doppler, ILIDS - Interferometric Laser Imaging for Droplet Sizing, ILIT - Interferometric Laser Imaging Technique, IPI - Interferometric Particle Imaging

5.7 UNCERTAINTIES

The results of noise measurements are usually expressed in decibels, as are the uncertainty of the hydrophones and measurement equipment. However, combining uncertainties of components in the measurement chain is not trivial as briefly shown in this section.

The expanded uncertainty u_i, expressed in percentage, for a given confidence level implies that the range of the signal with mean value x is given for that confidence level by $\left[(1-u_i)x,(1+u_i)x\right]$. In decibels, the upper range is given by

$$\begin{aligned}\Delta L_{u_i}^{+} &= 20\log_{10}\left[(1+u_i)x\right]-20\log_{10}\left[x\right],\\ &= 20\log_{10}\left[1+u_i\right],\end{aligned} \tag{13}$$

and the lower range by

$$\begin{aligned}\Delta L_{u_i}^{-} &= 20\log_{10}\left[x\right]-20\log_{10}\left[(1-u_i)x\right],\\ &= -20\log_{10}\left[1-u_i\right].\end{aligned} \tag{14}$$

For any given u_i, we have $\Delta L_{u_i}^{+} < \Delta L_{u_i}^{-}$.

However, for small values of the uncertainty, the expressions for the uncertainty in decibels can be linearized which leads to

$$\begin{aligned}\Delta L_{u_i}^{+} &= \frac{20}{\ln 10}\ln\left[1+u_i\right]\\ &\approx \frac{20}{\ln 10}u_i \quad \forall u_i \ll 1\end{aligned} \tag{15}$$

and similarly

$$\Delta L_{u_i}^{-} \approx \frac{20}{\ln 10}u_i \tag{16}$$

Hence, for small values of the uncertainty, the upper range and lower range are practically equal when expressed in decibels. Computing the combined uncertainty then also becomes straightforward:

$$\Delta L_{U_c} = \frac{20}{\ln 10}\sqrt{\sum_i u_i^2} = \sqrt{\sum_i \Delta L_{u_i}^2} \tag{17}$$

Alternatively, we may also start with a measurement in which the (expanded) uncertainty ΔL_U is directly provided in decibels. The upper and lower bounds, for a given confidence level, are then given by,

$$L_U = \bar{L} \pm \Delta L_U = 20\log_{10}(x) \pm \Delta L_U \tag{18}$$

If we insert the variable inside the logarithm, we find,

$$L_U = 20\log_{10}\left(x \times \left[10^{\Delta L_U/20}\right]^{\pm 1}\right) \tag{19}$$

The Taylor expansion of the power function 10^x gives (assuming that ΔL_U is small)

$$L_U = 20\log_{10}\left(x \times \left[1 \pm \Delta L_U \frac{\ln(10)}{20}\right]\right) \tag{20}$$

We retrieve here the term expressed in equations (15) and (16) available for small uncertainties u, that demonstrates the equivalence of the two approaches when the values are small. Figure 85 presents the relationship between the two situations, assuming a normal distribution of data in linear scale and a small value of the uncertainty u.

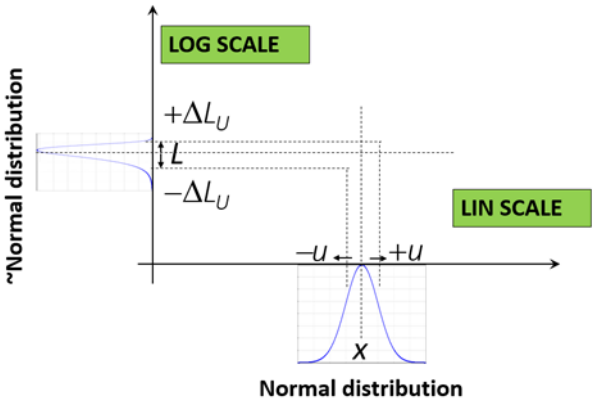

Figure 85. Example of the distributions equivalence between the linear and logarithmic scales, assuming a normal distribution of data in linear scale and a small value of the uncertainty.

Nevertheless, for higher values of the uncertainty, the equivalence is not obtained easily. In this particular case, the equations (15), or (19) if expressed in decibel, cannot be expanded. The equations for the transformation between statistical variables (see for example Papoulis, 2002) shows that one of the distributions is not symmetrical. As an example, Figure 86 presents the relationship between the two distributions assuming a normal distribution in the linear scale. In the logarithmic domain, the distribution looks like Gumbel or Weibull distribution. The upper ΔL^{+}_{U} and lower ΔL^{-}_{U} bounds are not equally spaced from the average in the logarithmic domain.

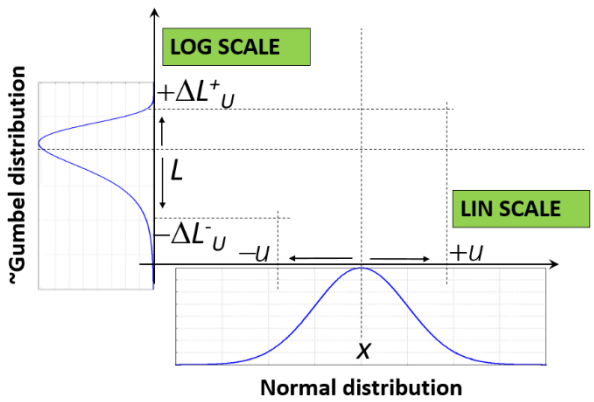

Figure 86. Example of a distribution modification between the linear and logarithmic scales, assuming a normal distribution of data in linear scale and large uncertainties.

Therefore, the distribution of a parameter around its mean value is of principal importance, especially if large uncertainties occur. Combination of uncertainties with equation (17) assumed that data are normally distributed. For small values of all uncertainties, this equation is available. Otherwise, the knowledge of distribution of signals/error of the chain should be used and improve the estimate of the final uncertainties for upper/lower bounds that are not equal.

5.8 REVIEW OF HTF BENCHMARK

In the last few years, a benchmarking activity has been carried out by the Community of Practice (CoP) "Noise" of the Hydro Testing Forum (https://www.hydrotestingforum.org/). This followed from the HydroTesting Alliance (European Network of Excellence) with the aim of gaining insight into the key aspects influencing the accuracy and reliability of URN measurements at model-scale, evaluating the impact of different experimental facilities and test procedures on full-scale noise predictions.

A round-robin test programme, involving different propeller scale factors and facility types and dimensions, has been carried out. The programme was carried out in cavitation tunnels of small (UNIGE, NMRI, UNEW) and large size (KRISO, SSPA), a free-surface cavitation channel (INM) and a depressurised wave basin (MARIN). The results of this activity are reported in various papers, such as Aktas *et al.* (2016a), Hallander (2017), Lafeber & Lloyd (2017), Sakamoto *et al.*, (2017), Tani *et al.* (2017), where tests in single facilities are reported, while in Tani *et al.*, (2020) the same results are summarised and compared. In Section 5.8.1 the testing campaign is briefly outlined, while in Section 5.8.2 the main results are summarised.

5.8.1 PRESENTATION OF THE ACTIVITY

The activity has been carried out using as test case the five bladed fixed-pitch propeller model (Figure 87) of the research vessel "The Princess Royal", belonging to Newcastle University and used also in the EU project SONIC. Four different models have been used during the campaign, with diameters ranging from 214 to 250 mm.

Figure 87. Model-scale propeller (Tani *et al*, 2020).

The propeller was tested in open water configuration and without shaft inclination (i.e., uniform inflow), with the aim of making the test as simple as possible. In addition to this, tests were also repeated with inclined shaft (5°) in order to induce non-stationary cavitation. The rather low angle considered did not result in very large variations in terms of radiated noise with respect to the results for 0° shaft inclination, thus the focus in the published articles is on the tests without shaft inclination. The propeller was tested in pulling condition in all cases, except by CNR-INM (pushing condition); this was due to an unexpected stop of tests (linked to the COVID emergency), which did not allow to fully complete the campaign as expected.

For each shaft inclination, six different operational conditions, resulting from two different values of the advance coefficient and three different values of the cavitation number, were considered (see Table 6).

Table 6. Operational conditions (zero shaft inclination)

Loading Condition	**J [-]**	σ_V **[-]**
C1	0.4	13.9
C2		8.1
C3		4.5
C4	0.5	13.9
C5		8.1
C6		4.5

This allowed to investigate considerably different cavitation extents, ranging from slightly after inception to fully developed tip vortex and sheet cavitation, as reported in Figure 88 (observations at SSPA).

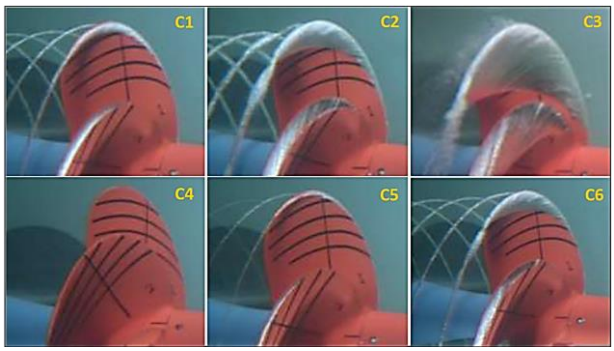

Figure 88. Cavitation extents at different conditions (Tani *et al*, 2020)

5.8.2 SUMMARY OF RESULTS

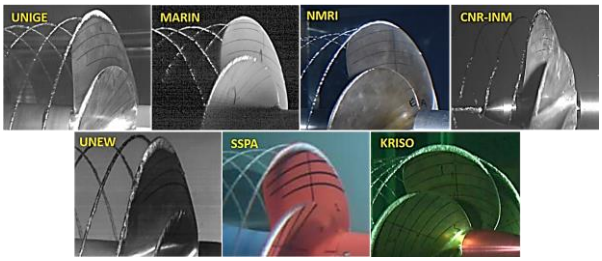

Figure 89. Cavitation extents at C1 condition for different facilities (Tani *et al*, 2020).

Propeller cavitation typologies and extents observed in the different facilities were fairly similar. As an example, in Figure 89 the observations for C1 condition in the different facilities are reported. In this case, the main difference is related to the extent of the sheet cavitation towards the inner radii, ranging from about 0.7*R* to about 0.8*R*.

Similar results were obtained also for other conditions, where the most important difference was the radial extent of cavitation (in particular for condition C3); in C4 condition (near inception) different tip vortex dimensions were observed.

These differences have been ascribed to different possible causes, i.e., small discrepancies in the operational conditions (thrust coefficient and cavitation number), different development of boundary layer (Reynolds number and turbulence stimulation), freestream turbulence, blade geometry finishing, and water quality.

For what regards the noise measurements, in Figure 90 and Figure 91, the results for condition C1 and C3 respectively, in terms of one-third octave spectra, are reported.[11]

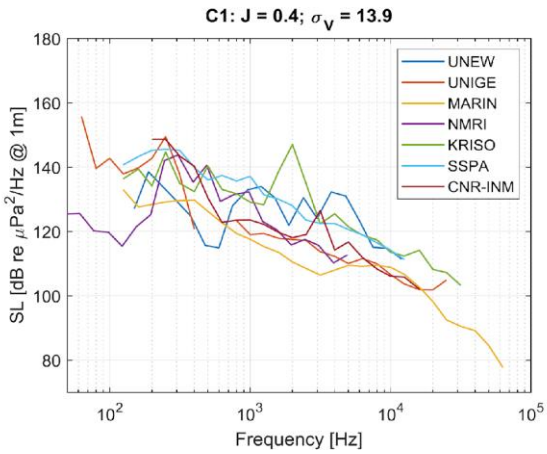

Figure 90. Noise spectra at C1 condition for different facilities (Tani *et al*, 2020).

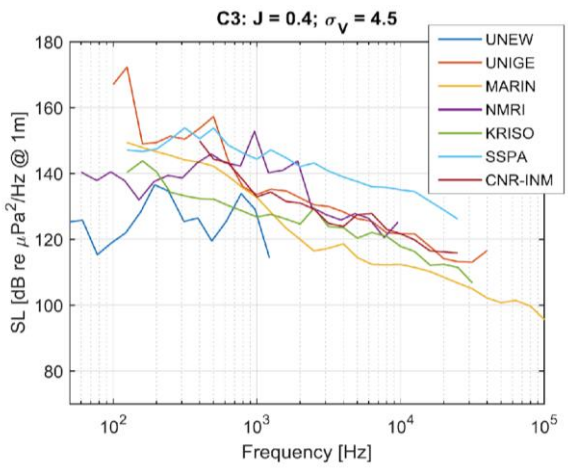

Figure 91. Noise spectra at C3 condition for different facilities (Tani *et al*, 2020).

As it can be seen, a band of variation of about 10 dB of predicted noise levels is observed on average, rising to about 20 dB for condition C3 (similar results were obtained also for condition C4).

Further analyses were devoted to specific parts of the spectra, i.e., the hump (centre

[11] In order to compare all the results of the campaign, noise spectra were scaled to a common condition in full-scale, resembling one of the functioning conditions of Princess Royal (D_s = 0.75 m, n_s = 19.025 rps, σ_{Ns} = 1.06).

frequency and level) and the high frequency part (decay slope and average power content).

Considering the centre frequency of the hump, the agreement observed was better than that visible from noise spectra, with the range of variation mainly below 100 Hz with few exceptions.

The agreement for correspondent peak level was worse, even if common trends might be found especially for conditions at J = 0.6 (C4-C6), while for conditions C1-C3 trends varied for different facilities. The spread in results was in most cases of about 10 dB (lower than the spread in the overall spectrum), except for condition C4, which showed larger variation due to incipient and intermittent cavitation.

Considering the high-frequency spectrum, the decay ratio resulted between 10 and 20 dB per decade, in good agreement with data on cavitation noise available in the literature (Ceccio & Brennen, 1991). However, the spread of results was again appreciable, and it seemed difficult to detect common trends.

Finally, considering the high frequency power content, the trends (for each single participant) agreed rather well with the observed cavitation extent, with higher levels measured in correspondence to higher propeller loading. However, differences of 10 dB are again present for all conditions, with higher discrepancies (up to 20 dB) found for condition C4 and C3, where minimum and maximum cavitation extents were present.

As a whole, the results of this activity are very interesting, providing an overview of the different sources of discrepancy. Among them, cavitation extent and cavitation dynamics, together with facility reverberation, are the most important ones.

Regarding cavitation extent and dynamics, the differences were related both to a not correct reproduction of the operational condition, in terms of thrust coefficient and cavitation number, and to water quality (nuclei content, turbulence levels). The first issue, despite being trivial, has to be considered carefully by each facility; water quality issues are less easy to be controlled, unless dedicated tools are available in the facilities, however it is important to collect as much data as possible in order to understand their effect. Regarding reverberation, not all facilities considered it in their measurements; it is very important in the future that all facilities measure the transfer function in accordance to the indications of the model-scale guidelines.

Other possible sources of discrepancy, such as model propeller geometry, bubble scattering, propeller singing, unwanted phenomena on structures inside the facility (e.g., hydrophone supports, screens, etc.), are discussed in Tani *et al*. (2020).

Overall, the HTF results underline that improvements have to be made in the near future and further investigations are needed in order to get a further insight into all the sources of discrepancy between different facilities, with the aim of reducing them. The proposed benchmark activity with the Nawigator ship (see Section 7) represents an opportunity with this aim, allowing to broaden the analysis and involve an even larger number of facilities with respect to those which participated to the HTF round robin. In order to obtain the largest amount of information, the experience of HTF, considering in particular the difficulties encountered, have to be considered carefully.

5.9 VALIDATION STUDIES

The accuracy of the model-scale measurements can be determined from a comparison between model-scale predictions and full-scale noise measurements, as described in the previous report of 28th ITTC specialist committee on hydrodynamic noise. The previous report addressed the importance of the aspects to consider in the model test such as ship wake field, propeller loading, cavitation extents and dynamics, noise measurements, background noise, propagation loss due to facility reverberation, and scaling. The above aspects are revisited in this report and some subjects such as facility reverberation are dealt with in detail.

The papers on the validation studies were reviewed in the previous report. A few papers have been published since the previous report in 2017. Instead of reviewing the individual paper, we summarized the recent validation studies in accordance with categories pertinent to the model-scale and the full-scale measurement methods. Some of papers were already reviewed in the report in 2017.

Ship type (full-scale):

Full-scale underwater radiated noise measurements were performed on various types of ships and the results were compared to model-scale predictions. Among the measured ships, the recently built commercial ships were also included.

Table 7. Review of validation studies of model-scale noise measurements: Arranged according to ship type.

Ship type	Validation studies
Crude Oil Tanker	Lee *et al.* (2012)
Product Carrier	Seol *et al.* (2015)
Oil/Chemical Tanker	Tani *et al.* (2016b), Li *et al.* (2018)
LNG carrier	Park *et al.* (2020)
Container Ship (3,600 TEU)	Kleinsorge *et al.* (2017)
Container Ship (14,000 TEU)	Park *et al.* (2020)
Combi-Freighter	Lloyd *et al.* (2018)
Research vessel (Princess Royal)	Aktas *et al.* (2016a), Gaggero *et al.* (2016), Labefer & Bosschers (2016), Tani *et al.* (2019a)
Research vessel (Nawigator XXI)	Traverso *et al.* (2017)

Cavitation extent observation (full-scale):

Full-scale cavitation extents were presented in many papers, which were helpful for analysis in validation studies. However, there were also some cases where full-scale noise was measured without cavitation observation.

Table 8. Review of validation studies of model-scale noise measurements: Arranged according to full-scale cavitation observations.

Full-scale cavitation	Validation studies
Observed	Aktas *et al.* (2016b), Seol *et al.* (2015), Gaggero *et al.* (2016), Labefer & Bosschers (2016), Tani *et al.* (2016b), Traverso *et al.* (2017), Li *et al.* (2018), Lloyd *et al.* (2018), Tani *et al.* (2019a)
Not observed	Lee *et al.* (2012), Kleinsorge *et al.* (2017), Park *et al.* (2020)

Propagation loss correction (full-scale):

To compare the full-scale measurement with the model-scale prediction, the measured full-scale noise was converted to either the radiated noise level (RNL) or the source level (SL) using various propagation loss corrections.

Table 9. Review of validation studies of model-scale noise measurements arranged according to correction for propagation loss for the full-scale measurements.

Propagation loss (full-scale)	Validation studies
Spherical spreading	Lee *et al*. (2012), Seol *et al*. (2015), Traverso *et al*. (2017), Park *et al*. (2020)
Spherical spreading & Lloyd mirror	Aktas *et al*. (2016b), Labefer & Bosschers (2016), Tani *et al*. (2019a)
Spherical spreading & bottom reflection	Lloyd *et al*. (2018)
Surface & bottom reflection	Kleinsorge *et al*. (2017)
Transmission loss (measured)	Tani *et al*. (2016b), Li *et al*. (2018)
Transmission loss (calculated)	Gaggero *et al*. (2016)

Facility (model-scale):

Most of the model tests were performed in the medium-size and the large cavitation tunnels. The depressurized wave basin in MARIN was also used for the model-scale noise measurement.

Table 10. Review of validation studies of model-scale noise measurements: Arranged according to facility.

Facility	Validation studies
Large cavitation tunnel	Lee *et al*. (2012), Seol *et al*. (2015), Tani *et al*. (2016b), Li *et al*. (2018), Park *et al*. (2020)
Medium-size cavitation tunnel	Aktas *et al*. (2016b), Gaggero *et al*. (2016), Tani *et al*. (2016b), Kleinsorge *et al*. (2017), Traverso *et al*. (2017), Tani *et al*. (2019a)
Depressurized wave basin	Labefer & Bosschers (2016), Lloyd *et al*. (2018)

Ship wake field (model-scale):

The wake fields were generated using a wake screen or a geometrically scaled model of the ship. In general, the former was used in medium-size cavitation tunnels, while the latter was used in the large cavitation tunnels and the depressurized model basin. Sometimes a hybrid method using the wake screen and the dummy body was used for the wake generation in the medium-size cavitation tunnels.

Table 11. Review of validation studies of model-scale noise measurements: Arranged according to simulation method for wake field.

Ship wake	Validation studies
Large-scale model	Lee *et al*. (2012), Seol *et al*. (2015), Labefer & Bosschers (2016), Tani *et al*. (2016b), Li *et al*. (2018), Lloyd *et al*. (2018), Park *et al*. (2020)
Wake screen	Aktas *et al*. (2016b), Gaggero *et al*. (2016), Tani *et al*. (2016b), Traverso *et al*. (2017), Tani *et al*. (2019a)
Dummy body/wake screen	Aktas *et al*. (2016b), Kleinsorge *et al*. (2017)

Propeller loading (model-scale):

In the model-scale measurements, the propeller loading was determined (or prescribed) from the powering tests or from both powering test and sea trial.

Table 12. Review of validation studies of model-scale noise measurements: Arranged according to applied propeller loading.

Propeller loading	Validation studies
Powering test	Lee *et al*. (2012), Labefer & Bosschers (2016), Tani *et al*. (2016), Traverso *et al*. (2017), Li *et al*. (2018)
Powering test + Sea trial	Aktas *et al*. (2016b), Seol *et al*. (2015), Gaggero *et al*. (2016), Kleinsorge *et al*. (2017), Lloyd *et al*. (2018), Tani *et al*. (2019a), Park *et al*. (2020)

Noise measurement (model-scale):

Propeller noise was mostly measured by multiple hydrophones except for Lee *et al.* (2012), Aktas *et al.* (2015b), and Lloyd *et al.* (2018), in which single hydrophone was used.

Propagation loss correction (model-scale):

The propagation loss correction was applied to the measured noise data in most of the validation studies. For the correction, the transfer function was measured or estimated using the spherical spreading of acoustic wave fields. A correction for the Lloyd mirror effect was applied to the measurement data of the Depressurized wave basin.

Table 13. Review of validation studies of model-scale noise measurements: Arranged according to applied correction method for propagation loss in the model-scale measurements.

Propagation loss (model-scale)	Validation studies
Transfer function (measured)	Seol *et al.* (2015), Gaggero *et al.* (2016), Tani *et al.* (2016b), Tani *et al.* (2019a), Park *et al.* (2020)
Spherical spreading	Lee *et al.* (2012), Aktas *et al.* (2016b), Traverso *et al.* (2017), Li *et al.* (2018), Tani *et al.* (2016b),
Transfer function & Spreading	Kleinsorge *et al.* (2017)
Lloyd mirror & spherical spreading	Labefer & Bosschers (2016), Lloyd *et al.* (2018)

Scaling method (model-scale):

Most of the validation studies adopted ITTC'87 low frequency scaling method to estimate the full-scale source level. However, Labefer & Bosschers (2016) applied ITTC'87 high frequency scaling method to the model-scale data. Park *et al.* (2020) and Lloyd et al. (2018) investigated the effects of two ITTC'87 scaling methods on the scaled results. According to their results, the low frequency scaling showed the better correlation to the full-scale measurements than the high frequency scaling. Kleinsorge et al. (2017) investigated both a correction factor for distance between hydrophone and propeller assuming spherical spreading and cylindrical spreading. The spherical spreading correction showed best performance for the low frequency range (f < 100 Hz) and the cylindrical spreading agreed well with full-scale measurement for the high frequency region (f > 100 Hz). Lee *et al.* (2012) scaled the tip vortex cavitation noise and compared the scaled results with the full-scale measured data. According to their study, McCormick exponents of 0.3 showed an acceptable correlation with the full-scale measurement.

Comparison of full-scale & model-scale:

Comparison of the full-scale measurement to the model-scale prediction involves some complexity such as machinery noise, which is only included in the full-scale. It should also be kept in mind that full-scale noise measurement has considerable uncertainty. By simply comparing the levels presented in validation studies, it seems that model-scale tests can predict full-scale noise levels within 5 to 10 dB.

This value of uncertainty is somehow lower than the band of uncertainty reported as a result of the round robin test carried out by Hydro Testing Forum (HTF) members, as reported in Section 5.6.2. That case is, however, different, since an open water propeller was used instead of a propeller operating in a wake field; Some possible reasons for these discrepancies are discussed in Section 5.6.2, showing areas that need further study. It is believed that, starting from that experience, the proposed benchmark study by the Committee will allow to obtain a deeper understanding.

6. COMPUTATIONAL PREDICTION

Some of the aspects on underwater noise prediction methods are discussed in the following sections, providing the *state of the art* in each category. Specifically, Section 6.1 shows hydrodynamic noise prediction, especially from propeller which is an important source of noise. Among of several approaches in Section 6.1, coupled CFD-FWHE technique is picked up as most important numerical approach and its guidelines for utilization are proposed in Section 6.2. Section 6.3 presents structural born noise as another important source of URN, and finally the propagation of URN is shown in Section 6.4.

6.1 HYDRODYNAMIC NOISE PREDICTION

6.1.1 EMPIRICAL AND SEMI-EMPIRICAL METHODS

Overview. Continued from previous committee (28th ITTC specialist committee on hydrodynamic noise), several studies about empirical and semi-empirical prediction methods have been observed. In addition to continuous efforts using classical approaches, adoption of data analysis technique has been rising. Although some of these approaches show fairly good results in the papers, careful attention should be needed to their application considering their modelling phenomena, assumption, based data etc. A schematic view of related phenomena and approach in prediction of URN is shown in Figure 92. Appropriate choice or combination of several methods might be essentially important for reasonable prediction, but no standard methodology has been established up to the present moment.

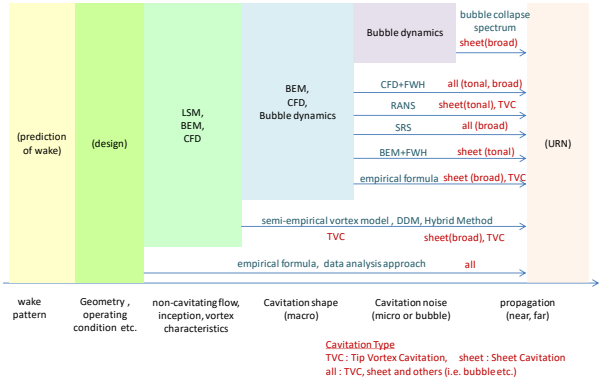

Figure 92. Approaches for predicting hydrodynamic noise from a propeller.

Continuing studies. As shown in previous committee, various approaches using empirical or/and semi-empirical methods have been studied so far. In this committee's period, there have been some further developments of these studies.

One is a combination of bubble dynamics theory and RANS CFD calculation by Ando *et al*. (2018). In this method, radiated noise from sheet cavitation and TVC was predicted by theoretical method modelling bubble collapse of free bubbles from cavitation. Mean initial size of bubble was assumed directly as 2.5 mm, and a normal distribution was adopted to bubble size distribution. Based on these assumptions, the number of bubbles was calculated from volume of sheet cavitation predicted by URANS CFD with cavitation model. For TVC, similar assumption for bubble size was adopted and the length of TVC is assumed as 1.5 D_p (propeller diameter), not based on CFD or other theoretical methods but from observation in model test. The predicted results with TVC showed better agreement to corresponding model test results, than the prediction without TVC.

Another study is by Bosschers (2018b). In this study, a hump-shaped pattern for the noise spectrum was assumed, and the centre frequency and level of this hump was described with an empirical model. This empirical model was obtained using model-scale and full-scale

measured hull-pressure data, and described as a function of cavity size, propeller diameter etc. To obtain the cavity size, BEM calculation and semi-empirical vortex strength model was adopted. Even though this method models only for TVC, the results showed some capability for cases with sheet cavitation with adjustment of the empirical parameters.

Both literatures mentioned in above show relatively good agreement between prediction and measurement, but careful attention should be paid to the assumptions or database which are essentially important to utilize these methods.

Adoption of data driven models. In addition to continuous studies in utilizing empirical knowledge and theoretical formulations or calculations, adoption of data driven models has appeared as new approach. This approach shows some possibility to improve the capability of empirical or/and semi-empirical methods.

A relative early study was a simple attempt by Aktas (2016), in which URN levels in several frequencies were modelled directly by Artificial Neural Network (ANN). As input variables, 12 simple parameters including propeller geometry, wake distribution and propeller operating conditions were used, and model tests results of series propeller were employed as training data. In this study, physical knowledge was utilized just in the choice of explanation variables, and only data analysis technique was used for creating prediction formulas. This simple application of ANN left large discrepancy between predictions and measurements.

Another approach was shown by Miglianti *et al.* (2019a,b). In this study, machine learning technique was adopted in following 2 ways. One is called "Data Driven Model" (DDM), which predicts URN directly using propeller geometry, operating conditions, occurring cavitation type etc. as input. Here the cavitation type might be estimated by CFD or other kind of calculation. The other way is called "Hybrid Model" (HM) which uses semi-empirical model similar with Bosschers (2018b), but a DDM approach was also adopted to predict model coefficients in the employed semi-empirical model. In both approaches, URN spectrum was simplified similar with Bosschers (2018b), i.e., characteristic values like URN centre peak frequency, level, etc. in hump-shaped pattern. The predicted results showed a relatively good agreement with measurements, especially in HM the error in centre peek noise level was within 5 dB. One additional interesting point was that HM showed some capability even if the input data for machine learning was only from the outside of range of operating conditions (i.e., thrust coefficient and cavitation number). This suggests the possibility of extrapolation of prediction, which should be useful to estimate the noise in the full-scale condition which is difficult to represent in model-scale.

6.1.2 POTENTIAL FLOW METHODS

Cavitation-free conditions

a) Bernoulli-based Formulation

Potential flows methods have been largely used in the past for the prediction of the noise field generated by simplified sources of sound like point-sources and vortices (Dowling & Ffowcs Williams, 1983; Howe, 2002). The extension to non-cavitating propellers is straightforward by assuming operating conditions where the theory of irrotational, inviscid, attached, incompressible three-dimensional (3D) flows is able to capture the flow-field features around lifting/thrusting bodies (Kerwin, 1986; Carlton, 2018) and applying the Bernoulli equation for the prediction of the pressure signals in the fluid medium. Undoubtedly, hydrodynamic solvers based on the Boundary Element Method (BEM) have been proven to be fast and accurate enough in capturing the tonal noise sources localized on

the blades and in the flow flow-field surrounding them, whenever the hydrodynamic environment is governed by vorticity fields exhibiting ordered vortex-flow patterns (see for instance: Morino & Gennaretti, 1992; Gennaretti *et al.*, 1997; Seol *et al*., 2002; Testa *et al*., 2008; Salvatore *et al*., 2009b; and Greco *et al*., 2014; just to cite a few). In this context, hydrodynamic effects induced by the hull wake (if present) may be fruitfully described by RANSE (Reynolds Averaged Navier Stokes Equation) computations yielding the main features of the onset-flow incoming the propeller disk, namely, the effective wake field (Rijpkema *et al*., 2013).

However, investigations based on the Bernoulli equation to compute the pressure disturbance in the flow-field have shown their weakness at the light of the recent advances on propeller hydroacoustics (Ianniello *et al*., 2013; Ianniello *et al*., 2014; Ianniello and De Bernardis, 2015; Ianniello *et al*., 2015) proving that non-cavitating propeller noise in open water is an inherently nonlinear problem governed (mainly) by the hydrodynamic sources of sound in the flow-field around the propeller like vortex released at the blade tip, vorticity, turbulence, etc.., which can be very intense and persisting around/downstream the propeller disk. Of course, BEM hydrodynamics is able to capture the noise contribution due to blade(s) kinematics and pressure distribution upon the propeller, including effects coming from the vorticity field convected downstream. Nonetheless, all those hydrodynamic sources of sound due turbulence and interaction among eddies spreading downstream the propeller, are completely lost. As shown in Testa *et al*. (2018b), for a marine propeller in open water at high advancing ratio, potential hydrodynamics is adequate to capture the tonal sources of sound due to cyclic blade passages and trailing vortices convected downstream for observers placed in the near field (0.75 diameters from the hub centre, along the vertical direction), upstream and downstream up to 0.5÷1 diameter far from the disk. Although turbulence-induced noise effects are not captured by BEM coupled with the Bernoulli approach, within this range the noise signals carried out by the potential flow-based approach seems to be a sort of *mean noise signal* with respect to predictions based on the acoustic analogy technique (Ffowcs Williams & Hawkings, 1969). Moving downstream, propeller hydroacoustics is not more dominated by potential wake vorticity effects: important vorticity contributions generated by complex interactions among vortices may give rise to stronger vortex structures inducing, in turns, higher level of noise behind the disk. In addition, the not modelled turbulent structures, evolving in the wake, make the use of BEM hydrodynamics data through the use of the Bernoulli equation inadequate for any hydroacoustic investigation. The range of 0.5÷1 diameter where the potential-flows based methods may provide reasonable results in terms of pressure pulses is expected to reduce for higher blade(s) loads, more intense wake and in the presence of non-uniform inflow to the propeller disk. In fact, in these circumstances the role assumed by the turbulent structures, downstream the propeller disk, grows-up and reduces the limits of applicability of potential methods for hydroacoustic purposes. Note that this approach based on BEM hydrodynamics and the Bernoulli equation does not account for the compressibility delays that, indeed, may alter the overall noise features with respect to prediction in which one assumes that all sources' contributions overlap simultaneously at the observer position. However, the low rotating blade tip Mach number, typical of marine propellers, allows to account for an instantaneous sound propagation because it does not alter the resulting signal in a significant way, at least within a distance of about 10 propeller diameters from the hub (Testa *et. al.*, 2008).

A field of applications where potential flows methods are still accurate for hydroacoustic

purposes is in the near field (few diameters from the propeller hub) where the tonal noise components, associated to the blades and vorticity convected downstream, may play an important role. Acoustic scattering problems in which hydro-borne propeller sound interacts with the hull structure, being spread out into reflected and diffracted noise components, fall within this field of application. Details are found in ITTC (2017a). The same considerations may be also valid in the far field, if the acoustic observers are far away from the propeller wake and the rotor blades are subject to a velocity field (due to blade-vortex interaction or high intense wake hull) with high-frequency changes both in time and space.

b) Ffowcs Williams & Hawkings Equation Approach – Linear Acoustics

Several hydroacoustic studies found in literature are based on the so-called *hybrid approach* where noise sources and sound radiation are investigated separately, with the former evaluated by fluid-dynamic computational tools (typically based on BEM) and the latter predicted through a post-processing step based on the use of acoustic analogies. Among them, the Ffowcs Williams & Hawkings Equation (FWHE) for impermeable surfaces has been widely applied for the analysis of rotating blade devices, by assuming that, nonlinear terms (the so-called quadrupole noise) can be neglected because of the low rotational speed of the blade.

For instance, in Seol *et al*. (2002) a noise prediction was carried out for a noncavitating propeller with and without a duct, by coupling the Farassat time-domain formulation 1A (Farassat, 1981) to a hydrodynamic BEM solver based on a potential approach. The robustness of the acoustic analogy and its advantages with respect to a direct pressure estimation by the Bernoulli equation were largely discussed in Testa *et.al*. (2008) by pointing out the role played by the numerical modeling of the propeller wake. From a general standpoint not depending on the CFD (Computational Fluid Dynamics) solver used to detect the sources of sound upon the blades, and for propellers in open-water conditions, the assumption that nonlinear terms can be neglected *a priori* has to be carefully applied, both for the comments at subsection *a)* and in view of the recent analytical study addressed in Ianniello (2016) on the acoustic efficiency of rotating sources in open water conditions, showing that the FWH surface terms from multibladed propellers may vanish underwater in a narrow region with relevant nonlinear phenomena occurring rather far from the body. In particular this paper shows that the blade tip vortex persists in an extended region, and, depending on both the operating conditions and external flow, it is inevitably destined to destabilize and break down, thus increasing the vorticity and turbulence. In other words, the flow nonlinear sources generated by the body motion (and occurring rather far from it) soon get the upper hand, and as a result the hydroacoustic far field may be dominated by the quadrupole term.

Differently, in behind-hull conditions the validity of hydroacoustic predictions based on the 1A Farassat Formulation is an open question because no consensus emerges. Specifically, a substantial margin of uncertainty on the role played by an unsteady loading noise component in case high unsteadiness of the tested operating conditions, remains. Akin to the Bernoulli-based approach, the 1A Farassat Formulation may be well suited in case of acoustic scattering problems in which hydro-borne propeller sound interacts with the hull. This issue is widely discussed in ITTC (2017).

Cavitating propellers

c) Bernoulli-based Formulation

Hydrodynamic cavitation concerns with the formation and collapse of partial vacuums in a liquid by a swiftly moving solid body. Under well-defined physical conditions, cavitation can occur in any hydrodynamic devices operating in liquid when pressure drops below the saturated vapor pressure. Acoustically speaking, cavitation is highly undesirable, as it induces and impulsive sound and deeply modifies the baseline acoustic signature of the propeller. These effects are inherently related to the spectrum of the high-energy radiated noise, that exhibits a low frequency range, governed both by tones (multiple of the blade passage frequency) and broadband hump (due to the large-scale cavity dynamics), and a higher frequency broadband range due to the collapse of vapor bubbles (Brennen, 1995). It is well recognized that the factors causing pressure fluctuation induced by a propeller are classified into three primary parts: changes in the blade loading, rotation of the blade thickness, and the volume change of the propeller cavitation (ITTC, 2014, 2017a; Carlton, 2018). However, pressure fluctuation due to changes in blade loading and blade thickness are very small compared with the pressure fluctuations caused by cavitation.

In principle the goal in the design of hydrodynamic devices is to avoid cavitation; however, few propellers in practice can operate entirely without cavitation due to the non-axisymmetric inflow or unsteady body motion. The occurrence of cavitation makes the detection of the sources of sound a very complicated and partially unsolved problem. In fact, the modern CFD is able to provide a satisfactory estimation of cavitation patterns (Salvatore *et al*., 2009a), but a reliable simulation of important underlying phenomena (especially those related to cavities collapsing stage) is still far from being achieved. Such a modelling uncertainty seems to be less critical in case of a *sheet cavitation*, which frequently occurs on conventional propellers operating in the hull wake field. It consists of a relatively *thin* vapor region which typically forms at blade leading edge, fluctuates in size in a limited azimuth range and eventually collapses, always remaining essentially attached to the blade surface. Under the assumption that: *i*) cavitation pockets remain attached to the blades surface and *ii*) the collapse of the cavity, due to condensation, does not imply violent implosions so that vapor bubble evolves in a smooth way (by progressively reducing its size up to disappear), a potential-flow hydro-dynamics analysis yields a reliable description of the cavity dynamics in terms of inception, growth and collapse (Knapp *et al*., 1970; Brown *et al*., 1976; Franc *et al*., 2004; Salvatore *et al*., 2009a).

In the framework of unsteady propeller cavitation tackled by 3D BEM hydrodynamics, the correlation between flow-field induced pressures and sheet cavitation pattern is obtained by integrating nonlinear sheet cavity models such those described in (Lee, 1987; Kinnas & Fine, 1992; Kinnas & Pyo, 1999; Salvatore & Esposito, 2001; Kinnas *et al*., 2003; Salvatore *et al*., 2003; Bosschers 2018b,) with a boundary integral methodology for the velocity potential (Morino *et al*., 1975) where propeller load-induced vorticity shedding is described by a trailing wake alignment model. In this approach, valid for leading edge cavitation attached to the blade suction side (partial sheet cavitation), the cavity trailing edge region is modelled via a closed–cavity scheme and the cavity shape is determined by a free–cavity length iterative technique. An extension to supercavitation is presented in (Young & Kinnas, 2003). Pressure pulses in the fluid medium is accomplished by means of the Bernoulli theorem once the velocity potential field is known (Gennaretti *et al*., 1997).

An approximated derivation to isolate the pressure field induced by the unsteady cavitation is obtained by noting that any cavity sheet over the blade surface affects the potential field through an additional source distribution known in literature as *cavity source sheet*, whose intensity is governed by the cavity dynamics (Salvatore & Ianniello, 2003). Other simplified approaches typically used to predict the tonal noise induced by the occurrence of sheet cavitation on the blade(s) surface rely on the use of a monopole model where propeller lifting surface methods are coupled to the solution of the Rayleigh-Plesset equation for the detection of the cavitation volume change (Okamura & Asano, 1998).

d) The Ffowcs Williams & Hawkings Equation Approach - Linear Acoustics

Unsteady flows generate pressure fluctuations that partially propagate as acoustic waves throughout the fluid medium. Lighthill's acoustic analogy (Lighthill, 1952) separates sound generation mechanisms from propagation phenomena by arranging the flow governing equations in the form of a wave equation; through the use of generalized functions theory, and by embedding the exterior flow problem in unbounded space, the most general form of the Lighthill's acoustic analogy recasts into the Ffowcs Williams & Hawkings equation (FWHE). In sheet cavitating conditions, a widely used approach followed in the literature (see for instance: Salvatore & Ianniello, 2003; Seol *et al*., 2005; Seol, 2013; Testa *et al*., 2018a) is to predict the noise field through the standard Farassat 1A formulation (Farassat, 2007). This is where: i) the pressure distribution upon blades is provided by a suitable panel code coupled with cavitation modelling such as those briefly mentioned in Section 6.2.2; ii) the bubble dynamics exhibits its noise effect through the variation of the blade shape during a revolution or by imposing suitable boundary conditions on the blade surface assumed as a porous, undeformable body. The two aspects represent the radiated noise by thickness-like effects (Testa *et al*., 2018a) and embody the current state of the art in this field.

In Belibassakis & Politis (2019), a numerical model is developed for the prediction of noise generated from cavitating or non-cavitating marine propellers operating in unsteady inflow conditions in the wake of the ship. The hydrodynamic part is analysed by a velocity-based vortex lattice method, providing the unsteady pressure on the blades and cavitation data. The latter are subsequently used, in conjunction with Farassat formulation, to calculate acoustic radiation from moving surfaces and predict the acoustic spectrum at a distance of several diameters from the propeller, representing the source of marine propeller noise. An approximate model is derived, exploiting information and integrated data concerning the time history of blade sheet cavity volume and the unsteady blade thrust. The latter are used to calculate the monopole and dipole forcing terms of the acoustic equation and derive the propeller acoustic spectrum in the low and moderate frequency band. Also, the directivity characteristics of the propeller noise are calculated, and the effect of nearby boundaries on underwater noise propagation are presented comparatively to the omnidirectional source assumption. In particular, the effect of the free surface as a pressure release boundary (Lloyd mirror effect), and of the ship hull, treated as hard and soft boundary, are illustrated.

In Lampe *et al*. (2019), interaction problems arising from the modelling of the dynamic behaviour of the flexible P1356 marine propeller are presented. The fluid domain is simulated through a potential theory based on BEM with an additional model to take into account sheet cavitation. The structural part of the problem is handled by a high-order finite elements method. Information exchange

between the respective sub-problems is managed by a separate coupling tool which employs the Quasi-Newton Least-Squares method to provide a stable and efficient computation method. Acoustic evaluation is performed in a postprocessing fashion using the Ffowcs-Williams Hawkings equation.

In the presence other cavitating phenomena localized in the flow field (bubble cavitation, tip vortex cavitation, etc.) the use of BEM is inadequate and the need of using a CFD solver is mandatory. However, the development and the assessment of reliable two-phase hydrodynamic solvers is well far to be achieved yet, making the prediction of cavitating propeller noise more a hydrodynamic issue than a hydroacoustic one. A brief description on relevant papers concerning the use of CFD solvers to provide the input data to the FWHE for cavitating propellers is found in ITTC (2017a).

6.1.3 HYDROACOUSTICS BY CFD-FWHE COUPLING

To capture noise induced by the nonlinear sources of sound occurring during the operating conditions for non-cavitating propellers, the FWHE for permeable surfaces is very attractive because no volume integration is needed. Starting from the identification of the sources of sound by high-fidelity CFD tools over a fictitious porous surface *S* that embeds all nonlinear flow effects and physical noise sources, the permeable FWHE yields the noise signatures outside *S* by solving an inhomogeneous wave equation through the Green function technique. However, its drawbacks are: i) the need of accurate CFD simulations as Large Eddy Simulation (LES) or Detached Eddy Simulation (DES) methods; ii) the occurrence of spurious signals when vortical/turbulent eddies pass through the downstream end of the control surface (namely, the end-cap problem); & iii) the need of a careful placement of the porous surface whose dimension must be tailored to enclose all the noise sources. Finally, for CFD finite-volume based solvers relying on the dual (or pseudo) time-stepping approach (Merkle & Athavale, 2012) the need of computations capable to avoid boundary conditions reflections is mandatory (Poinsot & Lele, 1992).

The end-cap problem is caused by truncation of the source terms at the integration boundary. From a physical standpoint, it is strictly related to the differences between acoustic and hydrodynamic pressure distributions that the FWHE describes (as an exact rearrangement of the Navier-Stokes equations). When vortical structures pass across the permeable surface, the integral formulation used to solve the FWHE radiates the hydrodynamic pressure field across it as sound waves, because the free space Green's function technique is applied to solve the FWH-P problem. By including the (neglected) volume term, these contributions are cancelled-out through the Lighthill's stress tensor.

In view of these issues, the use of the FWHE for permeable surfaces is widely applied. For instance, in Ianniello *et al*. (2014), the radiated noise of a complete scaled ship model using incompressible RANS simulation and the FW-H analogy is computed. The direct volume integration and permeable FW-H approach were both used. For the direct volume integration, the averaged contribution of the turbulent fluctuating velocity components to the Lighthill stress was also included. Different permeable surfaces enveloping the whole ship were studied. Good correlation between the acoustic pressures and the RANS pressure signals were obtained.

Lloyd *et al*. (2014), compared two different numerical solvers (ReFRESCO with porous FW-H and EXCALIBUR with Kirchhoff

formulation) for the two-bladed model propeller (S6666) in open water condition. The main aim of the study was to verify the FW-H application and investigate the behaviour of the porous surface. It was observed that FW-H results show good agreement with the measurement by underpredicting the first harmonic, whereas Kirchhoff formulation gives slightly better estimation to FW-H formulation.

Lloyd *et al*. (2015b), investigated the propeller hydroacoustic performance using RANS with porous FW-H equation in open water condition. In their study, different grid structure configurations were analysed in order to examine its effects on propeller hydrodynamic and hydroacoustic performance using the steady simulations for the receivers located at the propeller plane. The numerical results showed that both unsteady FW-H and RANS pressures seem to suffer from some numerical disturbances which are attributed to sliding interface or pressure correction methods.

Lloyd *et al*. (2015a), also examined the propeller hydroacoustic performance using RANS with porous FW-H formulation for two receivers located downstream with two different CFD codes (ReFRESCO and OpenFoam). The effects of the permeable surface closure on the propeller hydroacoustic performance were investigated. Testa *et al*. (2018b) examined the INSEAN E779A propeller using BEM and DES with a porous FW-H approach under uniform flow and non-cavitating conditions. The main aim of the study was to show the capabilities of BEM for propeller underwater radiated noise predictions. Due to the absence of capturing the turbulence-induced noise effects, BEM only provides acceptable results in the vicinity of the propeller (0.5-1D) and hence only tonal components can be predicted.

Lidtke *et al*. (2016), used URANS and the FW-H analogy to compute the tonal blade passage noise of the PPTC propeller and used LES (Large Eddy Simulation) and the FW-H analogy for the noise generated by a hydrofoil. In this case cavitation occurrence is simulated using the Schnerr-Sauer model. It was concluded that RANS is unable to accurately account for cavitation dynamics and the associated noise.

Lidtke *et al*. (2019), investigated the INSEAN E779A model propeller underwater radiated noise under non-cavitating and cavitating conditions in the presence of a wakefield with RANS and FW-H analogy. This systematic study might be the first study to test the capabilities of FW-H approach in the realistic configuration in the maritime field. Therefore, the main aim was to understand the definition of the porous surface as well as important parameters such as time step and grid resolution. The results showed that the porous surface definition is important for reliable acoustic simulations.

Li *et al*. (2018), used DDES (Delayed Detached Eddy Simulation) and the permeable FW-H approach to compute the radiated noise of a full-scale ship and compared the results with sea trial measurements.

In Cianferra *et al*. (2019) a numerical computation of the acoustic field generated by an isolated marine propeller, in open water is addressed. The propeller considered corresponds to a benchmark case, for which fluid dynamic data are available in literature and online. The fluid dynamic field, which represents the source of noise, is reproduced through a LES solver, the small scales of motion are modeled through the dynamic Lagrangian model and a wall-layer model allows to avoid the resolution of the viscous sublayer. The acoustic field is reconstructed by the Ffowcs Williams and Hawkings equation, which is composed of surface and volume terms indicating different noise generation mechanisms. By isolating each term

contribution, the paper shows that the shaft vortex constitutes a considerable source of low frequencies noise.

6.2 GUIDELINES FOR COUPLED CFD-FWHE

From the above cited literature works and referring to some relevant papers on jet-noise such as Mendez *et al*. (2009), Mendez *et al*. (2013) and Shur *et al*. (2005) where the use of the permeable FWHE is mature, some useful suggestions may be proposed.

Among them the optimal FWH surface location should be fairly tight around the rotor disk and the wake convected downstream. This would lead to calculating noise by information (only) from the high-quality region of the calculus domain.

Further, both the magnitude of Lighthill's source term and placement of the vorticity/turbulent field downstream the rotor disk should be used as good indicator of correctness of the FWH surface placement; a basic test would be to check that sound is not strongly dependent on the surface used, in terms of diameter and length.

Finally, a warning is made on the common use of open porous surface to overcome the end-cap problem. For observers downstream, omitting the closure disk from the permeable FWHE seems to yield slightly better results than closed surfaces, especially in terms of waveform. Note that several correction techniques have been proposed to alleviate this issue. Among them, the exit-flux concept introduced in Wang *et al*. (1996) has been successfully extended in Nitzkorski & Mahesh (2014) to the FWH methodology for the end-cap correction of porous surfaces in the near field.

For the sake of clarity Figure 93 depicts a sketch of marine propeller enclosed by a permeable closed cylindrical surface. Accounting for the above criteria and looking at the contour plot of the L_2 norm of the Lighthill stress tensor distribution inside the computational domain, the porous surface size (length and width), as well as the placement of closure-end are well suited to compute the noise induced by the propeller, in that outside the acoustic surface the noise sources are negligible, and no vortices cut its boundaries.

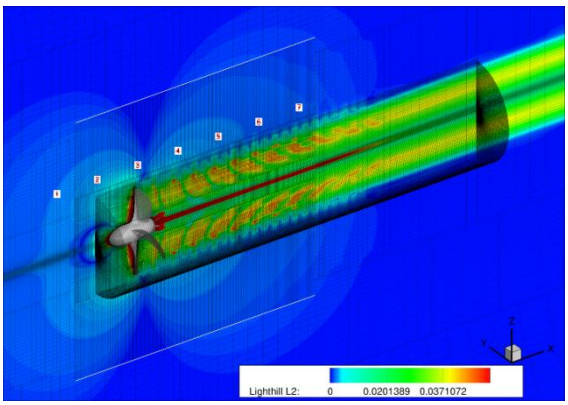

Figure 93. Sketch of FWH-P porous surface and contour of the L2 norm of Lighthill stress tensor.

6.3 STRUCTURAL BORNE NOISE

The noise caused by vibrating machinery onboard is called structural borne noise due to the fact that the vibrations are transmitted through the ship structure to the outer plating and emit as noise to the underwater environment. The most significant machinery noise sources are diesel engines and turbines, generators, propulsion gearboxes, and large pumps.

Any machinery will create both vibration and airborne noise. Figure 94 shows three main paths for noise generated by machinery (Spence *et al*., 2007). The first structure born path relates to the vibration excitation of machinery on the ship structures through the couplings between the source and the structure. The vibrations are

carried out through the entire hull. The low frequencies are controlled by the hull resonance modes which also affect the noise directivity (Arveson & Vendittis, 2000).

The secondary structure born path is excited by the airborne noise that impinges at the compartment boundaries and excite structures to vibrate. The vibrations then propagate to the outer plating causing underwater noise. The airborne path describes the noise that passes the ship's outer plating directly. The airborne path applies when the compartment containing machinery source is directly adjacent to the sea. When the machinery is located in the compartment next to the outer plating, the second structure born path has less significance than the airborne path. When the machinery is in inner compartments the situation is vice versa.

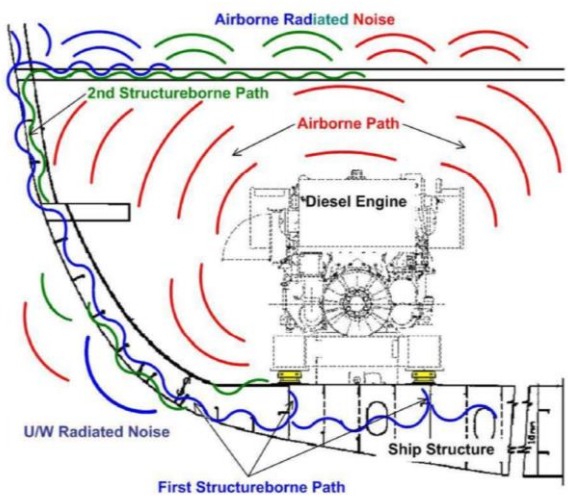

Figure 94. Main paths of structural born noise. Figure taken from Spence *et al.* (2007).

The source levels of vibrations in diesel engines usually scale as (power/weight)^2 (Fisher & Brown, 2005). The heavy low speed diesels have therefore lower source levels compared to medium speed engines. However, medium speed engines can be resiliently mounted which decrease their noise excitation level to water. Other well-known treatments to decrease structural born noise levels are to mount single or multiple items on a common floating deck, use hull decoupling materials, cladding treatments in machinery spaces, machinery enclosures, and flexible piping solutions. Air bubbling layers used to decrease flow friction under the hull also decrease the structural born underwater noise from the ship at a wide range of frequencies.

Vibroacoustic models are used to predict the structural born noise from ships. The models have been developed in other application areas and used for ships by specialist for dedicated purposes. Only few papers exist in open literature on vibroacoustics for underwater noise from ships.

At low frequencies, say up to 100 Hz depending on the size and complicity of the structure, the vibrations are first solved deterministic by FE method. The acoustic radiation is then solved by boundary element method (BEM) using the FEM solution as a forced response boundary condition. The two-step method is significantly less expensive computationally than a strongly coupled FEM-BEM solution.

At high frequencies from 500 Hz upwards, depending on the structure, the vibration behaviour is random. A statistical approach to model the vibrations on a structure is then a feasible choice. Statistical Energy Analysis (SEA) employs statistical descriptions of system components in order to simplify the analysis of complicated vibroacoustic problems (Lyon & De Jong, 1995).

In the frequencies between the feasible frequency limits for pure FEM and SEA approaches, a hybrid FEM/SEA approach can be utilized. FE and SEA subsystems are created for the structure. The FE part can be a larger system or a local junction between two SEA

subsystems. The coupling of the FE and SEA methods are described in detail for example in Shorter & Langley (2005a,b).

Not many papers are available in the open literature about underwater structural born noise from ships. Zhang *et al*. (2019) have published a study where they compared different radiation modelling methods for structural born noise of an oil tanker. They compared different acoustic radiation models at low and mid-frequencies with the FE method, namely BEM, infinite element method IFEM, and automatic matching layer AML. The latter two ones require volume mesh for the external acoustic field. All three methods gave relatively similar results, but the authors concluded that the FE-BEM hybrid model is the most suitable one for engineering purposes due to the lowest computational effort and robustness. The authors also studied the directivity of the noise at 50 m depth. The far field was reached at a radius of about half of the ship length around the vessel.

6.4 NOISE PROPAGATION

Noise propagation models are used to predict propagation loss due to surface and bottom reflections, bathymetry, and celerity profile. Propagation loss models were discussed in detail already in the report of the 28th ITTC specialist committee on hydrodynamic noise and are not repeated here.

NPL (Wang *et al*, 2014) reviewed the existing acoustic propagation models, see Table 14. The parabolic equation solution and the normal mode solution represent the most appropriate model choice at lower frequencies, for high frequency computations ray tracing or energy flux models are generally used.

Table 14. Review of propagation models (Wang et al, 2014)

Shallow water - low frequency	Shallow water - high frequency	Deep water - low frequency	Deep water - high frequency
Ray theory	*Ray theory*	*Ray theory*	*Ray theory*
Normal mode	*Normal mode*	*Normal mode*	*Normal mode*
Wave number integration	*Wave number integration*	*Wave number integration*	*Wave number integration*
Parabolic equation	*Parabolic equation*	*Parabolic equation*	*Parabolic equation*
Energy flux	*Energy flux*	*Energy flux*	*Energy flux*

Green – suitable; Amber – suitable with limitations; Red – not suitable or applicable

Within the project JOMOPANS (the Interreg Joint Monitoring Programme for Ambient Noise North Sea), a wide range of acoustic propagation model implementations from the JOMOPANS project partners are verified by means of a comparison of the output for two well defined benchmark scenarios based on the modelling scenarios developed for the Weston Memorial Workshop (Binnerts *et al*, 2019). The model types considered are based on energy-flux integration, analytical and numerical mode solvers, parabolic equation range step integration, ray tracking and wavenumber integration. Recommendations on the use of these models are given and limitations are discussed. The acoustic metric considered is the depth-averaged sound pressure level in one-third octave (base 10) bands from 10 Hz to 20 kHz. The results show that the majority of the tested models are in agreement for a range independent shallow water environment providing a reliable benchmark solution for the future verification of other propagation models. The observed agreement gives confidence that these models are correctly configured and able to provide numerically correct solutions. For a range-dependent environment however, a significant uncertainty remains. The solutions provided in this paper can be used as a reference to select the optimal compromise between reducing the computational complexity and increasing the model precision for the propagation of sound in shallow water.

Noise propagation models are commonly used for noise mapping. Typically, the modelled ranges are more than 10 km. For example, Cho *et al*. (2018) have modelled noise maps in Korean waters by combining empirical formula for source levels of ships, AIS data for shipping density, and propagation modelling. The transmission loss was calculated by a range-dependent ray-based propagation model. The authors found that the highest uncertainty in their calculation was the empirical model predicting the source level of ships. Halliday *et al*. (2017) simulated a region affected by underwater noise of a vessel in the western Canadian Arctic in order to estimate the potential impacts of underwater noise to whales. The source level was measured in the sea area and transmission loss was calculated by propagation models. A coupled normal modes model for a range-dependent environment (for frequencies between 50 Hz and 1.5 kHz), and a ray trace model (for frequencies between 1.5 and 24 kHz) were used in the study.

Propagation modelling can be used to predict transmission loss also at distances relevant in noise trials. Especially, the effect of shallow water on noise source level analyses can be estimated with propagation models. The Bureau Veritas (2014) URN rule notifications suggest as the first option to calculate the transmission loss at the noise trials at low frequencies (<1000 Hz) using a range independent wave integration model, and at higher frequencies (>1000 Hz) a range dependent ray trace-based model. One may also use other models if appropriate validation references are available.

Kozaczka & Grelowska (2018) have studied noise propagation in shallow water of about 20 meters using the normal mode theory. The authors have investigated the transmission loss at distances from 100 to 10 000 meters from the source. The paper investigates transmission loss at frequencies between 200 and 1000 Hz, and with different bottom sediment types. The bathymetry in the sea area was flat. The effect of shallow water on noise propagation is clearly seen in the simulations.

Sipilä *et al*. (2019) measured the propagation loss from noise measurements of an icebreaker. The noise measurements were repeated at varying by-pass distances of the ship and the measurement location. The propagation loss was calculated from the measurements. The water depth was about 25 meters in the measurement area. There was a slope in the seabed between the ship route and the measurement location. The propagation loss was also calculated using a range dependent parabolic equation model. Figure 95 shows comparison of geometrical transmission loss at a range of frequencies determined from the measurements and simulations. The two approaches show similar behavior for the transmission loss. The paper also studies the effect of different bottom sediment type and seabed slope on the transmission loss in shallow water.

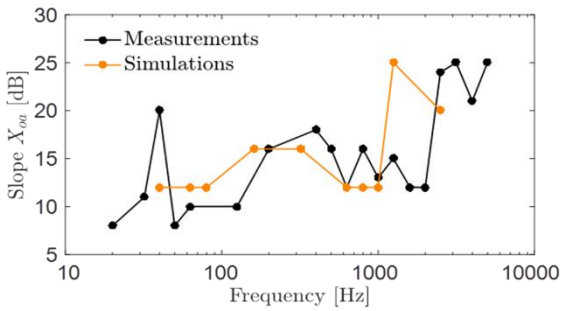

Figure 95. Measured and calculated propagation loss factor X , with propagation loss defined as X $\log_{10}$ R, at different frequencies determined for a distance of about 150 m. Figure taken from Sipilä *et al*. (2019).

Gaggero *et al*. (2016) calculated the transmission loss in shallow water to compare the model test results of noise emitting from a marine propeller to full-scale results. The conclusion was that careful determination of transfer function in model-scale and

transmission loss in full-scale is required to make comparisons of source level at different scales. However, more data is needed to gain further confidence on the procedures and on the complex mechanisms of cavitating propeller noise generation.

7. BENCHMARKING (MV)

The Specialist Committee on Hydrodynamic Noise of the 29th ITTC was tasked to identify a benchmarking case for model-scale underwater radiated noise (URN) measurements. The requirements for the test-case were that:

a. full-scale underwater radiated noise measurements are available.
b. it is a representative merchant vessel.
c. the geometry and measurement data can be shared with the whole ITTC community.

In the present paragraph, the proposed candidate ship is presented, reporting the reasons for the choice (Section 7.1). In order to setup the test matrix, two activities have been carried out, i.e., a questionnaire among a list of possible participants and some calculations carried out by members of the Committee; the results of both activities are summarised (Section 7.2). Finally, the complete structure of the proposed benchmark activity is described (Section 7.3).

7.1 Proposed candidate ship

A review of possible benchmark cases for model-scale noise measurements has been carried out by the Committee in order to propose a suitable candidate. The most relevant cases considered are summarised in the following:

- Olympus (AQUO Project) – Coastal Tanker - L = 116.9 m – Displacement 13250 t – Speed 14 kn – 1 CPP (D = 4.80 m): geometries not available to all participants, only separate agreements (ref.: Johansson *et al*, 2015; Tani *et al*, 2016b)

- Nawigator (EFFORT and AQUO Projects) – Research Vessel – L = 60.3 m – Displacement 1150 t – Speed 13 kn – 1 CPP (D = 2.26 m) (Ref.: Gaggero *et al*, 2016)

- Princess Royal (SONIC Project) – Research Vessel (catamaran) – L = 18. 9 m – Displacement 40 t – Speed 20 kn – 2 FPP (D = 0.75 m) (ref.: Aktas *et al.*, 2016b)

- Princess Royal (SONIC Project) propeller in open water conditions (Hydro Testing Forum test case) (ref.: Aktas *et al.*, 2016a; Hallander, 2017; Lafeber & Lloyd, 2017; Sakamoto *et al.*, 2017; Tani *et al.*, 2017; Tani *et al.*, 2020)

- Other cases were also considered, but they were either lacking URN data (REGAL used in LR CFD workshop), had noise measured with hull mounted transducers only (Seiun Maru), or URN measurements and geometries could not be made publicly available (Combi-Freighter)

Among the above mentioned cases, the research vessel Nawigator XXI has been selected, since it is the only case for which hull/propeller geometries and measurement data in full-scale can be shared with the ITTC Community. Moreover, Nawigator has a hull form and a propeller geometry that is representative of a merchant vessel. Therefore, despite its relatively small size, this ship is considered the best candidate for the benchmark activity.

In the following, a brief outline of the ship characteristics and the measurements available in full-scale is reported.

7.1.1 Ship characteristics

In Figure 96 a photograph of the ship is reported, while main ship characteristics are listed below.

Figure 96. Nawigator XXI Research Vessel.

- Ship name: Nawigator XXI
- Type / Year of building: Research Vessel built in 1998
- Owner: Maritime University of Szczecin
- Length overall: 60.3 m (LOS)
- Beam: 10.5 m
- Draft: 3.15 m
- Displacement: about 1150 t
- Speed: 13 kn (max)

Propulsion plant and other machineries characteristics are listed below:

- 1 Controllable Pitch Propeller (CPP), D = 2.26 m, P/D(design) = 0.942, 4 blades
- Main Engine: SULZER Cegielski 8S20D (4 stroke, 8 cyl L) resilient mounted, 1120 kW, 900 RPM, reduction rate: 3.75
- Auxiliary Engines: Caterpillar SR4: (4 stroke, 8 cyl L) resilient mounted, 2 x 240 kW + 1 x 85 kW, 1500 RPM
- Bow thruster: 110 kW, abt. 500 RPM (propeller)

7.1.2 Full-scale measurement campaign

URN measurements at sea have been carried out during the EU-FP7 AQUO project; the campaign took place in the Baltic Sea and the following data were recorded:

- Power, rpm, pitch, speed over ground
- Cavitation observations
- Vibrations
- URN
- Pressure pulses

Measurements have been performed at one ship draught (namely, 3.2 m at stern, 3.15 m at bow), mainly varying pitch at constant RPM (8 different pitch settings); in addition to this, in correspondence to one pitch setting two different propeller RPM have been considered (navigation and maximum)

It has to be kept in mind that the measurement campaign presents some shortcomings. In particular, information on blade pitch angle is only obtained from the bridge, thus there is some uncertainty on the exact value. Moreover, cavitation photographs using hull windows are available, but the quality is not enough to capture correctly the cavity extents. Finally, the URN measurements have been performed in shallow (24 m) water, requiring the use of a computational method to convert the radiated noise levels to source levels.

For what regards possible conditions of interest, considering the whole set of measurements, the signal to background noise ratio of the URN measurements is acceptable at maximum speed condition (maximum RPM) and for the conditions with lowest pitch tested. Model tests carried out during the AQUO project (propeller at UNIGE cavitation tunnel behind wake screen) suggest that in correspondence to maximum speed condition attached tip-vortex cavitation is present, plus

very limited sheet cavity at tip, as reported in Figure 97; in correspondence to the lower pitch condition pressure side cavitation is present (tip vortex, vortex from sheet face and pressure side sheet cavitation)

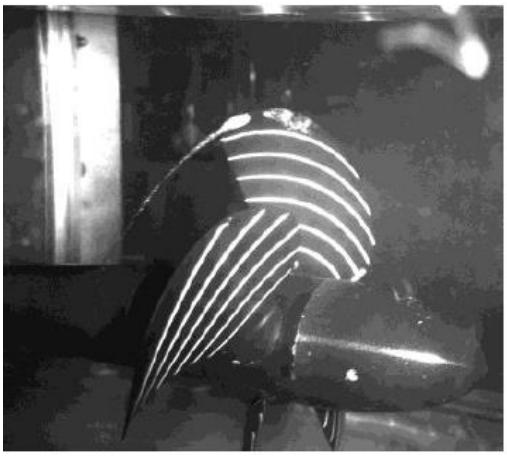

Figure 97. Cavitation observations at UNIGE cavitation tunnel (max. speed condition) (Gaggero *et al.*, 2016).

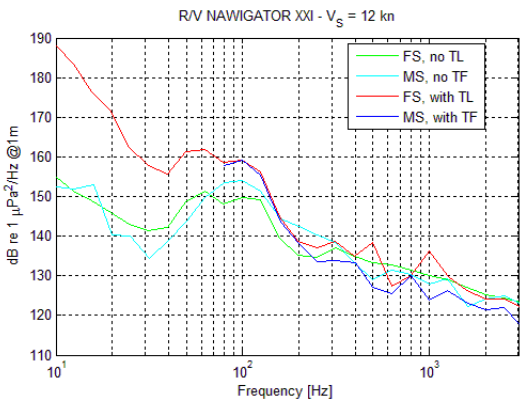

Figure 98. Model-scale vs Full-scale measurements (Gaggero *et al.*, 2016).

Notwithstanding the above-mentioned shortcomings, a good agreement between model tests and sea trials has been obtained, as reported in Figure 98. Therefore, the Committee considered it worthwhile to proceed with this candidate, keeping in mind that comparison between results of different cavitation test facilities is an important aspect of the benchmarking study.

7.2 Definition of the test matrix

In the following paragraphs, the results of the questionnaire and numerical calculations conducted by the Committee with the aim of defining the most suitable test matrix for the benchmarking activity are summarised.

7.2.1 Questionnaire

A questionnaire was circulated among possible participants to the benchmark activity, in order to get an insight into the number of facilities interested and the extent of their possible involvement in terms of number and complexity of tests.

The questionnaire obtained 20 answers, with 19 facilities confirming their interest in the benchmark activity. The Committee considers this result very encouraging in view of the forthcoming activity, with a large interest spread basically over the entire model testing community.

In particular, two conditions [12] were indicated as “mandatory”, as follows:

- Condition A: 79% pitch and max shaft rate (860 RPM) / full-scale data available
- Condition B: 79% pitch, identical propeller loading (thrust coefficient value) as Condition A, but reduced cavitation number

[12] For both conditions, tests have to be carried out reproducing ship wake (directly with models or with wake screens).

in order to enlarge sheet cavitation extent (together with tip–vortex cavitation) / no full-scale data available.

In addition to this, participants were asked to indicate their possible interest on different additional tests (e.g., at lower pitch[13], with reduced propeller loading, in different wakes).

Among the participants which provided a positive response, the following answers to specific questions were given:

- 100% agreed with the proposed "mandatory" conditions.
- 12 participants (63%) expressed interest in carrying out tests at reduced pitch; among these, 3 participants indicated the interest on the use of one additional pitch, 3 on two additional pitches, only one was in favour of more than two additional pitches; moreover, some participants proposed to use CPP model and not different FPP models in order to limit costs.
- 17 participants (89%) expressed interest in carrying out tests at constant pitch and reduced K_T; this kind of test of course does not reproduce the same phenomenon but has the advantage of investigating pressure side phenomena with low additional cost.
- 12 participants (63%) expressed interest in carrying out tests in open water condition; among these, all participants indicated interest in tests without shaft inclination, 6 participants indicated interest in investigating inclined shaft conditions (about 4° plus an higher inclination, with variable values); 1 participant indicated interest in testing propeller in pulling and pushing condition.
- Among facilities which use wake screens to reproduce the ship wake, 8 participants (42% of the total, 73% of facilities using wake screens) expressed interest in reproducing in addition to the full-scale wake also the model-scale wake.

Further possible interesting investigations suggested by some participants included the possibility to use the smart dummy concept (Schuiling *et al.*, 2011), to also measure propeller-induced hull-pressure fluctuations, and to increase the number of conditions in order to investigate tip vortex - sheet cavitation interactions.

Finally, considering all the participants (including the single negative answer), 58% confirmed to have an established procedure to determine the facility transfer function; this result confirms that this practice is becoming widespread, despite further efforts are still needed in order to make it a standard procedure for almost all facilities.

The results of the questionnaire have been utilised in order to propose the conditions for the benchmark activity.

7.2.2 Numerical calculations

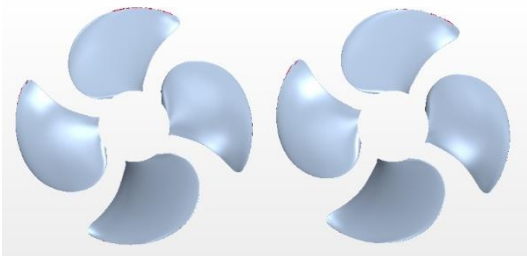

0° 12°

[13] Considering that a new propeller model for each additional pitch angle has to be manufactured to avoid uncertainties in the pitch setting.

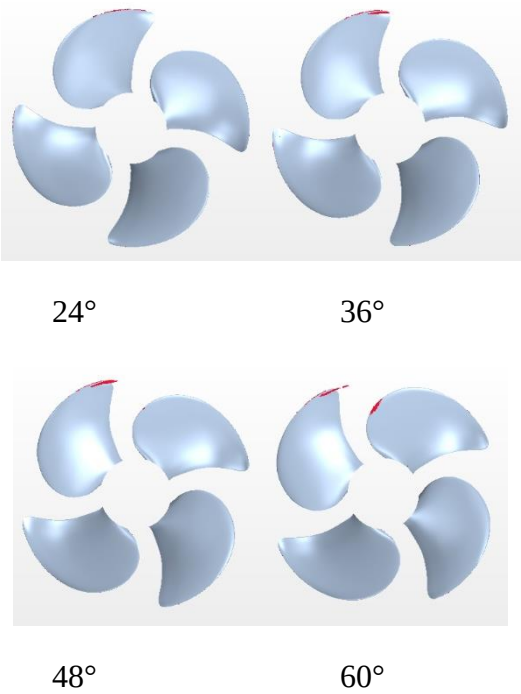

Figure 99. Cavitation predictions @ condition A1 with RANS code (courtesy of CSSRC).

In order to establish the conditions for the benchmarking activity, a series of numerical calculations have been carried out. In particular, Marin and UNIGE used BEM potential codes and CSSRC used a RANS code. The results of these calculation have been used to decide further conditions with respect to those tested at full-scale, reducing and increasing load to stimulate pressure side cavitation and increase suction side cavitation extent respectively. Moreover, calculations allowed to suggest a condition with very limited cavitation (slightly below inception) at rather large cavitation number.

In Figure 99 and Figure 100 results in correspondence to condition A1 only are reported. Numerical results confirm the expected extent of cavitation reported in Figure 97, with lower extent predicted by RANS calculations and higher extent predicted by BEM calculations.

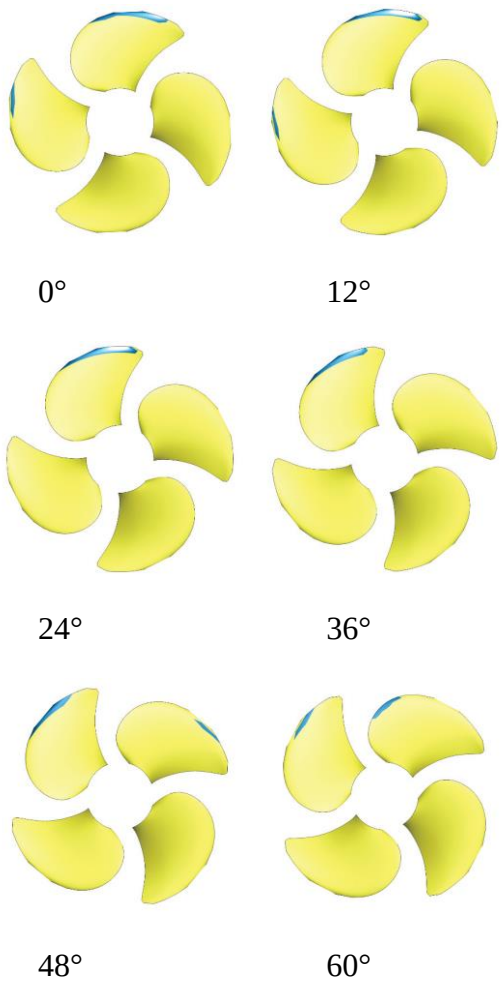

Figure 100. Cavitation predictions @ condition A1 with BEM code (courtesy of UNIGE).

7.3 Proposed benchmark

Considering the results of the questionnaire and of the numerical calculations, the Committee proposes the following conditions for the benchmark activity, as summarised in Table 15.

Table 15. Proposed test-conditions for the Nawigator XXI benchmarking studies.

Condition	P/D	K_T	σ_N (tip)	Type
A1[14]	0.91	0.22	2.79	Mandatory
A2	0.91	0.26	2.79	
A3	0.91	0.22	4.2	
A4	0.91	0.08	2.79	Suggested
B1[15]	0.464	0.08	3.58	Additional (lower pitch)
C1	0.91	0.22	2.79	Additional (uniform flow, no shaft inclination)
C2	0.91	0.26	2.79	
C3	0.91	0.22	4.07	
C4	0.91	0.08	2.79	
D1	0.91	0.22	2.79	Additional (uniform flow, 8° shaft inclination)
D2	0.91	0.26	2.79	
D3	0.91	0.22	4.07	
D4	0.91	0.08	2.79	
E1	0.91	0.22	2.79	Additional (wake sensitivity study)
E2	0.91	0.26	2.79	
E3	0.91	0.22	4.07	
E4	0.91	0.08	2.79	

The test-conditions consist of:

- Three "mandatory" conditions (condition A indicated above, named A1, condition A2 obtained with higher loading at constant cavitation number, condition A3 with reduced cavitation, near inception)
- One "suggested" condition (condition A4 with reduced loading at fixed pitch)
- Possible "additional conditions", such as:
  - tests at reduced pitch (31% in order to have reference full-scale tests), with a dedicated FPP model (condition B1)
  - tests in open water: basic tests with no shaft inclination (conditions C1-C4) plus additional tests at large shaft inclination, suggested value 8° (conditions D1-D4)
  - for smaller facilities using wake screens, additional tests with model-scale wake (conditions E1-E4

The tests must be performed according to normal procedures by all participants. For conditions A1-A4 and B1 the complete hull model or smart dummy will be used for larger facilities, dummy models or wake screens for smaller facilities. In the case of wake screens, the full-scale wake will be reproduced. For conditions E1-E4 (smaller facilities only), the model-scale wake will be reproduced.

Some further remarks must be considered when the benchmarking activity will be undertaken:

[14] For this condition full-scale measurements are available; propeller revolution rate at full-scale was 230 RPM, with a correspondent $\sigma_{N\,(shaft)} = 3.09$

[15] For this condition full-scale measurements are available; propeller revolution rate at full-scale was 203 RPM, with a correspondent $\sigma_{N\,(shaft)} = 3.96$

- in correspondence to lower pitch (condition B1), possible further conditions might be tested.
- for cases "C", "D", "E", all conditions proposed for case "A" are currently reproduced in the table, however the number of tests could be reduced.

8. SUMMARY AND CONCLUSIONS

The conclusions of the 29th Specialist Committee on Hydrodynamic Noise are presented here, ordered by the Terms of Reference.

1. An outline of the ITTC model-scale guidelines has been submitted to the IMO by the ITTC secretary in December 2017 without input from the Specialist Committee. The URN of shipping has until the moment of writing not been on the agenda of IMO MEPC meetings, even though a submission by Canada, Australia and the US, supported by the EU, asked for action. Therefore, the Specialist Committee did not consider another submission by the ITTC to be of value to the community within IMO.

2. Some progress on full-scale URN measurement procedures has been made, with an ISO regulation for shallow water noise measurements still in development. At present, a total of six classification societies have rules on URN emission with URN limits, some of which include procedures for the noise measurement in shallow water. Within the EU several URN monitoring programs have started in order to measure the present ambient noise levels in European waters needed for compliance with the Good Environmental Status. Some Canadian harbours have introduced measures to promote quieting ships which has resulted into an increase of the number of ships that hold an URN class.

3. A review of the recent published literature on model-scale noise measurements has been made in the areas of

   Facility reverberation: It appears that in the last years sufficient information has become available to measure and apply transfer functions. The Committee thus recommends that the determination of facility transfer functions becomes mandatory if the source level is to be determined. It should be noted that some issues are still present which need to be further studied.

   Tip-vortex scaling: Methods to account for the effect of Reynolds number on vortex cavity size and on the underwater radiated noise in model tests are proposed in the literature but further validation studies are required.

   Water quality: There is a general acknowledgement of the significance of water quality on cavitation behaviour and noise propagation, but this is generally not quantified. There is ongoing interest in the further development and application of, particularly optical based, techniques for the measurement of nuclei size distribution.

   Measurement techniques: Further progress has been made with respect to transducer calibration and in the use of pressure sensors, hydrophone arrays and dedicated signal processing techniques. Adding uncertainties in decibels of a measurement chain for noise measurements should be done with care.

   Benchmarking activity (HTF round robin test for a propeller in open water): Discrepancies between different facilities can be as high as 10 dB.

Validation studies for propellers operating behind a ship hull: It is found that full-scale noise levels can be predicted within 5 to 10 dB by model-scale tests.

4. Progress on computational prediction methods has been made, especially in modelling cavitation and turbulence structures in the flow field. Guidelines to couple CFD with FWHE are given to capture the relevant noise sources and to omit spurious noise in the simulations. Semi-empirical models predict noise from different cavitation patterns so appropriate combination of models is needed to deal with the whole spectrum of URN. Data driven models seem a promising option for cavitation noise predictions but should be applied carefully. Vibroacoustic models are used to predict the structure born noise from ships. The models are used by specialists for dedicated purposes and there is a limited number of papers in open literature. The models have matured from other application areas. Propagation loss models give more insight to propagation loss at different frequencies in shallow water (and in deep water). The approach seems promising and is recommended by Bureau Veritas for noise measurement analyses in shallow water. The propagation loss models are not yet widely used for ship source level determination but are more commonly used for noise mapping.

5. A review of possible benchmark cases for model-scale noise measurements has been carried out. Among them, the research vessel Nawigator XXI (considered during AQUO project) has been selected. As requested, hull/propeller geometries and measurements data in full-scale can be shared with the ITTC Community. Nawigator XXI ship has a hullform and propeller geometry that is representative of a merchant vessel, despite having a small size (L = 60.3 m – Displacement 1150 t). The ship has a maximum speed of about 13 kn and is equipped with 1 CPP (D = 2.26 m).

   A proposal for test conditions to be considered is presented by the Specialist Committee, considering also the results of a questionnaire among potential participants to the benchmarking activity and of ad hoc numerical calculations. The proposed conditions include minimal required tests corresponding to maximum speed at sea trials plus conditions with increased and decreased suction side cavitation and a condition with pressure side cavitation.

6. The guideline 7.5-02-01-05 for model-scale noise measurements has been updated, particularly with regards to facility reverberation and the facility transfer function describing the relation between acoustic source levels and measured radiated noise levels. New methods to account for the Reynolds number scaling of tip-vortex cavitation have been described. Note that guideline 7.5-02-01-05 has been renumbered to 7.5-02-03-03.9.

   The guideline 7.5-04-04-01 for full-scale noise measurements has been updated, particularly with regards to class rules on URN and corrections for the Lloyd-mirror effect.

9. RECOMMENDATIONS

The 29th Specialist Committee on Hydrodynamic Noise recommends adopting the following guidelines:

- ITTC guideline 7.5-02-01-05: Model-Scale Propeller Cavitation Noise Measurements.
- ITTC guideline 7.5-04-04-01: Underwater Noise from Ships, Full-Scale Measurements.

The recommendations for future work are:

- To organize the proposed round-robin test case.
- Further monitor and investigate specific aspects of model-scale noise measurements including reverberation, tip vortex scaling, water quality and the effect on uncertainty.
- Continue monitoring progress on shipping noise measurement procedures for shallow water and regulations as developed by ISO, classification societies and regulatory agencies.
- Continue monitoring progress on ship noise prediction by computational methods with emphasis on the prediction of cavitation noise using CFD methods and methods such as data driven models and machine learning techniques, and noise propagation modelling, especially for shallow waters.

10. REFERENCES

Aktas, B., 2016, "A Systematic Experimental Approach to Cavitation Noise Prediction on Marine Propellers", PhD Thesis (Newcastle University).

Aktas, B., Atlar, M., Turkmen, S., Korkut, E. and Fitzsimmons, P., 2016a "Systematic cavitation tunnel tests of a propeller in uniform and inclined flow conditions as part of a round robin test campaign", Ocean Engineering, Vol. 120, pp. 136–151.

Aktas, B., Atlar, M., Turkmen, S., Shi, W., Sampson, R., Korkut, E. and Fitzsimmons, P., 2016b, "Propeller Cavitation Noise Investigations of a Research Vessel Using Medium Size Cavitation Tunnel Tests and Full-Scale Trials", Ocean Engineering, Vol. 120, pp. 122-135.

Alexander, W.N., Hickling, C., Balantrapu, N.A. and Devenport, W.J., 2020, "Ingestion of non-uniform turbulent inflow by a rotor: sound production and propagation", 33rd Symposium on Naval Hydrodynamics, Osaka, Japan, October 2020.

Amailland, S., Thomas, J.-H., Pézerat, Ch. and Boucheron, R., 2018, "Boundary layer noise subtraction in hydrodynamic tunnel using robust principal component analysis", Journal of the Acoustical Society of America, Vol. 143, pp. 2152-2163.

ABS, 2018, Guide for the classification notation - Underwater Noise, American Bureau of Shipping.

Ando, S., Kimura, K., Segawa, K. and Yamamoto, K., 2018, "Study on the Hybrid Method of CFD and Bubble Dynamics for Marine Propeller Cavitation Noise Prediction", Tenth International Symposium on Cavitation (CAV2018).

ANSI/ASA S12.64-2009: Part 1, 2009, Quantities and procedures for description and measurement of underwater sound from ships, Part 1: General requirements.

AQUO-SONIC, 2015, Guidelines for regulation on UW noise from commercial shipping, Prepared by Bureau Veritas and DNV-GL.

Arndt, R.E.A. and Keller, A.P., 1976, "Free gas content effects on cavitation inception and noise in a free shear flow", Symposium on two phase flow and cavitation in power generation systems, Grenoble, France, Societe Hydrotechnique de France. Paris, pp. 3-16.

Arveson, P. T. and Vendittis, D. J., 2000, "Radiated noise characteristics of a modern cargo ship", Journal of the Acoustical Society of America, Vol. 107, no. 1, pp 118-129.

Audoly, C. and Meyer, V., (2017). "Measurement of radiated noise from surface ships – Influence of the sea surface reflection coefficient on the Lloyd's mirror effect", Acoustics 2017 Perth: Sound, Science and Society, Perth, The Australian Acoustical Society: Paper 20.

Bahtarian, M., 2019, "Quieting ships to protect the marine environment - workshop final report". ACENTECH Inc., Report #481 Cambridge, USA.

Baiter, H.J., 1989, "On cavitation noise scaling with the implication dissimilarity in cavitation inception", ASME International symposium on cavitation noise and erosion in fluid systems.

Baraniuk, R.G., Jones, D.L., 1995, "Unitary equivalence: a new twist on signal processing", IEEE Transactions on signal processing, Vol. 43, no. 10, pp. 2269-2282.

Bark, G., 1985, "Prediction of Propeller Cavitation Noise from Model Tests and its Comparison with Full Scale Data", Journal of Fluids Engineering, Vol. 107, pp. 112-119.

Belibassakis, K. and Politis, G., 2019, "Generation and propagation of noise from cavitating marine propellers", Sixth International Symposium on Marine Propulsors - smp'19, Rome, Italy.

Binnerts, B., Jong, C., Karasalo, I., Östberg, M., Folegot, T., Clorennec, D., Ainslie, M., Warner, G. and Wang, L., 2019, "Model Benchmarking Results for Ship Noise in Shallow water", https:// northsearegion.eu/ media/ 9884/binnerts-et-al-2019-uace-jomopans-model-benchmarking.pdf

Birvalski, M. and van Rijsbergen, M.X., 2018a, "Application of Interferometric Particle Imaging to cavitation nuclei measurements in a ship model basin", 19th International Symposium on the Application of Laser and Imaging Techniques to Fluid Mechanics, Lisbon, Portugal, July 2018.

Birvalski, M. and van Rijsbergen, M.X., 2018b, "Size and concentration measurements of cavitation nuclei in the wake of a ship model", 10th International Symposium on Cavitation – CAV2018, Baltimore, May 2018.

Blake, W.K., 2017, "Mechanics of flow-induced sound and vibration". 2nd edition, Academic Press.

Blake, W.K. and Sevik, M.M., 1982, "Recent developments in cavitation noise research", International Symposium on Cavitation Noise, Phoenix, Arizona.

Bosschers, J., 2018a, "Propeller Tip-Vortex Cavitation and its Broadband Noise". PhD Thesis, University of Twente, Enschede, The Netherlands.

Bosschers, J., 2018b, "A Semi-Empirical Prediction Method for Broadband Hull-Pressure Fluctuations and Underwater Radiated Noise by Propeller Tip Vortex Cavitation", Journal of Marine Science and Engineering, Vol. 6, art. 49.

Bosschers, J., 2020, "The effect of Reynolds number on a developed tip-vortex cavity and its radiated noise", 33rd Symposium on Naval Hydrodynamics, Osaka, Japan.

Bosschers, J. and van Wijngaarden, E., 2012,

"Scale effects on hull pressure fluctuations due to cavitating propellers", 10th International Conference on Hydrodynamics, St. Petersburg, Russia.

Boucheron R., 2016, "About Doppler-Fizeau effect on radiated noise from a rotating source in cavitation tunnel", 22nd International Congress on Acoustics, Buenos Aires, Argentina, September 2016.

Boucheron R., 2017, "Over-sampling improv ement for acoustic triangulation using Barker code or Schroeder code audio signals", 5th International Conference on Advanced Model Measurement Technology for the Maritime Industry AMT'17, Glasgow.

Boucheron, R., 2019a, "Adaptation of the Schroeder frequency to the case of acoustic propagation in duct", 6th International Conference on Advanced Model Measurement Technology for the Maritime Industry AMT'19, Rome, Italy.

Boucheron, R., (2019b), "Development of a demodulation method for acoustic propagation in ducts with unknown impedance conditions for both modal magnitude and wall impedance estimate", 26th International Congress on Sound and Vibration - ICSV26, Montreal, Canada.

Boucheron, R., 2020a, "About acoustic field characteristics in the test section of a cavitation tunnel", Ocean Engineering, Vol. 211, art. 107616.

Boucheron, R., 2020b, "Modal decomposition method in rectangular ducts in a test-section of a cavitation tunnel with a simultaneous estimate of the effective wall impedance", Ocean Engineering, Vol. 209, art. 107491.

Boucheron R., 2020c, "Influence of the warping time parameters on dedopplerization efficiency in the case of a rotating source in a cavitation tunnel", 179th Meeting of the Acoustical Society of America, Acoustics Virtually Everywhere, December 2020.

Boucheron, R., Amailland, S., Thomas, J.-H., Pézerat, Ch., Fréchou, D. and Briançon-Marjollet, L., 2017, "Experimental modal decomposition of acoustic field in cavitation tunnel with square duct section", 173rd Meeting of Acoustical Society of America – 8th Forum Acusticum, Boston, June 2017.

Boucheron R., Aumelas V., Donnet, M., Fréchou, D. and Poidatz, A., 2018, "Comparative study of optical experimental methods for micro-bubble sizing", 19th International Symposium on the Application of Laser and Imaging Techniques to Fluid Mechanics, Lisbon, Portugal, July 2018.

Breeding Jr., J.E., Pflug, L.A., Bradley, M., Walrod, M.H., McBride, W., 1996. "Research Ambient Noise Directionality (RANDI) 3.1 Physics Description". Naval Research Laboratory, Stennis Space Center, Report, No. NRL/FR/7176-95-9628.

Brennen, C.E., 1995, "Cavitation and Bubble Dynamics". Oxford University Press, New York.

Briancon-Marjollet, L. and Michel, J. M., 1990, "The hydrodynamic tunnel of I.M.G.: Former and recent equipments." Journal of Fluids Engineering, Vol. 112, no. 3, pp. 338-342.

Briançon, L., Fournier, P. and Frechou, D., 2013, "Marine propeller noise measurements techniques in hydroacoustics tunnel", 3rd International Conference on Advanced Model Measurement Technology for the EU Maritime Industry AMT'13.

Brown, N.A., 1976, "Cavitation noise problems and solutions", International Symposium on Ship-board Acoustics, Noordwijkerhout, The Netherlands.

BV, 2018, "Underwater Radiated Noise (URN)", Rule Note, NR 614 DT R02 E, Bureau Veritas.

Carlton, J.S., 2018, "Marine Propellers & Propulsion", Butterworth-Heinemann Ltd, Oxford, UK, 4th E.

CCS, 2018, "Guideline for ship underwater radiated noise", China Classification Society.

Ceccio, S.L. and Brennen, C.E., 1991, "Observations of the dynamics and acoustics of travelling bubble cavitation", Journal Fluid Mechanics, Vol. 233, pp. 633–660.

Chen L., Zhang L., Peng, X. and Shao X., 2019, "Influence of water quality on the tip vortex cavitation inception", Physics of Fluids, Vol. 31, art. 023303.

Chmelnitsky, E. and Gilbert, M., 2016, "Vessel quieting design, technology, and maintenance options for potential inclusion in EcoAction Program". Report 302-045.03, Hemmera Envirochem Inc.

Cho, S., Kang, D., Park, J.S. and Hahn, J., 2018, "Spatial mapping of underwater noise radiated from passing vessels using automatic identification system data", Japanese Journal of Applied Physics, Vol. 57, no. 7S1, art. 07LG07.

Cianferra, M, Petronio, A. and Armenio, V., 2019, "Numerical prediction of ship propeller noise through acoustic analogy", Sixth International Symposium on Marine Propulsors - smp'19, Rome, Italy.

Colbert, B.R., 2020, "Trends and developments in international regulation of anthropogenic sound in aquatic habitats". Journal of the Acoustical Society of America Vol. 147, no. 5, pp. 3100-3107.

Collins, M. D., 1993, " A split-step Padé solution for the parabolic equation method ", Journal of the Acoustical Society of America, Vol. 93, no. 4, pp. 1736-1742.

Collins, M. D., Cederberg, R. J., King, D. B. and Chin-Bing, S. A., 1996, "Comparison of algorithms for solving parabolic wave equations", Journal of the Acoustical Society of America, Vol. 100, no. 1, pp. 178-182.

Dinsenmeyer, A., Antoni, J., Leclère, Q. and Pereira, A., 2020, "A probabilistic approach for cross-spectral denoising: benchmarking with some recent methods", Journal of the Acoustical Society of America, Vol. 147, no. 5, pp. 3108-3127.

DNV-GL, 2019, Class Guideline DNVGL-CG-0313, Edition July 2019, "Measurement procedures for noise emission", Det Norske Veritas and Germanischer Lloyd.

DNV-GL, 2020, Rules for classification – Ships, DNVGL-RU-Ship Pt.6 Ch.7, Section 6 "Underwater Noise Emission – Silent", Det Norske Veritas and Germanischer Lloyd.

Dowling, A.P. and Ffowcs Williams, J.E., 1983, "Sound and Sources of Sound", John Wiley & Sons.

Duarte, C.M., Chapuis, L., Collin, S.P., Costa, D.P., Devassy, R.P., Eguiluz, V.M., Erbe, C., Gordon, T.A.C., Halpern, B.S., Harding, H.R., Havlik, M.N., Meekan, M., Merchant, N.D., Miksis-Olds, J.L., Parsons, M., Predragovic, M., Radford, A.N., Radford, C.A., Simpson, S.D., Slabbekoorn, H., Staaterman, E., Van Opzeeland, I.C.,

Winderen, J., Zhang, X. and Juanes, F., 2021, "The soundscape of the Anthropocene ocean", Science, Vol. 371, no. 6529, art. eaba4658.

Ebert, E., Kleinwächter, A., Kostbade, R. and Damaschke, N., 2018, "Dynamic water quality measurements on the full scale ferry ship "Loch Seaforth" by the Hydrodynamic Nuclei Concentration (HDNC) technique", 32nd Symposium on Naval Hydrodynamics, Hamburg, Germany, August 2018.

Erbe, C., Marley, S.A., Schoeman, R.P., Smith, J.N., Trigg, L.E. and Embling, C.B., 2019, "The Effects of Ship Noise on Marine Mammals—A Review", Frontiers in Marine Science, Vol. 6: art. 606.

Etter, P.C., 2013, "Underwater Acoustic modeling and simulation", 4th Edition, CRC Press.

Food and Agriculture Organization of the United Nations (FAO), 2019, Joint GFCM/ OceanCare Workshop on anthropogenic underwater noise and impacts on fish, invertebrates and fish resources, FAO headquarters, Rome, Italy, 21-22 February 2019.

Farassat, F., 1981, "Linear acoustic formulas for calculation of rotating blade noise", AIAA Journal, Vol. 19, no. 9, pp. 1122–1130.

Farassat, F., 2007, "Derivation of formulations 1 and 1A of Farassat", Technical Memorandum (TM) L-19318 NASA/TM-2007-214853.

Felli, M., Grizzi, S. and Falchi, M., 2014, "Novel approach for the isolation of the sound and pseudo-sound contributions from near field pressure fluctuation measurements: Analysis of the hydroacoustic and hydrodynamic perturbation in a propeller-rudder system", Experiment in Fluids, Vol. 55, no. 1, art. 1651.

Felli M., Falchi M. and Dubbioso, G., 2015, "Experimental approaches for the diagnostics of hydroacoustic problems in naval propulsion", Ocean Engineering, Vol. 106, pp. 1-19.

Feltane, A., Fayee, Boudreaux-Bartels, G. and Boudria, Y., 2018, "Using the Lambert-W function to create a new class of warped time-frequency representations", Circuits, Systems, and Signal Processing, Vol. 37, pp. 3191-3205.

Ffowcs Williams, J.E. and Hawkings, D.L., 1969, "Sound Generated by Turbulence and Surfaces in Arbitrary Motion", Philosophical Transactions of the Royal Society. Series A, Vol. 264, no. 1151, pp. 321-342.

Fischer, R. and Brown, N.A., 2005, "Factors affecting the underwater noise of commercial vessels operating in environmentally sensitive areas", OCEANS 2005, Proceedings of MTS/IEEE, Vol. 3, pp. 1982-1988.

Foeth, E.J. and Bosschers, J., 2016, 'Localization and Source-Strength Estimation of Propeller Cavitation Noise using Hull Mounted Pressure Transducers', 31st Symposium on Naval Hydrodynamics, Monterey, California.

Franc, J.-P. and Michel, J.-M., 2004, "Fundamentals of Cavitation", Kluwer Academic Press, Dordrecht.

Gaggero, S., Gaggero, T., Rizzuto, E., Tani, G., Villa, D. and Viviani, M., 2016, "Ship propeller side effects: pressure pulses and radiated noise", Noise Mapping, Vol. 3, no. 1, pp. 295-315.

Gao, J., Yu, L. and Jiang, W., 2019, "Extraction of target sources from incoherent and partially coherent background noise using low-rank and sparse decomposition of the cross-spectral matrix", Inter-noise 2019, Madrid, Spain, June 2019.

Gassman, M., Kindberg, L.B., Wiggins, S.M. and Hildebrand, J.A., 2017a, "Underwater noise comparison of pre- and post-retrofitted Maersk G-class container vessels", Marine Physical Laboratory, Scripps Institute of Oceanography, Report MPL-TM-616.

Gassmann, M., Wiggins, S.M. and Hildebrand, J.A., 2017b, "Deep-water measurements of container ship radiated noise signatures and directionality", Journal of the Acoustical Society of America, Vol. 142, no. 3, pp. 1563-1574.

Gedamke, J., Harrison, J., Hatch, L. et al. (2016). "Ocean noise strategy roadmap", NOAA report, USA.

Gennaretti, M., Luceri, L. and Morino, L., 1997, "A Unified Boundary Integral Methodology for Aerodynamics and Aeroacoustics of Rotors", Journal of Sound and Vibration, Vol. 200, no. 4, pp. 461–489.

Greco, L., Muscari, R., Testa, C. and Di Mascio, A., 2014, "Marine Propellers Performance and Flow-Field Features Prediction by a Free-Wake Panel Method", Journal of Hydrodynamics, Ser.B, Vol. 26, no. 5, pp. 780-795.

Hald, J., 2017, "Removal of incoherent noise from an averaged cross-spectral matrix", Journal of the Acoustical Society of America, Vol. 142, no. 2, pp. 846-854.

Hald, J., 2019, "Denoising of cross-spectral matrices using canonical coherence", Journal of the Acoustical Society of America, Vol. 146, no. 1, pp. 399-408.

Hallander, J., 2017, "Systematic cavitation tunnel tests with a propeller in uniform and inclined flow conditions as part of a round robin campaign", 5th International Conference on Advanced Model Measurement Technologies for the Maritime Industry - AMT'17 (Glasgow, UK).

Halliday, W., Insley, S., Hilliard, C., de Jong, T. and Pine, M., 2017, "Potential impacts of shipping noise on marine mammals in the western Canadian Arctic", Marine Pollution Bulletin, Vol. 123, pp. 73-82.

Hannay, D., MacGillivray, A., Wladichuk, J., Pace, F. and Frouin-Mouy, H., 2019, "Comparison of Class Society Quiet Notation maximum noise levels with ECHO program measurements" [presentation], Quieting Ships to Protect the Marine Environment: Technical Workshop. Hosted by the International Maritime Organization (IMO), 30 Jan to 1 Feb 2019, London, U.K.

Harrison, C.H. and Harrison, J.S., 1995, "A simple relationship between frequency and range averages for broadband sonar", Journal of Acoustical Society of America, Vol. 97, no. 2, pp.1314-1317.

Haver, S.M., Fournet, M.E.H., Dziak, R.P., Gedamke, J., Hatch, L.T., Haxel, J., Heppell, S.A., McKenna, M.F., Mellinger, D.K. and Van Parijs, S.M., 2019, "Comparing the underwater soundscapes of four US national parks and marine sanctuaries", Frontiers in Marine Science, Vol. 6, art. 500.

He, T., Humphrey, V.F., Mo S. and Fang, E., 2020, "The effect of water surface roughness on the measurement of radiated ship noise", Proceedings of Meetings on Acoustics, Vol. 40, no. 1, art. 070019.

Heinke, H.-J., 2003, "The influence of test parameters and wake field simulation on the cavitation and the propeller induced pressure fluctuations", STG-Sprechtag Kavitation, Hamburg.

Heinke, H.-J., Johannsen, C., Kröger, W., Schiller, P. and Weitendorf, E.-A., 2012, "On cavitation nuclei in water tunnels", Eighth International Symposium on Cavitation - Cav2012. Singapore: Paper No. 270.

Howe, M., 2002, "Frontmatter. In Theory of Vortex Sound" Cambridge Texts in Applied Mathematics, pp. I-Viii, Cambridge University Press. Cambridge.

Hynninen, A., Tanttari, J., Viitanen, V.M. and Sipilä, T., 2017, "On predicting the sound from a cavitating marine propeller in a tunnel", 5th International Symposium on Marine Propulsors, SMP'17, Espoo, Finland, June 2017.

Ianniello, S., 2015, "Sheet Cavitation Noise Prediction from A Marine Propeller", 22nd International Congress on Sound and Vibration (ICSV22), Florence, Italy.

Ianniello, S., 2016, "The Ffowcs Williams–Hawkings equation for hydroacoustic analysis of rotating blades. Part 1. The rotpole", Journal of Fluid Mechanics, Vol. 797, pp. 345-388.

Ianniello, S., Muscari, R. and Di Mascio, A., 2013, "Ship Underwater Noise Assessment by the Acoustic Analogy. Part I: Nonlinear Analysis of a Marine Propeller in a Uniform Flow", Journal of Marine Science and Technology, Vol. 18, no. 4, pp 547-570.

Ianniello, S., Muscari, R. and Di Mascio, A., 2014, "Ship Underwater Noise Assessment by the Acoustic Analogy part II: Hydroacoustic Analysis of a Ship Scaled Model", Journal of Marine Science Technology, Vol. 19, pp:52–74.

Ianniello, S. and De Bernardis, E., 2015, "Farassat's Formulations in Marine Propeller Hydroacoustics", International Journal of Aeroacoustics, Vol. 14, no. 1 & 2, pp. 87 – 103.

ISO, 2016, ISO 17208-1:2016, "Underwater acoustics – Quantities and procedures for description and measurement of underwater sound from ships – Part 1: Requirements for precision measurements in deep water used for comparison purposes", ISO Procedure.

ISO, 2019a, ISO 17208-2:2019, "Underwater acoustics – Quantities and procedures for description and measurement of underwater sound from ships – Part 2: Determination of source level from deep water measurements", ISO Procedure.

ISO, 2019b, ISO 20233-2:2019(E), "Ships and marine technology – Model test method for propeller cavitation noise evaluation in ship design – Part 2: Noise source localization", ISO Procedure.

ITTC, 2014, 27th ITTC Conference, Copenhagen, Denmark.

ITTC, 2017a, 28th ITTC Conference, Wuxi, China.

ITTC, 2017b, Recommended Procedures and Guidelines 7.5–04 04-01 Underwater Noise from Ships, Full Scale Measurements.

Jensen, F.B., Kuperman, W.A., Porter, M.B. and Schmidt, H., 2011, Computational Ocean Acoustics, 2nd Edition, Springer.

Jiang, P., Lin, J., Sun, J., Yi, X. and Shan, Y., 2020, "Source spectrum model for merchant

ship radiated noise in the Yellow Sea of China", Ocean Engineering, Vol. 216, art. 107607.

Johannsen, C., 1998, "Investigation of propeller-induced pressure pulses by means of high-speed video recording in the three-dimensional wake of a complete ship model", 22nd Symposium on Naval Hydrodynamics, Washington, D.C.

Johansson T, Hallander J, Karlsson R, Långström A. and Turesson, M., 2015 "Full scale measurements of underwater radiated noise from a coastal tanker". OCEANS 2015 MTS/IEEE Conference, Genova, May 18-21, 2015.

Joy, R., Tollit, D., Wood, J., MacGillivray, A., Li, Z., Trounce, K. and Robinson O., 2019, "Potential benefits of vessel slowdowns on endangered southern resident killer whales". Frontiers in Marine Science, Vol. 6, Article 344.

Kamiirisa, H., 2001, "The effect of water quality characteristics on cavitation noise", Fourth International Symposium on Cavitation, California Institute of Technology.

Kendrick, A. and Terweij, R. 2019, "Ship under-water radiated noise", Report Vard Marine Inc.

Kerwin, J.E., 1986, "Marine Propellers", Annual Reviews of Fluid Mechanics, Vol. 18, pp. 367–403.

Khoo, M. T., Venning, J. A., Pearce, B. W., Brandner, P. A. and Lecoffre, Y., 2016, "Development of a Cavitation Susceptibility Meter for Nuclei Size Distribution Measurements", 20th Australasian Fluid Mechanics Conference, Perth, Australia, AFMS.

Khoo, M. T., Venning, J. A., Pearce, B. W., Takahashi, K., Mori T. and Brandner, P. A., 2020a, "Natural nuclei population dynamics in cavitation tunnels", Experiments in Fluids, Vol. 61, art. 34.

Khoo, M. T., Venning, J. A., Pearce, B. W. and Brandner, P. A., 2020b, " Statistical aspects of tip vortex cavitation inception and desinence in a nuclei deplete flow", Experiments in Fluids, Vol. 61, art. 145.

Kim, D., Seong, W., Choo, Y. and Lee, J., 2015, "Localization of incipient tip vortex cavitation using ray based matched field inversion method", Journal of Sound and Vibration, Vol. 354, pp. 34-46.

Kinnas, S.A. and Fine, N.E., 1992, ''A Nonlinear Boundary Element Method for the Analysis of Propeller Sheet Cavitation,'' 19th Symposium on Naval Hydrodynamics, ONR, Seoul Korea, pp. 1–17.

Kinnas, S. and Pyo, S., 1999, "Cavitating propeller analysis including the effects of wake alignment", Journal of Ship Research, Vol. 43, pp. 38–47.

Kinnas, S., Lee, H.S. and Young, Y.L., 2003, "Modeling of Unsteady Sheet Cavitation on Marine Propeller Blades", International Journal of Rotating Machinery, Vol. 9, pp. 263–277.

Kleinsorge, L., Schemmink, S., Klose, R. and Greitsch, L., 2017, "Case study for the determination of propeller emitted noise by experimental and computational methods", 5th International Symposium On Marine Propulsors - SMP'17, Espoo, Finland, June 2017.

Knapp, R.T., Daily, J.W. and Hammitt, F.G., 1970, "Cavitation", McGraw-Hill Book Company, New York.

Kozaczka, E. and Grelowska, G., 2018. "Propagation of ship-generated noise in shallow sea", Polish Maritime Research, Vol. 25, pp. 37-46.

Kuttruff, H., 2009, "Room acoustics", Fifth edition, Spon Press, Taylor & Francis, U.K.

Lafeber, F.H., Bosschers, J., de Jong, C. and Graafland, F., 2015, "Acoustic reverberation measurements in the Depressurized Towing Tank", 4th International Conference on Advanced Model Measurement Technologies for the Maritime Industry AMT'15, Istanbul, Turkey.

Lafeber, F.H. and Bosschers, J., 2016, "Validation of Computational and Experimental Prediction Methods for the Underwater Radiated Noise of a Small Research Vessel", PRADS, Copenhagen, Denmark.

Lafeber, F.H. and Lloyd, T., 2017, "Round robin test on the underwater radiated noise of a cavitating ship propeller in open water". 5th International Conference on Advanced Model Measurement Technologies for the Maritime Industry -AMT'17, (Glasgow, UK).

Lampe, T., Radtke, L., Göttsche, U., Düster, A. and Abdel-Maksoud, M., 2019, "Evaluation of performance and acoustic signature of flexible marine propellers under consideration of fluid-structure interaction by means of partitioned simulation", Sixth International Symposium on Marine Propulsors - smp'19, Rome, Italy.

Lebrun, D., Allano, D., Méès, L., Walle, F., Corbin, F., Boucheron, R. and Fréchou, D., 2011, "Size measurement of bubbles in a cavitation tunnel by digital in-line holography", Applied Optics, Vol. 50, no. 34, pp. H1—H9.

Lecoffre, Y., 1987, "Procedures and Instrumentation for monitoring gas content in cavitation test loops", ASME International Symposium on Cavitation Research Facilities and Techniques, December 1987.

Lee, J.T., 1987, "A Potential Based Panel Method for the Analysis of Marine Propellers in Steady Flow", Tech. Rep. 87-13, Department of Ocean Engineering, MIT, Cambridge, Massachusetts USA.

Lee, J.H., Jung, J.K., Lee, K.J., Han, J.M., Park, H.G. and Seo, J.S., 2012, "Experimental Estimation of a Scaling Exponent for Tip Vortex Cavitation via Its Inception Test in Full- and Model-ship", Journal of Hydrodynamics, Vol. 24, no. 5, pp. 658-667.

Li, D.Q., Hallander, J. and Johansson, T., 2018, "Predicting underwater radiated noise of a full scale ship with model testing and numerical methods". Ocean Engineering, Vol. 161, pp. 121–135.

Lidtke, A.K., Humphrey, V.F. and Turnock, S.R., 2016, "Feasibility study into a computational approach for marine propeller noise and cavitation modelling", Ocean Engineering, Vol. 120, pp. 152–159.

Lidtke, A., Lloyd, T. and Vaz, G., 2019, "Acoustic modelling of a propeller subject to non-uniform inflow", Sixth International Symposium on Marine Propulsors, smp'19, Rome, Italy.

Lighthill M.J., 1952, "On sound generated aerodynamically: 1. general theory", Proceeding of The Royal Society A, Vol. 211, pp. 564–578.

Lloyd, T.P., Rijpkema, D. and van Wijngaarden, E., 2014, "Implementing the Ffowcs Williams-Hawkings acoustic analogy into a

viscous CFD solver", Numerical Towing Tank Symposium, Marstrand, Sweden.

Lloyd, T.P., Lidtke, A.K., Rijpkema, D., van Wijngaarden, E., Turnock, S.R. and Humphrey, V.F., 2015a, "Using the FW-H equation for hydroacoustics of propellers", 15th Numerical Towing Tank Symposium. Cortona.

Lloyd, T., Rijpkema, D. and van Wijngaarden, E., 2015b, "Marine propeller acoustic modelling: comparing CFD results with an acoustic analogy method". Fourth International Symposium on Marine Propulsors, spm'15, Austin, Texas.

Lloyd, T., Lafeber, F.H. and Bosschers, J., 2018, "Investigation and Validation of Procedures for Cavitation Noise Prediction from Model-Scale Measurements", 32nd Symposium on Naval Hydrodynamics, Hamburg, Germany, 5-10 August 2018.

Løvik, A., 1981, "Scaling of Propeller Cavitation Noise", Noise sources in ships, Nordforsk, Stockholm, Sweden.

LR, 2017, ShipRight - Design and Construction - Additional Design and Construction Procedure for the Determination of a Vessel's Underwater Radiated Noise, Lloyd's Register.

Lyon, R.H. and DeJong, R.G., 1995, "Theory and Application of Statistical Energy Analysis", Second Edition, Butterworth-Heinemann, Boston, 1995, 227 p.

McCormick Jr., B.W., 1962, "On cavitation produced by a vortex trailing from a lifting surface", Journal of Basic Engineering, Vol. 84, no. 3, pp. 369-379.

Méès, L., Lebrun, D., Allano, D., Walle, F., Lecoffre, Y., Boucheron, R. and Fréchou, D., 2010, "Development of interferometric techniques for nuclei size measurement in cavitation tunnel", 28th Symposium on Naval Hydrodynamics, Pasadena, California, September 2010.

Mendez, S., Sharma, A., Shoeybi, M. and Lele, S.K., 2009, "Post-processing of large eddy simulations for jet noise predictions," CTR Annual Research Briefs.

Mendez, S., Shoeybi, M., Lele, S.K. and Moin, P., 2013, "On the Use of the Ffowcs Williams-Hawkings Equation to Predict Far-Field Jet Noise from Large-Eddy Simulations", International Journal of Aeroacoustics, Vol. 12, no. 1, pp 1-20.

Merkle, C.L. and Athavale, M., 2012, "Time-accurate unsteady incompressible flow algorithm based on artificially compressibility". AIAA paper 87-1137.

Meyer, V. and Audoly, C., 2019, "A parametric study of the environment and the array configuration for underwater noise measurement from ships in shallow water", 26th International Congress on Sound and Vibrations, Montréal, Canada, 7-11 July 2019.

Meyer, V. and Audoly, C., (2020). "Accounting for sea floor properties in the assessment of underwater noise radiated from ships in shallow water." Proceedings of Meetings on Acoustics, Vol. 40, no. 1, art. 070007.

MacGillivray, A.O., Zizheng, L., Hannay, D.E., Trounce, K.B. and Robinson, O.M., 2019, "Slowing deep-sea commercial vessels reduces underwater radiated noise". Journal of the Acoustical Society of America., Vol. 146, no. 1, pp. 340-351.

McHorney, D.H., Pelella, G.M., Hilliard, L.C. and Palmieri, M.R., 2018, "Methods to

Minimize Commercial Vessel-Generated Marine Acoustic Pollution", Retrieved from https://digitalcommons.wpi.edu/iqp-all/5247

Miglianti, F., Cipollini, F., Oneto, L., Tani, G. and Viviani, M., 2019a, " Model scale cavitation noise spectra prediction: Combining physical knowledge with data science", Ocean Engineering, Vol. 178, pp. 185-203.

Miglianti F., Tani G., Viviani M., Cipollini F. and Oneto L., 2019b, "Data driven models for propeller cavitation noise in model scale", Sixth International Symposium on Marine Propulsors (smp'19).

Mitson, R.B., (Ed), 1995, "Underwater noise of research vessels: Review and recommendations", ICES Study Group Report.

Moreno, A., (Ed.), 2014, "European URN Standard Measurement Method", AQUO EU FP7 Project, Deliverable 3.1.

Morino, L., Chen, L.T. and Suciu, E.O., 1975, ''Steady and Oscillatory Subsonic and Supersonic Aerodynamics Around Complex Configurations,'' AIAA Journal, Vol. 13, pp. 368–374.

Morino, L. and Gennaretti, M, 1992, "Boundary Integral Equation Methods for Aerodynamics", Computational Nonlinear Mechanics in Aerospace Engineering, Atluri, S.N. (ed), Progress in Aeronautics & Astronautics, AIAA, Washington, DC, Vol. 146, pp. 279-320.

Morse, P.M. and Ingard, K.U., 1968, "Theoretical acoustics", Princeton University Press.

Nitzkorski, Z. and Mahesh, K., 2014, "A dynamic end-cap technique for sound computation using the Ffowcs Williams and Hawkings equations", Physics of Fluids Vol. 26, no. 11, art. 115101.

Okamura, N. and Asano, T., 1988, "Prediction of Propeller Cavitation Noise and Its Comparison with Full-Scale Measurements", Journal of Naval Architects of Japan, Vol. 164, pp.19-33

Oshima, A., 1990, "A study on correlation of vortex cavitation noise of propeller measured in model experiments and full scale". Journal of the Society of Naval Architects of Japan, Vol. 168, no. 1, pp. 89–96.

Oshima, A., 1994, "Scaling of Tip Vortex Cavitation Noise of Propeller", Technical report, Vol. 31, No. 3, Mitsubishi Heavy Industries, Ltd., Nagasaki, Japan.

Pang, Y., Liu, J., Yu, M. and Wu, W., 2020a, "Propagation loss analysis using ship radiated noise in shallow water." Proceedings of Meetings on Acoustics, Vol. 40, no. 1, art. 070010.

Pang, Y., Yu, M., Wu, W. and Wang, S., 2020b, "Ship noise source level measurement in shallow water based on experimental propagation loss", ResearchGate, Doi:10.13140/RG.2.2.31101.38883.

Papoulis, A., 2002, "Probability, random variables and stochastic processes", 4th edition, McGraw-Hill.

Park, C., Kim, G., Park, Y., Lee, K. and Seong, W., 2016, "Noise Localization Method for Model Tests in a Large Cavitation Tunnel Using Hydrophone Array", Remote Sensing, 2016, Vol. 8, no. 3, art. 195.

Park, C., Kim, G.-D., Park, Y.-H., Jang, H.-G. and Jang, Y.H., 2018, "A Study on the Model Test for the Twin Propeller

Cavitation Noise" (in Korean). Journal of the Society of Naval Architects of Korea, Vol. 55, no. 1, pp. 28-36.

Park, C., Kim, G. D., Yim, G.-T., Park, Y., and Moon, I.-S., 2019, "The validation of model test method for propeller cavitation noise prediction". 6th International Conference on Advanced Measurement Technology for the Maritime Industry, AMT'19, Rome, Italy.

Park, C., Kim, G.D., Yim, G.T., Park, Y.H. and Moon, I., 2020, "A validation study of the model test method for propeller cavitation noise prediction", Ocean Engineering, Vol. 213, art. 107655.

Park, J. and Seong, W., 2017, "Novel scaling law for estimating propeller tip vortex cavitation noise from model experiment". Journal of Hydrodynamics, Vol. 29, no. 6, pp. 962–971.

Poinsot, T.J. and Lele, S.K., 1992, "Boundary conditions for direct simulations of compressible viscous flows", Journal of Computational Physics, Vol. 101, no. 1, pp. 104-129.

Popper, A.N. and Hastings, M.C., 2009, "The effects of anthropogenic sources of sound on fishes", Journal of Fish Biology, Vol. 75, pp. 455-589.

Renilson, M. 2009, "Reducing underwater noise pollution from large commercial vessels". Report to IFAW, ISBN: 978-1-906920-02-9.

Rijpkema D., Starke B. and Bosschers J., 2013, "Numerical simulation of propeller-hull interaction and determination of the effective wake field using a hybrid RANS-BEM approach", Third International Symposium on Marine Propulsors smp'13, Launceston, Tasmania, Australia.

van Rijsbergen, M.X. and Beelen, S., 2019, "A Lagrangian analysis of scale effects on sheet cavitation inception", 6th International Symposium on Marine Propulsors SMP-19, Rome, Italy, May 2019.

RINA, 2017, Amendments to Part A and Part F of "Rules for the Classification of Ships" - New additional class notation: "DOLPHIN QUIET SHIP" and "DOLPHIN TRANSIT SHIP", Registro Italiano Navale.

Robinson, S.P., Lepper, P.A. and Hazelwood, R.A., 2014, "Good Practice Guide for Underwater Noise Measurement". NPL Good Practice Guide No. 133, National Measurement Office, Marine Scotland, The Crown Estate, ISSN:1368-6550.

Ross, D., 1976, "Mechanics of Underwater Noise", Pergamon Press.

Russell, P., Venning, J., Pearce, B.W. and Brandner, P.A., 2020a, "Calibration of Mie scattering imaging for microbubble measurement in hydrodynamic test facilities", Experiments in Fluids, Vol. 61, art. 93.

Russell, P.S., Barbaca, L., Venning, J.A., Pearce, B.W. and Brandner, P.A., 2020b, "Measurement of nuclei seeding in hydrodynamic test facilities", Experiments in Fluids, Vol. 61, art. 79.

Sakamoto, N., Fujisawa, J., Sawada, Y., Ukon, Y. and Kamiirisa, H., 2017, "Measurement of cavitation noise radiated from a marine propeller with and without shaft inclination" 5th International Conference on Advanced Model Measurement Technologies for the Maritime Industry - AMT'17, Glasgow, UK.

Salvatore, F. and Esposito, P.G., 2001, "An improved boundary element analysis of cavitating three-dimensional hydrofoils",

Fourth International Symposium on Cavitation - CAV2001, California Institute of Technology.

Salvatore, F. and Ianniello, S., 2003, "Preliminary Results on Acoustic Modelling of Cavitating Propellers", Journal of Computational Mechanics, Vol. 32, pp. 291–300.

Salvatore, F., Testa, C. and Greco, L., 2003, "A Viscous/Inviscid Coupled Formulation for Unsteady Sheet Cavitation Modelling of Marine Propellers", Fifth International Symposium on Cavitation - Cav2003, Osaka, Japan.

Salvatore, F., Streckwall, H. and van Terwisga, T., 2009a, "Propeller cavitation modelling by CFD-results from the VIRTUE 2008 Rome workshop", 1st International Symposium on Marine Propulsors, Trondheim, Norway.

Salvatore, F., Testa, C. and Greco, L., 2009b, "Coupled Hydrodynamics–Hydroacoustics BEM Modelling of Marine Propellers Operating in a Wakefield", 1st International Symposium on Marine Propulsors, Trondheim, Norway.

Schuiling, B., Lafeber, F.H., van der Ploeg, A. and van Wijngaarden, E., 2011, "The Influence of the Wake Scale Effect on the Prediction of Hull Pressures due to Cavitating Propellers", Second International Symposium on Marine Propulsors SMP'11, Hamburg, Germany, June 2011.

Seol H., 2013, "Time Domain Method for the Prediction of Pressure Fluctuation Induced by Propeller Sheet Cavitation: Numerical Simulations and Experimental Validation", Ocean Engineering, Vol. 72, pp. 287-296.

Seol, H., Jung, B., Suh, J-C. and Lee, S., 2002, "Prediction of Non–Cavitating Underwater Propeller Noise", Journal of Sound and Vibration, Vol. 257, no. 1, pp. 131–156.

Seol, H., Suh, J-C. and Lee S., 2005, "Development of Hybrid Method for the Prediction of Underwater Propeller Noise", Journal of Sound and Vibration, Vol. 288, pp 345–360.

Seol, H., Paik, B.G., Park, Y.H., Kim, K.Y., Ahn, J.W., Park, C., Kim, G.D. and Kim, K.S., 2015, "Propeller Cavitation Noise Model Test in KRISO Large Cavitation Tunnel and Its comparison with Full-Scale Results", 4th International Conference on Advanced Model Measurement Technology for the Maritime Industry, Gdansk, Poland.

Shorter, P.J. and Langley, R.S., 2005a, "Vibro-acoustic analysis of complex system", Journal of Sound and Vibration, Vol. 288, no. 3, pp. 669-699.

Shorter, P.J. and Langley, R.S., 2005b, "On the reciprocity relationship between direct field radiation and diffuse reverberant loading", Journal of the Acoustical Society of America, Vol. 117, no. 1, pp. 85-95.

Shur, M.L., Spalart, P.R., and Strelets, M.K., 2005, "Noise prediction for increasingly complex jets. Part I: Methods and tests", International Journal of Aeroacoustics, Vol. 4, no. 3, pp. 213–246.

Sipilä, T., Viitanen V., Uosukainen, S. and Klose, R., 2019. "Shallow Water Effects on Ship Underwater Noise Measurements", Proceedings of Internoise 2019.

Southall, B.L., Bowles, A.E., Ellison, W.T., Finneran, J.J., Gentry, R.L., Greene Jr., C.R., Kastak, D., Ketten, D.R., Miller, J.H., Nachtigall, P.E., Richardson, W.J., Thomas,

J.A. and Tyack, P.L., 2008, "Marine mammal noise exposure criteria: Initial scientific recommendations", Aquatic Mammals, Vol. 33, no. 4, pp. 411-521.

Spence, J., Fisher, R., Bahtiarian, M., Boroditsky, L., Jones, N. and Dempsey, R., 2007, "Review of existing and future potential treatments for reducing underwater sound from oil and gas industry activities", NCE Report 07-001, Noise Control Engineering, Inc., 185 p.

Strasberg, M., 1977, "Propeller Cavitation Noise after 35 Years of Study", ASME symposium on Noise and Fluids Engineering, Atlanta, USA.

Tani, G., Viviani, M., Armelloni, E. and Nataletti, M., 2016a, "Cavitation Tunnel Acoustic Characterisation and Application to Model Propeller Radiated Noise Measurements at Different Functioning Conditions", Proceedings of the Institution of Mechanical Engineers, Part M: Journal of Engineering for the Maritime Environment, Vol. 230, no. 2, pp. 250–266.

Tani, G., Viviani, M., Hallander, J., Johansson, T. and Rizzuto, E., (2016b), "Propeller underwater radiated noise: a comparison between model scale measurements in two different facilities and full scale measurements", Applied Ocean Research, Vol. 56, pp. 48–66.

Tani, G., Aktas, B., Viviani, M. and Atlar, M., 2017, "Two medium size cavitation tunnel hydro-acoustic benchmark experiment comparisons as part of a round robin test campaign", Ocean Engineering, Vol. 138, pp. 179-207.

Tani, G., Aktas, B., Viviani, M., Yilmaz, N., Miglianti, F., Ferrando, M. and Atlar, M., 2019a, "Cavitation tunnel tests for "The Princess Royal" model propeller behind a 2-dimensional wake screen", Ocean Engineering, Vol. 172, pp. 829–843.

Tani, G., Viviani, M., Ferrando, M. and Armelloni, E., 2019b, "Aspects of the measurement of the acoustic transfer function in a cavitation tunnel", Applied Ocean Research, Vol. 87, pp. 264–278.

Tani, G., Viviani, M., Felli, M., Lafeber, F.H., Lloyd, T., Aktas, B., Atlar, M., Turkmen, S., Seol, H., Hallander, J. and Sakamoto, N., 2020, "Noise measurements of a cavitating propeller in different facilities: results of the round robin test programme", Ocean Engineering, Vol. 213, art. 107599.

Testa, C., Ianniello, S., Salvatore, F. and Gennaretti, M., 2008, "Numerical approaches for hydroacoustic analysis of marine propellers", Journal of Ship Research, Vol. 52, no. 1, pp. 57–70.

Testa, C., Ianniello, S. and Salvatore, F., 2018a, "A Ffowcs Williams and Hawkings formulation for hydroacoustic analysis of propeller sheet cavitation", Journal of Sound and Vibration, Vol. 413, pp. 421-441.

Testa, C., Porcacchia, F., Greco, L. and Muscari, R, 2018b, "Effectiveness of Boundary Element Method Hydrodynamic", A. Yücel Odabaşı Colloquium Series 3rd International Meeting Progress in Propeller Cavitation and its Consequences: Experimental and Computational Methods for Predictions, 5th–16th November 2018, Istanbul, Turkey.

Thomson, D.J.M. and Barclay, D.R., 2020, "Real-time observations of the impact of COVID-19 on underwater noise", Journal of the Acoustical Society of America, Vol. 147, no. 5, pp. 3390-3396.

Traverso, F., Gaggero, T., Tani, G., Rizzuto, E., Trucco, A. and Viviani, M., 2017, "Parametric Analysis of Ship Noise Spectra", IEEE Journal of Oceanic Engineering, Vol. 42, no. 2, pp. 424-438.

UNCLOS, 2018, United Nation Convention of Law of the Sea.

Ward J. and Robinson S., 2019, "Low frequency hydrophone calibration with a Laser interferometer", Underwater Acoustics Conference and Exhibition (UACE) 2019, Hersonissos, Greece.

Wang, L., Heaney, K., Pangerc, T., Theobald, P., Robinson, S. and Ainslie, M., 2014, "Review of underwater acoustic propagation models", NPL Report. AC 12

Wang, M., Lele, S. and Moin, P., 1996, "Computation of quadrupole noise using acoustic analogy", AIAA Journal, Vol. 34, no. 11, pp. 2247-2254.

Weitendorf, E.-A., 1981, "Cavitation phenomena, propeller excited hull pressure amplitudes and cavitation scale effect." Ocean Engineering, Vol. 8, no. 5, pp. 517-539

Weitendorf, E.-A. and Tanger, H., 1999, "Cavitation Investigations in Two Conventional Tunnels and in the Hydrodynamics and Cavitation Tunnel HYKAT", Ship Technology Research, Vol. 46, pp. 43-56

Weston, D.E., 1971, Intensity-range relations in oceanographic acoustics. Journal of Sound and Vibration, Vol. 18, no. 2, pp. 271-287.

Urick, R.J., 1983, "Principles of Underwater Sound", McGraw-Hill.

Young, Y.L. and Kinnas S.A., 2003, "Numerical Modeling of Supercavitating Propeller Flows", Journal of Ship Research, Vol. 47, pp. 48-62.

Zhang, B., Xiang, Y., He, P., and Zhang, G.-J., 2019, "Study on prediction methods and characteristics of ship underwater radiated noise within full frequency", Ocean Engineering, Vol. 174, pp. 61-70.

Appendix A: Review of rules on full-scale noise measurements

Organization	Classification Societies						ISO	ANSI/ASA
	DNV-GL	BV	RINA	LR	ABS	CCS		
Rule number	**CG-0313**	**NR 614**	**/**	**/**	**295**	**GD28-2018**	**17208**	**S12.64**
Notation	Silent-E:Transit Silent-E:Quiet Silent-R / Silent-S Silent-F / Silent-A	URN - controlled vessel URN - advanced vessel URN - specified vessel	Dolphin Transit Dolphin Quiet	T for Transit Q for quiet R for research	UWN(Type) UWN+(Type)	Underwater Noise 1 Underwater Noise 2 Underwater Noise 3		
Year	2010 2019 v2	2014 2017 v2 2018 v3	2017	2018	2018	2016 2018 v2	2016 (part 1) 2019 (part 2)	2009
Water depth	Min 30 m under keel, and h> 0.64 v^2, with sloping seabed preferred	Shallow: 60 m <h <200 m and h> 0.3 v^2; Deep: >200 m and >1.5L	>150 m	Shallow: 60 m or 0,3v^2<h<150 m or 1.5L ; Deep: >150 m and >1.5L	Shallow: 60 m < h<150 m, h> 0.3 v^2; Deep: >150 m and >1.5L	Single Hydrophone: max(40 m , 0.64v^2); multiple hydrophone: max(60m , 0.3v^2).	>Max(150m,1.5L)	3 Grades A: >Max(300m,3L); B: >Max(150m,1.5L);; C: >Max(75m,1L);
Hydrophone depth(s)	0.2 m above seabed	Shallow: 3 hydrophones spaced at 15 m~20 m, with bottom 3 m~5 m from sea bottom Deep: 3 hydrophones spaced at more than 30 m, with top >40 m from surface	3 hydrophones at depths for: 15°, 30°, and 45°? below horizontal	Shallow: 3 hydrophones at h/10, h/2, and 5 m above seabed Deep: 3 hydro-phones at depths for: 15°, 30°, and 45° below horizontal	3 hydrophones at depths for: 15°, 30°, and 45° below horizontal	1 hydrophone:< 0.5 m above bottom; 3 hydrophones: spaced at 15 m~20 m, with bottom 3 m~5 m from sea bottom	3 hydrophones at depths for: 15°, 30°, and 45° below horizontal	Grade A and B: 3 hydrophone depth, 15°, 30°, and 45°; Grade C: 1 hydrophone, 20°.
CPA Distance	100 m~200 m	d_{CPA}=Max(200 m, 1L)(nominal), Max(100 m, 1L)(silent ship), 3 distances: d_{CPA},Min(400 m, 1.5 d_{CPA}), Min(500 m,2 d_{CPA})	Greater than 150 m	Greater than 100 m and ship length	Greater than 100 m and ship length	Transit:150m to 250m Quiet: d_{CPA}=Max(200 m, 1L)(nominal), Max(100 m, 1L)(silent ship),3 distances: d_{CPA},Min(400 m, 1.5 d_{CPA}), Min(500 m,2 d_{CPA})	Greater than 100 m or 1L	Greater than 100 m or 1L
Averaging time	≤ 5 kts, ship length/speed > 5 kts, 2 x ship length/speed	Time for passing ±45° of CPA, with a step of 5°	Time to travel 1.5 x ship length	Time for passing ±30° of CPA	Time for passing ±30° of CPA	2x ship length	Time for passing ±30°of CPA	Time for passing ±30°of CPA
Propagation adjustment factor	18 log r	Acoustic model ; 19 log r(water depth < 100 m);20 log r(water depth)>100 m);	20 log r	Shallow: measured or modelled Deep: 20 log r	20 log r	H<100m: 18 log r H>100m: 20 log r	20 log r	20 log r
Sea surface adjustment	None	Acoustic model	None	Shallow: measured or modelled Deep: Angle-dependent formula	None	none	angle dependent formulae (part 2)	none
Seabed reflection adjustment	-5dB	Acoustic model	None	Shallow: measured or modelled Deep: none	0.5 dB if hydrophone less than 20 cm off bottom	none	none	none
Number of passes	1 port + 1 starboard	6 port + 6 starboard, 2 at each of 3 CPA distances	2 port + 2 starboard	2 port + 2 starboard	2 port + 2 starboard	1 port + 1starborad	2 port + 2 starboard	2 port + 2 starboard
Frequency range	10 Hz to 100 kHz	10 Hz to 50 kHz	10 Hz to 40 kHz	10 Hz to 100 kHz	Commercial vessels:10 Hz to 50 kHz; Research vessels: 10 Hz to 100, 000 Hz	10 Hz to 50 kHz	10 Hz to 20 / 50 kHz	10 Hz to 10 / 25 / 50 kHz (depending on grade)
Vessel speed	Transit: 80% MCR Quiet Cruise: 11 knots for L>50 m;8 knots for L<50 m	According to the contract specifications or, by default, at NCR.	Not specified	Typically:85% MCR, Research vessels: 11 knots; Seismic vessels:5 knots; DP mode: 40% nominal load	Transit: 85% MCR Quiet: 3.1 m/s + 0.0084L	11 knots(L>50m), 8 knots (L<50m)	not specified	not specified
Measurement Result type	RNL (modified)	RNL	RNL	MSL	RNL(modified)	RNL	RNL(part 1) MSL(part 2)	RNL

L= Overall ship length; h= Water depth; RNL= Radiated Noise Level; MSL= Monopole Source Level; MCR= Maximum Continuous Rating

The Specialist Committee on Ice
Final Report and Recommendations to the 29th ITTC

1. INTRODUCTION

1.1 Membership and meetings

The members of the Specialist Committee on Ice of the 29th International Towing Tank Conference are as follows:

1. Topi Leiviskä (Chair), Aker Arctic Technology inc, Finland
2. Franz von Bock und Polach (Secretary), Hamburg University of Technology, Germany
3. John Wang, National Research Council of Canada, Canada
4. Yinghui Wang, China Ship Scientific Research Centre (CSSRC), China
5. Nils Reimer, Hamburgische Schiffbau-Versuchsanstalt GmbH (HSVA), Germany
6. Yan Huang, Tianjin University, China
7. Takatoshi Matsuzawa, National Maritime Research Institute (NMRI), Japan
8. Aleksei Alekseevich Dobrodeev, Krylov State Research Centre (KSRC), Russia
9. Jinho Jang, Korea Research Institute of Ships and Ocean Engineering (KRISO), Korea
10. Pentti Kujala, Aalto University, Finland (Mikko Suominen 2017-2018)

Four Committee meetings were held as follows:

1. January 24 – 25, 2018, Helsinki. Participants: Leiviskä (Chair), von Bock und Polach (Secretary), Reimer, Dobrodeev, Suominen, Jang, J.Wang, Y.Wang, Matsuzawa. Absent: Huang.
2. June 14, 2018, Skype meeting. Attendance: Leiviskä (Chair), Matsuzawa, Jang, Reimer, Suominen,

J.Wang, Dobrodeev. Absent: Huang, von Bock und Polach, Y.Wang.

3. November 21-22, 2018, Tianjin. Participants: all members, Leiviskä (Chair), von Bock und Polach (Secretary)
4. January 16-17, 2020, St John's Canada, Attendance: von Bock und Polach (Chair), Matsuzawa, Jang, Reimer, J.Wang, Dobrodeev, Kujala. (secretary) Absent: Leiviskä, Huang, Y.Wang.

2. MATERIALS

2.1 Terms of Reference

1. Continue to maintain, review and update existing accepted procedures and guidelines in accordance with current practice.
2. Review manoeuvring experiments in ice, and revise "7.5-02-04-02.3 Manoeuvring Tests in Ice" in cooperation with the Manoeuvring Committee.
3. Conduct survey of uncertainty in ice model experiments, and revise "7.5-02-04-02.5 Experimental Uncertainty Analysis for Ship Resistance in Ice Tank Testing."
4. Review of current analytical and numerical determination methods for the global ice load upon offshore structures of various types and compare to physical modelling.
5. Survey testing of platforms and monopiles in ice (such as wind turbine in frozen ocean) and consider establishing a new guideline or enhancing existing guidelines to cover such situation.
6. Update the Guideline 7.5-02-07-01.3 "Guidelines for Modelling of Complex Ice Environments" to cover additional complex conditions.

The tasks were divided into two groups. The committee decided to focus first on Tasks 1, 2, 3 and 6, and concentrate on Tasks 4 and 5 at later stage. A group leader was nominated to each task and group members were listed. Everyone had a possibility to join any of the groups.

3. UPDATES ON THE REVISED GUIDELINES

The following Guidelines were revised and updated. In addition to corrections and amendments the symbols in all Guidelines were reviewed and corrected follow the ITTC Symbols and Terminology List, Version 2017.

3.1 7.5-02-04-01 General Guidance and Introduction to Ice Model Testing

In this Guidelines there was only some minor spelling error corrections in Equations 1 and 2.

3.2 7.5-02-04-02 Test Methods for Model Ice Properties

In addition to spelling errors some corrections to the equations were made and, also one ice measurement method was added.

3.2.1 CORRECTION OF EQUATION 3 (ELASTIC MODULUS):

In Section 3 the definition of the Strain Modulus of Elasticity was faulty in Equation 3 and the exponent of thickness h was corrected from 2 to 3. The definition of the strain elasticity is:

$$E = \frac{3}{16}\frac{1-\nu^2}{kh^3}\left(\frac{F}{\delta}\right)^2 \quad (1)$$

where:

F = loading force,

g = gravitational acceleration,
k = foundation factor ($k = g\rho_w$).

3.2.2 CORRECTION OF EQUATION 6 (CHARACTERISTIC LENGTH)

In section 3.1.3 where the Infinite Plate-Bending Method C with Larger Load Radius is presented, the square root was changed to the 4th root in Equation 6 in order to be correct:

$$l_c = \sqrt[4]{\frac{Eh^3}{12(1-\nu^2)w}} \quad (2)$$

3.2.3 SECTION 3.2: CHANGING OF WORDING:

The strain modulus – which can be elastic or elastic-plastic - can be determined by cantilever beam tests and the use of the beam-bending differential equation.

The original wording was: “The elastic strain modulus can be determined by cantilever beam tests and the use of beam-bending differential equation”. The new wording is: The strain modulus – which can be elastic or elastic-plastic - can be determined by cantilever beam tests and the use of the beam-bending differential equation. The change of wording was done because purely elastic deformation cannot be stated with certainty for all cases.

3.3 Review manoeuvring experiments in ice, and revise "7.5-02-04-02.3 Manoeuvring Tests in Ice" in cooperation with the Manoeuvring Committee.

It was noticed that the previous guideline was very inadequate and in principle the whole document was re-written. It was also expected that the review will be done in cooperation with the Manoeuvring Committee.

The purpose of the procedure was defined: Definition of standards for performing manoeuvring tests in model ice. While manoeuvring test is a common name for all those tests in which the rudder is turned or the turning forces and moments are obtained by other means e.g. azimuthing thrusters or tunnel thrusters in bow. This procedure covers the most common manoeuvring tests for which standard methods exist in the different ice basins.

Typical manoeuvring tests in ice include turning circle tests, star manoeuvres and breaking out of channel. The model tests are often performed with a free model under its own propulsion. Sometimes, manoeuvring tests can be performed with a captive mode using x-y carriage or PMM (Planar Motion Mechanism). This allows force measurements, and it is mainly ad-hoc approach for certain cases.

The testing conditions of the model should be measured and documented similar as defined for Recommended Procedure for Free Running Model Tests 7.5-02-06-01. The loading condition of the model (draft fore/aft and GM) should be checked and documented. The GM should be as close as possible to the specified target value. If no value is specified, the actual value should be determined and reported. This value should at least be adjusted in a realistic range as full scale tests have revealed that the heeling angle of the ship has a large influence on the turning capability. For manoeuvring test with larger models at relatively low speed (e.g. turning circle) the correct adjustment of GM value is of lower relevance

3.3.1 TURNING CIRCLE TEST

In turning circle tests which are one of the most common manoeuvring tests, mainly the test procedures were clarified as follows:

The purpose of the turning circle test is to find out how much area is needed to turn the ship. In practice, the result of this kind of test may look as shown in Figure 1.

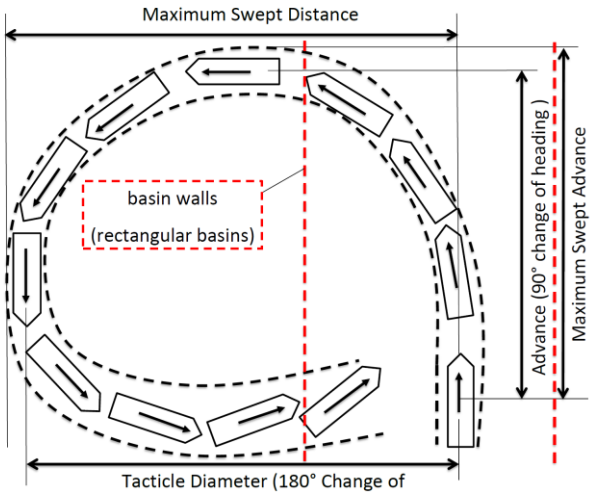

Figure 101: Definition of quantities used in turning circle tests

The test is started by proceeding the model straight ahead / astern at a certain speed into ice for at least one ship length. Thereafter a turning is induced by control of the rudder or thruster angles. The turning is continued until the maximum possible turning angle (with respect to basin restrictions) is achieved.

If the turning diameter, *Dc*, or radius, *Rc*, is determined, the method by which it was obtained should be described. The turning circle may be not a perfect circle, but a spiral.

Because majority of ice model test basins are long and narrow, also the determination of the turning radius was clarified especially, when a 180 degree turning is not possible. There are also several error sources in turning tests which were brought out:

It should be noted that there are several error sources (e.g. channel width variation) when determining the turning radius based on a limited number of measured points and limited turning angle. The relative error of turning radius clearly decreases for higher achieved turning angles. The main reason is the aforementioned asymmetry of the turning track.

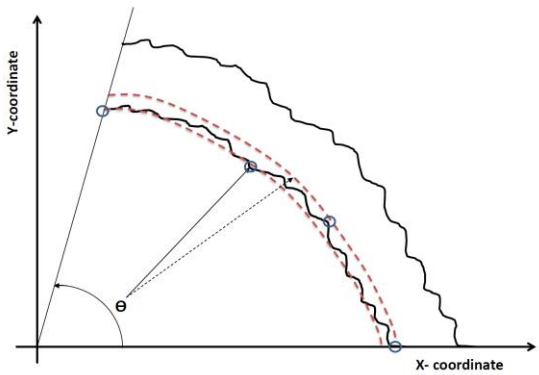

Figure 102: Broken channel of turning test

Considerable errors may appear, if the determination of *Dc* or *Rc* is based on a too small turn. Figure 2**Erreur ! Source du renvoi introuvable.** presents an example of the broken track left after a turning circle test. To illustrate the possible maximum error in diameter D_{inn}, when determined based on few points on the inner circle, as a function of the turning angle.

In many cases motion capture data can be used to alternatively derive the turning radius from the time series of models change of heading.

3.3.2 BREAKING OUT OF CHANNEL TEST AND STAR MANOEUVRE

Channel outbreaking test and star manoeuvre were reviewed and in principle totally rewritten. The procedures of the channel outbreaking test and star manoeuvre are written as follows:

Breaking out of channel is a test which can be performed from zero speed or some other specified speed. The model is typically accelerated to a certain speed or power in the

channel and thereafter the rudder / azimuth thrusters are turned. The model will change heading and the fore or aft shoulders will break ice from the channel edges. After achieving a certain yaw angle the model will be able to enter the surrounding ice sheet (Figure 3). The test is concluded by leaving the channel completely (or at a specified yaw angle). The success of breaking out of channel manoeuvre is significantly affected by the width of the broken channel (in relation to model width).

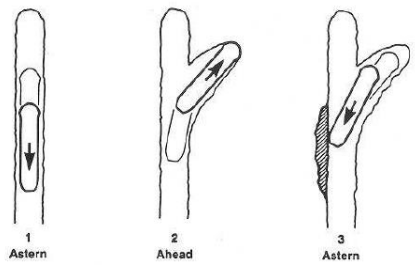

Figure 103: Sketch Break Out Manoevre, Quinton, Lau (2006)

The most relevant parameters that should be determined and reported are required distance in the channel (starting / end point), number of required attempts and time consumption.

Star Manoeuvre or Captain's turn is typically used when space and / or manoeuvring space is limited: The vessel turns around 180 deg by performing a series of channel breakouts fore and aft (Figure 4).

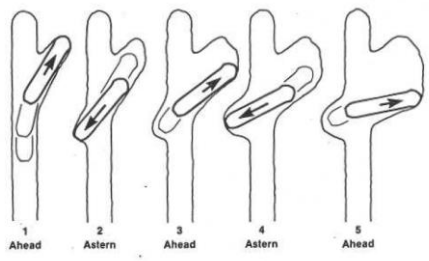

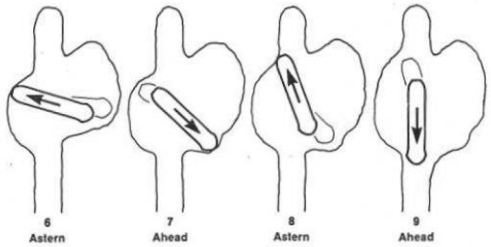

Figure 104: Sketch Star Manoeuvre, Quinton, Lau (2006)

Results to be obtained and reported for the star manoeuvre (captain's turn) are similar to those of break out tests.

3.3.3 ADDITIONAL COMMENTS WHICH WERE ADDED TO THE PROCEDURES

It should be noted that typically the behaviour of the model propulsion and manoeuvring / steering units does not exactly reflect the capability of the ships propulsion and manoeuvring systems. The reason is that stiffness and dynamic response of the model propulsion trains are not adjusted according to scaling similarities.

Further effects on manoeuvring tests resulting from restricted basin dimensions should be avoided.

As the results of manoeuvring tests are subject to the actual operating of manoeuvring systems the procedure for each manoeuvre should always be clearly documented and influence from operator should be limited to a minimum extent.

3.3.4 COOPERATION WITH THE MANOEUVRING COMMITTEE

The task obligated also cooperation with the Manoeuvring committee. There were discussions between the committees on relevance of captive model test for ice, harmonization of general introduction and description of required data between 75-02-06-01 (open water) and 7.5-02-04-02.3 (ice) and frequent updates between the two committees on what is modified in the ice manoeuvring guideline. Afterall, it was found that common ground between the two groups is limited, but cooperation and exchange will continue.

3.4 Conduct survey of uncertainty in ice model experiments, and revise "7.5-02-04-02.5 Experimental Uncertainty Analysis for Ship Resistance in Ice Tank Testing."

This task was not completed as planned. There are several uncertainty sources in ice model testing, some of which are not very well recognized. Most of the sources are related to ice properties. However, the following actions were taken for this task: Ice resistance test results using 4 ice sheets were used for the ITTC's present uncertainty analysis. For each ice sheet, two channels with three speeds were tested and 18 in-situ cantilever beam tests for each channel were performed. Ice resistance uncertainty as well as ice flexural strength uncertainty was investigated. Review of current analytical and numerical determination methods for the global ice load upon offshore structures of various types and compare to physical modelling.

3.5 Review of current analytical and numerical determination methods for the global ice load upon offshore structures of various types and compare to physical modelling.

Piled structures in ice

Prepared by Yan Huang

Piled structures in arctic and cold regions shall have the abilities to resist ice actions. Such structures generally include single pile structures (e.g., monopile foundations for offshore wind farms) and multi-pile structures (e.g., offshore jacket platforms, or multi-leg foundations for docks and wind turbines). Regarding single pile structures, global ice loads, ice induced vibrations and scaling methods for ice model testing are the key issues studied for many years. For multi-pile structures, influences of interference and sheltering effects, non-simultaneous failure, ice jamming and rubble building on global ice loads are the main topics in the published research programs.

1. Single pile structure

1.1. Global ice load

The global ice loads for single pile structures have been widely studied by many scholars through field observations, model tests and mathematical analyses, and several design formulas have been proposed. Despite the differences in the detailed expressions of the formulas, the global ice loads are generally treated as a function of ice thickness h, structural width w and ice strength σc. For now, the most applicable formula may be the ISO algorithm (ISO 19906, 2010) expressed as:

$$F_G = p_G \cdot h \tag{3}$$

$$p_G = C_R \cdot (h/h_1)^n \cdot (w/h)^m \quad (4)$$

where F_G is the global ice action normal to the surface, in MN; p_G is the global average ice pressure, in MPa; w is the projected width of the structure, in m; h is the thickness of the ice sheet, in m; h_1 is a reference thickness of 1 m; m is an empirical coefficient equal to −0.16; n is an empirical coefficient equal to $-0.50+h/5$ for $h < 1.0$ m, and to −0.30 for $h \geq 1.0$ m; C_R is the ice strength coefficient, in MPa.

The ISO algorithm considered the size effect in the ice pressure and obtained full-scale measurements data from Cook Inlet, Beaufort Sea, Baltic Sea and Bohai Sea. The ISO formulas have also been adopted by several design rules or guidelines in their latest versions, such as the API RP 2N (API, 2015) and the DNV OS J101 (DNV, 2014).

It should be noted that the Eq. (3) and Eq. (4) apply only for rigid structures and do not take into account the effects of ice-induced vibrations, which can arise in compliant structures.

1.2. Ice induced vibration

When ice breaks up, static and dynamic interactions will take place between the structure and the ice. For compliant structures, the natural vibrations of the structure will affect the break-up frequency of the ice, such that it becomes tuned to the natural frequency of the structure. This phenomenon is known as lock-in and implies that the structure becomes excited to ice induced vibrations in its natural mode shapes. The structure shall be designed to withstand the loads and load effects from dynamic ice loading associated with lock-in when ice induced vibration occurs.

There have been divergences on the mechanism that controls the procedure of ice induced vibrations on vertical structures. Some scholars such as Peyton (1968) and Neil (1976) have the opinion that steady state vibration caused by ice is a resonant vibration that relates to a concept known as the failure length of ice. Similar conclusions were obtained in field and lab tests by Michel (1978), Sodhi and Morris (1986) and Sodhi (2001). They reported that that the failure frequency of ice is directly proportional to ice velocity and inversely proportional to ice thickness. Resonant vibration may arise when the failure frequency is close to the natural frequency of the structure.

Other scholars took the interaction between ice and a flexible structure as the control mechanism of the procedure of ice induced steady vibration. Basing on the field observation in Kulk gulf, Matlock et al. (1969) established a numerical model on the consideration of the displacements and elastic deformations of ice sheet and structure. Some scholars hold the viewpoint that the break size of ice is controlled by structure, and the cause of ice induced vibration is the negative damping factor engendered in course of ice-structure interaction (Määttänen, 1977). Subsequently, this consideration was developed into the self-excited vibration theory, which is supported by quite a few scholars. On the basis of self-excited vibration theory, Yue (2004) analysed the problem from a new aspect that considered the material characteristics of ice and the feedback effect of the structure response. Some scholars also analysed the problem from the aspect of energy transition (Kärnä and Turunen, 1989, 1990).

Based on a series of single pile tests, Huang et al. (2007) established an interaction coefficient I (Eq. 5) to account for the influences of structure stiffness, natural frequency of the structure, ice elasticity and ice speed on the ice-

structure interaction and evaluate the response level of the structure under dynamic ice loading:

$$I = -\ln K / Eh \cdot \ln (Df_0) / V \cdot D / h \quad (5)$$

where K is the structure stiffness; E is the elastic modulus of ice; h is the ice thickness; D is the structural width; f_0 is the natural frequency of the structure; V is the ice drift speed. Based on the interaction coefficient I, Huang et al. (2007) proposed a range of 20–45 for the identification of violent ice induced vibrations. This range was later valid by field observation and multi-pile tests (Huang et al., 2013).

1.3. Scaling for ice model testing

The traditional Froude and Cauchy scaling approach for ice model testing is originated in the scaling of ships breaking ice (ITTC, 2017). Such approach is considered to be valid when the material behavior of the ice can be treated as linear elastic and inertia forces are significant under high speeds during ship-ice interaction.

For the interaction with pile structures, ice can fail in various ways, leading to the questioning on the applicability of Froude and Cauchy similarities. As known, the strength of the ice depends on the grain structure, temperature, degree of confinement and the loading rate, resulting in different behaviours of ice failure including creep, viscoplasticity, elasticity, or plasticity (Timco, 1987). Thus, in the interaction between a pile structure and a floating ice sheet, the ice may fail in creep, crushing, buckling, bending, etc.

Many investigators have conducted small-scale and medium-scale indentation tests to understand the ice crushing process, and the effects of indentation speed on the mode of crushing failure have been identified: creep deformation of ice at low speed, intermittent crushing against compliant structures at intermediate speeds, and continuous brittle crushing at high speeds (Sodhi et al., 1998). Sodhi (2001) presented a map of ice crushing failure during interactions with rigid and compliant structures (see Figure 5) and pointed out the existences of one transition speed (i.e., ductile to brittle) for rigid structures, and two transition speeds (i.e., ductile to intermittent and intermittent to brittle) for compliant structures. Huang et al. (2007) found that the two transition speeds for compliant structures are not constant but changing with different structure stiffness values.

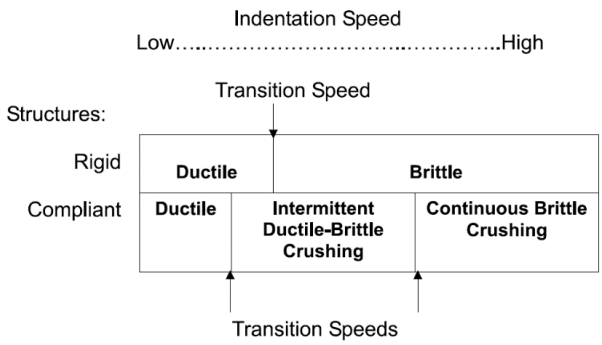

Figure 105: Ice crushing failure mode in terms of indention speed and type of structure (Sodhi, 2001)

Therefore, in the application of Froude-Cauchy scaling for the interaction between ice and pile structures, the following issues need to be addressed:

i. The transition interaction speed or loading rate for the definition of the elasticity for ice, which determines the applicability of Cauchy scaling. Derradji-Aouat (2003) proposed that ice behaves as a linear elastic material with a brittle mode of failure at high-speed impacts where the strain rates are higher than $10^{-3}s^{-1}$. Such threshold was obtained from triaxial tests (Derradji-Aouat, 2000) and can be applicable for rigid structures. For compliant structures, however, the two transition speeds are difficult to define with structural stiffness involved. Based on the interaction coefficient I, Huang et al. (2007) proposed a range of 20–45 for the

identification of violent ice induced vibrations, but the link between violent structural response and ice failure modes (i.e., intermittent ductile-brittle or continuous brittle) still needs to be clarified on the basis of specific structural dynamic characteristics.

ii. Alternative scaling methods for the ductile and intermittent ductile-brittle failure of ice. The Froude-Cauchy scaling is inapplicable for pile structures under low ice drift speed as the ice may fail in ductile or intermittent ductile-brittle mode and the inertia forces are small. As von Bock und Polach and Molyneux (2017) stated, specific similarities need to be developed for each single case (scenario), and the case-based scaling is considered more practical than the definition of one global scaling approach. Atkins and Caddell (1974) developed a non-dimensional ice number *In* to maintain both the Froude law and the cracking law, but the application of the In is still in the brittle regime. For small-scale laboratory tests on ice moving slowly against structures, Palmer and Dempsey (2009) proposed that the Froude scaling is unnecessary and can be abandoned and developed a dimensionless group lW/E (l is the characteristic length of the system, E is the elastic modulus and W is the weakening rate) based on nonlinear fracture mechanics to maintain the same notch sensitivity as the prototype, which inferred that the best material to model sea ice is the real saline ice itself, and artificial reduction of strength was not suggested. The suggestion of using real saline ice is consistent with the concept of replica modelling proposed by Sodhi (1998), but the latter is used for brittle crushing during edge indentation of ice sheets at high speeds.

iii. The elasticity of model ice. Recently, von Bock und Polach et al. (2013) found that model ice is not a linear elastic material, even at strain rates above $10^{-3}s^{-1}$, and the model ice could be rather represented by strain modulus than elastic modulus. Thus, for the application of the Cauchy scaling, studies are still needed to reduce the plasticity of the model ice and increase its stiffness.

2. Multi-pile structures

Differential and multi-directional ice actions on multi-pile structures shall be considered in design, and the accuracy of determining the ice load is of ultimate importance since it directly influence the operational safety and cost.

Studies concerning the ice actions on multi-pile structures are mainly from laboratory tests. According to the ISO 19906 (2010), the global ice load on a multi-leg structure can be defined as follows:

$$F_S=k_s k_n k_j F_1 \tag{5}$$

where k_s accounts for the interference and sheltering effect; k_n accounts for the effect of non-simultaneous failure; k_j accounts for the ice jamming; F_1 is the ice force on one leg that is not influenced by the above effects.

2.1. Interference and sheltering effect

When ice interacts with pile-groups, the ice failure mechanism and the ice load tend to alter when the lateral pile spacing is less than a certain value, which is commonly known as interference effect. On the other hand, the sheltering effect is that the ice sheet will first contact and mostly failed in the front piles when interacted with pile groups, leading to a reduction of the ice force on the back piles, and the value of k_s can be studied by the above two factors. In works of Kato and Sodhi (1984) and Saeki and Ono (1986), the interaction between multi-piled structure and ice sheet can be mainly studied in two modes:

i. The line connecting the adjacent piles is perpendicular to the ice moving direction.

ii. There is a certain angle between the line connecting two adjacent piles and the ice moving direction.

For the first interaction mode, the interference effect is significantly influenced by the lateral pile spacing *L* in the front row of legs. If this distance is large, each leg interacts with the ice sheet independently of the other legs. In this case, the sheltering factor, *ks*, approaches the number, *n*, of the legs. Where all legs are on a line perpendicular to the drift direction, data from limited model tests suggest that the legs act independently of each other if the ratio of the clear distance, *L*, between the legs and the width, *w*, of an individual leg is greater than 5. Field evidence from the Confederation Bridge suggests some interaction between piers for *L*/*w* ratios of about 10. For a typical multi-leg structure where the legs are not in a single line, the legs become independent at a higher value of *L/w*. For a typical multi-leg structure with four legs, the maximal sheltering factor varies from 3.0 to 3.5. But it should be mentioned that this is mainly for four leg structures, which maybe not suitable for other multi-piled structures.

For the second mode, the angle of incidence of the ice drift influences the ice action. Some guidance on the distribution of loads between legs for multi-leg structures based on model tests can be found in Wessels and Kato (1988). Li et al. (2017) also performed a series of model tests to evaluate the interference and sheltering effect, and an integrated reduction coefficient was introduced to describe these effects.

2.2. Non-simultaneous effect

Non-simultaneous failing effect tends to affect the ice loads and failure mechanisms for the multi-leg structures. Observations of non-simultaneous crushing failure of ice were proposed by several researchers on wide structures, on which appears several independent crushing zones during the ice failure process on wide vertical walls or cones (Kry, 1978; Kry, 1980; Kamesaki et al., 1997; Takeuchi, 1999). Jordaan (2001) developed the concept “independent zones” as “high-pressure zones” and studied the distributions of the hpz. Huang (2010) conducted a series of model tests to observe the ice bending failure before wide conical and pointed out the failures of ice wedges around the cone start to behave non-simultaneously when *D/h*>25 (*D* is the waterline diameter and h is the ice thickness).

For multi-pile structure, the non-simultaneous effect exists with similar but more complicated mechanism, and published studies mainly focus on the value of k_n when piles directly interact with the ice sheet. Kato et al. (1994) carried out a series of research works on multi-legged structure with vertical piles. It is noticed that non-simultaneous failure also caused the decreasing of ice loading, but the effect of non-simultaneous factor is not extensive discussed because of the insufficient test data, and the coefficient was recommended as 1.0. Shi et al. (2002) gave experimental investigations on the non-simultaneous failure of ice for two in a row and five piles in a row, respectively. The results showed that the k_n can be taken as 0.875 for two piles and 0.774 for five piles. ISO 19906 (2010) recommended 0.9 for the value of k_n but also mentioned such value is estimated with the absence of test data. Li et al. (2017) performed a series of model tests to investigate the maximum ice loads on a multi-pile structure with slightly sloping piles and found that the non-simultaneous failure of ice becomes more complicated in comparison with the vertical ones. This can be attributed to the mixed failure mode observed in the tests with the flexural failure of ice resulting in different loads than the normal compressive failure.

2.3. Ice jamming and rubble building

Ice jamming between the legs can be expected if L/w is less than 4. Huang et al. (2017) observed severe ice jamming between the conductor array of a jacket platform in Bohai Sea and carried out a series of model tests to investigate the ice pile-up process within the conductor array and the ice load acting on it. According to the ISO 19906 (2010), ice jamming may lead to an increase in the ice action. Results from Huang et al. (2017) agreed with such point of view, but also indicted a reduced R when using the ISO algorithm (Eq. 6 and Eq. 7) to calculate the horizontal ice load acting on the conductor array due to ice rubble building in front of the structure.

$$F_B = p_D D \tag{6}$$

$$p_D = Rh^{1.25}D^{-0.54} \tag{7}$$

where F_B is the horizontal ice force due to rubble building, in MN; p_D is the rubble building action per unit width, in MN/m; R is a coefficient; h is the ice thickness, in m; D is the width of the ice feature, in m.

Where there is any chance that ice can jam between the legs, both the jammed and unjammed cases should be considered, and the maximum value of ice action selected.

4. REFERENCES

ISO 19906, 2010. Petroleum and natural gas industries—Arctic offshore structures. International Organization for Standardization, Geneva.

API, 2015. Planning, Designing, and Constructing Structures and Pipelines for Arctic Conditions. ANSI/API Recommended Practice 2N Third Edition, American Petroleum Institute.

DNV, 2014. Design of Offshore Wind Turbine Structures. Offshore Standard DNV-OS-J101, Det Norske Veritas.

Peyton, H.R., 1968. Sea ice Forces. Ice pressure against structures. Technical Memorandum, vol. 92. National research Council of Canada, Ottawa, Canada, pp. 117–123.

Neil, C.R., 1976. Dynamic ice forces on piers and piles: an assessment of design guidelines in the lithe of recent research. Canada journal of civil engineering, vol. 3, pp. 305–341.

Michel, B., 1978. Ice Mechanics. Laval University Press, Quebec, P.Q., Canada, pp. 298–299.

Sodhi, D., Morri, C.E., 1986. Characteristic frequency of force variations in continuous crushing of sheet ice against rigid cylindrical structures. Cold regions Science and Technology, vol. 12, pp. 1–12.

Sodhi, D.S., 2001. Crushing failure during ice–structure interaction. Engineering Fracture Mechanics 68, 1889–1921.

Matlock, H., Dawkins, W., Panak, J., 1969. A model for the prediction of ice–structure interaction. Proc. 1st Offshore Tech. Conf., Houston, OTC 1066, vol. 1, pp. 687–694.

Määttänen, M., 1977. Stability of self-exited ice-induced structural vibration. Proceedings of 4th International Conference on Port and Ocean Engineering under Arctic conditions (POAC), vol. 2. St. John's Newfoundland, Canada, pp. 171–176.

Yue, Q.J., 2004. Crushing formed dynamic ice loads during interacting with vertical compliant structure. Engineering Mechanics 2, 200–208.

Kärnä, T., Turunen, R., 1989. Dynamic response of narrow structures to ice crushing. Cold Regions Science and Technology 17, 173–187.

Kärnä, T., Turunen, R., 1990. A straightforward technique for analysing structural response to dynamic ice action. Proceedings of the 9th International Conference of Offshore Mechanics and Arctic Engineering, vol. 4, pp. 135–142.

Huang, Y., Shi, Q.Z., Song, A., 2007. Model test study of the interaction between ice and a compliant vertical narrow structure. Cold Regions Science and Technology 49, 151–160.

Huang, Y., Yu, M., Tian, Y.F., 2013. Model tests of four-legged jacket platforms in ice: part 2. Analyses and discussions. Cold Reg. Sci. Technol. 95, 86–101.

ITTC, 2017. General Guidance and Introduction to Ice Model Testing. ITTC Recommended Procedures and Guidelines, International Towing Tank Conference.

Timco, G.W., 1987. Indentation and penetration of edge-loaded freshwater ice sheets in the brittle range. Journal of Offshore Mechanics & Arctic Engineering, 4(3), 287-294.

Sodhi, D.S., Takeuchi, T., Nakazawa, N., Akagawa, S., Saeki, H., 1998. Medium-scale indentation tests on sea ice at various speeds. Cold Reg. Sci. Technol. 28, 161–182.

Derradji-Aouat, A, 2003. Multi-surface failure criterion for saline ice in the brittle regime. Cold Regions Science and Technology 36: 47–70.

Derradji-Aouat, A., 2000. A unified failure envelope for isotropic freshwater ice and iceberg ice. ASME/OMAE-2000, Int. Conference on Offshore Mechanics and Arctic Engineering, Polar and Arctic section, New Orleans, US.

von Bock und Polach, R.U.F., Molyneux, D., 2017. Model ice: A review of its capacity and identification of knowledge gaps. Proceedings of the ASME 2017 36th International Conference on Ocean, Offshore and Arctic Engineering (OMAE2017), Trondheim, Norway.

Atkins, A.G., Caddell, R.M., 1974. The laws of similitude and crack propagation. International Journal of Mechanical Sciences, 16(8): 541–548.

Palmer, A., Dempsey, J., 2009. Model tests in ice. Proceedings of the 20th International Conference on Port and Ocean Engineering under Arctic Conditions, Luleå, Sweden.

Sodhi, D.A., 1998. Nonsimultaneous crushing during edge indentation of freshwater ice sheets. Cold Regions Science and Technology 27: 179–195.

von Bock und Polach, R., Ehlers, S., and Kujala, P., 2013. Model scale ice - part a: Experiments. Cold Regions Science and Technology, 94: 53–60.

Kato, K., Sodhi, D.S., 1984. Ice action on two cylindrical structures. Journal of Energy Resources Technology, 106: 107-112.

Saeki, H., Ono, T., 1986. Total ice forces on the clusters of cylindrical piles. In: 5th OMAE international conference on offshore mechanics and Arctic engineering, Tokyo, Japan.

Wessels, E., Kato, K., 1988. Ice Forces on Fixed and Floating Conical Structures, Proc. 9th IAHR Int. Symp. on Ice, Sapporo, Japan.

Li, W., Huang, Y., Tian, Y., 2017. Experimental study of the ice loads on multi-

piled oil piers in Bohai Sea. Marine Structures, 56: 1-23.

Kry, P.R., 1978. A statistical prediction of effective ice crushing stress on wide structure. Proc. 4th IAHR Symposium on Ice Problems, Lulea, Sweden, pp. 33–47.

Kry, P.R.,1980. Third Canadian geotechnical colloquium: Ice force on wide structures. Canadian Geotechnical Journal, 17(1):97-113.

Kamesaki, K., Tsukuda H., Yamauchi, Y., 1997. Experimental studies on non-simultaneous failure characteristic of vertical sided indentors. In: 7th ISOPE international offshore and polar engineering conference. Honolulu, USA.

Takeuchi, T., 1999. Indentation pressure in ice/structure interaction based on statistical generation of ice failure surface. Proceedings of the international offshore and polar engineering conference, 2: 505-511.

Jordaan, I.J., 2001. Mechanics of ice-structure interaction. Engineering Fracture Mechanics 68, 1923–1960.

Huang Y., 2010. Model test study of the nonsimultaneous failure of ice before wide conical structures. Cold Regions Science and Technology, 63(3): 87-96.

Kato, K., Adachi, M., Kishimoto, H., Hayashinguchi, S., 1994. Model experiments for ice forces on multi conical legged structures. In: 4th ISOPE international offshore and polar engineering conference, Osaka, Japan.

Shi, Q., Huang, Y., Song, A., Tong, J., 2002. Non-simultaneous failure of ice in front of multi-leg structures. China Ocean Engineering, 16:183-92.

Huang, Y., Sun, J., Wan, J., Tian, Y., 2017. Experimental observations on the ice pile-up in the conductor array of a jacket platform in Bohai Sea. Ocean Engineering, 140, 334-351.

4.1 Survey testing of platforms and monopiles in ice (such as wind turbine in frozen ocean) and consider establishing a new guideline or enhancing existing guidelines to cover such situation

The Technical Committee stress that the future procedure should include all stationary structures, including dynamic positioning in ice. Recently, very few tests have been conducted on this topic as the oil extrapolation in icy waters has practically stopped and the guideline might be outdated for the beginning. Therefore, the TC suggested just to write an outline for the future procedure. The outline is presented below:

Tests for Fixed Structures in Ice

1 PURPOSE OF PROCEDURE
2 TEST FOR FIXED STRUCTURES IN ICE
  2.1 Ice load tests for pile foundation structures
  2.2 Ice load tests for shallow foundation structures
  2.3 Ice induced vibration tests
3 PARAMETERS
  3.1 Parameters to be measured
  3.2 Ice parameters to be measured
4 VALIDATION
  4.1 Uncertainty analysis
  4.2 Benchmark tests
5 REFERENCES

4.2 Update the Guideline 7.5-02-07-01.3 “Guidelines for Modelling of Complex

Ice Environments" to cover additional complex conditions.

The group leader for this task was Alexey Dobrodeev. Guidelines for Modelling of Complex Ice Environments was earlier transferred for some reason under 7.5-02-07-01 Environmental Modelling. However, Ice committee asked that the same time the guideline was updated it would also be transferred back under 7.5-02-04 Ice Testing. The reason was that the development of ice environments and conditions should be in hands of Ice Committee because these features are typically only used in ice model testing of ships or structures.

Two chapters were added to the guidelines. They were Compressive ice and Snow-Cover ice. The other chapters were updated to correspond to the current practices.

5. COMPRESSIVE ICE

5.1 Background

The term compression in an ice cover refers to a situation where wind and/or current exert drag force on ice cover and the ice starts to drift. When wind drag acts on open pack ice, the ice floes start to move. If the ice motion is restricted by an obstacle like a shoreline, the ice cover starts to compact. First all the open water area closes. This is followed by rafting of ice at the contact points between ice floes. The rafting is followed by ridging. When the force required to ridging is larger than the driving forces, the ice drift stops and stresses i.e. compression in the immobile ice cover will be present.

Figure 106: A ship stuck in compressive ice

There is a definite relationship between the compression level the closing speed of the channel (Sazonov, 2010) on the basis of the full-scale tests processing, which can be presented as approximation:

$$V_C = 0{,}005\, S_{IC} + 0{,}03762\, S_{IC}^2 \qquad (8)$$

where V_C - the closing speed of the channel in m/s; S_{IC} – ice compression level measuring in numbers from 0 to 3. An ice compression from 0 to 3 on this scale can be described as:

0 – The ice is not compressed. There are channels, unclosed cracks and patches of ice-free water among the close ice.

1 – The ice is weakly compressed. In the compression zone separate patches of ice-free water and fresh cracks are observed. The brash ice between the ice floes is consolidated. There are rafted nilas and grey ice. There ice ridges among grey/white ice.

2 – The ice is distinctly compressed. In the compression zone only a few small patches of ice-free water and narrow cracks of variable width are preserved. This is an evidence of ice drift. The brash ice is partly extruded onto the ice channel edges. Fresh ice ridges are observed.

3 – The ice is strongly compressed. Open water and cracks are completely absent. Young ice is completely formed into ridges. The brash ice is completely extruded onto/under the ice channel edges. The channel is closed behind the icebreaker at once. There are ice ridges at the junctions of first- and multi-year ice.

5.2 Method for modelling compressive ice

An ice feature approximating a natural rubble field can be created by compressing ice floes within the tank, into a single- or multi-layered rubble field. The steps in this method are as follows:

The tests are performed with a self-propelled model or by towing the model across the basin. A ship model is driven or pulled through an open channel and one side of the ice field is pushed perpendicular towards the heading of the model (Figure 7). The model can be towed by a carriage only if both side of ice can compress the model symmetrically. The compression level is determined based on the closing speed of the channel in relation to the ship speed.

Added resistance in relation to the level ice resistance and open channel resistance determined with tests in these features without a compression.

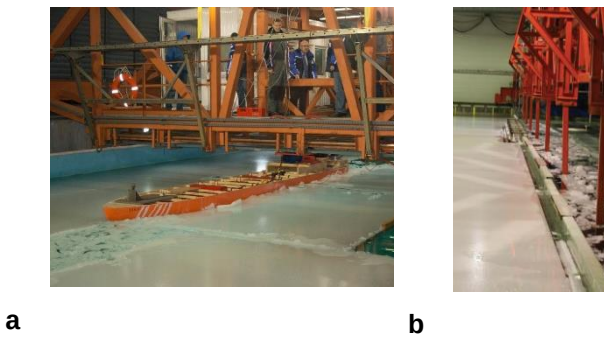

Figure 107: Towing tests of ship in compressive ice (a – the model towing with a winch across the KSRC basin during the pushing of ice sheet; b – the pushing plates lowered to the water level in AALTO basin)

5.3 Experiments and Testing

Resistance and propulsion tests can be performed in compressive level ice and closing channel see 7.5-02-04-02.1 “Resistance Test in Ice” and 7.5-02-04-02.2 “Propulsion Test in Ice”.

6. SNOW-COVERED ICE

6.1 General

Snow cover can have a significant effect on ice resistance and can increase the friction on a vessel's hull. It also provides an easily compressible layer, which consumes energy prior to fracturing the underlying ice, and entraps air which increases the buoyancy component. Such effects have been demonstrated through full-scale trials and model tests.

The results of full-scale sea trials provide conclusive evidence that snow cover on ice has significant effect on the ship’s ice resistance. Typically, this effect is taken into account by assuming some effective ice thickness so that the ship’s resistance in this effective ice thickness is equal to that in ice covered with snow.

6.2 PREPARATION

There are 3 approaches that could be used for preparing snow in model basin: modelling as an additional thickness to the ice sheet, artificially generating snow in basin (Huang 2018) and imitation by special chemical composition.

A so-called effective ice thickness h_I' , which is commonly introduced to include the snow effect on the ship’s performance in ice, is

defined as the ice thickness h_I plus some allowance for the snow-covered ice properties, primarily snow thickness h_{SN}. In this case it is assumed that the ice resistance of ship moving through continuous snow-free ice of thickness h_I' is equal to the ice resistance of the same ship moving through snow-covered ice of thickness h_I plus snow thickness h_{SN}. Calculations are performed using the following formula:

$$h_I' = h_I + k_e h_{SN} \tag{9}$$

where k_e is a certain empirical coefficient.

Different researchers suggested different values for this coefficient k_e based on scanty results obtained in full-scale trials. According to Ref. (Buzuev A.Ya., 1981) based on the analysis of the studies conducted by various researchers the values of this coefficient are in the range of 0.5 to 1.5, while A.Ya. Buzuev suggested it's equal to 1. Alternative suggestion was made by (Nyman, 1999 & Riska, 2001) to use a value of k_e equal to 1/3. For a fresh snow cover this coefficient could be assumed to be $k_e = 0$ (Belyashov, 2008 & Appolonov, 2011).

In Ref. (Ryvlin, Heisin, 1980), also based on full-scale results, it is shown that the value of this coefficient should depend on the snow density. These authors suggested the following formula for k_e:

$$k_e = k_e' \frac{\rho_{SN}}{\rho_I} \tag{10}$$

where ρ_{SN}, ρ_I – snow and ice density, respectively; k_e' - empirical coefficient (in the opinion of the authors, equal to 4.2 for icebreakers). The authors used the linear dependence as the first approximation. This dependence is apparently applicable to snow densities up to 400 kg/m^3.

The semi-empirical approach was further developed in Ref. (Gramuzov, 2011) that suggested the following formula for estimation of the coefficient k_e in Eq. (10):

$$k_e = 0.284 + 0.575 \cdot 10^{-3} S_{WB} - 0.164 h_I - 0.048 V \tag{11}$$

where V – ship speed, S_{WB}– wetted bottom area, m^2.

This formula was derived based on numerical calculations of the ship's ice resistance using the method of B.P.Ionov and E.M. Gramuzov (Ionov, 2001). In these calculations the snow thickness h_{SN} and some initial ice thickness h_I were assumed. The resistance due to snow-covered ice was calculated based on the data of Ref. (Gramuzov, 1986). Then the effective ice thickness h_I' was calculated to meet the equal resistance condition.

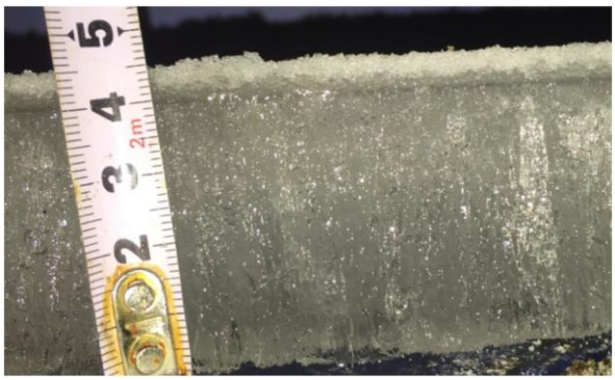

Figure 108: Artificially produced middle layer of depth hoar on model ice sheet (Huang, 2018)

The technique of artificially generating snow included in this method is forcing water vapour flowing over a cold snow surface to accelerate the formation of coarse-grained snow ice. A layer of snow ice is firstly produced on the model ice sheet by performing the two-order water pulverization procedure. Then a layer of coarse-grained snow ice with big crystal size (2–3 mm) is made by spraying the water vapour on the surface of new snow layer directly. As the wet snow particles are completely refrozen,

another new snow layer is sprayed on this base layer subsequently. In the next step, water vapour is driven to horizontally flow over the new snow surface to accelerate the formation of depth hoar (Figure 8). Then a layer of dense and close-grained depth hoar is quickly developed on the base snow ice layer. The last step of the layered snow cover generation is spraying a layer of new snow over the middle layer of depth hoar (Huang et al, 2016).

6.3 Experiments and Testing

Resistance and propulsion tests can be performed in snow cover ice see 7.5-02-04-02.1 "Resistance Test in Ice" and 7.5-02-04-02.2 "Propulsion Test in Ice".

7. REFERENCES

Appolonov, E.M., Belyashov, V.A. et al., 2011, "The Ice performance researching of icebreaker "Sankt-Peterburg" in the Kara Sea", Sudostroenie, Issue 4, pp 9 - 12.

Belyashov, V.A., Sazonov, K.E. et al., 2008, "Yury Topchev" and "Vladislav Strizhov" multipurpose ice-breaking vessels for Prirazlomnaya platform maintenance: field and model tests. Proceedings of International Conference and Exhibition on Performance of Ship and Structures in Ice 2008", ICETECH 2008, pp 105 - 113.

Buzuev, A.Ya., 1981, "Influence of environmental conditions on ship navigation in ice-covered waters", Hydrometeoizdat, Leningrad, 200 p (in Russian).

Eriksson, P. et al., 2009. Research Report No 59, Helsinki: Winter Navigation Research Board.

Finnish Transport Safety Agency (TraFi) (2010), ICE CLASS REGULATIONS 2010 FINNISH-SWEDISH ICE CLASS RULES 2010, TRAFI/31298/03.04.01.00/2010.

Finnish Transport Safety Agency (TraFi) and Swedish Transport Agency (2011), GUIDELINES FOR THE APPLICATION OF THE FINNISH-SWEDISH ICE CLASS RULES, TRAFI/21816/03.04.01.01/2011.

Frederking, R and Timco, G., 1983, "On measuring flexural properties of ice using cantilever beams", Annals of Glaciology 4.

Gramuzov, E.M., 1986, "Snow resistance of moving icebreaker", The design of tools for navigation extension: interuniversity collection, Gorkovskiy politechncal institution, Gorkiy, pp 59 - 71. (in Russian).

Gramuzov, E.M., Tikhonova, N.E., 2011, "The method of taking account of snow on icebreaker resistance by means of present thickness of level ice sheet", The proceedings of Nizhniy Novgorod State Technical University n.a. R.E. Alekseeva, Issue 4(91), pp 178 - 183.

Hamilton, J., Holub, C., et al., 2011, "Ice Management for Support of Arctic Floating Operations", In Proc. of the Arctic Technology Conference.

Huang, Y. et al., 2018, "Experiments on navigating resistance of an icebreaker in snow covered level ice", Cold Regions Science and Technology, Issue 152 (2018), pp 1 - 14.

Ionov, B.P., Gramuzov, E.M., 2001, "Ships ice performance", Sudostroenie, St. Petersburg, 512 p (in Russian).

Tuhkuri, J., and Lensu, M., "Laboratory tests on ridging and rafting of ice sheets", J. Geophys. Res., Issue 107(C9), 3125.

Leppäranta, M. and Hakala, R., 1992, "The structure and strength of first-year ice ridges in

the Baltic", Cold Regions Sciences and Technology, Volume 20, pp 295 - 311

Molyneux, D. and Spencer D., 2013, "Predicting Ice Loads on Offshore Structures", Proceedings, 18th Offshore Symposium, Texas Section, SNAME, Houston, February 7.

Nyman, T., Riska, K. et al., 1999, "A. The ice capability of the multipurpose icebreaker Botnica – full scale results", POAC 99, Espoo, Finland, Volume 2, pp 631 - 343.

Prodanovic, A., 1979. "Model tests of ice rubble strength. Proc. Port and Ocean Engineering under Arctic Conditions", The University of Trondheim, The Norwegian Institute of Technology, Trondheim, Norway, pp 89 - 105.

Riska, K., Leiviskä, T. et al., 2001, "Ice performance of the swedish multi-purpose icebreaker Tor Viking II", POAC 01, Ottawa, Ontario, Canada, Volume 2, pp 849 - 866.

Ryvlin, A.Ya., Heisin, D.E., 1980, "Ship ice trials", Sudostroenie, Leningrad, 208 p (in Russian).

Sazonov, K. E., 2010, "Theoretical principles of ship navigation in ice", Krylov Shipbuilding Research Institute, St. Petersburg, Russia, 274 p.

Strub-Klein, L., and Sudom, D., 2012, "A comprehensive analysis of the morphology of first-year sea ice ridges", Cold Regions Science and Technology 82, pp 94 - 109.

Suominen, M. & Kujala, P., 2012, "Ice Model Tests in Compressive Ice", 21st IAHR International Symposium on Ice, Dalian, China.

Timco, G. W. and Burden, R. P., 1997, "An Analysis of the Shapes of Sea Ice Ridges", Cold Regions Science and Technology, Volume 25, pp 65 - 77.

Timco, G. W., Croasdale, K. and Wright, B., 2000, "An Overview of First-Year Sea Ice Ridges", Canadian Hydraulics Centre, Technical Report HYD-TR-047, PERD/CHC Report 5-112, August

Wang, J., Sayeed, T. et al., 2016, "Ice Model Tests for Dynamic Positioning Vessel in Managed Ice", In Proc. of the Arctic Technology Conference.

8. FUTURE WORK

1. Guidelines for tests with offshore structures –

2. Guideline for ice trials – It is suggested to prepare in principle a new guideline because the previous guideline cannot be considered applicable anymore as it is outdated. In. The guideline should include the performance of the tests, ice measurement practises and analysis methods.

3. Review on numerical methods to predict the performance of ships in ice in cooperation with ISSC.

4. Guideline or proposal for waves in ice, which is a topic gaining increasing attention.

5. Uncertainty analysis

The Specialist Committee on Manoeuvring in Waves

Final Report and Recommendations to the 29th ITTC

1. INTRODUCTION

1.1 Membership

The 29th ITTC Specialist Committee on Manoeuvring in Waves consisted of:

- Prof. Hironori Yasukawa (Chairman). Hiroshima University, Japan
- Dr. Manasés Tello Ruíz (Secretary). HSVA, Germany, formerly, Ghent University (UGent) and Flanders Research Hydraulics (FRH), Belgium
- Dr. Evgeni Milanov. BSHC, Bulgaria
- Dr. Young-Jae Sung. Hyundai Heavy Industries, Korea
- Dr. Yeongyu Kim. Korea Research Institute of Ships & Ocean Engineering (KIOST), Korea
- Dr. Xiechong Gu. Shanghai Jiao Tong University, China
- Prof. Wenyang Duan. Harbin Engineering University, China
- Dr. Marc Steinwand. SVA Potsdam, Germany (left in 2019)

1.2 Meetings

The committee met four times:

1. BSHC, Varna, Bulgaria, February 2018

2. Shanghai Jiao Tong University, China, October 2018

3. Ghent University and Flanders Research Hydraulics, Antwerp, Belgium, May 2019

4. Hiroshima University, Japan, January 2020

1.3 Tasks and Report Structure

The following lists the tasks given to the 29th ITTC, the Specialist Committee on Manoeuvring in Waves (SC-MW). Originally, we planned to add the results of the SIMMAN workshop, but we did not mention it because it was postponed due to the influence of the Corona-virus.

1. Define the overall framework for what manoeuvring in waves means. (*section 2*)
2. Present the state of the art based on a comprehensive literature review. (*section 3*)
3. Create a guideline for benchmark tests on manoeuvring in waves. Consideration should be given to the generation of data for the validation of numerical tools. (*Publication of the new guideline was postponed*)
4. Investigate the methodology needed to combine experimental tests and numerical tools. (*section 3*)
5. Investigate new manoeuvres to assess minimum power requirements (e.g. return to head waves). (*section 4*)
6. Address the issues brought about from IMO-MEPC71 and following meetings concerning the minimum power requirements, including issues on manoeuvrability under adverse weather. (*section 4*)
7. Validate the Level 2 – Simplified Assessment Method of the 2013 Interim Guidelines (MEPC.1/Circ.850). (*section 4*)
8. Liaise with IMO and/or IACS to address manoeuvring in waves. (*section 5*)
9. Liaise with the Manoeuvring Committee, the Seakeeping Committee and the Stability in Waves committee. (*section 5*)
10. Establish a mathematical model for manoeuvring in waves. (*section 3*)

2. GENERAL

2.1 Overview on the Ship Manoeuvring in Waves

Over the years the ship's manoeuvring qualities have been traditionally analysed, predicted and normalized for calm and deep water by means of 3DOF manoeuvres, assuming negligible influence of external sea conditions. However, the assumption of negligible external effects such as wind, current, shallow water and waves is not strict. Several studies have focused on the first three factors, because accounting for them fits well into the time-domain studies of ship manoeuvrability.

In real navigation conditions, the two problems overlap. When performing manoeuvre in waves the wave induced ship motions interacts with the ship's manoeuvring motion, thus waves may substantially influence the hydrodynamic forces and thereby change the manoeuvring behaviour, and vice versa. The need to evaluate the manoeuvring behaviour in such scenarios leads to a necessity to combine the knowledge gained in the two separate approaches. This is not an easy task as even in the study of the ship's controllability in calm water the mathematical model in calm water is still in the horizontal plane. Note that research on manoeuvrability and seakeeping intersects in two fields, on one hand the frequency dependency of hydrodynamic coefficients and

ship motions and on the other the fluid memory effects.

Regarding the frequency dependency, a number of works have been devoted to justify the use (in the task of predicting ship manoeuvrability in still water the PMM) of "slow motion derivatives" under the assumption of quasi-steady flow. This approach is still applied as a standard in PMM data analysis. Such assumption, however, is rather questionable because in a conventional towing tank, the length of run is quite short and the frequency of captive motion is quite high. The effect of past history of the motion in view of "slow motion derivatives" is assumed negligible. Some approaches have been used for separation of fluid memory effects by adequate PMM data post-processing.

Since the introduction of the Energy Efficiency Design Index (EEDI), serious concerns regarding the manoeuvrability of ships in waves have been brought to the forefront. IMO Marine Environment Protection Committee issued determined a "Minimum propulsion power to maintain manoeuvrability of ships in adverse conditions" (MEPC 232(65), 2013). The definitions of adverse conditions and minimum power line requirements in the document were stated. However, the question what means to "maintaining manoeuvrability" remains open. Research into the problem has been initiated in a number of centres, using experimental, numerical and hybrid approaches.

In the frame of SHOPERA project development, added resistance and ship manoeuvrability have been studied experimentally and numerically focusing on second order wave forces (Shigunov and Papanikolaou, 2015). A subset of benchmark data was established relating to added resistance in regular an irregular waves; drift forces, turning and zig-zag manoeuvres in regular waves at 4 and 6 knots approach speed. Particular attention was paid to developments in the area of the problem of additional criteria for manoeuvrability in waves. In this regard, three critical scenarios were proposed for consideration, where the ship operation functional requirements, the practical criteria and the environmental conditions have been specified. As the ship may fall into each of the scenarios, it would be appropriate to identify the most critical one. In principle, the question of simplifying the set of requirements regarding the ship's manoeuvrability in waves is on the agenda.

In this context, SHOPERA and JASNAOE in 2016 submitted to IMO a coordinated proposal which contains unique description of adverse seas and one most critical scenario ("escape from coastal area"). During a meeting organized by ITTC Manoeuvring Committee workshop at LR in London, 2016 all aspects of ship manoeuvring in waves were discussed and opinion on the subject by participants have been presented. Due to the complexity of the problem there were more questions than answers. The corresponding panel discussion focused on five main topics: a) methods and procedures to work on; b) how to simplify and still be relevant; c) how to improve simulations; d) environmental or input conditions; e) manoeuvres to consider; f) general comments. Based on above, the discussion covers many issues of varying complexity and importance to considered research area.

On the basis of the so far considered requirements of the regulatory authorities and the results of previous studies, a general and preliminary definition of the sufficient ship manoeuvring in adverse sea conditions we can accept: "The ship has ability to maintain certain advance speed and change and keep the course in most unfavourable waves and wind conditions".

2.2 Indices Representing Manoeuvring in Waves

The manoeuvrability of a ship in waves can be classified, as shown in Table 1, based on that in calm water. The major difference from calm water is that ships sailing straight in waves at an average constant ship speed generally require a check helm, which leads to a hull drift angle and a ship speed drop. The condition of the ship moving in waves is called "steady sailing condition" here.

The turning circle in the presence of waves does not become a circular trajectory as in the case of the calm water. During turning, the ship drifts to a different direction from the incident waves. Two indices representing the drift characteristics during turning, the drifting distance H_D and the drifting direction μ_D, are used (Ueno et al., 2003). Here, the successive ship positions in ψ=90°, 450°, 810°, etc. are numbered as 1, 2, 3, and so on, as shown in Figure 1. Then, H_{D1} and H_{D2} are defined as the distances of ship drifting from 1 to 2 and 2 to 3, respectively. Similarly, μ_{D1} and μ_{D2} are defined as angles of the ship drifting from 1 to 2 and 2 to 3, respectively (Hasnan et al., 2020).

Table 109: Indices representing manoeuvring in waves

	straight moving	small/medium rudder angle	large rudder angle
calm water	propulsive peformance	10/10 or 20/20 zig-zag maneuvers	35deg turning
waves	steady sailing performace		
indices in waves	check helm, drift angle, speed drop, etc.	overshoot angles	advance, tactical dia., drifting distance, drifting direction

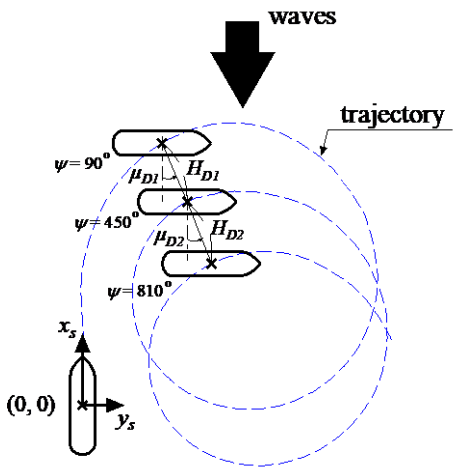

Figure 1: Definition of drifting distance H_D and drifting direction μ_D (Hasnan et al. 2020)

As manoeuvring in waves other than those shown in Table 1, it should be considered stopping in waves and crabbing in waves.

3. STATE-OF-THE ART OF PREDICTION METHODS OF SHIP MANOEUVRING IN WAVES

3.1 Experimental Methods

3.1.1 Free running tests in waves

General: Free running model tests are commonly used to investigate the manoeuvring of a ship directly. Their results can also be used as validation data for developing a computer simulation model. Traditionally, free running model tests are conducted in calm water condition, but those can also be conducted in waves.

Free running tests should be designed for the ship model to move autonomously. For measuring the position of the ship model, three methods are frequently used: a) a method of using an acoustic measurement equipment installed at the bottom of the tank (Hirano et al., 1980), (Ueno et al., 2003), b) a method in which

a carriage in the tank automatically tracks and measures the position according to the movement of the ship (Yasukawa and Nakayama, 2009), and c) a method of measuring the ship position by an optical method (Yasukawa et al., 2015), (Kim et al., 2019a). Commonly, the inclination angle of the ship is measured using a gyro. Figure 2 shows a measurement system by an optical method (total station system) in KRISO, Ocean Engineering Basin.

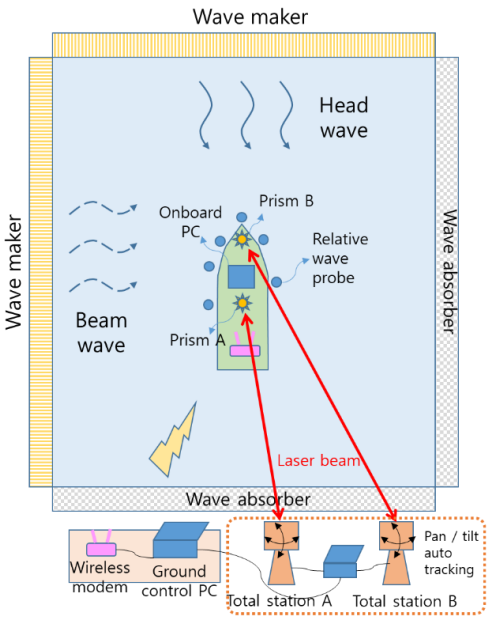

Figure 2: Measurement system for free-running tests in KRISO Ocean Engineering Basin (Kim et al., 2019a)

Most manoeuvring tests start from a straight course condition with as steady as possible values of heading, speed, rpm and rudder angle. Speed trial tests should be carried out in order to find the propeller rpm corresponding to the desired test speed. Methods for accelerating the ship model to the target speed are summarized as follows:

- A propeller revolution scheduling system which is usually used at acceleration phase to reduce acceleration time and distance. But relatively long distance is required. (Kim et al., 2019a)
- A catapult system (Yasukawa et al., 2015) (Hasnan et al., 2020)
- A carriage releasing system: the ship model is released after acceleration phase. (Yasukawa and Nakayama, 2009) (Sanada et al., 2013)

Free running tests in regular waves:

In 1980, Hirano et al. (1980) conducted a free running test in regular waves using a self-propelled Ro-Ro ship model to investigate the effects of waves on the turning trajectory. The drifting behaviour during turning in regular waves was studied. Ueno et al. (2003) performed free running tests for turning, zig-zag, and stopping manoeuvres in regular waves using a VLCC tanker model. It was shown that the drifting direction of a ship was different from the incoming wave direction. In addition, a large drift of the ship during turning was observed for shorter wavelengths.

Yasukawa (2006a), Yasukawa (2008), and Yasukawa and Nakayama (2009) conducted free running tests for turning, zig-zag, and stopping manoeuvres using the S-175 container ship model. Lee et al. (2009) conducted turning and zig-zag manoeuvre tests in regular waves using a VLCC model to capture the wave height effect. However, details such as wave-length were not revealed.

Sanada et al. (2013) performed turning tests for the ONR Tumblehome in calm water and regular waves and presented time histories of 6-DOF motions during turning in waves. Moreover, Sanada et al. (2019) performed repeat tests of turning and zig-zag manoeuvres for the same ONR Tumblehome in regular waves and discussed the effect of ship speed and wave-length on manoeuvring with the measured accuracy.

Sprenger et al. (2017) performed turning and zig-zag manoeuvre tests for a DTC container ship and KVLCC2 tanker models in regular waves with variations in wave directions, wave-length, etc. The obtained data was mainly used to validate the calculation method for manoeuvring in waves.

Kim et al. (2019a) carried out the turning tests in regular waves using KVLCC2 model. Figure 3 shows the turning trajectories with variations of the ratio of wave-length of ship length (λ/L). The rudder angle was 35°. While turning, the ship model drifts in the direction near the steering point. The drifting distance becomes larger at shorter wave-lengths, and the angle drifted obliquely to the incident wave direction becomes smaller at shorter wave-lengths. Such characteristics are similar to the results of the S-175 model (Yasukawa and Nakayama, 2009).

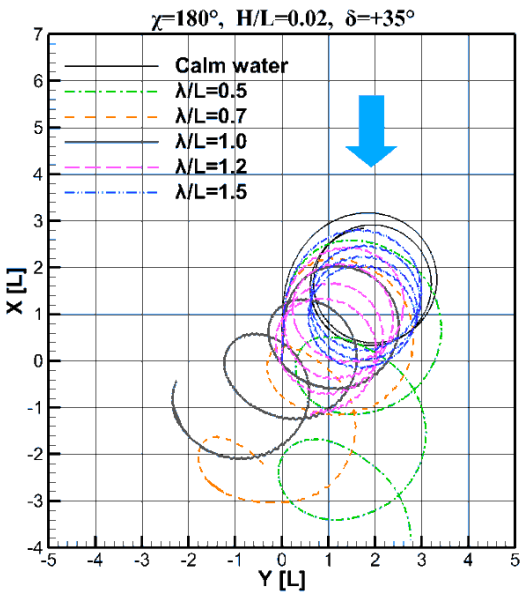

Figure 3: Turning trajectories in regular head waves with variations of λ/L for KVLCC2 (Kim et al., 2019a)

Free running test results in irregular waves:

Yasukawa et al. (2015) conducted free-running model tests using a KVLCC2 model in short-crested irregular waves. Turning tests, and 10/10 zig-zag manoeuvre tests were carried out to obtain the validation data of the manoeuvring simulation method in irregular waves.

Hasnan et al. (2020) conducted the turning tests in short-crested irregular waves using two ship models of KVLCC2 tanker and KCS container ship. The tests were performed in head waves at the time of approaching with the significant wave height 4.5 m for KVLCC2 and 3.0 m for KCS at full-scale. With a decrease in the approach speed of the ships sailing in the same wave condition, advance A_D decreases but tactical diameter D_T does not change significantly. With a decrease in the approach speed, both drifting distance H_D and drifting direction μ_D increase significantly, and the tendency of the ship drifting to the rudder execution point in space becomes remarkable.

Kim et al. (2019b) conducted turning tests with various seeds using KVLCC2 model in long-crested irregular waves for different propeller revolutions (n_P). Figure 4 shows comparison of turning trajectories in irregular waves. The trajectories at n_P=8.2 rps (corresponding to 7.0 kn in calm water) are significantly different with changing the seeds of the irregular waves. At n_P=4.0 rps (corresponding to 4.0 kn in calm water), the ship cannot turn in waves. It is necessary to study more for better understanding of the ship behaviour in irregular waves.

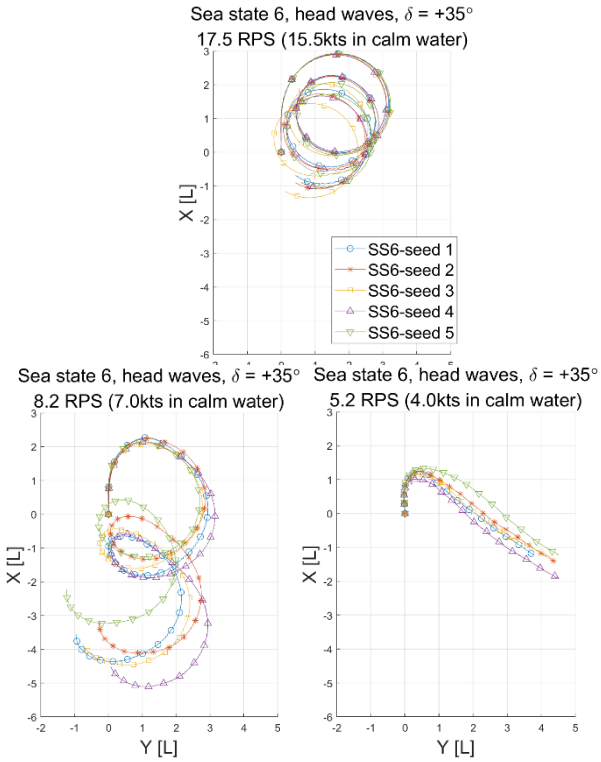

Figure 4: Comparison of turning trajectories in irregular waves for KVLCC2 model (Kim et al.,2019b)

Free running test results in wind and waves:

Fujiwara, T. et al. (2008) carried out free-running model test on a large container ship under heavy wind and regular wavs at the 400m towing tank, NMRI, Japan. Averaged navigation conditions and time fluctuations of the ship speed, hull drift angle, rudder angle, ship motions and propeller thrust etc. were captured in the experiments.

3.1.2 Captive model tests in waves

General: Captive model tests in waves are performed to verify the forces and moments induced by waves. Up to date, the mathematical model for interpreting manoeuvring performance in waves is largely divided into two problems, a) a mathematical model that interprets the force induced by waves by linear superposition on the calm water manoeuvring equations of motion, and b) a mathematical model that incorporates all elements of seakeeping and manoeuvring. In the former case, the method of analysis through model testing and other verification is well set-up for the calm water manoeuvring analysis model, but in the latter case, interpretation and verification methods through model testing are not well set-up yet.

In case of static straight or oblique tests, in which the incident direction of waves is fixed, both 1st and 2nd order wave forces can be obtained by fitting and averaging. But in case of dynamic tests such as PMM, wave incident direction is changed, so it is difficult to obtain 1st and 2nd order wave forces by fitting and averaging. Even at steady circular motion test (CMT), it is impossible to obtain test results with the same wave condition such as wave direction and wave encounter frequency, even more, those are not affected by the wave

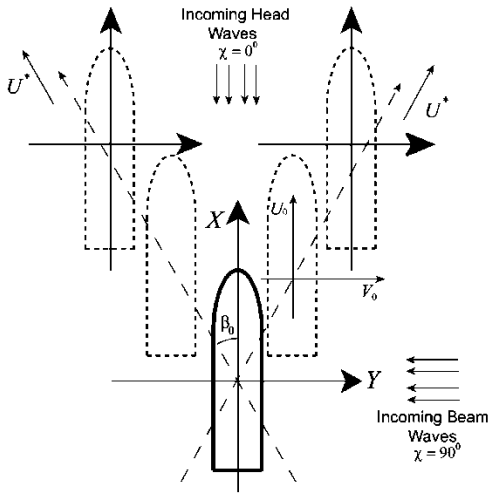

Figure 5: Schematic diagram of horizontal motions of ship in oblique tests in waves (Yasukawa and Adnun, 2006)

produced by the model ship. Therefore, only static straight or oblique tests are performed. In the oblique tests in waves, the wave encounter angle to the incident waves has to be kept with the drift angle as shown in Figure 5.

Ship motions and measured forces in waves:

Yasukawa and Adnan (2006), and Yasukawa et al. (2010) measured the ship motions in regular waves for an obliquely moving ship. The experiments were carried out for S-175 container ship in head waves and beam waves. Figure 6 shows the amplitude of the wave-induced motions (sway, roll, heave and pitch) in regular head waves. Due to the effect of the hull drift angle (β_0), the lateral motions such as sway, roll and yaw are induced even in pure heading waves. Their amplitudes become larger with increase of absolute value of the hull drift angle. On the other hands, the influence of the hull drift angle on the motions of surge, heave and pitch is not remarkable.

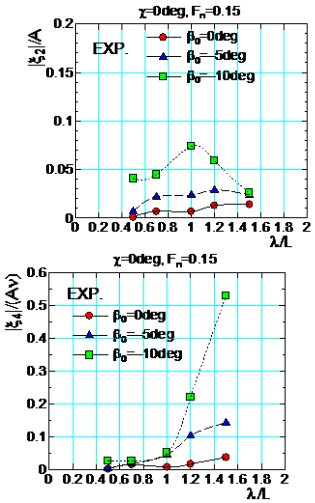

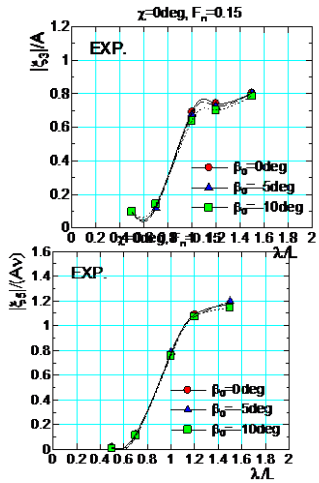

Figure 6: Amplitude of wave-induced motions (sway, roll, heave and pitch) for an obliquely moving ship in regular head waves (Yasukawa and Adnun, 2006)

Choi et al. (2019) presented test results of average value of lateral force and yaw moment acting on a KCS model obtained at oblique tests in regular waves. The ship model was fixed in the tests. Therefore, the measured forces represent the sum of hydrodynamic forces acting on the obliquely moving ship and mean wave drift forces (only diffraction component).

For a limited combination of wave amplitudes and wave lengths, drift angles and in shallow water conditions tests with a scaled model of ULCS have been investigated in Tello Ruíz et al. (2019). In Figure 7 a sample of their findings for the mean forces obtained for fully captive model tests are shown. The influence of waves at lower speeds were found to be significant important (see vertical offset of the square markers in Figure 7). For intermediate to larger speeds the wave influence was found to be less relevant for all tested wave lengths. Similar observation were found in following waves (see Figure 8)

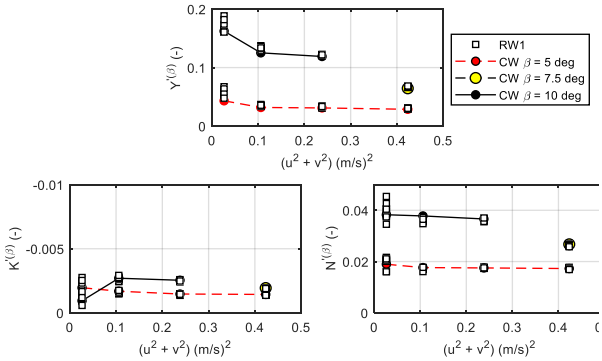

Figure 7: Mean sway force (top), roll moment (bottom left) and yaw moment (bottom right) in calm water (CW) and in head waves at T_M=13.1m, 50% UKC, ζ_a=1m (RW1) and at three drift angles, model fully captive. Results are plotted as function of V^2 only (from 0.2 to 0.8 $/Lpp$) (Tello Ruíz et al. 2019a,b)

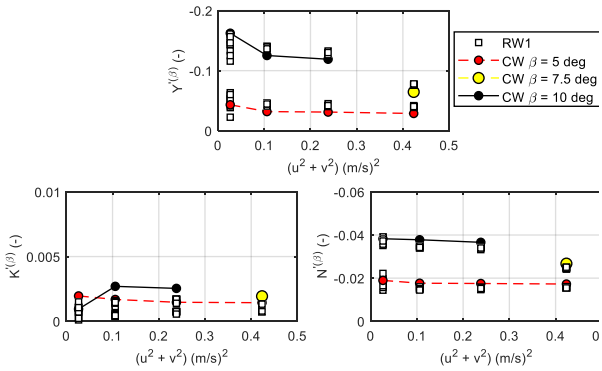

Figure 8: Mean sway force (top), roll moment (bottom left) and yaw moment (bottom right) in calm water (CW) and in following waves at T_M=13.1m, 50% UKC, ζ_a=1m (RW1) and at three drift angles, model fully captive. Results are plotted as function of V^2 only (from 0.2 to 0.8 $/Lpp$) (Tello Ruíz et al. 2019a,b)

<u>Mean wave drift forces:</u>

Ueno at al. (2001) measured mean wave drift forces and moment in turning motion. The wave encounter angle changes gradually during turning motion in the tests.

Yasukawa and Adnan (2006) measured the mean wave drift forces and moment in regular waves for an obliquely moving ship. Figure 9 shows added resistance, mean lateral force, and mean yaw moment in regular head waves. The influence of the hull drift angle (β_0) on the mean lateral drift force and mean yawing moment is large, although the influence on the added resistance is small.

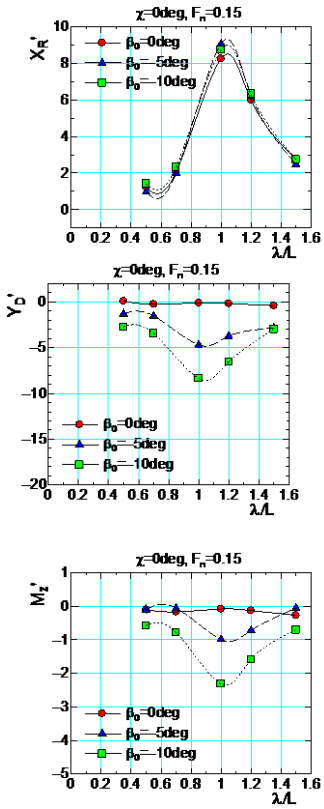

Figure 9: Added resistance, mean lateral force, and mean yaw moment for an obliquely moving ship in regular head waves (Yasukawa and Adnun, 2006)

3.2 Numerical methods

3.2.1 Framework

In literature several works addressing the topic of manoeuvring in waves can be found. In spite of the differences encountered, they all can be classified in four main groups:

(a) Mean wave force methods

(b) Two-time scale methods

(c) Unified methods

(d) CFD based direct simulation methods

The main consideration for each one is summarised in the sections below.

3.2.2 Mean wave force methods

To analyze the problem of ship maneuvering in waves, the coupling effects between the high-frequency wave-induced quantities and low-frequency steering-induced quantities should be considered. Notably, the mean wave force, known as the second-order mean force, is the most critical coupling effect.

In predicting ship maneuvering in waves, a simple method is known which takes only mean wave force into account to the existing prediction method in calm water (Hirano et al.,1980). Such a treatment is theoretically acceptable on the assumption of a slender ship (Nonaka, 1990). This method is widely used for predicting the various maneuvering motions in regular and irregular waves, for instance, by Yasukawa (2006a), Yasukawa (2008), Yasukawa et al. (2015), Papanikolaou et al. (2016), Yasukawa, et al., (2017), Tello Ruíz at al. (2019a), and Aung and Umeda (2020).

In the method, the mean force is obtained from a pre-computed database for various operation conditions by using the fast computation method (for example, the frequency domain computation based on the 2D strip theory or the 3D panel method). Cura-Hochbaum and Uharek (2016) used CFD to construct a database for the mean wave force. Chillcce and El Moctar (2018) used a 3D Rankine source based boundary element method.

The major drawback of works using this method is that they cannot handle the wave-induced motions such as heave, pitch, roll, etc. during ship maneuvering.

3.2.3 Two-time scale methods

In the methods the basic motion equations are separated into two groups: a) the high frequency wave-induced motion and b) the low frequency manoeuvring motion. The motion equations for manoeuvring and seakeeping are solved considering the mutual motion interaction in time-domain. This method is called the two-time scale method (Skejic and Faltinsen, 2008). The two-time scale method was proposed by Yasukawa (2006b), and Skejic and Faltinsen (2008). Skejic and Faltinsen (2013) also extended the method to predicting the ship manoeuvring in irregular waves. Figure 10 shows a calculation flow for ship manoeuvring in waves by the two-time scale method. In the low frequency manoeuvring model, the mean wave force method mentioned in sub-section 3.2.2 is normally used. Based on the calculated results of the ship manoeuvring, wave-induced motions are calculated by the seakeeping method.

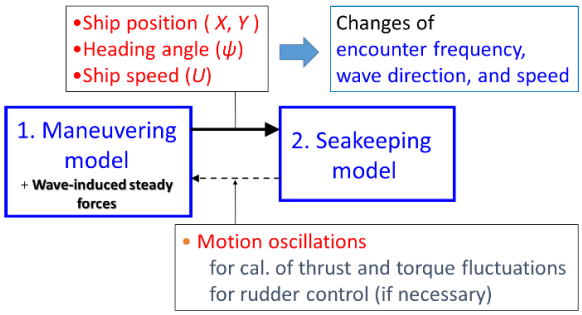

Figure 10: A calculation flow for ship manoeuvring in waves by the two-time scale method

Yasukawa and Nakayama (2009) calculated both manoeuvring and wave-induced motions by the two-time scale method. To verify their model's accuracy, the simulation results were compared with the results obtained during free running model test in waves. The scale model of a S175 container ship was used for this purpose. Figure 11 shows the comparison of the ship trajectories in regular beam waves with λ/L=0.7. Figure 12 shows the time histories of yaw rate,

drift angle, and heave during turning in the same condition as Figure 12. Although the accuracy of the turning trajectory in beam waves is not sufficient, the calculation captures qualitative tendency well. This calculation also captures the qualitative tendency of the time history results.

Hasnan and Yasukawa (2020) calculated both manoeuvring and wave-induced motions of KVLCC2 tanker model in short-crested irregular waves and compared the calculation with the turning test results provided by Hasnan et al. (2020). This method can simulate with practical accuracy in short computational time.

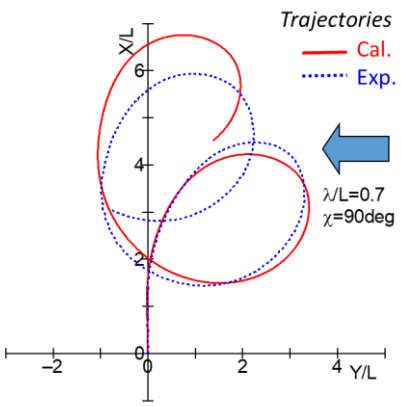

Figure 11: Comparison of ship trajectories for S-175 in regular beam waves at λ/L=0.7 (Yasukawa and Nakayama, 2009)

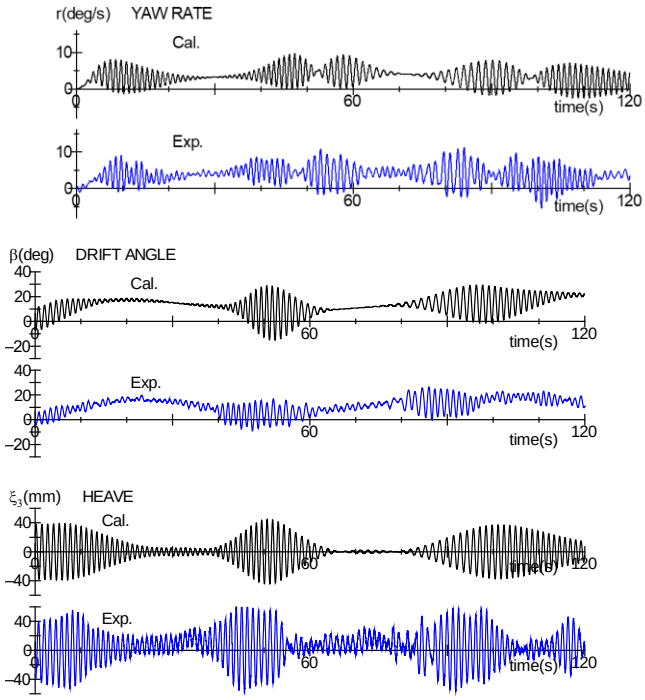

Figure 12: Time histories of yaw rate, drift angle, and heave during turning in regular beam waves (Yasukawa and Nakayama, 2009)

Seo and Kim (2011) introduced a coupling method based on the time-domain Rankine panel method to integrate the seakeeping and maneuvering quantities. In this approach, the seakeeping analysis was performed considering the instantaneous operating velocity of the ship and incident direction of the wave, and the computed wave-induced motions and forces were incorporated in the maneuvering equation of motion. Zhang and Zou (2016), Zhang et al. (2017), and Lee and Kim (2020) extended this approach by using double-body linearization, and the modeling for vortex flows that may occur at the end of the hull was introduced for the analysis of the double-body flow. Lee et al. (2020) extended the method to consider the weakly non-linear effect induced by hull geometry on the ship maneuvering in regular waves, but this effect was not significant.

Piro et al. (2020) proposed a hybrid method that combines a Reynolds-averaged Navier-Stokes (RANS) solver with a potential flow boundary-element method (BEM). The low-frequency manoeuvring problem mostly handled with the RANS method, and the relatively high-frequency seakeeping problem with the BEM. This method was applied for predicting the ship turning of KCS model in calm water and waves.

3.2.4 Unified methods

This method aims to propose a more general formulation for the ship's hydrodynamic problem. Thus, disregarding the assumptions, partially or totally, taken for the independent analysis of manoeuvring in calm water and seakeeping. In this manner, avoiding the same computation of the same hydrodynamic problem twice, for instance, added masses in seakeeping codes and acceleration derivatives in manoeuvring models.

As the manoeuvring is a time domain problem, all phenomena is aimed to be represented in the time domain, thus avoiding (wherever possible) frequency domain computations. Up to date works using this method have mainly covered the body reaction forces (the radiation problem), e.g. Ankudinov (1983), Bailey et al. (1998). Other approaches attempt to model the entire problem directly in the time domain, e.g. Subramanian and Beck (2015).

All works considering the unified method differ in the selection of the mathematical model to account for the manoeuvring forces due to viscous, cross flow effects, and lift effects. But they all agree treating the potential contribution apart and expressed in the time domain. Note, however, that wave exciting forces and moments (first and second order) are mostly computed by the sum of the components obtained in the frequency domain and over the mean wetted surface. At most, because of its simplicity, only Froude-Krylov forces have been incorporated taking into account the real time variation of the wetted surface.

Ankudinov (1983) used this method to predict the ship response in irregular waves. In his work the radiation problem is model using memory terms proposed by Cummins (1962). Due to computational limits, the kernel functions were simplified by using higher order differential equation with constant coefficients. Exciting wave forces were also intended to be evaluated by convolution integrals for the first order and second order, but resulted in larger computing times, they were model instead by the sum of the frequency components.

In Bailey et al. (1998) the unification of the fluid phenomena was also extensively discussed for the body reaction forces. In addition, they introduced corrections to the kernel functions in order to account for viscous effects. First order wave forces were also computed by convolution integrals. They work, however, did not extend to incorporate second order wave forces, and only considered linear manoeuvring forces given by the velocities and acceleration derivatives.

Other approaches such as the works of McCreight (1986), Lee (2000), Nishimura and Hirayama (2003), Ayaz, et al. (2006), Sutulo and Guedes Soares (2006) , Yen et al. (2010), Araki et al. (2011), Subramanian and Beck (2015) and Tello Ruíz (2018) fall into the classification of unified methods. Most of the above works avoid to solve the convolution integral problem by directly computing the radiation each time step, increasing considerably computation times.

Works on this method have enjoyed less attention that the simplify method of considering second order wave forces only. Some results following the works on Ankudinov (1983) and Subramanian and Beck (2015) are

presented in Figure 13 and Figure 14, respectively.

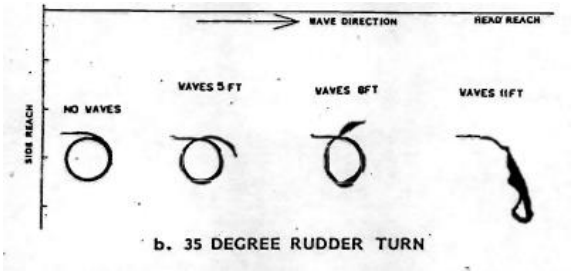

Figure 13: Turning circle trajectory of Mariner in calm water and in different irregular waves, Ankudinov (1983)

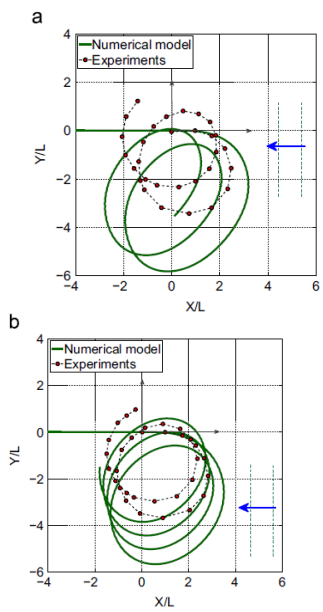

Figure 14: Turning circle trajectory of S-175 in waves. Rudder angle of -35 deg (starboard turns) (a) at λ/L of 1, in head seas and H/λ of 1/50. (b) at λ/L of 1:2, in head seas and H/λ of 1/60. (Subramanian and Beck, 2015)

3.2.5 CFD based direct simulation methods

Direct simulation using computational fluid dynamics (CFD) is the most promising method which can solve specific local flow details around the hull and its appendages and then provide a better understanding of the hydrodynamic problem of ship manoeuvring. Most of CFD studies on ship manoeuvre solves the Reynolds-Averaged-Navier-Stokes (RANS) equations for unsteady turbulent flows around complex geometries. For free running ship models, the propeller body force model or the sliding mesh method and most the overset grid method coupled with full 6-DoF motion are used. However, a precise simulation of ship manoeuvring in waves has to consider large-amplitude ship motions with more violent free surface deformation and more notable hull-propeller-rudder interactions, which is more difficult than the simulation in calm water.

Carrica et al. (2012) performed numerical simulations of ship manoeuvring in waves by using a simplified body force propeller model and applied overset grid to handle the ship motions and rudder steering. It is found that the main discrepancy between the CFD and experiments can possibly be tracked to the simplistic propeller model.

Shen and Korpus (2015) used dynamic overset grid technique and performed simulations of free running ship in head and quartering waves under course keeping control.

Wang et al. (2016, 2018a, 2018b) using naoe-FOAM-SJTU to simulate the free running course-keeping problem， zigzag manoeuvre and turning circle manoeuvre under various wave conditions for a fully appended twin-screw ship (ONR Tumblehome). The trajectory and main parameters agree well with the experiment, which show that the RANS dynamic overset grid is a reliable approach to directly simulate of such ship manoeuvre in waves. Figure 15 shows the local grid distribution for CFD simulations. Figures 16 and 17 shows free-surface elevation and vorticial structures around ship hull during turning in waves, respectively.

The above research shows the capability of CFD approach in directly simulating free running ship model in deep water regular waves. However, due to the high computational cost and even more long-time simulation requirement, direct CFD manoeuvring simulations in irregular waves, certainly for manoeuvring in shallow water waves are still a changeling problem.

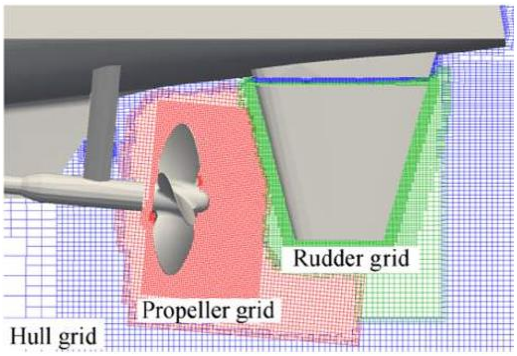

Figure 15: Local grid distribution for CFD simulations of ONR Tumblehome model ship (Wang et al. 2018b)

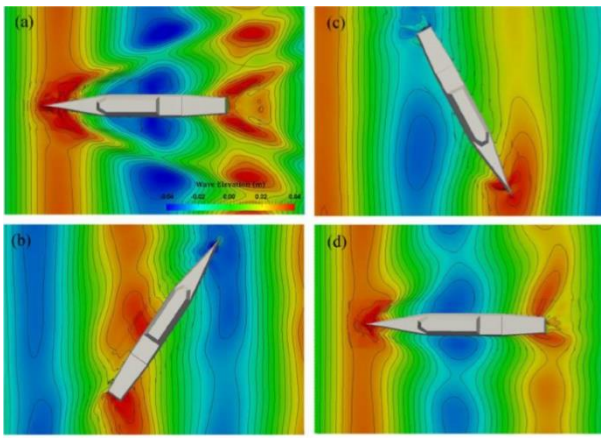

Figure 16: Free-surface elevation during turning in waves (a–d correspond to heading change of 0°, 120 °, 240 ° and 360 °, respectively) (Wang et al. 2018b)

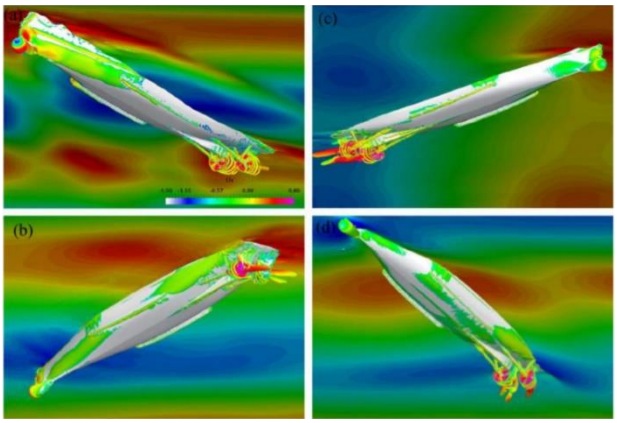

Figure 17: Vorticial structures around ship hull during turning in waves (a–d correspond to heading of 0 °, 120 °, 240 ° and 360 °, respectively) (Wang et al. 2018b)

3.3 Steady Sailing Performance and Manoeuvring Limit in Wind and Waves

For discussing the manoeuvring limit in adverse weather conditions, it is useful to evaluate the average steady sailing conditions (SSC), such as check helm, speed drop, hull drift angle, etc., of a ship moving straight in steady wind and waves. In addition, the dynamic stability, or course stability (CS), of the ship should be checked at the SSC. Both the SSC and the CS of ships under external disturbances are called the steady-sailing performance (SSP). For this analysis, the mean wave force methods mentioned in 3.2.2 are normally used.

The basic principle to conveniently obtain the SSP of the ships in steady wind and waves has already been presented by Eda (1968) and Ogawa (1969) as follows:

1. By setting acceleration, angular acceleration, and angular velocity to zero in the motion equations, the equilibria equations, that is, the balance with respect to forces and moments acting on the ship can be obtained. The check helm, speed drop, hull drift angle, and so on are obtained

by solving the equilibria equations after setting the environmental condition.

2. The course stability of the ship under adverse conditions is adjudged by evaluating the eigenvalues of the linearized motion equations.

According to the aforementioned ideas, many studies have been performed on the SSP of ships under external disturbances. However, a remarkable difference can be observed in the existing studies.

The difference exists in the base model of the hydrodynamic forces acting on the manoeuvring ship, which can be classified as follows:

- Original MMG-model (Ogawa et al.,1977)
- Models expressing the hydrodynamic forces acting on the ship by the polynomial function with respect to ship motions and operation parameters such as rudder angle and propeller revolution (perturbation method), (Eda, 1968) (Ogawa, 1969)
- Simplified model based on the models mentioned above (Ishibashi, 1975) (Tanaka et al., 1980) (Martin, 1980)

In addition, the following points must be considered. There are two methods to solve the equilibria equations: one is an exact method (Hirano et al., 1984) (Kadomatsu et al., 1990), (Spyrou, 1995) (Naito and Takagishi, 1998) (Fujiwara et al., 2005) (Fujiwara et al., 2006) (Umeda et al., 2016), and the other is an approximate method. For solving the equilibria equations precisely, an iterative calculation is required, with the usage of a computer, since the equilibria equations are mathematically non-linear. In order to obtain the solution in a short time, it is useful to employ approximations, although the calculation accuracy becomes worse. In particular, the approximation that the ship speed is known has been often employed in several studies (Tanaka et al., 1980) (Asai, 1981) (Yasukawa et al., 2012).

Spyrou (1995) and Spyrou et al. (2007) presented a method to investigate the course stability of ships in steady wind by locally linearized stability analysis at the equilibria condition based on the Jacobean matrix expression that is obtained from the motion equations. This is a general method for solving the problem numerically regardless of the expression of the base hydrodynamic force model. Umeda et al. (2016) applied this method for investigating the manoeuvring limit of a full hull ship in wind and waves based on the low speed hydrodynamic force model presented by Yoshimura et al. (1988) and Yoshimura et al. (2009).

Yasukawa and Sakuno (2020) presented a method for conveniently obtaining the SSP under external disturbances in deep and shallow water based on `4D MMG method' (Yasukawa et al., 2019). Yasukawa (2020) extended the method to the SSP problem for a ship moving in a shallow channel. Figure 18 shows the results of the SSCs, including the longitudinal ship velocity component u_0, the check helm δ_0 and the hull drift angle β_0 at the average wave period T_P=10s for a pure car carrier (PCC) with a ship length of 180 m as calculation examples. The horizontal axis represents the absolute wind direction θ_W (wave direction χ is the same).

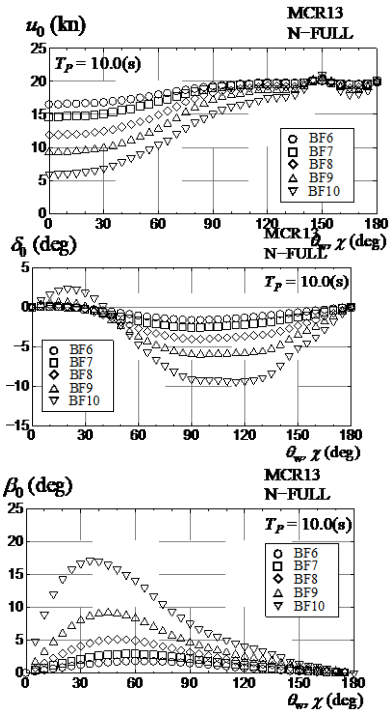

Figure 18: Results of the SSCs, including the longitudinal ship velocity component u_0, the check helm δ_0 and the hull drift angle β_0 at the average wave period T_P=10s for a pure car carrier (PCC) (Yasukawa et al., 2019)

Table 2 shows the conditions of wind and waves in the predictions of the SSP. The conditions are classified by the Beaufort (BF) Scale. The u_0 drops significantly at the head waves (wind) direction with an increase of the BF scale. The absolute value of δ_0 reaches the maximum at about 100° in θ_W (χ). However, the maximum value is almost 10° in BF10, and there is a safety margin for maximum rudder angle 35°. β_0 is over 15° in BF10 with the region of 15° to 60° of θ_W. In addition, it was shown that the studied ship had no problem in maintaining the course stability in adverse weather conditions.

Table 2: Conditions of wind and waves

Beaufort Scale	BF6	BF7	BF8	BF9	BF10
$H_{1/3}$ (m)	3	4	5.5	7	9
U_W (m/s)	13.9	17.2	20.8	24.5	28.5

Cura-Hochbaum and Uharek (2019) presented a procedure for analysing the sway-yaw-heading stability of a ship in regular waves. RANS computations for the container ship DTC in calm water and in regular waves of diverse lengths coming from several directions have been used to determine all coefficients of the mathematical model. Cura-Hochbaum and Uharek (2020) extended their study to the problem including wind with waves for the S-175 container ship.

3.4 Wave Effect on Ship Manoeuvring in Shallow Water

Manoeuvring in waves in shallow water has only been addressed by few in literature. In Tello Ruíz et al. (2019b) an extensive discussion on the experimental analysis is presented. The work investigates the effect of waves on the manoeuvring behaviour in shallow water, and also proposes a method for its modelling based on the unified method. This work has been discussed in more detail in Tello Ruíz et al. (2016) and Tello Ruíz (2018). The two-time scale method has also been applied for shallow water in Tello Ruíz et al. (2019a) for an ultra large container vessel. Validation of such results, however, still a future work.

The applications to solve the manoeuvring in waves problem in shallow water are still at an early stage of research. The problem is highly nonlinear and one must bear in mind that from

the point of view of seakeeping codes along, not only speeds effects are important but the correct simulation of squat is also needed. Even in the studies of seakeeping in shallow water, applications such as the Rankine panel method (see Mei et al., 2019) and CFD studies (see Martić et al., 2019 and Chillcce et al., 2019) require yet significant improvements.

3.5 Additional Aspect of Manoeuvring Simulation in Waves

When a vessel navigates in rough weather, it experiences a clear drop in the propulsion performance. The effects of waves on ship propulsion can be summarized as shown in Figure 19. Unfortunately, these effects are not fully understood yet.

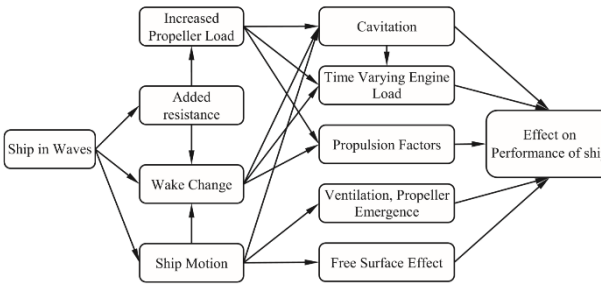

Figure 19: Effects of waves on ship propulsion (Taskar et al., 2016)

In this section to the main focus is on the effects of waves related to ship motions and ventilation on the propeller performance. Especially, propeller thrust and torque fluctuations during ship manoeuvring in waves are important when discussing the manoeuvring limit in adverse weather conditions. Furthermore, some recent researches on the simulation of two-stroke diesel engine will be introduced.

3.5.1 Effects of waves and motions on propeller performance

Fluctuations in propeller thrust and torque caused by the changes of flow field due to wave effects were observed by Nakamura and Naito (1975), Lee (1983) and Amini (2011). Propeller inflow velocity is mainly affected by pitching motion of a ship (Faltinsen et al., 1981).

By assuming the bottom of the ship to be a flat plate, the mean inflow velocity (V_{mean}) due to the pitching motion (η_5) can be calculated as:

$$V_{mean} = \sqrt{\left(1 - \frac{\Delta\overline{p}}{0.5\rho U^2}\right)} \cdot U \quad (1)$$

where,

$$\Delta\overline{p} \sim -\frac{\rho}{4}\omega_e^2 |\eta_5|^2 x^2 \quad (2)$$

Ueno et al. (2013) modelled the fluctuating velocity ($V_{fluctuating}$) due to the regular waves induced particle motion and the surge motion of a ship as follows:

$$V_{fluctuating} = (1 - w_P)\{U - \omega_e \xi_a \sin(\omega_e t - \zeta_\xi)\} + \alpha\omega h_a e^{-kz_P} \cos\chi \cos(\omega_e t - kx_P \cos\chi) \quad (3)$$

Where w_P is wake fraction, ω_e is encounter wave frequency, ξ_a is surge amplitude, ζ_ξ is phase shift of the surge motion, h_a is incident wave amplitude, k is wave number of incident waves, χ is wave direction, x_P is propeller longitudinal coordinate, z_P is propeller immersion depth. α is a correction factor defined as

$$\alpha = \begin{cases} 0.2\left(\frac{\lambda}{L|\cos\chi|}\right) + 0.5, & \text{for } \frac{\lambda}{L|\cos\chi|} \leq 2.5 \\ 1, & \text{for } \frac{\lambda}{L|\cos\chi|} > 2.5 \end{cases}$$

(4)

Based on Eqs. (1) and (3), Taskar et al. (2016) modelled the time varying total velocity (V_{total}) in waves as:

$$V_{total} = \sqrt{\left(1 - \frac{\Delta\overline{p}}{0.5\rho U^2}\right)} \cdot V_{fluctuating} \quad (5)$$

Using this formula, it is possible to simulate the propeller thrust and torque of the ship manoeuvring in waves.

By RANS simulations, Guo et al. (2012) observed significant changes in wake filed in the presence of waves and ship motions. Similar results were observed by using PIV by Sadat-Hosseini et al. (2013).

3.5.2 Effect of ventilation in propeller performance

Vertical motions of a vessel and waves bring the thruster closer to the surface and make more susceptible to ventilation. Kempf (1934) was one of the pioneers on the study of ventilation effects on propellers. He studied the torque and thrust loss due to ventilation using similar propellers of different diameters as well as different immersion ratios and rate of revolutions. Shiba (1953) discussed the influence of different propeller design parameters e.g. expanded area ratio, contour of blade, radial variation of pitch, skewback, effect of rudder, turbulence of inflow on ventilation. Gutsche (1967) presented the test results of partially submerged propellers and suggested a procedure for calculating the out-of-water effect on average thrust. Fleischer (1973) presented average thrust and torque measurements that demonstrated interaction between propeller and hull when the propeller is partially submerged.

The effect of ventilation on average thrust and torque of propellers operating in waves has been discussed by Faltinsen et al. (1981) and Minsaas et al. (1983). Kaushan (2006) performed extensive model tests on an azimuth thruster with 6 DOF measurements of forces on one of the four blades. Based on the experiments, Kozlowska et al. (2009) observed three different types of ventilation inception mechanism and investigated influence of several factors on ventilation and thrust loss.

Thrust and torque loss factors, β_T and β_Q are defined as follows,

$$\beta_T = \frac{T_t}{T_n} \quad \text{where } T_n = K_{Tn} \cdot \rho n^2 D^4 \quad (6)$$

$$\beta_Q = \frac{Q_t}{Q_n} \quad \text{where } Q_n = K_{Qn} \cdot \rho n^2 D^5 \quad (7)$$

where T_t and Q_t are propeller thrust and torque including the ventilation effect, respectively. T_n and Q_n are propeller thrust and torque in open water, respectively. The n is propeller revolution, and D is the propeller diameter. K_{Tn} and K_{Qn} are open water characteristics of propeller thrust and torque, respectively. Here we introduce a model of the thrust loss factor by Minsaas et al. (1983). β_T was modelled as:

$$\beta_T = \beta \cdot \beta_V \quad (8)$$

where β is the thrust loss factor due to loss of propeller disc area, the Wagner effect and wave making, except the effects of ventilation, was approximated as follows:

$$\beta = 1 - 0.657 \cdot [1 - 0.0769(h/R)]^{1.258}$$

$$\text{for } h/R < 1.3 \quad (9)$$

where h is the propeller submergence from the shaft centre to the free surface and R is the propeller radius.

β_V is the thrust loss for a fully ventilated propeller, and approximated as follows:

$$\beta_V = \frac{1.5 \cdot \mathrm{EAR}}{K_{Tn}} \cdot \left(\frac{\pi}{2} \cdot \alpha + \frac{2gh}{V_\infty}\right) \tag{10}$$

where α is angle of attack of a propeller blade and V_∞ is velocity of propeller blade at 0.7*R*. EAR is expanded area ratio of the propeller.

The result of these empirical relations was compared with measurements by Kozlowska et al. (2009) as shown in Figure 20. These formulas can roughly capture the thrust loss factors β_T.

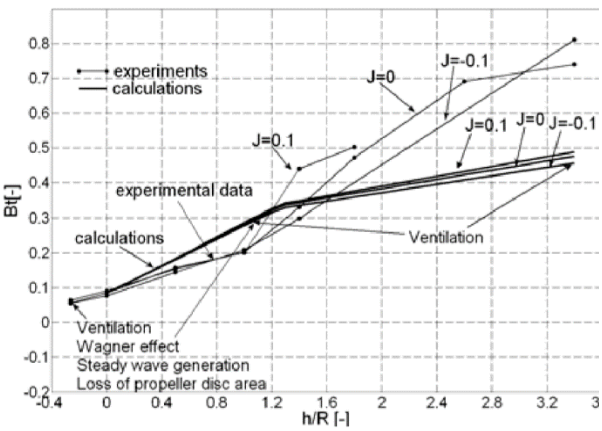

Figure 20: Comparison between calculated and experimental thrust loss factors at different advance ratios (Kozlowska et al., 2009)

3.5.3 Engine dynamics for simulation

Fluctuations of propeller loads also affect the engine performance due to shaft speed variations. Variable loads on the propeller in waves can cause mechanical failure (Amini, 2011). Livanos et al. (2006) and Theotokatos and Tzelepis (2013) studied coupled dynamics for a vessel-propeller-diesel engine system. Tanizawa et al. (2012) developed a methodology to include realistic engine response in the self-propulsion test to emulate real condition and get accurate estimates of fuel consumption in waves. Taskar et al. (2016) and Yum et al. (2017) studied unsteady interaction between engine and propeller caused by the waves from different directions by using the propeller inflow model of Eq. (5).

A generic equation of torque balance applied on propeller shaft has been described as

$$2\pi I_E \cdot \frac{dn_E}{dt} = Q_E - Q_f - Q_n \tag{11}$$

where, I_E is mass moment of inertia of the total propulsion system including main engine crank shaft, a main shaft and a propeller. n_E is rotating speed of engine. In case of no reduction gear, number of propeller rotation is identical to that of engine rotation. Q_E and Q_f stand for the engine torque and frictional torque of shaft bearing, respectively. Q_n is propeller torque. Engine torque could be given by the following non-dimensional form (Tanizawa et al., 2012):

$$\begin{cases} \bar{Q}_E = 0.5 \cdot \bar{h}_p^{\frac{2}{3}} + 1.5 \cdot \bar{h}_p^{\frac{1}{3}} \cdot \bar{n} + \bar{n}^2 \\ \bar{Q}_E = \frac{Q_E}{Q_E\,MCR},\ \bar{h}_p = \frac{h_p}{h_p\,MCR},\ \bar{n} = \frac{n}{n\,MCR} \end{cases} \tag{12}$$

where, $Q_E MCR$, $h_P MCR$, $nMCR$ are engine torque, stroke of fuel pump rack and rotating speed at the Maximum Continuous Rating, respectively.

Details on fuel flow, parameters of engine speed control system and characteristics of air and exhaust gas were described by Bondarenko et al. (2009) and Yum et al. (2017).

In the future, it is necessary to complete a simulation method that couples the equation of motion for manoeuvring in waves with the equation of motion for propeller speed considering engine characteristics, Eq. (11).

4. MINIMUM ENGINE POWER REQUIREMENT

4.1 General

To reduce the shipping's green house gases emissions via improved ship design and operation, the International Maritime Organization (IMO) adopted two mandatory mechanisms as energy efficiency standards for ships: Energy Efficiency Design Index (EEDI) for new ships and Ship Energy Efficiency Management Plan (SEEMP) for all ships.

The EEDI is an index that indicates the energy efficiency of a ship in terms of gCO_2 (generated) / tonne.mile (cargo carried); calculated for a specific reference ship operational condition. The intention is that, by imposing limits on this index, IMO will be able to drive ship technologies to more energy efficient ones over time. EEDI is thus a goal-based technical standard that is applicable to new ships. Ship designers and builders are free to choose the technologies to satisfy the EEDI requirements in a specific ship design.

There was a concern that one of the most effective ways of reducing a ship's EEDI is simply by choosing a smaller main engine or main propulsion motor for the ship, thus consequently reducing the ship's design speed. Within IMO a debate took place on how far speed reduction could be used to attain low levels of EEDI? As a result, it was decided to limit the use of this method of EEDI reduction so that it does not lead to unsafe and underpowered ships that may lose manoeuvring capability under adverse weather condition. These guidelines effectively define a methodology for estimating the minimum propulsion power for each ship for safe manoeuvring, thus ensuring that choice of the main propulsion engines/motors that satisfies these minimum requirements.

Accordingly, the purpose of the guidelines is to assist administrations in verifying that ships, complying with EEDI, have sufficient installed propulsion power to maintain the manoeuvrability in adverse weather conditions (Resolution MEPC.232(65), as amended by resolutions MEPC.255(67) and MEPC.262(68)). The guidelines currently apply to tankers, bulk carriers and combination carriers.

4.2 Assessment

The guidelines proposed for estimating the minimum power are based on two assessment levels or methods;

<u>Assessment Level 1, Minimum power lines assessment</u>: This is a simple approach and involves calculation of the minimum power from a specific line as a function of ship deadweight. For this purpose, the verifier should check if the ship has an installed power not less than the minimum power defined by the line represented by the following equation:

$$\text{Minimum Power Line Value [MCR, kW]} = a \times (DWT) + b \qquad (13)$$

where "a" and "b" are constants and vary with ship type. There had been some discussion on the determination of these parameters (Table 3), and present values were decided at the 68th MEPC meeting (MEPC.262(68)).

The effects of these parameters can be reviewed by applying the minimum power lines to the recently built bulk carriers and tankers. From the IHS Sea web database (https://maritime.ihs.com), 1,517 bulk carriers and 874 tankers, which were built after 2000, were selected, and the minimum power lines are applied as shown in Figure 21. MCR power of the recently built ships (red circles) are a little bit smaller than the ships built before 2014. Most of the ships are compatible with the

previous criteria. But some ships cannot satisfy the strengthened present criteria.

Table 3: Parameter a and b for determination of the minimum power line values for the different ship types

Reference	Ship Type	a	b
MEPC 64/4/13 (IACS et al.)	BC (DWT<275,825 ton) BC (DWT≥275,825 ton)	0.0606 0.0273	4195.2 13366.0
	Tankers	0.0603	5495.5
MEPC 64/4/42 (Japan & ROK)	BC (DWT<275,825 ton) BC (DWT≥275,825 ton)	0.0606 0.0273	2648.0 11818.8
	Tankers	0.0603	3294.0
Resolution MEPC.232(65)	BC	0.0687	2924.4
	Tankers	0.0689	3253.0
Resolution MEPC.262(68)	BC (DWT<145,000 ton) BC (DWT≥145,000 ton)	0.0763 0.0490	3374.3 7329.0
	Tankers	0.0652	5960.2

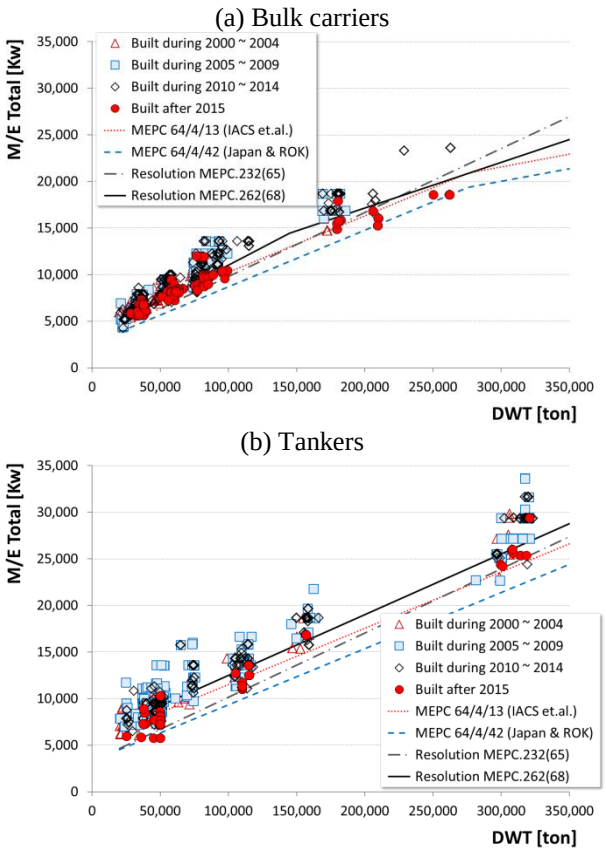

Figure 21: Application of minimum power lines.

Assessment Level 2, Simplified assessment: This is a more mathematically involved method. The assessment procedure consists of two steps:

Step 1: Definition of the required advance speed in head wind and waves, ensuring course-keeping in all wave and wind directions.

Step 2: Assessment whether the installed power is sufficient to achieve the above required advance speed.

Details of the assessment methods are given in the 2013 Interim Guidelines (MEPC.262(68)).

4.3 Subsequent Discussions on the Assessment

(1) DISCUSSION IN IMO MEPC71

At MEPC 71, two issues were discussed; China (MEPC 71/5/8, 2017) proposed amendments in light of the thrust deduction factor and the added resistance in wave. Although numerical and experimental results on the four tankers were submitted, it was not sufficient to draw support for the amendment. The second one was related to providing information on the progress and present status of the work of developing a draft revision of 2013 Interim Guidelines based on the research projects of SHOPERA and JASNAOE (MEPC 71/5/13, 2017, MEPC 71/INF.28, 2017). The project proposed the amendments shown in Table 4. Note that more severe adverse weather conditions were proposed than 2013 Interim Guidelines and more relaxed ship propulsion ability was proposed. For the latter, from previous 4 knots to 2 knots under the scenario of weather-vanning in coastal area under strong gale (see Table 5.)

Table 4: Proposed amendments on the adverse weather conditions (MEPC 71/5/13)

	Existing Guidelines	Draft revised Guidelines

Beaufort number	BF7 for L_{PP} < 200m BF8 for L_{PP} ≥ 250m	BF8 for L_{PP} < 200m BF9 for L_{PP} ≥ 250m
Wind speed	15.7m/s for L_{PP} < 200m 19.0m/s for L_{PP} ≥ 250m	19.0m/s for L_{PP} < 200m 22.6m/s for L_{PP} ≥ 250m
Hs	4m for L_{PP} < 200m 5.5m for L_{PP} ≥ 250m	4.5m for L_{PP} < 200m 6.0m for L_{PP} ≥ 250m

Table 5: Proposed amendments on the scenario for the evaluation of the sufficiency of ship's propulsion power to maintain the manoeuvrability in the adverse condition (MEPC 71/5/13)

Area	Coastal area
Weather condition	BF8 (gale) for L_{PP} < 200m BF9 (strong gale) for L_{PP} ≥ 250m, linear over L_{PP} between 200m to 250m
Encountered wave and wind angle	Head seas to 30 degrees off-bow for a situation of weather-vanning
Propulsion ability	Speed through water at least 2 knots
Steering ability	Ability to keep heading into head seas to 30 degrees off-bow

However, considering that there were still different views on the adverse environmental conditions, it was further proposed that finalizing the draft revised guidelines at MEPC 71 would be premature and the Committee continue the discussion in parallel with the discussion of the EEDI review for phase 3 EEDI requirements. The Committee decided to consider the issue further at MEPC 72 and to extend the applicability of the 2013 Interim Guidelines to phase 2 EEDI requirements as an interim solution (MEPC 71/17, 2017).

(2) DISCUSSION IN IMO MEPC72

At MEPC 72, China proposed that thrust deduction factor can be conservatively defined as 0.1 and wake fraction can be defined as 0.15, based on the model test results of wake fraction and thrust deduction at low speeds of a ship (MEPC 72/5/9, 2018).

China also provided information on an alternative numerical method for calculating quadratic transfer function of the added resistance in regular waves applied in the 2013 Interim Guidelines (MEPC 72/INF.16, 2018).

However, it was discussed that more background data should be provided to validate the proposed method. So, a further submission was requested for MEPC 73 (MEPC 72/17, 2018).

(3) DISCUSSION IN IMO MEPC73

At MEPC 73, two issues were proposed. One is allowing for a shaft power limitation in order to resolve potential conflict between EEDI requirement and minimum required propulsion power (MEPC 73/5/1, 2018). The other is providing information on the work done on the minimum power requirements for ships in adverse conditions in the Netherlands (MEPC 73/INF.13, 2018).

Germany et al. proposed to limit the ship's shaft power for normal operation to meet the EEDI target whilst reserving extra power for adverse weather conditions (MEPC 73/5/1, 2018). Whilst there was general support, concerns were also expressed on the proposed idea on actual implementation mechanism and, especially when the use of reserve power is appropriate and allowed, and further consideration on how to certify NOx EIAPP scheme under the regulation 13 of MARPOL Annex VI if the reserved power for an engine is allowed. To improve the idea and for further discussion, it was agreed to keep consideration at next session (MEPC 73/19, 2018).

(4) DISCUSSION IN IMO MEPC74

China provided further validation of the numerical method for calculating the quadratic transfer function of the added resistance in regular waves (MEPC 74/INF.38)

Denmark introduced a concept to increase engine torque at low engine loads called the "adverse weather condition" function, by which an engine could ensure sufficient power to the ship in adverse condition as shown in Figure 22. It was concluded that the load diagram extension offers a potential solution that will enable fulfilment of the required minimum propulsion power at adverse weather conditions without negative impacts on emissions and within the current regulatory framework (MEPC 74/5/17, 2019).

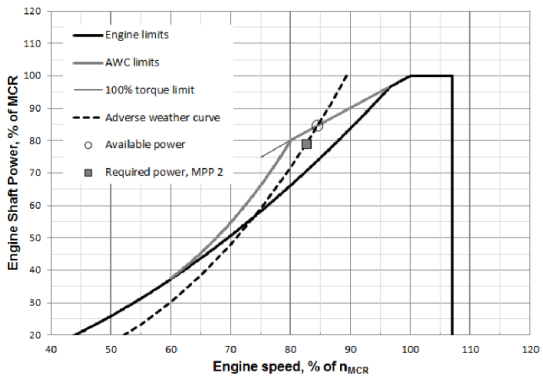

Figure 22: Extension of engine load limit by "Adverse Weather Condition" functionality (Denmark, MEPC 74/5/17, 2019)

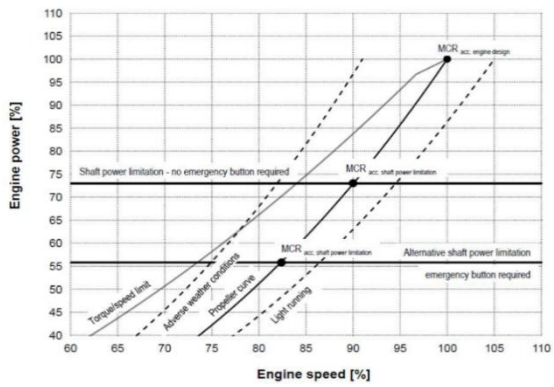

Figure 23: Concept of Shaft/Engine Power Limitation (France et al., MEPC 74/5/5, 2019)

France et al. proposed a refined proposal for Shaft Power Limitation ("ShaPoLi") related to the minimum propulsion as shown in Figure 23. (MEPC 74/5/5, 2019). The use of power reserve can be proceeded as follows:

1. In case of emergency (e.g. manoeuvrability in adverse conditions) the master can press / release an "emergency button" to use the power reserve (full installed engine power or torque reserve whatever the technical details of the power reserve provided);
2. In case of pressing the "emergency button", some defined conditions of the ship and of the engine will be automatically recorded in a tamper proof system which is part of the Shaft / Engine Power Limitation – device. Afterwards, the condition can be checked by the Administration or by a port State inspector;
3. Thereby, the installed engine power will remain as high as needed to maintain a ship's manoeuvrability in adverse condition, but for normal operation the power will be limited to the level set by the EEDI requirements; and
4. For calculation of attained EEDI for new ships, P_{ME} with the concept of power limitation would be on 75% of $MCR_{limited}$, and minimum propulsion power would be provided with some margins for reserved power.

Meanwhile, some objections and comments against the "ShaPoLi" was presented as (1) The proposal on "ShaPoLi" should not be agreed until the draft minimum propulsion power guidelines have been finalized and agreed by the Committee (MEPC 74/5/26, 2019), (2) The proposal on "ShaPoLi" should not be accepted as such a change to the power definition would undermine the intended goals of EEDI and would not result in improved energy efficiency for ships and (3) The shaft power limitation should be set with 15% sea margin (i.e. P_{ME} = 0.75 × 0.85 MCR ~ 0.64 MCR), so as to be in line with the recent shipbuilding practice (MEPC 74/5/31, 2019).

There were many supports on the application of "ShaPoLi" in resolving the improvement in energy efficiency with concerns over minimum

power especially for large bulk carriers and oil tankers. However, there were still significant technical barriers to be addressed including which engine power should be used for NOx certification of marine diesel engine, etc; and there were concerns that "ShaPoLi" concept could discourage technical innovation as the same engine would have a lower EEDI, also there would be challenges for port State control. Hence, the Committee decided to further consideration at next session with concrete proposals on the shaft power.

(5) DISCUSSION IN IMO MEPC75

France et al. proposed an updated proposal for shaft power limitation (MEPC 75/6/6). For further discussion to improve the concept, it was agreed to consider this matter at a future session. It was also agreed to proceed with the revision work for the finalization of the Interim Guidelines.

For the finalization at MEPC 76, Corresponding Group was established. Definition of the "Adverse conditions" and assessment procedure (Deletion/Retention of Appendix 2, assessment Level 2) are being discussed.

4.4 Investigation on the effects of other factors for the assessment

The issues brought from MEPC 71 and following meetings can be categorized into four items. The first is the definition of adverse weather condition, the second is the calculation of added resistance in wave, the third is the determination of self-propulsion factors, and the last is the selection of the engine operation limits. The first three items are related with the Level 2, Simplified assessment. The effects of these items are reviewed by applying the assessment to KVLCC2. KVLCC2 is the second variant of the KRISO tanker which has been used as a benchmark test vessel for manoeuvrability study.

For the Simplified assessment, some parameters, such as the windage areas, dead weight, MCR power and RPM, are necessary. These parameters are assumed as Table 6. (Deadweight and MCR power are the averaged values of the VLCC built between 2000~2004, windage area are estimated from the similar ships). Under these assumptions, KVLCC2 complies with the minimum power line assessment criteria.

Table 6: Assumed parameters of KVLCC2 for the application of simplified assessment

Windage area		Deadweight / MCR	
Frontal, A_{FW} [m^2]	920	Deadweight [ton]	302,273
Lateral, A_{LW} [m^2]	3,300	Power $_{MCR}$ [kW]	26,341
		RPM $_{MCR}$ [-]	81

4.4.1 EFFECT OF ADVERSE WEATHER CONDITIONS

There have been four suggestions on the definition of adverse weather conditions. For ships whose length is larger than 250m, it can be summarized in Table 7.

Table 7: Adverse weather conditions for ships with L_{PP} > 250 m ($H_{1/3}$: Significant wave height, T_P: Peak period, V_W: Mean wind speed)

References	$H_{1/3}$ [m]	T_P [s]	V_W [m/s]
Resolution MEPC.262(68)	5.5	7.0~15.0	19.0
MEPC 64/4/13 (IACS)	6.0	8.0~15.0	19.0
MSC 93/21/5 (Greece)	7.0	-	23.0
MEPC 71/5/13 (Denmark)	6.0	8.8~12.2	22.6

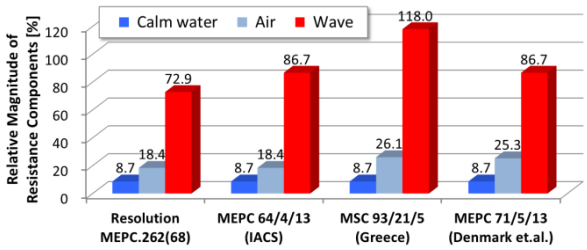

Figure 24: Relative magnitude of resistance components under different adverse weather conditions (100% means the total resistance by the Resolution MEPC.262(68))

Figure 24 shows the relative magnitudes of each resistance components with respect to the total resistance calculated by the present Interim Guidelines, Resolution MEPC.262(68). For this comparison, the wave added resistance were estimated by i-STAP. i-STAP is an ISO 15016 based speed trial analysis program develop by KRISO (Shin et al., 2016). The ratios of wind and wave added resistances are increased as the wind speed and the significant wave height are increased. In all cases, the wave added resistance amounts to more than 70% of the total resistance. This means that the accurate estimation of low speed wave added resistance can be one of the decisive factors for the simplified assessment.

The ratio of required power over the available power is shown as Figure 25. If this ratio is large than 100%, it means that the vessel is not compatible with the simplified assessment. Except the worst weather condition, MSC 93/21/5, the vessel satisfy the simplified assessment criteria with 6~12% power margin.

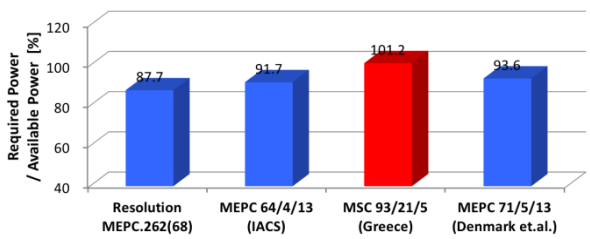

Figure 25: Ratio of the required power over the available power under different adverse weather conditions

4.4.2 EFFECT OF WAVE ADDED RESISTANCE ESTIMATION

According to the 2013 interim guidelines for determining minimum propulsion power, the added resistance in waves can be calculated by the quadratic transfer function. This function can be obtained from the added resistance test in regular waves at the required ship advance speed as per ITTC procedures 7.5-02 07-02.1 and 7.5-02 07-02.2 or from equivalent method verified by the Administration.

The required ship speed for the minimum power assessment usually ranges between 4 and 6 knots. Hence, due to the reflected waves, it is quite difficult to perform the model tests in the conventional towing and the square basin tests have been preferred. For the KVLCC2, Sprenger et al. (2017) performed the model test at F_n = 0.055 (corresponding to 6 knots in full scale) as a part of the SHOPERA project. This kind of model tests are possible but may not practicable for routine ship design purposes, as few such facilities exist. Therefore, the empirical formulae or the potential based calculations have been used as a practical alternative. Table 8 shows some estimation methods for the added resistance in waves for comparison study.

Table 8: Estimation methods for the added resistance in waves for comparison

Types	Name	Motion induced	Reflection correction
Empirical	STAWAVE2 (Boom et al., 2013)	Jenkine's method	Experimental data
	MEPC 70/INF.33		
2D strip	SLE	Maruo method	Faltinsen
	i-STAP (Shin et al., 2016)		NMRI emprical
	PrimeShip (Class NK)		
3D panel	WISH (Park et al., 2014)	Pressure integration	

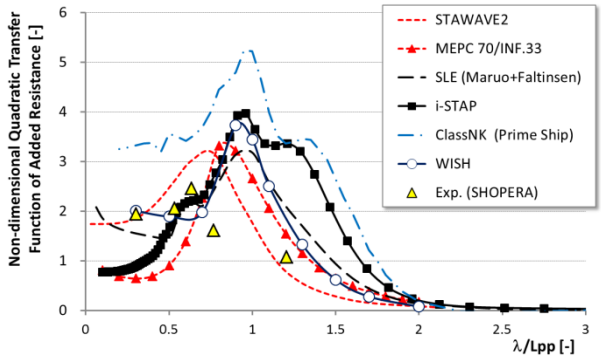

Figure 25: Non-dimensional quadratic transfer function of the wave added resistance for KVLCC2 at F_n = 0.055

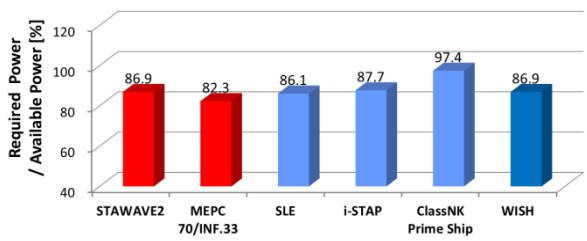

Figure 26: Ratios of the required power over the available power by the various different wave added resistance estimates

The non-dimensional quadratic transfer functions are compared with the results of empirical formulae or potential based calculations in Figure 25. Appreciable variances between the estimation methods could be found. The ratios of required power over the available power are shown in Figure 26. All the estimation methods comply with the simplified assessment criteria in the assumed KVLCC2 case. The MEPC 70/INF.33, which is an empirical formulae based on SHOPERA project, satisfies the criteria with a relatively large margin, while the PrimeShip gives the most conservative result.

4.4.3 EFFECT OF SELF-PROPULSION FACTORS

According to the Interim Guidelines, self-propulsion factors (wake fraction, *w*, and thrust deduction factor, *t*) can be obtained either from model tests or empirical formula. The recommended conservative estimates are given in the Interim Guidelines.

China noted that the values of thrust deduction factor and wake fraction obtained from the model test are fairly lower than those obtained from the Interim Guidelines. China was of the view that the value of thrust deduction factor should be obtained from required ship advance speed. That is it should be higher than the value in bollard pull state (about 0.04 for single screw ships), and lower than the value in calm water condition with design speed (about 0.2 for single screw ships). China proposed that the thrust deduction factor can be set to 0.1 (MEPC 71/5/8, 2017), and wake fraction can be conservatively defined as 0.15 (MEPC 72/5/9, 2018).

Table 9 shows four sets of the wake fraction and thrust deduction factors for KVLCC2. As was noted by China, the estimates for *t* and *w* by the Interim Guidelines are similar to those values at calm sea design speed. Considering that the required ship advance speed is about 4~6 knots and the added resistances are about ten times larger than the calm water resistance, the estimates by the Interim Guidelines do not seem to be realistic ones.

Table 9: Estimates on wake fraction and thrust deduction factors for KVLCC2

References	Wake fraction, *w*	Thrust deduction factor, *t*
Resolution MEPC.262(68)	0.350	0.245
Calm sea at F_n=0.141	0.347	0.233
MEPC 71/5/8 (China)	0.350	0.100
MEPC 72/5/9 (China)	0.150	0.100

Figure 27 shows the available power (dashed line) and the required powers for the different self-propulsion factors of Table 9. As the estimated values of the Interim Guidelines (△)

and the calm sea design speed (◆) are similar, the required powers are almost the same. When only the small thrust deduction factor (□) is used, the required RPM and power are lower than the Interim Guidelines, but the available power margin is almost the same. When the both self-propulsion factors are changed (●), the required RPM and power are higher than the Interim Guidelines and the power margin is smaller than the Guidelines. This shows that the simplified assessment result can be affected by the estimates of self-propulsion factors and the estimates of the Guidelines are not the most conservative case. Hence, the more realistic estimates on these factors may results in the more reliable simplified assessment.

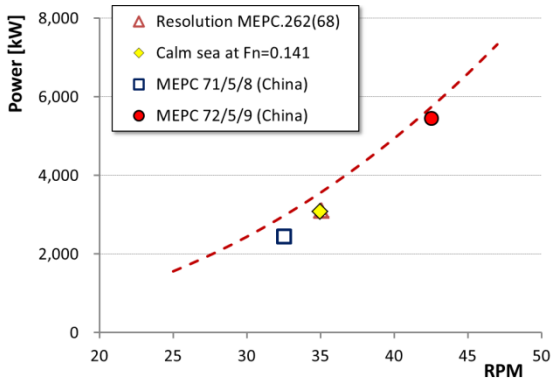

Figure 27: Effects of wake fraction and thrust deduction factors for KVLCC2 (Dashed line is a power limit curve under the assumed MCR condition)

5. CONCLUSIONS

5.1 Prediction Methods of Ship Manoeuvring in Waves

A large number of works on manoeuvring in waves methods have been published during in this period. Experimental research remains valuable and is being used complementary to numerical research. Due to technological developments in progress, tests in irregular waves with large wave height are becoming more feasible.

Direct CFD simulations of ship maneuvering in waves were presented by several authors. Using CFD simulations of self-propulsion and turning motions as well as zig-zag maneuvers of a free running ship model in regular waves can be conducted. However, due to the high computational cost and even longer time simulation requirement, direct CFD maneuvering simulations in irregular waves are still a changeling problems.

Until now, the problem of manoeuvring in deep water waves has been mainly treated, but the problem has been extended to shallow water area.

As an application example of the calculation of manoeuvring in waves, there are many studies on the manoeuvring limit of ships by analysing the steady sailing performance.

5.2 Benchmark data

The SIMMAN research project has facilitated new data for the KCS and the ONRT in regular waves. These data is quite valuable to support the validation and certification of numerical simulation method.

5.3 Minimum Engine Power Requirement

The issues brought about from IMO-MEPC71 and following meetings were addressed concerning the minimum power requirements. The accurate estimations of the wave added resistance and the self-propulsion factors in higher propeller load condition are a decisive factor for the simplified assessment.

6. RECOMMENDATIONS

Update the following guidelines:

- Free Running Model Tests in Waves
- Captive Model Tests for Measuring Forces in Waves

To improve the numerical method for manoeuvring in waves, the following actions are needed:

- Validate the numerical methods for mean wave drift forces, especially steady lateral force and steady yaw moment acting on an advancing ship in cooperation with the seakeeping committee.

- Provide the captive test data on the hydrodynamic forces acting on the ship in waves, such as
    - ✓ Oblique towing test data in waves
    - ✓ Circular motion test data in waves
    - ✓ PMM test data in waves
    - ✓ Rudder force data in waves when ship is straight moving.

for validation of CFD in cooperation with the manoeuvring committee.

- Investigate the effect of wave height on the propeller performance and the coupling with the main engine in cooperation with the propulsion committee.

Validate the Level 2 – Simplified Assessment Method of the 2013 Interim Guidelines (MEPC.232(65)) by enhanced and comprehensive methods.

Investigate the concept of "Shaft Power Limitation" (ShaPoLi) introduced for the first time at MEPC 73 (MEPC 73/5/1) and deliberated at following sessions (MEPC 74/5/5, MEPC 75/6/6), as a measure to overcome intrinsic conflict between safety and environmental regulatory requirements.

7. REFERENCES

Amini, H., 2011, "Azimuth Propulsors in Off-design Conditions", Norges teknisk-naturvitenskapelige universitet, Trondheim.

Ankudinov, V, 1983, "Simulation Analysis of Ship Motion in Waves", International Workshop on Ship and Platform Motions. Berkeley, California.

Araki, M., Umeda, N., Hashimoto, H., and Matsuda, A., 2011, "An Improvement of Broaching Prediction with a Nonlinear 6 Degrees of Freedom Model", J. Japan Society of Naval Architects and Ocean Engineers, 14, 85–96.

Asai, S., 1981, "A Study on Check Helms for Course Keeping of a Ship under Steady External Forces", J. Society of Naval Architects of Japan 150, 245-253.

Aung, M. Z., and Umeda, N., 2020, "Manoeuvring Simulations in Adverse Weather Conditions with the Effects of Propeller and Rudder Emergence Taken into Account", Ocean Engineering 197, 106857.

Ayaz, Z., Vassalos, D., and Turan, O, 2006, "Parametrical Studies of a New Numerical Model for Controlled Ship Motions in Extreme Astern Seas", J. Marine Science and Technology 11(1), 19–38.

Bailey, P. A., Price, W. C., and Temarel, P., 1998, "A Unified Mathematical Model Describing the Manoeuvring of a Ship Travelling in a Seaway", RINA, 140, 131–149.

Bondarenko, O., Kashiwagi, M., and Naito, S., 2009, "Dynamics of Diesel Engine in the Framework of Ship Propulsion Plant", Conference Proceedings, The Japan Society of Naval Architects and Ocean Engineers, Vol.8, 335-338.

Boom, H. Van den, Huisman, H. and Mennen, F., 2013, "New Guidelines for Speed Power Trials, Level Playing Field Established for IMO EEDI", SWZ Maritime.

Carrica, P. M., Ismail, F., Hyman, M., Bhushan, S. and Stern, F., 2012, "Turn and Zigzag Maneuvers of a Surface Combatant using a URANS Approach with Dynamic Overset Grids", J. Marine Science and Technology 18, 166–181.

Chillcce, G., and El Moctar, O., 2018, "A Numerical Method for Manoeuvring Simulation in Regular Waves", Ocean Engineering 170, 434-444.

Chillcce, G., Martić, I., Tello Ruíz, M., Ramirez, J., Degiuli, N., and el Moctar, B., 2019, "Rans Evaluation of the DTC's Vertical Motion Sailing in Finite Water Depth Waves". MASHCON2019. Ostend, Belgium.

Choi, H., Kim, D. J., Kim, Y. G., Yeo, D. J., Yun, K., and Lee, G. J., 2019, "An Experimental Study on the Captive Model Test of KCS in Regular Waves," MASHCON2019. Ostend, Belgium.

Cummins, W. E., 1962, "The Impulse Response Function and Ship Motions". Schiffstechnik 9, 101–109.

Cura-Hochbaum, A. and Uharek, S., 2016, "Prediction of Ship Manoeuvrability in Waves based on RANS Simulations", 31st ONR Symp. on Naval Hydrodynamics, Monterey, CA.

Cura-Hochbaum, A. and Uharek, S., 2019, "On the Heading Stability of a Ship in Waves", Ship Technology Research 66:2, 75-82

Cura-Hochbaum, A. and Uharek, S., 2020, "Prediction of Heading Stability under Wind and Waves", 33rd Symposium on Naval Hydrodynamics, Osaka, Japan.

Eda, H., 1968, "Low-Speed Controllability of Ships in Wind", J. Ship Research 12(3):63, 181-200.

Faltinsen, O. M., Minsaas, K. J., Liapis, N., Skjørdal, S. O., 1981, "Prediction of Resistance and Propulsion of a Ship in a Seaway", 13th Symposium on Naval Hydrodynamics, Tokyo, Japan.

Fleischer, K.P., 1973, "Untersuchungen über das Zusammenwirken von Schiff und Propeller beiteilgetauchten Propellern" Publication 35/73 of Forschungszentrum des Deutschen Schifbaus, Hamburg, Germany.

Fujiwara, T., Ueno, M. and Ikeda, Y., 2005, "Cruising Performance of Ships with Large Superstructures in Heavy Sea --1st report: Added resistance induced by wind—", J. Japan Society of Naval Architects and Ocean Engineers 2, 257-269.

Fujiwara, T., Ueno, M. and Ikeda, Y., 2006, "Cruising Performance of Ships with Large Superstructures in Heavy Sea --2nd report: Added resistance induced by wind and waves, and optimum ship routing—", J. Japan Society of Naval Architects and Ocean Engineers 3, 147-155.

Fujiwara, T., Ninura, T., Minami, Y., Sasaki, N., and Takagi, K., 2008, "Free-running Model Test on a Large Container Ship Under Wind and Waves at Towing Tank", J. Japan Society of Naval Architects and Ocean Engineers 8, 155-162.

Guo, B. J., Steen, S., Deng, G. B., 2012, "Seakeeping Prediction of KVLCC2 in Head Waves with RANS", Applied Ocean Research 35, 56-67.

Gutsche, F., 1967, "Einfluss der Tauchung auf Schub und Wirkungsgrad von Schiffspropellern", Shiffbauforschung 6 5/6/67, 256-277, Berlin, Germany.

Hasnan, M. A. A., Yasukawa, H., Hirata, N., Terada, D. and Matsuda, A., 2020, "Study of Ship Turning in Irregular Waves", J. Marine Science and Technology 25(4), 1024–1043

Hasnan, M. A. A. and Yasukawa, H., 2020, "6-DOF Motion Simulation of a Ship Turning in Irregular Waves", 33rd Symposium on Naval Hydrodynamics, Osaka, Japan.

Hirano, M., Takashina, J., Takeshi, K., and Saruta, T., 1980, "Ship Turning Trajectory in Regular Waves", Trans. West-Japan Society of Naval Architects 60, 17–31.

Hirano, M., Takashina, J. and Moriya, S., 1984, "Ship Maneuverability in Wind", J. Society of Naval Architects of Japan 155, 122-131.

Ishibashi, K., 1975, "On Course Stability and Manoeuverable Range of Wind Velocity in the Uniform Wind", J. Society of Naval Architects of Japan 138, 165-177.

Kadomatsu, K., Inoue, Y. and Takarada, N., 1990, "On the Required Minimum Output of Main Propulsion Engine for Large Fat Ship with Considering Manoeuverability in Rough Seas", J. Society of Naval Architects of Japan 168, 171-182.

Kempf, G., 1934, "The Influence of Viscosity on Thrust and Torque of a Propeller Working Near the Surface", Trans. the Institution of Naval Architects, 321-326, London, UK.

Kim, D. J., Yun, K., Park, J. Y., Yeo, D. J., and Kim, Y. G., 2019a, "Experimental Investigation on Turning Characteristics of KVLCC2 Tanker in Regular Waves", Ocean Engineering 175(1), 197-206.

Kim, D. J., Yun, K., Choi, H., Yeo, D. J., and Kim, Y. G., 2019b, "Turning Characteristics of KVLCC2 Tanker in Long-crested Irregular Head Waves", International Conference on Advanced Model Measurement Technology for the Maritime Industry (AMT19).

Koushan, K, 2006, "Dynamics of Ventilated Propeller Blade Loading on Thrusters" World Maritime Technology Conference, ISBN 1-902536-54-1, London, UK.

Kozlowska, A. M., Steen, S. and Koushan, K., 2009, "Classification of Different Type of Propeller Ventilation and Ventilation Inception Mechanisms", First International Symposium on Marine Propulsors, SMP09, Trondheim, Norway.

Lee, C. S., 1983, "Propeller in Waves", The 2nd International Symposium on Practical Design in Shipbuilding (PRADS), Tokyo & Seoul.

Lee, S.-K., 2000, "The calculation of Zig-Zag Maneuver in Regular Waves with Use of the Impulse Response Functions", Ocean Engineering 27(1), 87–96.

Lee, S., Hwang, S., Yun, S., Rhee, K. and Seong,

W., 2009, "An Experimental Study of a Ship Manoeuvrability in Regular Waves", International Conference on Marine Simulation and Ship Manoeuvrability (MARSIM'09), Panama City.

Lee, J-H., and Kim, Y., 2020, "Study on Steady Flow Approximation in Turning Simulation of Ship in Waves", Ocean Engineering 195, 1-19.

Lee, J-H., Kim, Y., Kim, D-J., and Kim, Y-G., 2020, "Numerical Investigation and Experimental Validation on Maneuverability of KVLCC2 Tanker in Regular Waves", 33rd Symposium on Naval Hydrodynamics, Osaka, Japan.

Livanos, G. A., Simotas, G. N., Dimopoulos, G. G., and Kyrtatos, N. P., 2006, "Simulation of Marine Diesel Engine Propulsion System Dynamics During Extreme Maneuvering", ASME 2006 Internal Combustion Engine Division Spring Technical Conference, American Society of Mechanical Engineers.

Martin, L. L., 1980, "Ship Maneuvering and Control in Wind", SNAME Trans. 88, 257-281.

Martić, I., Chillcce, G., Tello Ruíz, M., Ramirez, J., Degiuli, N., and el Moctar, B., 2019, "Numerical Assessment of Added Resistance in Waves of the DTC Container Ship in Finite Water Depths". MASHCON2019. Ostend, Belgium.

McCreight, W. R., 1986, "Ship Manoeuvring in Waves". 16th Symposium on Naval Hydrodynamics, 456–469.

Mei, T. L., Delefortrie, G., Ruiz, M. T., Lataire, E., Vantorre, M., Chen, C., and Zou, Z. J., 2019, "Numerical and Experimental Study on the Wave-Body Interaction Problem with the Effects of Forward Speed and Finite Water Depth in Regular Waves", Ocean Engineering 192.

MEPC.232(65), 2013, "2013 Interim Guidelines for Determining Minimum Propulsion Power to Maintain the Manoeuvrability of Ships in Adverse Conditions".

MEPC.255(67), 2014, "Amendments to the 2013 Interim Guidelines for Determining Minimum Propulsion Power to Maintain the Manoeuvrability of Ships in Adverse Conditions (Resolution MEPC.232(65))" .

MEPC.262(68), 2015, "Amendments to the 2013 Interim Guidelines for Determining Minimum Propulsion Power to Maintain the Manoeuvrability of Ships in Adverse Conditions (Resolution MEPC.232(65), As Amended by Resolution MEPC.255(67))".

MEPC 71/5/8, 2017, "Proposed amendments to the 2013 Interim Guidelines for determining minimum propulsion power to maintain the manoeuvrability of ships in adverse conditions".

MEPC 71/5/13, 2017, "Progress and present status of the draft revised Guidelines for determining minimum propulsion power to maintain the manoeuvrability of ships in adverse conditions".

MEPC 71/INF.28, 2017, "Draft revised Guidelines for determining minimum propulsion power to maintain the manoeuvrability of ships in adverse conditions".

MEPC 71/17, 2017, "Report of the Marine Environment Protection Committee on Its Seventy-First Session".

MEPC 72/5/9, 2018, "Proposed amendments to the 2013 Interim Guidelines for determining minimum propulsion power to maintain the

manoeuvrability of ships in adverse conditions".

MEPC 72/INF.16, 2018, "An alternative numerical method for calculating quadratic transfer function of the added resistance in regular waves applied in the 2013 Interim guidelines for determining minimum propulsion power to maintain the manoeuvrability of ships in adverse conditions".

MEPC 72/17, 2018, "Report of the Marine Environment Protection Committee on Its Seventy-Second Session".

MEPC 73/19, 2018, "Report of the Marine Environment Protection Committee on Its Seventy-Third Session"

MEPC 73/5/1, 2018, "Proposal for an Option to Limit the Shaft Power while ensuring a Sufficient Safety Power Reserve in Adverse Weather Conditions".

MEPC 73/INF.13, 2018, "Information on further work on minimum power requirements for ships".

MEPC 74/5/5, 2019, "Updated proposal for an option to limit the shaft / engine power while ensuring a sufficient safety power reserve in adverse weather conditions".

MEPC 74/5/17, 2019, "Adverse weather condition functionality".

MEPC 74/INF.38, 2019, "Further validation of the method proposed in document MEPC 72/INF.16 for calculating quadratic transfer function of the added resistance in regular waves applied in the 2013 Interim Guidelines for determining minimum propulsion power to maintain the manoeuvrability of ship in adverse".

MEPC 74/5/26, 2019, "Comments on documents MEPC 74/5/5".

MEPC 74/5/29, 2019, "Comments on document MEPC 74/5/5".

MEPC 74/5/31, 2019, "Comments on document MEPC 74/5/5".

MEPC 75/6/6, 2019, "Updated Proposal for the Shaft/Engine Power Limitation Concept (SHaPoLi)".

Minsaas, K., Faltinsen, O. M., Persson, B., 1983, "On the Importance of Added Resistance, Propeller Immersion and Propeller Ventilation for Large Ships in a Seaway", Second International Symposium on Practical Design in Shipbuilding (PRADS), 149-159. Seoul and Tokyo.

Naito, S. and Takagishi, K., 1998, "Time Mean Behavior of Large Full Ships in the Sea", J. Kansai Society of Naval Architects, Japan, No.229, pp.57-68.

Nakamura, S. and Naito S., 1975, "Propulsive Performance of a Container Ship in Waves", J. Kansai Society of Naval Architecture, Japan 158.

Nishimura, K., and Hirayama, T., 2003, "Manoeuvring and Motion Simulation of a Small Vessel in Waves". MARSIM2003, pp. RC-10(1)-RC-10(9), Kanazawa, Japan.

Nonaka, K., 1990, "Manoeuvring Motion of a Ship in Waves", International Conference on Marine Simulation (MARSIM1990), Tokyo, 422-430.

Ogawa, A., 1969, "Calculation on the Steered Motion of a Ship under the action of External Forces (1)", J. Society of Naval Architects of Japan 126, 107-120.

Ogawa, A., Koyama, T. and Kijima, K., 1977, "MMG report-I, On the Mathematical Model of Ship Manoeuvring", Bulletin of Society of Naval Architects of Japan 575, 22-28.

Papanikolaou, A., Fournarakis, N., Chroni, D., Liu, S., and Plessas, T., 2016, "Simulation of the Maneuvering Behaviors of Ships in Adverse Weather Conditions", 31st Symposium on Naval Hydrodynamics, Monterey, CA.

Park, D.M., Seo, M.G., Lee, J., Yang, K.K. & Kim, Y., 2014, "Systematic experimental and numerical added analyses on added resistance in waves", Journal of the Society of Naval Architects of Korea, Vol.51(6), pp.459-479

Piro, D., White, P., Knight, B., Maki, K. and Kring, D., 2020, "Prediction of Ship Maneuvering in Waves Using a Combined RANS and Potential Flow Approach", 33rd Symposium on Naval Hydrodynamics, Osaka, Japan.

Sadat-Hosseini, H., Wu, P.C., Carrica, P.M., Kim, H., Toda, Y., and Stern, F., 2013, "CFD Verification and Validation of Added Resistance and Motions of KVLCC2 with Fixed and Free Surge in Short and Long Head Waves", Ocean Engineering 59, 240-273.

Sanada, Y., Tanimoto, K., Takagi, K., Gui, L., Toda, Y., and Stern, F., 2013, "Trajectories for ONR Tumblehome Maneuvering in Calm water and Waves", Ocean Engineering 72, 45-65.

Sanada, Y., Elshiekh, H., Toda, Y., and Stern, F., 2019, "ONR Tumblehome Course Keeping and Maneuvering in Calm Water and Waves", J. Marine Science and Technology 24(3), 948-967.

Seo, M.-G., and Kim, Y., 2011, "Numerical Analysis on Ship Maneuvering Coupled with Ship Motion in Waves". Ocean Engineering 38, 1934–1945.

Shen, Z. and Korpus, R., 2015, "Numerical Simulations of Ship Self-Propulsion and Maneuvering Using Dynamic Overset Grids in OpenFOAM", Workshop on CFD in Ship Hydrodynamics, Vol. III, Tokyo.

Shiba, H., 1953, "Air Drawing of Marine Propellers", Trans. Technical Research Institute, Report no. 9.

Shigunov, V., and Papanikolaou, A., 2015, "Criteria for minimum powering and maneuverability in adverse weather conditions", Ship Technology Research 62(3), 140-147.

Shin, M.S, Park, B.J., Lee, G.J. & Ki, M.S., 2016, "Revision of ISO15016 for the EEDI and Analysis Program(i-STAP)", Bulletin of the Society of Naval Architects of Korea, Vol.53(1), 17-21

Skejic, R. and Faltinsen, O. M., 2008, "A Unified Seakeeping and Maneuvering Analysis of Ships in Regular Waves", J. Marine Science and Technology 13(4), 371-394.

Skejic, R. and Faltinsen, O. M., 2013, "Maneuvering Behavior of Ships in Irregular Waves", Proc. ASME 32nd International Conference on Ocean, Offshore and Arctic Engineering (OMAE2013), Nantes, France.

Sprenger, F., Maron, A., Delefortrie, G., van Zwijnsvoorde, T., Cura-Hochbaum, A., Lengwinat, A. and Papanikolaou, A., 2017, "Experimental Studies on Seakeeping and Maneuverability of Ships in Adverse Weather Conditions", J. Ship Research 61(3), 131-152.

Spyrou, K., 1995, "Yaw Stability of Ships in Steady Wind", Ship Technology Research 42, 21-30.

Spyrou, K. J., Tigkas, I. and Chatzis, A., 2007, "Dynamics of a Ship Steering in Wind Revisited", J. Ship Research 51(2), 160-173.

Subramanian, R., and Beck, R. F., 2015, "A Time-Domain Strip Theory Approach to Maneuvering in a Seaway", Ocean Engineering, 104, 107–118.

Sutulo, S., and Guedes Soares, C., 2006, "A Unified Nonlinear Mathematical Model for Simulating Ship Manoeuvring and Seakeeping in Regular Waves", MARSIM 2006, Terschelling, The Netherlands.

Tanaka, A., Yamagami, Y. Yamashita, Y. and Misumi, E., 1980, "The Ship Manoevrbility in Strong Wind", J. Kansai Society of Naval Architects, Japan 176, 1-10.

Tanizawa K., Kitagawa Y., Takimoto T., and Tsukada Y, 2012, "Development of an Experimental Methodology for Self-Propulsion Test with a Marine Diesel Engine Simulator", Twenty-second International Offshore and Polar Engineering Conference, Rhodes, Greece, 921-928.

Taskar, B., Koosup Yum, K., Steen, S. and Pedersen, E., 2016, "The Effect of Waves on Engine-Propeller Dynamics and Propulsion Performance of Ships", Ocean Engineering 122, 262-277.

Theotokatos, G. and Tzelepis, V., 2013, "A Computational Study on the Performance and Emission Parameters Mapping of a Ship Propulsion System", Proceedings of the Institution of Mechanical Engineers, Part M: Journal of Engineering for the Maritime Environment: 1475090213498715.

Tello Ruíz, M., Delefortrie, G., and Vantorre, M., 2016, "Induced Wave Forces on a Ship Maneuvering in Coastal waves," Ocean Engineering 121, 472-491.

Tello Ruíz, M., 2018, "Manoeuvring Model of a Container Vessel in Coastal Waves", Ghent University, PhD thesis.

Tello Ruíz, M., Mansuy, M., Donatini, L., Villagómez, J. C., Delefortrie, G., Lataire, E., and Vantorre, M., 2019a, "Wave Effects on the Turning Ability of an Ultra Large Container Ship in Shallow Water". OMAE2019. Glasgow, UK.

Tello Ruíz, M., Mansuy, M., Delefortrie, G., and Vantorre, M., 2019b, "Modelling the Manoeuvring Behaviour of an ULCS in Coastal Waves", Ocean Engineering 172, 213–233.

Ueno, M., Nimura, T., Miyazaki, H., and Nonaka, K., 2001, "On Steady Horizontal Forces and Moment due to Short Waves Acting on Ships in Manoeuvring Motion", Practical Design of Ships and Other Floating Structures (PRADS2001), 671-677.

Ueno, M., Nimura, T., and Miyazaki, H., 2003, "An Experimental Study on Manoeuvring Motion of a Ship in Waves", MARSIM'03, RC-13-1 -RC-13-7

Ueno, M., Tsukada, Y. and Tanizawa, K., 2013, "Estimation and Prediction of Effective Inflow Velocity to Propeller in Waves", J. Marine Science and Technology 18(3), 339-348

Umeda, N., Kawaida, D., Ooiwa, S., Matsuda, A. and Terada, D., 2016, "Tank Test Results and Simulations in Adverse Weather Conditions", Symp. Minimum Engine Power Requirement of Ships, Japan Institute of Navigation, Japan Society of Naval

Architects and Ocean Engineers, Tokyo, 51-56.

Wang, J., and Wan, D., 2016, "Investigations of self-propulsion in waves of fully appended ONR Tumblehome model", Appl. Math. Mech. 37, 1345–1358

Wang, J., Zou, L. and Wan, D., 2018a, "Numerical Simulations of Zigzag Maneuver of Free Running Ship in Waves by RANS-Overset Grid Method", Ocean Engineering 162, 55–79.

Wang, J. and Wan, D., 2018b, "Direct Simulations of Turning Circle Maneuver in Waves Using RANS-Overset Method", OMAE2018, 17-22, Madrid, Spain.

Yasukawa, H., 2006a, "Simulations of Ship Maneuvering in Waves (1st report: turning motion)", J. Japan Society of Naval Architects and Ocean Engineers 4, 127-136.

Yasukawa, H., 2006b, "Simulation of Wave-Induced Motions of a Turning Ship", J. Japan Society of Naval Architects and Ocean Engineers 4, 117-126.

Yasukawa, H. and Adnan, F. A., 2006, "Experimental Study on Wave-Induced Motions and Steady Drift Forces of an Obliquely Moving Ship", J. Japan Society of Naval Architects and Ocean Engineers 3, 133-138

Yasukawa, H., 2008, "Simulation of Ship Maneuvering in Waves (2nd report: zig-zag and stopping maneuvers)". J. Japan Society of Naval Architects and Ocean Engineers 7, 163-170.

Yasukawa, H., and Nakayama, Y., 2009, "6-DOF Motion Simulations of a Turning Ship in Regular Waves", MARSIM'09, Panama City. M-13-M-22.

Yasukawa, H., Adnan, F. A., and Nishi, K., 2010, "Wave-Induced Motions on a Laterally Drifting Ship", Ship Technology Research 57(2), 84-98.

Yasukawa, H., Hirono, T., Nakayama, Y. and Koh, K. K., 2012, "Course Stability and Yaw Motion of a Ship in Steady Wind", J. Marine Science and Technology 17(3), 291-304.

Yasukawa, H., Hirata, N., Yonemasu, I., Terada, D. and Matsuda, A., 2015, "Maneuvering Simulation of a KVLCC2 Tanker in Irregular Waves', MARSIM2015, Newcastle, UK.

Yasukawa, H. Zaky, M., Yonemasu, I. and Miyake, R., 2017, "Effect of Engine Outpu on maneuverability of a VLCC in Still Water and Adverse Weather Conditions", J. Marine Science and Technology 22, 574-586.

Yasukawa, H., Sakuno, R. and Yoshimura, Y., 2019, "Practical Maneuvering Simulation Method of Ships Considering the Roll-Coupling Effect", J. Marine Science and Technology 24(4), 1280-1296.

Yasukawa, H., and Sakuno, R., 2020, "Application of the MMG-Method for Prediction of Steady Sailing Condition and Course Stability of a Ship under External Disturbances", J. Marine Science and Technology 25(1), 196-220.

Yasukawa, H., 2020, "Steady Sailing Performance of a Ship in the Proximity to the Bank under Windy Conditions", J. Marine Science and Technology 25(4), 1246–1265

Yen, T. G., Zhang, S., Weems, K. and Lin, W. M., 2010, "Development and Validation of Numerical Simulations for Ship Maneuvering in Calm Water and in Waves",

28th Symp. on Naval Hydrodynamics, Pasadena, 12-17.

Yoshimura, Y., 1988, "Mathematical Model for Manoeuvring Ship Motion in Shallow Water (2nd Report), -- Mathematical Model at Slow Forward Speed", J. Kansai Society of Naval Architects, Japan 210, 77-84.

Yoshimura, Y., Nakao, I. and Ishibashi, A., 2009, "Unified Mathematical Model for Ocean and Harbour Manoeuvring", MARSIM'09, Panama City, M116-M124.

Yum K.K., Taskar, B., Pedersen E., and Steen S., 2017, "Simulation of a Two-Stroke Diesel Engine for Propulsion in Waves", International Journal of Naval Architecture and Ocean Engineering 9, 351-372.

Zhang W. and Zou, Z.-J., 2016, "Time Domain Simulations of the Wave-Induced Motions of Ships in Maneuvering Condition", J. Marine Science and Technology 21, 154-166.

Zhang W., Zou, Z.-J and Deng, D.-H., 2017, "A Study on Prediction of Ship Maneuvering in Regular Waves", Ocean Engineering 137, 367-381.

The Specialist Committee on Modelling of Environmental Conditions

Final Report and Recommendations to the 29th ITTC

1. GENERAL

1.1 Membership and Meetings

The Specialist Committee on Modelling of Environmental Conditions appointed by the 29th International Towing Tank Conference consisted of the following members:

- Alessandro Iafrati, CNR-INM, Italy (Chairman)
- Toshifumi Fujiwara, NMRI, Japan
- Hyun Joe Kim, Samsung Heavy Industries, Korea
- Yuxiang Ma, Dalian University of Technology, China
- Jule Scharnke, MARIN, The Netherlands (Secretary)
- Prof. Solomon C. Yim, Oregan State University, USA
- Pedro Cardozo de Mello, University of Sao Paolo, Brazil
- Xinshu Zhang, Shanghai Jiao Tong University (SJTU)
- Marcin Drzewiecki, Ship Design and Research Centre (CTO S.A.)

Four Committee meetings were held respectively at:

- CNR-INSEAN, Rome, Italy, January 2018
- NMRI, Tokyo, Japan, January 2019
- OMAE, Glasgow, June 2019
- CTO S.A., Gdansk, Poland, January 2020

Additional short meetings were held in the form of web conferences.

1.2 Tasks based on the Recommendations of the 28th ITTC

1. Complete tasks originally assigned to the committee i.e. propose and develop guidelines for generation of waves, wind and current in model scale. Each

guideline should address the following problems:

Waves:

- Non-linear effects – analysis, control
- Interactions with current and wind
- Distribution of extremes
- Wave grouping (characterization and reproduction)
- Short-crested wave modelling
- Deterministic generation of extreme waves
  - Confinement
  - Wave frequency and low frequency reflections
- Radiation and reflection from model, beach, etc.
- Measurement and analysis of long- and short-crested waves
- Non-stationary power spectrum (time and space)
- Wave breaking – influence on statistics and kinematics
- Geographical consistency of wave spectrum selection
- Investigate techniques for modelling those aspects of the extreme wave environment that are important in the determination of dynamic instability of intact vessels. Coordinate and exchange information with the Stability in Waves Committee on this task.

Wind:

- Interaction with waves
- Gusting (including squalls)
- Turbulence
- Vertical profiles
- Horizontal variation
- Measurements
- Geographical consistency of wind conditions

Current:

- Interaction with waves
- Turbulence
- Vertical profiles (including current reversal)
- Horizontal variation
- Measurements

2. Continue work of modelling extreme wave environment including design wave groups.
3. Continue work on breaking waves
   a. Breaking kinematics and typology
   b. Effects of breaking waves on spectral content
   c. Statistics of breaking occurrence and spectral shape
   d. Extreme wave generation and statistics
4. Investigate and review state-of-the-art of wind-wave interactions and the effects on wave breaking
5. Investigate and review state-of-the-art of wave-current interactions and the effects on the generation of extreme waves

1.3 Structure of the report

The work carried out by the committee is presented as follows:

<u>Modelling of extreme wave environments</u>

<u>Breaking waves</u>

<u>State-of-the-art review of wind-wave interactions and the effects on the generation of extreme waves</u>

<u>State-of-the-art review of wave-current interactions and the effects on wave breaking</u>

2. MODELLING OF EXTREME ENVIRONMENTS

In Bitner-Gregersen et al. (2019), a comparison of temporal and spatial statistics of non-linear waves is presented. In the past, it was most common to derive wave parameters and their statistics from time series of wave elevation. The duration of the wave records has been usually restricted to 20 or 30 minutes. Recently, increasing attention has started to be given to spatial wave data and wave statistics, particularly due to introduction in oceanography of stereo camera systems for collecting space–time ensemble of sea surface elevation. Using numerical linear, 2nd and 3rd order simulations this study compares temporal and spatial statistics of wave parameters. The 3rd order wave data are simulated by a numerical solver based on the Higher Order Spectral Method (HOSM) which includes the leading order nonlinear dynamical effects, accounting for the effect of modulational instability. The study demonstrates differences between the temporal and spatial statistics of wave parameters based on unidirectional numerical linear, 2nd order and HOSM simulations for the JONSWAP gamma parameter γ=1, 3.3 and 6. The maximum surface elevation, skewness and kurtosis are considered. It is shown that the higher order nonlinear wave field including dynamical effects is more sensitive to sampling variability than the 2nd order and linear ones. The dynamical effects have significant impact on the analysed parameters, particularly on η_{max}/H_s. The discrepancies between the estimators of the wave parameters derived from the HOSM simulations and the linear ones are much larger than the ones obtained from the 2nd order and linear simulations. The shape of a wave spectrum does not affect much skewness, being primarily a second order effect, but impacts kurtosis and the maximum surface elevation. Further, it is shown that, consistent with earlier findings, directionality reduces kurtosis significantly. The HOSM means over all random realizations of the same sea state of the temporal skewness and kurtosis estimators are approximately equal to the spatial ones. In contrast with it, as expected, the mean maximum temporal surface elevation is significantly lower than the spatial one, since the spatial calculation covers many more waves than the single point measurement. There is large spreading around the mean values due to sampling variability, being larger for the temporal data than the spatial data. This should be considered in design work and in forecasting of rogue waves.

Recently, some studies were performed for crossing sea states, for instance by Liu et al. (2019). Numerical simulations for crossing seas were performed and investigated on the occurrence of rogue waves using HOS. A number of non-collinear systems with different total wave steepness were investigated, and for each case, 10 repetitions with different random phases were performed. The temporal evolution of directional and omnidirectional wave spectra, wave crest distribution, as well as the kurtosis and skewness of free surface elevations were obtained and analysed. Their results show that the skewness and kurtosis are found to increases quickly from the initial Gaussian value within a small time scale and then stay rather stationary. The theoretical third-order crest distribution tends to underestimate the probability of extreme crest height for the crossing sea states with large wave steepness.

An experimental study was reported in Luxmoore et al. (2019). Their study shows that the third-order nonlinearity was more affected by varying the directional spreading of the components instead of the crossing angles between components. They also found that the kurtosis, which quantitatively describes the third-order nonlinearity, can be estimated from the directional spreading using an empirical relationship based on the two-dimensional Benjamin-Feir index (BFI2_d), proposed by

Mori et al. (2011). More recently, Liu et al. (2020) derived a new coupled two dimensional Benjamin-Feir index (CBFI_2d) for crossing seas to quantify the third-order nonlinearity effects. Their results show very good agreement with experiments for a broad of wave spreading functions.

In Ross et al. (2019), a review of the current practice of the application of environmental contours is discussed. Environmental contours are used in structural reliability analysis of marine and coastal structures as an approximate means to locate the boundary of the distribution of environmental variables, and to identify environmental conditions giving rise to extreme structural loads and responses. There are different approaches to estimate environmental contours, some directly linked to methods of structural reliability. Each contouring approach has its pros and cons. Although procedures for applying contours in design have been reported in articles and standards, there is still ambiguity about detail, and the practitioner has considerable flexibility in applying contours. It is not always clear how to estimate environmental contours well. Over four years, DNV-GL, Shell, the University of Oslo and HR Wallingford worked together to review current practice regarding the use of design contours.

In Huang et al. (2018), a semi-empirical distribution for long-crested non-linear waves is proposed. In comparison with simulations as well as measurement data the proposed distribution function appears to give promising results. However, at this point wave breaking is not yet included in the semi-empirical distribution function, which may result in an over prediction of the highest crests for very steep sea states. Wave breaking can cause a reduction of the amplification of the extreme crest heights with respect to linear or 2nd order theory, as described in Buchner et al. (2011).

Liu et al. (2019) developed a Higher-order Spectral (HOS) model by combing with wave breaking model based on eddy-viscosity to study the extreme wave occurrence for long-crested random waves. They compared the numerical results with the measurements in wave basin and satisfactory agreement was found. In addition, they also developed a semi-empirical distribution based on extensive 3-hour simulations using HOS. The semi-empirical formula may be used to obtain criteria for wave calibration before model tests in a wave basin.

In Klein et al. (2019), the systematic experimental validation of high-order spectral method for deterministic wave prediction is presented. The aim is to identify and evaluate possible areas of application as well as limitations of use. For this purpose, irregular sea states with varying parameters such as wave steepness and underlying wave spectrum are addressed by numerical simulations and model tests in the controlled environment of a seakeeping basin. In addition, the influence of the propagation distance is discussed. For the evaluation of the accuracy of the HOSM prediction, the surface similarity parameter (SSP) is utilized, allowing a quantitative validation of the results. The results obtained are compared to linear wave prediction to discuss the pros and cons of a non-linear deterministic short-term wave prediction. In conclusion, this paper shows that the non-linear deterministic wave prediction based on HOSM leads to a substantial improvement of the prediction quality for moderate and steep irregular wave trains in terms of individual waves and prediction distance.

Fujimoto et al. (2018) developed a four-dimensional variational method (4DVAR) for wave reconstruction to study the generation of freak waves. The 4DVAR methods performs perturbed ensemble simulations to evaluate the gradient of the squared error and is easy to parallelize and implement. They also adopted

HOS to predict the nonlinear wave evolution, which is essential for freak wave generation. They found that considering the nonlinearity in HOSM was crucial to estimate the freak wave accurately.

McAllister et al. (2019) performed physical tests in FloWave basin to recreate the Draupner wave with an equivalent surface elevation time series and demonstrate that a wave of the same and greater steepness than the Drauper wave can arise as a results of crossing seas at large angles (between 60 and 120 degrees). They also investigated the role of wave breaking.

In Essen (2019), the variability of encountered waves during deterministically repeated seakeeping tests at forward speed is discussed. In this paper a steep wave condition over the longitudinal basin axis (waveA) and a less steep oblique wave condition (waveB) were studied. Overall similarity as well as individual crest height, steepnesses and timing variability are discussed, because ship response is not equally sensitive for every point in the wave time series. It was concluded that the variability of the measured incoming wave crests and their timing increases with distance from the wave generator for waveA. The crest height variability for waveB is lower and more constant over the basin length (because the propagation distance to the model is constant in oblique waves and wave breaking is less likely). It was shown that only a small part of the variability close to the wave generator is caused by 'input' uncertainties such as the accuracy of the wave generator flap motions, measurement carriage position, their synchronisation and measurement accuracy. The rest of the variability is caused by wave and basin effects, such as wave breaking instabilities and small residual wave-induced currents from previous tests. The latter depend on previous wave conditions, which requires further study.

Kim et al. (2019) proposed a heuristic approach to develop an optimal grid system for a numerical wave tank by investigating the characteristics of the numerical waves propagating in various CFD-based NWT set-ups. Linear dispersion relations of the waves in a Cartesian grid system are derived analytically. The analytic results lead to an optimal grid aspect ratio for the best dispersion approximation. Extensions of the analytic approach to determine an optimal set up of the grid system of CFD-based NWT are discussed. A roadmap to develop CFD modelling practices based on these heuristic approaches and further numerical verification is proposed for the on-going industry efforts to develop the guidelines for numerical wave tanks, such as the Joint Industry Project on "Reproducible CFD Modeling Practices for Offshore Applications", Koop et al. (2020).

Baquet et al. (2019) examined the effect of the non-Gaussian distribution in the fully-nonlinear wave on offshore platform responses. In this study, linear wave components with randomly distributed wave phases and fully nonlinear irregular waves using a potential numerical wave tank were used as input to the global performance analysis of two kinds of floating platforms. In the results, the response spectra, the probability distribution and the extreme responses of motions and air gaps are compared, and the way using nonlinear waves could give more realistic motion responses with less uncertainty in the airgap estimation.

Watanabe et al. (2019) developed a stereo camera system to reconstruct three-dimensional wave fields and assimilated into a phased resolved nonlinear wave model to construct a dynamically consistent wave field in a much wider domain. The newly developed scheme named as SWEAD was successfully used to reconstruct wave field. The scheme was tested for different tunable parameter values and model setting to improve the reproducibility of

the reconstruction outside of the imaging domain. The SWEAD is not restricted to be used for the stereo imaging system and seems also suitable to analyze surface elevations from ship-borne radars.

Ducrozet et al. (2020) applied the time reversal (TR) methodology to reconstruct real-ocean rogue waves in a laboratory environment conditions. As the purpose to validate the method, three literature real wave recorded were used in experiments conducted in a wave flume. The waves selected for the experiments are known very steep and highly nonlinear, being challenging to be reproduced in controlled environmental conditions in a laboratory. The wave flume characteristics and wave breaking during propagation could be introducing changes to the wave shape. Aspects related to the selected position for the wave reproduction in the flume is also an issue investigated in the paper. It was reported that the TR method presented was robust to reproduce the selected waves with good quality for a unidirectional wave, also in comparison to other methods described in the literature.

Xie et al. (2019) analysed 1-year of wave data measured in the South China Sea at depth from 200m to 1500m. The results showed that JONSWAP spectrum is suitable in the South China Sea and the mean value of peak enhancement factor is about 2.15. The ratio between the maximum wave height and the significant wave height is about 1.7.

In Niu et al., 2020, an improved focusing method named the All Phase Correction Method (APCM) was developed to produce accurate extreme waves at a predefined position in wave flumes. An improved phase estimation algorithm and second-order wavemaker theory was employed to iteratively correct the phases and amplitudes of the generated waves. Compared with the self-correction method which was proposed by Fernández et al. (2014), a faster convergence rate and higher correlation coefficient were obtained utilizing the APCM.

Hidetaka et al. (2018) present a new wave generation method based on the higher order spectral method (HOSM) used to calculate the wave maker control signal. This method was validated for unidirectional spatially-periodic modulated wave trains. Moreover, freak waves were generated in unidirectional irregular waves and in directional irregular waves to obtain time series of the surface elevation, frequency spectra and spatial wave profiles. The measurements generated based on the higher order spectral method compared well with simulations based on the higher order spectral method.

Khait and Shemer (2019) suggest an alternative analytic method of determination of nonlinear correction to the wavemaker motion that allows definition of the target wave field in either Fourier or physical space. Rather than starting the derivation from the governing potential flow equations as in the theory by Schäffer, advantage is taken here of the existing nonlinear wave models supplemented by the nonlinear boundary condition at the wavemaker. Since the existing nonlinear water wave theories are accurate to the 3rd and higher orders, the present approach makes possible to circumvent the 2nd-order limitation of the Schäffer theory. This approach allows significant simplification of the procedure needed for determination of the nonlinear correction to the wavemaker driving signal, which is critical in many practical applications. Particular attention was given to significant deviation of the linear wavemaker transfer function obtained in the fully-nonlinear numerical simulations from the theoretical predictions. This deviation was observed in numerous experimental works. The existence of such a deviation in fully nonlinear simulations of potential flow indicates that viscous friction and possible leakages at the wavemaker that were suggested as a possible source for this effect can only play a minor role. The quadratic

dependence on the wave steepness of the relative deviation of the transfer function from the linear predictions suggests that the mean current at the 2nd order that results from the nonlinear interaction of the velocity field of the propagating waves with the wavemaker surface oscillations of finite amplitude is a possible reason for this inaccuracy. A more careful investigation is needed to clarify the reasons for this behaviour of the transfer function.

3. BREAKING WAVES

3.1 Breaking kinematics and typology

In Duz et al. (2020) kinematics under spilling and plunging breakers are investigated using both experimental and numerical methods. In a modular laboratory flume, the breakers were generated using dispersive focusing, and the kinematics underneath them were measured utilizing the Particle Image Velocimetry (PIV) technique. Using the state-of-art high-speed video cameras, the kinematics were measured at a high sampling rate without needing phase-locked averaging. Afterwards, computational fluid dynamics (CFD) simulations were carried out for comparison purposes. These simulations were run in single-phase using a finite volume based Navier-Stokes solver with a piecewise-linear interface reconstruction scheme. The spilling and plunging breakers from the measurements were reconstructed in the computational domain using an iterative scheme. As a result a good match with the measured waves was obtained in the simulations. Results indicate that even though measured kinematics are somewhat higher than the simulated ones especially in the spilling and overturning regions, the CFD simulations can accurately capture the relevant details of the flow and produce reasonably accurate kinematics in comparison with the PIV results.

Comparisons between numerical simulation and experimental measurements of wave breaking flows are presented in Alberello et al. (2019). A two-fluid numerical model is used to simulate the multiphase flow. The flow field in the Navier-Stokes solver is initialized by using the HOSM solution computed shortly before the onset of the breaking and the flow is simulated up to the breaking. Experimental measurements are given in terms of the velocity field computed by particle image velocimetry and comparisons with numerical data are established. A rather satisfactory agreement between measurements and numerical data has been found, although some limits still exists very close to the crest where the numerical data seem to underestimate the measurement. This may be due some numerical limits, e.g. grid resolution or thickness of the interface, or to the use of slightly different initial conditions.

3.2 Effects of breaking waves on spectral content

In Huang et al. (2018), a reduction of energy in the high-frequency range of steep measured and simulated wave spectra in with respect to the target wave spectrum is discussed. As this reduction in energy only occurs for steep wave spectra, this may be related to wave breaking.

The changes operated by the occurrence of breaking are discussed in Iafrati et al. (2015) and in De Vita et al. (2018). In Iafrati et al. (2015), a JONSWAP spectrum is initialized and its evolution is followed by using a HOS method. Shortly before the breaking, the HOS solution is used to initialize a two-fluids Navier-Stokes solver which is used to simulate the flow beyond the breaking. By comparing the spectra provided by the HOS and Navier-Stokes results, it is possible to distinguish between the changes operated by the time evolution and those associated to the breaking process. Results

clearly indicate that the breaking acts mostly on the higher harmonics.

In De Vita et al. (2018), a careful numerical study on the breaking induced by the modulational instability is presented. As already discussed in Tulin et al. (1999), results shows that the modulational instability causes a downshifting of the energy from the fundamental component to the lower sideband and the occurrence of breaking freezes the energy transfer

In Ewans et al. (2019) the identification of higher order interactions in wave time-series are described. Reliable design and reanalysis of coastal and offshore structures requires, amongst other things, characterisation of extreme crest elevation corresponding to long return periods, and of the evolution of a wave in space and time conditional on an extreme crest. Extreme crests typically correspond to focussed wave events enhanced by wave-wave interactions of different orders. Higher-order spectral analysis can be used to identify wave-wave interactions in time-series of water surface elevation. The bispectrum and its normalised form (the bicoherence) have been reported by numerous authors as a means to characterise three-wave interactions in laboratory, field and simulation experiments. The bispectrum corresponds to a frequency-domain representation of the third order cumulant of the time-series, and can be thought of as an extension of the power spectrum (itself the frequency-domain representation of the second order cumulant). The power spectrum and bispectrum can both be expressed in terms of the Fourier transforms of the original time-series. The frequency domain analysis therefore provides an efficient means of estimation. However, there are a number of important practical considerations to ensuring reasonable estimation. To detect four-wave interactions, the trispectrum and its normalised form (the tricoherence) needs to be considered. The trispectrum corresponds to a frequency-domain (Fourier) representation of the fourth-order cumulant of the time-series. In the paper it is concluded that the T-tricoherence provides the capability to detect phaselocked four wave interactions of the form $f_4=f_1+f_2+f_3$, that is where three waves interact to force a bound fourth component. However, the estimates of the T-tricoherence on nonlinear wave simulations, and measured laboratory and field (Draupner) records did not indicate significant four wave interactions of this type. While this result is expected for deep-water cases, larger T-tricoherence values for the HOS5 (Table 2) case, for which k_P d≈1 might have been expected. Estimates of V-tricoherence produce high values at frequency triplets that correspond to high harmonics. It is not possible to conclude whether these indicate the occurrence of actual four wave interactions of the type $f_1+f_2=f_3+f_4$, or whether they simply indicate combinations of independent pairs of Fourier components that happen to satisfy the frequency relationship. It is likely though that these four-wave interactions are present, in some of the sea states that were investigated. Alternative tricoherence estimators to differentiate between these two possibilities or to exclude contributions from trivial combinations in the moment estimates are currently being investigated.

In Dong et al. (2019), a new experimental study was presented in which large isolated focusing wave groups were generated in a special “X” configuration. By varying the initial wave steepness, wave groups ranging from near-linear to violent breaking were generated. Essentially, the experimental results suggested that the nonlinear energy transfer during wave-wave interactions is particularly sensitive to the directional spread. Similar to unidirectional laboratory data, nonlinear energy transfers between the first harmonic and second harmonic bands for the non-breaking case, while energy loss comes from the high-frequency components of the first harmonic band when

breaking occurs. However, it is the directional interaction that dictates the severity of breaking, i.e. greater breaking occurs when the wave packets propagate with larger approach angle, and hence the energy loss increases generally with an increase of the approach angle.

3.3 Statistics of breaking occurrence and spectral shape

In Babanin (2009) a complete overview of the state-of-the-art knowledge on breaking of ocean surface waves including details regarding the definitions and onset of breaking and wave breaking probability and occurrence are presented. In the paper, variety of definitions related to the wave breaking are discussed and formulated, and methods for breaking detection and measurements are examined. Most of attention is dedicated to the research of wave-breaking probability and severity. Experimental, observational, numerical, analytical and statistical approaches and their outcomes are reviewed. Present state of the wave-breaking research and knowledge is analysed and main outstanding problems are outlined.

In Toffoli et al. (2010) the maximum steepness of oceanic waves is analyzed through filed and laboratory experiments. In this paper it is stated that intuitively, waves break when they become too steep. Unfortunately, a general consensus on the ultimate shape of waves has not been achieved yet due to the complexity of the breaking mechanism which still remains the least understood of all processes affecting waves. To estimate the limiting shape of ocean waves, here we present a statistical analysis of a large sample of individual wave steepness. Data were collected from measurements of the surface elevation in laboratory facilities and the open sea under a variety of sea state conditions. Observations reveal that waves are able to reach steeper profiles than the Stokes' limit for stationary waves. Due to the large number of records this finding is statistically robust.

4. STATE-OF-THE-ART REVIEW OF WIND-WAVE INTERACTIONS AND THE EFFECTS ON THE GENERATION OF EXTREME WAVES

4.1 CFD Modelling Practice for Wind Load Estimation

Wind load is an important parameter to be considered in the design of hull and mooring systems of offshore floating structures. The first step to minimize the uncertainties in wind load is generating an accurate wind profile that satisfies design requirements. Recently, there were some joint-industry effort to implement wind profiles accurately and develop a CFD modelling practice on wind-load estimation. In SNAME OC-8 CFD Task Force, Kim et al. (2018) and Kim et al. (2019), a modelling practice was developed and successfully validated for a semi-submersible topside with several independent participants. In a joint development project, TESK JDP by TechnipFMC, EURC, Samsung Heavy Industries and Korea Research Institute of Ships & Ocean Engineering (KRISO), the procedure was further verified for hulls with more complicated topsides, Yeon et al. (2019). As shown in Figure 1, sustainability, i.e. the capability of a wind profile at the inlet boundary in retaining its shape anywhere in the wind direction, was verified with an NPD (Norwegian Petroleum Directorate) profile in API (2005) and DNV (2014). The sustainable wind profile was applied to a semi-submersible and the calculated wind loads showed good agreement with model test data. Further an exhaustive study was conducted with an FPSO hull in order to determine uncertainties between CFD and model tests in the course of the TESK JDP, Xu et al. (2019). One of the findings was that the gap between FPSO bottom and turntable of the

wind tunnel has some impact on the vertical force, roll and pitch moment. In the same study, the effect of the topside modules' porosity on wind loads was explored with several simplified models from original shape, Huang et al. (2020). In another joint development project which was initiated by TechnipFMC, Chevron, and Samsung Heavy Industries, a sustainable atmospheric boundary layer was implemented and extended to ESDU (Engineering Science Data Unit) (1982,1983) as well as NPD profile. The NPD profile is a neutral atmospheric boundary layer which was proven to be an analytic solution of the Navier-Stokes equations by Richard et al. (1993). Thus, the NPD profile inherently satisfies sustainability conditions. ESDU profile is an unstable atmospheric boundary layer but it was shown that the sustainability could be achieved with modified sustainability conditions as shown in Figure 2.

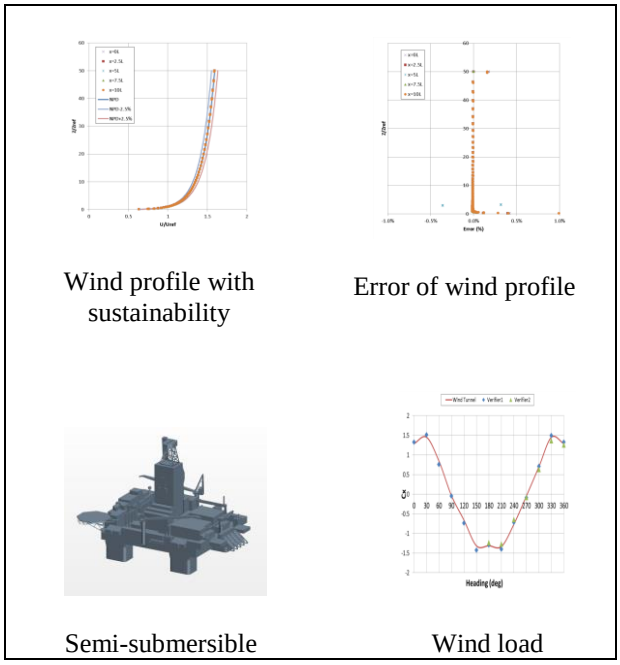

Figure 1. sustainable NPD profile and its wind load on semi-submersible, Yeon et al. (2019)

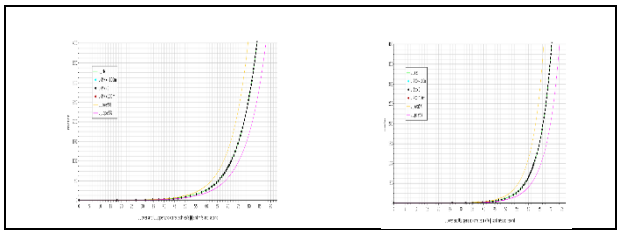

Figure 2. sustainable wind profile implementation: NPD (*left*), ESDU (*right*)), ESDU (1982, 1983)

4.2 Vertical Wind Profiles in strong wind conditions

Vickery (2014) presents the examination of the suitability of the models for atmospheric turbulence used in the draft of API RP 2MET, (2013), for describing the characteristics of hurricane winds offshore, using data collected in Gulf of Mexico from recent (post-2000) hurricanes. The investigation found that the API RP 2MET model yields an underestimate of the true gust factors for the height range examined, and it exhibits a trend for the gust factor to increase as wind speed increases which is not seen in in the data because the model is based on North Sea data. The ESDU (1982, and 1983) models give the gust factors more consistent with the measured field data.

4.3 Wind Load Simulation in Model Test

Tsukada et al. (2017) developed a wind load simulator (WiLS), which simulates forces and moments directly using three pairs of light and small duct fans, not generating environmental wind loads. The wind load simulator can be used to the free-running model tests for evaluating ship performance at actual seas. A feedback control was adopted to take into account the supposed true wind speed and direction, and instantaneous model ship speed, drift and heading angle. Fan inertial forces measured from the accelerometers were corrected in the fan control.

4.4 Wind and Wave Interaction effects on breaking waves and induced loading

Kristoffersen et al. (2019) presented a series of experimental studies on the spatially localized influence of wind on wave induced load on a flexible circular cylinder, which were conducted in a wave-wind-current flume at Newcastle University. These tests were motivated from other experimental and numerical investigations showing air flow separation on the leeward side of steep waves that can lead to added wind energy transfer resulting in an increase of impulsive wave loading. In the tests, the maxima of the force acting on the body are compared for the tests with and without wind. For low wave amplitudes, there was a decrease in force response when wind was introduced. For the largest wave amplitude, the maximum of the force response was increased by 6.5 % when wind was introduced. Some differences in the time series of the free surface elevation were observed when wind was present, but the maximum of the surface elevation did not change notably, and the slope was only minimally changed, meaning that this should not give basis for the differences in the loads.

A numerical investigation of the effects of the wind on the development of modulational instability is provided in Iafrati et al. (2019). Therein, the evolution of a modulated wave train under a uniform wind profile is simulated and comparisons with the corresponding evolution in no-wind solution are established. The occurrence of flow separation at the crest similar to that found experimentally in Buckley et al. (2019), is observed. Results indicate that the presence of wind have a stabilizing effect on the steep waves that delays the onset of the breaking and the allows the waves to reach larger steepnesses. Such results are in general agreement with what found in Touboul et al. (2006) and Kharif et al. (2008).

4.5 Tropical cyclones: modelling and characterization

Grey et al. (2019) proposed a new probabilistic method to increase the sample of tropical cyclones by producing 10,000 years of synthetic cyclone tracks with a range of paths, intensities and sizes based on Hall et al. (2007) and Casson et al. (2000)]. From this set of synthetic tracks, the tropical cyclones that most likely affect the site of interest are modelled using time varying wind fields based on the Holland model in Holland (1980) with surge, current and waves then simulated by the hydrodynamic model TELEMAC-2D coupled to the SWAN wave model. As it is impractical to model 10,000 years of tropical cyclones, a Gaussian process emulator is employed to relate the resultant conditions to parameters defining the cyclones, such as track position, heading, intensity and radius to maximum wind. The result is a synthesized 10,000 years of cyclone events from which design conditions for a range of return periods can be predicted with a greater degree of certainty than by extrapolating from historical events.

Tao et al. (2019) performed a statistical study on the duration of each tropical cyclone that attacked Hong Kong, the time interval between every two continuous tropical cyclones during the year, and the time interval between the last cyclone of each year and the first cyclone of the following year.

4.6 Gust parameters and wind spectrum

Xie et al. (2019) studied the parameters of the gust factor and wind spectra during typhoon and monsoon period by using the observational data of long-term wind on a platform in South China Sea. It has been found that there was no significant positive correlation between the gust factor and turbulence with the wind speed. The gust factor decreased with increase of the gust duration, and the turbulence intensity increased

with the duration. The weather system has a significant impact on the wind factor and the turbulence intensity. A seasonal trend of gust turbulence has been observed: the turbulence changes greatly in summer and the gust factors are relatively stable with high wind speed in winter and typhoon processes. After comparison, the NPD spectrum was recommended in SCS according to the observed data.

4.7 The wave climate of the southern ocean

Young (2019) presented an analysis of field measurements of wind and waves in the Southern Ocean based on a combination of more than 30-years of satellite altimeter data plus insitu buoy measurements at 5 locations. The analysis shows that the Southern Ocean is a unique environment where there are strong winds year-round with only a relatively small variation with season which blow over exceptionally long distances, in contrast to the Northern Hemisphere, which is relatively calm at high latitudes in Summer, The strong persistent winds of the Southern Ocean generate swell which propagates across the South Pacific, South Atlantic and Indian Oceans. Therefore, the wave climate of the Southern Ocean impacts half the oceans of the world. As a result, the fact that wind speed and wave heights, particularly the extremes, are changing, is of importance for wave setup and coastal erosion around these oceanic basins. The unique environment is a continuous “race track” of winds generating waves which give rise to spectral forms seen in no other ocean at these latitudes. The spectra are unimodal, with spectral parameters very similar to actively wind generated seas. This is despite the fact that the energetic waves are almost always propagating faster than the local wind. The spectra are a clear indication of the important role of nonlinear interactions in wind.

5. STATE-OF-THE-ART REVIEW OF WAVE-CURRENT INTERACTIONS AND THE EFFECTS ON WAVE BREAKING

5.1 Current Load Estimation using CFD

Current load is an important parameter to be considered in the design of hull and mooring systems of offshore floating structures. To accurately predict the motions of moored vessels, current load should be determined with confidence in the results. To improve the confidence level, there were several joint studies performed recently. One of the working group in Xu et al. (2019) developed a modelling practice and verified the practice. the developed modelling practice was further tested with more participants and various CFD solvers in a blind manner. The compared result following the modelling practice gave good match with model test data within 10% tolerance, Koop et al. (2020).

5.2 Stochastic models of waves and current for prediction of structural design loads

In Bruserud (2018) a simultaneous stochastic model of waves and currents for prediction of structural design loads is presented. In the paper it is discussed that Simultaneous data of metocean parameters, such as wind, waves and current, of sufficient quality and duration are necessary to establish reliable, joint models of metocean loads and load effects on marine structures. In lack of such joint models, the Norwegian design standard, NORSOK N-003, recommends combinations of metocean parameters for load estimations assumed to be conservative. However, the degree of conservatism is rather uncertain. The possible conservatism in NORSOK N-003 for combinations of wave and current conditions in the northern North Sea has been assessed. To perform such an assessment, precise knowledge

about the wave and current conditions is required, as well as simultaneous wave and current data of high quality and long duration.

Available measured wave and current data during nearly five years, at selected locations in the northern North Sea, are described. A thorough assessment of the current conditions at these locations is given, with the following important findings;

(1) the quality of measured current data is poorer than anticipated

(2) the dominating current conditions at some locations is wind-generated inertial oscillations

(3) the seasonality of current conditions at these locations is very distinct due to the inertial oscillations and

(4) significant interannual variations in current conditions is found.

For waves in the northern North Sea, both measured and hindcast data are found to be of appropriate quality and duration for joint considerations, but neither current measurements nor hindcast have the required quality or duration. To generate adequate current data, a simple model for wind-generated inertial oscillations is applied and validated at one location in the northern North Sea. With that, simultaneous wave and current data of sufficient quality and duration for joint modelling are available and a joint conditional model for waves and currents is proposed. The anticipated conservatism in NORSOK N-003 for load estimations is assessed by a case study. A simplified model for a generic static load on a jacket, caused by waves and currents, is assumed. For the northern North Sea, metocean loads are estimated first according to the NORSOK N-003 recommendation, and then directly from a load times series. Comparison of the two different approaches gives a clear indication that the NORSOK recommendation is not necessarily conservative in the northern North Sea. Due to several simplifications in the steps leading up to the load estimations, this result is intended to be illustrative.

5.3 Wave current interaction on rogue waves

In the ocean, negative horizontal velocity gradients (i.e. an accelerating opposing current or a decelerating following current) make waves shorten and heighten which enhances wave steepness. As a result, a nonlinear mechanism known as modulational instability develops, leading to the formation of large amplitude waves (the so-called rogue waves), even if they would otherwise be unexpected. In Toffoli et al. (2019), laboratory experiments and numerical simulations with a current-modified version of the Euler equations are presented to assess the role of an opposing current in changing the statistical properties of unidirectional random wave fields. Results demonstrate in a consistent and robust manner that an opposing current induces a sharp and rapid transition from weakly to strongly non-Gaussian properties with a consequent increase of the probability of occurrence of rogue waves. The tests were conducted with irregular unidirectional waves in a wave flume and a directional wave basin at Plymouth University. The initial conditions at the wave maker were given in the form of an input JONSWAP-like wave spectrum to model waves in the frequency domain. As the wave field entered into a region of opposing current, the wave height was observed to increase. Evident breaking dissipation was observed for very strong current fields for $U/Cg > 0.3$ (breaking appeared with even less strong currents in the wave basin). The presence of the current also accelerated the downshift of the spectral peak, with energy migrating from high to low frequencies bands within scales of tens of

wavelengths, in agreement with modulational instability effects, Onorato et al. (2009). The analysis of the statistical properties of extreme (rogue) waves with an aid of kurtosis, the fourth-order moment of the probability density function of the surface elevation. The kurtosis expresses the probability of extreme events in a record (this assumes the value of 3 for Gaussian sea states). The sea state rapidly transitioned from a weakly to a strongly non-Gaussian condition as current speed increased; maximum values of kurtosis were detected to reach 3.5 or higher, which are remarkably high for water waves. These features were evident in both facilities. However, the wave basin exhibited much higher kurtosis (> 4) than the wave flume. Agreement with numerical simulations confirms that this transformation can be attributed to quasi-resonant nonlinear interactions triggered by the background current.

Liao et al. (2017) derived a nonlinear Schrödinger equation for the propagation of two-dimensional surface gravity waves on linear shear currents in finite water depth. Using the equation, the properties of the modulational instability of gravity waves on linear shear currents were investigated. It is showed that shear currents modify significantly the modulational instability properties of weakly nonlinear waves. Furthermore, the influence of linear shear currents on the Peregrine breather which can be seen as a prototype of freak waves was also studied. In intermediate water depth, both currents and the corresponding vorticity have significant influence on the structure of a Peregrine breather. It was demonstrated that depth-uniform opposing currents can reduce the breather extension in both time and spatial domain, but following currents has the adverse impact, indicating that a wave packets with freak waves formed on following currents contains more hazardous waves in finite water depth. However, the corresponding and coexisting vorticity can counteract the influence of currents. Additionally, if the water depth is deep enough, shear currents have negligible effect on the characteristics of Peregrine breather.

Liao et al. (2018) conducted a series of laboratory experiments on the Peregrine breather (which is often considered as prototypes of oceanic freak waves) evolution in a wave flume with a background opposite current. In the experiment, the cases were selected with the relative water depths k_0h (k_0 is the wave number and h is the water depth) varying from 3.11 through 8.17 and the initial wave steepness k_0a (a is the background wave amplitude) ranges between 0.065 and 0.120. The experimental results showed that the persistence of the breather evolution dynamics even in the presence of strong current. The spectrum of the PB persisted at the current, thus making it a viable characteristic for prediction of freak waves. It was also found that the opposing currents tend to shift the focusing point upstream compared to the cases without currents. Furthermore, it was found that depth-uniform opposing currents can reduce the breather extension in time domain.

6. REFERENCES

Alberello, A., Iafrati, A., 2019, “The Velocity Field Underneath a Breaking Rogue Wave: Laboratory Experiments Versus Numerical Simulations”, Fluids, Vol. 4, 68.

American Petroleum Institute (API), 2005, “Design and Analysis of Stationkeeping Systems for Floating Structures”, Recommended Practice 2SK, 3rd Edition, pp.59-62.

American Petroleum Institute, 2013, “Derivation of Metocean Design and Operating Conditions”, API RP 2MET, Committee draft, September 2013.

Babanin, A., 2009, "Breaking of Ocean Surface Waves", Acta Phys. Slovaca, 56(4), 305-535.

Baquet A., Lim, H., Kim, J., 2019, "Effect of Non-Gaussian Distribution of Fully-Nonlinear Waves on Offshore Platform Motion Responses", In Proceedings of the ASME 38th International Conference on Ocean, Offshore & Arctic Engineering, OMAE2019-96465, Glasgow, UK.

Bitner-Gregersen, E., Gramstad, O., 2019, "Comparison of Temporal and Spatial Statistics of Nonlinear Waves", In Proceedings of the ASME 38th International Conference on Ocean, Offshore & Arctic Engineering, OMAE2019-95357, Glasgow, UK.

Bruserud, K., 2018, "Simultaneous Stochastic Model of Waves and Currents for Prediction of Structural Design Loads", In Proceedings of the ASME 37th International Conference on Ocean, Offshore & Arctic Engineering, OMAE2018-77219, Madrid, Spain.

Buchner, B., Forristall, G., Ewans, K., Christou, M., Hennig, J., 2011, "New Insights in Extreme Crest Height Distributions (A Summary of the ‚CresT' JIP)", In Proceedings of the ASME 30th International Conference on Ocean, Offshore and Arctic Engineering, OMAE2011-49846, 2011, Rotterdam, The Netherlands.

Buckley, M.P., Veron, F., 2019, "The Turbulent Airflow Over Wind Generated Surface Waves", European Journal of Mechanics/B-Fluids, Vol. 73, 132-143

Casson, E., Coles, S. , 2000, "Simulation and Extremal Analysis of Hurricane Events" Journal of Royal Statistical Society, Series C, Vol. 49, No. 3, pp 227-245.

De Vita, F., Verzicco, R., Iafrati, A., 2018, "Breaking of Modulated Wave Groups: Kinematics and Energy Dissipation Processes", Journal of Fluid Mechanics, Vol. 855, 267-298.

Dong, G., Liu, D., Ma, Y., Perlin, M., 2019. Experimental investigation of weakly three-dimensional nonlinear wave interactions. European Journal of Mechanics B/Fluids, 77, 239-251.

Ducrozet, G., Bonnefoy, F., Mori, N., Fink, M., & Chabchoub, A., 2020, "Experimental Reconstruction of Extreme Sea Waves by Time Reversal Principle", Journal of Fluid Mechanics, 884, A20, doi:10.1017/ jfm.2019.939

Duz, B., Scharnke, J., Hallmann, R., Tukker, J., Blanchard, K., Khurana, S., 2020, "Comparison of the CFD Results to PIV Measurements in Kinematics of Spilling and Plunging Breakers", In Proceedings of the ASME 2020 39th International Conference on Ocean, Offshore and Arctic Engineering, OMAE202-19268, 2020, Florida, USA.

Engineering Sciences Data Unit (ESDU), 1982, "Strong Winds in the Atmospheric Boundary Layer", Part 1: Mean hourly wind speed, Item No. 82026, London, England.

Engineering Sciences Data Unit (ESDU), 1983, "Strong Winds in the Atmospheric Boundary Layer", Part 2: Discrete gust speeds, Item No. 83045, London, England.

Essen, S., 2019, "Variability in Encountered Waves During Deterministically Repeated Seakeeping Tests at Forward Speed", In Proceeding of the ASME 2019 38th International Conference on Ocean, Offshore and Arctic Engineering, OMAE2019-95065, 2019, Glasgow, UK.

Ewans, K., Christou, M., Ilic, S., Jonathan, P., 2019, "Identifying Higher-Order Interactions in Wave Time-Series", In Proceeding of the ASME 2019 38th International Conference on Ocean, Offshore and Arctic Engineering, OMAE2019-95378, 2019, Glasgow, UK.

Fujimoto, W., Waseda, T., 2018, "Reproduction of Freak Waves Using Variational Data Assimilation and Observation", In Proceedings of the ASME 37th International Conference on Ocean, Offshore & Arctic Engineering, OMAE2018-77771, Madrid, Spain.

Grey, S., Liu, Y., 2019, "A Probabilistic Approach to Tropical Cyclone Modelling.", In Proceeding of the ASME 2019 38th International Conference on Ocean, Offshore and Arctic Engineering, OMAE2019-96245, 2019, Glasgow, UK.

Hall, T.M., and S. Jewson., 2007, "Statistical Modeling of North Atlantic Tropical Cyclone Tracks", Tellus, Vol. 59A (2007), pp 486-498.

Hidetaka H., Takuji W., Wataru F., Keiji K., Katsuji T., 2018, "Generation of a Spatially Periodic Directional Wave Field in a Rectangular Wave Basin Based on Higher-Order Spectral Simulation", Ocean Engineering, Vol. 169, pp 428 – 441.

Holland, G., 1980, "An Analytic Model of the Wind and Pressure Profiles in Hurricanes" Monthly Weather Review, Vol. 108, pp 1212-1218.

Huang, J., Zhang, Y., 2018, "Semi-Empirical Single Realization and Ensemble Crest Distributions of Long-Crest Non-Linear Waves", In Proceedings of the ASME 2018 37th International Conference on Ocean, Offshore and Arctic Engineering, OMAE2018-78192, 2018, Madrid, Spain.

Huang, J., Kim, H., 2020, "Physical Modeling and Simplification of FPSO Topsides Module in Wind Tunnel Model Tests.", In Proceedings of the ASME 39th International Conference on Ocean, Offshore & Arctic Engineering, OMAE2020-19058, Florida, USA.

Iafrati, A., De Vita, F., Alberello, A., Toffoli, A., 2015, "Strongly Nonlinear Phenomena in Extreme Waves", SNAME Transactions, Vol. 123, 17-38

Iafrati, A., De Vita, F., Verzicco, R., 2019, "Effect of the Wind on the Breaking of Modulated Wave Trains", European Journal of Mechanics/B-Fluids, Vol. 73, 6-23

Khait, A., Shemer, L., 2019, "Nonlinear Wave Generation by a Wavemaker in Deep to Intermediate Water Depth", Ocean Engineering, Vol. 182, pp 222 – 234.

Kharif, C., Giovanangeli, J., Touboul, J., Grare, L., Pelinovsky, E., 2008, "Influence of Wind on Extreme Wave Events: Experimental and Numerical Approaches", Journal of Fluid Mechanics, Vol. 594, 209-247

Kim, J. W., Jang, H., Xu, W., Shen, Z., Kara, M., Yeon, S., Yan, H., 2018, "Numerical Modeling of Neutrally-Stable and Sustainable Atmospheric Boundary Layer for the Wind Load Estimation on an Offshore Platform", In Proceedings of the ASME 37th International Conference on Ocean, Offshore & Arctic Engineering, OMAE2018-78699, Madrid, Spain.

Kim, J. W., Jang, H., Xu, W., Shen, Z., Yeon, S., 2019, "Developing Industry Guidelines for the CFD-Based Evaluation of Wind Load on

Offshore Floating Facilities", Offshore Technology Conference, OTC-29270-MS.

Kim, J. W., Jang, H., Yeon, S., Kim, H., 2020, "Numerical Modeling of Sustainable Atmospheric Boundary Layer for Offshore Floaters.", In Proceedings of the ASME 39th International Conference on Ocean, Offshore & Arctic Engineering, OMAE2020-10747, Florida, USA.

Kim, J., Baquet A., Jang, H., 2019, "Wave Propagation in CFD-Based Numerical Wave Tank", In Proceedings of the ASME 38th International Conference on Ocean, Offshore & Arctic Engineering, OMAE2019-96460, Glasgow, UK.

Klein, M., Dudek, M., Clauss, G., Hoffmann, N., Behrendt, J., Ehlers, S., 2019, "Systematic Experimental Validation of High-Order Spectral Method for Deterministic Wave Prediction", In Proceedings of the ASME 2020 39th International Conference on Ocean, Offshore and Arctic Engineering, OMAE202-95063, 2020, Florida, USA.

Koop, A., Yeon Seong, M., Yu, K., Loubeyre, S., Xu, W., Huang, J., Vinayan, V., 2020, "Development and Verification of Modeling Practice for CFD Calculations to Obtain Current Loads on FPSO", In Proceedings of the ASME 39th International Conference on Ocean, Offshore & Arctic Engineering, OMAE2020-19173, Florida, USA.

Kristoffersen, J. C., Bredmose, H., Georgakis, C.T., Tao, L., 2019, "Preliminary Experimental Study on the Influence of the Local Wind Field on Forces from Breaking Waves on a Circular Cylinder", In Proceedings of the ASME 38th International Conference on Ocean, Offshore & Arctic Engineering, OMAE2019-95179, Glasgow, UK.

Liao, B., Dong, G., Ma, Y., Gao, J., 2017, "Linear-shear current modified Schrodinger equation for gravity waves in finite water depth", Physical Review E, 96: 043111.

Liao, B., Ma, Y., Ma, X., Dong, G., 2018, "Experimental study on the evolution of Peregrine breather with uniform-depth adverse currents", Physical Review E, 97: 053102.

Liu, Y., and Grey, S., 2019, "A probabilistic Approach to Tropical Cyclone Modelling", In Proceedings of the ASME 38th International Conference on Ocean, Offshore & Arctic Engineering, OMAE2019-96245, Glasgow, UK.

Liu, S., Zhang X., 2019, "Numerical Investigation on the Rogue Wave Occurrence in Crossing Wave Fields", In Proceedings of the ASME 38th International Conference on Ocean, Offshore & Arctic Engineering, OMAE2019-96029, Glasgow, UK.

Liu, S., Zhang, X., 2019, "Extreme Wave Crest Distribution by Direct Numerical Simulations of Long-crest Nonlinear Wave Fields", Applied Ocean Research, 86, 141-153.

Liu, S., Zhang, X., 2020, "A Modified Benjamin-Feir Index for Crossing Sea States", 35th International Workshop on Water Waves and Floating Bodies, Seoul, Korea.

Luxmoore, J., Ilic, S. & Mori, N. 2019, "On Kurtosis and Extreme Waves in Crossing Directional Seas: A Laboratory Experiment". Journal of Fluid Mechanics 876, 792-817.

McAllister, M.L., Draycott, S., Adcock, T.A.A, Taylor, P.H., Bremer, T.S. van den, 2019, "Laboratory Recreation of the Draupner

Wave and the Role of Breaking in Crossing Seas". Journal of Fluid Mechanics 860, 767-786.

Mori, N., Onorato, M. & Janssen, P. A. E. M., 2011, "On the Estimation of the Kurtosis in Directional Sea States for Freak Wave Forecasting." Journal of Physical Oceanography 41 (8), 1484-1497.

Niu, X. Ma, X., Ma, Y., Dong, G., 2020, "Controlled extreme wave generation using an improved focusing method", Applied Ocean Research, 95: 102017.

Onorato, M., Cavaleri, L., Fouques, S., Gramstad, O., Janssen, P. A., Monbaliu, J., Osborne, A. R., Pakozdi, C., Serio, M., Stansberg, C., Toffoli, A., Trulsen, K., 2009, "Statistical properties of mechanically generated surface gravity waves: a laboratory experiment in a three-dimensional wave basin", Journal of Fluid Mechanics, Vol. 627, 235-257.

Richard, P. and Hoxey, R., 1993, "Appropriate Boundary Conditions for Computational Wind Engineering Models Using the k-e Turbulence Model", Journal of Wind Engineering Industrial Aerodynamics 46, 145-153.

Ross, E., Astrup, O.C., Bitner-Gregersen, E., Bunn, N., Feld, G., Gouldby, B., Huseby, A., Liu, Y., Randell, D., Vanem, E., Jonathan, P., 2019, "On Environmental Contours for Marine and Coastal Design", Proceeding of the ASME 2019 38th International Conference on Ocean, Offshore and Arctic Engineering, OMAE2019-96587, 2019, Glasgow, UK.

Tao, S., Song, J., Wang, Z., Liu, Y., Dong, S., 2019, "Statistical Analysis for the Duration and Time Intervals of Tropical Cyclones, Hong Kong", In Proceedings of the ASME 38th International Conference on Ocean, Offshore & Arctic Engineering, OMAE2019-95791, Glasgow, UK.

Toffoli, A., Babanin, A., Onorato, M., Waseda, T., 2010, "Maximum Steepness of Oceanic Waves: Field and Laboratory Experiments.", Geophysical Research Letters, Vol. 37, L05603.

Toffoli, A., Ducrozet, G., Waseda, T., Onorato, M., Abdolahpour, M., Nelli, F., 2019 "Ocean Currents Trigger Rogue Waves", In Proceedings of the Twenty-ninth International Ocean and Polar Engineering Conference, Honolulu, Hawaii, USA

Touboul, J., Giovanangeli, J.P., Kharif, C., Pelinovsky, E., 2006, "Freak Waves Under the Action of Wind: Experiments and Simulations", European Journal of Mechanics/B-Fluids, Vol. 25, 662-676

Tsukada, Y., Suzuki, R., Ueno, M., 2017, "Wind Loads Simulator for Free-Running Model Ship Test", In Proceedings of the ASME 36th International Conference on Ocean, Offshore & Arctic Engineering, OMAE2017-61158, Oslo, Norway.

Tulin, M.P., Waseda, T., 1999, "Laboratory Observation of Wave Group Evolution, Including Breaking Effects", Journal of Fluid Mechanics, Vol. 378, 197-232

Vickery, P. J., 2014, "Analysis of Hurricane Winds", In Proceedings of Offshore Technology Conference, OTC-25244-MS.

Watanabe, S., Fujimoto, W., Kodaira, T., Davies, G., Lechner, D., Waseda, T., 2019, "Data Assimilation of the Stereo Reconstructed Wave Fields to a Nonlinear Phase Resolved Wave Model", In Proceedings of the ASME 38th International Conference on Ocean, Offshore & Arctic

Engineering, OMAE2019-95949, Glasgow, UK.

Yeon, S., Jang, H., Kim, J.W., Kim, J., Nam, B.W., O' Sullivan, J., Huang, Z., Kim, H.J., Hong, S.Y., 2019, "Numerical Modeling Practice and Verification of the Wind Load Estimation for FPSO and Semi-submersible", In Proceedings of the ASME 38th International Conference on Ocean, Offshore & Arctic Engineering, OMAE2019-96429, Glasgow, UK.

Xie, B., Ren, X., Li, J., Duan, W., Wang, J., and Zhao, B., 2019, "Study on Gust Parameters and Wind Spectrum of South China Sea", In Proceedings of the ASME 38th International Conference on Ocean, Offshore & Arctic Engineering, OMAE2019-95779, Glasgow, UK.

Xie, B., Ren, X., Xu, J., Li, Z., 2019, "Research on wave spectrum and parameter statistics in the northern South China Sea", Offshore Technology Conference, OTC29547

Xu, W., Huang, J., Kim, H. , 2019, "Thorough Verification and Validation of CFD Prediction of FPSO Current Load for Confident Applications", In Proceedings of the ASME 38th International Conference on Ocean, Offshore & Arctic Engineering, OMAE2019-95017, Glasgow, UK.

Xu, W., Huang, J., Kim, H., 2019, "Thorough Verification and Validation of CFD Prediction of FPSO Wind Load for Confident Applications", In Proceedings of the ASME 38th International Conference on Ocean, Offshore & Arctic Engineering, OMAE2019-95018, Glasgow, UK.

Young, I. R., 2019, "The Wave Climate of the Southern Ocean", In Proceedings of the ASME 38th International Conference on Ocean, Offshore & Arctic Engineering, OMAE2019-95168, Glasgow, UK.

The Specialist Committee on Ships in Operation at Sea (SOS)

Final Report and Recommendations to the 29th ITTC

1. INTRODUCTION

1.1 Membership and Meetings

The members of the Specialist Committee on Ships in Operation at Sea (SOS) of the 29th International Towing Tank Conference are as follows:

- Jinbao Wang (Chairman), MARIC, China
- Florian Kluwe (Secretary), HSVA, Germany.
- Dominic Hudson, University of Southampton, UK
- Henk van den Boom, MARIN, The Netherlands
- Sebastian Bielicki, CTO, Poland
- Koutaku Yamamoto, Mitsui, Japan
- Kenichi Kume, NMRI, Japan
- Hideo Orihara, JMUC, Japan
- Se-Myun Oh, SHI, South Korea
- Gongzheng Xin, CSSRC, China

Four Committee meetings were held as follows.

- 17~19, Jan, 2018 CTO, Poland. All members except Henk van den Boom from MARIN attended.
- 10-12, Sep, 2018, Mitsui, Japan. All members except Gongzheng Xin from CSSRC attended.
- 8-10, May, 2019, HSVA, Germany. All members attended.
- 15-17, Jan, 2020, Samsung Ship Model Basin, Daejeon, South Korea. All members attended.

The AC representative to IMO Prof. Gerhard Strasser attended all the four meetings in order to keep close eye on the progress of the speed/power trial procedure, C_A guideline and provide feedback from IMO/MEPC meetings.

Figure 110: SOS committee photo with Prof. Strasser (4th meeting)

1.2 Contact with ITTC committees

The 29th SOS committee has coordinated and exchanged information with the CFD/EFD, Resistance and Propulsion, and Manoeuvring in waves Committees on relevant issues.

1.2.1 CONTACT CFD/EFD COMMITTEE

The committee has contacted CFD/EFD committee on the following aspects: Establish guideline for CFD to get wind coefficient. Initiate and conduct benchmark study for evaluation of CFD applicability to determine the wind resistance coefficients. Shallow water correction using CFD calculations at model and full scale. Monitoring the development of CFD methods for added resistance due to waves.

CFD/EFD committee chair Sofia Werner recommended Prof. Takanori Hino, for expertise in CFD calculations, to attend SOS meeting and provided valuable guidance on how to proceed. SOS will refer to new guideline 7.5-03-01-02 Quality Assurance in Ship CFD Application in guideline on CFD based determination of wind resistance coefficients.

1.2.2 CONTACT OTHER COMMITTEES

SOS committee has Contacted R&P committee regarding Load Variation Coefficient example. Contact was made to Prof. Hironori Yasukawa from Manoeuvring in waves committee regarding combined current correction method. Contact Quality Systems Group to obtain instruction on Uncertainty Analysis matters.

1.2.3 JOINT MEETING WITH CFD/EFD AND R&P COMMITTEE

Accurate performance prediction from model test is very important for sea trial, especially those ships performed sea trial usually at ballast condition. For this purpose, during AC meeting in France (2019), a joint meeting with CFD/EFD and R&P committee chair was held on a new method to predict delivered power using CFD/EFD combination. The method obtained k from CFD while other data from model test. Relative factors which may influence k have been extensively studied numerically, including grid shape and size, temperature, large speed range, posture, rudder etc. Model tests were carried out intensively according to ITTC procedure in MARIC towing tank. Delivered power prediction using this method agrees well with sea trial results on two typical sister ships-208k bulk carrier and 20k container ship. It shows that the combination of CFD/EFD method is practical and feasible.

After face to face discussion and Email contact, CFD/EFD and R&P committee agree to refer paper (by Jinbao Wang et al), Feasible study on full scale delivered power prediction using CFD/EFD combination method, in their final reports to full conference.

1.3 Contact with AC chairman about IMO issues

The AC representative to IMO Prof. Gerhard Strasser, attended IMO MEPC 71-74 during this term. Major outcome/comments related to fluid dynamic issues are as follows.

(1) Major outcome/comments from IMO MEPC 71 meeting.

- IMO has received submission from ITTC with overview on all procedures that have changed after the 28th ITTC
- Either Raven method should be improved with sufficient validation, or a new method should be proposed

(2) Major outcome/comments from IMO MEPC 72-73 meeting

- China has submitted a proposal on Evaluation of ISO15016_2015 MEPC 72-INF.15
- Submission by ITTC on sea trial procedure(7.5-04-01-01:2017) proposed to MEPC73 (MEPC 73/5/7) was accepted by the meeting
- IACS 2014 industry guidelines shall be updated to reflect the new ITTC sea trial procedure

(3) Major outcome/comments from IMO MEPC 74 meeting

- Amendments to MARPOL Annex VI adopted
- Discussions on introduction of EEDI phase 3 and early implementation for container ships as they are far below the current baseline. Without data, the reduction rate cannot be adjusted for container vessels
- Intense discussion on alternative fuels and main focus on new fuels, marine plastic litter
- Some people raised questions about Raven-method unofficially

1.3.1 COMMENTS FROM AC

Sea trial procedure（2017 version） was highly appreciated by AC – gained much maturity.

ITTC shall have a representative in ISO committee on 15016 sea trial procedures to coordinate.

All modification to guidelines shall be done in word using tracking mode; track-changes version shall be submitted together with clean version; modified guideline to be sent to QSG Chairman.

1.4 Terms of Reference (TOR) Assigned by the 28th ITTC

1. Address the following aspects of the analysis of speed/power sea trial results:

(1) Shallow water correction

Formulate, validate and recommend a single method for correcting speed/power sea trial measurements for shallow water effects based on first principles, using full scale and model scale tests and CFD analyses of a suitable range of vessel designs and sizes, water depths and ship speeds.

(This task is considered the highest priority for the specialist committee and shall be commenced immediately. If possible, the procedure 7.5-04-01-01.1 shall be updated to incorporate the new procedure. If this is not possible, the specialist committee shall liaise with the Advisory Council on which action to take).

(2) Wave correction

a. More extensive validation of the present wave correction methods and expand range of application, introduce other methods where necessary.

b. Monitoring the development of CFD methods for added resistance due to waves.

(3) Wind correction

a. Guidance on the location and height of the anemometer and whether a dedicated anemometer is necessary.

b. Investigate limitations of averaging wind correction method and suggest improvements.

c. Establish guideline for CFD to get wind coefficient.

d. Extend wind coefficient database for more ships.

e. Initiate and conduct benchmark study for evaluation of CFD applicability to determine the wind resistance coefficients.

(4) Current correction

a. Further validation on the present current correction methods.

b. To find the possibility of using long track on 2 double runs.

(5) Comprehensive correction

a. Further validation on Extended-Power-Method

b. More investigation on existing methods for the speed/power sea trial analysis, including the Combined Correction Method presented by H. Yasukawa (Ship Technology Research, Vol.62, No. 3, 2015, pp.173-185.)

(6) Study and validate model-ship correlation factors at different drafts when possible.

(7) Provide a practical guidance for installation of measuring equipment on a propeller shaft with regard to the shaft material properties (e.g. G modulus), shaft geometry and alignment.

(8) Other

a. Water temperature and density influence on ship's performance

b. Noise in the measured data during the ship performance assessment and identify the method for filtering it.

c. Measurement error and influence on power

2. Update the speed/power sea trial procedures 7.5-04-01-01.1 where appropriate.

3. Update guideline to determine model-ship correlation factors at different draft.

4. Explore 'ship in service' issues, to get feed-back to towing tanks with respect to:

a. Key performance indicators identifying and establishing performance baseline when appropriate.

b. More accurate measurement of environmental data, including wind, waves, current, etc, and comparison with hindcast data when available.

c. Speed power related info monitoring, including fuel consumption, shaft torque, speed, draught, trim and rudder angle etc.

d. On board recording.

e. To find possibilities to analyse ship performance, including speed power relation, decrease of ship speed, etc. on a single run.

f. The applicability of unmanned (flying, floating or underwater...) vehicles and devices.

5. Monitor the new information and communication (ICT) technologies applied on board ships to collect and process data as well as ship control systems, and identify their influence on ship performance prediction.

2. SHALLOW WATER CORRECTIONS

2.1 General

Speed power trials are preferably conducted in deep water because the EEDI and contract speed are specified for ideal conditions. Especially for large or fast ships, the actual water depth at the trial's location may be such that a speed loss is incurred. In such cases trial procedures such as ISO 15016:2015 and ITTC 2017, allow for a speed correction according to a formula proposed by Lackenby (1963).

In 2004 at the start of the STA-Joint Industry Project (Boom, Huisman and Mennen 2014), comparisons of trial results conducted by the same ship in both deep- and shallow water clearly indicated that the formula published by Lackenby cannot be considered accurate.

The verification of the Lackenby formula by means of model tests is complicated due to the limited width of model basins which affects the results in shallow water far more than in deep water.

Raven (2012) studied the effects of shallow water on resistance by means of both model testing and potential flow calculations, in order to develop a correction method for the limited width of the model basin. He found that much of the resistance increase in shallow water is actually viscous resistance rather than wave resistance.

Based on these results, Raven (2016) developed a new correction method for shallow water effects in speed power trials. In this so-called "Raven method", the main dimensions and block coefficient determine the viscous resistance of the ship and its increase in shallow water is estimated. The wave resistance is supposed unaffected as long as the depth Froude number is limited; but an additional correction for the effect of the increased dynamic sinkage is applied. This effect on the power increase has been formulated by Raven based on the Tuck formula for squat (Tuck & Taylor 1970), extended by an estimate for deep water sinkage. The Raven procedure thus estimates the power increase in shallow water at equal speed. This procedure fits in the "Direct Power Method" utilized by both ITTC2017 and ISO15016:2015 to correct the measured power for shallow water effects.

With the continued support of the STA-Group, systematic full scale speed power trials were conducted by MARIN on board three vessels. Two vessels were trialled in 4 water depths and one vessel was trialled in 3 water depths.

The trials were conducted in full compliance with ISO 15016:2015 and ITTC2017 and the measured results were analysed with the freeware STAIMO (www.staimo.org). The weather conditions during each of these trials were close to ideal; corrections for wind and waves were negligible to small.

For each ship and each water depth, the shallow water effects were computed with both the old method of Lackenby and the new Raven method. The results demonstrated that the Raven method consistently provides more accurate results. These results are presented in

the 28th ITTC (2017) Proceedings. Figure 111 to Figure 114 wrap up these results.

Based on this information the 28th ITTC included the Raven method in the Procedure 7.5-04-01-01.1 for speed/power trials next to the existing Lackenby method.

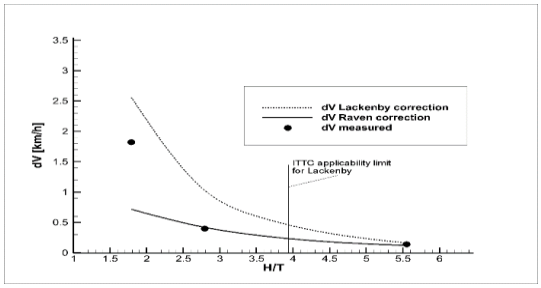

Figure 111 Raven and Lackenby compared to trial results for inland vessel [ITTC 2017]

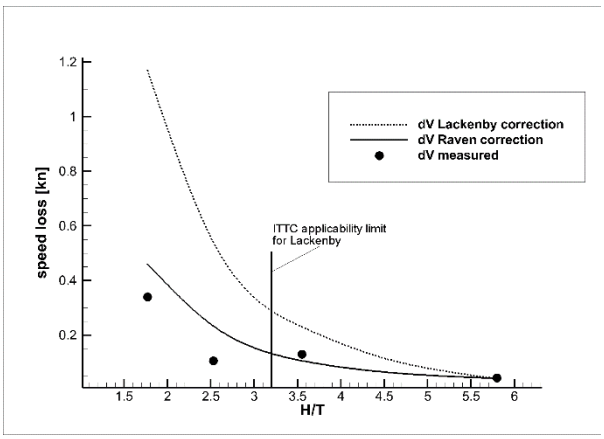

Figure 112 Raven and Lackenby compared to trial results for hopper suction dredger [ITTC2017]

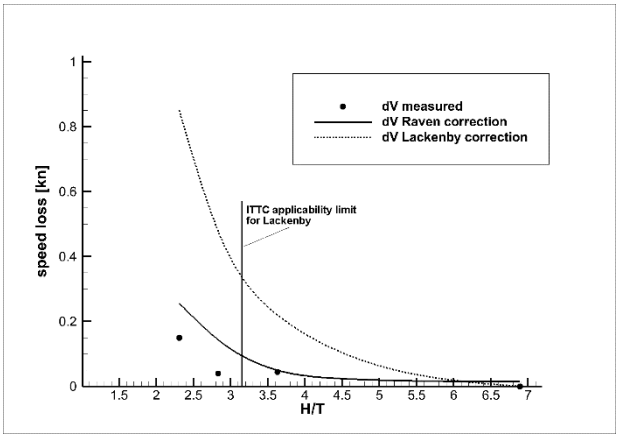

Figure 113 Raven and Lackenby compared to trial results for research vessel [ITTC2017]

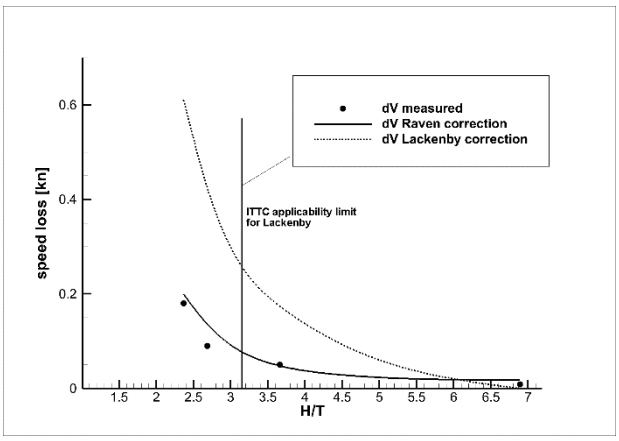

Figure 114 Raven and Lackenby compared to trial results for LPGC on single run [ITTC2017]

2.2 Scope of 29th ITTC SOS

In 2017 the 28th ITTC assigned the new SOS Committee with the following tasks:

Further validation of Raven (2016) method and comparison with Lackenby

More investigation of model tests on shallow water correction

To study the possibility of CFD method on shallow water correction

The three vessels deployed by MARIN and STA-Group for the speed power trials to validate the Raven method, comprised an inland tanker, a hopper suction dredger and a research vessel. These vessels comprised a series of different hull geometries and the trials covered a solid range of water depths.

Although scaling of measurement results to larger sizes is still considered reliable by the ITTC community, the Conference desired a more extensive validation with full scale trials with representative large merchant vessels to be conducted by multiple members.

The 29th ITTC SOS Committee noted that the trial results of the fourth vessel, presented to the 28th ITTC, a 80,000 m3 LPG carrier trialled on two water depths by HHI, should be rejected. Although the results were reasonably in line with those of the other three vessels, the trials on the 80 k LPGC did not comply with ITTC2017 procedure as they were conducted with single runs and therefore the effect of current was not eliminated in the presented results. Therefore, these results have to be neglected.

To further validate the Raven method and compare it with Lackenby, the 29th ITTC SOS Committee aimed for an additional extensive and dedicated speed power trial campaign on various large merchant vessels such as ultra large container vessels, very large bulkers and LNG carriers in both deep and shallow water.

At the same time it was envisaged that these trials would be accompanied by systematic model tests on both deep and shallow water and by in-depth CFD analysis. In this way a better understanding of the shallow water effects on speed power was anticipated and a solid shallow water correction method for speed power trials would be achieved. This work was to be shared by the key members of the ITTC SOS Committee.

2.3 Evaluation

Several Chinese institutes lead by SSSRI evaluated ISO 15016:2015 and the ITTC 2017 Procedures for speed power trial analysis. Comparisons between the Raven and Lackenby methods were made by applying them to the results of existing speed power trials. In most cases the corrections provided by Raven were found to be smaller than those from Lackenby.

It was concluded by the participating institutes that the Raven method has a solid scientific background and has been validated by the dedicated speed power trials on different water depths (MEPC72/INF.15, 2018).

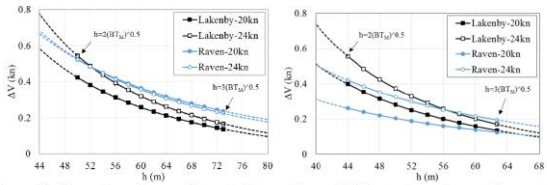

Correction of speed through shallow water of a Container at EEDI(Left) and light load(right) condition

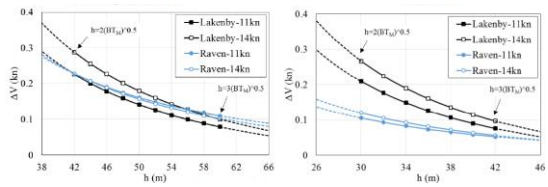

Correction of speed through shallow water of a Bulk carrier at EEDI(Left) and light load(right) condition

Figure 115 Evaluation of Raven method (MEPC72/INF 15, 2018)

2.4 Model Tests & Physics

The extensive numerical and experimental work of Raven (2012, 2016, 2019) on shallow-water effects in resistance and propulsion over the last decade has been closely reviewed by the

SOS Committee. The published results provided a good basis for the understanding of the physics involved. It also presented the concerns and limitations of model testing for shallow water conditions. The width of most basins used for shallow water testing is too small for reliable results and test results thus require a sophisticated correction and extrapolation method.

The large difference of the measured model resistance in deep and shallow water was presented and explained by Dr Hoyte Raven to the ITTC SOS Committee in their Hamburg meeting in May 2019. The Committee solutions for the long-standing problem of the power and speed of ships in shallow water including the correction method for speed power trials.

In 2011 Raven introduced a first step to correct for the effect of the limited width of model basins. At that time no method was available to correct for this, i.e. to translate the model resistance in the tank to that in a waterway of unlimited width and equal depth. By analyzing the flow field from several computations, the nature of the tank wall effect was established, and a new theoretical method developed. It requires a single potential flow computation; evaluation of some fluxes from the result, and solution of an algebraic equation to obtain corrected model speeds. Thus, the measured resistance points are shifted to a slightly higher speed by an amount that depends on water depth, speed and hull form. It then appears that the limited tank width exaggerates the apparent water depth dependence. After the correction, the true water depth effect appears to be a lot smaller.

But there is another important aspect. Model tests are 'extrapolated' to full scale to derive a ship performance prediction. The straightforward application of common model-to-ship extrapolation methods would include the shallow water resistance increase entirely in the 'wave' or 'residual' resistance component, which is assumed equal for model and ship. Much of the resistance increase in shallow water is actually viscous resistance.

Computational studies (Raven 2019) have indicated that this viscous resistance increase is in most cases a similar percentage for model and ship, and should be included in an increase of the form factor. This is the method now applied at MARIN. It reduces the assumed water-depth dependency of the ship resistance. Both steps have substantially improved the power predictions for ships in shallow water.

Starting with the deep water resistance curve, the two dominant empirical contributions from the shallow water correction method were added: the increase of the viscous resistance, and the increase of resistance due to the additional dynamic sinkage. In Figure 116 this process is visualized and results for the actual ship model are presented.

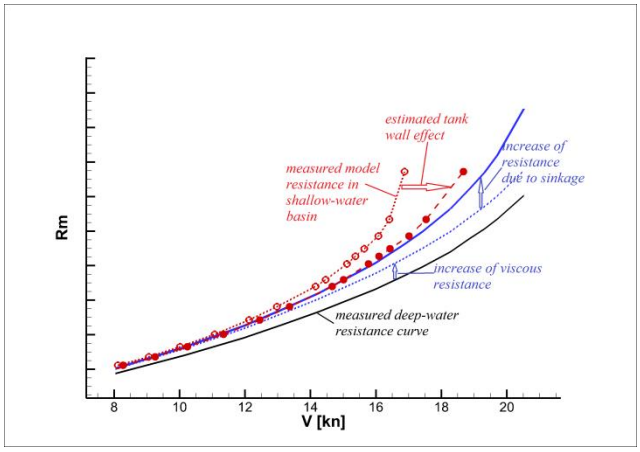

Figure 116 Model test results in deep water corrected to shallow water and compared with model tests results in shallow water [Raven]

A good correlation was obtained with results of the model tests in MARIN's Shallow Water Basin (220 x 16 x 1.0 m), corrected for the tank wall effect.

The remaining discrepancy was the shallow water increase of the wave resistance, which, contrary to previous insights, turns out to be small.

2.5 Full Scale Trials

Although serious plans were developed in China to contribute with dedicated speed power trials with large merchant vessels on different water depths, these plans did not materialize over the past three years due to lack of confidence, costs and time constraints.

Dedicated systematic trials on large merchant vessels happen to be more complicated and cumbersome than anticipated.

Effectively over the term of the ITTC SOS Committee, no new results of shallow and deep water trials have been delivered or collected.

2.6 CFD Analysis

As part of the agreed validation effort, CTO conducted a correlation study comparing the Raven correction method with CFD results.

The CFD analysis were conducted with the RANS-code STARCCM for the KRISO-containership in 6 water depths ranging from real shallow to deep water. The numerical flow analyses were conducted with double body and free surface effects. The computational domain is presented in the adjacent Figure 117.

For each of the water depths, the resistance was computed and also calculated with the Raven method in combination with the available deep water model test results.

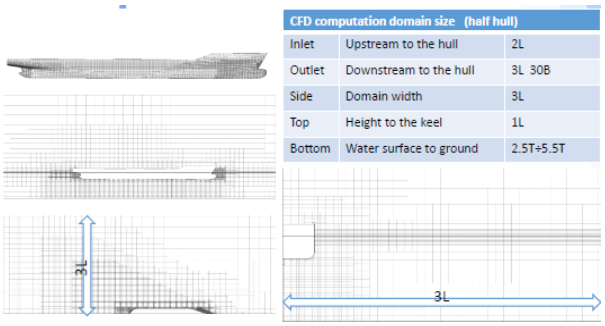

CFD computation domain size (half hull)		
Inlet	Upstream to the hull	2L
Outlet	Downstream to the hull	3L 30B
Side	Domain width	3L
Top	Height to the keel	1L
Bottom	Water surface to ground	2.5T+5.5T

Figure 117 Domain used for KCS in shallow water

The correlation is summarized in the graph below. It is noted that some water depths are outside the application limits of the Raven method. These cases are therefore excluded from the validation conclusion.

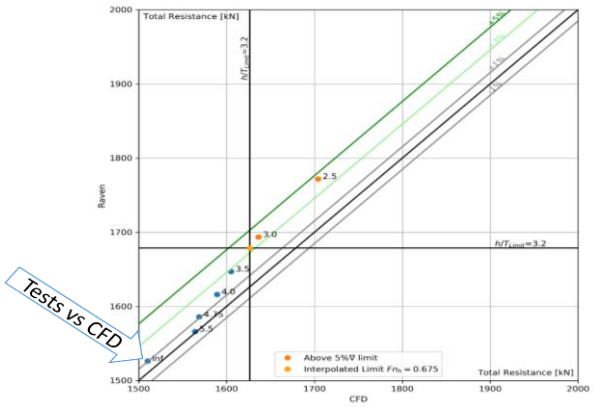

Figure 118 Correlation between Raven (vertical axis) and CFD (horizontal axis) for KCS.

It was concluded by CTO that the difference of the Raven correction compared to the CFD resistance does not exceed 3% below cases with $Fr_h = 0.675$. It was also noted that the estimated sinkage has a significant result on the results.

This implicates that if a better practical empirical sinkage prediction method would be available, the results of Raven could even be improved further.

Although this correlation study included only one vessel design, this important contribution by CTO supported the correlation

data obtained from the full scale trials as well as the correlation work conducted by Raven based on model tests and full scale data.

It was also concluded by ITTC SOS that RANS CFD can be used for computing the effects of shallow water on the resistance and propulsion and offers a powerful tool for extrapolating model test results in physically restricted model test facilities.

At the same time, it is noted that RANS CFD unfortunately does not offer a practical correction method for shallow water effects experienced during speed power trials as the geometry of the vessel on trial is normally not disclosed by designers and yards.

2.7 Water Depth Limits

In the current Procedure there is an upper limit for water depth. This limit has no rational background and causes discontinuity in the speed trial results after correction for water depth.

For the Raven method the minimum water depth limits have been investigated: The corrections may be applied for water depths compliant with: $h \geqslant 2.5\ T$ and $h \geqslant 2.4\ V^2/g$

Furthermore, the displacement change due to dynamic sinkage is limited to 5%.

2.8 Propeller Efficiency

An increased resistance normally leads to an increased propeller loading, resulting in a decrease of the propulsive efficiency. For the resistance increase due to wind and waves, this is evaluated using results of overload tests.

Some members noted that it would be consistent to do the same for a shallow water resistance increase. However, as discussed by Raven (2012), the situation is a bit different. In shallow water, not only the resistance increases, but also the wake fraction increases markedly. On the one hand the propeller loading increases more quickly than just due to the resistance increase, normally causing a drop of the open-water efficiency η_0; on the other hand also the hull efficiency

$$\eta_H = (1-t)/(1-w) \quad (1)$$

increases, which partly compensates the drop of the open-water efficiency. Therefore, only counting the drop of the open-water efficiency may not be an improvement.

Based on several model tested cases evaluated, it was concluded that the propulsive efficiency η_D should be considered unaffected by water depth, so no use should be made of the propeller load variation tests for shallow water effects.

2.9 Conclusion

Based on the available validation results from dedicated full scale trials, model tests and RANS CFD analysis, and appreciating the physically rational background of the method, ITTC SOS Committee concluded that the Raven method adopted by ITTC2017, together with the new application limits for water depth, speed and sinkage, provides a consistently more accurate correction for the effect of shallow water on the speed power performance of ships compared with the method presented by Lackenby in 1965.

Therefore, the Lackenby method shall be considered outdated and obsolete and is therefore removed in ITTC 2021 Procedure 7.5-04-01-01.2021.

ITTC shall actively propose to ISO to revise ISO15016:2015 accordingly and to implement the Raven method as the single method for

correction of the effects of water depth in analysis of measured speed-trial results.

3. WAVE CORRECTION

3.1 Introduction

There are several empirical methods to correct wave-added resistance at full scale in the sea trial procedure of ITTC (2017) version. However, the STA methods are limited to head waves. For wave encounter angles beyond 45 degrees, the NMRI method can be used, but the method needs the ship's lines. For this reason, an open and transparent semi-empirical SNNM method has been developed. It considers the full range of wave directions and can be applied when a lines plan is not available.

The SNNM method originated in the framework of EU funded FP7-SHOPERA project (2013-2016) (Papanikolaou et al., 2015) at the National Technical University of Athens, which has carried out long research on nonlinear seakeeping and added resistance (see, e.g., Papanikolaou & Nowacki, 1980; Papanikolaou & Zaraphonitis, 1987& 1993; Liu et al., 2011; Liu& Papanikolaou, 2016). The method was extended at the Nanyang Technological University (Liu & Papanikolaou, 2020) and verified by the Marine Design and Research Institute of China (MARICAR, 2016-2018; Liu et al., 2019).

An early version of the ensuing formula was submitted to IMO for consideration by member states in support of the research undertaken in SHOPERA (MEPC 70/INF.30, 2016). The formula has been undergoing continuous update with the growing data sample of the established experimental database, as documented in various publications (Liu et al., 2015; Liu et al., 2016; Liu & Papanikolaou, 2016a & 2019 & 2020).

The formula considers the main ship dimensions, global hull form characteristics and speed, along with the ensuing wave conditions, which are directly related to the wave-induced added resistance. This leads eventually to an approximation of the transfer function of the added resistance R_{AW} in regular waves of amplitude ζ_A and of any direction (head to following), which can be used in power correction during sea trial.

A database of experimental data for the added resistance of about 130 ships of all types has been established to support the development of this formula. The database, which has been continuously enriched over the last 10 years, includes at the moment about 1,500 data points for head wave conditions and another 1,500 data points for other headings, thus, in total slightly more than 3,000 experimental data points. The majority of this data refers to public domain model experimental data and the rest to confidential data from funded research and Joint Industry Projects of the developers.

Figure 119 shows the breakdown of the ships in the database per ship type, which fairly represents the breakdown of the world fleet.

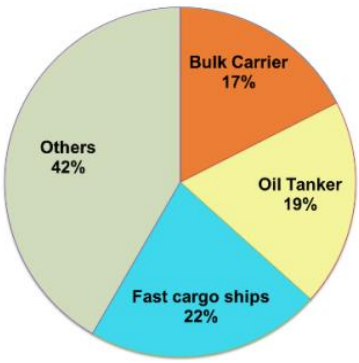

Figure 119 Breakdown of ship types in the database

Figure 120 shows several main particulars and coefficients of the ships in the database. The majority of the ships in the SNNM database are within the range of: 75 m < L_{PP}< 383 m; 5.0 < L/B < 7.5; 2.0 < B/T < 8.0; 0.54 < Cb<0.87. The

Froude number covers the typical range of ships in sea trial, i.e., from 0.10 to 0.30. Regarding the associated wave heading, most of the tank tests cases were for head waves (180 degree) only, whereas for bow waves, 21 sets of data were available and for astern waves 11 sets. Attention should be paid in the application of the formula in case the subject ship or type is not within the set limits and the coverage of the database.

The application of the SNNM formula requires 9 input parameters, as listed in Table 16.

Table 16 Example of input file of sample bulkcarrier

#	Item	Values
1	Lpp (m)	280.0
2	Beam B (m)	45.0
3	Draft at F.P. Tfore(m)	16.5
4	Draft at A.P. Taft (m)	16.5
5	Block coefficient Cb	0.86
6	kyy; radius of gyration of pitch, % Lpp	0.25
7	Length of waterline entrance(m)	42.0
8	Length of waterline run(m)	60.9
9	Froude number	0.13

Main features of the ships, and the tested Froude numbers and the wave headings in the added resistance database are illustrated in following figures.

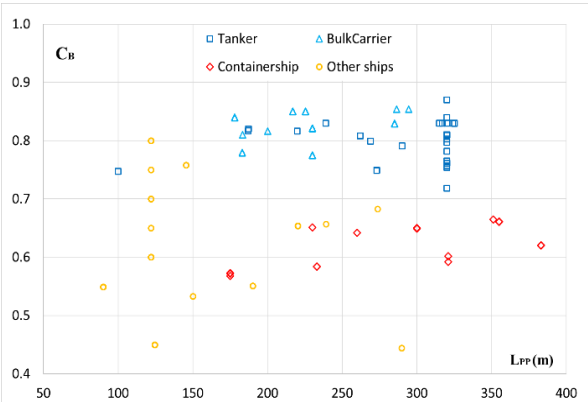

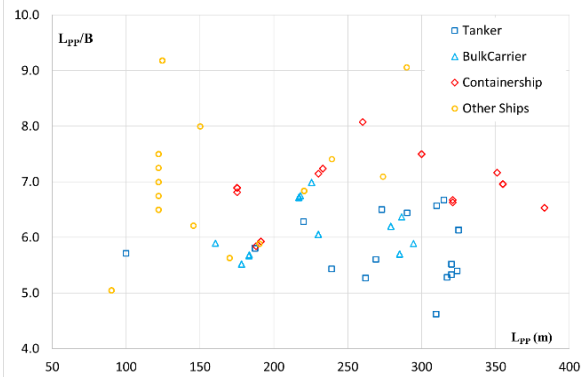

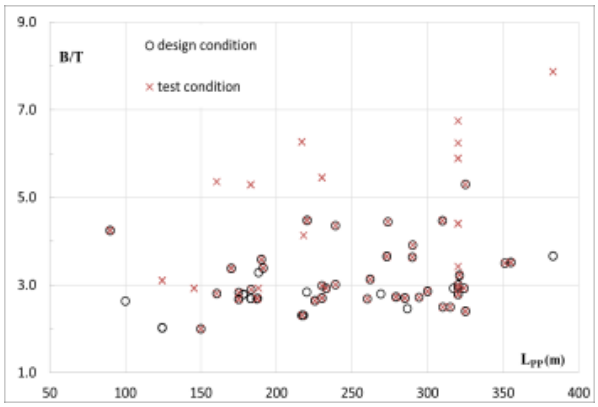

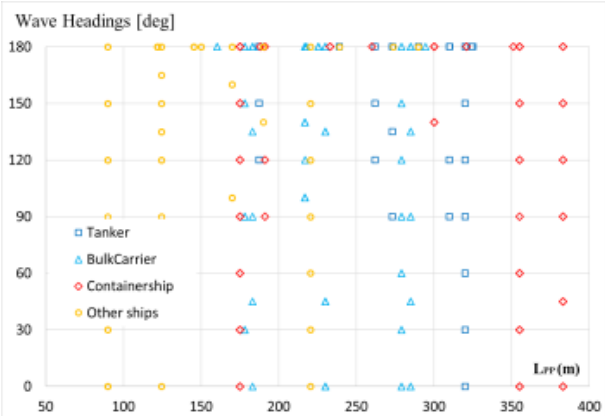

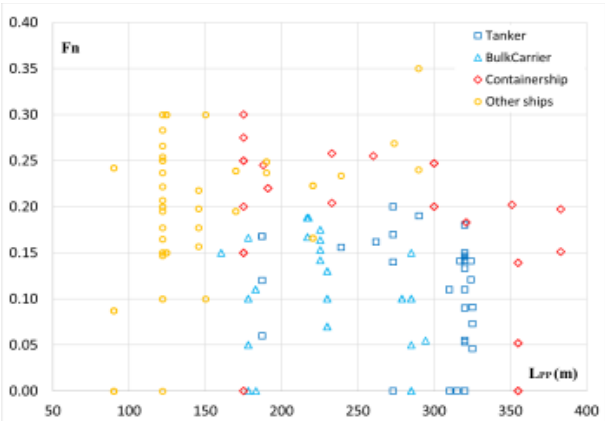

Figure 120 Main features of the ships, and the tested Froude numbers and the wave headings in the added resistance database.

3.2 SELF-VALIDATION STUDY

Figure 121 (top) shows the obtained results of the SNNM formula for the added resistance of the S-cb84 ship at Fn=0.12 in comparison with experimental results (Yasukawa et al., 2019). Figure 121 (bottom) shows the obtained results for the added resistance of a large container ship in ballast condition Fn=0.197 in comparison with experimental results obtained at MARIN, Netherlands. An overall good agreement has been observed for two cases.

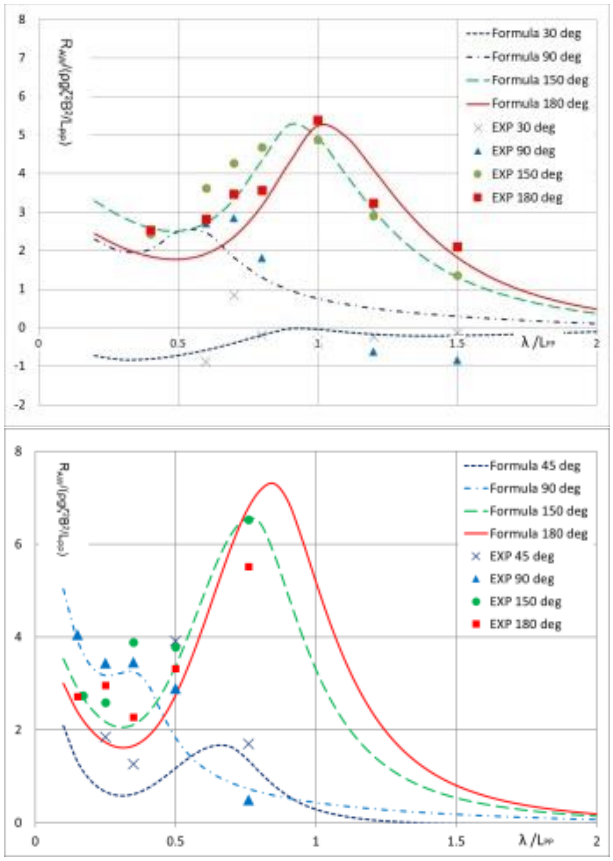

Figure 121 Added resistance of the Scb84 (top) and a large containership (bottom) in regular waves.

Some typical results of the SNNM method in comparison to other methods recommended by ITTC are shown Figure 122.

(a)

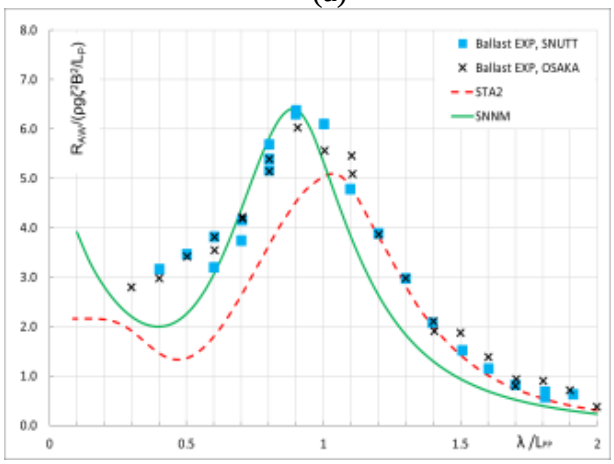

(b)

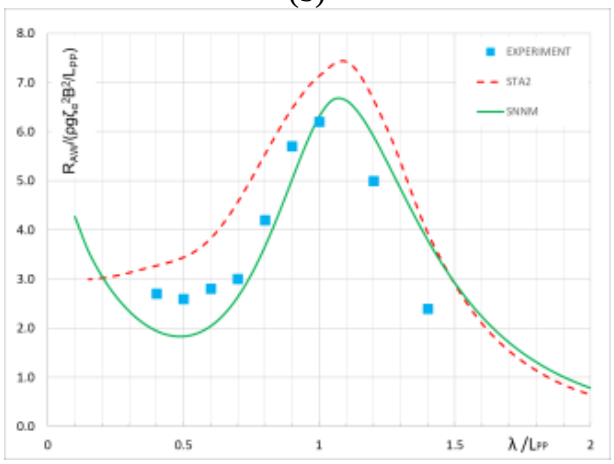

(c)

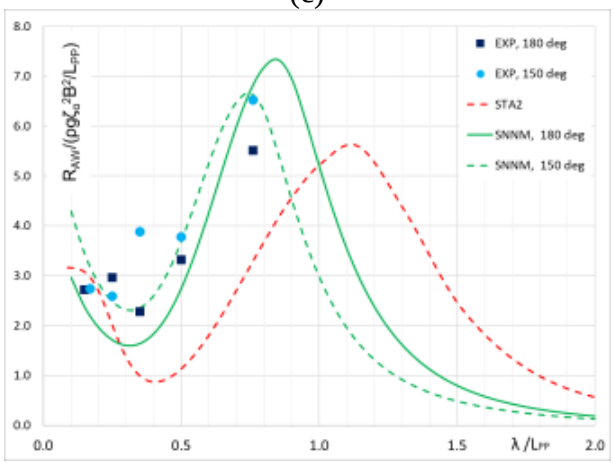

(d)

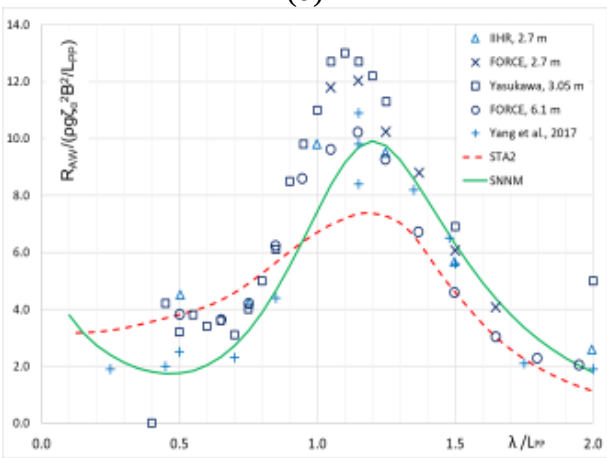

Figure 122 Added resistance of several ships in regular waves: (a) KVLCC2 in ballast condition, Fn=0.142; (b) a LNG carrier, Fn=0.20; (c) a containership in ballast condition, Fn=0.197; (d) KCS in design condition, Fn=0.26.

A more systematic validation study is presented in Figure 123 below.

(a)

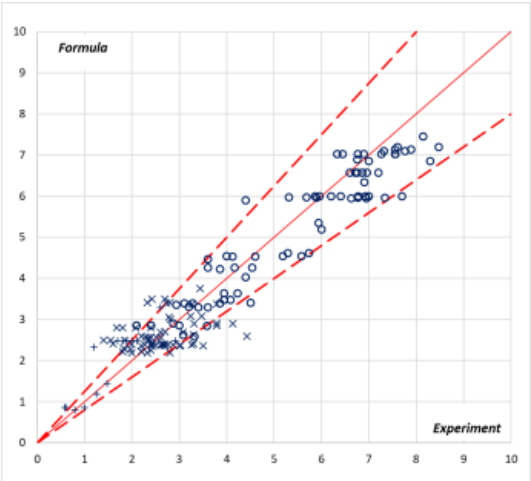

(b)

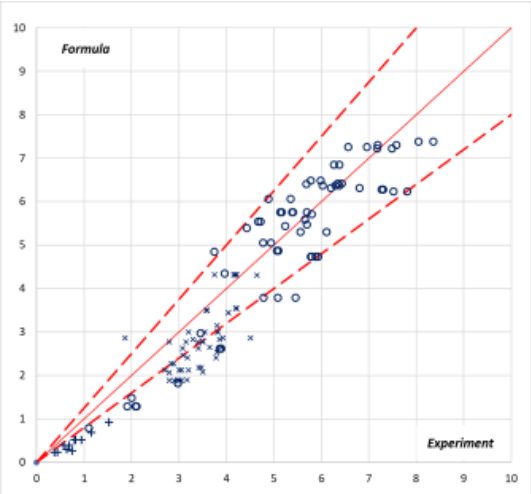

(c)

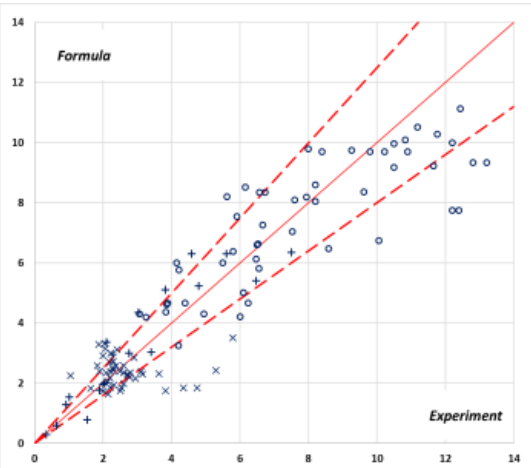

(d)

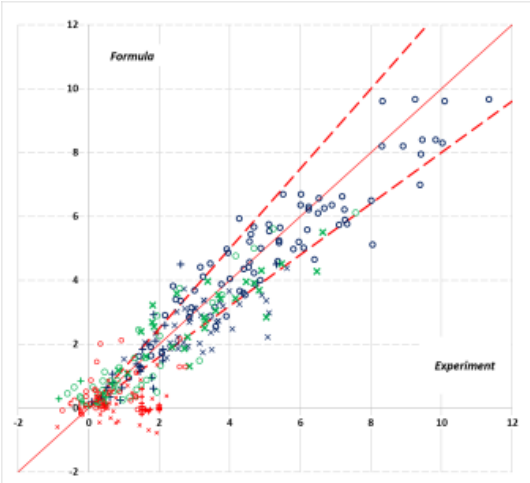

Figure 123 Predicted versus experimental non-dimensional added resistance of ships of different categories in regular waves.(×:λ/L ≤ 0.7; ○: 0.7 <λ/L < 1.5; +:λ/L ≥ 1.5).

Figure 123 (a) presents the correlation of the predicted added resistance of eight (8) full type ships (tankers and bulkers) in design load condition in regular head waves at design speed with the experimental results, with the mean percentage error being εmean = -1.3%;the Pearson's R correlation coefficient R = 0.956; the standard deviation σ = 0.624; and the Mean Absolute Error MAE = 0.499. Note that σ and MAE are calculated in terms of the non-dimensional added resistance

$$\sigma = \mathrm{R_{AW}}/(\rho g \zeta_{\mathrm{A}}{}^{2} \frac{B^2}{L_{PP}}) \qquad (2)$$

Figure 123 (b) presents the correlation of the predicted added resistance of six (6) full type ships in ballast condition in regular head waves at design speed in comparison with experimental results, with the obtained εmean = -21.9%; R = 0.948; σ = 0.777; MAE = 0.657. Note that the majority of the herein used experimental data is from tested models of small length, namely 2.9 m, thus some uncertainty may be inherent in the experimental data.

Figure 123 (c) is the correlation of the predicted added resistance of seven (7) fast cargo ships in design load or ballast condition in regular head waves at moderate speeds (Fn=0.183-0.3) with the experimental results., with the obtained εmean = 1.6%; R = 0.918; σ = 1.37; MAE = 0.999.

Figure 123 (d) shows the predicted added resistance of six ships (6) of lengths 175 m ~ 383 m in design load or ballast conditions in regular waves of random headings at moderate speeds (Fn=0.183-0.3) in comparison with experimental results. The comparison in bow waves with $120^o < \alpha \leq 180^o$ is presented in blue with obtained εmean = -4.8%; R = 0.939; σ = 0.846; MAE = 0.640. The comparison in beam waves with $60^o < \alpha \leq 120^o$ is presented in green with obtained εmean = 6.4%; R = 0.869; σ = 1.017; MAE = 0.703. The comparison in stern waves with $0^o \leq \alpha \leq 60^o$ is presented in red with εmean = -10.2%; R = 0.462; σ = 0.742; MAE = 0.542. Note that the measurements of the added resistance in astern waves are prone to large uncertainties, hence, the obtained rather low correlation R. However, the achieved σ = 0.614 and MAE = 0.459 are even smaller than that in other headings.

3.3 Preliminary Validation by Some Members of ITTC SOS Committee

Dr. Orihara from JMUC presented the validation results of a 160k DWT crude oil carrier at the 4th Meeting of the SOS Specialist Committee held at Daejeon. Figure 124 shows the results in head to beam waves. Note that here

$$K_{\mathrm{AW}} = \mathrm{R}_{\mathrm{AW}}/(4\rho g \zeta_{\mathrm{A}}{}^{2} \frac{B^2}{L_{PP}}) \quad (3)$$

Overall, predictions based on the SNNM formula are slightly lower than the experimental results. This is a satisfactory outcome, considering that in prediction a 15% error in added resistance is generally acceptable, as the added resistance is a derived seakeeping quantity of higher numerical and experimental uncertainties are expected. For more accurate predictions, high-fidelity methods (frequency and time-domain 3D panel codes, CFD or model testing) can be employed.

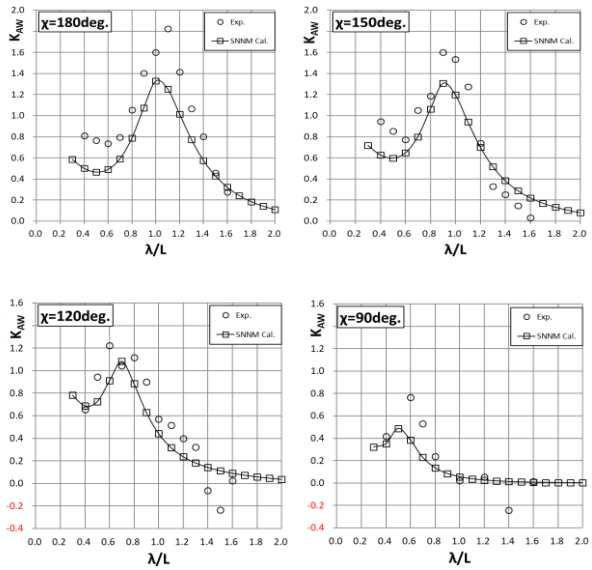

Figure 124 Added resistance of a 160k DWT crude oil carrier in regular waves of various directions, Fn=0.13.

MARIN also conducted a correlation study(Grin 2014, Grin & Boom, 2020), comparing the SNNM method with MARIN's STA- & SPAWAVE methods and the 3D panel code FATIMA, using 2 ROPAX, 1 cruise ship and 2 VLCCs(including the well-known KVLCC2).

Figure 125 shows the prediction of the added resistance for MARIN's VLCC in 2 loading conditions in head waves. For the design condition, SPAWAVE considerably under-predicts the peak value. STA2 and SNNM yield comparable peak values but the location of the peak value from STAWAVE2 shifts towards shorter wave region. On VLCC, the SNNM results show an asymptotic increase towards

short waves, while the other two methods assume a constant tail value. In ballast condition, similar performance has been observed in the very short waves region. All three methods capture well the transition of the added resistance from short wave to the peak value. However, available tank tests stop at about $\lambda/Lpp \approx 0.8$, hence, the peak value and its location cannot be identified by this experiment.

Similar phenomenon is also observed for the KVLCC2 case and the results based on SNNM method agree with model test results quite well.

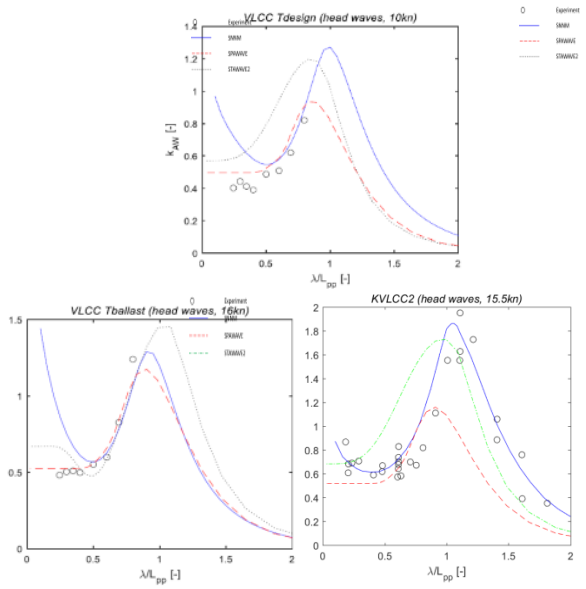

Figure 125 Added resistance of a VLCC at design and ballast conditions and KVLCC2 at design condition in regular head waves.

Two RoPaxs were studied by MARIN and Figure 126 shows the case where the results of added resistance in waves of various headings are available. In head waves, the performance of three methods in short waves is similar to that of the VLCC case. They capture well the added resistance in the transition region, with small deviations in capturing the peak value and its location. In the long waves region, SNNM underpredicts the added resistance and the other two methods have better performance. In bow quartering waves, SNNM underpredicts the added resistance in the long waves region. SPAWAVE captures herein well the experimental results; the result of STAWAVE2 is herein not included. In stern oblique waves, SNNM captures well the experimental results, while SPAWAVE results are a bit lower. There is no experimental data available in the long waves region.

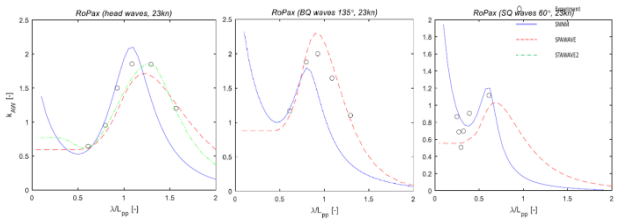

Figure 126 Added resistance of a RoPAX ship in regular waves of various directions, Fn=0.30.

Dr. Bielicki from CTO, Poland supplied the validation results of KCS containership model in following waves of λ/Lpp=0.4~1.8 at two speeds corresponding to Fn=0.13 and 0.22. As presented in Figure 127, at Fn=0.13 the added resistance is rather small and the SNNM method, besides showing the same tendency as model test, slightly underpredicts the added resistance in longer waves. At Fn=0.22, the SNNM method predicts the added resistance with high accuracy except for the point at λ/Lpp=0.4. Overall, the prediction based on SNNM method for this standard model in following waves is very encouraging.

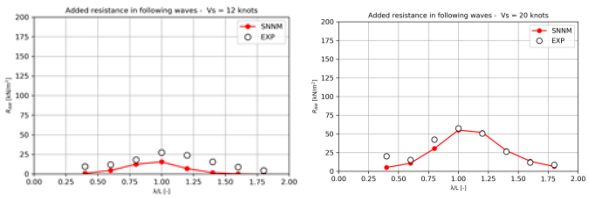

Figure 127 Added resistance of the KCS model in regular following waves, Fn=0.13 and 0.22.

Overall, the validation results from ITTC members demonstrated that the proposed SNNM method well predicts the added resistance of common cargo ship types,

particularly bulk carriers, tankers and containerships, which represent the main bulk of the world fleet, in wave of arbitrary directions, and it is fully transparent and readily applicable by engineers in practice. Its performance in predicting the added resistance of passenger ships seems less satisfactory, but may be further improved by enriching the background database. In very short waves, the new SNNM method shows an increasing asymptotic behaviour, which is observed in the experimental results of a large container ship, a 160K oil tank and the KVLCC2. This is different from other empirical methods.

3.4 Open Validation by ITTC SOS Committee

Encouraged by AC to make more valuable contribution, SOS has carried out more extensive and intensive validation of SNNM method.

After two months' discussion, criterion have been set in [0,45°] and (45° ,180°] with Pearson's correlation coefficient not less than 0.78 and 0.70 respectively. And relative error between SNNM and experiment over total resistance was also proposed as voluntary index.

Eight SOS members contributed 1477 data points for 29 ships, covering different ship types with different draft, speed and wave direction. Data analysis and report were performed by CTO and HSVA. Pearson's correlation coefficient has reached 0.86 in both wave regions. The relative error distribution has a Gaussian distribution character with average estimated expected value nearly 0% and 75% of samples are within ±2% interval.

After full discussion, SOS agreed to include SNNM method into the sea trial procedure.

4. MONITORING THE DEVELOPMENT OF CFD METHODS FOR ADDED RESISTANCE DUE TO WAVES

As stated in the final report to the 28th ITTC (ITTC 2017), CFD methods have developed to the point where they can be routinely applied to the prediction of wide range of aspects relating to ship hydrodynamic performances.

For the application of CFD methods to the wave correction in the analysis of speed/power sea trials, it is necessary for the methods to be able to predict the added resistance due to waves over a range of wave frequencies sufficient for covering encountered conditions anticipated during speed/power sea trials and in arbitrary wave headings from head to following directions.

Based on the considerations mentioned above, some examples of recent research works were reviewed to assess the state of the art of CFD application to the prediction of added resistance due to waves.

Kim M. et al. (2017a) presented CFD simulations using a commercial code STAR-CCM+ with an unstructured grid system for KVLCC2 in fully loaded condition under regular head wave conditions. The results were compared with the published model test data (Lee et al. 2013 and Sadat-Hosseini, 2013). It is showed that while the variation of added resistance with incident wave lengths are reasonably reproduced in CFD results, the quantitative agreement in added resistance of CFD results with model tests were not good in particular in short wave lengths where differences are in the order of 20%. (see Figure 128).

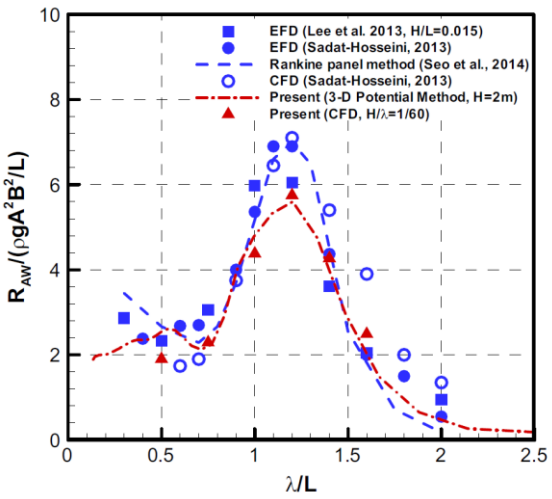

Figure 128 Added resistance (Vs = 15.5 knots, θ = 180°). (Kim M. et al. 2017, KVLCC2 in head waves)

Kim Y.-C. et al. (2017) presented CFD simulations using a code WAVIS with a structured grid system for KVLCC2 in fully loaded condition under regular head wave conditions. The results were compared with their model tests results and the published model test data (Sadat-Hosseini, 2013). It is showed that while the variation of added resistance with incident wave lengths are reasonably reproduced in CFD results, the quantitative agreement in added resistance of CFD results with model tests were not good in particular in short wave lengths where differences are in the order of 10～20%. (see Figure 129).

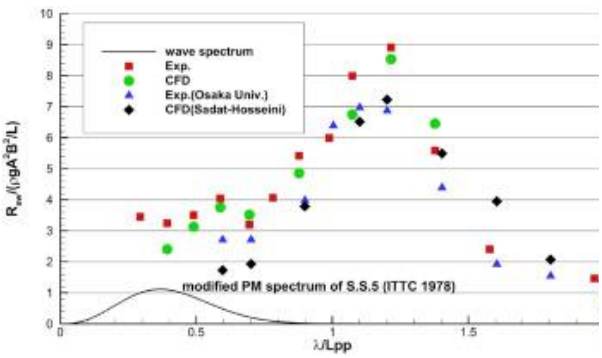

Figure 129 Added resistance in waves. (Kim Y.-C.et al. 2017, KVLCC2 in head waves)

Hossain M.A. et al. (2018) presented CFD simulations using a code CFDSHIP-IOWA with an overset structured grid system for KRISO container ship in fully loaded condition under regular head wave conditions. The results were compared with their model tests results and the published model test data (Simonsen 2013, Sadat-Hosseini, 2015). It is showed that while the variation of added resistance with incident wave lengths are reasonably reproduced in CFD results in the same way as the previous KVLCC2 cases, the quantitative agreement in added resistance of CFD results with model tests were not good in particular in short wave lengths where differences are in the order of 40%. (see Figure 130). Also noted is that the differences among model tests data were quite large corresponding to the order of 50% in short waves.

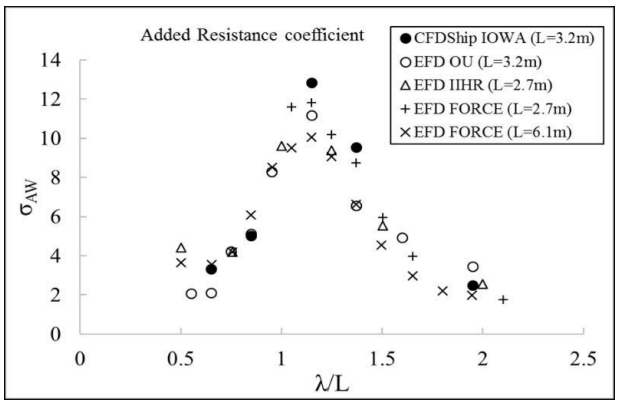

Figure 130 Added resistance coefficient. (Hossain M. A. et al. 2018, KCS in head waves)

Ohashi K. et al. (2019) presented CFD simulations using a code CFDSHIP-IOWA with an overset structured grid system for KRISO container ship in fully loaded condition under regular head wave conditions. The results were compared with their model test results. It is showed that while the CFD results agree reasonably well with model tests results in longer waves (λ /L>1.0), the quantitative agreement in added resistance of CFD results with model tests were not good in short wave

lengths where differences are in the order of 20%. (see Figure 131).

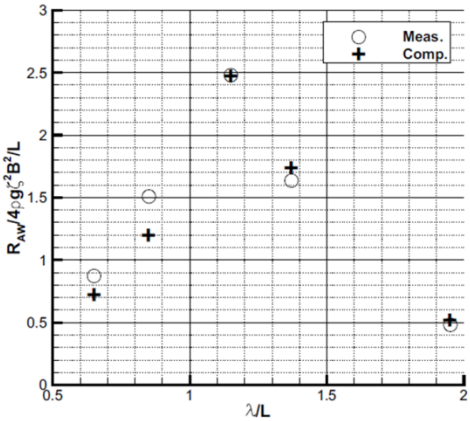

Figure 131 Comparison of an added resistance coefficient. (Ohashi et al. 2019, KCS in head waves)

Guo and Wan (2019) presented CFD simulations using a code naoe-FOAM-SJTU with an unstructured grid system for KRISO container ship in fully loaded condition under regular head wave conditions. The results were compared with the published model test data (Simonsen 2013, Sadat-Hosseini, 2015). It is showed that while the CFD results agree reasonably well with model tests results in longer waves (λ /L>1.0), the quantitative agreement in added resistance of CFD results with model tests were not good in short wave lengths where differences are in the order of 20% at the shortest wave case (λ /L=0.65). (see Figure 132).

Kim M. et al. (2017b) presented CFD simulations using a commercial code STAR-CCM+ with an unstructured grid system for S175 container ship in fully loaded condition under regular head wave conditions. The results were compared with the published model test data (Fujii and Takahashi 1975, Nakamura and Naito 1977).

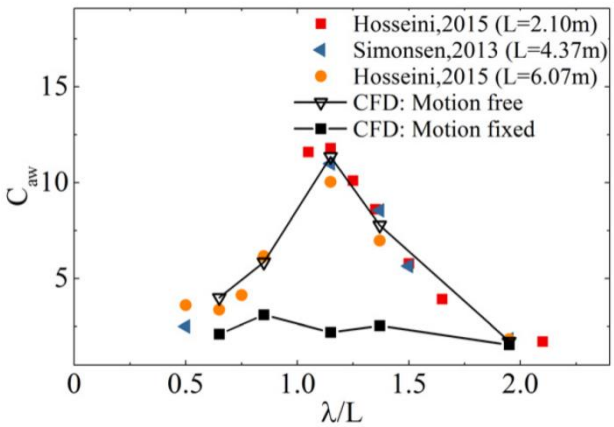

Figure 132 Added resistance coefficient of KCS. (Guo and Wan 2019, in head waves)

It is showed that while the variation of added resistance with incident wave lengths are reasonably reproduced in CFD results, the quantitative agreement in added resistance of CFD results with model tests were not good in particular in shorter waves where differences are in the order of 50% at the shortest wave case (λ /L=0.7). (see Figure 133).

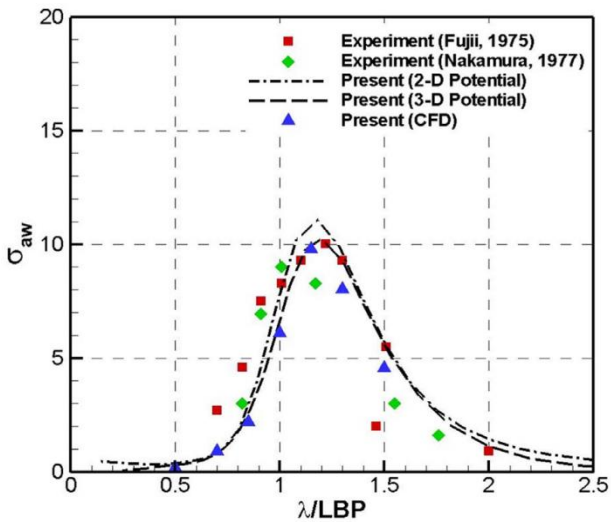

Figure 133 Added resistance comparison (Fn = 0.25, θ = 0°). (Kim M. et al. 2017b, S175 in head waves)

Orihara and Yoshida (2018) presented CFD simulations using a code WISDAM-X with an overset structured grid system for a non-public tanker form (called SR221C) in ballast

condition under regular head wave conditions. The results were compared with their model test results. It is showed that while the CFD results reproduce the trends of model test results, the quantitative agreement in added resistance of CFD results with model tests were not good in short wave lengths where differences are in the order of 20%. (see Figure 134).

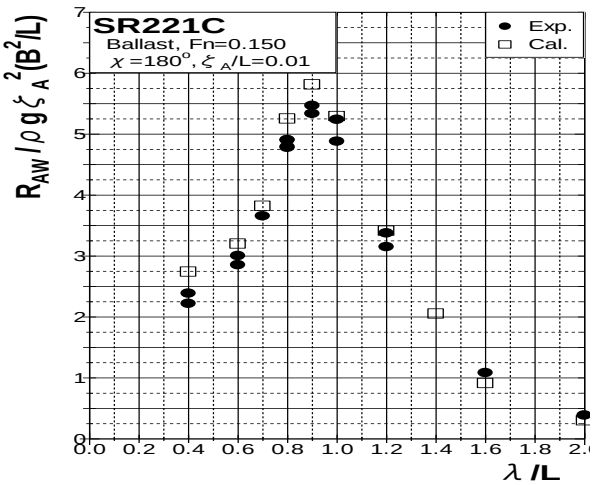

Figure 134 Comparison of normalized added resistance for a SR221C model in ballast condition, Fn=0.15, ζA/L=0.01. (Orihara and Yoshida 2018, in head waves)

As described in the above reviews, most of the CFD studies are conducted only for the case of head waves and fully loaded condition for a limited number of open-source hull forms (e.g., KVLCC2, KRISO container ship). This may be mainly due to the unavailability of suitable model test data for the validation of CFD methods. For wave conditions other than head waves, available tank test data suitable for the validation in speed/power sea trial applications, that is, those at forward speeds corresponding to the speed range of speed/power sea trials are limited to the data of Fujii and Takahashi (1975) for S175 container ship and Sadat-Hosseini et al. (2015) for KRISO container ship. Since these data are for the relatively old hull forms and container ships, validation data for other ship types (e.g. tankers, bulk carriers) are needed for the general examination of the CFD applicability to wave correction in speed/power sea trials. Another issue in the validation of CFD method is that most of them are made for fully loaded conditions and not for the actual trial conditions, although speed/power sea trials are conducted only in trial (lightly loaded) conditions, except for the case of tankers. Model test data for the actual trial conditions and validation with these data are considered indispensable for the rigorous assessment of the applicability of CFD methods to wave correction in speed/power trials analysis. In addition, the accuracy of the model test results must be examined in detail before the validation of CFD methods. As seen in the model test data shown in Figure 128 through Figure 134, variation of model test data for the specific hull forms among different testing facilities are quite large and greater than the difference between the CFD and model test results. Establishment of high-fidelity model test data with small bias and random errors is strongly desired.

It is thus considered that according to the results of present monitoring the development of CFD methods for added resistance due to waves, CFD methods have not matured to the point where they can be generally applicable to the speed/power sea trial analysis for the purpose of correction of wave effects mainly due to the lack of validation under wave conditions other than head waves and trial (lightly loaded) displacement conditions. It should also be emphasized that CFD methods must be validated against high-fidelity model test data obtained from multiple model testing facilities in order to remove the uncertainty due to inter-facility bias in the model test data.

5. WIND CORRECTION - GUIDANCE ON THE LOCATION AND HEIGHT OF THE ANEMOMETER

Given the importance of estimating accurately the wind effect for correction of measured power from a sea trial, as accurate a determination of the encountered wind speed as possible is essential.

Ideally the undisturbed wind speed encountered by the vessel should be measured, if at all possible. This may be accomplished by deployment of a dedicated measurement buoy equipped to measure wind speed. The results of measuring wind at a buoy and the effects on the speed performance analysed from trials is shown in section 6 (table 3) and seems to indicate that differences are reduced when buoy data are utilised. Technology is developing to allow direct measurement from the ship of the undisturbed wind speed outside the region where airflow is distorted by the presence of the ship. One example of such technology is the use of LIDAR (light detection and ranging), which is used routinely in the offshore wind industry and being tested for use in ship sea trials by MARIN, as described further in section 23. It is therefore strongly encouraged to adopt techniques that measure undisturbed airflow wherever possible for the correction of sea trials.

It is recommended that investigations are conducted to compare such remote measurement techniques with wind speed and direction as measured onboard in order to better recommend the instrumentation necessary for making wind measurements during trials.

Comparison of wind speeds predicted using weather hindcast models with those measured by standard ship anemometers indicate that onboard measurements are considerably in excess of those from a hindcast model, even accounting for the difference in vertical location of the anemometer and the reference height of model predictions (Lakshmynarayanana and Hudson, 2018). Adopting a standard power-law in correcting for vertical location is a further source of uncertainty when comparing measurements from buoys, other vessels and weather models.

If an anemometer is to be used for trials measurements then it should be positioned so as to minimise the effect of airflow distortion on the measured wind speed. Siting on a foremast away from superstructures is preferable, although it should be appreciated that even at the foremast the airflow is still disturbed by the presence of the ship. Within certain bounds agreement is found between wind speed measured by a foremast anemometer and as measured by an anemometer at the superstructure, as shown in section 6.

Computational fluid dynamics (CFD), or wind tunnel experiments, may be used to assist with anemometer positioning. Any error in measurement is highly dependent on the anemometer position and the shape of the ship's superstructure. Shipboard anemometers on typical tankers/bulk carriers may not be well-exposed and the wind could be accelerated by over 10% or decelerated by 100% (Moat et al, 2005a). There have been studies using wind tunnels and CFD aimed at improving measurement of wind speed on research vessels and on providing guidance for the correction of wind speed measured by merchant ships participating in the Voluntary Observing Ship (VOS) programme of the World Meteorological Organisation (WHO) (Moat et al, 2005a.b, 2006 a,b).

Moat et al (2006 b) provide non-dimensionalised predicted wind speed bias data that may be used directly to guide placement of anemometers onboard vessels.

In general, the anemometer should be sited as close to the upwind leading edge of

superstructures and as high above them as possible. Directly above the leading edge is not recommended due to greater distortion effects at oblique wind angles. Sonic anemometers are to be used in preference to cup anemometers due to the reduced effect of oblique flow angles on reliable measurements. Any anemometer should be sited more than 3x mast diameter away from masts.

6. LIMITATIONS OF AVERAGING WIND CORRECTION METHOD

6.1 General

Estimation of the wind effect is important for the powering performance analysis of the ships. During speed trials, it is common that the wind speed and directions change significantly. Therefore, accurate and reliable on-board measurement of the wind speed and direction is essential for the evaluation of the wind resistance.

The characteristics of wind speed and direction have been investigated for LNG carriers, tankers and large container were performed as shown in Table 17. The ultrasonic anemometers in addition to the shipborne anemometer were installed on radar mast and foremast. Based on these measurements and the influence of the measurement locations and the characteristics of relative wind direction depending on ship headings are investigated.

Table 17 Overview of Measurement Duration and Installation Position

	160K LNGC	180K LNGC	115K Tanker 1st	115K Tanker 2nd	20000TEU Container
Duration	2017.05.01 ~05	2017.06.08 ~13	2017.06.23 ~.26	2017.08.22 ~24	2017.05.20 ~.22
Loading Condition	Ballast	Ballast	Full Load	Ballast	Ballast
Measure Position (Foremast-FM, Radarmast-RM)	FM	FM	FM	FM	FM
	RM	RM	RM	RM	RM

Figure 135 and Figure 136 are comparison of wind measurement results. The distributions of the unfiltered wind measurement have large scatter throughout the range (Figure 135).

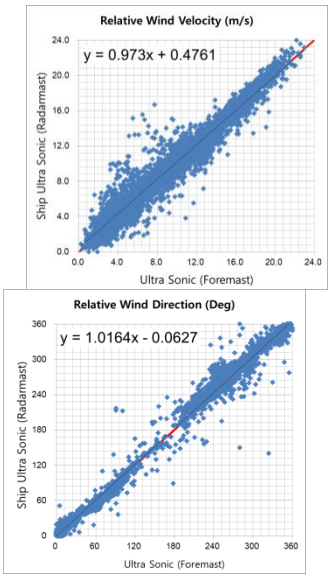

Figure 135 Comparison of Wind Measurement Results: Ultrasonic Foremast VS Shipborne Anemometer

The agreements between wind data from foremast and radar mast are improved by the filtering, confirming that this is an important step in the elimination of the disturbance by super structure. To avoid the influence of structures, measured data are filtered, and limit values for filtering are as follows:

- Rate of Turn < 5 deg / min

- Ship Speed > 5.0knots

As a result of the wind observations, the influence of the position of the anemometer is not significant when the ship's speed is over 5 knots and rate of turn is less than 5 degrees as shown in Figure 136.

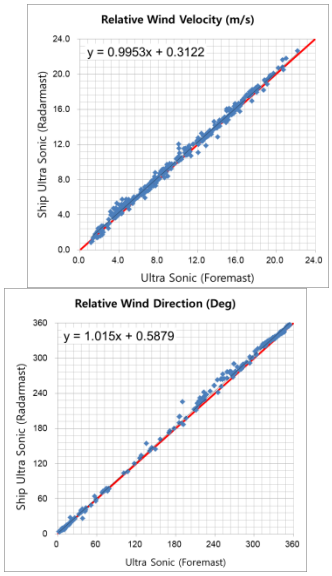

Figure 136 Comparison of Wind Measurement Results after Filtering: Ultrasonic Foremast vs Ship Anemometer

In order to investigate the influence on speed performance analysis by wind averaging process, wind observations from GEOJE weather buoy moored near sea trial area in Korea, and data from on-board measurements were compared. As shown in Table 18, approximately 10% of wind data from GEOJE buoy shows that the speed difference between

measurement and calculated by averaging process is over 1 m/s. And more than 30% of wind data from on-board shows over 1 m/s speed difference. For the wind direction, more than 10% of wind data indicate that the difference between measurement and calculated by averaging process is over 40 degrees both from buoy and from ship. The maximum difference of wind direction is about 180 degrees from GEOJE buoy. It means that head wind becomes follow wind.

Table 18 Difference of Wind by Averaging Process for 180K LNGC

	Speed Difference (m/s)				Direction Difference (degree)		
	> ± 0.5	> ± 1.0	> ± 2.0	Max.	> ± 20	> ± 40	Max.
GEOJE Buoy	31%	10%	4%	3.4	7%	4%	179
Shipborne Radar mast	78%	56%	19%	6.6	20%	9%	139
Ultrasonic Radar mast	60%	39%	15%	5.5	23%	12%	148
Ultrasonic Foremast	64%	37%	13%	6.2	23%	11%	138

Table 19 shows the influence of the speed power performance by wind data from different anemometer position.

The relative wind speed difference between the positions of anemometer is estimated in range of -0.03knots to +0.06knots for the 4 cases of speed power trials. The effect of the wind averaging process on speed power performance is mostly around -0.04knots.

Table 19 Effect on the Speed - Power Analysis

Based on ISO15016;2015		Differences by Measurement Location (Relative Wind)		Speed Difference (knots)	
		Direction (Deg)	Velocity (m/s)	Anemometer Location	Averaging Process ***
180K LNGC	Shipborne Ultrasonic	Base	Base	Base	-0.14
	Radar	5.60	1.42↓	0.01↓	-0.07
	Fore	1.01	2.80↓	0.03↓	-0.02
115K Tanker 1st	Shipborne Ultrasonic	Base	Base	Base	-0.07
	Radar	1.22	0.93↓	0.02↓	-0.03
	Fore	0.72	0.66↓	0.02↓	-0.05
115K Tanker 2nd	Shipborne Ultrasonic	Base	Base	Base	-0.07
	Radar	0.20	0.77↓	0.03↓	-0.04
	Fore	2.20	0.92↓	0.02↓	-0.04
20,000 TEU	Shipborne Ultrasonic	Base	Base	Base	-0.04
	Radar	8.17	0.85↑	0.04↑	-0.04
	Fore	6.81	0.95↑	0.06↑	-0.04

Notes:*** is Wind data by averaging process - wind data by each speed run

6.2 Limitations of Averaging method

(1) When wind speed is close to the design speed, and the angle between ship direction and wind direction is small, then the relative wind speed approaches zero in tailwind, which is not easy to measure accurately. This will influence the averaging accuracy over double run.

(2) When wind speed reaches BF5, ranging from 17-21kn, for those ships such as Oil tank, Bulk carriers, some Gas carriers, 'real' tailwind will occur, in these cases, averaging method tends to underpredict the ship speed.

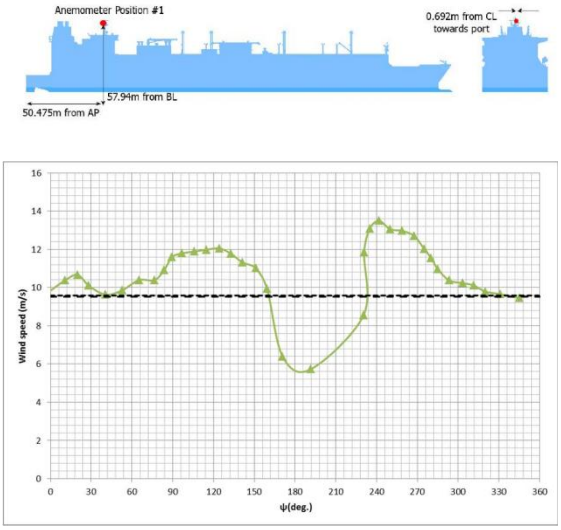

Figure 137 LNG carrier tested in FORCE

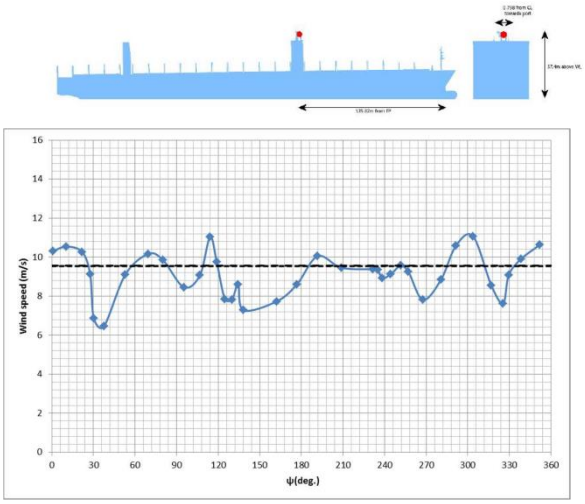

Figure 138 Container ship tested in FORCE

(3) When wind speed reaches BF6, ranging from 22-27kn, for almost all commercial vessels, including container ships, averaging method tends to underpredict the ship speed.

(4) When head wind speed is less than tailwind, averaging method tends to predict higher ship speed than without averaging.

6.3 Conclusions

The Committee decided to retain the present wind correction method. The reason for averaging method is imperfection of on board wind measurements caused by wind disturbances of the vessel i.e the wheelhouse as well as the inaccuracies of instruments such as "cup-type" anemometers. In case the average true wind speed from two subsequent runs is within 5% or 0.5m/s whichever is larger, or the undisturbed (not affected by any part of the ship) wind speed encountered by the vessel is measured remotely by a certified instrument accurately, the averaged single run wind speed may be used.

7. GUIDELINE FOR CFD-BASED DETERMINATION OF WIND RESISTANCE COEFFICIENTS

The guideline for CFD- based determination of wind resistance coefficients was established during the current period of SOS ITTC committee works. The document comprises general practices for computational approach and evaluation methods of CFD based calculations aimed at finding the corrections from wind forces acting on a vessel during sea trials. It is suggested to use as a complementary document to method of Appendix F in 7.5-04-01-01.1.

8. STUDY ON CFD COMPUTATIONS OF WIND FORCES

8.1 Introduction

The influence of wind forces on corrections of Sea Trials measurements plays an important role in the assessment of sea trial ship's performance. Thus, the committee of the current ITTC term has focused on the applicability of established wind force corrections by use of CFD methods. For this purpose, AC proposed an exercise in which several participants were invited to run CFD computations on two selected cases: a Handy Size Bulk Carrier (HSBC) and a Japan Bulk Carrier (JBC). Both represent the above water parts of non-existing vessels.

There were four participants working on the HSBC case and seven participants on the JBC case. Both cases were provided by two of the participants and they had differently defined flow conditions. HSBC had free domain size and conditions with uniform velocity on the inlet whilst the JBC focused on the modelling domain in a way to represent wind tunnel conditions. The detailed CFD computation conditions and domain sizes as well as solvers used in the computations are presented in Table 20 and Table 21.

Table 20 HSBC computations parameters

P#N	TS	NE [106]	TM	BC
1	2e-4	9.6	SST	I:V, O:P, N-S on hull, F-S on remaining boundaries
2.1	Steady	19.9	k-ε, realizable	I:V, O:P, N-S on hull, F-S on remaining boundaries
2.2		4.2	SST k-ε	
3		1.5	EASM	I:V, O:P, Top, Side – symmetry, remaining N-S
4		9.6	RSM	I:V, O:P, N-S on hull, F-S on remaining boundaries

Table 21 JBC computations parameters

P#N	TS	NE [106]	TM	BC
1	Steady	9.6	EASM	N-S: bottom, hull
2	Steady	8.2	k-ω, SST 2003	N-S(W-F): bottom, hull
3.1	0.05	8.2	EASM	N-S: bottom
3.2	0.01	11.3	k-ε, realizable	
3.3			k-ω, SST	
3.4			RSM QPS	
4.1	Steady	27.2	k-ω, SST	N-S: bottom, hull
4.2		16.9		
4.3		11.7		
4.4	0.0002	27.2		
5		11.2	SST	N-S(W-F): hull, F-S: other boundaries
6.1	Steady	1.7	RSM	N-S(W-F): hull, F-S: other boundaries
6.2	Steady	4.1	k-ω, SST	N-S: bottom
7	Steady	0.6	k-ω, SST-Menter	N-S(W-F): bottom, hull

P#N – participant number, TS – time step, NE – number of elements, TM – turbulence model, BC – boundary condition, I:V-Velocity inlet, O:P-Pressure outlet, F-S -free slip, N-S –no slip wall, W-F – wall function

The participants were numbered in random order and the number behind the dot refers to the calculated cases. Most of the participants elaborated one computational case, however, some provided results for more cases differing in domain details or turbulence models used in the analyses.

8.2 Geometry of Analysed Cases

The geometry of the vessels selected for the computations differ significantly from each other, although the ship type is the same. HSBC (Figure 139) had a smaller number of hatches and a pair of cranes above two of five hatches whilst JBC (Figure 140) was simplified to a version without outfits but with nine hatches on the deck. The superstructure of JBC was modelled by simple blocks and HSBC is characterized by more detailed and realistic geometry. It is worth noting that all participants were free to decide about geometry simplifications for meshing purposes.

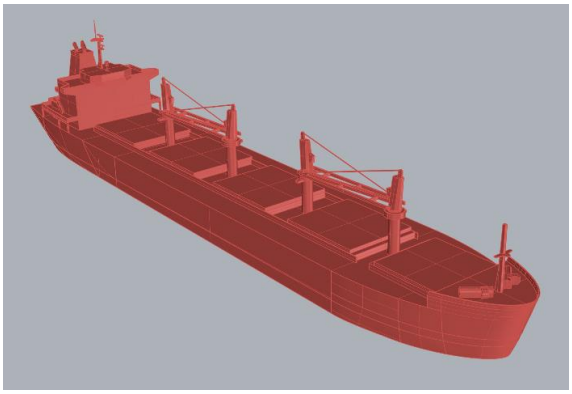

Figure 139 HSBC model

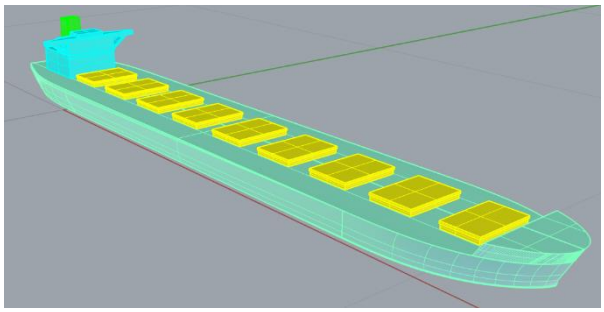

Figure 140 JBC model

8.3 Coordinate System

All calculated results were converted to the unified coordinate system presented in Figure 141. The direction of wind is 0° from aft and 180° for head wind.

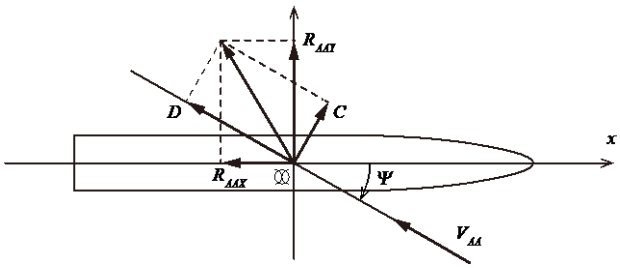

Figure 141 Unified coordinate system

8.4 Post-Processing of Calculated Forces

The most important wind force in Sea Trial analyses is the air resistance acting along the longitudinal axis of the ship, however, the lateral force was also examined. Typically, the wind tunnel results are presented in a normalized form as coefficients – the forces are related to a dynamic pressure multiplied by a reference area. The air force coefficients are computed according to formulas:

$$C_{DAX} = \frac{R_{AAX}}{q_A A_{VX}} \quad (4)$$

$$C_{DAY} = \frac{R_{AAY}}{q_A A_{VY}} \quad (5)$$

where:

C_{DAX}, C_{DAY} – are normalized wind force coefficients

A_{VX} –Transverse projected (frontal windage) area [m2]

A_{VY} – Lateral projected (side windage) area [m^2]

$$q_A = \frac{1}{2}\rho_A {V_{AA}}^2 \quad (6)$$

– dynamic pressure

V_{AA} – reference air velocity, [m/s]
ρ_A – air density, [kg/m^3]

These values of coefficients are presented as a function of the wind velocity direction.

8.5 Calculation Parameters

The study was carried out at model scale corresponding to the model size used in wind tunnel tests (Kaiser, 2016) (Kume, 2019). This approach is necessary to avoid any scale effects. The length of the HSBC model is L_{PP} = 0.867m and of the JBC is L_{PP}=1.200m. The angles of the wind velocity vectors were set in the ranges from 0° to 30° and 150° to 180° with equal steps of 10°. The inlet velocities were set to 20m/s for HSBC and 25m/s for JBC respectively.

8.6 Averaging Wind Profile

The reference velocity used in normalization of forces measured in the wind tunnel is always captured at a certain level (typically 10 m above sea level at full scale) and may cause some additional discrepancies in comparison between measurements and CFD results. To avoid this effect Kume et al. proposed a method for averaging the wind profile at the centre of the rotation of the model to find the reference speed in a more appropriate way. The details of this method can be found in the new ITTC guideline on the CFD-based Determination of Wind Resistance Coefficients (submitted to this full conference) or Kume (2019, 2020).

8.7 Forces Coefficients

The CFD results for the HSBC model were obtained using uniform flow, except for one of the participants whilst the majority of the calculations of the JBC case were carried out in a velocity profile caused by the boundary layer. The CFD and wind tunnel longitudinal C_{DAX} and lateral C_{DAY} values of the wind force coefficients plotted over the wind directions showed some scatter of the results in comparison to wind tunnel results. However, all normalized values are within the doubled standard deviation and the averaged values are close to the experimental curves. The percentage of deviation from the measurements is presented by plotting CFD based normalized values against experiment at the same direction of wind velocity vector.

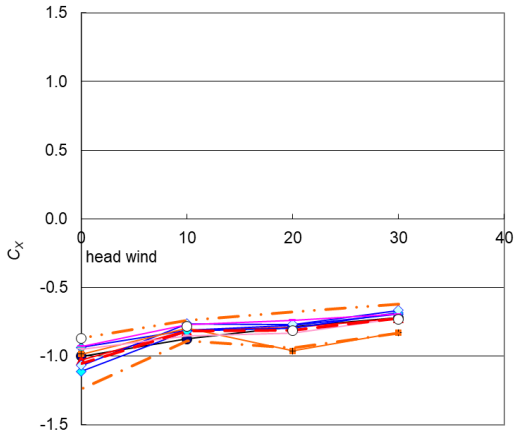

(a) Headwind side

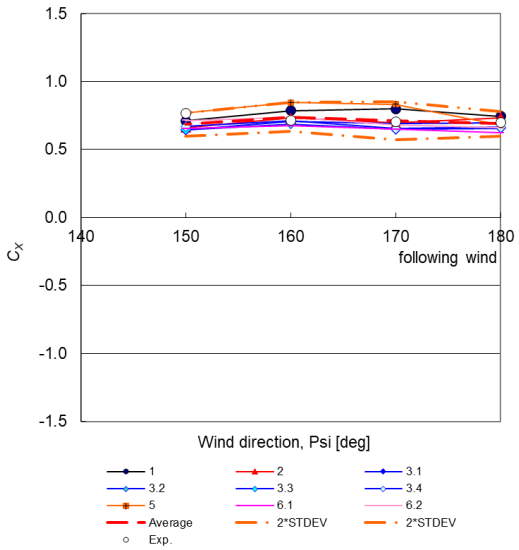

(b) Following wind side

Figure 142 Comparison of C_X coefficients for JBC

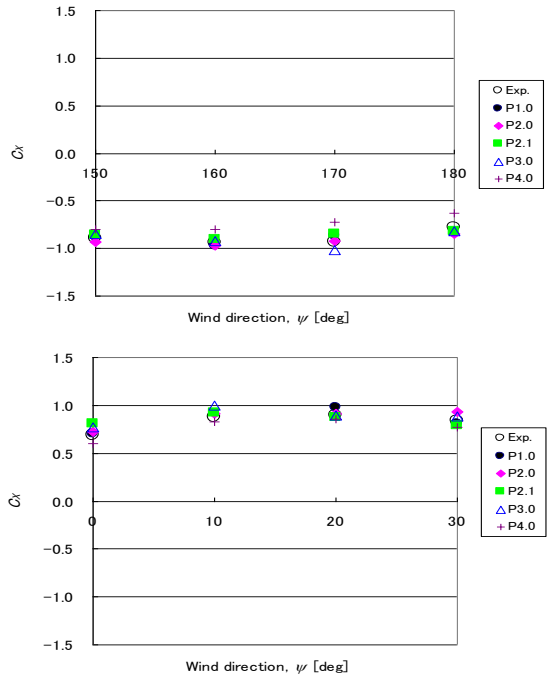

Figure 143 Comparison of C_X coefficients for HSBC

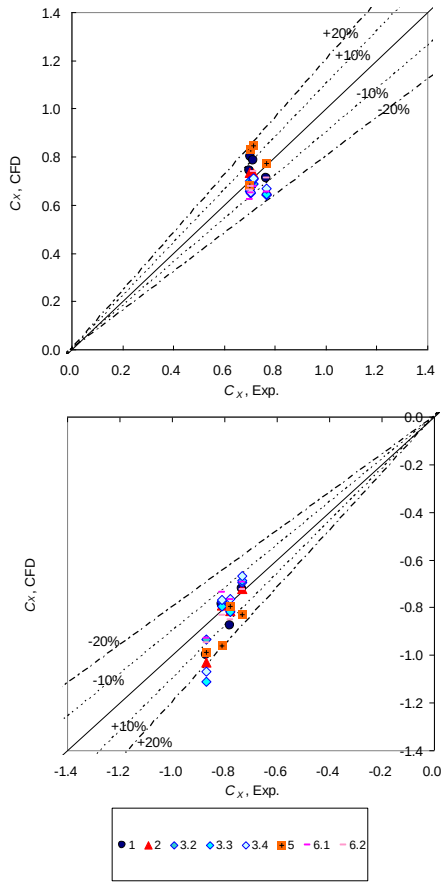

Figure 144 Results of CFD against Wind Tunnel, JBC

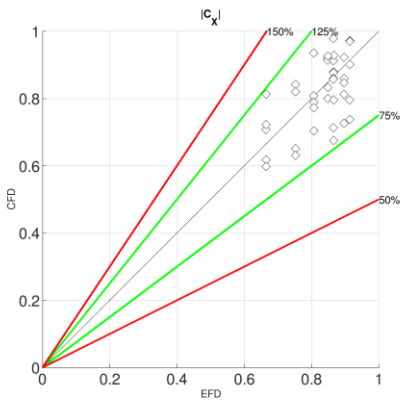

Figure 145 Results of CFD against Wind Tunnel, HSBC

8.8 Discussion of The Results

CFD based normalized wind forces are within ±20% of the experimentally achieved values. This level of deviation means that ITTC allows the use of CFD analyses in the wind correction of a Sea Trials only when the corrected value of the wind force does not exceed 2% of the total corrected power.

8.9 Conclusions

The scattered distribution of results does not lead to a conclusion which methodology of CFD computations is preferable. The main profit of the study is the normalization method of both experimental and calculation forces. This approach allows minimizing the impact of a velocity distribution on the analysed quantities.

8.10 Acknowledgements

The ITTC SOS Committee would like to express heartful thanks for all participants of this study followed in alphabetic order of company/institution name: CSSRC (China), CTO (Poland), Lloyd's Register (Korea), MARIC (China), MARIN (the Netherlands), NMRI (Japan), SJTU (China), SSPA (Sweden), SVA GmbH. (Vienna Model Basin)

9. CURRENT CORRECTION

The current correction in speed trials is conducted by assuming a current variation using the measured ship's speeds.

In general, current speed is considered to change against not only time and but also place. Therefore, in principle, the measurements of speed trial are conducted at almost the same position by repeating double runs, as shown in Figure 146, to eliminate the effect of place.

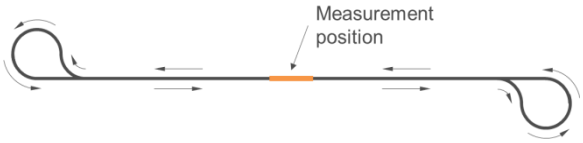

Figure 146 Path for the repetition of double run

The most primitive current correction method is to average the ship's speeds obtained by double run at the same engine output setting (mean method), in which current variation is assumed to be constant during the double run and current speeds are eliminated by averaging ship's speeds of the double run. As the method assuming that the current speed varies against time, mean of means method and iterative method are adopted in the ITTC RP 7.5-04-01-01.1 ver. 2017. The mean of means method assumes that current speed varies parabolically and eliminates the current speeds at each run. On the other hand, in the iterative method, current variation against time is explicitly estimated using all measured ship's speeds and the ship's speeds are corrected by subtracting the estimated current speeds. The Iterative method was newly adopted in the ITTC RP, after validation using a lot of fabricated cases by Strasser et al. (2015). This method has been used in a lot of actual speed trials by a lot of shipyards for three years after being adopted. To date, no implementation problem has been informed to ITTC.

To decrease repetition of double runs, a run procedure called "long track" was proposed. This procedure allows to conduct the conduct of multiple measurements at different points in each run (between turnings) along the run course, as shown in the Figure 147. The committee discussed this procedure.

If the long track procedure would be adopted, it is required that current variations against time at different measurement positions should be the same as each other to eliminate the effect of place. However, in general, it is difficult to find such area.

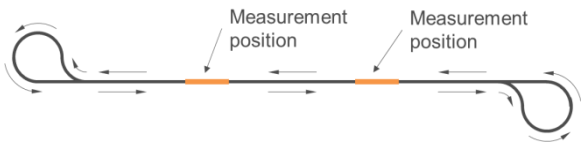

Figure 147 an Example of path for long track

To address this issue, though the concept to make measuring positions close to each other, as shown in Figure 148, was proposed, it was pointed out that such procedure has the following problems.

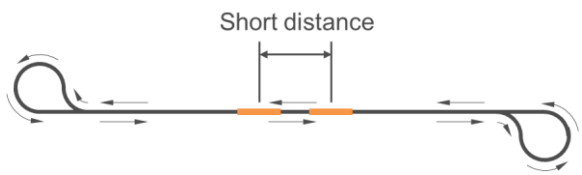

Figure 148 an Example of path for long track

1. As shown in Figure 149, the current variation derived in this procedure might be less reliable than the one derived in normal procedure.

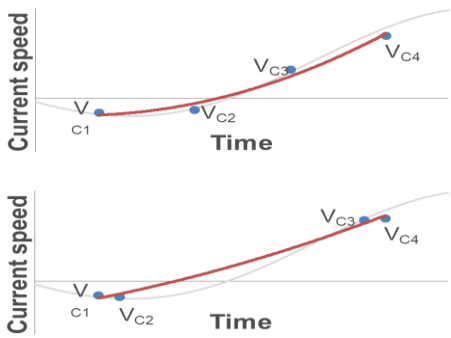

Figure 149 schematic charts describing the difference of current variation between normal procedure (upper) and long track with closed points (lower)

2. Even current speeds at close points might be different from each other. Two current variations derived by analysing the results of actual trial, in which, as shown in Figure 150,

two consecutive 1-mile-measurements at almost the same positions in each run were conducted at the same engine output setting for redundancy purpose. The measured data were analysed individually for each position A and B. These results show that the difference of current speeds at two position only 1-mile away was more than 0.1knots.

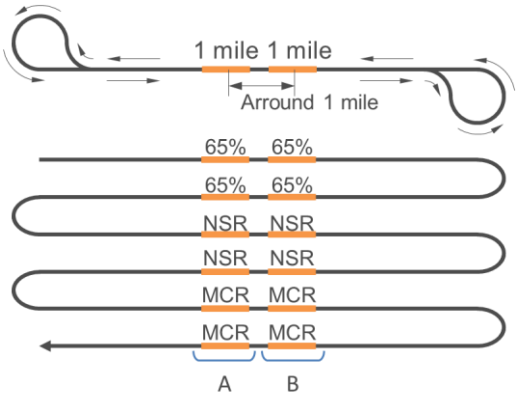

Figure 150 schematic diagram of two consecutive 1-mile-mesurements for redundancy purpose

The committee also discussed the order of engine output in long track method. Engine output setting for each measurement should be determined to avoid a deceleration approach, as shown in Figure 152. The data measured after a deceleration approach as shown in Figure 151 might include some uncorrectable gain due to insufficient deceleration, since it is impossible to confirm whether the ship's speed reached the one corresponding to the engine output setting and the sea condition during the measurement.

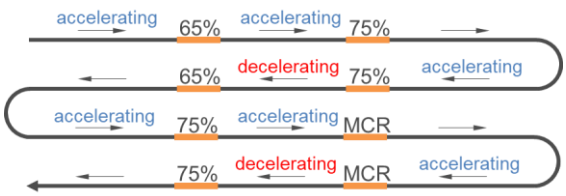

Figure 151 schematic diagram of long track including deceleration approach

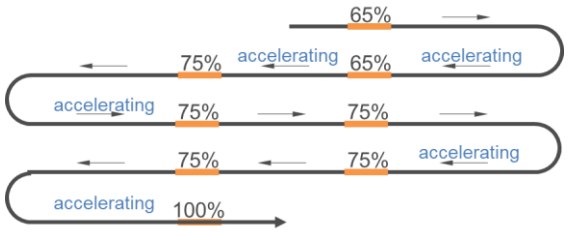

Figure 152 schematic diagram of long track without deceleration approach

The committee concluded that it is premature to adopt the long track procedure at this stage.

10. COMPREHENSIVE CORRECTION

At present, some trial analysis methods are proposed to eliminate the added resistances, such as wind and wave. In this section, the methods directly correcting delivered power by the following equation are reviewed:

$$P_{\mathrm{Did}} = P_{\mathrm{Dms}} - \Delta P \tag{7}$$

$$\Delta P = \frac{\Delta R V_S}{\eta_{\mathrm{Did}}} - P_{\mathrm{Dms}} \frac{\Delta\eta}{\eta_{\mathrm{Did}}} \tag{8}$$

Where P_{Did} is the delivered power in ideal condition, i.e. the delivered power after added resistances have been eliminated, P_{Dms} is the delivered power in trial condition and ΔP is the added power due to all added resistances.

The lower equation is derived considering that the delivered power is derived from ship's speed through the water, V_S, resistance, R, and propulsive efficiency, η_D. In the equation, $\Delta\eta$ is the difference between η_{Did} and η_{Dms}, which are the propulsive efficiencies in ideal and trial conditions respectively.

10.1 DPM

Direct Power Method (DPM) has been already adopted in the ITTC RP 7.5-04-01-01.1. In this method, propulsive efficiency is assumed

to vary linearly with the added resistance, as written below:

$$\frac{\Delta\eta}{\eta_{\mathrm{Did}}} = \xi_{\mathrm{P}} \frac{\Delta R}{R_{\mathrm{id}}} \tag{9}$$

Where ΔR is total added resistance estimated from the measured data and ξ_P is slope of linear function which should be derived from self-propulsion tests (SPT) and load variation tests (LVT) in advance.

From equations (8) and (9), the following quadratic equation for P_{Did} is derived and P_{Did} can be obtained by solving the equation:

$$P_{\mathrm{Did}} = P_{\mathrm{Dms}} - \frac{\Delta R V_{\mathrm{S}}}{\eta_{\mathrm{Did}}}\left(1 - \frac{P_{\mathrm{Dms}}}{P_{\mathrm{Did}}}\xi_{\mathrm{P}}\right) \tag{10}$$

10.2 EPM

In Appendix J of the ITTC RP 7.5-04-01-01.1, Extended Power Method (EPM) is described as informative. The advantage of this method is to be able to give full scale wake fraction.

In the EPM, propulsive efficiencies for both ideal and trial conditions in equation (), η_{Dms} and η_{Did} respectively, are estimated from the propeller open characteristics (POCs) and self-propulsion factors (SPFs) considering both with and without load variation effects.

Especially, propeller efficiencies for ideal and trial conditions, η_{Oid} and η_{Oms}, are derived by estimating the propeller loading points for each condition from propeller open chart of the subject vessel, as follows (see also Figure 153).

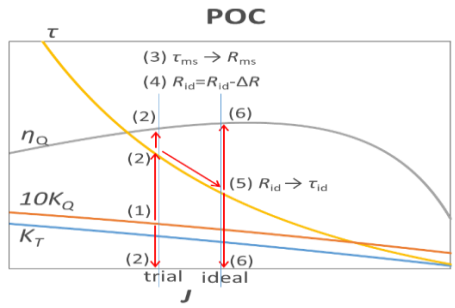

Figure 153 propeller open chart in which how to derive propeller efficiencies as well as propeller advance coefficients, propeller load factors and so on are shown.

The torque coefficient in trial condition, KQms, is calculated from the data measured in speed power trial with the following formula:

Propeller advance coefficient, propeller load factor and propeller efficiency in trial condition, Jms, τms and η_{Oms}, corresponding to the above KQms are derived from the propeller open chart. (J_{ms} is used to estimate full scale wake fraction)

Ship's resistance in trial condition, R_{ms}, is calculated from the obtained τ_{ms}.

Ship's resistance in ideal condition, Rid, is calculated by subtracting the total added resistance due to disturbances, ΔR, from R_{ms}.

Propeller load factor in ideal condition, τ_{id}, is calculated.

Propeller advance coefficient and propeller efficiency in ideal condition, J_{id} and η_{Oid}, corresponding to the above τid are derived using the propeller open chart.

Full scale wake fraction, w_S, can be estimated in the following process:

Full scale wake fraction in trial condition, wSms, can be derived from the already obtained J_{ms}, n_{ms} and V_S with the following formlae:

$$1 - w_{\mathrm{Sms}} = \frac{J_{\mathrm{ms}} n_{\mathrm{ms}} D}{V_{\mathrm{S}}} \tag{11}$$

The scale correlation factor, e_i, can be estimated from the above w_{Sms} and the w_{Mms} with the following formula:

$$e_i = \frac{1-w_{\mathrm{Sms}}}{1-w_{\mathrm{Mms}}} \quad (12)$$

Sid shall be derived from w_{Mid} and the above e_i with the following formula:

$$1 - w_{\mathrm{Sid}} = (1 - w_{\mathrm{Mid}})e_i \quad (13)$$

As to validation of the EPM, as already reported in the 28th ITTC proceedings, the differences of the power corrected by between the DPM and the EPM were less than 1% of that corrected by DPM, as shown in Figure 154.

Figure 154 Comparison between the corrected powers by DPM and EPM normalised by the corresponding value by DPM (% DPM)

10.3 Power-based Taylor Expansion Method (PTEM)

Yasukawa (2019) proposed a new method that he calls Power-based Taylor Expansion Method (PTEM).

This method requires ξ_P, and SPFs in both with and without propeller load effects. In this method, P_{Did} (at n = n_{id}) as the function of propeller shaft speed is expressed by Taylor series about n = n_{ms}, as follows:

$$P_{\mathrm{Did}} = P_{\mathrm{Dms}} - \Delta n \frac{\partial P}{\partial n} + \Delta n^2 \frac{\partial^2 P}{\partial n^2} + O(\Delta n^3) \quad (14)$$

Where

$$\Delta n = n_{Did} - n_{Dms}. \quad (15)$$

$\partial P/\partial n$ and $\partial^2 P/\partial n^2$ are derived from POCs, SPFs considering the load variation effect and V_S.

The advantage of this method is to require neither added resistances nor current speed to eliminate the influence of disturbances. Total added resistance is estimated by the following function derived by rewriting the equation (10).

$$\Delta R = \frac{\Delta\eta P_{\mathrm{Did}}}{\xi_{\mathrm{P}} V_{\mathrm{S}}} \quad (16)$$

V_S is estimated by the following equation:

$$V_{\mathrm{S}} = \frac{P_{\mathrm{Did}}\eta_{\mathrm{Did}}}{(1-t_{\mathrm{id}})T_{\mathrm{id}}} \quad (17)$$

Where Tid is also derived by Taylor series at n = n_{ms}.

The above ΔR, V_S, n_{id} and P_{Did} as well as related intermediate information, such as POCs and SPFs and so on, are derived with iterative process.

In order to obtain Δn, the following equation derived by substituting equation (16) and also equation (14) for basic equation (8) is solved:

$$\Delta n^2 \frac{\partial^2 P}{\partial n^2} - \Delta n \frac{\partial P}{\partial n} = \frac{\Delta\eta(1-\xi_{\mathrm{P}})}{\Delta\eta+\xi_{\mathrm{P}}\eta_{\mathrm{Did}}} P_{\mathrm{Dms}} \quad (18)$$

Verification results conducted using virtual trial data are presented. It is concluded that the error of corrected propeller shaft speed an corrected delivered power were less than 1% and 2% respectively within the disturbances taken into account in the verification.

Furthermore, the analysis results by this method using the actual trial data are also presented. It is mentioned that as a result of comparison with other methods, scatter of the results analysed using this method is smaller than that of others.

11. MODEL-SHIP CORRELATION FACTORS AT DIFFERENT DRAFTS

This topic deals with the question whether correlation factors should be determined draft-dependent or not. This has been put on the agenda already several years ago as there has been a certain indication from ships in service that performance on loaded draughts showed a different relation to the prediction as on ballast draught.

The phenomenon is mainly prevalent for ship types where sea trials under normal conditions cannot be performed at design draughts. This in particular affects container vessels. One very sparse example of a container vessel at full load draught is shown in Park, J. et.al. (2016)

Additional relevance is generated by the calculation procedure for the Energy Efficiency Design Index (EEDI) as a statutory instrument for emission control in shipping. Here, the attained EEDI performance is calculated utilizing the predicted relation between speed power performance on ballast draughts and loaded draught.

Gaining evidence in this question has been proven very difficult and in the last couple of years no concluding answers could be found. The reasons are manifold, but primarily the lack of appropriate full scale data of sufficient quality is prohibiting an evaluation.

As statistical evidence is not available to date an alternative approach is to look into physical effects that potentially generate a dependency between the scaling procedure and draught, which subsequently would require draft dependent correlation. The following factors could establish such kind of relationship:

- Varying relation between wave making resistance and viscous resistance components on different draughts.
- Form factor k: In case a ship and draught dependent form factor is applied, the influence of the draught is incorporated in the draught dependent k, while this is not the case for those cases where no specific form factor is used for the prediction.
- Influences from submerged transoms
- Flow separation – varying behaviour on different draughts.
- Effect of trim in ballast cases
- Wind resistance of model
- Treatment of wind resistance in prediction procedure

Some insights on this can be found in Wang, J. (2019)

As the question remains important both for performance prediction as well as for the evaluation of sea trials results, ITTC has decided to address this topic in a more focussed way by setting up a dedicated working group. The work will be based on the fundamental goal based standards that have been established by ITTC's Guideline on the determination of model-ship correlation factors (see also Section 16). The main goal of the newly established working group is providing benchmark relationships between speed power performance at different draughts. These can be used to check the validity of correlation approaches.

12. SHAFT G-MODULUS

12.1 Introduction

The G-Modulus of the propulsion shaft is one of the key uncertainties in assessing the speed power characteristics of ships by speed trials. The shaft power is derived from the shaft torsional deflection measured by strain gauges or optical sensor systems and multiplied by the G-modulus to obtain torque and thence power. This material property defines the ratio between the shear stress and the shear strain and can be expressed in the Young's E-modulus by means of the Poisson ratio ν viz.

$$G=E/(2(1+\nu)) \tag{19}$$

In theory the G-modulus can be derived for the full shaft section. In reality, for the size and weight of today's propulsion shafts such tests are not practical and reliable. Also, the testing of shaft samples in tensile or torsion configurations has demonstrated large uncertainties.

For this reason, a default value of 82,400 MPa is used in ISO 15016:2015 and in the ITTC 2017 Procedure.

In this section both results from the recent work of ITTC PSS (2017) as well as from earlier research is reviewed.

12.2 Previous Work

Prior to 1970 several organizations proposed various values for the G-Modulus:

ITTC: 81,400 MPa based on the value presented by Mr. Sakuichi Togino (1936), based on tests of 36 shafts with a diameter in the range of 260-455 mm.

SNAME: 82,000 MPa based on the value found by Mr. John H. Brandan (1962) from specimen tests with Molybdenum-Vanadium steel at 27 degr. Celsius.

BSRA: 81,900 MPa based on measurements of 68 shafts by means of ultrasonic equipment.

In 1969-1971 the Japanese organization JSTRA (Japanese government MOT & Japanese Shipyards) conducted an extensive test campaign with 76 intermediate shafts. The shafts were conventionally twisted by weights on a torsion arm. This resulted in an average G-modulus of 82,200 MPa

The same group of Shipyards also measured 43 shafts by using ultrasonic equipment manufactured by Electronic Consultant Company that was also involved in the BSRA campaign. It was concluded that the ultrasonic measurement is more accurate than the conventional twisting method. Finally, the Shipyard group recommended 82,000 MPa.

In 2015 ISO and ITTC agreed to use a default value for the G-modulus equal to 82,400 MPa. This figure harmonized the values from ITTC 2014 and from ISO15016:2001 and corresponds to the value proposed by Fincantieri Shipyard in that same meeting in London.

12.3 Recent Research

Inspired by ISO and ITTC, Hyundai Heavy Industries (Lee, Tae-Il (2016)) conducted extensive material tests on propulsion shafts to establish the G-Modulus for use in speed power trials analysis. This work was executed in compliance with Class rules and regulations and supervised by DNV-GL in 2015-2016.

As the mechanical twisting of actual propulsion shafts for today's merchant ships was considered practically impossible due to the size and mass of the intermediate shaft sections, the shear modulus was derived from tensile tests of material specimens taken from actual shafts.

Three shafts were used; a 650 mm diameter intermediate shaft for a 162,000 m3 LNGC and two 480 mm diameter shafts for a 174,000 m3 LNGC.

In consultation with Class, the specimens were taken at several locations and orientations of the shaft cross sections at both ends of the shafts.

The test specimens were produced in compliance with ASTM E111-04 and DNV Ship Rule Pt.2, Ch.1, Sec.1. The tensile testing machines and technicians complied with KOLAS.

From the measured stress-strain curves the linear part between 40 and 65% of yield stress were used to derive the Young's E-modulus. For the derivation of the shear G-modulus a Poisson ratio of 0.29 was taken from ASME Sec. II, Part D (2013).

The average results over multiple specimens per shaft as presented by Dr. Tae-Il Lee to ITTC-PSS Committee in their meeting on June 15, 2016, are presented in Table 22.

Table 22

Shaft #	No of test specimen	Average G-modulus [Mpa]	Standard Deviation [Mpa]
1	6	85,691	9,858
2	8	83,123	4,190
3	8	89,571	18,381

It was stated by HHI that torsion tests on actual size propulsion ships is often impossible. HHI concluded that derivation of G-modulus from tensile tests of shaft specimen results in unacceptably large variation.

12.4 Conclusions

Based on the above results, SOS concluded that the default value of the G-modulus to be used for speed power trials remains 82,400 MPa.

As stated in the Procedure, measured values of the actual propulsion shaft may be accepted provided that an adequate measurement procedure and certified equipment is used by qualified test engineers.

13. WATER TEMPERATURE AND DENSITY CORRECTION

13.1 General

The water temperature and density correction should be carried out in the same manner as ISO 15016. Sea water temperature and density may be measured by taking water samples at the trial site and from an inlet which is located at the same level as the ship's bottom. It is difficult to determine where the sample should be obtained, as discussed in the final report of the 28th ITTC.

The degree of the effect may be evaluated by some cases of sea trial and the environmental condition of the sea. For example, in some of the sea trial areas of China, water temperature normally changes within 3℃ in different season (Table8).

From the sea trial records of VLOC series vessel(Table9), water temperature has about 20 ℃ change.

Table 23 Water Temperature changing with different season and depth

		East China sea		Yellow sea	
		Temperature changing amplitude every day	Average Temperature (℃)	Temperature changing amplitude every day	Average Temperature (℃)
Surface layer	Winter	0.6	9~12	0.5	2~10
	Spring	1.3	17~23	0.8	13~17
	Summer	0.9	26~29	2.1	24~27
	Autumn	0.5	17~26	2.0	13~14
Middle layer (5m~10m)	Winter	0.4	9~11	0.4	2~10
	Spring	1.4	16~23	0.4	12~15
	Summer	0.2	20~22	2.4	18~20
	Autumn	0.2	15~23	2.4	13~14

Table 24 Water Temperature conditions for the trials of VLOC series vessel at Ballast Condition

Ship No.	Sea Trial Area	Water Temperature（℃）
1#	Yellow sea	5.5
2#	East China sea	15.0
3#	East China sea	14.0
4#	East China sea	17.5
5#	Yellow sea	19.5
6#	Yellow sea	24.4
7#	Yellow sea	25.0

According to the correction formula of ISO 15016, the power correctional values of different water temperature for 39000 DWT and 60000 DWT B.C were calculated and compared with the test results of power (Figure 155). When the temperature is higher than the reference value (15℃), the speed correction is about -0.02kn interval per 2.5℃. If the temperature is lower than the reference value, the speed correction is about +0.02kn interval per 2.5℃.

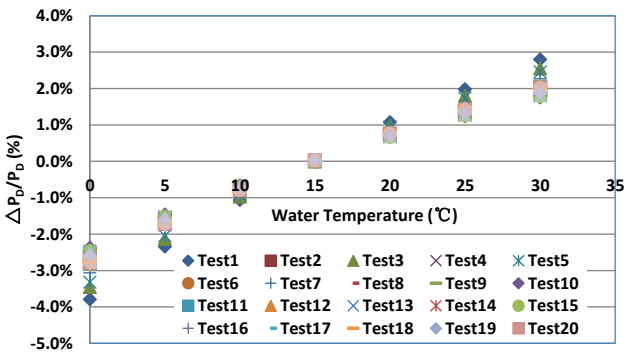

Figure 155 Correction of power for different water temperature (39000DWT B.C & 60000DWT B.C)

13.2 Conclusions

The Committee considered that the present correction method for the water temperature and density correction should be retained.

14. NOISE IN THE MEASURED DATA AND MEASUREMENT ERROR

14.1 General

The uncertainty of the speed and power performance is determined by the accuracy level of the measured values of shaft power and environmental disturbances. To reduce the uncertainty of the speed and power performance analysis during speed trial, it is recommended to use a reliable measurement system and to perform it in an ideal environmental condition such as still water, but it is not easy to conduct speed trials under ideal environmental conditions. Therefore, all results of speed and power performance include both the uncertainty of the measuring system and the uncertainty of added resistance from environmental conditions. The uncertainty analysis of speed / power performance was carried out based on raw data in sea trials. The speed power performance was estimated through the guideline of ISO15016, and Monte Carlo simulation was used for the analysis of uncertainties.

The results of the uncertainty analysis of the ship speed power performance during a double run test at the MCR 75% condition showed expanded uncertainty due to the added resistance by wind (R_{AA}) which was ±2% and ±12% at each run. The uncertainty of added resistance due to waves (R_{AW}) was ±16%, respectively (at a 95% confidence interval, k=2).

Table 25 Uncertainty of Resistance increase due to wind and waves

Engine Load	Wind		Waves	
	RAA	U (%) (95%, K=2)	RAW	U (%) (95%, K=2)
50% 1st Run	-66.5	± 6	-	-
50% 2nd Run	110.1	± 15	56.9	± 1.2
75% 1st Run	-89.8	± 2	-	-
75% 2nd Run	152.6	± 12	81.3	± 1.2
90% 1st Run	-48.2	± 14	-	-
90% 2nd Run	32.1	± 39	83.3	± 1.2

The expanded uncertainty of the measured delivered power (P_{Did}) converted to the ideal conditions was about ±1.2% as shown in Table 26. The uncertainty of the delivered power can be converted to an uncertainty of ship speed of about ±0.1knots.

Table 26 Uncertainty for corrected ideal power

Engine Load	U (95%, K=2) (kW)	U (95%, K=2) (%)
50% of MCR	± 164	± 1.2
75% of MCR	± 227	± 1.2
90% of MCR	± 265	± 1.2

The dominant component among the uncertainty factors for the delivered power in ideal conditions is the shaft power measurement system which accounts for about 60% of the total uncertainty. Hence, it is necessary to measure the shaft torque more precisely to reduce the uncertainty of the shaft power in sea trials.

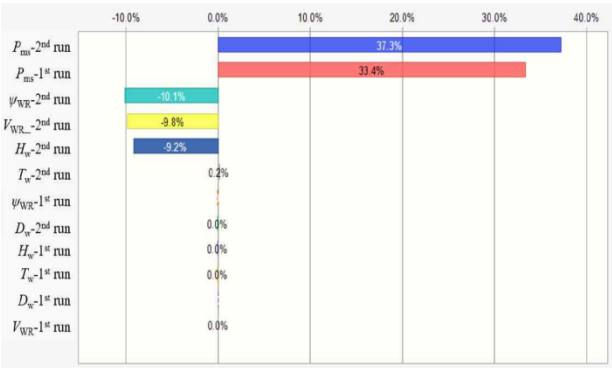

Figure 156 Sensitivity of corrected shaft power on basic input parameters (MCR 75％)

14.2 Conclusions

It is found that the expanded uncertainty of ideal power performance is about ±1.4% at the 95% confidence level (k=2). The influence of the uncertainty in the added resistance was minor due to moderate weather conditions, and thus the shaft power measurement system (standard uncertainty of the shear module) was the dominant effect.

15. UPDATE THE SPEED/POWER SEA TRIAL PROCEDURES 7.5-04-01-01.1

Main updates of the procedure during this term are as follows.

Shallow water correction. The committee accepted the Raven method exclusively concerning shallow water corrections and new water depth limitations for the applicability of shallow water corrections were established. Additionally, the appropriate formulae correcting vessel's speed achieved during speed trials were replaced by corrections of delivered power. The shallow water speed corrections based on the Lackenby method are excluded from the procedure.

Wave correction. A new wave-added resistance prediction method-SNNM was developed and validated extensively to adapt the situation when wave angle is larger than 45° from heading and shipline is not available. After open validation in SOS and full discussion, SOS agreed to include SNNM into the sea trial procedure.

Wind averaging method. Limitations of wind averaging method were detected. The reasons for averaging method and exceptional case for averaged single run were presented (refer to 6.2).

Guidance on the location of anemometer was recommended (refer to part5)

Additional runs for sister vessels due to current change were updated. If after evaluation the vessel speed deviates more than 0.3 knots compared to the first ship of the series and "Mean of Means" method is used, the full run program as specified for the first ship shall be followed.

Finally, there was an update of the wind force coefficient database applied in the relevant appendix.

16. UPDATES TO THE GUIDELINE ON THE DETERMINATION OF MODEL-SHIP CORRELATION FACTORS

The guideline 7.5-04-05-01 had been first introduced by the 28th ITTC, so the last term has seen the first revision-period for this new guideline. Generally, the guideline addresses the standards and procedures according to which institutes shall derive their individual

correlation schemes. The guideline in this sense defines minimum requirements and general guidance for this task. The major changes that have been incorporated into the new revision of the guideline are as follows.

The procedures and standards provided in the guideline are explicitly no longer limited to physical model testing. The general rules and requirements set out in the guideline may also be used for correlation in the context of CFD-calculations. Consequently, the wording was changed to “prediction” in general.

More detailed description of iterative approach for determination of a resistance-based correlation factor (i.e. C_A).

The description of the background and general approach has been extended giving a clearer explanation of the purpose of the guideline.

Furthermore, an example implementation of the procedure in Excel format was provided to the committee members for testing

16.1 Practical Procedure to Derive a Resistance-Base Correlation Factor (C_A)

The determination of C_A requires an iterative process as shown in Figure 157. This is necessary as the propulsive efficiency η_D represents a non-linear relationship between effective power P_E and delivered power P_D. For the determination of the correlation factor C_A, the values for η_H and η_R are taken from the model tests while the propeller efficiency η_0 is obtained from the propeller open water characteristics.

16.2 Required Size of Samples for a Reliable Determination of Correlation Factors

Each towing tank is using its own, specific regression model for the correlation scheme. The correlation formulae depend on a number of m variables.

The regression model may be derived by multivariate regression analysis. The significance of the individual parameters has to be tested by statistical instruments. In order to obtain statistical significant results, the sample has to be of a certain minimum size. This depends on the number of parameters used for the correlation scheme. According to Green (1991) the following rule of thumb may be used for the determination of required sample sizes:

$$n > 50 + 8 \cdot m \tag{20}$$

n number of samples, m number of independent variables in the regression formula.

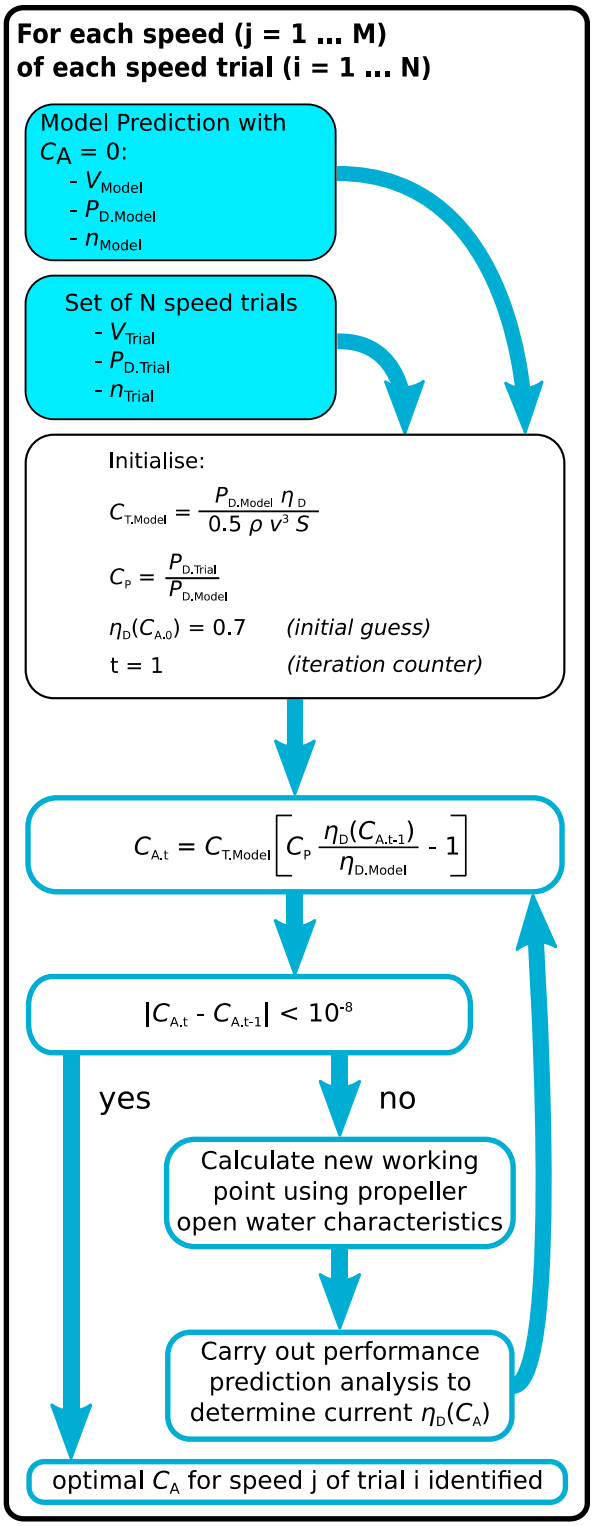

Figure 157. Determining optimal C_A iteratively

17. KEY PERFORMANCE INDICATORS FOR SHIPS IN SERVICE

There are multiple reasons for monitoring ship powering performance in service. A primary reason is to track increases in hull and propeller fouling, such that efficient performance of the vessel is ensured through appropriate timing of maintenance interventions, whether hull and/or propeller cleanings, or application of new coatings.

Other reasons may include weather routing for improved fuel efficiency, real-time 'optimisation' of draught and trim, feedback to designers for estimation of sea margin and feedback to towing tank organisations for correlation and research purposes. Recently, attempts to reduce fuel consumption by operators for environmental reasons as well as economic have placed greater emphasis on vessel fuel efficiency and hence performance monitoring.

The IMO mandating assignment of an Energy Efficiency Design Index (EEDI) and adoption of a Ship Energy Efficiency Management Plan (SEEMP) have placed greater regulatory focus on this area, in particular in requiring the verification of speed and power for the EEDI through accurate sea trials results.

Ongoing discussions at IMO on 'short term measures' to reduce Greenhouse Gas (GHG) Emissions from shipping are likely to increase the focus on operational measures to reduce fuel consumption. These discussions may result in a form of Carbon Intensity Index (CII) that will require determination of a ship's powering performance in service as well as when newly built, for regulation. This will further increase emphasis on trustworthy measures of in-service power and speed and methods to compare fairly between loading, and encountered environmental, conditions. These measures – as with EEDI – are likely to require ongoing %

reductions relative to a baseline performance. These baseline performances are derived through statistical analysis of fleet data pertaining at a particular time.

These baselines are distinct from those adopted by ship operators in managing hull and propeller fouling and associated maintenance interventions. In this latter case a baseline is usually established by monitoring powering performance when the ship is newly out of dry-dock and comparing subsequent performance to this baseline. The emphasis is therefore often on relative, rather than absolute, determination of performance. The challenge with modern coatings is in detecting relatively small changes in performance over a number of years, given the inherent scatter in measured data points arising from variations in vessel loading condition, ship speed, weather, sea currents, water temperature and salinity, engine performance and operational practices.

Traditionally, so-called 'noon reports' were the primary source of in-service data – consisting of a manual report of ship's position, fuel consumed in 24hr period and an estimate of the prevailing wind and wave conditions made by an experienced mariner. In recent years these data are increasingly being supplanted by automatically recorded data at much smaller time intervals – often referred to as 'high frequency' or 'continuous monitoring' data. Examples of typical systems are given in section 19. Aldous et al (2015) compare uncertainties from these approaches and demonstrate that a continuous monitoring approach has much lower uncertainty than using noon reports, such that similar levels of uncertainty in power are determined from continuous monitoring data after 90 days at sea as from noon report data after 270 days at sea. It is considered that noon report data has too much uncertainty to be of great value to the ITTC community, although with automated collection of parameters it retains some value for long term monitoring of ship performance.

One problem with all measurements and analysis is the characterisation of the encountered wind and wave environment. Noon reports are often reliant on manual observation. Continuous monitoring systems typically record the anemometer as the means to determine wind speed and direction. The measured relative wind requires correction to true wind, but this is a measurement of a disturbed wind field. Wave height is generally not recorded, but may sometimes be available from a MetOcean hindcast model. Potential uses of these data are discussed in Boom and Hasselaar (2014) and Lakshmynarayanana and Hudson (2018). Recent developments in shipboard measurement of wave height are discussed in section 18.

Standards derived for analysis of ship performance data (ISO19030) therefore recommend a continuous monitoring approach. Most such analyses rely on monitoring performance through the derivation of speed power curves, or using Key Performance Indicators (KPIs) over time. Typically, these approaches focus on filtering and 'binning' data to derive a calm water condition. This reduces the influence of weather by filtering out data points for wind speed and wave heights above a threshold value and by retaining narrow ranges of draught and trim conditions (see, for example, Dinham-Peren and Dand, 2010). Such methods filter out a large amount of data, typically retaining only about 9-11% of the total dataset.

A major problem with such methods is the transparent and consistent definition of threshold values for data filtering (i.e. "less than x m wave height represents 'calm water'"). These choices greatly affect derived speed power curves due to changes in the size of the resulting dataset. For this reason, the derivation of speed power curves should be avoided if possible unless accompanied by clear

presentation of applied threshold values and justification for their selection.

An alternative approach is to correct or normalise the data by applying shaft power corrections for the effects of wind and waves. Boom and Hasselaar (2014) discuss the improvements that applying methods derived initially for sea trials correction can make to in-service performance assessment. Further recent developments in this approach are reviewed in section 21.

If sufficient data are available for analysis then a pure data-driven approach using machine learning techniques has been shown capable of predicting power with a mean error of 2% compared to measured power across the full range of ship loading condition, operational speed and encountered wind and waves for an LNGC carrier (Parkes et al, 2018).

Developments in data collection and processing techniques are covered well in the 'Hull Performance and Insight Conference (HullPIC)' series, annually since 2016.

For the monitoring of hull and propeller fouling it is common to use 'speed loss' as a performance indicator or KPI, as recommended in ISO19030 and aligned with some onboard systems and coating manufacturers. An alternative is to use 'power (or resistance) increase'. Given the approximately cubic relationship between power and speed, the latter is more sensitive to small variations. With these performance indicators it is not possible to separate effects of hull fouling from propeller fouling, which can result in sub-optimal decisions around maintenance interventions. A complete separation of hull and propeller fouling is not possible without separate thrust and torque measurement on the propeller shaft. The small deflection of the propeller shaft due to thrust makes this extremely difficult, recent progress is discussed in section 20. Partial separation of propeller and hull effects is possible through careful consideration of the torque, propeller revolutions and ship speed.

Analysis of continuous monitoring data is key to realising operational efficiencies (draught, trim optimisation, weather routing, coating and maintenance strategies) and is likely to be central to international efforts to reduce Greenhouse Gas emissions from shipping. Presently there are few standards for the automated collection and analysis of such data. ISO19030 offers one standard, but is focused on filtering data, such that the dataset size is greatly reduced. There is potential in methods that correct, or normalise, data (as discussed in section 21) to increase useful data and accuracy. Such methods offer the potential to provide insights into ship performance when combined with data from towing tank tests and CFD. Uncertainties remain regarding encountered wind and wave conditions and further investigation is recommended in these areas.

18. MORE ACCURATE MEASUREMENT OF ENVIRONMENTAL DATA

For the reliable evaluation of Ship's speed/power performance from in service performance monitoring, accurate measurement of encountered environmental conditions is of primary importance. Among the environmental data, encountered waves are the most difficult to obtain from onboard ships in service. For the routine recording of wave conditions in on-board log books, visually observed wave data have been used and is still normal practice today.

In recent years with the advancement of wave radar analysing technologies which evaluate wave directional power spectrum by analysing the scattering of the X-band radar signal caused by Bragg backscattering from the sea surface ripples (so-called "sea clutter") (e.g. Plant and Keller (1990), Lee et al. (1995),

Nomiyama and Hirayama (2003), Giron-Sierra and Jimenez (2010)), so-called "wave radar" systems provide by several manufactures (e.g. Miros WAVEX system, Ocean Waves WaMos II system) have increasingly employed as a wave measuring device in on-board performance monitoring. Some examples of wave measurements on ships in service are presented in the following and their effectiveness for ship performance monitoring is discussed.

Yoshida et al. (2015) presented results of wave-radar measurements on an iron ore carrier and comparison with the forecast and on-board visually observed data, see Figure 158. It is found that the agreement among the data is reasonably good but the wave-radar data tend to underestimate relative to other data, in particular in rough wave conditions (wave height greater than 4m). In addition, they validated the wave radar data by comparing short-term estimations of pitch and roll motion calculated using the wave-radar data with measured ship motions. It is shown that estimations from radar wave data agree well with measured motion data except for higher wave cases.

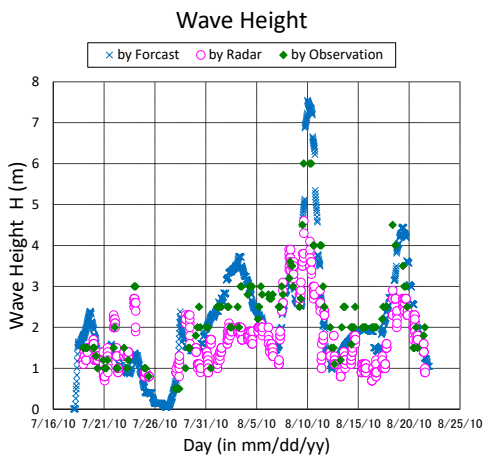

Figure 158 Comparison of wave-radar measured data with forecast and visually observed data. (Yoshida et al. 2015)

Lu et al. (2017) presented results of wave-radar measurements on a 28k DWT bulk carrier and comparison with the hindcast data calculated with NOAA's 3rd generation WW3 model (Stopa et al. (2016)). In their study, the hindcast wave data are firstly validated by comparing the short-term frequency spectra of ship's pitch motion in a similar way as Yoshida et al (2015) which is calculated using them, then comparison is made with the frequency spectra calculated from measured pitch data. Their comparison show good agreement between the short-term results with the measured data. Then they compared time-historical variations of wave statistical parameters (height, period, direction). They found that radar measured wave height and spectra lack reliability when significant wave heights exceed 4m, see Figure 159(WRF-Weather Research and Forecasting model , NCEP-National Center for Environmental Prediction model , ERA-European center for medium-range weather forecasts Re-Analysis model). As for the reliability, they considered that the deficiency of the wave radar can be attributed to the large amplitude ship motions under which conditions the microwave radiation cannot accurately detect the sea surface ahead of the ship.

One of the drawbacks of the wave radar measurements is in that it cannot evaluate quantitatively the wave height or magnitude of wave energy by itself. That is, the measured reflection intensity of radar wave signal is not directly relating to the wave heights but roughness of the sea surface (ripples). Thus, the wave height is in most cases indirectly determined from the signal to noise (S/N) ratio of the radar in conjunction with calibration of the S/N ratio with wave height obtained from other devices or data sources. (e.g. Giron-Sierra and Jimenez (2010))

To deal with this drawback and reduce uncertainty arising from the use of S/N ratio,

Iseki et al (2013) developed the hybrid Bayesian wave estimation method in which wave-radar data is incorporated into the ordinary Bayesian wave estimation method which estimate wave environment based on the wave buoy analogy with input of ship motion responses. It is shown that by using wave-radar data estimated directional wave energy spectrum can be improved and results in higher accuracy of wave period and direction. In this hybrid method, wave height, that is the magnitude of wave energy spectrum, is evaluated principally from the ship motions in a physically consistent manner without the need for empirical calibration. In their study, wave measurements were conducted on a 6,500 TEU class container ship on the north pacific route in winter of 2010.

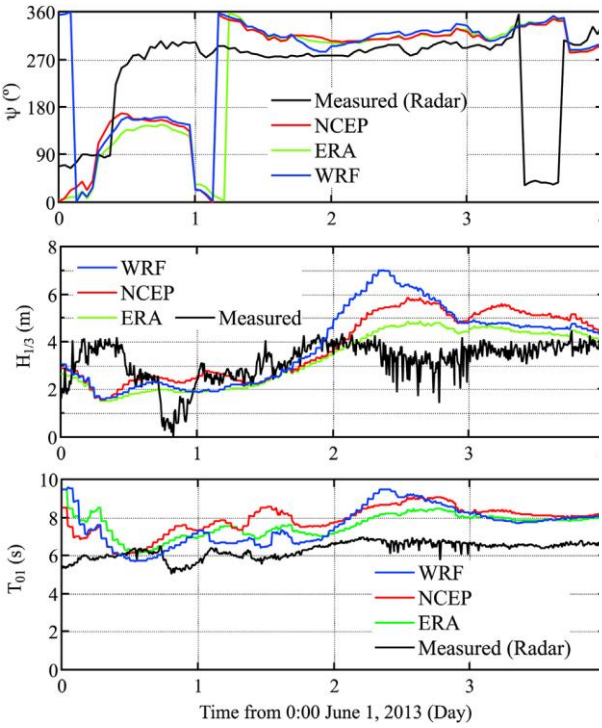

Figure 159 Comparison of observed and simulated (hindcast) wave directions, significant wave heights and periods. (Lu et al. 2017)

The wave statistical parameters estimated by the wave radar system using the proposed hybrid Bayesian system are compared with NOAA buoy data which is evaluated by referencing data from the nearest three NOAA wave buoys. Figure 160 shows the comparison of the estimated data (Bayes) and the buoy data. While the Bayes data well reproduce the time-historical variation, differences are relatively large in the order of 1 to 2m.

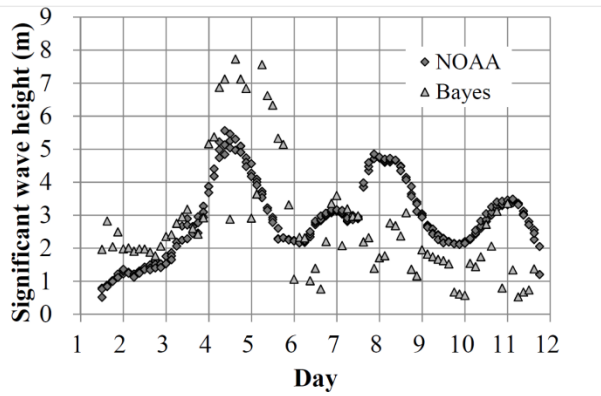

Figure 160 Comparison of estimated and measured wave heights. (Iseki et al. 2013)

As described in the above, the effectiveness of wave radar system as an onboard wave measuring device has not been thoroughly verified so far. Most of the verifications are made by the comparison with forecast or hindcast data. In addition, the agreement between the wave-radar data and forecast/hindcast data is not satisfactory. Comparison with the measured data from a wave buoy deployed close to the ship course is indispensable to conduct more detailed validations, in particular for the assessment of wave height estimation.

19. SPEED POWER PERFORMANCE RELATED MONITORING

Ship's speed/power performance evaluation in service conditions has been of greater importance in recent years due to several reasons, including the introduction of EEOI (Energy Efficiency Operational Indicator). To achieve this on practical basis, reliable on-board monitoring of performance related parameters

should be realized within reasonable costs justified from operational and financial point of view.

Contrary to the situations in builder's speed/power sea trials conducted before delivery, performance monitoring on in-service ships need to be made automatically or by unskilled crews without assistance of experienced specialists normally attending the builder's sea trials. Thus simplification of the monitoring procedures and robustness of the monitoring equipment are indispensable. To achieve this, most of the recent performance monitoring on in-service ships have employed system configurations connected to normal rule-mandate on-board operational data recording equipment including Voyage Data Recorder (VDR) and engine-room Monitoring System (EMS). (see Kim 2018, Orihara et al. 2019) Normally, most of the performance-related parameters are obtained from VDR and EMS except for encountered waves, ship motions and propeller/shaft thrust and torque for which special measuring devices is needed. Use of the equipment obviates the need for the installation of special sensors and dedicated cabling for the performance monitoring. One example of these on-board monitoring systems is shown in Figure 161.

This monitoring system consists of a suite of sensors and a system's PC to acquire, analyse and display data. Most of hull-related data (ship's speed, course, heading wind, rudder angle etc.) are obtained from VDR as a LAN output data. Machinery-related data (fuel-oil flow rate, fuel-oil temperature, shaft power etc.) are obtained from engine-room data-logger (equivalent of EMS). Ship motions and encountered waves are optional monitoring items and measured by using dedicated motions sensors and a radar wave analyser.

Measured data are merged as a time-history data file of 20-min length containing all the monitored items. Then, statistical analysis of the time histories are conducted on the system's on-board PC. Average, minimum, maximum, standard deviation, significant value and zero-up-cross period are calculated for all the data items. Statistically analysed data are automatically transmitted to the on-shore data server via satellite communication. Examples of performance analysis using the analysed data will be given in 5.5.

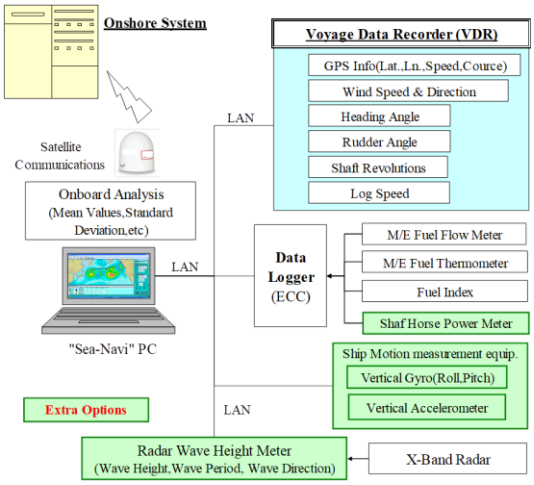

Figure 161 Configuration of "Sea-Navi" on-board monitoring system. (Orihara et al. 2019)

A set of on-board monitored parameters mentioned are basically common with those measured in the builder's speed/power sea trials except for the speed through water (STW). Measurement of STW is normally made by a speed log (Doppler or Electro-magnetic type) and routinely in ship's operation. However, it is well known that the accuracy of a speed log is quite sensitive to environmental disturbances and is prone to bias significantly.

To improve the accuracy of STW measurement, Sudo et al. (2018) developed Multi-Layered Doppler Sonar (MLDS) and evaluated its effectiveness through on-board measurements. Principles of MLDS are as follows. It transmits wideband ultrasonic waves which have multiple spectral peaks (= N). By

doing so, about N times amount of data can be obtained by measuring Doppler shifts of each spectral peak at the same time independently. MLDS has been developed by using this function, which is continuously measuring the relative flow velocity at multi-layer of water as shown in Figure 162.

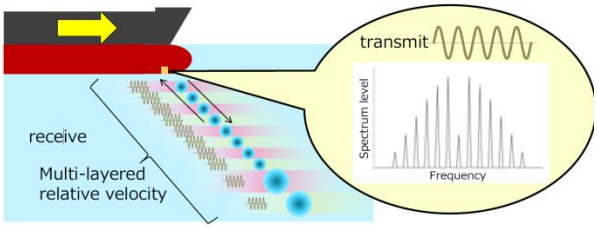

Figure 162 Multi-layered Doppler sonar. (Sudo et al. 2018)

Sudo et al. (2018) presented results of STW measurement using MLDS on a PCC and a tanker. Since draft/trim conditions affect flow field around a hull and measured STWs, measurements were made for a variety of draft/trim conditions. From the measured data depth-wise distribution of STW is established and the physically consistent STW value without effects of viscous and potential wake of the hull is obtained as a quasi-constant value at a depth sufficiently away from the hull. Figure 163 show an example of normalized depth-wise STW distribution for a specific draft/trim case. Although MLDS can eliminate the effects of viscous and potential wakes, it cannot cope with the effect of depth-wise variation in tidal and ocean currents. Since the depth of STW measurement is 3 to 4 times a draft of ships, measured STWs may differ from those at depths from water surface to the bottom of a ship for the case of deep draft ships.

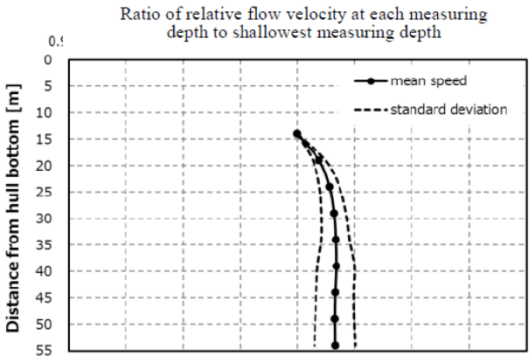

Figure 163 Overall average of relative flow velocity ratio at every layer to the shallowest layer. (Sudo et al. 2018)

MLDS were also applied to the near field flow measurements. Inukai et al. (2018) applied the MLDS for the full scale stern wake fields on a large container ship. Flows close to an operating propeller are measured and CFD simulation results.

On board monitoring thrust and torque. Observing the performance of the propeller and ship hull retrofits, it is important to measure the propeller performance from the hull resistance separately. For this, it is needed to measure propeller power, also the propeller thrust.

Application of an optical Propeller Thrust and Torque sensor, is a useful method to avoid unpredicted degradation of hull coating or propeller performance and able to separate the hull and propeller performance. In case the underwater area of the vessel's hull or the propeller is fouled or damaged, the monitoring system will indicate the cause and negative effects immediately. This is particularly useful when the propeller and bulbous bow are modified at the same time.

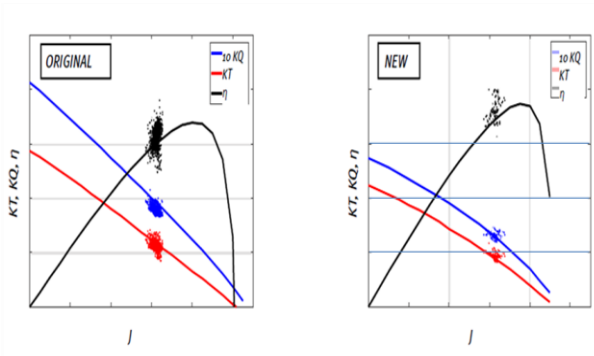

Figure 164 Monitoring the performance of different propeller

20. POSSIBILITIES TO ANALYSE SHIP PERFORMANCE ON A SINGLE RUN

Ship's speed/power performance evaluation in service conditions is normally conducted on a single run basis using speed through water (STW) as a reference speed. Since the on-board measured STWs frequently suffer from the bias and random errors, effective correcting procedures for these errors in STW are principal issues for achieving performance analysis on a single run. The other issue is the correction for the encountered disturbances to the standard or reference weather conditions. Since the weather conditions (wind & waves) and ship responses in service vary significantly depending on the operating requirements, monitored data should be corrected to unified reference conditions so that consistent evaluations can be made on the same basis.

For the correction of encountered disturbances, attempts employing the approach similar to ISO15016:2015 have been proposed, for instance, Kim et al. (2018), Orihara and Tsujimoto (2018). Among them, Kim et al. (2018) measured speed/power performance of the 300K bulk carrier in service. Measured data were analysed by their newly developed method based on ISO15016:2015 and compared with that of model test result under still water conditions without wind and wave effects. Figure 165 shows an example of speed/power monitoring results.

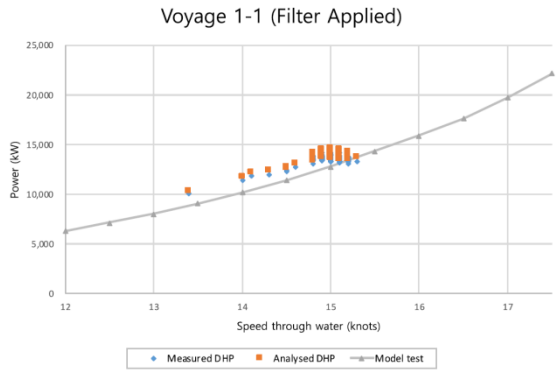

Figure 165 Analysis results of voyage 1-1 (after filtering). (Kim et al. 2018, 300K bulk carrier)

Orihara and Tsujimoto (2018) proposed full scale speed/power performance analysis method for the evaluation of performance under standard weather conditions according the Beaufort scale (BF) on a single run approach using STW as a reference ship speed. Corrections for wind and waves are similar to those in ISO15016:2015.

Orihara etc. (2019) presented speed/ power performance in service analysis results for a VLCC, a large bulk carrier and a PCTC using the method of Orihara and Tsujimoto (2018). In this study, analysed results were compared with estimated speed/power curves for conditions equivalent to BF=4, 5, 6. Examples of comparison are shown in Figure 166 and

Figure 167 for a VLCC and PCTC respectively. It is shown that analysed results agree reasonably well with the estimated curves for a range of weather conditions. In these comparisons bias error of STW measurement is corrected as a combination of fouling/aging effect by subtracting the power difference between analysed speed/power curve for BF=0 (no wind & wave effects) and estimated curve

from still-water resistance/self-propulsion model test results.

Limelette et al (2018) presented results of a comparison between filtering and normalisation approaches to determine calm water performance, for an LNGC vessel from measured data over an 18 month period. Filtering criteria were applied to determine calm water performance, namely that significant wave height (from MetOcean hindcast model) <1.5m, true wind speed <10 knots and the difference between the STW and SOG <1 knot. Correction, or normalisation, of the data using STAWAVE-1 and STAWAVE-2 was performed for comparison purposes, respecting the wave correction limits of these methods and neglecting correction for wind resistance. For this ship, which is considered as large and where encountered ship motions within the wave limit ranges was considered small, correction of data exhibited less scatter using STAWAVE-1 as compared to STAWAVE-2. Within the ship operating range of 9-19 knots, there was a maximum difference of 6% between results for calm water power derived by filtering and normalisation. This further suggests that correction may be a suitable alternative to filtering to obtain calm water power for vessels at sea from measured data.

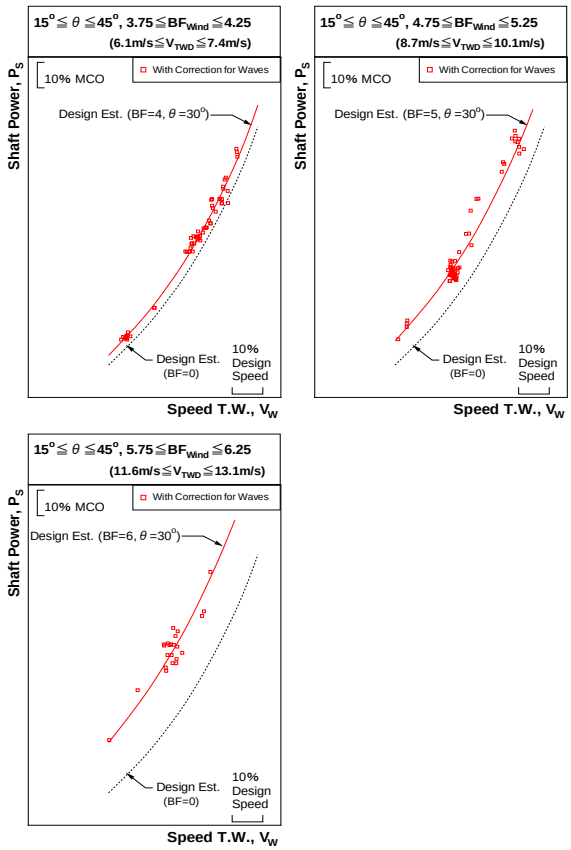

Figure 166 Measured and corrected speed/power performance for Ship A, 15 $deg. \leqq \theta \leqq 45 deg.$ (Orihara et al. 2019, VLCC in bow sea conditions)

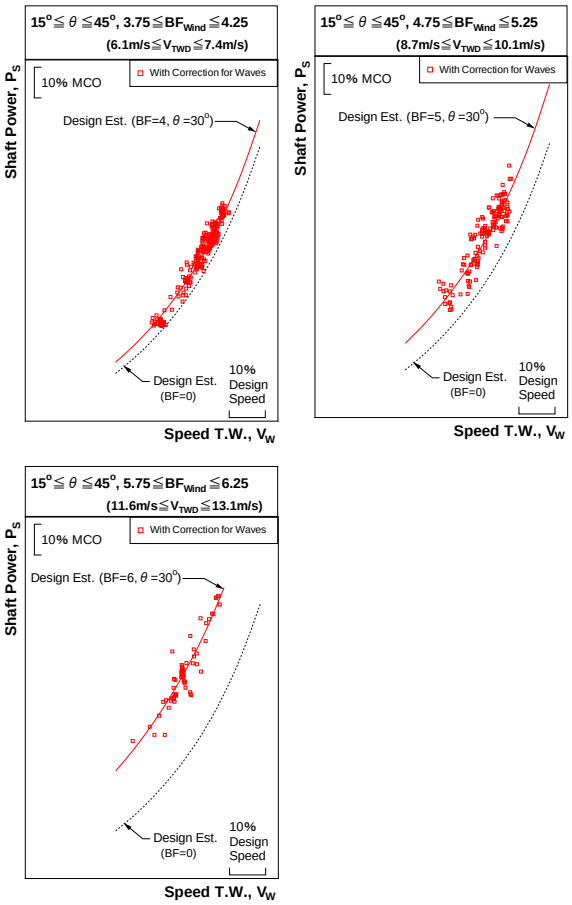

Figure 167 Measured and corrected speed/power performance for Ship C, 15° ≦θ≦45° . (Orihara et al. 2019, PCTC in bow sea conditions)

Speed/power performance monitoring and analysis methods described above can be readily conducted on in-service ships without small additional cost and considered as one of the viable approach to the analysis of the ship performance on a single run. In addition, they can cope with the ship's conditions not evaluated in the builder's trials such as fully loaded conditions for dry cargo ships or in rough weather conditions. So, their verification on a wide range of ships with an improvement of STW measurement is expected in the future.

21. EXPLORE 'SHIP IN SERVICE' ISSUES TO GET FEEDBACK TO TOWING TANKS

21.1 Applicability of Unmanned Vehicles and Devices

Airborne, underwater and floating devices are examples of unmanned vehicles that are effective in evaluating the performance of ships in service. Air drones are often used to monitor exhaust gas emissions, while underwater drones are used for water quality surveys and mapping the floors of the oceans. Although floating drones are used in the same way as underwater ones, and the drones have not obtained enough information that will be useful for providing feedback on actual operational performance, "Aquatic Drones (Aquatic Drones, 2018)" is introduced as an example of a floating drone that can be used to collect information that may be useful for estimating actual ship performance. Aquatic Drones are maritime robots that collect data autonomously. It is a multi-use platform with a wide range of sensors such as the radar for detection of ships, AIS system for ship tracking, camera and LIDAR for distance calculation and GPS for positioning. It can operate at sea in 10-18 hours on lithium batteries. If the seakeeping ability would be improved, it may be possible to measure wave height and directions or wind speed and directions or current information which are valuable for performance evaluation in actual seas.

Figure 168 An image of Aquatic Drones' surface platform.

22. MONITORING THE NEW INFORMATION AND COMMUNICATION TECHNOLOGIES APPLIED ON BOARD SHIPS

22.1 Overview

Although on board ICT of recent date is often used to confirm the integrity of the hull structure and main engine from land, the main purpose is to prevent accidents and respond quickly to breakdowns. Thanks to that, the communication environment between ship and land has improved dramatically. However, there are few introductions of the noticeable progress of the on-board monitoring instruments. LIDAR laser scanner technology is one of the few promising technologies.

22.2 Practical Example of LIDAR System

MARIN is conducting a demonstration test of wind velocity distribution measurement using LIDAR (Light Detection and Ranging) system in WINDLASS-JIP and aiming for practical use. Measurement campaign at exposed berth including 3-D wind field measurement by LIDAR wind scanner and mooring line loads by load cells will be implemented (WINDLASS-JIP, 2019). In addition, Pichugina measured the vertical wind velocity distribution using a LIDAR system installed on board a ship (Pichugina, 2012). The comparisons with more conventional measurement systems, such as rawinsondes, are shown and the effectiveness of LIDAR system are presented. However, such published and actual examples are limited, technologies for the prediction of ship performance need to be continually investigated.

Figure 169 Doppler LIDAR scanner on a vessel [Pichugina, 2012]

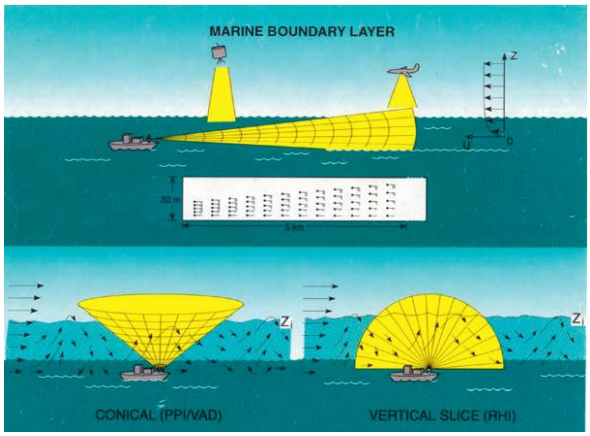

Figure 170 Common scanning patterns used by LIDAR system [Pichugina, 2012].

23. CONCLUSIONS AND RECOMMENDATIONS

23.1 Main Conclusions

a) Raven (2016) method has been accepted exclusively as a shallow water correction method, and upper limit of shallow water has been cancelled to avoid discontinuity

and low limit redefined on the basis of study. Lackenby method has been skipped.

b) Detailed survey on the development of CFD methods for wave-added resistance shows that the deviation in comparison to results obtained from model tests is found to be in the range of 20%. In tendency short wave lengths are affected by higher errors. Most of the comparisons are made in head wave cases only. Assessment of the accuracy in waves other than head waves is scarce.
c) A new full directional wave-added resistance method has been openly and intensively validated by SOS committee. The proposed method is included in the final report of the committee and the sea trial procedure.
d) Limitations of averaging wind correction method investigated and discussed extensively. Averaging method has considered the influence of superstructure. However, for large ships, when double run takes long time, the accuracy of averaged method decreases. To overcome this disadvantage, new testing instrumentation such as Lidar is proposed.
e) Guidance on the location, and type of the anemometer suggested.
f) A comparative study with CFD on wind resistance coefficient has been initiated and conducted. New approach for non-dimensionalising wind resistance coefficients has been proposed and implemented.
g) A new guideline for the CFD-based Determination of Wind Resistance Coefficients has been established. It provides guidance for CFD based derivation of wind resistance coefficients.
h) Number of double runs for sister ships has been clarified.
i) The guideline for derivation of correlation factors has been reviewed and updated by the committee.
j) The committee has reviewed the state of the art related to in-service performance monitoring including collection of data, analysis methods as well as filtering of data.
k) The speed/power sea trial procedure 7.5-04-01-01 has been further updated to reflecting all research findings so far.
l) For shallow water model testing towing tanks are normally too limited in width. Therefore, results need to be corrected for tank wall effects.

23.2 Recommendations to the Full Conference

a) Adopt the revised Procedure 7.5-04-01-01: Preparation, Conduct and Analysis of Speed/Power Trials (2021)
b) Adopt the revised Guideline 7.5-04-01-02: Guideline on the determination of model-ship correlation factors at different draughts (2021)
c) Adopt the new Guideline on the CFD-based Determination of Wind Resistance Coefficients (2021)

23.3 Recommendations for future work

1. Address issues related to hull and propeller surface roughness such as:

a) Definition of roughness properties
b) Components of roughness
c) Measurement of roughness
d) Effects of roughness on in-service performance including filtering and analysis methods for evaluating hull and propeller performance separately
e) Roughness usage in performance prediction and cross effects with correlation

2. Provide technical support to ISO and IMO in further development of approaches to in-service performance monitoring (e.g. ISO19030)

3. Address the following aspects of the analysis of speed/power sea trial results:

a) Initiate and conduct speed trials on commercial ships on deep and shallow water to further validate Raven method.
b) More validation on wave-added resistance methods, and recommend better method if appropriate.
c) Investigate the influence of water depth on the hull-propeller interaction (thrust deduction, relative rotative efficiency)
d) Continue reviewing state-of-the-art of added resistance assessment by means of CFD.
e) Explore and monitor new developments in instrumentation and measurement equipment relevant for sea trials and in-service performance assessment (e.g. wind, waves, thrust, speed through water).

4. Further investigate and validate draft dependency of model-ship correlation.

5. Study accuracy of CFD for shallow water applications.

6. Update the speed/power sea trial procedures 7.5-04-01-01.1 where appropriate.

7. Support ISO in updating ISO15016 in compliance with 7.5-04-01-01.1(2021).

8. Update guideline for determination of model-ship correlation factors.

9. Update guideline on CFD-based wind coefficient; in particular re-assess database of wind resistance coefficients and update it according to the new procedure for non-dimensionalising.

24. REFERENCES

Aldous, L., Smith, T., Bucknall, R., Thompson, P., 2015, “Uncertainty Analysis in Ship Performance Monitoring”, Ocean Engineering, Vol. 110, pp. 29-38.

Aquatic Drones, 2018, https://www.aquaticdrones.eu/

Boom, H.J.J. v. d., Huisman, H. & Mennen, F., "New Guidelines for Speed/Power Trials", SWZ-Maritime, January and February 2013.

Boom, H.J.J. and Hasselaar, T.W.F., 2014, “Ship Speed power Performance Assessment”, SNAME Maritime Convention, Houston, Texas, USA, 12pp.

Brandan, John H., 1962, D.T.M.S. Report No. 1517.

Dinham-Peren, T.A. and Dand, I.W., 2010, “The need for full scale measurements”, RINA William Froude Conference: Advances in Theoretical and Applied Hydrodynamics – Past and Future, Portsmouth, UK.

D.W. Seo., M.S. Kim., S.Y. Kim, 2019. “Uncertainty Analysis for Speed and Power Performance in Sea Trial using Monte Carlo Simulation” in Korean, Journal of the Society of Naval Architects of Korea, Vol. 56, No. 3, pp. 242-250

Fujii, H. and Takahashi, T., 1975, "Experimental study on the resistance increase of a ship in regular oblique waves", Proceedings, 14th International Towing Tank Conference, Ottawa, CANADA, Vol. 4, pp 351-360.

Giron-Sierra, J. M. and Jimenez, J. F., 2010, "State-of-the-Art of Wave Measurement for Ship Motion Prediction", Proceedings, 8th IFAC Conference on Control Applications in Marine Systems, Rostock-Warnemunde, Germany.

Green, S. B., 1991, "How many subjects does it take to do a regression analysis?", Multivariate Behavioral Research, 26(3), 499–510. https://doi.org/10.1207/s15327906mbr2603_7

Grin R. "On The Prediction Of Wave Added Resistance With Empirical Methods", Journal of Ship Production and Design, Vol. 30, No. 4, November 2014, pp. 1–11

Grin R. and Boom H. Van den, 2020, "Correlation study SNNM - SPAWAVE - FATIMA", MARIN memo.

Guo, H., and Wan, D., 2019, "Study of Wave Added Resistance and Motions of KCS in Waves with Different Wave Lengths", Proceedings, 38th International Conference on Ocean, Offshore and Arctic Engineering, Glasgow, Scotland, UK.

Hoffmann, P., 2017, "CFD Analysis, ship model HSBC", Technical Report No. RH-2017/T-008E, CTO S.A., Gdansk, Poland

Hossain, M.A., Wu, P.-C., Shibano, Y. and Toda, Y., 2018, "Forces, Ship Motions and Velocity Wake Field for KRISO Container Ship Model in Regular Head Waves", Proceedings, 28th International Ocean and Polar Engineering Conference, Sapporo, JAPAN.

International Maritime Organization, MEPC 70/INF.30. 2016. "Supplementary information on the draft revised Guidelines for determining minimum propulsion power to maintain the maneuverability of ships in adverse conditions", London, UK.

International Standards Organisation (ISO), 2015, ISO 19030, "Ship and Marine Technology – Measurement of Changes in Hull and Propeller Performance".

Inukai, Y., Sudo, Y., Osaki, H., Yanagida, T., Mushiake, M. and Kawanami, S., 2018, "Extensive Full scale Measurement on Propeller Performance of 14000 TEU Container Ship", Proceedings, 3rd Hull Performance & Insight Conference, Redworth, UK, pp 27-35.

Iseki, T., Baba, M. and Hirayama, K., 2013, "Hybrid Bayesian wave Estimation for Actual Merchant Vessels", Proceedings, 10th International Conference on Marine Navigation and Safety of Sea Transportation, Gdynia, Poland.

ITTC Procedures, "Preparation, Conduct and Analysis of Speed/Power Trials, Procedure", 7.5-04-01-01.1, 2017.

Kaiser, M., 2016, "Results of aerodynamic model tests for HSBC", Technical Report No. RH-2016/T-104E, CTO S.A., Gdansk, Poland

Kaiser, M., 2019, "Results of model tests in wind tunnel, ship model JBC", Technical Report no. RH-2019/T-078E, CTO S.A., Gdansk, Poland.

Kim, H., Park, B.- J. and Van, S.- H., 2018, "Analysis for the Powering Performance of Dry Cargo Ship in Operation", Proceedings, 28th International Ocean and Polar Engineering Conference, Sapporo, JAPAN.

Kim, M., Hizirb, O., Turana, O. and Incecika, A., 2017, "Numerical studies on added resistance and motions of KVLCC2 in head seas for various ship speeds", Ocean Engineering, Vol. 140, pp 466-476.

Kim, M., Hizirb, O., Turana, O., Day, S. and Incecika, A., 2017, "Estimation of added resistance and ship speed loss in a seaway", Ocean Engineering, Vol. 141, pp 465-476.

Kim, Y.-C.., Kim, K.-S., Kim, J., Kim, Y., Park, I.-R. and Jang, Y.-H., 2017, " Analysis of added resistance and seakeeping responses in head sea conditions for low-speed full ships using URANS approach", International Journal of Naval Architects and Ocean engineers, Vol. 9, pp 641-654.

Kume, K., Ohba, H., Orihara, H., Mizokami, S., "Wind Velocity Profile and Representative Wind Velocity for Wind Resistance Measurement of Ship Models", Journal of JASNAOE, Vol.30, pp.1-13, 2019.

Kume, K., Bielicki, S., Kobayashi, H., Ohba, H., "Validation of dimensionless method using height average wind velocity for wind forces", Journal of JASNAOE, Vol.31, 2020.

Lakshmynarayanana, P.A. and Hudson, D.A., 2018, "Is Wave Height Necessary to Determine Ship Performance in Calm Water from Measurements?", Proceedings of 3rd Hull Performance and Insight Conference: HullPIC '18, Redworth, UK, pp. 335-346.

Lee, P. H. Y., Barter, J. D., Beach, K. L., Hindman, C. L., Lake, B. M., Rungaldier, H. and Yuen, H. C., 1995, "X Band Microwave Backscattering from Ocean Waves", Journal of Geophysical Research, Vol. 100(C2), No.16, pp 2591-2611.

Lee, J.H., Seo, M.G., Park, D.M., Yang, K.K., Kim, K.H. and Kim, Y., 2013, "Study on the effects of hull form on added resistance", Proceedings, 12th International Symposium on Practical Design of Ships and Other Floating Structures, Changwon, KOREA, pp 329-337.

Lee, Tae-Il, 2016, Presentation in 28th ITTC PSS Committee meeting on June 15.

Limelette, M., Lakshmynarayanana, P.A. and Hudson, D.A., 2018, "Derivation of the Calm Water Performance of a Ship Through Normalisation of Shaft Power from Full Scale Measurements", Proceedings of RINA International Conference on Full Scale Ship Performance, London, 7pp.

Liu S., PapanikolaouA. and ZaraphonitisG. (2011), "Prediction of Added Resistance of Ships in Waves", Ocean Engineering, Vol. 38, pp.641–650.

Liu S., Papanikolaou A. and Zaraphonitis G. (2015),"Practical approach to the added resistance of a ship in short waves", Proceedings of the 25th International Offshore and Polar Engineering Conference, KONA-USA, Vol. 3, pp. 11-18.

Liu S. and Papanikolaou A. (2016a), "Fast approach to the estimation of the added resistance in head waves", Ocean Engineering, Volume: 112, pp. 211-225.

Liu S. and Papanikolaou A., (2016b), "Prediction of the added resistance of ships in oblique seas", Proceedings of the 26th International Offshore and Polar Engineering Conference, Rhodes, Greece.

Liu S., Shang B., Papanikolaou A. and Bolbot V. (2016), "Improved formula for estimating the added resistance of ships in engineering applications", Journal of Marine Science and Applications, Vol. 15(4), pp. 442-451.

Liu S. and Papanikolaou A. (2019), "Approximation of the added resistance of ships with small draft or in ballast condition by empirical formula", Proceedings of the Institution of Mechanical Engineers, Part M: Journal of Engineering for the Maritime Environment, Vol. 233(1), pp. 27-40.

Liu S., Papanikolaou A., Feng P., and Fan S. (2019), "A multi-level approach to the prediction of the added resistance and

powering of ships in waves", Proceedings of the 38th International Conference on Ocean, Offshore and Arctic Engineering, Glasgow, Scotland.

Liu S. and Papanikolaou A., (2020), "Regression analysis of experimental data for added resistance in waves of arbitrary heading and development of a semi-empirical formula", Ocean Engineering, https://doi.org/10.1016/ j.oceaneng.2020.107357 .

Lu, L. F., Sasa, K., Sasaki, W., Terada, D., Kano, T. and Mizojiri, T., 2017, "Rough wave simulation and validation using onboard ship motion data in the Southern Hemisphere to enhance ship weather routing", Ocean Engineering, Vol. 144, pp 61-77.

MARICAR (2016-2018). Seakeeping and added resistance in waves. Joint Industry Project of NTUA-Ship Design Laboratory and MARIC, Athens/Shanghai.

MARIN, WINDLASS-JIP, 2019, https://www.marin.nl/jips/windlass

MEPC 72/INF.15, Study on application of ISO 15016:2015 during the implementation of amendments to the Guidelines on survey an certification of the Energy Efficiency Design Index (EEDI), 2 February 2018.

Moat, B.I., Yelland, M.J. and Molland, A.F., 2005a, "The effect of ship shape and anemometer location on wind speed measurements obtained from ships", 4th International Conference on Marine Computational Fluid Dynamics, pp 133-139.

Moat, B.I., Yelland, M.J., Pascal, R.W. and Molland, A.F., 2005b, "An Overview of the Airflow Distortion at Anemometer Sites on Ships", International Journal of Climatology, Vol. 25., pp 997-1006.

Moat, B.I., Yelland, M.J. and Molland, A.F., 2006a, "Quantifying the Airflow Distortion over Merchant Ships. Part I: Validation of a CFD Model", Journal of Atmospheric and Oceanic Technology, Vol. 23, pp 341-350.

Moat, B.I., Yelland, M.J. and Molland, A.F., 2006b, "Quantifying the Airflow Distortion over Merchant Ships. Part I: Application of the Model Results", Journal of Atmospheric and Oceanic Technology, Vol. 23, pp 351-360.

Nakamura, S., and Naito, S., 1977, "Propulsive Performance of a Container Ship in Waves", Naval Architecture & Ocean Engineering, Vol. 15, pp 24-48.

Nomiyama, D. H. and Hirayama, T., 2003, "Evaluation of marine radar as an ocean-wave-field detector through full numerical simulation", Journal of Marine Science and Technology, Vol. 9, No.2, pp 88-98.

Ohashi, K., Hino, T., Kobayashi, H., Onodera, N. and Sakamoto, N., 2019, "Development of a structured overset Navier–Stokes solver with a moving grid and full multigrid method", Journal of Marine Science and Technology, Vol. 24, No.3, pp 884-901.

Orihara, H. and Yoshida, H., 2018, "A validation study of CFD simulations of a tanker in ballast condition advancing in waves ", Proceedings, 28th International Ocean and Polar Engineering Conference, Sapporo, JAPAN.

Orihara, H. and Tsujimoto, M., 2018, "Performance Prediction of Full scale Ship and Analysis by means of On-board Monitoring. Part 2: Validation of Full scale Performance Predictions in Actual Seas", Journal of Marine Science and Technology, Vol. 23, No.4, pp 782-801.

Orihara, H., Yoshida, H. and Takagishi, K., 2019, "Full scale Performance Monitoring of Large Merchant Ships and Comparison with Theoretical Predictions", Proceedings, 29th International Ocean and Polar Engineering Conference, Honolulu, Hawaii, USA.

Papanikolaou A., and Nowacki Z. (1980), "Second-Order Theory of Oscillating Cylinders in a Regular Steep Wave", Proc. l3th ONR Symp., Tokyo, pp. 303-333.

Papanikolaou A. and Zaraphonitis G., (1987), "On an improved method for the evaluation of second-order motions and loads on 3D floating bodies in waves," Journal Schiffstechnik, Vol. 34, pp.170-211.

Papanikolaou, A., Bitner-Gregersen E., El Moctar, O., GuedesSoares, C., Reddy, R., Spengler, F., Shigunov, V., Zaraphonitis, G., Energy Efficient Safe Ship Operation (SHOPERA) (2015), Proc. 12th Int. Marine Design Conference IMDC2015, University of Tokyo and Soc. Of Naval Arch. And Ocean Engineers of Japan, 11-14 May 2015, Tokyo, Vol. I, pp.132, ISBN 978-4-930966-04-9.

Park, J., Jang, J., Kim, S. (2016). Full load speed trial of 8000TEU container vessel, Proceedings of the 13th International Symposium on Practical Design of Ships and Other Floating Structures (PRADS' 2016). Technical University of Denmark.

Parkes, A.I., Sobey, A.J. and Hudson, D.A., 2018, "Physics-based shaft power prediction for large merchant ships using neural networks", Ocean Engineering, Vol. 166, pp. 92-104.

Pichugina,Y., "Doppler Lidar-Based Wind-Profile Measurement System for Offshore Wind-Energy and Other Maritime Boundary Layer Applications", Journal of Applied Meteorology and Climatology, pp.327-349, 2012.

Plant, W. J. and Keller, W. C., 1990, "Evidence of Bragg Scattering in Microwave Doppler Spectra of Sea Return", Journal of Geophysical Research, Vol. 95(C9), pp 299-310.

Raven, H.C., "A computational study of shallow water effects on ship viscous resistance.", 29th Symp. Naval-Hydrodynamics, Gothenburg, Sweden, 2012.

Raven, H.C., "A new correction procedure for shallow water effects in ship speed trials", PRADS 2016, Copenhagen, Denmark, 2016.

Raven, H.C., "Shallow water effects in ship model testing and at full scale", 5th MASHCON, Oostende, Belgium, 2019.

Raven, H.C., "A method to correct shallow water model tests for tank wall effects." Jnl Marine Science Techn., Vol.24-2, June 2019.

Sadat-Hosseini, H., Wu, P., Carrica, P., Kim, H., Toda, Y. and Stern, F., 2013, "CFD verification and validation of added resistance and motions of KVLCC2 with fixed and free surge in short and long head waves", Ocean Engineering, Vol. 59, pp 240-273.

Sadat-Hosseini, H., Sanada, Y., Stocker, M., Stern, F., Toxopeus, S., Castiglione, T., Simonsen, C. and Otzen, J. F., 2015, " KCS Added Resistance for Variable Heading ", Proceedings, Workshop on CFD in Ship Hydrodynamics, Tokyo, JAPAN.

Sadat-Hosseini, H., Toxopeus, S., Kim, D. H., Sanada, Y., Stocker, M., Simonsen, C., Otzen, J. F., Toda, Y. and Stern, F., 2015, "Experiments and Computations for KCS Added Resistance for Variable Heading",

Proceedings, 5th World Maritime Technology Conference, Providence, Rhode Island, USA.

SHOPERA (2013-2016). "Energy Efficient Safe Ship Operation", EU funded FP7 project, Grant Agreement number 605221, http://www.shopera.org, coordination by NTUA-Ship Design Laboratory.

Simonsen, C., D., Otzen, J., F., Joncquez, S. and Stern, F., 2013, " EFD and CFD for KCS heaving and pitching irregular head waves ", Journal of Marine Science and Technology, Vol. 18, pp 435-459.

S.M Oh., D.Y. Kang., S.H. Choi., D.Y. Lee., B.K. Kim, 2018. "Characteristics of wind speed and direction during sea trials of ships", Proceedings of the 28th International OCEAN and POLAR Engineering Conference, Vol. 4, pp. 879-886.

Stopa, J. E., Ardhuin, F, Babanin, A. and Zieger, S., 2016, "Comparison and validation of physical wave parameter-izations in spectral wave models", Journal of Ocean Modelling, Vol. 103, pp 2-17.

Strasser, C., 2018, "Wind tunnel tests, ship model HSBC", Technical Report No. 2789/01, SVA GmbH, Vienna, Austria.

Strasser, G. et. al, 2014 "A Verification of the ITTC/ISO Speed/Power Trials Analysis", Journal of Marine Science and Technology.

Sudo, Y., Igarashi, N., Yonezawa, T., Mushiake, M. and Kawanami, S. and Hino, T. 2018, "Improvement of Measuring Accuracy of Ship's Speed through Water by using MLDS (Multi-Layered Doppler Sonar)", Proceedings, 3rd Hull Performance & Insight Conference, Redworth, UK, pp 275-284.

Togino, Sakuichi, 1936, title unknown, Japanese Society of Naval Architects and Ocean Engineers, No. 59.

Tuck, E.O. and Taylor, P.J., 1970, "Shallow Water Problems in Ship Hydrodynamics", Proceedings 8th Symposium on Naval Hydrodynamics, Washington DC.

Wang, J., Yu, H. & Feng, Y. Feasible study on full scale delivered power prediction using CFD/EFD combination method. J Hydrodynamics 31, 1250–1254 (2019). https://doi.org/10.1007/s42241-019-0075-4

Yasukawa, H., 2019, "Speed Trial Analysis Method Eliminating the Need for External Disturbance Data", Ship Technology Research, Vol. 66, pp 135-149.

Yasukawa H., Hirata N., Matsumoto A., Kuroiwa R., Mizokami S. (2019), "Evaluations of wave-induced steady forces and turning motion of a full hull ship in waves", Journal of Marine Science and Technology, Vol. 24(1), pp. 1-15.

Yoshida, H., Orihara, H. and Yamasaki, K., 2015, "Long-term Wave Measurement by an Onboard Radar Wave Meter and Prediction of Ship Motions based on the Onboard Wave Measurement", Proceedings, 34th International Conference on Ocean, Offshore and Arctic Engineering, St. John's, Newfoundland, CANADA.

Zaraphonitis, G., Papanikolaou, A., (1993) "Second-Order Theory and Calculation of Motion and Loads of Arbitrarily Shaped 3D Bodies in Waves", Marine Structures, Vol. 6, pp. 165-185.

The Specialist Committee on Hydrodynamic Modelling of Marine Renewable Energy Devices

Final Report and Recommendations to the 29th ITTC

1. INTRODUCTION

This report summarises the work of the Specialist Committee on Hydrodynamic Modelling of Marine Renewable Energy Devices for the 29th ITTC.

1.1 Membership

The 29th ITTC Specialist Committee on Hydrodynamic Modelling of Marine Renewable Energy Devices (SC-HMMRED) has been organized into three focus groups: Offshore wind turbines (OWT); current turbines (CT); and wave energy converters (WEC).

The committee consisted of the following members, divided into their respectively focus group:

Offshore Wind turbines:

- Dr. Petter Andreas Berthelsen (Committee Chair), SINTEF Ocean, Norway.
- Dr. Maurizio Collu (Committee Secretary), University of Strathclyde, UK.
- Prof. Hyun Kyoung Shin, University of Ulsan, South Korea.

Current turbines:

- Prof. Ye Li, Shanghai Jiaotong University, China.
- Dr. William M. Batten, QinetiQ, UK.
- Mr. Willam A. Straka, Pennsylvania State University, USA.

Wave energy converters:

- Dr. Giuseppina Colicchio, CNR, Italy.
- Dr. Keyyong Hong, Korea Research Institute of Ships and Ocean Engineering, South Korea.
- Dr. Jean-Roch Nader (replacing Assoc. Prof. Irene Penesis mid-term), Australian Maritime College, University of Tasmania, Australia.
- Dr. Sylvain Bourdier, LHEEA, Centrale Nantes, France.

1.2 Meetings

The Committee has met four times during the three-year mandate:

- SINTEF Ocean, Trondheim, Norway, 24-26 January 2018.
- AMC, UTAS, Launceston, Australia, 12-14 February 2019.
- University of Strathclyde, Glasgow, UK, 4-7 June 2019.
- University of Ulsan, Ulsan, South-Korea, 11-13 February 2020.

1.3 Acknowledgement

The Committee would also like to acknowledge the contributions from Maxime Thys (SINTEF Ocean) and Katarzyna Patryniak (University of Strathclyde) for the support provided in writing up this report.

2. TASKS

The following lists the tasks given to the 29th Specialist Committee on Hydrodynamic Modelling of Marine Renewable Energy Devices:

2.1 Report on Full Scale installations

a. Type of device
b. Problems in installation
c. Success of energy extraction
d. Survivability

2.2 Wave Energy Converters

a. Monitor and report on new concepts for WEC's (focus on new WEC's with high TRL).
b. Develop guidelines for physical and numerical modelling of WEC's.
c. Review and report on the progress made on the modelling of arrays.
d. Continue to monitor developments in PTO modelling both for physical and numerical prediction of power capture.
e. Investigate Survivability for WEC.

2.3 Current Turbines

a. Develop specifications for benchmark tests (EFD and CFD) for current turbines.
b. Investigate effects and reproduction at model scale of inflow turbulence and unsteadiness to the turbine.
c. Review and report on the progress made on the modelling of arrays elaborating on wake interactions and impact on performance.

2.4 Offshore Wind Turbines

a. Monitor and report on recent developments of testing methodology for offshore wind turbines.
b. Report on other existing regulations related to model tests of offshore wind turbines (e.g., IEC, classification societies, DoE) and draw on these regulations if considered relevant.
c. Develop a guideline for uncertainty analysis for model testing of offshore wind turbines.

3. PROCEDURES AND GUIDELINES

3.1 Existing guidelines

This committee is responsible for maintaining the following ITTC procedures and guidelines:

- 7.5-02-07-03.7 Wave Energy Converter Model Test Experiments

This procedure addresses designing and performing hydrodynamic model tests of wave energy converters. The guideline provides a careful consideration of the differences and complexities in testing a device at various TRLs where for example the power take-off (PTO) system should be representative of the full-scale PTO and survivability tests where extreme load fatigue analysis is required. No major revision has been performed during the 29th ITTC.

- 7.5-02-07-03.8 Model tests for Offshore Wind Turbines

This procedure addresses designing and performing hydrodynamic model tests of offshore wind turbines. The guideline describes different methods for modelling of the wind loads on the wind turbine in a hydrodynamic testing facility as well as test procedures for offshore wind turbines. No major revision has been performed during the 29th ITTC.

- 7.5-02-07-03.9 Model tests for Current Turbines

This procedure addresses designing and performing model tests of ocean and tidal current turbine devices at various scales in a reproducible environment at a hydrodynamic test facility and suitability for testing such devices. The procedure was revised to address current best practices. This included the addition of a section on noise measurements. Definitions and parameters were added as were additional relevant equations. The procedure was also updated to use current ITTC nomenclature and symbols.

- 7.5-02-07-03.12 Uncertainty Analysis for a Wave Energy Converter

The procedure addresses guidelines for the application of uncertainty analysis to the small-scale testing of wave energy converters provided by ITTC procedure 7.5-02-07-03.7, "Wave Energy Converter Model Test Experiments". Details about the energy capture performance have been added to the procedure. Because of the relative importance of the PTO system in the different stages of development, three macro categories for the applications of the uncertainty have been identified: the concept validation stages (TRL 1-3), the design validation stages (TRL 4-5) and the system validation, prototype, and demonstration stage (TRL 6-9). For each of these stages, the sources of uncertainty to consider are listed as well as guidelines for their reliable evaluation.

- 7.5-02-07-03.15 Uncertainty Analysis – Example for horizontal axis turbines

The procedure addresses guidelines for the application of uncertainty analysis to the small-scale testing of current turbines provided by ITTC procedure 7.5-02-07-03.9, "Model Tests for Current Turbines". The guideline's scaling discussion was combined, reduced, and simplified. The uncertainty example was updated to better align to Type A and B uncertainty nomenclature and ITTC standards. Errors in a few equations were corrected.

3.2 New guidelines

The following two new guidelines were developed during this term:

- 7.5-02-07-03.17 Uncertainty Analysis for Model Testing of Offshore Wind Turbines

The purpose of the guideline is to provide guidance on the application of uncertainty analysis to the model scale testing of offshore wind turbines following the ITTC Procedure 7.5-02-07-03.8, "Model Tests for Offshore Wind Turbines". The model scale testing of offshore wind turbines focuses on the environmental loads and global response of the

structure, similar to the testing of other offshore structures (floating or fixed).

See also Section 9.3 for more details.

- 7.5-02-07-03.18 Practical Guidelines for Numerical Modelling of Wave Energy Converters

The purpose of this guideline is to provide a methodology to assess the fidelity of the numerical simulation for Wave Energy Converters (WECs) at different stages of development, to set up numerical calculations and to analyse the obtained results. Therefore, they have been classified as a function of the objectives of the study, of the Technology Readiness level (TRL) of the WEC and the numerical facility on which they can be run has been detailed.

See also Section 7.2 for more details.

4. COOPERATION WITH OTHER COMMITTEES

The International Electrotechnical Commission (IEC) is a key international body which addresses standards in all field of electrotechnology. The work is organized through technical committees (TCs). The TC of particular relevance for this ITTC SC are IEC TC88 (Wind Turbines) and IEC TC114 (Marine Energy – Wave, tidal and other water current converters). Through the 28th ITTC term, there were informal collaboration that resulted in cross-referencing of draft and existing ITTC guidelines and procedures, further assisting dissemination of ITTC Procedures and establishing best practice. This collaboration is still ongoing for the 29th ITTC through direct contact with IEC TC88 (MT3-2 – FOWT and WG3 – OWT), IEA Wind Task 30 and an informal contact with IEC TC114.

In particular, committee members have been involved in IEC TC 88 MT 3-2 with the task to transform IEC TS 61400-3-2; 2019 into IEC IS 61400-3-2, a technical specification and guideline for floating offshore wind turbines (FOWTs) which all FOWT industry can refer to.

5. BENCHMARK DATA

The SC-HMMRED committee was tasked to report and identity benchmark datasets that are readily available for comparison for future experiments or to validate computational and performance models.

5.1 Wave Energy Converters

In the WECs field, the development of both numerical and experimental benchmark cases is still under development. Numerical and experimental test cases have been devised by IEA OES in its task 10 “Wave Energy Converters Modelling Verification and Validation” presenting the comparison among linear, weakly nonlinear, fully nonlinear codes and experimental data. The first experimental heave decay test data of a heaving floating sphere are available (Wendt et al., 2019). These tests aimed at providing rigorous benchmark dataset and were performed with high level of accuracy and precision as well as being supplemented with thorough uncertainty analysis. Some preliminary study of the numerical analysis of a heaving sphere are also available (Nielsen et al., 2019). For further update, this information can be found in: https://www.ocean-energy-systems.org/oes-projects/wave-energy-converters-modelling-verification-and-validation/.

The European H2020 project MARINET2 round robin is still ongoing. These tests focus on two kinds of WECs to identify the uncertainty deriving from the facility bias. However, no

further updates on its progress have been publicised.

The same goes with the pan-European cost action WECANET with the planning of another round robin tests looking this time at different model scales. Once again, no further updates on its progress have been publicised.

On the other hand, in recently published article, (Orphin et al., 2021) have presented a comprehensive and detailed methodology to apply uncertainty analysis to the design and results of WEC model scale experiment using the Monte Carlos method. Example of the method is applied to a 1:30 scale experiment of a case study oscillating water column WEC in both regular and irregular waves.

At present, all the available databases are all relatively new and very few results have been published until now. However, they apply to different types of WEC technologies and address different features of uncertainties. This makes the different efforts even quite valuable for the numerical model validations. It is still to be seen if the published data are sufficiently detailed to be used by people not directly involved in the project.

5.2 Current turbines

There are a few benchmark studies currently available for verification of testing and simulations of current turbines. These include but are not limited to tow tank and water tunnel tests completed by Bahaj et al., (2007); a series round-robin experiments in multiple facilities conducted by Gaurier et al. (2015, 2018); and multiple-scale contra-rotating studies by Clarke, et al. (2007). Currently, the most complete benchmarking database for current turbines may be from the U.S. Department of Energy (USDOE) sponsored Reference Model (RM) project. Details of this project can be found at https://tethys-engineering.pnnl.gov/signature-projects/reference-model-project. This project included scaled turbine studies on a horizontal-axis and cross-flow hydrokinetic turbines (Neary et al. 2014). The largest database (relative to the types of available data) used a single three-blade horizontal-axis turbine (Fontaine, et al. (2013, 2020)). Other research included a dual rotor two-blade horizontal-axis (RM1) (Hill et al. (2020)) and a cross-flow turbine (RM2) (Bachant et al. (2014) and Wosnik et al. (2015)).

Each of these existing studies and many others provide a pool of data for comparison to other experiments or to verify other computational models. However, almost all published studies, to date, have limitations that hinder them from being considered a complete benchmark database. In most cases, details needed for validation and verification of modelling are not readily available. This includes open platform geometry definition of the turbine and test configuration within the facility; digital data files; and documented data uncertainty and hardware tolerances. An issue with current benchmark datasets in general is the range of turbine configurations that can exist including horizontal axis, vertical axis, kite and shrouded turbines to name a few. The proposed environment for each design is also often unique. Although similar, each configuration or application will have unique characteristics that may require different modelling and benchmark criteria.

Figure 171: Three-bladed “round-robin” horizontal instrumented turbine in water flume and tow tank (From Gaurier et al. (2015))

In many prior studies, performance parameters and turbine geometries used for experimental studies have been considered propriety or not readily available in the public domain. Often the data is presented in literature but not further. This is more evident with multi-scale studies or fielded installations. Multi-scale databases are important to confirm performance assessments and to validate scaling of performance of sub-scale models evaluated in experimental facilities and with computational predictions tools with fielded installations. A contra-rotating current tidal device (Clarke, et. al. (2007a, b)) was tested in tow tanks at 1/30th scale and in the Cylde estuary at 1/10th scale. However, detailed geometry information and digital measurement data for those designs do not appear to be available. Similarly, many current turbine experiments have been used to validate CFD predictions in literature. Very little of the data appears to be available in published online or accessible databases. The cavitation data of Bahaj et al. (2017) for instance has been successively used to validate computations predictions such as of Gharrere (2015) among others. Most of these data appears to be shared by personal communications.

A few databases are now or appear soon to be available online and publicly assessable. One of the first was a ‘‘round robin’’ study on three-bladed 0.7m diameter horizontal-axis turbine that was conducted in order to evaluate the impact of different experimental facilities on test results (Gaurier et al., 2015). This work tested the same model tidal turbine in two towing tanks, of very different size, and two circulating water channels. Performance assessments for TSR from 0 to 7 were conducted in each facility. Measurements included power, thrust/drag and inflow velocity. In general results in the various facilities were very similar. Due to the effect of inflow turbulence, the largest differences between the different facilities (circulating and towing) were observed in the fluctuations of torque and drag measurements. These tests highlighted the significant effect of blockage yielding high thrust coefficients, even at relatively small blockage ratios. The data from these tests can be found online (Gaurier et al., 2018a). To date, no uncertainty analysis has been present on these experiments. It also does not appear that the available data set include standard CAD files of the turbine or support structure. A second phase of this work comparing wave and current interactions is included in Gaurier et al. (2018b) so more data may be available in the near future.

The U.S. DOE Reference Model (RM) project created marine energy prototypes as reference models to benchmark performance and cost for the marine energy community. One objective stated for this project was to provide non-propriety turbine design for the marine energy community. For current turbines, this resulted in available studies for a single and dual rotor subscale horizontal-axis turbine and a subscale cross-flow turbine (Neary et al. 2014). Some details of these benchmark experiments follow.

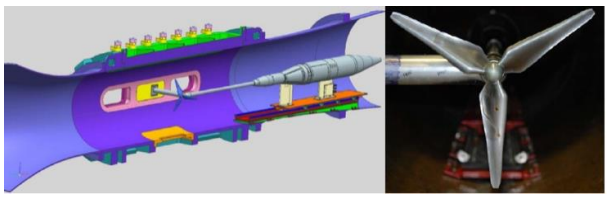

Figure 172: A 1:8.7 scale horizontal-axis current turbine (DOE-MHKF1) in cavitation tunnel (from Fontaine et al. (2013))

Fontaine et al. (2013, 2020) conducted a verification and validation study using a 1:8.7 single-rotor 0.575m diameter three-bladed horizontal-axis current turbine (Sandia turbine rotor, MHKF1, Figure 172) in a closed loop cavitation tunnel. The objective of this work was to generate a database that would provide a better understanding of the current turbine technology and means to validate analytical and

numerical models. As such, this experiment provides one of the most detailed model-scale benchmark database to date for a horizontal-axis turbine. The measured data includes device power, steady and unsteady shaft loads, tower unsteady pressures, blade strain, device acoustic measurements, nacelle vibration levels, and oil paint flow visualization photographs. Flow mapping upstream and up to one rotor diameter downstream was measured using laser Doppler velocimetry (LDV) and stereo particle image velocimetry (SPIV). The flow measurements as well as much of the other data were synced with rotor blade position. The data and geometry files are reported to be provided on the USDOE Marine and Hydrokinetic Data Repository but do not seem to be available yet. The model scale turbine was tested for operating conditions for TSR from 2 to 6 for both cavitating and non-cavitating water conditions. This database will also include blade inspection data and general uncertainty estimates.

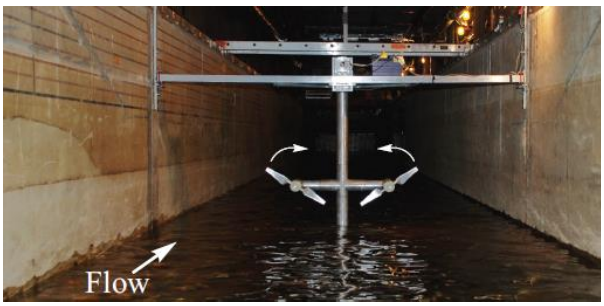

Figure 173: A 1:40 scale dual rotor horizontal-axis current turbine (DOE-RM1) channel facility (from Hill et al. (2020))

As part of the same U.S. DOE reference project, a dual rotor two-bladed horizontal-axis turbine was designed and tested at 1:40 scale in an open channel flume to evaluate power performance and wake flow recovery (Hill et al. (2020, Figure 173). Each rotor was 0.5m in diameter and evaluations completed for TSR from 1 to 9. Acoustic Doppler velocimeters were used to collect flow velocity up to 5 diameters upstream and downstream up to 10 diameters to record synchronized turbulent flow characteristics. This study included uncertainty estimates and should provide a robust dataset for numerical model validation.

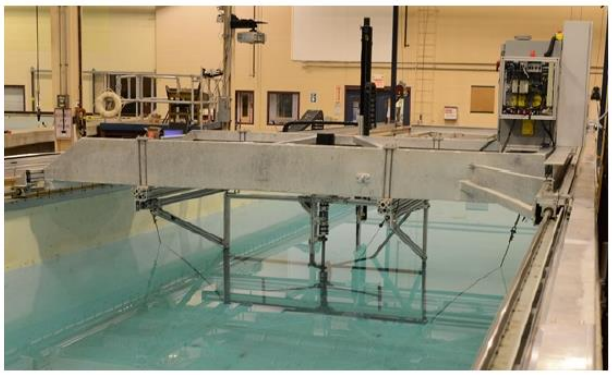

Figure 174: A 1:6 scale cross-flow turbine (DOE-RM2) setup up in tow tank (from Wosnik et al. (2015))

A 1:6 scale model of a cross-flow hydroturbine. RM2 (Barone et al. (2011)) was tested in a tow tank (Bachant et al. (2014) and Wosnik et al. (2015)). The scaled three-bladed turbine had a height of 0.807m and a diameter of 1.075m (Figure 174). Performance data such as turbine torque, drag and angular velocity were measured along with inflow speed and wake velocities at approximately one turbine diameter downstream. The data were obtained for Reynolds numbers, Re_D, from 0.4 to 1.3×10^6. CAD STEP files for the 1:6 scale model geometry are available online (Bachant et al. (2015a)). A digital measurement database is also available for download ((Bachant et al. (2015b)).

5.3 Offshore Wind Turbines

The International Energy Agency Wind Technology Collaboration Programme (IEA Wind TCP) aims at advancing the accuracy of the coupled numerical modelling tools for offshore wind turbines. Tasks 23 and 30 include a few large-scale initiatives.

IEA OC3 - Offshore Code Comparison Collaboration (Jonkman and Musial, 2010) focused on testing the newly developed aero-hydro-servo-elastic codes for modelling the fixed-bottom and floating OWT. The main emphasis was given to the verification of the dynamics of different support structures including a monopile in shallow water, a tripod at an intermediate depth, and a floating spar buoy in deep water.

IEA OC4 - Offshore Code Comparison Collaboration Continuation (Musial et al., 2009) was established to verify OWT modelling codes through code-to-code comparisons. Phase I of the project analysed the complex hydrodynamics of a jacket foundation and its local vibration phenomena, while phase II investigated the implications of different hydrodynamic theories applied to a semi-submersible floating platform.

IEA OC5 - Offshore Code Comparison Collaboration, Continuation, with Correlation (U.S. Department of Energy, 2021) extended the previous two projects providing the validation of modelling tools through comparison of the numerical results to experimental response data from both scaled tank testing and full-scale, open-ocean testing. Phase I covered the dynamics of rigid and flexible cylinders, with no wind turbine present, while phase II focused on the DeepCwind floating semi-submersible with a 1:50 scale model of a 5-MW horizontal-axis turbine.

The most recent campaign, IEA OC6 - Offshore Code Comparison, Collaboration, Continued, with Correlation and unCertainty (IEA Wind, 2021) employs a three-way validation process where both the engineering-level modelling tools and higher-fidelity numerical models are compared to experimental results. The project involves validation of the nonlinear hydrodynamic and aerodynamic loading on FOWT undergoing large motion, as well as the development of an advanced pile/foundation interaction model and the development of a hybrid potential-viscous hydrodynamic solver for innovative floating OWT support structures.

Comprehensive information about the models and results of the OC3-OC6 projects are publicly available at IEA (2021) and at the webpages indicated in **Table 27**.

Two experimental campaigns were conducted by the DeepCwind consortium at the MARIN offshore wave basin. The 1:50 scale models of a spar, a semi-submersible, and a tension-leg platform (TLP) were tested in the first campaign, followed by additional testing of the semi-submersible floater using different turbine and tower. The emphasis was given to capturing the coupling between the floating platform and the wind turbine dynamics in the operational, design, and survival seas states. Results were published in Goupee et. al (2013) and Goupee et. al (2014).

INNWIND.EU Task 4.2 partially financed by the MARINET project carried out several wave tank test campaigns. In the campaigns at the LHEEA and DHI facilities, a 1:45 model of DeepCwind semi-submersible and a 1:60 model of TLP with three different mooring lines configurations were tested with the same Froude-scaled 10MW rotor and individual pitch control. The effects of the directionally spread wave conditions, misaligned wind/ waves and extreme waves were studied. The final report and results were published in INNWIND.EU (2021) under deliverables 4.22-4.25.

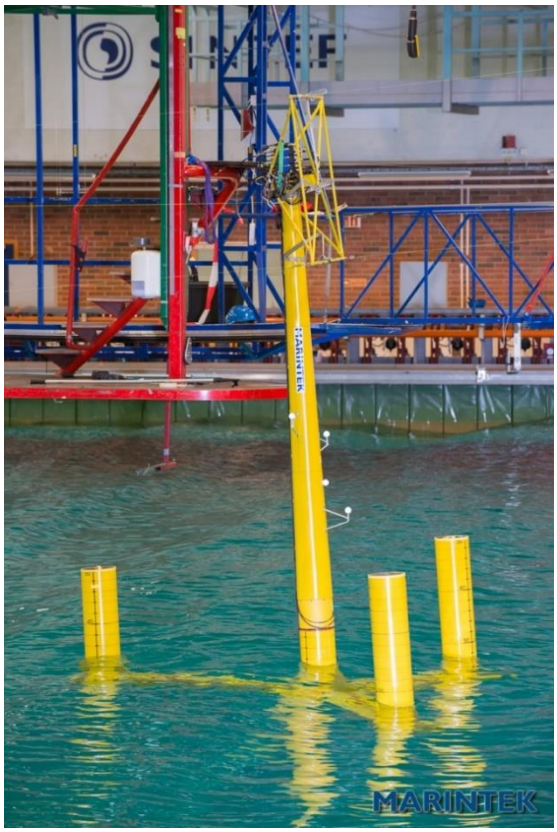

Figure 175: NOWITECH model test of a 5MW FWT (courtesy of SINTEF Ocean).

NOWITECH (Norwegian Research Centre for Offshore Wind Technology) carried out a test campaign for a 5MW semisubmersible floating wind turbine. The tests applied real-time hybrid model (ReaTHM) testing with a cable driven robot for modelling of the wind turbine (Sauder et al. 2016; Bachynski et al. 2016). The test results have been used as benchmark data for calibration of simulation models, e.g., Berthelsen et al. (2016) and Karimirad et al. (2017). The tests were performed at MARINTEK's (SINTEF Ocean) Ocean Basin in 2015 (see Figure 175).

A second NOWITECH test campaign was carried out in 2017 with a fully flexible bottom-fixed offshore wind turbine (Bachynski et al. 2019). The response of a monopile subject to irregular wave loads were investigated for a range of sea states during the tests (see Figure 176). The NOWITECH test data for benchmarking can be made available upon request.

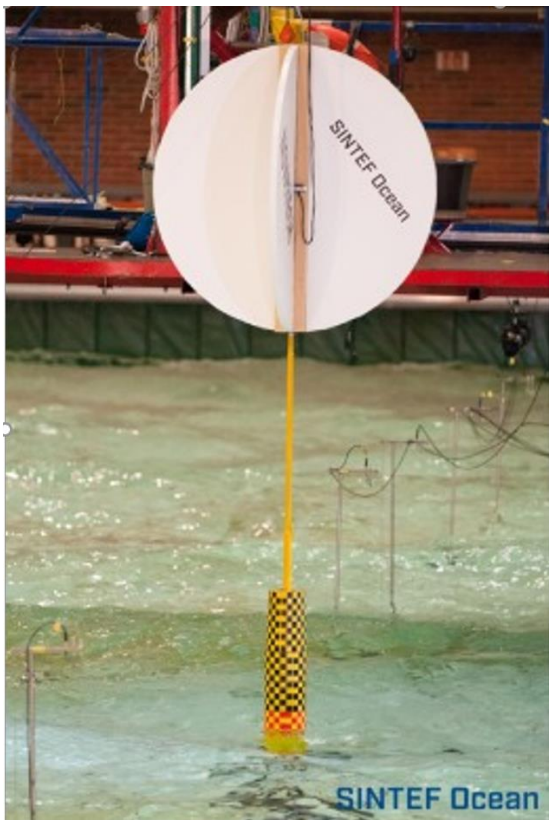

Figure 176: NOWITECH monopile test (courtesy of SINTEF Ocean).

Finally, a series of detailed aerodynamic and load measurements on a 4.5m diameter wind turbine model was conducted in the largest European wind tunnel DNW within the project 'Mexico' partly funded by the European Fifth Framework Programme. The campaign concerned a wide range of operational conditions, including multiple operational tip speed ratios, blade pitch angles, yaw misalignment angles and several unsteady cases. Information about the model and measurements was published in the report by Schepers and Snel (2007). The extensive results were subsequently analysed under the IEA Wind Task 29 and can be accessed at ECN (2021).

Table 27: Offshore Wind Turbines numerical and experimental test campaigns

INITIATIVE	LEADING ORGANISATION	YEARS	REPOSITORY WEBSITE/ REFERENCE
IEA OC3	International Energy Agency (IEA)	2004-2009	https://drive.google.com/drive/u/0/folders/0B0KGNSHvXXgCMmVsU3RkZ3FHVlE
IEA OC4	International Energy Agency (IEA)	2010-2013	https://drive.google.com/drive/u/0/folders/0B0KGNSHvXXgCSDBlREZLdDRxX2s
IEA OC5	International Energy Agency (IEA)	2014-2017	https://community.ieawind.org/task30/t30benchmarkproblems
IEA OC6	International Energy Agency (IEA)	2019-2023	Data will be made available upon completion of the project
Experimental Comparison of Three Floating Wind Turbine Concepts	DeepCwind consortium	2012-2014	https://doi.org/10.1115/OMAE2014-24172 https://www.nrel.gov/docs/fy13osti/58076.pdf https://doi.org/10.1115/1.4024711
INNWIND.EU Task 4.2	CENER	2014-2015	http://www.innwind.eu/publications/deliverable-reports
NOWITECH Semisubmersible	MARINTEK (SINTEF Ocean)/NTNU	2015	https://doi.org/10.1115/OMAE2016-54435 https://doi.org/10.1115/OMAE2016-54437 https://doi.org/10.1115/OMAE2016-54640
NOWITECH Monopile	SINTEF Ocean/NTNU	2017	https://doi.org/10.1016/j.apor.2019.05.002
Mexico	Energy Research Centre of the Netherlands (ECN)	2006-2007	http://iopscience.iop.org/1742-6596/75/1/012014
Mexnext (IEA Wind Task 29)	International Energy Agency (IEA)	2012-2018	https://www.mexnext.org/results status/

6. FULL SCALE INSTALLATIONS

6.1 Wave Energy Converters

For wave energy converters, only the Mutriku Wave Power Plant in Basque Country Spain, in operation since 2010, has demonstrated long term consistent power production (Magagna, 2019). Table 28 lists deployed or planned projects collected with information related of their type of technology, rated power, developer, and development status. Not all of those projects are full scale where the industry are still mostly at demonstration stages. Furthermore, very few data and information are available on these tests as well as virtually no information about installation issues, and

survivability. The industry is still at early stage with very few commercial products meaning that they still rely heavily on investment and grant funds. Any issues or data obtained are therefore used sensitively and not publicised. Hopefully, more information on these tests will be available in the future especially in the lesson-learnt domain to help the development of the overall industry.

Table 28 Wave Energy Converter deployment worldwide (2017-2020).

PROJECT NAME	COUNTRY	YEAR ONLINE	DEVELOPMENT STATUS	DEVELOPER	Scale	RATED POWER [MW]	TYPE	REFERENCE
LAMWEC	Belgium	2020/2021	At Sea Prototype	Laminaria	1:7	0.2	Point Absorber	Lamaniria, 2021
Wavepiston	Denmark	2017-2019	Demonstration Scale	Wavepiston A/S	1:9	0.2	Oscillating Wave Surge Converter	WavePiston, 2021
mWave	Wales	2021	Development	Bombora	1:7	1.5	Gravity Based Pressure Differential	Bombora, 2021
King Island Project	Australia	2020	Installed Waiting Connection	Wave Swell Energy	Full Scale	0.2	Oscillating Water Column	WaveSwell, 2021
OE Buoy	Ireland/USA	2020	Arrived at Hawaii Test Site	Ocean Energy (Ireland)	Full Scale	0.5	Oscillating Water Column	Offshore Energy, 2019
PowerBuoy	North Sea	2020	Operational	Ocean Power Technologies	Full Scale	0.003	Point Absorber	Ocean Power Technologies, 2021
NEMOS Wave Energy Converter	Belgium	2019	At Sea Prototype	NEMOS	Large Scale	unknown	Point Absorber	NEMOS, 2021
Tordenskiold	Denmark	2019	Half-Scale Open Sea	Crestwing	1:2	unknown	Attenuator	Crestwing, 2021
WAVEGEM	France	2019	At Sea Prototype	GEPS Techno	Full Scale	0.15	Point Absorber	GEPS Techno, 2021
WaveSub	United Kingdom	2018	At Sea Prototype	Marine Power Systems	1:4	4.5 full scale (Prototype rated power unknown)	Submerged Point Absorber	Marine Power Systems, 2021
WaveRoller	Portugal	2018	At Sea Prototype	AW-Energy	unknown	0.25	Oscillating Wave Surge Converter	AW-Energy, 2019
C3	Sweden	2018	At Sea Prototype	CorPower	1:2	unknown	Point Absorber	CorPower Ocean, 2021
Oneka Buoy	Canada	2018	At Sea Prototype	Oneka	unknown	5/10 cubic meter of fresh water	Point Absorber	Oneka, 2021
Penguin	Finland	2017	Grid Connected Test	Wello Oy	unknown	1	Internal Rotating Mass	Wello, 2021

6.2 Current Turbines

6.2.1 TYPES OF TURBINE

The type of tidal turbine still has not converged to a single type of system (Greaves & Iglesias, 2019). There are also developers investigating vertical axis devices and tidal fences. Both options may have advantages in shallower and restricted currents.

However, the majority of the devices are horizontal-axis turbines with either two or three blades. These can be mounted either on the seabed or floating with a tethered system.

One of the most successful turbines is the AR1500 turbine (SIMEC ATLANTIS ENERGY ,2020) as shown in Figure 177. This 1.5 MW turbine has a substantial tripod foundation.

Figure 177: AR1500 tidal turbine test fitting on the dock. (SIMEC ATLANTIS ENERGY, 2019).

As an example of a floating device, Orbital marine power devices is shown in Figure 178. This is 2MW device has two rotors with shared power electronics on one platform. This type of floating device allows for easier installation and maintenance.

Figure 178: Orbital marine power twin 2MW device. (Orbital marine power, 2021)

As an example of a different type of technology, a kite-based system has been developed by Miesto, (2021). This orbital path of this device shown in Figure 179. The additional motion increases the inflow speed but at increased complexity.

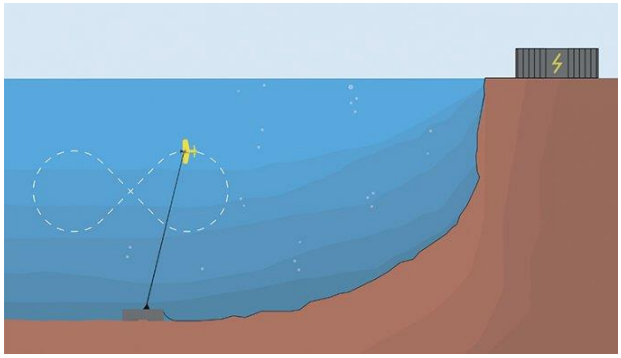

Figure 179: The orbital path of Deep Green device, Minesto (2021) turbine.

6.2.2 SUCCESS OF ENERGY EXTRACTION

From 2010 to 2019, almost 60 current turbines have been deployed in Europe. The total rated power is 27.7 MW of which 10.4 MW of this is currently operating. The remainder of 17.3 MW has now been decommissioned following the successful completion of testing programmes (Ocean Energy Europe 2019).

These installations have mainly been for medium and full-scale demonstrations to

increase the technology readiness level. The most successful project is MeyGen Phase 1A which has installed four 1.5 MW turbines and had delivered 31GWH to the grid by the end of 2019. (SIMEC ATLANTIS ENERGY, 2019). After the demonstration phase, the total farm planed size is 86 MW.

Although most of the installation has been in Europe, the Canadian province of Nova Scotia boasts the highest Feed-In Tariff which has attracted European developers. In the United States, various smaller commercial and demonstration projects have been ongoing since around 2012. These include but are not limited to the Roosevelt Island and Cobscook Bay tidal energy projects (https://openei.org/wiki/PRIMRE/Databases/Technology_Database/Projects). China has also been investing heavily in and now has a similar high feed-in tariff. (Ocean Energy Europe 2019). Other demonstration project examples include the Tasmania Turbo and Singapore Tidal demonstrations. Both were fielded for about a year each. One summary of the total installed capacity is shown in Figure 180.

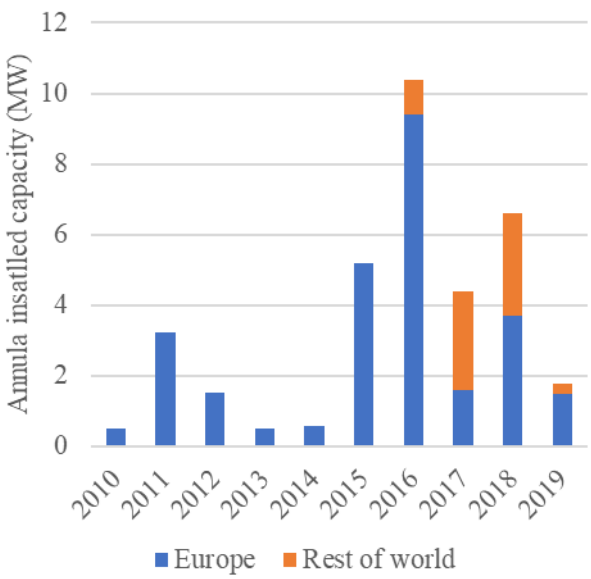

Figure 180: Global annual instated capacity (Ocean Energy Europe 2019)

There have been two main sources of failure with current turbine developers. Firstly, technical problems have been encountered. These have mainly been a fundamental structural or manufacturing issue of rotor blades or survivability issues causing rapid wearing or corrosion due to fatigue or inadequate designs/materials (EC, 2017).

Another source of failure has been due to financial problems. For example, producing the matching funds for public grants at demonstration scale or having to increase the shareholder contribution from private equity due to not meeting milestones (EC, 2017).

6.2.3 INSTALLATION ISSUES

The installation of the current turbines support structure on the seabed has a lot of uncertainties in it due to the highly variable seabed morphologies. This remains a significant technological and, therefore, also a cost challenge. Each CT farm installation normally requires tailoring to adapt to the subsoil conditions. The techniques from the offshore oil and gas have also required a considerable amount of adaptation before they will provide viable solutions for tidal installations.

For example, fairings have had to be installed on jack-up barge legs as although the installation is done in slack water when the tide is changing the barge must go through a tidal cycle.

Lessons learned from marine operations in the Nova Scotia (FORCE, 2019) have highlighted issues with tugs requiring maximum thrust during turbine installs and limitations on

towing in the tides. At Nova Scotia site the window for safe diving is approximately 20 minutes which limits the type of installation and mitigation options if automated installation systems fail.

In order to mitigate some of these installation issues of turbines firmly mounted to the seabed, there have been recent developments in floating moored systems. This also improves the ability to do maintenance. However, this increases the complexity of the device and in most cases the amount of fabrication.

6.2.4 SURVIVABILITY

A significant number the early installation of turbines had issues with survivability. As of consequence, guidelines have been released to help developers EMEC (2009).

Also, over the last ten years, the understanding of the nature of the unsteadiness flow in tidal current test sites has improved. This has been mainly due to better quality measurements and analysis of tests sites which has improved the understanding of magnitude and frequency unsteadiness due to large scale turbulence structures and waves. (See for example McCaffrey et al. 2015 and Milne et al., 2016).

Some of the failures may also be due to not replicating enough of the environment in the test facility. This is further reviewed in Section 8.2 where the issues of the reproduction of inflow turbulence and unsteadiness in test facilities is discussed. As an example, recent experimental data, which has shown delayed separation and dynamic stall can result in blade root bending moments that exceeds the steady value by 25%, (Milne et al., 2016).

These additional loads have been the main cause of tidal turbine rotor blade fractures. This has resulted in the optimisation method to address these structural issues with increased blade thickness and improved fatigue life (Liu & Veitch 2012). This knowledge has led to improved predictions of the magnitude of unsteady hydrodynamic loading and there have been fewer failures.

The recent developments in floating current turbines have yet to become mature enough to show any patterns in survivability.

6.3 Offshore Wind Turbines

As the floating offshore wind turbine (FOWT) technology matures, the projects are starting to move from demonstration pilots to full commercial wind farms. Since the last (28th) ITTC report, in 2017, the number of operational floating wind turbines has more than doubled, quadrupling the total installed capacity (**Table 29**). Spar and semisubmersible platforms remain the most widely applied concepts, however, new designs, such as the damping pool by Ideol, have gained some momentum. The major large-scale installations in Europe and Japan are described below and summarised in Table 29.

The world's first FOWT, Hywind Demo, remained operational in Norwegian waters for eight years. During that time, it produced more than 40 GWh, proving the survivability of the concept in a harsh environment (Equinor, 2021a). Taken over by Unitech, this wind turbine is still operational, and it is used for research purposes (UNITECH, 2021) at the test site of the Marine Energy Test Centre (MET Centre) off the coast of Karmøy, Norway.

The three FOWT of the Fukushima FORWARD project (2,5 and 7MW) were installed in the years 2013-2016 to assess their safety, reliability, and economic efficiency (Fukushima Offshore Wind Consortium, 2021). Although they provided a valuable early experience, the wind farm is currently being decommissioned; the project turned out not to

be enough profitable due to its low availability, low output, and expensive maintenance of the two larger turbines (Randall-Smith, 2021). Having learned the lessons, Japan pursued another floating project (Kitakyushu Hibiki), successfully deploying a 3MW wind turbine supported by the Ideol's barge. Shortly after installation, the turbine survived three category 5 typhoons (Ideol, 2021b). Next, significantly larger wind farms are being developed in Pacific (e.g., Goto Sakiyama Oki Oki Huangdao Pilot A - 22MW, and Fukushima Phase 3 - 1GW).

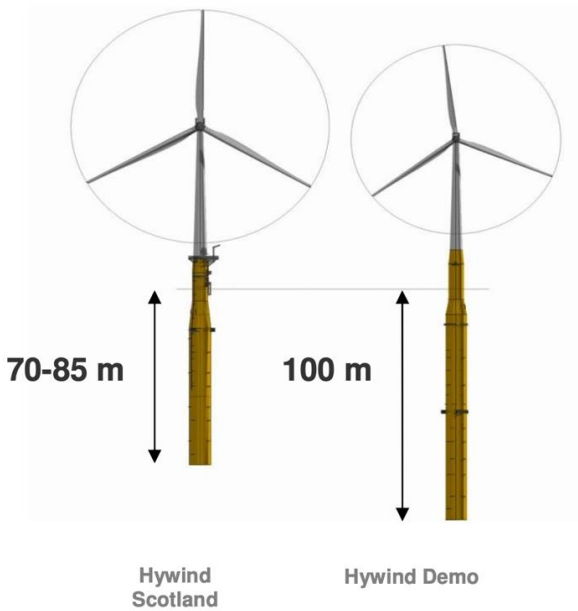

Figure 181: Hywind Scotland (2017) and Hywind Demo (2009) Spar floating offshore wind turbines (xodus group, 2013).

The world's first and largest floating wind farm, the Hywind Scotland Pilot Park, started producing power in 2017 (Equinor, 2021b). Five 6-MW turbines were mounted on the Equinor's spar platforms, achieving around 65% capacity factor in the first 3 months of operation. Importantly, according to Equinor, the cost reduction of 60 - 70% was reached as compared to the first Hywind project in Norway (Equinor, 2021b).

The second-largest floating wind farm was installed 20 kilometres away from the shore of Portugal within the WindFloat Atlantic project. Following the earlier 5-years trial of the Principal Power's semisubmersible, three world's largest floating wind turbines were connected to the grid, featuring the Vestas 8.4MW turbines with 164m diameter rotors (EDP, 2021).

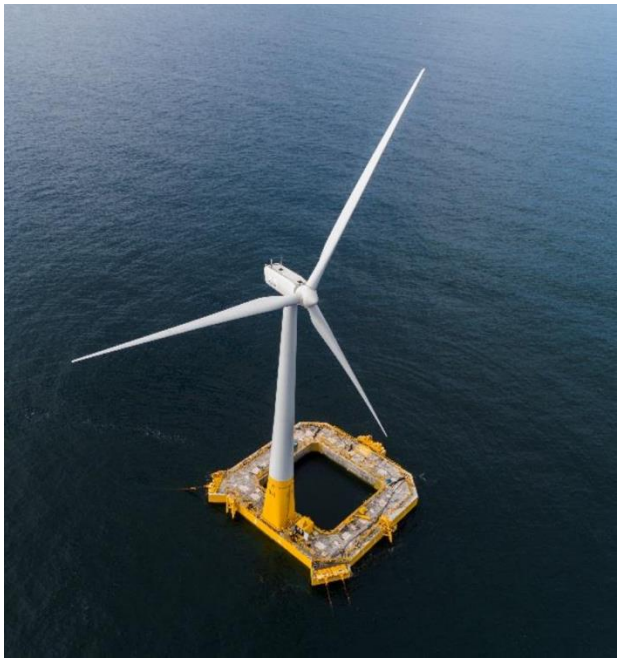

Figure 182: Floatgen by Ideol (Ideol, 2019).

The year of 2018 saw four major installations, with two semisubmersible platforms and two spar buoys. The project Floatgen installed one 2MW floating WT, allowing France and Ideol to join the floating wind industry (Ideol, 2021c). Following this success, French Eolink deployed a 1:10 scale prototype of a 12MW turbine which provided the basis for the future development of 10MW+ floating systems (Eolink, 2021). Finally, Kincardine Phase 1 project added another 2MW to the British offshore grid. This demonstrator of the Principal Power's semisubmersible is the first of 6 turbines to be installed. Ultimately, the

wind farm's total capacity will reach almost 50MW (Group Cobra, 2021).

Another important project in the construction phase is the TetraSpar Demo at the MET Centre in Norway (Stiesdal, 2021). By focusing on the modularity of the design and its suitability for mass production, the project developers' goal is to switch from one-off foundation design, based on the oil and gas industry, to designs thought to be mass-produced, eventually lowering the CAPEX levels.

Another demo project planned at the MET Centre is the EU-financed H2020 project FLAGSHIP, a European collaboration led by Iberdrola. The consortium will design, build, install and operate a semisubmersible (OO-Star Wind Floater) type floating wind turbine with minimum a 10MW turbine. The project was established in 2020, and construction time is estimated to be 2 years with a test period of 2 years after that (Dr. Techn.Olav Olsen, 2021). The main objective of the project is to demonstrate cost-effective large floating wind turbines to ensure a reduction in LCOE to a range of 40-60€/MWh in 2030.

In 2021, the vast majority of the installations are planned to take place in France:

- EOLMed (30MW)
- Les éoliennes flottantes de Groix et Belle-Ile (28.5MW)
- Les éoliennes flottantes du Golfe du lion (30MW)
- Les éoliennes flottantes du Provence Grand Large (25.2MW)

All these projects have recently upgraded their choice of turbines to 8.4-10MW, taking the advantage of fast-developing wind technology and pushing the boundaries of the floating platforms' performance (EOLMed, 2021, EOLFI, 2021, EFGL, 2021 and PGL, 2021).

Hywind Tampen will be the largest floating wind farm when commissioned late 2022 (Equinor, 2021c). The project, consisting of 11 Hywind spar platforms, intends to provide electricity for the Snorre and Gullfaks offshore fields in the Norwegian North Sea. It is expected that the wind farm will reduce the annual emissions from the gas turbine power of the offshore fields by 200.000 tonnes CO_2 and 1000 tonnes NO_x. Each spar platform will be equipped with a Siemens Gamesa SG 8MW turbine providing a total capacity of 88MW. The Tampen wind farm will be the first to power oil and gas platforms, and due to the large size, it will be an essential step towards industrialization of floating wind technology and reducing costs for future projects.

Table 29: Completed installations of offshore floating wind turbines worldwide.

PROJECT NAME	COUNTRY	YEAR ONLINE	DEVELOPMENT STATUS	DEVELOPER	UNITS	RATED POWER [MW]	TYPE	REFERENCE
Hywind Demo (KARMØY)	Norway	2009	Operational	Equinor (sold to Unitech)	1	2.3	Spar	Equinor, 2021b
WindFloat Atlantic Phase 1	Portugal	2011	Decommissioned in 2016	Windplus Consortium	1	2	Semisub.	EDP, 2021
WindFloat Atlantic	Portugal	2020	Operational	Windplus Consortium	3	25.2	Semisub.	
Fukushima Demo 1 (Mirai)	Japan	2013	Operational	Mitsui	1	2	Semisub.	
Fukushima Demo 2 A (Shimpuu)	Japan	2015	Decommissioned in 2020	Mitsubishi	1	7	Semisub.	Fukushima Offshore Wind Consortium, 2021
Fukushima Demo 2 B (Hamakaze)	Japan	2016	Operational	JMU Corporation	1	5	Spar	
GOTO FOWT – Kabashima 2	Japan	2013	Operational	Toda	1	2	Spar	Utsunomiya et al., 2014
Hywind Scotland Pilot Park	UK	2017	Operational	Equinor/ Masdar	5	30	Spar	Equinor, 2021b
Floatgen	France	2018	Operational	Ideol	1	2	Barge (damping pool)	Ideol, 2021c
Kincardine Phase 1	UK	2018	Operational	Principle Power	1	2	Semisub.	Group Cobra, 2021
Kitakyushu Hibiki NEDO	Japan	2018	Operational	Ideol	1	3	Barge (damping pool)	Ideol, 2021b
Eolink (prototype)	France	2018	Decommissioned in 2019	Eolink	1	1.2	Semisub.	Eolink, 2021

7. WAVE ENERGY CONVERTERS

7.1 New concepts

There are many concepts of wave energy convertors. In fact, no technology convergence has been observed and every companies have developed their own technologies of devices and power take off systems: internal rotating mass from the Penguin (Wello, 2021), vertical plates attached to sea water pumps in the WavePiston (WavePiston, 2021), the uni-directional airflow system in the Uniwave (WaveSwell, 2021), the closed internal water circulation system in the WAVEGEM (GEPS Techno, 2021) or the pressure differential energy harvester through air-inflated rubber membranes as in the mWave (Bombora, 2021). A list of the most developed devices and their type of system can be found in Table 28.

7.2 Guideline for physical and numerical modelling of WEC's

The new guideline on numerical modelling of wave energy converters have been issued, the purpose is to provide a methodology to assess the fidelity of the numerical simulation for Wave Energy Converters (WECs) at different stages of development. Because of the WECs variety, it was impossible to draw a general procedure. Instead, the different numerical solvers that are available at the moment have been described and their range of applicability has been detailed as a function of: the TRL, the wave conditions, the non-hydrodynamic features that have to coupled and the numerical facility availability. More in particular, the numerical methods have been described and grouped in analytical, potential flow and computational fluid-dynamics models, eventually coupled with hybrid strategies.

In the fashion of the ITTC procedure 7.5–03 02–03 "Practical Guidelines for Ship CFD Applications", the main steps of the applications of all the numerical models have been detailed for the pre-processing stage (description of the body, setting of the boundary and environmental conditions), the computations (time and spatial discretization, device response to external loads as mooring, PTO and controls) and post-processing (collection and analysis of the data, verification and validation of the solution).

7.3 Physical and numerical modelling of arrays

WECs are reaching such a level of development to be appetible to electric utilities to replace fossil-fuel energy sources. To become truly commercial though, they have to be deployed in array or farms so that the cumulative production can be of the order of a few MW.

In these farm settings, the interactions between close by WECs (near field effects) will give rise to a complex wave field that affects the power extracted by each device and consequently the total power output of the farm. Moreover, at large distances behind WECs (far field effects), the farms alter the wave field affecting the coastal processes, such as: other users at sea, coastal ecosystems and the coastline.

The numerical and experimental methods commonly used for the analysis of the array configuration were already thoroughly described in the former committee final report. The limits that were stated in that report have been only partially overcome. Below, just a few of the more outstanding examples of advancement from the experimental and numerical points of view are given.

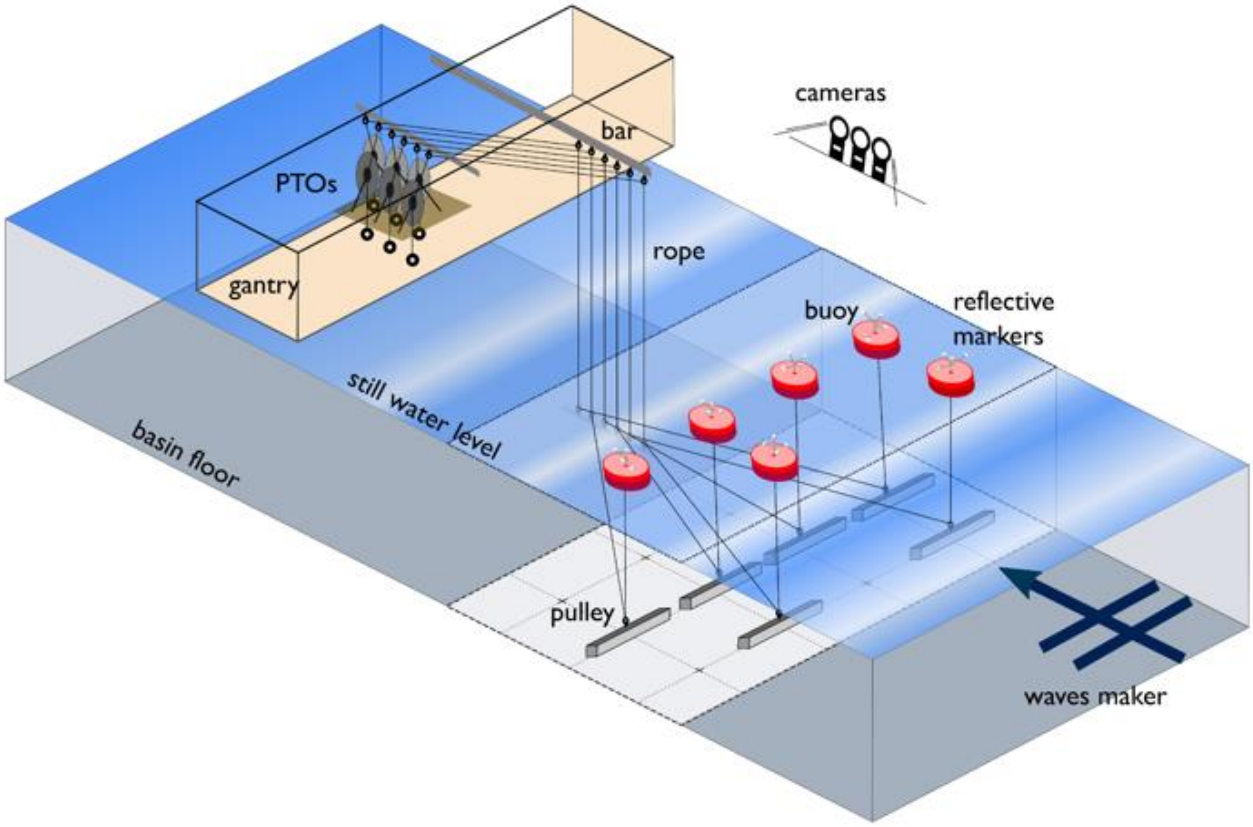

Figure 183: Layout of the array with each WEC moving in 6DOF (from Giassi et al., 2020)

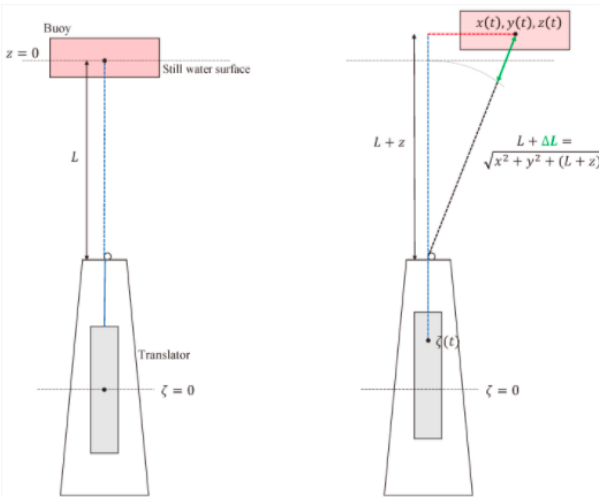

Figure 184: Relative displacement of the floater with respect to the PTO from Giassi et al., 2020.

Advancement in experimental analysis of the WECs farms can be found in Giassi et al., 2020; their work stands out because the analysed six point-absorbers can move in six DoFs. The array is tested both in regular and irregular waves in three different layouts. The full motion of the WECs highlighted that the floats moving also in sway cause the reduction of the shadowing effect. Moreover, as in the single WEC with multiple degree of freedom, the importance of non-linear behaviours is stressed for: 1) the two-body dynamics with different relative displacement of float and PTO due to slack and elasticity in the connection as shown in Figure 184 (mostly in irregular waves) and 2) Mathieu-type instability (mostly in regular waves) (Orszaghova et al., 2019).

From an experimental point of view, tests can be performed either in model test wave tanks or at sea. The two choices have opposite advantages and drawbacks. As for the single device, in the former case, facility biases are magnified (reflexion, incident wave field variations, blockage effects, etc.) and large uncertainties may occur when trying to quantify the relative interactions with the surrounding devices. In the latter case, full scale or large-scale tests can be performed limiting the errors induced by the different scaling laws relative to the different parts of WECs (hydrodynamic behaviour, viscosity, PTO system, mooring system) but it is very expensive, and the environment is difficult to control. For this reason, the recent work on arrays described in Yang et al., 2019, is noticeable because it is one of the few examples of quite well detailed large-scale experimental analysis of an array of WECs. The array is composed of point-raft WECs into three layouts with ten, six or two buoys deployed in real sea conditions in Taiwan Strait, China. Unfortunately, the importance of this paper is diminished by the lack of information about the PTO that is based on mechanical gear transmission of the rotation from the raft to the shaft to a permanent magnet generator (see Figure 185). However, neither the mechanical nor the electrical parts of the PTO are fully detailed and characterized.

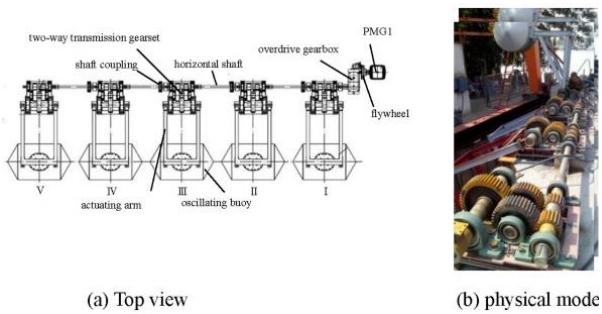

Figure 185: Array drive mode from Yang et al., 2019.

Advancement in numerical simulations of WECs arrays can be found in the full CFD simulations described in Devolder et. al., 2018. There, the numerical simulations of two, five and nine heaving Floating Point Absorbers (FPA) WECs arranged in a geometrical array configuration show the capability of state-of-the-art numerical models to predict the independent motion of closely-spaced WECs in regular waves. The results are compared to the WECwakes project experimental dataset. The paper presents also a percentage evaluation of the differences between numerical and experimental data for different sizes of array and for the heave motion, surge force and wave height in several location inside the array and around it.

7.3.1 RELIABILITY OF THE RESULTS

As underlined in Göteman et al., 2020, the qualification of the reliability of both numerical and experimental data and models is fundamental to further proceed towards the optimization of farms.

In Devolder et. al., 2018., the CFD simulations are carried on with OpenFOAM that fully models the viscous and turbulent effect. There, the largest differences between numerical and experimental data are found in the case with the largest array (9 elements). They are respectively 18% on the surge force, 30% in the wave height and 64% in the heaving motion. Even though, the author claims that the largest difference in the heaving motion were due to different the frictional forces in the PTOs; this paper is one of the few examples where the comparison between numerical and experimental data are used to state the reliability of the adopted numerical models. Moreover, the authors give useful advices on the experimental procedures. For example, they state that fouling can alter the characteristics of sliding mechanism and they highlight the importance of their daily cleaning. They also recommend the validation of the numerical studies with the free

decay tests for each individual WEC of the array to estimate the frictional forces due to the sliding mechanisms.

Another important step forward in the assessment of the numerical methods and, in particular, of the Phase-Averaging Wave Propagation Array Models is given in McNatt et al., 2020. There, the spectral wave action balance code SNL-SWAN is compared to the Boundary Element Methods code WAMIT. The comparisons are performed for three types of WECs (pitching flaps, points absorbers, and hinged rafts), for the single WECs or array layouts, in short, medium and long crested waves and with various amounts of directional spreading, Figure 186 compares the solutions for arrays of different types of WECs and WAMIT solutions is as assumed as reference.

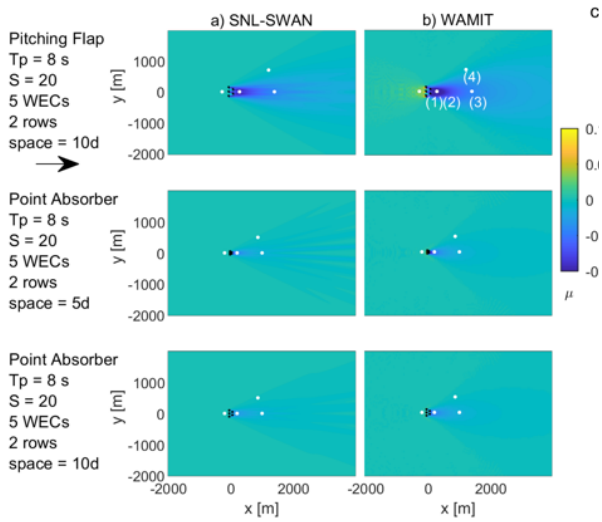

Figure 186: Example of wave field difference between SNL-SWAN and WAMIT from McNatt et al., 2020.

From their analysis, the authors draw the following guidelines for the use of SNL-SWAN:

1. For arrays, the impact of the park on the wave field differs from 20% to 60% between WAMIT and SNL-SWAN, the differences vanish 30 characteristic WEC dimensions away.

2. SNL-SWAN works better for larger spreading of the wave spectrum, consequently unidirectional waves are not well captured.

3. SNL-SWAN application has to be careful in shorter waves where it does not model wave reflection or scattering (including reflections in SNL-SWAN is underway).

7.3.2 PARK OPTIMIZATION

The performance of a WECs-park depends on many parameters (layout, number of devices, mooring system, control strategies) that will have a deep influence on the LCOE, reliability of the installation, power production, electricity quality. For these reasons, the late development of the WEC-parks analysis is the introduction of optimization techniques (Sharp et al., 2018, McCarthy et al., 2019, Göteman et al., 2020).

The first studies related to the array optimization described the comparison among several configurations, but little explanations were given on the choices. It further evolved into a *parameter sweep* method, where one single parameter was regularly varied to find the optimal array layout as a function either of the power fluctuation or of the power output (Falvià et al. 2017, Lòpez-Ruiz et. al., 2018).

Because of the many parameters influencing the array performance, the simple sweep over single parameters is not suitable to find the optima, more complex solutions are needed.

The field of array optimization is quite new and there is no winning technique for it. Here we report the most used. One of them is the *nonlinear programming* (NLP) optimization, it

is based on constraints and objective function that are nonlinear.

Another approach consists in the *Metaheuristic Algorithm* that looks for the solution space of sufficiently good solution. It is used when the optimization problem is too large to look for all the possible solutions and when the solution space is multi-peaked or when imperfect information is available. Among these methods there are the *genetic algorithms*, the *covariance matrix adaption*, the *differential evolution*, the *particle swarm algorithms* (for a complete description see Göteman et al., 2020).

Moreover, there is the *Bayesian Network approach for a Risk based optimization*, used in McCarthy et al., 2019, that is adopted to analyse the probability of a collision accident within the farm as well as the likelihood of meeting the desired level of power production. It is based on probabilistic techniques, that are well suited to take into account the many uncertainties associated with the WEC-farms analysis and enables to obtain the desired level of production while minimizing the risks associated with the proximity of several WECs.

7.4 Developments in PTO modelling both for physical and numerical prediction of power capture

The WEC PTO systems harvest wave energy through a series of hydrodynamic, mechanical, and electrical processes. In general, WEC devices are classified according to their primary energy conversion principles such as oscillating water column (OWC), overtopping, oscillating wave surge convertor (OWSC), point absorber, attenuator, submerged pressure differential (SPM). There are WECs based on flexible membrane and rotating mass as well. A primary energy conversion of OWC and overtopping type devices transforms wave energy into kinetic and potential energy of fluid respectively, while other WEC devices convert it into dynamic motion of submerged or floating body. The following process and composition of PTO systems varies depending on the characteristic of the primary energy conversion. A typical PTO composition includes appropriate generator and power control system in common and it is distinguished according to WEC devices such as OWC (air chamber, air turbine), overtopping (water reservoir, hydraulic turbine), OWSC (hydraulic pump, accumulator, hydraulic motor), point absorber (heaving buoy), etc.

The WEC PTO modelling is still far from a standardization mainly because of diverse WEC systems. The difference in PTO simulation results can be significant depending on modelling methods. Recent studies on PTO systems includes the nonlinear, unsteady, and viscous properties of the PTO components, which are critical for the accurate performance evaluation. A series of benchmark tests to compare the numerical tools for hydrodynamic modelling of WEC PTOs have been carried out by IEA-OES group since 2016 (Bingham et al, 2021). Research on coupling effects between integrated PTO components has increased as well. The optimal operation considering those interactions may increase wave energy extraction significantly, and it raises the need to develop an integrated WEC simulation tools (So et al., 2016, Penelba et al., 2018).

The OWC devices convert wave energy into oscillating water column in the pneumatic chamber and subsequently produces air flow in the connected duct that runs air turbine. Recent studies of pneumatic chamber include the CFD simulation of resonant sloshing with nonlinear PTO (Xu et al., 2019, Connell et al., 2018), the investigation of air compressibility effect inside chamber by Falcao et al. (2019) and Simonetti et al. (2018). A self-rectifying bi-radial air turbine was examined experimentally by Carrelhas et al. (2020), showing significant improvement of efficiency over a wide range of

flow coefficients. An unsteady analysis of a bi-directional impulse turbine coupled with permanent magnet synchronous generator (PMSG) and its controller was carried out by Ezhilsabareesh et al. (2019), suggesting the maximum efficiency tracking for different axial velocities. Kim et al. (2020) analysed the hydrodynamic performance of pneumatic chamber interacting with air turbine based on 3-D potential flow in time domain, addressing that nonlinear flow characteristics depend on incident wave height.

The point absorbers transform wave energy into a moving body that is commonly connected to a direct electrical drive system, and the accurate estimation of its damping parameter is critical in the PTO design of point absorbers. Rodriguez et al. (2019) analysed the damping coefficient affected by wave conditions based on a hybrid method of numerical simulation and experimental measurement. Li et al. (2020) proposed a mechanical PTO using a ball screw and mechanical motion rectifier, converting wave energy into the unidirectional rotational of PMSG. Kong et al. (2019) developed a PTO control method for the optimization of an axisymmetric point absorber in irregular waves and compared the average capture width ratios obtained by time and frequency domain analyses. The latching control of direct mechanical derive PTO system may significantly increase the power extraction by point absorbers, while it raises practical challenges control caused by excessive peak-to-average power ratio (Shadman et al., 2021, Temiz et al., 2018).

The OWSC uses a hydraulic PTO system featured with lower flow rate and higher pressure, and it is commonly equipped with a breaking system to constrain an excessive motion of oscillating structural elements. Calvario et al. (2020) simulated the performance of OWSC concepts with different PTO layout configurations, and compared it to point absorbers, insisting that OWSC devices have less constraint in design optimization and advantage in operational wave condition. Senol et al. (2019) simulated the PTO model of bottom-hinged OWSC equipped with a braking system, proposing a PTO technique enhancing energy harvesting by minimizing engagement of the braking system.

7.5 Survivability for WEC

There are still a lot of unknown related to survivability for WECs. Very few companies who have deployed at full scale have shared any data or information related to the device survival response. There are essentially no publications comparing experimental and/or numerical model testing of survival conditions to full scale applications. And due to the complexity of WEC systems compared to other offshore structures, there is still a strong need to update guidelines, best-practices documents, and standards for the survivability testing of WECs.

The guidelines for Wave Energy Converter Model Test Experiments, the survivability section, has been further extended. Advices have been added regarding the full design framework to obtain the load characteristic of the WEC (fatigue and extreme response statistics) prior to the tests. Once the environmental conditions are identified depending on the type of state conditions (Ultimate Limit States or Accidental Limit States), the details of specific test conditions, the relevant parameters to be included and the quantities to be measured are listed.

8. CURRENT TURBINES

8.1 Benchmark Specifications

To date, much of the data and design geometries for marine renewable devices including current or tidal turbines have been

considered propriety or not readily available in the public domain. More recently, for current turbines, a few experimental programs have been conducted for the purpose of validation of CFD predictions or to evaluate the impact of different facilities on test results and turbine performances. The databases for some of these studies are currently or will soon be available online in the public domain. A few of these were summarized in section 5.2. Although each of these databases provide valuable resources, specification for more complete future benchmark studies are needed. Planning for a benchmark should follow guidelines addressed in ITTC 4.0-0.

8.1.1 OBJECTIVES

The three key objectives for current turbine benchmarking evaluation would be to

- Understand the bias between experimental testing facilities
- Provide geometry configuration, boundary conditions and performance data for CFD validation and verification
- Provide data to assess performance scaling and predictions tools of full-scale devices.

8.1.2 FACILITY AND TURBINE CONFIGURATION

The choice of experimental facility or facilities for current turbines is anticipated to have a more significant effect than for standard open water propellers. This is a result of a higher influence of blockage and the effect of inlet turbulence due to the shorter blade chords. The type of facility used would be dependent on the type of turbine that is needed for the benchmark data. It is also recommended that multi-scale data been considered for any benchmark database in order to develop and confirm scaling both for computational models and for facility performance scaling. The benchmark turbine needs to be non-proprietary and ideally be or already been fielded in order to obtain full-scale data to compare.

The choice of a turbine for any benchmark test will depend on the range of test facility or facilities that would be used. ITTC Procedure and Guideline 7.5-02-07-03.9 has good advice that must be used and followed when planning a current turbine benchmark evaluation. The range of configuration of tidal and current devices can include horizontal-axis, vertical-axis, kite, and shrouded turbines. Although similar, each configuration will have unique characteristics that may need different modelling criteria and hardware and measurement requirements. Benchmarking can and should be accomplished for single rotors, multiple rotors and arrays as flow and wake interactions are important. The horizontal-axis turbine configuration appears to be one of the more popular fielded configurations. The U.S. DOE RM project used two horizontal-axis turbine designs. Given its detailed database, RM turbine (MHKF1) would provide a good candidate to be used for further benchmark studies as the turbine design and details should be soon in the public domain. Other existing turbines databases such as used in round-robin testing (such as Gaurier et al. (2015)) would also provide a good candidate provided further geometry, facility/setup details and data uncertainty were provided.

As tidal/current rotors usually consist of two to three blades with short chord lengths and small amounts of skew or rake, the Reynolds number (Re) based on chord length can be low. Consequently, a section profile with predictable transition is necessary. Some tests have specificity used low Re glider sections (Stallard et al. (2012)) or specially tailored MHK design sections (Shui et al. (2012)). The material choice for the benchmark rotor should be stiff and must exhibit similar deflections at all scales of proposed tests. Inspection and QA

measurements of the rotor should be made to ensure that the sections are built to within ITTC propeller model accuracy (ITTC 7.5-01-01-02). For instance, the section form tolerance of 0.05 mm is recommended for the entire blade given these short chord lengths. If tests are performed in facilities of different sizes ("round-robin" style) it would be preferable to also test rotors of different scales to help provide data to access performance scaling assessments and tool validation.

The support structures on which the turbine is attached are usually device dependent. The benchmark testing and any computational evaluations must properly consider and represent faithfully as possible the intended superstructures including the nacelle, PTO housings, supports, and towers of the turbine configuration. The benchmark experiment needs to minimize any hardware needed to support the turbine and measurements as documented those items for digital reproduction. The computational benchmarking should "model-the-model" including all support structures and facility boundary.

8.1.3 BOUNDARY AND INFLOW CONDITION

Turbines typically operate in areas of strong velocity gradients with moderate to extreme turbulence levels and at times oscillating flow patterns. In most facilities, it is difficult to replicate these conditions and by design free stream turbulence levels can be small in most test facilities. Very small-scale turbines have been tested in facilities with roughness elements on the floor of the tank or tunnel but this is difficult to replicate between EFD facilities and to model in CFD so it might not be feasible for in any round-robin benchmarking tests. Removable turbulence generating grids (symmetric and/or asymmetric) or similar devices should be considered in a closed-loop flume or tunnel benchmark test to quantify the sensitivity of turbulent inflow variations on device performance parameters including wake structures and blade forces. These issues are further discussed Section 8.2.

This data would be used to verify CFD tool development. Inflow condition measurements are of upmost importance for the benchmark database. It is recommended that upstream measurements of velocity, velocity profiles and gradients (if applicable) and turbulence quantities be completed as part of the benchmark experiment. This should be accomplished at multiple locations upstream of the turbine. CFD modelling needs to use these measurements as boundary conditions during the evaluation along with all facility boundaries. If the benchmark includes a large-scale fielded device, site surveys need to be completed or collected to provide adequate comparisons to facility configurations and computational model boundary conditions.

8.1.4 DATA MEASUREMENTS

It is key for a successful benchmark test that the inflow conditions of all EFD and CFD tests are measured / predicted correctly. In order to confirm data needs the test planning team must include some CFD end users. These end users need to review the test plan and be actively involved with any test readiness review to confirm adequate data quantity and locations. The key components for performance are measurements will be rotor torque, thrust and RPM. Measurements of the direct power generation is highly recommended as is inflow quantities as discussed in prior section. The following measurements should be considered for any benchmark database. These include

- Oil paint visualization of blades and key components to show limiting streamlines to highlight flow structures and separations

- Wake measurements behind the turbine and support structures using PIV, LDV or ADV. These measurements should if possible be synced with rotor position.
- Steady and unsteady loads on single blades using multi-component forces cells or strain gages
- Steady and unsteady loads on support structures such as the tower
- Dynamic pressure measurements on tower to provide load fluctuation data
- Dynamic loads included unsteady rotor torque, thrust and hub side forces. These data will be especially important during any turbulence inflow sensitivity studies
- Flow visualization including mini-tuft
- Cavitation measurements (if applicable for configuration or facility)
- Broadband noise measurements.

8.1.5 OPERATING CONDITIONS

Measurements in unsteady flow are strongly dependent on the PTO system. Most experiment setups use a constant RPM control as it is easier to setup. However, full-scale device will be power or torque controlled. It is recommended that care be taken in datum methodology. The tests should be conducted over a range of TSR achievable for the turbine design and facility. In most cases, this will be done by setting the inlet flow or carriage speed and varying the motor-generator RPM systematically. For closed-loop facilities with pressure control, it is recommended that the pressure be set to at minimum to suppress cavitation and reduce its effect on blade loading during some data runs.

8.1.6 DATABASE

A key to any benchmark database is a well-documented and accessible digital record. This database must include standard neutral format CAD representative (e.g., STEP) of the turbine, support structure and testing facility to allow the computational modelling of the entire configuration. The key data should be processed to provide averages, standard deviations and have uncertainty estimates. The experimental data results should combine Type A and B uncertainties to aid in comparisons. In order to compare the data among different facilities, blockage corrections (e.g., Bahaj et al., 2007) should be applied and documented. The blockage correction can be tested as part of the CFD benchmarking. All data must be provided in a neutral data format.

8.1.7 EVALUATION CRITERIA AND TEAMING

It is important for consistent and useful benchmarking that the process includes input from all parties including experimental staff from each facility and computational analysts and tool developers that will use data. This will start with the downselect of turbine design and configurations; baseline data needs and measurement locations. Guidelines for benchmarking are provided in ITTC 4.0-01 (2002). To succeed a set of definitions, evaluation criteria and items like document standard, design and test reviews and data storage need to be agreed upon early in the process. It would be overwhelming to attempt to summarize all the benchmark criteria for both facility and computational efforts in this document. Good practices in QA, data uncertainty analysis, and thorough documentation of the experiment and data is needed from the test team(s). Similarly, the computational and tool end-users must define and use standard criteria such as mesh, grid, convergence and exercising turbulence models (Oberkampf & Trucano, 2002)

8.2 Reproduction at Model Scale of Inflow Turbulence and Unsteadiness

8.2.1 REQUIREMENTS AND CONSTRAINTS

For current turbines to become a commercially viable technology, they must maintain high levels of reliability in the hostile ocean environment as discussed at full scale in Section 6.2.4. Consequently, the turbines must be designed to withstand large unsteady hydrodynamic loads introduced by the presence of waves, turbulence and velocity shear and flow misalignment (e.g., Milne et al., 2017; MacEnri et al., 2013 and Payne et al. 2018).

Of these, the peak loads induced by waves has been suggested to be most significant and can be several orders of magnitude larger than ambient turbulence (Lust et al., 2013). This is however strongly dependent on the type of tidal site. For fatigue both the high cycles due to turbulence and low cycles due to waves and velocity profile need to be understood. The higher frequency associated with turbulence also cause flicker in the output from the generator (MaxEnri at al., 2012).

These key causes of unsteady loads are shown in Figure 187. Unsteady loads result from turbulence, shear flows, waves, surge and flow directionality changes. There are also unsteadiness due flow misalignment (yawed condition) and due to interactions between current turbines within an array.

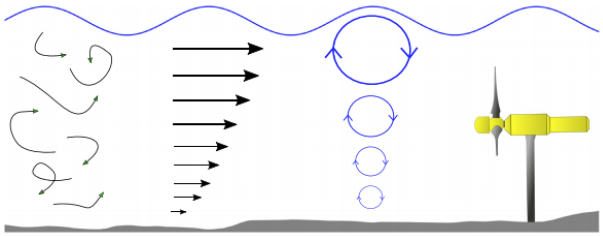

Figure 187: Diagram of the key causes of unsteady loads on tidal turbines (Draycott et al. 2019).

Fully replicating all the unsteady flow features is not considered a realistic option for a single test facility. Consequently, tests are done with simplifications of the environment to produce unsteady flows for validation data.

Experiments with unsteady inflow are typically done to develop and validate the numerical methods than cover a full set of conditions. As an example, Galloway et al. (2014) performed a set of experiments in order to validate Blade Element Momentum Theory (BEMT) code in the presence of waves and yawed flow.

When performing these types of experiments in model test facilities, the most significant considerations, due to operating at lower flow velocities, is the reduced Reynolds number. This is particularly important when reproducing combined current and wave tests that are also Froude number dependent. It, therefore, may be necessary to modify the blade geometry to obtain the correct power and thrust coefficients in the reduced Re regime (Whelan & Stallard 2011).

The other key consideration when performing these experiments is the control strategy. It is typical to use speed control (e.g., Guo et al. 2018), however, implementation of torque control could significantly alter the expected peak thrust, Ordonez-Sanchez et al.

(2019). These uncertainties are further discussed in the ITTC Horizontal Axis Turbine Uncertainty Analysis Recommended Procedure and Guideline (7.5-02-07-03.15).

8.2.2 REPLICATING VELOCITY PROFILE

The use of surface roughness on the bed of long flumes. This produces some non-isotropic turbulence, but these facilities are generally limited to tests with small model scale turbines or turbine simulators. These tests are generally done to help validate simulation tools for modelling CT wakes for array modelling and validation.

8.2.3 REPLICATING FLOW MISALIGNMENT

Several developers have investigating cost saving by design devices that are bi-directional in design and not requiring a yaw mechanism. This has been successfully achieved by pitching the blades 180 degrees and running in reverse. However, most tidal sites have some bias due to the bathymetry and consequently, the flow is not truly bi-directional. This unsteady effect can be readily replicated in the test facility by changing the angle of the model is to the flow direction (E.g., Galloway et al., 2014).

8.2.4 REPLICATING TURBULENCE

When developing a velocity profile in a circulating water channel or tunnel with bed roughness the background turbulence in the facility will also increase. This may resemble some parts of the turbulence spectrum.

The use of screens and grids to generate turbulence has been used (E.g., Blackmore et al., 2016). However, the turbulence generated may have intensity values at the turbine location close to real conditions but isotropic in nature and with different length scales. The non-isotropic nature of tidal flow is particularly dominant in shallow water.

The inverse of the normal configuration is done at IFREMER's circulating water channel where the flow conditioning units are removed. This increased the level of streamwise turbulence intensity from 3% to 12%. Payne et al. (2018) experiments using this facility found that for frequencies below the rotational frequency, load spectra are correlated to spectral density of the onset flow velocity. Above the rotational frequency, loads are mainly affected by turbine operation phenomena. The tower shadowing effect is clearly identified through frequency and angular analysis.

8.2.5 REPLICATING COMBINED WAVES AND CURRENT

The use of circulating water channels with combined with currents. This is limited to very few facilities such as the FlowWave tank at the University of Edinburgh. In this facility an experimental assessment was conducted on tidal turbine loading from irregular waves over a tidal cycle (Draycott et al., 2019b). During this experiment, the standard deviations of measured turbine parameters for the opposing condition range between 215 and 260% of the following case, and between 340 and 565% of the current-only measurements. An example set of results is shown in **Erreur ! Source du renvoi introuvable.**. This confirms that greater fatigue damage will be accumulated during one-half of the tidal cycle. The mean values, however, appear to be unaffected by the presence of waves suggesting that the overall turbine performance is unaltered.

Similar effects were also demonstrated in Guo et al. (2018) experiments in a towing tank. Although the range of standard deviations in torque and thrust were noticeability less. This may be due towing tank tests not replicating the

interaction between the current and wave that is only possible in circulating water facilities.

This is also evident in the experiments of Ordonez-Sanchez et al. (2019) performed in a towing tank with waves where the effect of two different power control strategies were included.

The influence of combined turbulence and opposing waves has also been studied as an example of an extreme case (Fernandez-Rodriguez et al., 2014). Wave kinematics are not strictly sinusoidal due to interaction between waves and large-scale turbulence of the opposing flow, but linear theory provides velocity at hub height to within 77%. Applying this force prediction method with a thrust coefficient of 2.0 provides extreme thrust forces.

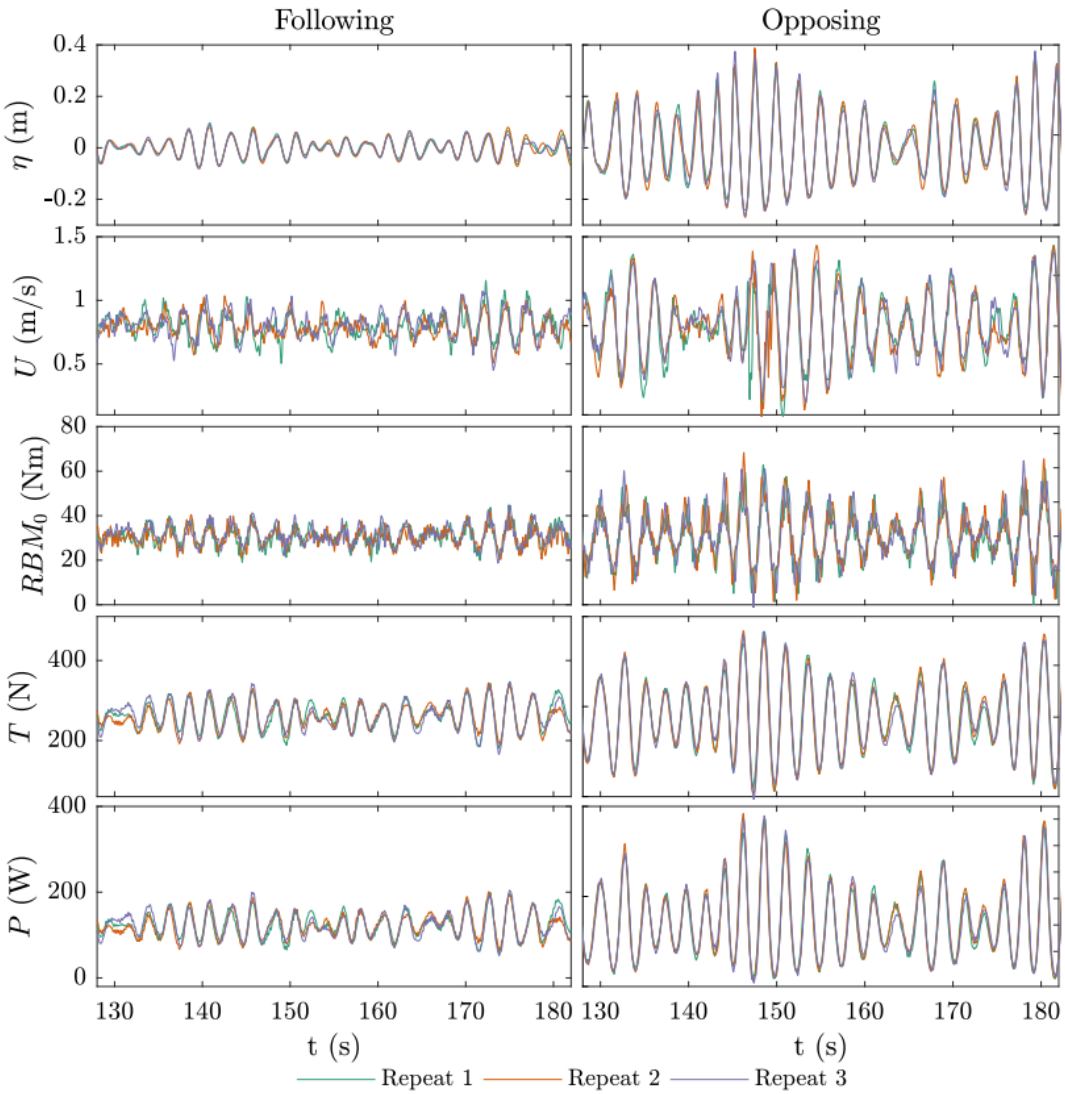

Figure 188: Time-domain results of key environmental and turbine parameters for the opposing and following wave conditions. The three repeats of each conditions are shown for each parameter; H is the surface elevation; U is the streamwise velocity, 0.4 m beneath the surface;. RBM_0 is streamwise blade root bending moment sensors; T is rotor-based thrust measurement; P is rotor power.

8.2.6 INTERACTIONS WITHIN AN ARRAY

Within an array of current turbine there can be both flow acceleration due to blockage and unsteady wakes. This interactions with the background turbulence have recently been studied for an arrangement of three turbines (Gaurier et al. 2020). For the configuration tested the analysis of the power spectral density functions of the downstream turbine torque and thrust showed no signature of the upstream turbines. Numerical modelling of this interaction is discussed in Section 8.3.

8.2.7 NUMERICAL MODELLING TURBULENCE

The key point in inflow turbulence is more on the real spectrum of the site data. How to recreate the inflow in the numerical tool. For example, Ebdon et al. (2021), analysed inflow turbulence extensively by conducting a wake flume experimental test and then introducing them into a RANS code. Ahmed et al. (2017) tried to implement the EMEC site data into RANS and LES code to analyse the inflow impact. Stevens (2017) presented an overall analysis on Cook Straight in New Zealand. Du et al. (2016) presented a site survey on the turbulence impact in Zhoushan Site, China). They all concluded that the site measurement with ADCP is not sufficient for detailed analysis for turbulence load on rotor blades.

Several papers have reported numerical investigations on inflow turbulence that site data might not cover. For example, Togneri et al. (2021) compared a few different numerical methods for modelling inflow turbulence. Arini et al. (2018) proposed a 2D numerical method to analyse inflow turbulence impact on vertical axis tidal current turbine. Hu et al. (2017) conducted a comprehensive analysis of the relationship between inflow turbulence condition and array performance by utilizing LES method. This research provides important support for modelling tidal current turbine array.

8.3 **Current** TURBINE ARRAY **Modelling**

With the improvement of tidal current turbine technology, there have been extensive studies on tidal current turbine modelling (Nachtane et al., 2020). A number of researchers still focused on improving the standard array modelling approaches. They extend these approaches by introducing new descriptions of physics or trying to combine different sub-categories methods together. For example, Gajardo et al.(2019) developed an approach combining BEM and DES to study tidal current turbine wake. Ma et al. (2018) proposed both a theoretical and CFD combined methods for vertical axis tidal current turbine array performance evaluation. Bonar et al. (2017) developed a theoretical method to analyse the performance of a non-uniform array in a uniform inflow. Hu et al. (2017) improved the LES-ALM methods to study tidal turbine array with different inflow conditions. Nuernberg & Tao (2017) demonstrate the utilization of the dynamic mesh with RANS to simulate tidal current turbine array.

Some researchers have also started to work on the free surface impact on the array performance. This is a particularly important physics, which was only evaluated theoretically in the past. Li et al. (2021) presented a recently developed high efficiency RANS code that can evaluate the wave impact on tidal current turbine array wake and quantified the wave impact. Kolekar et al. (2019) improved an existing theoretical assessment method on free surface effect on turbine array performance. Draycott et al. (2019) presented their recent experimental investigation on wave effect's impact on array performance. Sufian et al. (2017)

have shown numerical simulation on the wave impact by introducing wave induced velocity into the CFD model.

Furthermore, researchers have begun to also introduce turbine control algorithm within array modelling. These are implemented either numerically or experimentally. For example, Delafin et al. (2021) discussed the array performance with variable active pitch control. Zhao et al. (2020) introduced a torque control algorithm into actuator line method. Gu et al (2018) demonstration a blade pitch control algorithm with field test. Wang et al. (2018) developed a new approach combining the vortex method and geometrically exact beam theory to study the dynamic response on turbine blades in an array. Mannion et al. (2018) showed a numerical simulation result on a vertical axis turbine array with variable pitch control.

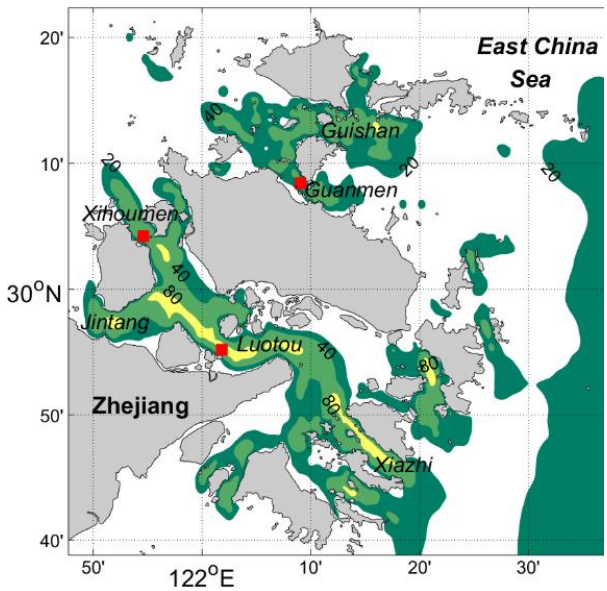

Figure 189: Tidal Power and Local Flow:A-Zhoushan Site-China(Deng et al 2019).

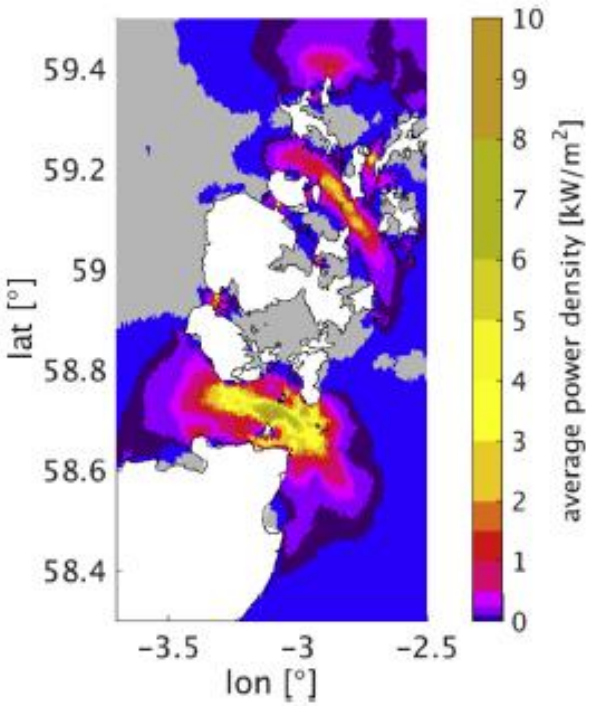

Figure 190: Tidal Power and Local Flow: Pentland Firth,UK(De Dominicis et al. 2017).

Interaction between ambient flow and tidal current turbine array also becomes a hot topic. Tidal current turbine array may affect the local channel flow and even regional ocean current. For example, Deng et al. (2019) discussed a tidal array performance in Zhoushan area China with realistic local ocean flow by utilizing (Regional Ocean Modelling System). They found that when the scale of the tidal current turbine farm is large enough, the array will pose noticeable impacts on the local environment. Musa et al. (2018) conducted a large eddy simulation to investigate the array performance in a channel with large migrating fluvial bedforms. Du Feu et al. (2017) introduced a new approach for investigating trade-offs different objectives of developing tidal current turbine array with a focus on impact on the local flow. In this study, they developed a numerical tool. De Dominicis et al. (2017) utilized Finite Volume Community Ocean Modelling to simulate the performance of UK tidal current

turbine farm Pentland Firth and its environmental impact.

9. OFFSHORE WIND TURBINES

9.1 Development of testing methodology for offshore wind turbines

Offshore Wind Turbines are complex dynamical systems, exposed to both hydrodynamic and aerodynamic loads, and their global response is also strongly influenced by the wind turbine controller (Goupee et al. 2014; Goupee, Kimball, and Dagher 2017).

There are two major challenges related to wave tank testing of offshore wind turbines (Sauder 2018):

- Generation of high-quality wind in tank facilities.
- Incompatibility between Froude and Reynolds scaling laws.

The wind field in hydrodynamic facilities is generally of poorer quality than what can be obtained in wind tunnels (Wendt, Robertson, and Jonkman 2017; Allen and Goupee 2017). Although efforts are being made to increase the capacity of wind generation in such facilities (e.g., Wind-Wave basin at the University of Maine), there is still a quality imbalance between the waves/current and the wind generation. Wind tunnel facilities with towing tank below exist but the size of the basin and the capacity to generate waves are significantly reduced compared to state-of-the-art ocean basins.

As for the latter, the similitude relationships (through scaling laws) are essential for interpretation of experimental data and for scaling up results for the prediction of how the prototype will behave. Hydrodynamic tests are usually governed by Froude scaling due to the dominant gravity and inertia loads, but viscous loads are important for the modelling of aerodynamic loads on a wind turbine. For practical purposes, however, it is not possible to satisfy all scaling laws simultaneously and there will be a mismatch of flow conditions between the prototype and the model. This difference is referred to as scale effects and is mostly related to difference in Reynolds number in model and full scale.

Until recently, these two challenges have been addressed by improving the capacity of wind generation in hydrodynamic laboratories, and by re-designing the rotors models with the aim to model full-scale aerodynamic loads (Borg 2018; Courbois 2013; de Ridder et al. 2014). Allen and Goupee (2017) noted that large uncertainties remain regarding the aerodynamic loads generated with such approaches, in particular the representation of rotor torque and gyroscopic effects. In addition, a performance scaled rotor will require a redesign of the model scale wind turbine controller to provide the same control characteristics as the prototype due to the differences in the rotor performances and inertial characteristics (Fontanella et al. 2019; Yu et al. 2017)

The two challenges can also be addressed by using Hardware-In-the-Loop (HIL) testing, also known as Real-Time Hybrid Model testing. The problem is then broken down into several physical and numerical substructures, which are interconnected in real-time. For model testing of offshore wind turbines, the structure is broken into one substructure for hydrodynamic loads and one for aerodynamic loads. Depending on the testing facility (hydrodynamic laboratory or wind tunnel), one substructure is physically represented and the other represented by a numerical model.

In the following subsections, the most common approaches of modelling the wind turbine in scaled model tests are further

discussed, namely using physical rotors or hybrid methods. Simplified and passive methods such as simulating the steady wind load by weights connected via wires or drag discs are discussed in e.g., ITTC Recommended Guidelines 7.5-02-07-03.8.

9.1.1 GEOMETRICALLY SCALED ROTORS

The need to model the wind turbine controller has been the motivation for including a physical rotor in hydrodynamic experiments. Other advantages with a physical rotor are the inclusion of 3p excitation, as well as better modelling of aerodynamic damping and the influence of the platform motions on the aerodynamic rotor loads. Initially, these tests used geometrical and Froude scaling of the rotor, (e.g., Molin, Remy and Facon 2004, Nielsen, Hanson, and Skaare 2006, Robertson et al. 2013).

The DeepCwind consortium studied three different floaters (spar, semi, and TLP) in their test campaign (Robertson et al. 2013). Detailed analysis of the aerodynamic performance of the scaled rotor is given in (Martin 2011; Martin et al. 2014) and is summarised below.

The main parameters characterising the performance of a rotor are the thrust coefficient $C_T=T/(½\rho_a U^2 A)$ and the power coefficient $C_P=Q\Omega/(½\rho_a U^3 A)$, where U is the wind speed, A is the swept rotor area, ρ_a is air density, T is the rotor thrust force, Q is the rotor torque and Ω is the rotational speed. These characteristics are usually given as function of the tip speed ratio TSR=$\Omega R/U$ where R is the rotor radius. Maintaining the TSR ensures the correct rotor rotational speed as well as any system excitations related to the rotor rotation. Using Froude scaling, where ratio between inertial and gravitational forces are preserved between prototype and model scale, will scale wind speed to maintain the ratio between wind speed and wave celerity.

For aerodynamic performance testing of a wind turbine, the scaling is aimed at preserving the Reynolds number, which is the ratio between inertial and viscous loads. A large difference in Reynolds number was found when performing model tests in a hydrodynamic facility based on Froude scaling. Initially, it was expected that the difference in Reynolds number between model and prototype scale would only have a minor effect on the aerodynamic performances of the rotor due to the potential nature of the lift at small angles of attack. However, the wind turbine profiles that were originally designed for high Reynolds numbers operated now at low Reynolds number, where the blade lift and drag coefficient were found to be much smaller. Since the blade lift is nearly perpendicular to the rotor plane, reduction of the lift force causes a reduction in rotor thrust. Since blade drag is nearly in the rotor-plane, increase in the blade drag will cause a significant reduction in the rotor torque and therefore a lower power coefficient.

To overcome this scaling incompatibility, three different solution were proposed by Martin et al. (2014): adjustment of the thrust by increasing wind speed, addition of roughness on the blade profile, or redesign of the wind turbine blade, where combinations can be considered.

In the first phase of the DeepCwind model tests they adjusted the wind speed to match the thrust force on the rotor (Robertson et al. 2013). The main load components transmitted from the wind turbine to the supporting structure are the gyroscopic moment, the rotor torque, and the rotor thrust. The gyroscopic moment is conserved as long as the mass of the rotor is correctly modelled, and the rotational speed is Froude scaled. To match the rotor thrust, the wind speed was increased by approximately a factor of two. The rotor torque was accepted to

be much smaller than specified since it is considered to be less important than the thrust.

Although it is possible to achieve proper mean thrust by increasing mean wind speed, it does not necessarily preserve the same change in thrust due to platform motions, inflow wind speed, and blade pitch angle, as the prototype. The influence of the increased wind speed on the aerodynamic damping due to the platform pitch motions close to the natural frequency was described as representative by Martin et al. (2014). On the contrary, Hall and Goupee (2017) reported a reduced damping due to relatively smaller changes in the relative wind speed due to the pitch motions. The TSR could no longer be maintained when the wind speed was increased. The excitations increased for tests with dynamic winds due to the increased mean wind speed (Kimball et al. 2014).

Adding roughness to the rotor blades to trigger a transition from laminar to turbulent boundary layer flow was tested by Martin et al. (2014) and Courbois (2013). It was found to have a positive, but not sufficient, influence on the rotor thrust at high TSR. Use of artificial roughness should be done with care due to the sudden nature of the transition away from laminar stall.

9.1.2 PERFORMANCE SCALED ROTOR

Redesign the model blade profile was the third approach proposed by Martin et al. (2014). In this case, low-Reynolds number profile with lift and drag coefficients equivalent to the prototype blade profile is used for the model tests. This type of scaling is called performance scaling. More details about the performance scaling method are given in Martin (2011) and Fowler et al. (2013). It was also used by de Ridder et al. (2014) for the building of the MARIN Stock Wind Turbine (MSWT) model which was used for the DeepCwind phase 2 model tests (Goupee et al. 2014).

Redesigning the blades according to performance scaling will allow for Froude-scaled wind and will give realistic modelling of variations in thrust due to platform motions, variations in wind speed, and blade pitch angle. In the scaling process, the blade mass, blade length and rotor rpm are scaled according to Froude scaling preserving gyroscopic loads. The blade profiles, cord length and twist angle are then modified to achieve the Froude scaled rotor thrust over the range of TSR of interest.

The rotor torque is only a secondary target in the blade redesigning step as it is considered less important for the overall dynamics. For instance, the overturning moment due to the turbine torque is approximately 5% of that due to rotor thrust at rated wind speed for the 5MW NREL turbine (Fowler et al. 2013). On the other hand, approximate modelling of the power coefficient is required to study the controller performance on the power production. The power coefficient is smaller at model scale due to the larger drag observed at model scale, which affect the torque and therefore the power.

A combination of increasing the wind speed and redesigning the rotor was used by Courbois (2013) to model the correct wind turbine thrust. The blade profile was similar to the prototype, but the blade twist was adapted to better replicate the rotor thrust. The wind speed was higher than Froude-scaled values, and consequently, the TSR was not correctly modelled.

Borg (2018) presented a different approach for performance scaling where the goal was to maintain the slope of the thrust as function of TSR, not only the thrust. This ensures better modelling of the unsteady aerodynamic loads that comes from the platform motions, wind fluctuations, and blade pitch control.

9.1.3 CHALLENGES AND LIMITATIONS WITH PHYSICAL ROTORS

In addition to the Froude and Reynolds scaling law incompatibility described above, there are a few other challenges and limitations related to using a physical rotor for wave tank testing of offshore wind turbines. These includes:

- Mass of the model RNA (Rotor-Nacelle Assembly).
- Interference from the instrumentation cable.
- Model scale wind turbine controller.
- Generation of high-quality wind field.

A fully instrumented physical rotor in model scale is likely to be heavier than the down-scaled mass of the prototype RNA (Gueydon 2016, DNV 2019). This is a larger challenge for smaller model scales. To overcome this problem, masses in the support structure can be shifted around to maintain the global moments of inertia and CoG. Also, elements from the RNA model such as motor, transducer and encoder can be moved to the base of the tower with the rotor connected via a shaft in the tower in order to meet target design mass (Ward et al. 2018). Deviations from the target mass distribution can be of importance for the structural modes and force measurements of the tower if an elastic model of the tower is applied. The influence of this deviation can be investigated numerically to determine which results from the model tests that will be inaccurate due to the mass deviation (DNV 2019).

The instrumentation and power cables can influence the motion response of a floating wind turbine model. A free-hanging cable will contribute with additional weight and aerodynamic drag forces in the experiments. Cable influence on the platform response has been reported for the first phase of the DeepCwind model tests (Robertson et al. 2013). It is recommended to use a thin, flexible, and light cable instead. Else, the cables influence on the floater motion should be evaluated in the model set-up, e.g., by comparing free decay tests with and without the cables present (DNV 2019).

The model scale wind turbine controller must be re-designed to account for the differences between model scale and prototype rotor aerodynamic behaviour and inertial characteristics (Fontanella et al. 2019). A reduced order model can be used to tune the model scale wind turbine controller to achieve the same operating behaviour between the model scale and prototype wind turbine (Fontanella, Bayati, and Belloli 2018; Yu et al. 2017).

Wind generation in hydrodynamic facilities are not as consistent as can be expected in a wind tunnel. As reported from the DeepCwind model tests (Robertson et al. 2013), drop-offs in the wind velocity, increased turbulence at the edges of the rotor plane, and low-level swirling behaviour induced unwanted excitation in the system.

Molin, Remy, and Facon (2004) investigated the importance of the quality of the wind generation in hydrodynamic facilities. Their main concern was that unwanted turbulences and spatial-temporal in-homogeneities in the wind field could give rise to parasitic excitations triggering resonant modes. They compared tests with fans setup in an offshore basin with tests in a wind tunnel-wave basin facility at IRPHE , based in Luminy (France). Unfortunately, the experiments were inconclusive because the results were affected by an imbalanced rotor.

Courbois (2013) developed a wind generating system based on centrifugal pumps at the testing facilities of the Ecole Centrale de Nantes (ECN) to avoid twisted flows caused by

axial fans. The system was developed to operate at higher wind speeds than typically Froude-scaled wind speeds. Due to the weight of the centrifugal fans, they had to be mounted on land and attached to the diffuser in front of the model via a flexible tube.

More advanced systems use a set of screens and honeycomb to enhance the quality of the wind field. Screens have the same effect as a section reduction, by minimizing longitudinal turbulence and spatial homogenisation of the mean velocity. The honeycomb reduces the lateral turbulence components. For the DeepCwind tests (Robertson et al., 2013) the wind was generated by a set of 35 fans with a honeycomb front plate to reduce swirl and a nozzle to reduce turbulence. Counter rotating fans were used to reduce swirls generated by the fans.

Hall and Goupee (2017), Goupee et al. (2017) and Thys et al. (2018) demonstrated the significance of turbulent wind in tank testing of floating wind turbines. The wind turbulence was observed to introduce substantial low-frequency excitation. The behaviour of the wind turbine and its controller is also sensitive to the type of wind field (steady vs turbulent) as shown by Goupee et al. (2014). The blade pitch controllers tended to increase the platform's pitch response in steady wind cases compared to similar tests with no blade pitch controller. On the other hand, for tests in dynamic wind the damping levels were found to be similar for cases with and without controller.

Advanced fan-based wind systems can produce wind spectrums by adapting the power input frequencies. As indicated by Goupee et al (2017), the current state-of-the-art of open-jet wind generation machines is limited to temporal variations with no spatial variations. The NPD spectrums are well suited for this, since only the temporal variations in the longitudinal direction are prescribed and no realistic spatial variations in the wind characteristics are given. Allen and Goupee (2017) observed from numerical and experimental studies that using the NPD spectrum gave lower responses than a more realistic Kaimal spectrum for very low frequencies. They indicated that it could be wise to develop better means of generating full-field, turbulent winds in model testing of floating wind turbines. Wind turbulence may also excite responses at higher frequencies. Significant blade-root and tower-top bending excitation at 1p and 3p frequencies, respectively, reflect the spatial wind speed variations in the turbulent wind field (Hall and Goupee, 2017).

The use of a combined wind-wave testing facility, such as LHRI (France), NMRI (Japan), Newcastle University (UK), and the Harbin Institute of Technology (China), presents an alternative to installing the wind-generating system in an existing hydrodynamic testing facility. While these facilities represent the advantage of high-quality wind production, the small size, and the limited capacity to generate waves are significant disadvantages.

9.1.4 HYBRID TESTING

The limitations and challenges mentioned above have led to alternative methods for model testing of floating offshore wind turbines in the form of hardware-in-the-loop or real-time hybrid model testing. For consistency, these types of tests will be referred to as hybrid testing.

As summarised by Chabaud et al. (2013), early interest in hybrid testing, and the possibility to combine experiments with numerical simulations, goes back to the 1970's for testing of buildings under seismic loads. Other applications can be found in the automotive industry but also within renewable energy. The earliest reference to hybrid testing in marine technology is made in Buchner (1999) and Cao and Tahchiev (2013) where hybrid

testing is proposed as a solution to overcome the wave tank depth limitations when testing moored structures in ultra-deep water.

The Ecole Centrale de Nantes performed in 2013 a hybrid tests with a floating wind turbine where the rotor thrust was modelled by use of a ducted fan (Azcona et al., 2014). Numerical simulations computed the aerodynamic thrust in real-time which then was applied to the model using a ducted fan. The thrust from the fan was controlled using an open-loop system where the relation between fan speed and thrust was obtained from static tests. Figure 191 shows the ducted fan from the EU FP7 INNWIND tests (Aszcona et al. 2016).

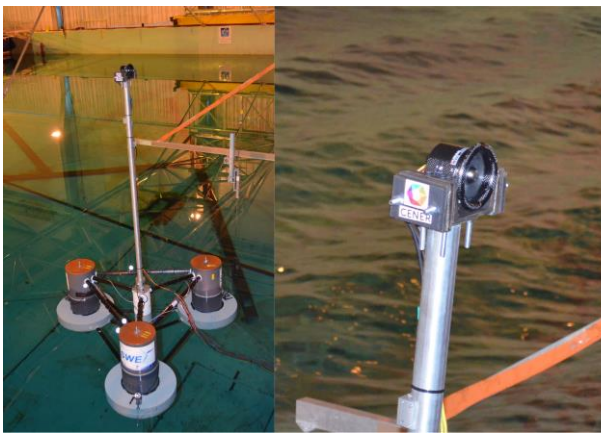

Figure 191: Hybrid testing with a single ducted fan used in the EU INNWIND-project (courtesy of CENER).

A sensitivity study showed that other rotor loads than the thrust could have a significant impact on the tower loads, motions, and mooring line tensions of a semi-submersible FOWT (Bachynski et al., 2015). To include additional rotor loads, Sauder et al. (2016) used a cable driven parallel robot connected to a frame at the tower top of the FOWT model. The robot was controlled based on a closed loop system, and all the rotor loads except for the vertical rotor loads, were applied on the model. The performance of the hybrid method, referred to as ReaTHM (Real-Time Hybrid Model) testing, is verified by means of calm water decay tests with the hybrid system in following mode (i.e. connected to the model with zero net load applied), by repetition tests and by comparison of requested and measured rotor loads. The system was found to work for the main frequencies of interest (up to 2Hz model scale). Furthermore, fault conditions including blade failure and emergency shutdown were tested.

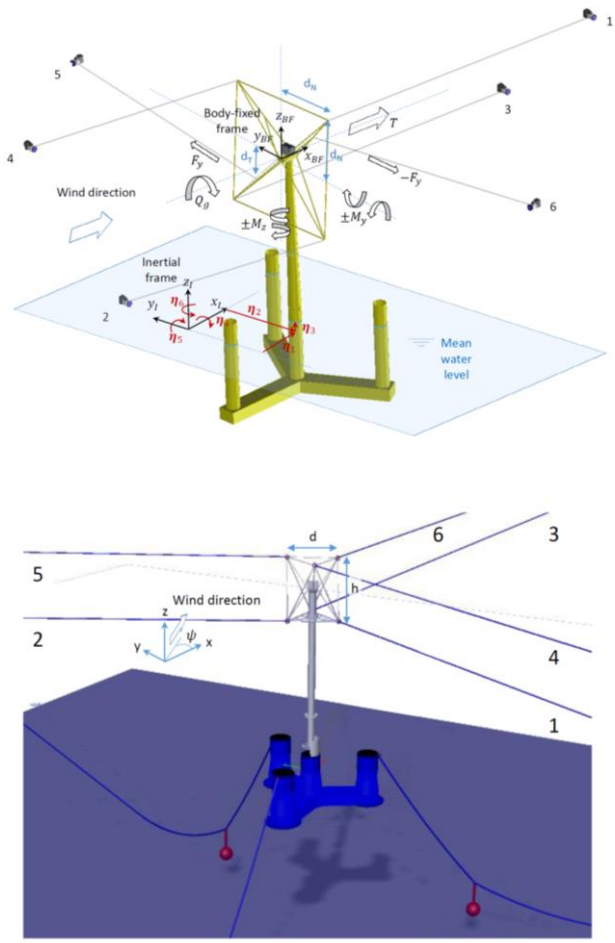

Figure 192: Real-Time Hybrid Model (ReaTHM) testing setup with cable driven parallel robots: NOWITECH (top); LIFES50+ (bottom). From Chabaud et al. 2018.

The hybrid testing with cable driven robots, initially developed for the NOWITECH CSC FOWT tests, was further improved for the EU H2020 LIFES50+ ocean basin tests (Chabaud et al., 2018; Thys et al., 2018). The frame for the

cable attachment points on the wind turbine tower was reshaped into a square pyramid frame, which allowed for more flexible multidirectional modelling of the wind loads, including the effect of rapid changes of wind direction during the tests (see Figure 192). The bandwidth of the LIFES50+ tests was increased to blade sweeping (3p) frequency or up to 3-4Hz in model scale, while the bandwidth of the NOWITECH tests were set to wave frequency or up to 1-2Hz in model scale. The cable driven parallel robot setup was also applied in the WINDMOOR project for testing a 12MW floating wind turbine, see Figure 193 (Thys et al., 2021).

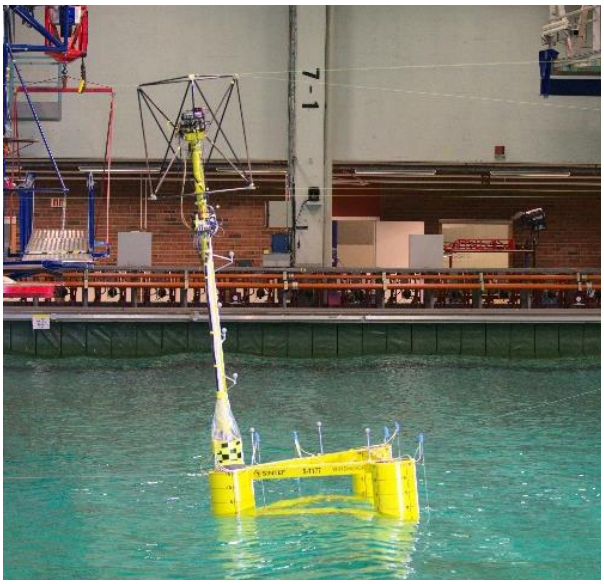

Figure 193: Real-Time Hybrid Model (ReaTHM) tests of the INO WINDMOOR 12MW FOWT (courtesy of SINTEF Ocean).

As an alternative to cable driven robots, a multi-fan or multi-prop actuator can be applied for emulation of multiple degrees of rotor loads. The idea is an extension of the single ducted fan actuator, which is limited to the modelling of thrust force only. By applying multiple propellers spread out in a similar configuration as a drone it is possible to include out-of-plane rotor moments (see Figure 194). Such system has been developed and tested for a four-propeller actuator (e.g., Pires et al., 2020; Fontanella et al., 2020; Vittori et al., 2021) and for a six-propeller actuator (e.g., Urbán and Guanche, 2019, Jurado et al., 2017).

Hall et al. (2017) validated the hybrid testing technique by comparing model tests with a semisubmersible FOWT using two different rotor thrust modelling techniques: 1) hybrid testing with a single cable driven robot and 2) physical wind-driven performance scaled rotor. The agreement between both methods was found to be good, but the importance of true-to-scale turbulent wind demonstrated the value of hybrid testing.

Figure 194: MARINET2 tests with CENER's multi-fan actuator system tested at MARIN (courtesy of CENER).

The hybrid testing technology for hydrodynamic tank tests has a clear advantage over conventional methods when it comes to modelling of a realistic three-dimensional turbulent wind field. Together with the improved rotor loads emulation, hybrid testing methodology offers an effective tool for the development and validation of control strategies for floating offshore wind turbines (Fontanella et al., 2020). Hybrid testing is also very suitable for calibration of hydrodynamic coefficients in numerical simulations models since the aerodynamics loads can be controlled and documented from the tests with high accuracy. It does also have the flexibility to model various load cases with fault conditions.

Hybrid testing of FOWT in wind tunnel facilities has been developed in parallel with hybrid wave tank testing (Bayati et al., 2013). In these tests the wind turbine aerodynamic rotor loads are reproduced by a scaled rotor model exposed to physical wind combined with a numerical hydrodynamic model of the platform providing real-time rigid-body motion. The computed platform displacements are imposed to the wind turbine model using a parallel kinematic robot (see Figure 195). The hybrid wind tunnel tests were initially performed for 2DOF floater motion but was later expanded to 6DOF (Bayati et al., 2014; Belloli et al., 2020). The wind field in a wind tunnel is of higher quality than what can be achieved by an open-jet wind generating system normally used in a hydrodynamic test facility. Thus, hybrid testing in a wind tunnel is a good alternative way of investigating unsteady aerodynamic loads and wind turbine controller actions on the overall dynamics of the floating wind turbine.

Figure 195: 6DOF hybrid setup of a floating wind turbine in a wind tunnel (from Belloli et al., 2020; courtesy of Politecnico di Milano).

Hybrid testing opens new opportunities, but it should also be applied with care. Documentation and verification of the setup should be carried out prior to testing, and the performance of the hybrid system should be closely monitored during testing. Time delays from simulations, data transfer and actuator response may cause additional damping or introduce spurious energy into the system. The capacity of the actuators must be carefully considered for relevant ranges of frequencies and magnitudes of load components when designing the experimental setup. As demonstrated by Gueydon et al. (2018), the use of a hybrid system outside its bandwidth may lead to unwanted responses in the system. Also, the accuracy of the wind loads is limited by the accuracy and correctness of the numerical simulation model.

9.2 Existing regulations related to model tests of offshore wind turbines

This status report presents the existing guidelines and standards addressing the model tests of offshore wind turbines published by classification societies, including ABS, BUREAU VERITAS, DNV, and Class NK as well as IEC IS 61400-3-1, IEC TS 61400-3-2 and ISO 29400.

These regulations are as follows:

- IEC TS 61400-3-2, Design requirements for floating offshore wind turbines, April 2019;
- IEC IS 61400-3-1, Design requirements for offshore wind turbines, April 2019;
- ISO 29400, Ships and marine technology - Offshore wind energy - Port and marine operations, May 2020;
- ABS, Guide for Building and Classing Bottom-Founded Offshore Wind Turbine Installations, July 2020;
- ABS, Guide for Building and Classing Floating Offshore Wind Turbine Installations, July 2020;
- BUREAU VERITAS NI 572, Classification and Certification of Floating Offshore Wind Turbines, January 2019;
- Class NK, Guidelines for Offshore Floating Wind Turbine Structures, July 2012;

- Class NK, Guidelines for Certification of Wind Turbines and Wind Farms, May 2014;
- DNV, DNVGL-RU-OU-0512, Floating offshore wind turbine installations, October 2020;
- DNV, DNVGL-ST-0126, Support Structures for Wind Turbines, July 2018;
- DNV, DNVGL-ST-0119, Floating Wind Turbine Structures, July 2018;
- DNV, DNVGL-SE-0422, Certification of Floating Wind Turbines, July 2018;
- DNV, DNVGL-RP-0286, Coupled analysis of floating wind turbines, May 2019;

Societies have acted in competition with one another and in concert with the national and international standards agencies to provide sets of rules and design appraisals for the offshore wind turbine (floating or fixed) industry. A more nebulous, but nevertheless crucial, role has been as a central 'repository' of knowledge and experience. (Garrad, 2012) The development of the standards and rules and their application to offshore wind turbines (floating or fixed) have allowed the offshore wind turbine industry to gain confidence in the designs. Also, the standards and certification on offshore wind turbines (floating and fixed) address how they are about to change from addressing prototype installations with a few unit to large scale floating offshore wind farms consisting of many identical units.

Utilizing the experience and lessons learned from certifying based on standards can make the offshore wind turbine (floating or fixed) industry to know where the largest cost savings can be found and how standards and certification can be used to eliminate risk from the project while maintaining the same level of confidence.

It has been found that the other regulations do not include the guidelines or procedures for the model tests, but they referred to the need of model tests for specific topics like air gap, verification of coupled analysis codes, etc. Model tests may be carried out to assess a wide range of issues. The items listed in DNVGL-RP-C205, Environmental conditions and environmental loads, December 2020 are also relevant for offshore wind turbines:

- Hydrodynamic load characteristics
- Global system concept and design verification
- Individual structure component testing
- Marine operations, demonstration of functionality
- Validation of numerical models
- Estimation of extreme loads and response.

In addition to these, model tests of FOWTs are carried out to understand the loading mechanisms and relative importance of and coupling between different environmental loads. A good control of the loading conditions makes it possible to investigate rare but critical conditions. Also, control of the relative importance of different environmental loadings is a desirable benefit provided in a model basin.

9.3 Guideline for uncertainty analysis for model testing of offshore wind turbines

The following new guideline was developed during this term:

- 7.5-02-07-03.17 Uncertainty Analysis for Model Testing of Offshore Wind Turbines

The purpose of the guideline is to provide guidance on the application of uncertainty analysis to the model scale testing of offshore wind turbines.

A first step in uncertainty analysis is to identify all significant sources of uncertainty. The sources of uncertainty related to model testing of offshore wind turbines can be grouped

into these main blocks: model, installation, control system and actuators, measurement and data processing, environmental condition modelling, and initial test conditions. Additional sources of uncertainties due to the scaling can be grouped into the mismatch of Reynolds number and viscous effects on the hull and mooring lines (Bachynski et al., 2019).

In this guideline, an example of the uncertainty analysis to offshore wind turbine model test is shown and it suggests Type B uncertainties (estimated through a simplified analytical uncertainty propagation) for the estimation of RAOs were found to be of importance compared to Type A uncertainties (estimated through repetition tests).

10. CLOSING SUMMARY

10.1 Wave energy converters

At the present level of development, the commercial exploitation of wave energy is only economically viable if WECs are used in other multi-use costal structure such as coastal protection, off-grid applications or if they are deployed in large arrays. In these farm settings, the interactions between close by WECs (near field effects) will give rise to a complex wave field that affects the power extracted by each device and consequently the total power output of the farm. Moreover, at large distances behind WECs (far field effects), the farms alter the wave field affecting the coastal processes: other users at sea, coastal ecosystems, and the coastline. Advancement in the numerical and experimental modelling of arrays have been done and summarized in the report. The most significant advancement is the introduction of park optimization techniques that allow a multi-criteria choice of the WECs position in the array.

In the WEC PTO system modelling, more efforts have been made to identify nonlinear effects, unsteady characteristics and viscous effects in recent years. Understanding on coupling effects between components of a PTO system is critical to improve the performance evaluation and more attention is being given to develop the integrated simulation tools that can include interactions between PTO components. A series of benchmark tests on various WEC PTO models have been carried out by the WEC modelling group of IEA-OES and it may identify the capability and potential improvement of the current WEC PTO modelling.

However, wave energy technology is certainly one of the most diverse in terms of ocean renewable energy systems. In fact, most companies possess very unique and different ways to harnessing ocean wave energy. This can arguably explain the slow development of the sector where lessons learn from failures or successes, supply chain, component manufacturing etc. cannot be easily transfer from one device to another. To date, no company has reached the full commercial stage and only the Mutriku Wave Power Plant has demonstrated consistent power production with commercial implications. In order to increase their competitiveness, companies are slowly moving towards niche markets, off-grid applications and integration in current or future ocean structures (breakwaters, multipurpose platforms, harbours etc.).

It is therefore important to ensure thorough guidelines and procedures to help developers through the TRLs. There are still many unknowns around accounting for scale effects, hydrodynamic PTO impacts or survivability tests and much of the data available are very new. As further information slowly become available, continuing improvement of these guidelines and procedures will be important if not necessary.

10.2 Current turbines

General specifications for both experimental and computational benchmarks for current turbine have been laid out and outlined for current turbine. To date, much of the data and design geometries for marine renewable devices including current or tidal turbines has been considered propriety or not readily available in the public domain. In the past few years, for current turbines, there are a few experimental programs that have been conducted for the purpose of validation of CFD predictions or to evaluate the impact of different facilities on test results and turbine performances. The databases for a few of these studies are currently available online. Each of these databases appear to provide valuable resources for future studies. However, in most cases the available data is not adequate as a benchmark for validation of CFD or verification and confirmation of experimental processes. Generally, there is a lack of needed information available with published databases such as detailed geometry definitions needed for CFD to model the experiment; documented digital data files or uncertainty analysis. The U.S. DOE had developed a reference turbine project in which included three current/tidal turbine designs and subscale evaluation. One was a 1:8.7 scale a three-bladed horizontal-axis turbine. A design report was completed and electronic database for this design should soon be available online.

Large- and full-scale CT are being deployed throughout the world with increasing success. Between 2010 and 2018 almost 60 CT has been deployed in the sea around Europe. These have mainly been for medium and full scale tests. The most successful project is MeyGen Phase 1A which has installed four 1.5 MW turbines and had delivered 17GWH to the grid by mid-2019. After the demonstration phase the total farm planed size is 86 MW.

Over the last ten years the understanding of the nature of the unsteadiness flow in tidal current test sites has improved. This has been mainly due to better quality measurements and analysis of tests sites which has improved the understanding of magnitude and frequency unsteadiness due to large scale turbulence structures and waves. This has led to improved predictions of the magnitude of unsteady hydrodynamic loading. With this knowledge, the survivability has improved and there has been a reduction in the occurrence of blade and drive train failures. The improved understanding of the tidal sites has also led to a reduction in the installation time combined with experience gained through learning-by-doing.

Replicating all the unsteady flow features is not realistic for a single test facility. Consequently, tests are done with simplifications of the environment to produce unsteady flows for validation data. The following techniques have been reviewed in the literature:

- The use of a towing tank with waves. Due to matching Froude similarities the carriage speed is often low, so consequently the blade Re numbers are low which may cause large regions of laminar flow and separation.
- The use of planner motion type mechanisms in towing tanks. This is generally limited to generic simulation of key vibration magnitudes and frequencies.
- The use of screens and grids to generate turbulence in circulating water channels and cavitation tunnels. The turbulence generated may have intensity values at the turbine location close to real conditions but isotropic in nature and with different length scales.
- The use of circulating water channels with combined with currents. This is limited to very few facilities and the range of quality of the waves can be limited.

- The use of surface roughness on the bed of long flumes. This produces some non-isotropic turbulence, but these facilities are generally limited to tests with small model scale turbines or turbine simulators. These tests are generally done to help validate simulation tools for modelling CT wakes for array modelling and validation.

Regarding the numerical simulation on turbine array, some researchers still focus on improving existing method to tune the accuracy of the wake structure, but a good number start to develop method to study other aspects of array such as free surface effect and control algorithm. It can be understood that the accuracy of the wake under free surface effect is in the same level of that of the traditional methods while that of the control study is less. Nevertheless, they require further experimental test for validation. Additionally, like wind energy, tidal energy's potential impact on environment receives attention lately while they are conducted in small regions. Further investigations are expected to be conducted to understand this impact clearly with a greater scale and higher accuracy.

10.3 Offshore Wind turbines

Due to the scarcity of publicly available experimental results, especially relative to full-scale fixed and floating offshore wind turbines, a number of initiatives have been carried out by the research community to fulfil this gap, including numerical code-to-code comparisons and physical experiments at scaled model level.

A series of important initiatives, organised under the IEA Task 23 and Task 30, have been the OC3 (Offshore Code Comparison Collaboration), focusing on the code-to-code comparison of a number of aero-hydro-servo-elastic codes, considering a monopile, a tripod, and a Spar, the OC4 (Offshore Code Comparison Collaboration Continuation), focused on the complex hydrodynamics of a jacket foundation and of semisubmersibles, the OC5 (Offshore Code Comparison Collaboration Continuation, with Correlation), which extended the previous OCx initiatives by validating the numerical tools considered against experimental data (fixed flexible cylinder and semisubmersible), and the currently ongoing OC6, which expanded the verification and validation adopting a three ways approach: engineering level modelling tools, higher-fidelity numerical tools, and experimental data, analysing more complex problems such as aerodynamics and hydrodynamics of FOW undergoing large motion, hybrid potential-viscous approaches, and advanced pile/foundation interactions.

In addition to the above, a series of experimental campaigns have been conducted on scale models of FOWT, typically at a scale around 1:50, modelling the three main FOWT substructure types: spar, semi-submersible, and TLPs (DeepCwind, INNWIND.EU), and also adopting real-time hybrid model approaches (NOWITECH) to address the fundamental conflict between Reynolds scaling of aerodynamic forces and Froude scaling of hydrodynamic forces.

As far as full-scale installations are concerned, the focus has been on floating offshore wind farms. Since the last (28th) ITTC report, in 2017, the number of operational floating wind turbines has more than doubled, quadrupling the total installed capacity.

The most adopted configurations, so far, have been the spar and the semisubmersible configurations, but new ones (e.g., the damping pool barge by Ideol, the ballast-stabilised "pendulum" Tetraspar, by Stiesdal) are also emerging. After a number of demonstrators, with rated power around 2 MW, the first floating wind farms, with 3-5 wind turbines, for a total

of 25-30MW rated power, have been commissioned, with many more in the pipeline.

The survivability and the success of energy extraction has been fully proven for the spar and semi-submersible configurations, with two demonstrators having operated for a number of years in harsh conditions and delivering to the electric utility grid tens of GWh (e.g., Hywind demo in Norway, and WindFloat Atlantic Phase I), and two floating wind farms with rated power 25-30 MW successfully delivering electricity (Hywind Scotland pilot Park – spar, and WindFloat Atlantic – semi-submersible). Also, the 3MW demonstrator by Ideol, installed in Japan, managed to survive three category 5 typhoon shortly after its installation. To date, there are still no MW-scale Tension Leg Platform (TLP) demonstrators tested in an offshore environment. Between 2009, when the first demonstrator was installed by Statoil (now Equinor), and now, the most active countries have been Norway, Portugal, Japan, the UK, and France.

Significant challenges still remain in terms of scaled aero-hydrodynamic model testing of floating wind turbines due to the scaling challenges associated with the Reynolds number dissimilitude. Real-time hybrid testing techniques have been further developed and applied in more tank tests, i.e. platform responses are measured experimentally and passed into numerical simulations, whereas actuators, or other means, apply the appropriate aerodynamic loads according to simultaneous simulations of the wind turbine. Performance scaling is still widely used where the main objective of the scaling procedure is the representative modelling of the aerodynamic thrust. Some of the challenges related to the aerodynamic modelling of wind turbines loads include:

- Assessing and documenting the accuracy and uncertainty related to modelling of the aerodynamic wind turbine loads in hydrodynamic model testing of floating wind turbines, both for tests with physical modelling of the wind turbine and for hybrid testing.
- Generating high quality physical wind fields in open air in a wave tank and measure/document the spatial and temporal variations.

As the turbines become bigger, the design of the support structures has become relatively slender, and the significance of structural elasticity may be more important in future model testing.

During this term ITTC developed the new guideline 7.5-02-07-03.17 'Uncertainty Analysis for Model Testing of Offshore Wind Turbines'. Generally, the development of the standards, rules, and guidelines known as regulations and their application to offshore wind turbines (floating or fixed) have allowed the industry to gain confidence in designs. Also, the standards, guidelines and certifications address how they are about to change from addressing prototype installations with a few unit to large scale (floating or fixed) offshore wind farms consisting of many identical units. As a central 'repository' of knowledge and experience in the field of offshore wind turbine, IEC published both IEC IS 61400-3-1 'Design requirements for offshore wind turbines' and IEC TS 61400-3-2 'Design requirements for floating offshore wind turbines' in April 2019. Also ISO published ISO 29400 'Ships and marine technology - Offshore wind energy - Port and marine operations' in May 2020.

11. RECOMMENDATIONS

The 29th Specialist Committee on Hydrodynamic Modelling of Marine Renewable Energy Devices has the following recommendations for future work:

11.1 General recommendations

5. Continue interactions with IEC.
6. Review interactions between model scale and moderate/full scale test sites.
7. Review of testing of deployment (transportation, installation) and O&M for marine renewable devices.
8. Review testing of multipurpose platforms (e.g., combined WEC/OWT/ Solar/Aquaculture platforms).

11.2 Recommendations for wave energy converters (WECs):

1. Continue to monitor development of new concepts of WECs.
2. Continue to monitor developments in PTO modelling both for physical and numerical prediction of power capture.
3. Assess the feasibility of developing specific guidelines for numerical and experimental survival testing of WECs.
4. Assess support to using the benchmark round robin data for numerical comparison and/or for evaluating facility biases and scale related uncertainties.
5. Update the uncertainty analysis of WEC testing to include the uncertainties of the power capture and potentially of a different type of device technology.
6. Update and extend array section of the guidelines for numerical modelling of WECs.
7. Review and report on the different PTO control strategies for power optimisation and survivability modes.
8. Review and report on comparisons between full scale data and numerical work/experimental model testing.

11.3 Recommendations for current turbines (CTs):

1. Continue to monitor development in physical and numerical techniques for prediction of performance of current turbines.
2. Assess the support for round robin test of a 3-blade horizontal axis turbine (such as the DoE turbine). If there are enough willing participants develop a technical delivery plan.
3. Review and report the techniques use for CFD modelling current turbines. This should include the use of combined EFD/CFD techniques for scaling and blockage corrections and methodologies for replicating environmental conditions.

11.4 Recommendations for offshore wind turbines (OWTs):

1. Continue monitoring and report on the development in full-scale installation of floating offshore wind turbines.
2. Report on possible full-scale measurement data available and address how these data can be utilized for validation of simulation tools and evaluation of scaling effects from model scale tests.
3. Continue monitoring and report on the development in model testing methodology for offshore wind turbines.
4. Review and report on recent development of physical wind field modelling in open space with application for wave tank testing of floating offshore wind turbines, including modelling of turbulence and measuring and documentation of the wind field.
5. Review and report on the development of numerical offshore wind farm modelling.

12. REFERENCE

Ahmed, U., Apsley, D.D., Afgan, I. , Stallard, T., Stansby, P.K., 2017 "Fluctuating loads on a tidal turbine due to velocity shear and turbulence: comparison of CFD with field data", Renewable Energy, Vol 112, pp 235-246.

Allen, C.K., Goupee, A.J., 2017, "Assessment of Wind/Wave Basin Capability for Emulating Active Blade Pitch and Generator Control Influence on Floating Wind Turbine Response", In Proceedings of the 27th International Ocean and Polar Engineering Conference. International Society of Offshore and Polar Engineers.

Arini, N. R. , Turnock, S. R. , & Tan, M. 2018, "2D fluid structure interaction analysis of a vertical axis tidal turbine blade using periodic inflow equivalence model", Proc of the Inst of Mech Eng, Part M: Journal of Engineering for the Maritime Environment, Vol 232(1), pp 5-18.

Azcona, J., Bouchotrouch, F., González, M., Garciandía, J., Munduate, X., Kelberlau, F., Nygaard, T.A., 2014, "Aerodynamic Thrust Modelling in Wave Tank Tests of Offshore Floating Wind Turbines Using a Ducted Fan", Journal of Physics: Conference Series (Torque 2014), Vol. 524.

Azcona, J., Lemmer F., Matha, D., Amann, F., Bottasso, C.L., Montinari, P., Chassapoyannis, P., Diakakis, K., Voutsinas, S., Pereira, R., Bredmose, H., Mikkelsen, R., Laugesen, R. Mandrup Hansen, A., 2016, " Results of wave tank tests - Description of Floating Wind Model Tests at ECN and DHI", Technical report D4.2.4, INNWIND.EU.

Bachant, P., Wosnik, M., Gunawan, B., and Neary, V., 2014 "Experimental test plan - 1:6 scale reference model 2 cross-flow turbine", Technical Report, University of New Hampshire Center for Ocean Renewable Energy, December.

Bachant, P., Wosnik, M., Gunawan, B., Neary, V., 2015a "1:6 scale RM2 cross-flow turbine CAD package", figshare.com http://dx.di.org/10.6084/m9.figshare.1373870.

Bachant, P., Wosnik, M., Gunawan, B., Neary, V., 2015b, "1:6 scale RM2 cross-flow turbine CAD package", figshare.com http://dx.di.org/10.6084/m9.figshare.1373870Bachynski, E.E., Chabaud, V., Sauder. T., 2015, "Real-Time Hybrid Model Testing of Floating Wind Turbines: Sensitivity to Limited Actuation", Energy Procedia, 12th Deep Sea Offshore Wind R&D Conference, EERA DeepWind'2015, 80 (January), pp 2–12.

Bachynski, E. E., Thys, M., Delhayec,, V., 2019, "Dynamic response of a monopile wind turbine in waves: Experimental uncertainty analysis for validation of numerical tools", Applied Ocean Research, Vol. 89, pp 96-114.

Bachynski, E.E., Thys, M., Sauder, T., Chabaud, V., Sæther, L.O., 2016, "Real-time hybrid model testing of a braceless semi-submersible wind turbine. Part II: Experimental results", In Proceedings of the International Conference on Ocean, Offshore and Arctic Engineering, Busan, South Korea: ASME.

Bahaj, A.S., Molland, A.F., Chaplin, J.R., Battan, W.M.J., 2007 "Power and thrust measurements of marine current turbines under various hydrodynamic flow conditions in a cavitation tunnel and a towing tank", Renewable Energy Vol. 32, pp. 407–426.

Bayati, I., Belloli, M., Facchinetti, A., Giappino, S., 2013, "Wind Tunnel Tests on Floating Offshore Wind Turbines: A Proposal for Hardware-in-the-Loop Approach to Validate Numerical Codes", Wind Engineering 37 (6), pp 557–68.

Bayati, I., Belloli, M., Ferrari, D., Fossati, F., Giberti, H., 2014, "Design of a 6-DoF Robotic Platform for Wind Tunnel Tests of Floating Wind Turbines", Energy Procedia 53. pp 313–23.

Belloli, M., Bayati, I., Facchinetti, A., Fontanella, A., Giberti, H., La Mura, F., Taruffi, F., 2020, "A hybrid methodology for wind tunnel testing of floating offshore wind turbines", Ocean Engineering, Vol. 210.

Berthelsen, P.A., Bachynski, E.E., Karimirad, M., Thys, M., 2016, "Real-time hybrid model tests of a braceless semi-submersible wind turbine. Part III: Calibration of a numerical model", In Proceedings of the International Conference on Ocean, Offshore and Arctic Engineering, Busan, South Korea: ASME.

Bingham, H.B., Yu, Y-H., Nielsen, K., Tran, T.T., Kim, K-H., Park, S., Hong, K., Said, H.A., Kelly, T., Ringwood, J.V., Read, R.W., Ransley, E., Brown, S., Greaves, D., 2021, "Ocean energy systems wave energy modelling task 10.4: Numerical modelling of a fixed oscillating water column", Energies (MDPI), Vol. 14, No 6(1718).

Blackmore, T., Gaurier B., Myres, L., Germain G., Bahaj A.S., 2015, "The Effect of Freestream Turbulence on Tidal Turbines", 11th European Wave and Tidal Energy Conference, Nantes, France

Bombora, 2021, " Pembrokeshire project, Available at: https://www.bomborawave.com/latest-news/project/1-5mw-pembrokeshire-project/, Accessed 1st February 2021.

Borg, M., 2018, "Physical Model Testing of the TetraSpar Floater in Two Configurations." presented at the EERA Deepwind, Trondheim, Norway.

Buchner, B., 1999, "Model Test Challenges for Deep Water Floaters".

Calvario, M., Gaspar, J.F., Kamarlouei, M., Hallak, T.S., Soares, C.G., 2020, "Oil-hydraulic power take-off concept for an oscillating wave surge converter", Renewable Energy, Vol. 159, pp 1297–1309.

Cao, Y., Tahchiev, G., 2013, "A Study on an Active Hybrid Decomposed Moor-ing System for Model Testing in Ocean Basin for Offshore Platforms", In Proceedings of the International Conference on Ocean, Offshore and Arctic Engineering, Nantes, France.

Carrelhas, A.A., Gato, L.M.C., Henriques, J.C.C., Falcao, A.F.O., 2020, "Experimental study of a self-rectifying biradial air turbine with fixed guide-vanes arranged into two concentric annular rows", Energy, Vol. 198(117211).

Chabaud, V., Eliassen, L., Thys, M., Sauder, T., 2018, "Multiple-degree-of-freedom actuation of rotor loads in model testing of floating wind turbines using cable-driven parallel robots", Journal of Physics: Conference Series (EERA DeepWind 2018), Vol. 1104.

Chabaud, V., Steen, S., Skjetne, R., 2013, "Real-Time Hybrid Testing for Marine Structures: Challenges and Strategies", In Proceedings of the International Conference on Ocean, Offshore and Arctic Engineering, Nantes, France.

Clarke, J.A., Connor, G., Grant, A.D., and Johnstone, C.M., 2007a "Design and testing of a contra-rotating tidal current turbine", Proceedings of the Institution of Mechanical Engineers, Part A: Journal of Power and Energy, Vol. 221, Issue 2, pp. 171-179.

Clarke, J., G. Connor, A. Grant, C. Johnstone and D. MacKenzie., 2007b "Development of a contra-rotating tidal current turbine and analysis of performance", Proceeding of European Wave and Tidal Energy Conference, EWTEC, September.

Connell, K.O., Thiebaut, F., Kelly, G., Cashman, A., 2018, "Development of a free heaving OWC model with non-linear PTO interaction", Renewable Energy, Vol. 117, pp 108–115.

Courbois, A., 2013, "Étude expérimentale du comportement dynamique d'une éolienne offshore flottante soumise à l'action conjuguée de la houle et du vent." Phd thesis, Ecole Centrale de Nantes (ECN), France.

De Dominicis, M. , O'Hara Murray, R. , & Wolf, J., 2017, "Multi-scale ocean response to a large tidal stream turbine array", Renewable Energy, Vol. 114, pp 1160-1179.

Delafin, P.L., Deniset, F., Astolfi, J.A., Hauville. F, 2021, "Performance improvement of a darrieus tidal turbine with active variable pitch", Energies, Vol. 14(3), pp 667.

Deng, G., Zhang, Z., Li, Y., Liu, H., Pan, Y., 2020, "Prospective of development of large-scale tidal current turbine array: an example numerical investigation of zhejiang, china", Applied Energy, Vol. 264, 114621.

Devolder, B., Stratigaki, V., Troch, P., Rauwoens, P., 2018, "CFD Simulations of Floating Point Absorber Wave Energy Converter Arrays Subjected to Regular Waves", Energies, 11, 641.

DNV 2019, "Coupled analysis of floating wind turbines", Recommended Practice DNVGL-RP-0286.

Dr. Techn.Olav Olsen 2021, "Breakthrough for OO-Star Wind Floater". Available at: https://www.olavolsen.no/en/aktuelt/post-hdQPQ-breakthrough-for-oo-star-wind-floater, Accessed 18th February.

Draycott, S., et al. 2019a, "An experimental investigation into non-linear wave loading on horizontal axis tidal turbines", J. Fluids and Structures, Vol. 84, pp 199-217.

Draycott, S., et al. 2019b., "Experimental assessment of tidal turbine loading from irregular waves over a tidal cycle", J. Ocean Eng. Mar. Energy, Vol. 5, pp 173–187.

Du, M., Hou, E., Wang, B., Li, Y., Wang, H., Duan, L., 2016, "The effect of tidal stream characteristic and mechanical support structure on horizontal axis tidal turbine performance", Oceans. IEEE,

Du Feu, R.J., Funke, S.W., Kramer, S.C., Culley, D.M., Hill, J.M., Halpern, B.S.,, 2017, "The trade-off between tidal-turbine array yield and impact on flow: a multi-objective optimisation problem", Renewable Energy, Vol. 114, pp. 1247-1257.

Ebdon, T., Allmark, M.J., O'Doherty, D.M., Mason-Jones, A., O'Doherty, T., Germain, G., 2021), "The impact of turbulence and turbine operating condition on the wakes of tidal turbines", Renewable Energy, Vol. 165, pp 96-116.

EC, 2017, "Study on Lessons for Ocean Energy Development", Directorate-General for Research and Innovation. Publications

Office of the European Union. EUR 27984 EN.

ECN, 2021, "IEA Wind Task 29 Maxent. Results/status". Available at: https://www.mexnext.org/resultsstatus, Accessed 25th January 2021.

EDP, 2021, "Innovation at edp: WindFloat Atlantic" Available at: https://www.edp.com/en/innovation/windfloat, Accessed 1st February 2021.

EFGL, 2021, "Les Eoliennes Flottantes du Golfe du Lion. Le Projet" Available at: https://info-efgl.fr/le-projet/eolienne-mhi-vestas/, Accessed 1st February 2021.

EMEC, 2009, "Guidelines for Reliability, Maintainability and Survivability of Marine Energy Conversion Systems", The European Marine Energy Centre Ltd.

EOLFI, 2021, "Les Eoliennes Floattantes de Groix & Belle-Île", Available at: https://eoliennes-groix-belle-ile.com/en/project/#technique, Accessed 1st February 2021.

Eolink, 2021, "Eolink Cost-effective Floating Wind Farms. First Prototype", Available at: http://eolink.fr/en/article-fp-en, Accessed 1st February 2021.

Equinor, 2021a, "Hywind Scotland", Available at: https://www.equinor.com/en/what-we-do/floating-wind/hywind-scotland.html, Accessed 1st February 2021.

Equinor, 2021b, "Hywind Demo". Available at: https://www.equinor.com/en/what-we-do/floating-wind/hywind-demo.html, Accessed 1st February 2021.

Equinor, 2021c, "Hywind Tampen: the world's first renewable power for offshore oil and gas". Available at: https://www.equinor.com/en/what-we-do/hywind-tampen.html, Accessed 18th February 2021.

Ezhilsabareesh, K., Suchithra, R., Samad, A., 2019, "Performance enhancement of an impulse turbine for OWC using grouped grey wolf optimizer based controller", Ocean Engineering, Vol. 190(106425).

Falcao, A.F.O., Henriques, J.C.C., 2019, "The spring-like air compressibility effect in oscillating-water-column wave energy converters: Review and analyses", Renewable and Sustainable Energy Reviews, Vol. 112, pp 483-498.

Flavià, F., Mcnatt, C., Rongère, F., Babarit, A., and Clément, A. (2018). A numerical tool for the frequency domain simulation of large arrays of identical floating bodies in waves. Ocean Eng. 148, 299–311.

Fernandez-Rodriguez, E. Stallard T.J., Stansby, P.K., 2014, "Experimental study of extreme thrust on a tidal stream rotor due to turbulent flow and with opposing waves", Journal of Fluids and Structures, Vol. 51, pp 354-361.

Fontaine, A.A., Straka, W.A., Meyer, R.S., Jonson, M.L., 2013, "A 1:8.7 scale water tunnel verification and validation test of an axial flow water turbine", Penn State/Applied Research Laboratory Technical Report, TR 13-002.

Fontaine, A.A., Straka, W.A., Meyer, R.S., and Jonson, M.L., Young, S.D., Neary, V.S., 2020, "Performance and wake flow characterization of a 1:8.7-ccale reference USDOE MHKF1 hydrodynamic turbine to establish a verification and validation test database", Renewable Energy Vol. 159, pp. 451–467.

Fontanella, A., Bayati, I., Belloli, M., 2018, "Control of Floating Offshore Wind Turbines: Reduced-Order Modeling and Real-Time Implementation for Wind Tunnel Tests", In Proceedings of the International Conference on Ocean, Offshore and Arctic Engineering, Madrid, Spain.

Fontanella, A., Liu, Y., Azcona, J., Pires, O., Bayati, I., Gueydon, S., de Ridder, E.J., van Wingerden, J.W., Belloli, M., 2020, "A hardware-in-the-loop wave-basin scale-model experiment for the validation of control strategies for floating offshore wind turbines", Journal of Physics: Conference Series (TORQUE2020), Vol. 1618.

Fontanella, A., Taruffi, F., Bayati, I., Belloli, M., 2019, "Variable-Speed Variable-Pitch Control for a Wind Turbine Scale Model", Journal of Physics: Conference Series (EERA DeepWind 2019), Vol. 1356.

FORCE, 2019 "Lessons learned, Marine Operations Minas Passage", Operational Excellence Consulting Inc.

Fowler, M.J., Kimball, R.W., Thomas III, D.A., Goupee, A.J., 2013, "Design and Testing of Scale Model Wind Turbines for Use in Wind/Wave Basin Model Tests of Floating Offshore Wind Turbines", In Proceedings of the International Conference on Ocean, Offshore and Arctic Engineering. Nantes, France.

Fukushima Offshore Wind Consortium, 2021, "Fukushima Floating Offshore Wind Farm Demonstration Project", Available at: http://www.fukushima-forward.jp/english/index.html, Accessed 1st February 2021.

Gajardo, D., Escauriaza, C., Ingram, D.M.. 2019, "Capturing the development and interactions of wakes in tidal turbine arrays using a coupled bem-des model", Ocean Engineering, Vol. 181, pp. 71-88.

Garrad A., 2012, "The lessons learned from the development of the wind energy industry that might be applied to marine industry renewables", Philosophical Transactions of the Royal Society A, Vol. 370, pp 451-471.

Gaurier, B., Germain, G., Facq, J.V., Johnstone, C.M., Grant, A.D, Day, A.H., Nixon, E., Di Felice, F., Constanzo, M., 2015 "Tidal energy round-robin tests – comparisons between towing tank and circulating tankresults", International Journal of Marine Energy, Vol. 12, pp. 87 - 109.

Gaurier, B., Germain, G., Facq, J.V., Day, S., Johnstone, C., Grant, A.D, Di Felice, F., Constanzo, M., 2018a "Towing and circulating tanks tidal energy converter test results", SEANOE, Sea scientific open data edition https://www.seanoe.org/data/00463/57450/.

Gaurier, B., Ordonez-Sanchez, S., Germain, G., Facq, J.V., Johnstone, C., Salvatore, F. and Santic, I., 2018b, "MaRINET2 Tidal "Round Robin" dataset: comparisons between towing and circulating tanks test results for a tidal energy converter submitted to wave and current interactions", SEANOE, Sea scientific open data edition https://www.seanoe.org/data/00471/58265/

Gaurier, B., Carlier, C., Germain G., Pinon, G., Rivoalen, E., 2020 "Three tidal turbines in interaction: An experimental study of turbulence intensity effects on wakes and turbine performance," Renewable Energy, Vol. 148, pp 1150-1164.

Gaurier, B., Davies, P., Deuff, A., Germain, G., 2013, "Flume tank characterization of marine current turbine blade behaviour

under current and wave loading", Renewable Energy, Vol. 59, pp 1–12.

GEPS Techno, 2021, " Autonomous hybrid offshore platforms, Available at: https://www.geps-techno.com/en/autonomous-hybrid-platforms/, Accessed 1st February 2021.

Germanischer Lloyd, 2015, "Draft of guideline for the certification of ocean energy converters, part 1: ocean current turbines", available from: www.gl-group.com/pdf/ OCT-Guideline_draft_R10.pdf

Gharraee, B., 2015, "Numerical Simulation of Cavitation on a Tidal Turbine using ReFRESCO", Master's Thesis, Chalmers University of Technology, Sweden.

Giassi, M., Engström, J., Isberg, J., Göteman, M., 2020, "Comparison of Wave Energy Park Layouts by Experimental and Numerical Methods", Journal of Marine Science and Engineering, 8,750 Galloway, P.W., Myers, L.E, Bahaj, A.S., 2014, "Quantifying wave and yaw effects on a scale tidal stream turbine", Renewable Energy, Vol. 63, pp 297–307.

Göteman, M., Giassi, M., Engström, J., Isberg, J., 2020, "Advances and Challenges in Wave Energy Park Optimization—A Review", Front. Energy Res, 8:26.

Goupee, A.J., Koo, B.J., Lamrakos, K.F., Kimball, R., 2013, "Offshore Wind Energy: Model Tests for Three Floating Wind Turbine Concepts", In Proceedings of the Offshore Technical Conference, April 30 – May 3, 2012, Houston, TX.

Goupee, A.J., Fowler, M.J., Kimball, R.W., Helder, J., de Ridder, E.-J., 2014, "Additional Wind/Wave Basin Testing of the DeepCwind Semi-Submersible with a Performance-Matched Wind Turbine", In Proceedings of the International Conference on Offshore Mechanics and Arctic Engineering, San Francisco, California, USA.

Goupee, A.J., Kimball, R.W., Dagher, H.J., 2017, "Experimental Observations of Active Blade Pitch and Generator Control Influence on Floating Wind Turbine Response." Renewable Energy 104 (April). pp. 9–19.

Greaves D, Iglesias G. 2018. Wave and Tidal Energy. Chichester, UK: Wiley

Group Cobra, 2021, "Kincardine Offshore Floating Wind Farm. Available at: https://www.grupocobra.com/en/proyecto/kincardine-offshore-floating-wind-farm/, Accessed 1st February 2021.

Gu, Y.J., Lin, Y.G., Xu, Q.K., Liu, H.W., Li, W., 2018, "Blade-pitch system for tidal current turbines with reduced variation pitch control strategy based on tidal current velocity", Renewable Energy, Vol. 115, pp 149-158.

Gueydon, S., Lindeboom, R., van Kampen, W., de Ridder, E.-J., 2018, "Comparison of Two Wind Turbine Loading Emulation Techniques Based on Tests of a TLP-FOWT in Combined Wind, Waves and Current", In Proceedings of the International Offshore Wind Technical Conference, San Francisco, California, USA.

Guo, X., Yang, J., Gao, Z., Moan, T., Lu, H., 2018, "The surface wave effects on the performance and the loading of a tidal turbine", Ocean Engineering, Vol. 156, pp 120-134,

Hall, M., Goupee, A., 2017, "Comparing fatigue loads in floating wind turbine basin tests: geometric-scaled, performance-scaled, and hybrid approaches," in Proceedings of the

27th International Ocean and Polar Engineering Conference, San Francisco, California.

Hall, M., Goupee, A.J., 2018, "Validation of a Hybrid Modeling Approach to Floating Wind Turbine Basin Testing." Wind Energy 21 (6).

Hill, C., Neary, V., Gualu, M. and Sotiropoulos, F. 2020, "Performance and Wake Characterization of a Model Hydrokinetic Turbine: The Reference Model 1 (RM1) Dual rotor Tidal Energy Converter", Energies, Vol. 13, Issue 19, 21.

Hu.Q, Li Y., Di Y. and Chen J. (2017) "A large-eddy simulation study of horizontal axis tidal turbine in different inflow conditions", Journal of Renewable and Sustainable Energy, Vol. 9, pp 064501

Ideol, 2019 "Ideol Press Kit", Available at: https://www.ideol-offshore.com/sites/default/files/2019-10/Ideol%20-%20Press%20kit_0.pdf, Accessed 15th March 2021.

Ideol, 2021a, "EOLMed Project.", Available at: https://www.ideol-offshore.com/en/eolmed-project, Accessed 1st February 2021.

Ideol, 2021b, "Ideol Offshore. News", Available at: https://www.ideol-offshore.com/en/ideols-floating-wind-turbine-japan-officially-inaugurated-after-months-sea, Accessed 1st February 2021.

Ideol, 2021c, "Floatgen Demonstrator", Available at: https://www.ideol-offshore.com/en/floatgen-demonstrator, Accessed 1st February 2021.

IEA, 2021, "Benchmark Problems. Available at: https://community.ieawind.org/task30/t30benchmarkproblems, Accessed 25 th January 2021.

IEA Wind, 2021, "Task 30: Offshore Code Comparison Collaboration, Continuation with Correlation, and unCertainty (OC6)". Available at: https://community.ieawind.org/task30/home, Accessed 1st February 2021

INNWIND.EU, 2021, "Deliverable reports", Available at: http://www.innwind.eu/publications/deliverable-reports, Accessed 25 th January 2021.

Jonkman, J., Musial, W., "Offshore Code Comparison Collaboration (OC3) for IEA Task 23 Offshore Wind Technology and Deployment", NREL/TP-500-48191, Golden, Colorado: National Renewable Energy Laboratory, 2010.

Jurado, A., Sarmiento, J., Armesto, J.A., Meseguer, A., Guanche, R., Couñago, B., Urbano, J., Serna, J., 2017, "Experimental Modelling and Numerical Model Calibration of Telwind: An Innovative Floating Wind Offshore Concept," in Marine Energy Week, Bilbao, Spain.

Karimirad, M., Bachynski, E.E., Berthelsen, P.A., Ormberg, H., 2017, " Comparison of Real-Time Hybrid Model Testing of a Braceless Semi-Submersible Wind Turbine and Numerical Simulations", In Proceedings of the International Conference on Ocean, Offshore and Arctic Engineering, Trondheim, Norway: ASME.

Kennedy, C.R., Leen, S.B., Brádaigh, C., 2012, "A preliminary design methodology for fatigue life prediction of polymer composites for tidal turbine blades", Proc IMechE Part L: J Mater: Des Appl, Vol. 226(3), pp. 203-218.

Kim, J-S., Nam, B.W., Kim, K-H., Park, S. Shin, S-H., Hong, K., 2020, "A Numerical Study on Hydrodynamic Performance of an Inclined OWC Wave Energy Converter with Nonlinear Turbine-Chamber Interaction based on 3D Potential Flow", J. of Marine Science & Engineering (MDPI), Vol. 8, No. 3(176).

Kimball, R., Goupee, A.J., Fowler, M.J., de Ridder, E.-J., Helder, J., 2014, "Wind/Wave Basin Verification of a Performance-Matched Scale-Model Wind Turbine on a Floating Offshore Wind Turbine Platform", In Proceedings of the International Conference on Ocean, Offshore and Arctic Engineering, San Francisco, California, USA.

Kolekar, N., Vinod, A., Banerjee, A., 2019, "On blockage effects for a tidal turbine in free surface proximity", Energies, Vol. 12(17), 3325.

Kong, F., Su, W., Liu, H., Collu, M., Lin, Z., Chen, H., Zheng, X., 2019, "Investigation on PTO control of a Combined Axisymmetric Buoy-WEC (CAB-WEC)", Ocean Engineering, Vol. 188(106245).

Li, X., Chen, C., Li, Q., Xu, L., Liang, C., Ngo, K., Parker, R.G., Zuo, L., 2020, "A compact mechanical power take-off for wave energy converters: Design, analysis, and test verification", Applied Energy, Vol. 278(115459).

Li, Z., Ghia, K., Li.Y., Fan, Z., Shen L., 2021, "Unsteady Reynolds-averaged Navier-Stokes investigation of free surface wave impact on tidal turbine wake", Phil Trans Royal Soc A, Vol. 477, Issue 2246.

Liu, P., Veitch, B., 2012, "Design and optimization for strength and integrity of tidal turbine rotor blades", Energy, Vol. 46, pp 393-404.

López-Ruiz, A., Bergillos, R., Raffo-Caballero, J., and Ortega-Sánchez, M. (2018a). "A risk-based approach to layout implementation of WEC array by addressing accidental constraints" J. Ocean. Eng. And Marine Eng. 5, 73-84.

Lust, E.E., Luznik, L., Flack, K.A., Walker, J.M., Van Benthem M.C., 2013, "The influence of surface gravity waves on marine current turbine performance", International Journal of Marine Energy, Vol. 3-4, pp 27–40.

Ma Y. et al, 2018. "Theoretical vertical-axis tidal-current-turbine wake model using axial momentum theory with CFD corrections." Applied Ocean Research, Vol. 79, 113-122.

MacEnri J., Reed M., Thiringer T., 2013, "Influence of tidal parameters on SeaGen flicker performance", Phil Trans Royal Soc A, Vol 371: 0120247.

Magagna, D., 2019, "Ocean Energy Technology Development Report 2018," Luxembourg.

Mannion, B., Seán B. Leen, Mccormack, V., Nash, S., 2018, "Numerical Modelling of a Variable-Pitch, Vertical Axis Tidal Turbine Incorporating Flow Acceleration", ASME 2018 37th International Conference on Ocean, Offshore and Arctic Engineering

Martin, H.R., 2011, "Development of a Scale Model Wind Turbine for Testing of Off-shore Floating Wind Turbine Systems." University of Maine.

Martin, H.R., Kimball, R.W., Viselli, A.M., Goupee, A.J., 2014, "Methodology for Wind/Wave Basin Testing of Floating Offshore Wind Turbines", Journal of

Offshore Mechanics and Arctic Engineering 136 (2): 020905.

McCaffrey, K., Fox-Kemper, B., Hamlington, P.E., Thomson, J, 2015, "Characterization of turbulence anisotropy, coherence, and intermittency at a prospective tidal energy site: Observational data analysis," Renewable Energy, Vol 75, pp. 441-452.

McCarthy, R.J., Arzaghi, E., Abaei, M.M., Abbassi, R., Garaniya, V., Penesis, I., 2019, A risk-based approach to layout implementation of WEC array by addressing accidental constraints.

McNatt, J.C., Porter, A., Ruehl, K., 2020, "Comparison of Numerical Methods for Modeling the Wave Field Effects Generated by Individual Wave Energy Converters and Multiple Converter Wave Farms", J. Mar. Sci. Eng., 8, 168

Milne, I.A., Day, A.H., Sharam, R.N., Flay, R.G.J., 2016, "The characterisation of the hydrodynamic loads on tidal turbines due to turbulence", Renewable and Sustainable Energy Reviews, Vol. 56, pp. 851–864.

Minesto, 2021, www.minesto.com

Molin, B., Remy, F., Facon, G., 2004, "Etude Expérimentale du comportement Hydro-Aéro- Elastique d'une Eolienne Offshore sur Ancrages Tendus", In Proceedings of the Ocean Energy Conference. Brest, France.

Musa M., Hill C, Sotiropoulos, F. Guala, M., 2018, "Performance and resilience of hydrokinetic turbine arrays under large migrating fluvial bedforms", Nature Energy, Vol. 3, pp. 839-846.

Musial, W., Jonkman, J., Vorpahl, F., Quesnel, L., "Annex 30 Task Proposal Comparison of Dynamic Computer Codes and Models Offshore Code Comparison Collaboration Continuation (OC4) Project", International Energy Agency, 2009.

Nachtane, M., Tarfaoui, M., Goda, I., Rouway, M., 2020, "A review on the technologies, design considerations and numerical models of tidal current turbines", Renewable Energy, Vol 157, pp 1274-1288.

Neary, V.S., Fontaine, A.A, Bachant, P., Gunawan, B., Wosnik, M., Michelen, C., Meyer, R.S., Straka, W.A., 2013, "US Department of Energy (DOE) national lab activities in marine hydrokinetics: Scaled model testing of DOE reference turbines", Proceedings of European Wave and Tidal Energy Conference, EWTEC.

Nielsen, F.G., Hanson,T.D., Skaare, B., 2006, "Integrated Dynamic Analysis of Floating Offshore Wind Turbines", In Proceedings of the International Conference on Ocean, Offshore and Arctic Engineering, Hamburg, Germany.

Nielsen, K., Wendt, F., Yu, Y. H., Ruehl, K., Touzon, I., Nam, B. W., Kim, J. S., Kim, K. H., Crowley, S., Sheng, W., Kurniawan, A., Ogden, D., Girardin, S., Babarit, A., Costello, R., Giorgi, S., Roy, A., Bingham, H., Read, R., … Thomas, S., 2018, Oes task 10 wec heaving sphere performance modelling verification. Advances in Renewable Energies Offshore - Proceedings of the 3rd International Conference on Renewable Energies Offshore, RENEW 2018, 265–272.

Nuernberg, M., Tao, L., 2017, "Three dimensional tidal turbine array simulations using openfoam with dynamic mesh", Ocean Engineering, Vol. 147, pp. 629-644.

Ocean Energy Europe, 2019, "Ocean Energy: Key Trends and Statistics 2019" , Brussels.

Oberkampf, W.L, Trucano, 2002, "Verification and Validation in Computational Fluid Dynamics", Progress in Aerospace Sciences, Vol. 38, Issue 3, pp. 209-272.

Ordonez-Sanchez, S., Allmark, M., Porte,r K., Ellis, R., Lloyd, C., O'Doherty, T., Johnstone, C, 2019, "Analysis of a horizontal axis tidal turbine performance in the presence of regular and irregular waves using two control strategies", Energies, Vol. 12(3):367.

Orbital Marine Power (2021), www.orbitalmarine.com

Orphin, J., Nader, J. R., & Penesis, I. (2021). Uncertainty analysis of a WEC model test experiment. Renewable Energy, 168, 216–233.

Orszaghova, J., Wolgamot, H., Draper, S., Eatock Taylor, R., Taylor, P., and Rafiee, A (2019). Transverse motion instability of a submerged moored buoy. Proc. R. Soc. A 475:20180459

Pacheco A., Grobena E., Plomaritis T., Goncalves J., 2018, "Lessons learned from E1 Evopod Tidal Energy Converter deployment at Ria Formosa, Portugal", 7th International Conference on Ocean Energy, Cherbourg, France

Payne S.P., Stallard, T., Martinez R., Bruce, T., 2018, "Variation of loads on a three-bladed horizontal axis tidal turbine with frequency and blade position", Journal of Fluids and Structures, Vol. 83, pp 156-170.

Penalba, M., Davidson, J., Windt, C., Ringwood, J.V., 2018, "A high-fidelity wave-to-wire simulation platform for wave energy converters: Coupled numerical wave tank and power take-off models", Applied Energy, Vol. 226, pp 655-669.

PGL, 2021, "Provence Grand Large. Le Projet", Available at: https://www.provencegrandlarge.fr/, Accessed 1st February 2021.

Pires, O., Azcona, J., Vittori, F., Bayati, I., Gueydon, S., Fontanella, A., Liu, Y., de Ridder, E.J., Belloli, M., van Wingerden, J.W., 2020, "Inclusion of rotor moments in scaled wave tank test of a floating wind turbine using SiL hybrid method", Journal of Physics: Conference Series (TORQUE2020), Vol. 1618.

Randall-Smith, B., 2021, "Japan's floating trio to be decommissioned next year", Available at: https://www.4coffshore.com/news/japan27s-floating-trio-to-be-decommissioned-next-year-nid20670.html, Accessed 1st February 2021.

de Ridder, E.-J., Otto, W., Zondervan, G.-J., Huijs, F., Vaz, G., 2014, "Development of a Scaled-Down Floating Wind Turbine for Offshore Basin Testing." In Proceedings of the International Conference on Ocean, Offshore and Arctic Engineering, San Francisco, California, USA.

Robertson, A.N., Jonkman, J.M., Goupee, A.J., Coulling, A.J., Prowell, I., Browning, J., Masciola, M.D., Molta, P., 2013, "Summary of Conclusions and Recommendations Drawn from the DeepCwind Scaled Floating Offshore Wind System Test Campaign", In Proceedings of the International Conference on Ocean, Offshore and Arctic Engineering, Nantes, France.

Rodríguez, C.A., Rosa-Santos, P., Taveira-Pinto, F., 2019, "Assessment of damping coefficients of power take-off systems of wave energy converters: A hybrid approach", Energy, Vol. 169, pp 1022-1038.

Sauder, T., 2018, "Fidelity of Cyber-Physical Empirical Methods." PhD-Thesis,

Norwegian University of Science and Technology (NTNU), Norway.

Sauder, T., Chabaud, V., Thys, M., Bachynski, E.E., Sæther, L.O., 2016, "Real-Time Hybrid Model Testing of a Braceless Semi-Submersible Wind Tur-bine: Part I — The Hybrid Approach", In Proceedings of the International Conference on Ocean, Offshore and Arctic Engineering, Busan, South Korea: ASME.

Schepers, J.G., Snel, H., "Mexico, Model experiments in controlled conditions", ECNE-07-042, Energy Research Center of the Netherlands, 2007.

Senol, K., Raessi, M., 2019, "Enhancing power extraction in bottom-hinged flap-type wave energy converters through advanced power take-off techniques", Ocean Engineering, Vol. 182, pp 248-258.

SIMEC ATLANTIS ENERGY, 2019, "Annual report 2019", SIMEC Atantis Energy Limited.

Simonetti, I., Cappietti, L., Elsafti, H., Oumeraci, H., 2018, "Evaluation of air compressibility effects on the performance of fixed OWC wave energy converters using CFD modelling", Renewable Energy, Vol. 119, pp 741-753.

Shadman, M., Avalos, G.O.G., Estefen, S.F., 2021, "On the power performance of a wave energy converter with a direct mechanical drive power take-off system controlled by latching", Renewable Energy, Vol. 169, pp 157–177.

Sharp. C., DuPont, B., 2018, "Wave energy converter array optimization: A genetic algorithm approach and minimum separation distance study". Ocean Engineering, 263, 148-156.

Shui, H., van Dam, C.P., Johnson, E., Barone, M. Phillips, R., Straka, W., Fontaine, A. and Jonson, M., 2012, "A design of a hydrofoil family for current driven marine Hydrokinetic Turbines", 20th International Conference on Nuclear Engineering and ASME 2012 Power.

So, R., Simmons, A., Brekken, T., Ruehl, K., Michelen, C., 2015, "Development of PTO-Sim: A power performance module for the open-source wave energy converter code WEC-Sim", Proceedings of the 34th International Conference on Ocean, Offshore and Arctic Engineering, St. John's, Canada.

Stallard, T., Collings, R., Feng, T., and Whelan, J., 2012, "Interactions between tidal turbine wakes: experimental study of a group of three-bladed rotors", Phil Trans Royal Society. A: Math. Phys. Eng. Sci. Vol. 371.

Stiesdal, 2021, "The potential of offshore windpower is enormous", Available at: https://www.stiesdal.com/offshore-wind power/, Accessed 1st February 2021.

Stevens, C., 2017, "Scales of Marine Turbulence in Cook Strait (New Zealand) in the Context of Tidal Energy Turbines", Egu General Assembly Conference. EGU2017, in Vienna, Austria.

Sufian, S. F., Li, M., O'Connor, B.A., 2017, "3d modelling of impacts from waves on tidal turbine wake characteristics and energy output", Renewable Energy, Vol. 114, pp 308-322.

Tatum, S.C, Frost, C.H. Allmark, M., D.M. O'Doherty, Mason-Jones, A. Prickett, P.W. Grosvenor, R.I., Byrne, C.B., O'Doherty, T. "Wave–current interaction effects on tidal stream turbine performance and loading

characteristics", International Journal of Marine Energy, Vol. 14, pp 161-179.

Temiz I., Leijon, J., Ekergard, B., Bostrom, C., 2018, "Economic aspects of latching control for a wave energy converter with a direct drive linear generator power take-off", Renewable Energy, Vol. 128, pp 57–67.

Thys, M., Chabaud, V., Sauder, T., Eliassen, L., 2018, "Real-Time Hybrid Model Testing of a Semi-Submersible 10MW Floating Wind Turbine and Advances in the Test Method", In Proceedings of the ASME 2018 1st International Offshore Wind Technical Conference, San Francisco, California, USA.

Thys, M., Souza C., Sauder, T., Fonseca, N., Berthelsen, P.A., Engebretsen, E., Haslum, H., 2021, "Experimental investigation of the coupling between aero- and hydrodynamical loads on a 12 mw semi-submersible floating wind turbine", In Proceedings of the International Conference on Ocean, Offshore and Arctic Engineering.

Togneri, M., Grégory, P., Clément, C., Choma, C., Masters, B., 2020, "Comparison of synthetic turbulence approaches for blade element momentum theory prediction of tidal turbine performance and loads", Renewable Energy, Vol. 145, pp 408-418.

UNITECH, 2021, "Press Release January 8th 2019", Available at https://unitechenergy.com/2019/01/08/press-release-january-8th-2019/, Accessed 1st February 2021.

Urbán, A.M., Guanche, R., 2019, "Wind Turbine Aerodynamics Scale-Modeling for Floating Offshore Wind Platform Testing", Journal of Wind Engineering and Industrial Aerodynamics 186 (March): 49–57.

U.S. Department of Energy, 2021, "OC5 Offshore Code Comparison Collaboration, Continued, with Correlation, Overview", Available at: https://a2e.energy.gov/projects/oc5, Accessed 1st February 2021.

Utsunomiya, T., Shiraishi, T., Sato, I., Inui, E., & Ishida, S., 2014, "Floating offshore wind turbine demonstration project at Goto Islands, Japan". In OCEANS 2014 – TAIPEI, Institute of Electrical and Electronics Engineers Inc.

Vittori, F., Pires, O., Azcone, J., Uzunogly, E., Guedes Soares, C., Zamora Rodríguez, R., Souto-Iglesias, A., 2020, " Hybrid scaled testing of a 10MW TLP floating wind turbine using the SiL method to integrate the rotor thrust and moments", In book Developments in Renewable Energies Offshore, 1st edition, CRC Press.

Wang, Q., Zhang, P., Li, Y.. 2018, "Structural dynamic analysis of a tidal current turbine using geometrically exact beam theory", Journal of Offshore Mechanics & Arctic Engineering", Vol. 140(2), 021903.

Ward, J.C., Fowler, M.J., Viselli, A.M., Goupee, A.J., Dagher, H.J, 2018, "Design and Validation of a Multi-Scale Model Floating Offshore Test Wind Turbine" In Proceedings of the International Offshore Wind Technical Conference, San Francisco, California, USA.

WavePiston, 2021, "WavePiston", Available at: https://www.wavepiston.dk/#our-services, Accessed 1st February 2021.

WaveSwell, 2021, "King Island project", Available at: https://www.waveswell.com/king-island-project-2/, Accessed 1st February 2021.

Wello, 2021, " The Penguin Wave Energy Converter ", Available at: https://wello.eu/the-penguin-2/, Accessed 1st February 2021.

Wendt, F., Nielsen, K., Yu, Y. H., Bingham, H., Eskilsson, C., Kramer, M., Babarit, A., Bunnik, T., Costello, R., Crowley, S., Gendron, B., Giorgi, G., Giorgi, S., Girardin, S., Greaves, D., Heras, P., Hoffman, J., Islam, H., Jakobsen, K. R., … Yasutaka, I., 2019, Ocean energy systems wave energy modelling task: Modelling, verification and validation of wave energy converters. Journal of Marine Science and Engineering, 7(11), 379.

Wendt, F.F., Robertson, A.N., Jonkman, J.M., 2017, "FAST Model Calibration and Validation of the OC5-DeepCwind Floating Offshore Wind System Against Wave Tank Test Data", In Proceedings of the 27th International Ocean and Polar Engineering Conference. International Society of Offshore and Polar Engineers.

Whelan J.I., Stallard T.J., 2011, "Arguments for modifying the geometry of a scale model rotor", In Proceedings of the 9th European Wave and Tidal Energy Conference, Southampton, UK.

Wosnik, M., Bachant, P., Gunawan, B., 2015, "Performance measurements for a 1:6 scale model of the DOE reference model 2 (RM2) cross-flow hydrokinetic turbine", In Proceedings of 3rd Marine Energy Technology Symposium.

Xodus group, 2013, "Hywind Scotland Pilot Park Project - EIA Scoping Report", Available at: http://marine.gov.scot/sites/default/files/00435569.pdf , accessed 15 March 2021.

Xu, C., Huang, Z., 2019, "Three-dimensional CFD simulation of a circular OWC with a nonlinear power-takeoff: Model validation and a discussion on resonant sloshing inside the pneumatic chamber", Ocean Engineering, Vol. 176, pp 184-198.

Yang, S.H., He, H.Z., Chen, H., Wang, Y.Q., Li, H., Zheng, S.G., 2019, "Experimental study on the performance of a floating array-point-raft wave energy converter under random wave conditions", Renewable Energy, Vol. 139, Pages 538-550

Yu, W., Lemmer, F., Bredmose, H., Borg, M., Pegalajar-Jurado, A., Mikkelsen, R.F., Stoklund Larsen, T., Fjelstrup, T., Lomholt, A.K., Boehm, L., Schlipf, D., Azcona Armendariz, J., Cheng, P.W., 2017, "The Triple Spar Campaign: Implementation and Test of a Blade Pitch Controller on a Scaled Floating Wind Turbine Model", Energy Procedia, 14th Deep Sea Offshore Wind R&D Conference, EERA DeepWind'2017, 137 (October), pp 323–38.

Zhao, R., Creech, A.C.W., Borthwick, A.G.L., Nishino, T., Venugopal, V., 2020, "Numerical Model of a Vertical-Axis Cross-Flow Tidal Turbine", In ASME 2020 39th International Conference on Ocean, Offshore and Arctic Engineering.

The Quality Systems Group
Final Report and Recommendations to the 29th ITTC

1. GENERAL

1.1 Membership and Meetings

Benedetti, Lanfranco, CNR-INM (Secretary)
Chen, Weimin, SSSRI
Derradji-Aouat ,Ahmed, NRCC
Ferrando, Marco, Genova Univ. (Chair)
Grigoropoulos, Gregory, NTUA
Kitazawa, Daisuke, Tokyo University
Park, Joel, NSWCCD
Reed, Arthur M., NSWCCD
Sena Sales, Joel Jr., UFRJ
Valle, Jesus, CEHIPAR

As of August 8th 2019, Ahmed Derradji-Aouat Joined the Quality Systems Group

On September 1st 2020, Jesus Valle left the Quality Systems Group

The Group held four meetings as follows:

September 22nd 2017, Wuxi,
June 25th to 26th 2018, Madrid
September 2nd to 3rd 2019, Athens
February 20th to 21st 2020, Rome

From here on, in order to save space in the report, the Quality Systems Group will be addressed as QSG.

1.2 Terms of Reference given by the 29th ITTC to the QSG.

7. Update all ITTC Recommended Procedures and Guidelines to conform to the requirements of Recommended Procedure 4.2.3-01-03, Work Instruction for Formatting ITTC Recommended Procedures and Guidelines.
8. Support the Technical Committees in their work on Recommended Procedures. Supply the chairmen of the new committees with the MS Word versions of the relevant procedures.
9. Maintain the Manual of ITTC Recommended Procedures and Guidelines. Co-ordinate the modification and re-editing of the existing procedures according to the comments made by ITTC member organizations at the Conference and by the Technical Committees.
10. Observe the development or revision of ISO Standards regarding Quality Control.

11. Update the ITTC Symbols and Terminology List.
12. Update the ITTC Dictionary of Hydromechanics.
13. Revise and update the existing ITTC Recommended Procedures according to the comments of Advisory Council, Technical Committees and the Conference.
14. After the third AC Meeting, review and edit new ITTC Recommended Procedures with regard to formal Quality System requirements including format and compliance of the symbols with the ITTC Symbols and Terminology List.
15. Support the Technical Committees with guidance on development, revision and update of uncertainty analysis procedures.
16. Observe ISO standards for uncertainty analysis, in particular the uncertainty analysis terminology.
17. Review developments in metrology theory and uncertainty analysis and issue appropriate Procedures.
18. Continue to maintain the online Wiki keeping it up to date and in line with the adopted documents of the ITTC.
19. At the beginning of the period, organize an electronic repository of information and data on the benchmarks cases. ITTC member organizations should then be invited to participate in the adoption of the benchmark and contribute to the data-base.

2. TASKS PERFORMED

2.1 Update all ITTC Recommended Procedures and Guidelines to conform to the requirements of Recommended Procedure 4.2.3-01-03, Work Instruction for Formatting ITTC Recommended Procedures and Guidelines.

This task was performed during the 28th ITTC. Its insertion into the 29th QSG ToR is probably due to a “Cut and Paste” error in drafting 29th ITTC QSG ToR

2.2 Support the Technical Committees in their work on Recommended Procedures. Supply the chairmen of the new committees with the MS Word versions of the relevant procedures.

A total of 58 MS Word files containing the procedures to be updated, together with the template to be used for drafting new procedures was sent to the Chairmen of the various ITTC Committees.

QSG cooperated with 29th Conference Chairman to produce the template for Committee report to be distributed for the next Conference

2.3 Maintain the Manual of ITTC Recommended Procedures and Guidelines. Co-ordinate the modification and re-editing of the existing procedures ac-cording to the comments made by ITTC member organizations at the Conference and by the Technical Committees.

The revision of the Manual of ITTC Recommended Procedures and Guidelines included 84 documents:

- 9 existing procedures were deleted
- 13 new Procedures/Guidelines have been approved
- 62 existing procedures have been reviewed or updated.
- 125 disclaimers have been inserted in ITTC recommended Procedures and Guidelines as per Executive Committee request

- 82 equations in Recommended Procedures and Guidelines have been translated from the old MathType format to the MS Word equation editor format.

During the activity connected with this ToR the QSG realized that a number of procedures need further revision; especially when dealing with UA. Some procedures require extensive updates to conform to BIPM (2008) GUM. Some procedures still refer to the ISO GUM.

A proposal for future work has been added to this effect.

The table of "revision outcomes" is illustrated in Appendix A.

2.4 Observe the development or revision of ISO Standards regarding Quality Control.

QSG reviewed the current work of the ISO Technical Committees (TC) and Sub-Committees (SC), and established a list of those Working Groups (WG) which are working on items within the scope of ITTC. Eleven relevant documents were under preparation by ISO/TC008 ("Ships and marine technology"), one by ISO/TC043 ("Acoustics") and three by ISO/TC188 ("Small craft"). To be more specific, the following ISO documents under preparation may take into account uncertainty:

ISO/TC 008/SC 02 "Marine environment protection"
ISO/TC 008/SC 02/WG 03 "Environmental response"
ISO/TC 008/SC 02/WG 05 "Anti-fouling systems on ships"
ISO/TC 008/SC 02/WG 08 "Shaft power measurement for ships"
ISO/TC 008/SC 02/WG 11 "Ships' energy efficiency data collection"
ISO/TC 008/SC 06 "Navigation and ship operations"
ISO/TC 008/SC 06/WG 17 "Speed trial data analysis"
ISO/TC 008/SC 08/WG 14 "Propeller"
ISO/TC 008/SC 08/WG 20 "Antifouling paints"
ISO/TC 008/SC 08/WG 23 "Buoyancy support system"
ISO/TC 008/SC 12 "Ships and marine technology - Large yachts"
ISO/TC 008/SC 12/WG 05 "Quality assessment and acceptance criteria"
ISO/TC 008/SC 13 "Marine technology"
ISO/TC 008/SC 13/WG 01 "Submersibles"
ISO/TC 008/WG 09 "Polar (Arctic/Antarctic) regions"

There are another 66 ISO/WG working on Uncertainty Analysis on procedures not directly associated with ITTC scope of interest.

2.5 Update the ITTC Symbols and Terminology List.

As regards the Symbols & Terminology List QSG decided to start a systematic check to be

sure that symbols used in the standing procedures are contained in the S&T List.

The documents belonging to the following sections of the Register have been checked for symbol usage:

- 7.5-02-01
- 7.5-02-02
- 7.5-02-03
- 7.5-02-04
- 7.5-02-05
- 7.5-02-06
- 7.5.02-07-01
- 7.5-02-07-03

A total of 70 documents have been checked. The result of the check has been disappointing, since many documents make use of symbols not included into the Symbols and Terminology list or of incorrect symbols with respect to those included in the List.

The observations regarding symbols have been sent to the relevant committees requesting action to rectify this situation.

Changes made to the Symbols & Terminology List are as follows:

- The definition of C_{DA} has been updated following an AC suggestion.
- *Hw1/3, Hw1/3d, Hw1/3u* need to be checked against the procedures and eventually deleted as non-necessary symbols. The new symbols will be: $H_{w1/3}$, $H_{1/3w}$ (for waves) and $H_{1/3s}$ (swells), in procedure 7.5-04-01-01.1.
- The left-hand coordinate axes system has been removed from the Symbols and Terminology List.
- Several other symbols have been added, including: Linear momentum (**P**) and Angular momentum (**L**).
- A number of new symbols have been added according to a Resistance and Propulsion Committee proposal.

2.6 Update the ITTC Dictionary of Hydromechanics.

A new section has been developed and added to the ITTC Dictionary of Hydrodynamics, it is: Offshore Engineering. This initial version of the new section has focused on offshore oil and gas production, all from the perspective of hydrodynamics—those platforms, vessels and components for which model testing and/or performance related calculations would be performed. Those components for which no hydrodynamic issues or requirements would be expected (e.g., blowout preventers) are not included, which is not to say that these components are not critical parts of the entire system.

The Offshore Engineering additions start with a definition of offshore platforms, in general and specifically those related to oil and gas drilling and production. It then contains definitions and descriptions of various types of drilling platforms, fixed and mobile (Fixed Platforms, Compliant Towers, Jack-up rigs, Mobile Offshore Drilling Units, (MODUS), Semi-submersible drilling units, Drill ships and Ultradeep water drilling units). It then presents the various systems used for production (Gravity-based structure (GBS); Tension Leg Platform—Conventional, New Generation; Semisubmersible floating production units (semi-FPU); Spar Platforms—Classic, Truss, Cell, Mini-Doc; Floating production systems (FPS); Floating, production, storage and offloading (FPSO) vessels—Shipshape, circular; and Floating liquefied natural gas (FLNG) vessels), and specialty vessels, particularly Anchor Handler Vessels (AHV) and Anchor Handling Tug Supply Vessels (AHTS). Illustrations or photographs are provided for many of many of the above platforms and vessels.

The contributions to the new section end with specific components involved in offshore

platforms and some of the performance issues that they may experience. The particular components included are: Risers, Strakes, Bottom Templates or Guides, and Mooring systems. The particular issues particular to offshore platforms are Vortex induced vibration (VIV) and Vortex Induced motion (VIM).

2.7 Revise and update the existing ITTC Recommended Procedures according to the comments of Advisory Council, Technical Committees and the Conference.

The QSG updated 8 documents, as listed in Appendix C.

The following 11 documents were reviewed:

- 4.2.3-01-01 — Guide for the Preparation of ITTC Recommended Procedures
- 4.2.3-01-03 — Work Instruction for formatting ITTC Recommended Procedures and Guidelines
- 7.5-02-01-06 — Determination of a type A uncertainty estimate of a mean value from a single time series measurement
- 7.5-02-01-07 — Guideline to Practical Implementation of Uncertainty Analysis
- 7.5-02-02-02 — General Guidelines for Uncertainty Analysis in Resistance Tests
- 7.5-02-02-02.1 — Example for Uncertainty Analysis of Resistance Tests in Towing Tanks
- 7.5-02-05-05 — Evaluation and Documentation of HSMV
- 7.5-02-06-04 — Uncertainty Analysis for Manoeuvring Predictions based on Captive Manoeuvring Tests
- 7.5-02-06-05 — Uncertainty Analysis for Free Running Model Tests
- 7.6-02-01 — Calibration of a Steel Ruler
- 7.6-02-08 — Calibration of Weights
- 7.6-02-09 — Calibration of Load Cells

As regards the outcome of the review:

4.2.3-01-01: this procedure did not contain a reference section and consequently has been updated.

4.2.3-01-03: this work instruction has been updated to correct minor errors and inconsistencies.

7.5-02-01-06: the first version of the document only included the equations for analog computations and the purposes of this revision was to include the equations for digital data processing. Martin van Rijsbergen, one of the original authors agreed to participate to the revision process. This procedure has been updated and includes the most recent recommendations of the Manoeuvring Committee.

7.5-02-01-07: Equations (9) and (12) have been corrected; data were correct in tables; a Central finite difference form was added as Equation (4); the Reference list has been updated

7.5-02-02-02: this guideline has been reviewed for consistency with guideline 7.5-02-02-02.1 and updated. Significant revisions have been made, and some editorial changes by the Resistance and Propulsion Committee were included. The following sections were added:

- Outlier and non-linear detection methods
- Force computation from mass loading for dynamometers in a calibration fixture
- Distinction between methods for confidence and prediction limits with relevant equations
- Running sinkage and trim
- List of symbols was added. A running sinkage and trim section was added.

7.5-02-02-02.1: The guideline has been reviewed for consistency with guideline 7.5-02-

02-02 and updated. The main changes are as follows:

- Force reported in Newton (N) rather than kilogram force (kgf)
- Uncertainty estimates in expanded uncertainty, *U*, rather than standard uncertainty, *u*.
- Sinkage and trim data processing equations with uncertainty analysis
- Equations for confidence and prediction limits
- List of symbols
- Reference list updated

For repeat tests, a distinction is made between confidence limit and prediction limit. An uncertainty estimate for a series of tests is computed from the standard deviation of the mean value. The uncertainty estimate for total resistance, R_T, is from the 95 % confidence limit

$$U_{\bar{R}_T} = k\, s_{R_T}/\sqrt{N} \tag{21}$$

where k is the coverage factor, s the computed standard deviation of N samples. For a small number of samples, the coverage factor k can be the Student-t distribution $t_{0.025,\, N\text{-}1}$ at the 95 % confidence level. However, if the uncertainty is applied to some future event such as an uncertainty estimate for a single sample from a previous estimate of the standard deviation or estimate at full-scale from model-scale, then the uncertainty from the prediction limit is

$$U = ks\sqrt{1 + 1/N} \tag{22}$$

or for a large number of samples at the 95 % prediction limit $U = 2s$.

7.5-02-05-05: this procedure was updated regarding symbols usage. The revision number remains 02 and the date of approval 2014.

7.5-02-06-04: this procedure has been reviewed by QSG as regards format issues. The updated document has been forwarded to the Manoeuvring Committee for further review.

7.5-02-06-05: this procedure has been reviewed and updated by QSG as regards format issues. The updated document has been forwarded to the Manoeuvring Committee for further review.

7.6-02-01: After a long discussion QSG reconsidered its proposal to review the document. Considering that UA procedures prescribe traceability to a National Metrology Laboratory, internal calibration of steel rulers cannot be used anymore. To this effect, QSG proposed to delete the document. That proposal has been rejected by the AC, which asked QSG to prepare a procedure on the internal calibration of steel rulers or a practical way to check length measurement devices in towing tanks.

QSG did not manage to produce this document in time and this task has been inserted into the Recommendations for Future Work

7.6-02-08: This working instruction has been updated with modifications for consistency with other documents. The minimum tolerance for weights was changed to OIML Class M_2.

7.6-02-09: This working instruction has been greatly simplified. A calibration example is included that compares random to sequential loading of weights on a calibration stand. The following equation is included for the conversion of mass in kg to force in N.

$$F = mg(1 - \rho_A/\rho_M) \tag{23}$$

where m is the mass in kg, g is local acceleration of gravity in m/s^2, ρ_A is air density, and ρ_M is the density of the weight in kg/m^3. The nominal values for Equation (23) are as follows:

g	9.80665 m/s^2 for standard gravity
ρ_A	1.2 kg/m^3
ρ_M	8000 kg/m^3

Local gravity is typically less than standard gravity. The last term in Equation (23) is an air buoyancy correction from Archimedes principle and is typically 0.017 %. The mass in Equation (23) is the sum of the weights added to the calibration stand.

$$m = \sum_{i=1}^{n} m_i \tag{24}$$

If the tolerance of the weights is applied as the uncertainty estimate, the uncertainty is the tolerance of the total mass, *m*.

The procedure also includes an example for the comparison of sequential loading to random loading. An example of the loading is given in Figure 196.

The calibration result is presented in Figure 197 as a residual plot. By a hypothesis test, the calibration constants are statistically the same for the two methods, but the uncertainty is significantly less by the random method.

2.8 After the third AC Meeting, review and edit new ITTC Recommended Procedures with regard to formal Quality System requirements including format and compliance of the symbols with the ITTC Symbols and Terminology List.

The QSG review process regarded 56 existing and 13 new procedures adding to a total of 69 documents, as illustrated in Appendix B.

The document 0.0 Register has been updated accordingly.

A template in word format has been prepared to write new procedures during the next ITTC period. To write a new procedure, an author will open the new file with the following template: ProcTemplate.dotx. The file will be available on the ITTC Web site.

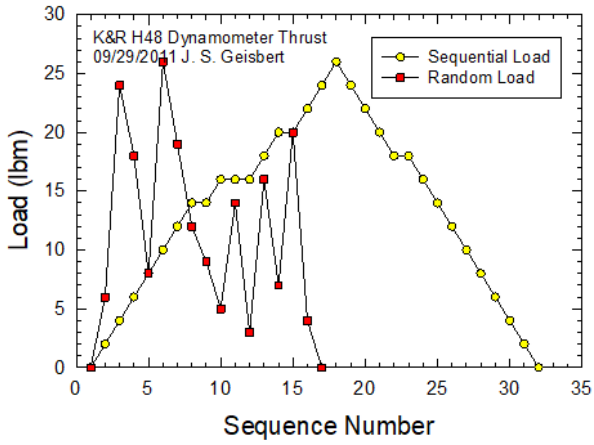

Figure 196. Loading sequence for Kempf & Remmers H48 dynamometer in thrust.

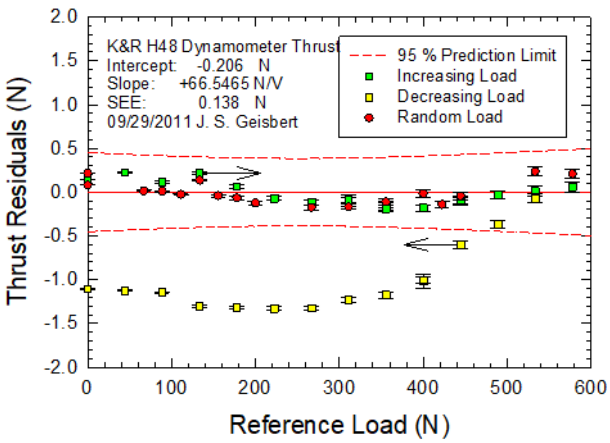

Figure 197. Calibration data for Kempf & Remmers H48 dynamometer in thrust.

2.9 Support the Technical Committees with guidance on the development, revision and update of uncertainty analysis procedures.

QSG liaised with Stability in Waves committee on the revision of procedures 7.5-02-07-04.3, 7.5-02-07-04.4, 7.5-02-07-04.5, their proposed change of formulation in ITTC Procedure 7.5-03-02-03, Practical Guidelines for ship CFD application, and the development of new ITTC Procedures: Inclining Tests, and Extrapolation for direct assessment stability in waves

7.5-02-01-06; Manoeuvring Committee supplied a revised version for QSG check

QSG assisted the Ocean Engineering Committee on the uncertainty analysis of a benchmark test.

2.10 Observe ISO standards for uncertainty analysis, in particular the uncertainty analysis terminology.

The responsibility for the ISO Guide to the Uncertainty in Measurement (GUM) is now the Bureau International des Poids et Mesures (BIPM). The focus in the future should be with BIPM not ISO. The Joint Committee for Guides in Metrology (JCGM) within BIPM is now tasked with the GUM. JCGM is divided into two working groups as follows:

- Working Group on the Expression of Uncertainty in Measurement (JCGM-WG1: GUM)
- Working Group on the International Vocabulary of Metrology (JCGM-WG2: VIM)

Each working group meets twice per year.

The following are the documents issued by WG1:

- JCGM 100:2008, "Evaluation of measurement data—Guide to the expression of uncertainty in measurement," GUM 1995 with minor corrections
- JCGM 101:2008, "Evaluation of measurement data—Supplement 1 to the 'Guide to the expression of uncertainty in measurement'—Propagation of distributions using a Monte Carlo method"
- JCGM 102:2011, "Evaluation of measurement data—Supplement 2 to the 'Guide to the expression of uncertainty in measurement'—Extension to any number of output quantities"
- JCGM 103:2020, "Evaluation of measurement data—Concepts and basic principles," in review
- JCGM 104:2009, "Evaluation of measurement data – An introduction to the 'Guide to the expression of uncertainty in measurement' and related documents"
- JCGM 106:2012, "Evaluation of measurement data—The role of measurement uncertainty in conformity assessment"

The following will be developed in the future:

- JCGM 107, "Applications of the least-squares method"
- JCGM 108, "Bayesian methods"
- JCGM 109, "Statistical Models and Data Analysis for Inter-Laboratory Studies (with application to Key Comparisons)"
- JCGM 110, "Examples of uncertainty evaluation"

A revision to the GUM was circulated at the end of 2014. After a rejection of the draft revision, the effort is now focused on the development of the supplements to the GUM. The current version of the VIM is version 3: JCGM 200:2012, "International vocabulary of metrology—Basic and general concepts and associated terms (VIM)." WG2 anticipates publishing version 4 in the near future. The web page for JCGM is as follows: https://www.bipm.org/en/committees/jc/jcgm/ .

2.11 Review developments in metrology theory and uncertainty analysis and issue appropriate Procedures.

On 20 May 2019, a new International System of Units (SI) was adopted. Details are described in Bureau International des Poids et Mesures (BIPM). The new logo for SI units is in Figure 198, which consists of seven constants,

and the following definitions are from BIPM (2019).

"The definitions below specify the exact numerical value of each constant when its value is expressed in the corresponding SI unit. By fixing the exact numerical value the unit becomes defined, since the product of the ***numerical value*** and the ***unit*** has to equal the ***value*** of the constant, which is postulated to be invariant.

The seven constants are chosen in such a way that any unit of the SI can be written either through a defining constant itself or through products or quotients of defining constants.

The International System of Units, the SI, is the system of units in which

- the unperturbed ground state hyperfine transition frequency of the caesium 133 atom $\Delta\nu_{Cs}$ is 9 192 631 770 Hz,
- the speed of light in vacuum c is 299 792 458 m/s,
- the Planck constant h is $6.626\,070\,15 \times 10^{-34}$ J s,
- the elementary charge e is $1.602\,176\,634 \times 10^{-19}$ C,
- the Boltzmann constant k is $1.380\,649 \times 10^{-23}$ J/K,
- the Avogadro constant N_A is $6.022\,140\,76 \times 10^{23}$ mol^{-1},
- the luminous efficacy of monochromatic radiation of frequency 540×10^{12} Hz, K_{cd}, is 683 lm/W,

where the hertz, joule, coulomb, lumen, and watt, with unit symbols Hz, J, C, lm, and W, respectively, are related to the units second, metre, kilogram, ampere, kelvin, mole, and candela, with unit symbols s, m, kg, A, K, mol, and cd, respectively, according to Hz = s^{-1}, J = kg m^2 s^{-2}, C = A s, lm = cd m^2 m^{-2} = cd sr, and W = kg m^2 s^{-3}." Since the numerical values are exact, no uncertainty is associated with these values.

The web page for BIPM and the new standard for SI units is as follows:

https://www.bipm.org/en/measurement-units/ .

Two tools are available for the computation of uncertainty estimates, which are based on the GUM, JCGM (2008) and include the Monte Carlo method. The first is located on the National Physical Laboratory (NPL) web page: https://www.npl.co.uk/resources/software/measurement-uncertainty-evaluation . The software consists of MATLAB routines that are downloaded from the web page. NPL is the National Metrology Institute (NMI) of the United Kingdom (UK). The user manual is included in the software.

Figure 198. BIPM logo for SI units.

The second is on-line software at the National Institute of Standards and Technology (NIST), the NMI of the USA. The web page for the NIST Uncertainty Machine is as follows: https://uncertainty.nist.gov/. Lafarge and Possolo (2018) is the latest version of the user's manual.

The NIST web page also includes an on-line Engineering Statistics Handbook. That web page is as follows and was last updated October

2013: https://www.itl.nist.gov/div898/handbook/ .

The journal Metrologia is published by IOP Science for BIPM. Metrologia should be reviewed for articles on uncertainty analysis. The American Society of Mechanical Engineers (ASME) also a journal dedicated to uncertainty analysis and verification and validation (V&V), Journal of Verification, Validation, and Uncertainty Quantification. The first issue was published in March 2016.

ASME continues to host an annual "Verification and Validation Symposium". The first was in Las Vegas, Nevada, on 2-4 May 2012. Presentations are accepted on the basis of an abstract. No technical papers are published, but presentations are available on the ASME conference web page.

ASME has also published two standards related to uncertainty analysis. ASME V&V 20-2009 is one of the more detailed documents on the application of V&V to computational fluid dynamics (CFD). ASME PTC 19.1-2018 is on test uncertainty and is compatible with the GUM, JCGM (2008).

A value of the local acceleration of gravity is necessary for the calculation of force in a calibration stand from mass per Equation (23). Previously, a global tool was available for the computation of local gravity at the Physikalisch-Technische Bundesanstalt (PTB), Braunschweig, Germany, but that on-line calculation tool is no longer available. PTB provides a link another calculation tool, but it is applicable only to locations within Germany. That calculation tool is located at Bundesamt für Kartographie und Geodäsie (BKG) in Frankfurt, Germany, on the following web page: http://gibs.bkg.bund.de/geoid/gscomp.php?p=s. The input parameters are latitude and longitude in degrees and elevation in metres.

The USA has a similar web page at the National Geodetic Survey (NGS) as follows: https://geodesy.noaa.gov/cgi-bin/grav_pdx.prl. The default elevation for NSWCCD in that tool is 78.95 m. Another tool, which provides the elevation from the latitude and longitude, yields an elevation of 40 m, and different value in local gravity is obtained. The NGS tool also provides an uncertainty estimate. Elevation is determined from the address in the following web page globally: https://elevation.maplogs.com/. When a laboratory is located on the GPS map, the latitude and longitude may be adjusted for a location within the facility.

Another tool, which appears to provide international data, is at the Bureau Gravimétrique International (BGI), Toulouse, France. That web page is as follows: http://bgi.obs-mip.fr/data-products/outils/prediction-of-gravity-value/ . It does not provide data for CSSRC. A comparison of the values of local gravity, g, is summarized in Table 30 for example ITTC laboratories by the different tools. The PTB values in the table are from ITTC (2017), Table 1.

As a final note, the QSG observes that the ITTC focuses on uncertainty, while neglecting the incorporation of confidence bands in the results from committees dealing with stochastic processes. The size of the confidence bands will in general be significantly larger than the uncertainty bounds. And half or more (if the Manoeuvring Committee is dealing with manoeuvring in waves) of the General Committees are working with stochastic processes.

2.12 Continue to maintain the online Wiki keeping it up to date and in line with the adopted documents of the ITTC.

In ITTC (2011), when the ITTC-wiki was established, some positive feedbacks visits and returning visitors were counted, as time has

passed, the level of feedback has been continuously decreasing. The thrust of the wiki tool has been to build, refine and review concepts and notions around the definitions contained in the Dictionary of Hydromechanics through collective knowledge. However, because the content of the Dictionary of Hydromechanics is endorsed by the Conference such interactions and modification of the wiki tool were quite limited, defeating the wiki approach. Furthermore, the Wiki server was down for various technical problems during most of the period between the two ITTC conferences.

In view of the abovementioned considerations it is proposed to discontinue the wiki tool and to maintain the Dictionary updated, maintained and furtherly expanded as necessary; and freely available for download on the ITTC website.

2.13 At the beginning of the period, organize an electronic repository of information and data on the benchmarks cases. ITTC member organizations should then be invited to participate in the adoption of the benchmark and contribute to the data-base.

The ITTC web page now contains a link to the Benchmark repository.

The data structure to host data pertaining to benchmarks was defined during the 26th ITTC and is illustrated in Figure 199.

According to the 29th QSG TOR, one task is to organize an electronic repository of information and data on the benchmark cases at the beginning of the period. Then, ITTC member organizations shall be invited to participate in the adoption of the benchmarks and contribute to the database.

To date, the work of 29th QSG has been to review the benchmarks and their data as much as possible. After discussing with relative technical committee members and ITTC community, the frequently used benchmarks are listed in Table 31. As the survey has only engaged with a small part of ITTC community, and information has been collected from several conference websites, QSG would like to describe the situation at the current time.

Table 32 shows the sources of the benchmarks and their applications, including the website and conference name. Some of the benchmarks are somewhat obsolete, however, others are still widely referenced. Data cleaning and data sorting needs to be performed in the future. This work should be performed together with the relevant technical committee.

Take the 'KCS' from Tokyo 2015 A Workshop on CFD in Ship Hydrodynamics as an example, it is describe as following.

"The KCS was conceived to provide data for both explication of flow physics and CFD validation for a modern container ship with a bulbous bow (i.e., ca. 1997). The Korea Research Institute for Ships and Ocean Engineering (KRISO) performed towing tank experiments to obtain resistance, mean flow data and free surface waves (Van et al, 1998a,b, Kim et al, 2001). Self propulsion tests were carried out at the Ship Research Institute (now NMRI) in Tokyo and are reported in the Proceedings of the CFD Workshop Tokyo in 2005 (Hino, 2005). Later, resistance tests were also reported by NMRI (See Zou and Larsson, 2014). Data for pitch, heave, and added resistance are available from Force/Dmi measurements reported in Simonsen et al. (2008)."

The keywords is "Resistance Test, Self-propulsion test, Added resistance test, CFD simulation", and manoeuvring as well as SIMMAN.

Therefore, QSG would like to setup a questionnaire to all the ITTC committees at the start of the next term to obtain the definition, objective, data format and other information of the various benchmarks.

Many of the technical committees are engaged in collecting benchmarks. Therefore, an inter-committee liaison mechanism shall be established to communicate the demands and application of benchmarks, as well as the data sources. The QSG shall be involved in this organization, and will establish a standard format for the use of all the ITTC committees and community.

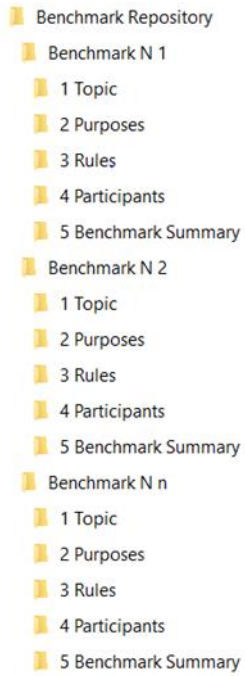

Figure 199. Benchmark Repository data structure.

Table 30. Comparison of local gravity for Example ITTC laboratories.

ITTC Laboratory	**Elevation (m)**	**Acceleration of Gravity, g (m/s²)**			
		BGI	**BKG**	**NGS**	**PTB**
AMC, Newnham, TAS, Australia	21.0	9.80282			
CSSRC, Wuxi, China	5.0				9.79439
HSVA, Hamburg, Germany	13.0	9.81378	9.80378		
CNR-INM, Rome, Italy	55.0	9.80347			
NSWCCD, Bethesda, MD, USA	41.2 40.0	9.80112		9.80108	9.80106

Table 31. Benchmark data used in technical fields.

Fields	**KCS**	**JBC**	**ONRT**	**DTC**	**DTMB 5415**	**KVLCC 1**	**KVLCC 2**
Resistance and Propulsion	●	●				●	●
Maneuvering			●	●	●	●	●
Seakeeping	●					●	●
Ocean Engineering							
Stability in Waves			●	●			

Notes: the information is collected from several conference website, needed to be updated

Table 32. Benchmark data used in technical fields.

	website	Conference
KCS	http://www.t2015.nmri.go.jp/kcs.html	Tokyo 2015 A Workshop on CFD in Ship Hydrodynamics
JBC	https://t2015.nmri.go.jp/jbc.html	Tokyo 2015 A Workshop on CFD in Ship Hydrodynamics
ONRT	https://t2015.nmri.go.jp/onrt.html	Tokyo 2015 A Workshop on CFD in Ship Hydrodynamics
DTC	http://www.mashcon2019.ugent.be/EN/mashcon2019_call_EN.htm	5th International Conference on Ship Manoeuvring in Shallow and Confined Water
dtmb 5415	https://simman2014.dk/ship-data/us-navy-combatant/	SIMMAN 2014
KVLCC 1	http://www.simman2008.dk/KVLCC/KVLCC1/tanker1.html	SIMMAN 2008
KVLCC 2	https://simman2014.dk/ship-data/moeri-kvlcc2-tanker/	SIMMAN 2014
Series	http://www.shipstab.org/index.php/data-access (needs register)	International Ship Stability Workshop

So far, the benchmark is mostly focused on model scale. However, due to the future demand from several technical committees and research from the community, full-scale benchmarks are also of great interest.

3. CONCLUSIONS

The format of S.I. units should be considered with a view to achieving consistency with respect to the use of a multiplication symbol when referring to sub-units, such as when referring to milliseconds, ms versus meter seconds, m s (separated by a hard space (Ctrl+Shift+space) or by a half-high center dot).

It is necessary to complete the list of symbols used for Uncertainty Analysis.

A new section addressing new techniques such as ASME Validation and Verification methodology should be added to procedure 7.5-02-01-01 Guide to the Expression of Uncertainty in Experimental Hydrodynamics.

Consideration should be given by the Conference to new emerging technologies in artificial intelligence (such as machine learning techniques) with respect to data quality assessment.

Consideration should be given by the Conference to further development of liaison with International Ship and Offshore Structures Congress (ISSC) for the purpose harmonization and common understanding of the state of the art in Uncertainty Analysis.

QSG noted that many procedures do not comply with the format required by 4.2.3-01-01 Guide for the Preparation of ITTC Recommended Procedures, in particular many documents do not include the sections:

3. PARAMETERS; SYMBOLS

3.1 parameters to be taken into account,

3.2 recommendations of ITTC for parameters if there are any (e.g. friction line 57).

An effort should be made to resolve this inconsistency.

4. RECOMMENDATIONS TO THE CONFERENCE

The QSG recommends to the Full Conference to:

Adopt the revised procedures and guidelines and work instructions:

- 4.2.3-01-01 – Guide for the Preparation of ITTC Recommended Procedures.
- 4.2.3-01-03 – Work Instruction for Formatting ITTC Recommended Procedures
- 7.5-02-01-06 – Determination of a type A uncertainty estimate of a mean value from a single time series measurement
- 7.5-02-01-07 – Guideline to Practical Implementation of Uncertainty Analysis
- 7.5-02-02-02 – General Guidelines for Uncertainty Analysis in Resistance Tests
- 7.5-02-02-02.1 – Example for Uncertainty Analysis of Resistance Tests in Towing Tanks
- 7.6-02-08 – Calibration of Weights
- 7.6-02-09 – Calibration of Load Cells

Adopt the revised Symbols and Terminology List Version 2021;

Adopt the revised ITTC Dictionary of Hydromechanics Version 2021;

5. RECOMMENDATIONS FOR FUTURE WORK

The following future work is recommended:

20. Support the Technical Committees in their work on Recommended Procedures. Supply the chairmen of the new committees with the MS Word versions of the relevant procedures.
21. Maintain the Manual of ITTC Recommended Procedures and Guidelines. Co-ordinate the modification and re-editing of the existing procedures according to the comments made by ITTC member organizations at the Conference and by the Technical Committees.
22. After the third AC Meeting, review and edit new ITTC Recommended Procedures and Guidelines with regard to formal Quality System requirements including format and compliance of the symbols with the ITTC Symbols and Terminology List.
23. Revise and update existing ITTC Recommended Procedures according to the comments of Advisory Council, Technical Committees and the Conference.
24. Prepare a procedure on the internal calibration of steel rulers or a practical way to check length measurement devices in towing tanks.
25. Introduce New Uncertainty Analyses Guidelines to include data anomalies in Machine Learning Algorithms for Autonomous and Intelligent ships.
26. Update ITTC procedures and Guidelines still referring to the ISO GUM to conform to BIPM (2008) GUM
27. Observe the development or revision of ISO Standards regarding Quality Control.
28. Update the ITTC Symbols and Terminology List.
29. Update the Uncertainty Analysis section of the Symbols & Terminology List.
30. Update the ITTC Dictionary of Hydromechanics.
31. Expand the content of current ITTC dictionary version, considering CFD, MASS, etc.
32. Support the Technical Committees with guidance on development, revision and update of uncertainty analysis procedures.
33. Support the Technical Committees dealing with stochastic processes with guidance on development, revision and update of procedures for the inclusion of confidence bands on their computational and experimental results.
34. Observe BIPM/JCGM standards for uncertainty analysis, in particular the uncertainty analysis terminology.
35. Review developments in metrology theory and uncertainty analysis and issue appropriate Procedures.
36. Setup an effective way to collect benchmark data.
37. Upload all the collected and verified benchmark data into the ITTC benchmark data repository
38. Liaise with relative technical committees to complete a questionnaire about the demand and use of benchmarks, not be limited in model scale
39. Cooperate with Technical Committees to establish the ITTC benchmarks, including definition, raw data, data format, etc.

Appendix A. OUTCOME OF THE MANUAL OF ITTC RECOMMENDED PROCEDURES AND GUIDELINES MAINTENANCE.

New/ Rev./ Del	Number	P /G	Title	Effective Date
R	1.0-06	G	Guidelines for ITTC Conference Organisers	2021
R	4.2.3-01-01	P	Guide for the Preparation of ITTC Recommended Procedures	2021
R	4.2.3-01-03	W	Work Instruction for Formatting ITTC Recommended Procedures	2021
D	7.5-02-01-05	G	(Model-Scale Propeller Cavitation Noise Measurements) Moved to 7.5-02-03-03.9	2021
R	7.5-02-01-06	P	Determination of a type A uncertainty estimate of a mean value from a single time series measurement	2021
R	7.5-02-01-07	G	Guideline to Practical Implementation of Uncertainty Analysis	2021
R	7.5-02-02-01	P	Resistance Tests	2021
R	7.5-02-02-02	G	General Guidelines for Uncertainty Analysis in Resistance Tests	2021
R	7.5-02-02-02.1	G	Example for Uncertainty Analysis of Resistance Tests in Towing Tanks	2021
R	7.5-02-02-02.2	G	Practical Guide for Uncertainty Analysis of Resistance Measurements in Routine Tests	2021
N	7.5-02-02-04		Wave Profile Measurement and Wave Pattern Resistance Analysis	2021
R	7.5-02-03-01.1	P	Propulsion/ Bollard pull Test	2021
D	7.5-02-03-01.2	P	(Uncertainty Analysis Example for Propulsion Test) Deleted	2021
R	7.5-02-03-01.3	PC	Podded Propulsor Tests and Extrapolation	2021
R	7.5-02-03-01.4	P	1978 ITTC Performance Prediction Method	2021
R	7.5-02-03-01.7	P	Performance Prediction Method for Unequally Loaded, Multiple Propeller Vessels	2021
R	7.5-02-03-01.8	G	Scaling Method for ship wake fraction with pre-swirl devices	2021
R	7.5-02-03-02.1	P	Open Water Test	2021
D	7.5-02-03-02.2	P	(Uncertainty Analysis, Example for Open Water Test) Deleted	2021
R	7.5-02-03-03.9	G	Model-Scale Propeller Cavitation Noise Measurements	2021
R	7.5-02-04-01	G	General Guidance and Introduction to Ice Model Testing	2021
R	7.5-02-04-02	P	Test Methods for Model Ice Properties	2021
R	7.5-02-04-02.3	PC	Manoeuvring Tests in Ice	2021
R	7.5-02-04-03	G	Guidelines for Modelling of Complex Ice Environments	2021
R	7.5-02-05-04	P	Seakeeping Tests	2021

R	7.5-02-05-06	P	Structural Loads	2021
D	7.5-02-05-07	P	(Dynamic Instability Tests) Withdrawn	2021
R	7.5-02-06-01	P	Free Running Model Tests	2021
R	7.5-02-06-02	P	Captive Model Test Procedure	2021
R	7.5-02-06-03	P	Validation of Manoeuvring Simulation Models	2021
R	7.5-02-06-04	P	Uncertainty Analysis for manoeuvring predictions based on captive manoeuvring tests	2021
R	7.5-02-06-05	G	Uncertainty Analysis for free running model tests	2021
N	7.5-02-06-06	G	Benchmark Data for Validation of Manoeuvring Predictions	2021
N	7.5-02-06-07	G	Captive Model Test for Underwater Vehicles	2021
R	7.5-02-07-01.2	G	Laboratory Modelling of Waves	2021
D	7.5-02-07-01.3	G	(Guidelines for Modelling of Complex Ice Environments) Moved to 7.5-02-04-03	2021
N	7.5-02-07-01.5	G	Laboratory Modelling of Wind	2021
N	7.5-02-07-01.6	G	Laboratory Modelling of Currents	2021
R	7.5-02-07-02.1	P	Seakeeping Experiments	2021
R	7.5-02-07-02.2	P	Predicting of Power Increase in Irregular Waves from Model Tests	2021
R	7.5-02-07-02.3	P	Experiments on Rarely Occurring Events	2021
R	7.5-02-07-02.5	P	Verification and Validation of Linear and Weakly Nonlinear Seakeeping Computer Codes	2021
R	7.5-02-07-02.6	P	Global Loads Seakeeping Procedure	2021
R	7.5-02-07-02.7	P	Sloshing Model Tests	2021
R	7.5-02-07-02.8	P	Calculation of the weather factor fw for decrease of ship speed in waves	2021
R	7.5-02-07-03.1	P	Floating Offshore Platform Experiments	2021
R	7.5-02-07-03.2	P	Analysis Procedure for Model Tests in Regular Waves	2021
D	7.5-02-07-03.4	P	(Active Hybrid Model Tests of Floating Offshore Structures with Mooring Lines) Deleted	2021
R	7.5-02-07-03.5	P	Passive Hybrid Model Tests of Floating Offshore Structures with Mooring Lines	2021
R	7.5-02-07-03.6	P	Dynamic Positioning System Model Test Experiments	2021
R	7.5-02-07-03.7	G	Wave Energy Converter Model Test Experiments	2021
R	7.5-02-07-03.8	P	Model Tests for Offshore Wind Turbines	2021
R	7.5-02-07-03.9	P	Model Tests for Current Turbines	2021
R	7.5-02-07-03.10	G	Guideline for VIV Testing	2021
R	7.5-02-07-03.11	G	Guideline for Model Tests of Stationary Multi-Bodies Operating in Close Proximity	2021
R	7.5-02-07-03.12	G	Uncertainty Analysis for a Wave Energy Converter	2021
R	7.5-02-07-03.13	G	Guideline for VIM Testing	2021

R	7.5-02-07-03.14	P	Analysis Procedure of Model Tests in Irregular Waves	2021
R	7.5-02-07-03.15	G	Uncertainty analysis - Example for horizontal axis turbines	2021
N	7.5-02-07-03.16	G	Model Construction of Offshore Systems	2021
N	7.5-02-07-03.17	G	Uncertainty Analysis for Model Testing of Offshore Wind Turbines	2021
N	7.5-02-07-03.18	G	Practical guidelines for numerical modelling of wave energy converters	2021
R	7.5-02-07-04.3	G	Predicting the Occurrence and Magnitude of Parametric Rolling	2021
R	7.5-02-07-04.4	P	Simulation of Capsize Behaviour of Damaged Ships in Irregular Beam Seas	2021
R	7.5-02-07-04.5	P	Estimation of Roll Damping	2021
N	7.5-02-07-04.6	P	Extrapolation for Direct Stability Assessment in Waves	2021
N	7.5-02-07-04.7	P	Inclining Tests	2021
R	7.5-03-01-01	P	Uncertainty Analysis in CFD, Verification and Validation Methodology and Procedures	2021
R	7.5-03-01-02	G	Quality Assurance in Ship CFD Applica-tion	2021
D	7.5-03-01-03	P	(CFD User's Guide) Deleted	2021
D	7.5-03-01-04	P	(CFD Verification) Deleted	2021
R	7.5-03-02-02	P	Benchmark Database for CFD Validation for Resistance and Propulsion	2021
R	7.5-03-02-04	G	Practical Guidelines for Ship Resistance CFD	2021
N	7.5-03-02-05	G	Use of CFD methods to calculate wind resistance coefficient	2021
R	7.5-03-04-01	G	Guideline on Use of RANS Tools for Manoeuvring Prediction	2021
R	7.5-03-04-02	G	Validation and Verification of RANS Solutions in the Prediction of Manoeuvring Capabilities	2021
R	7.5-04-01-01.1	P	Preparation, Conduct and Analysis of Speed/Power Trials	2021
R	7.5-04-02-01	P	Full Scale Manoeuvring Trials Procedure	2021
N	7.5-04-02-02	G	UV Full Scale Manoeuvring Trials	2021
R	7.5-04-04-01	G	Underwater Noise from Ships, Full Scale Measurements	2021
R	7.5-04-05-01	G	Guideline on the determination of model-ship correlation factors	2021
D	7.6-02-01	W	Calibration of Steel Rulers	2021
R	7.6-02-08	W	Calibration of Weights	2021
R	7.6-02-09	W	Calibration of a Load Cells	2021

Appendix B. Recommended Procedures and guidelines reviewed with regard to formal Quality System requirements

Procedure No.	Procedure title	Committee
1.0-06	Guidelines for ITTC Conference Organisers	EC
7.5-02-02-01	Resistance Tests	R&P
7.5-02-02-02	General Guidelines for Uncertainty Analysis in Resistance Tests	R&P
7.5-02-02-02.1	Example for Uncertainty Analysis of Resistance Tests in Towing Tanks	R&P
7.5-02-02-02.2	Practical Guide for Uncertainty Analysis of Resistance Measurements in Routine Tests	R&P
7.5-02-02-04	Wave Profile Measurement and Wave Pattern Resistance Analysis	R&P
7.5-02-03-01.1	Propulsion/ Bollard pull Test	R&P
7.5-02-03-01.3	Podded Propulsor Tests and Extrapolation	R&P
7.5-02-03-01.4	1978 ITTC Performance Prediction Method	R&P
7.5-02-03-01.7	Performance Prediction Method for Unequally Loaded, Multiple Propeller Vessels	R&P
7.5-02-03-01.8	Scaling Method for ship wake fraction with pre-swirl devices	ESM
7.5-02-03-02.1	Open Water Test	R&P
7.5-02-03-03.9	Model-Scale Propeller Cavitation Noise Measurements	HN
7.5-02-04-01	General Guidance and Introduction to Ice Model Testing	ICE
7.5-02-04-02	Test Methods for Model Ice Properties	ICE
7.5-02-04-02.3	Manoeuvring Tests in Ice	ICE
7.5-02-04-03	Guidelines for Modelling of Complex Ice Environments	ICE
7.5-02-05-04	Seakeeping Tests	SKC
7.5-02-05-06	Structural Loads	SKC
7.5-02-06-01	Free Running Model Tests	MAN
7.5-02-06-02	Captive Model Test Procedure	MAN
7.5-02-06-03	Validation of Manoeuvring Simulation Models	MAN
7.5-02-06-04	Uncertainty Analysis for manoeuvring predictions based on captive manoeuvring tests	MAN
7.5-02-06-05	Uncertainty Analysis for free running model tests	MAN
7.5-02-06-06	Benchmark Data for Validation of Manoeuvring Predictions	MAN
7.5-02-06-07	Captive Model Test for Underwater Vehicles	MAN
7.5-02-07-01.2	Laboratory Modelling of Waves	MEC
7.5-02-07-01.5	Laboratory Modelling of Wind	MEC
7.5-02-07-01.6	Laboratory Modelling of Currents	MEC
7.5-02-07-02.1	Seakeeping Experiments	SKC
7.5-02-07-02.2	Predicting of Power Increase in Irregular Waves from Model Tests	SKC
7.5-02-07-02.3	Experiments on Rarely Occurring Events	SKC
7.5-02-07-02.5	Verification and Validation of Linear and Weakly Nonlinear Seakeeping Computer Codes	SKC
7.5-02-07-02.6	Global Loads Seakeeping Procedure	SKC
7.5-02-07-02.7	Sloshing Model Tests	SKC
7.5-02-07-02.8	Calculation of the weather factor fw for decrease of ship speed in waves	SKC
7.5-02-07-03.1	Floating Offshore Platform Experiments	OEC
7.5-02-07-03.2	Analysis Procedure for Model Tests in Regular Waves	OEC

7.5-02-07-03.5	Passive Hybrid Model Tests of Floating Offshore Structures with Mooring Lines	OEC
7.5-02-07-03.6	Dynamic Positioning System Model Test Experiments	OEC
7.5-02-07-03.7	Wave Energy Converter Model Test Experiments	MRED
7.5-02-07-03.8	Model Tests for Offshore Wind Turbines	MRED
7.5-02-07-03.9	Model Tests for Current Turbines	MRED
7.5-02-07-03.10	Guideline for VIV Testing	OEC
7.5-02-07-03.11	Guideline for Model Tests of Stationary Multi-Bodies Operating in Close Proximity	OEC
7.5-02-07-03.12	Uncertainty Analysis for a Wave Energy Converter	MRED
7.5-02-07-03.13	Guideline for VIM Testing	OEC
7.5-02-07-03.14	Analysis Procedure of Model Tests in Irregular Waves	OEC
7.5-02-07-03.15	Uncertainty analysis - Example for horizontal axis turbines	MRED
7.5-02-07-03.16	Model Construction of Offshore Systems	OEC
7.5-02-07-03.17	Uncertainty Analysis for Model Testing of Offshore Wind Turbines	MRED
7.5-02-07-03.18	Practical guidelines for numerical modelling of wave energy converters	MRED
7.5-02-07-04.3	Predicting the Occurrence and Magnitude of Parametric Rolling	SIW
7.5-02-07-04.4	Simulation of Capsize Behaviour of Damaged Ships in Irregular Beam Seas	SIW
7.5-02-07-04.5	Estimation of Roll Damping	SIW
7.5-02-07-04.6	Extrapolation for Direct Stability Assessment in Waves	SIW
7.5-02-07-04.7	Inclining Tests	SIW
7.5-03-01-01	Uncertainty Analysis in CFD, Verification and Validation Methodology and Procedures	R&P
7.5-03-01-02	Quality Assurance in Ship CFD Applica-tion	R&P
7.5-03-02-02	Benchmark Database for CFD Validation for Resistance and Propulsion	R&P
7.5-03-02-04	Practical Guidelines for Ship Resistance CFD	R&P
7.5-03-02-05	Use of CFD methods to calculate wind resistance coefficient	SOS
7.5-03-04-01	Guideline on Use of RANS Tools for Manoeuvring Prediction	MAN
7.5-03-04-02	Validation and Verification of RANS Solutions in the Prediction of Manoeuvring Capabilities	MAN
7.5-04-01-01.1	Preparation, Conduct and Analysis of Speed/Power Trials	SOS
7.5-04-02-01	Full Scale Manoeuvring Trials Procedure	MAN
7.5-04-02-02	UV Full Scale Manoeuvring Trials	MAN
7.5-04-04-01	Underwater Noise from Ships, Full Scale Measurements	HN
7.5-04-05-01	Guideline on the determination of model-ship correlation factors	SOS

Appendix C. DOCUMENTS UPDATED BY QSG

Number	P / G	Title
4.2.3-01-01	P	Guide for the Preparation of ITTC Recommended Procedures
4.2.3-01-03	W	Work Instruction for formatting ITTC Recommended Procedures and Guidelines
7.5-02-01-06	P	Determination of a type A uncertainty estimate of a mean value from a single time series measurement
7.5-02-01-07	G	Guideline to Practical Implementation of Uncertainty Analysis
7.5-02-02-02	G	General Guideline for Uncertainty Analysis in Resistance Tests
7.5-02-02-02.1	G	Example for Uncertainty Analysis of Resistance Tests in Towing Tanks
7.6-02-08	W	Calibration of Weights
7.6-02-09	W	Calibration of Load Cells

P = Procedure
G = Guideline
W = Work Instruction